



**Humberto Salazar  
Amorim Varum**

**Avaliação, reparação e reforço sísmico de edifícios  
existentes**

**Seismic assessment, strengthening and repair of  
existing buildings**



**Humberto Salazar  
Amorim Varum**

**Avaliação, reparação e reforço sísmico de edifícios  
existentes**

**Seismic assessment, strengthening and repair of  
existing buildings**

dissertação apresentada à Universidade de Aveiro para cumprimento dos requisitos necessários à obtenção do grau de Doutor em Engenharia Civil, realizada sob a orientação científica do Prof. Doutor Aníbal Costa, Professor Associado com Agregação da Faculdade de Engenharia da Universidade do Porto e do Prof. Doutor Paulo Vila Real, Professor Associado com Agregação da Universidade de Aveiro

## **o júri**

presidente

**Prof<sup>a</sup>. Doutora Maria Helena Vaz de Carvalho Nazaré**  
Reitora da Universidade de Aveiro

vogais

**Prof. Doutor Aníbal Guimarães da Costa**  
professor associado com agregação da Faculdade de Engenharia da Universidade do Porto

**Prof. Doutor Paulo Jorge de Melo Matias Faria de Vila Real**  
professor associado com agregação da Universidade de Aveiro

**Doutor Artur Vieira Pinto**  
chefe do sector de Construção e Engenharia Sísmica do Laboratório ELSA do Centro Comum de Investigação da Comissão Europeia, Ispra, Itália

**Prof. Doutor Raimundo Moreno Delgado**  
professor catedrático da Faculdade de Engenharia da Universidade do Porto

**Prof. Doutor João José Rio Tinto de Azevedo**  
professor catedrático do Instituto Superior Técnico da Universidade Técnica de Lisboa

**Prof. Doutor José Claudino de Pinho Cardoso**  
professor associado da Universidade de Aveiro

**Prof. Doutor Paulo Barreto Cachim**  
professor auxiliar da Universidade de Aveiro

## acknowledgements

The present work has been developed at the Civil Engineering Department of Aveiro University and at the ELSA laboratory of the Joint Research Centre at Ispra, in Italy. I gratefully acknowledge the generous help of the following organisations and many individuals, for their generous support, which made this work possible:

To Professor Aníbal Costa and Professor Paulo Vila Real for their invaluable supervision. To Professor Aníbal Costa I would like to express my gratitude for the encouragement over these years. Without his constructive advice on the contents, I would have never got to finish the thesis.

To Dr. Artur Pinto for directing me towards such an interesting project, and for making my work at JRC so stimulating. He was largely responsible for the conception and success of this project. His contribution, comments and patient supervision are gratefully acknowledged.

The financial support provided by the Portuguese Science and Technology Foundation (PRAXIS XXI BD/15875/98 grant) is gratefully acknowledged.

Thanks go to Dr. Javier Molina, Dr. Rui Pinho, Professor Michael Griffith, Dr. Pierre Pegon, Dr. José Jara, Dr. António Arêde, Dr. João Guedes, Dr. Rui Faria and Professor Raimundo Delgado for their friendship, supportive interest and constructive comments to my work. The contributions from European institutions and researchers involved in the ICONS TMR-Network research programme are also acknowledged. Special thanks are due to Dr. Eduardo Carvalho and Dr. Ema Coelho from LNEC.

The successful preparation and execution of the complex testing campaign is a result of the exceptional joint effort of the ELSA laboratory staff and researchers. Their technical assistance, professionalism and welcoming environment are gratefully acknowledged. Particular thanks to Professor Michael Geradin, Mr. Guido Verzeletti, Ms. Jeanne-Paule Ambrosetti and Ms. Paola Schaack.

I would like to address special thanks to all my undergraduate and master professors from the Engineering Faculty of University of Porto. Their example was always a precious positive reference to me. My work reflects what I have learned from them, from an academic, professional and human point of view.

To my colleagues from the Civil Engineering Department at University of Aveiro, I express my thanks for their friendship, comments and suggestions. Particular thanks to Professor Claudino Cardoso, Professor Luís Magalhães, Mr. Celestino Quaresma, Nuno Lopes and Ms. Ana Maria.

Thanks are due to Mr. Manuel Carvalho for his assistance in the final arrangement of the figures.

To the great friends I have made while at the JRC, I am also very grateful for their genuine friendship. I am also eternally indebted to my sincere friends in Portugal, particularly to Paulo Fidalgo and Daniel Oliveira for their endless friendship, tolerance and encouragement.

Lastly, I would also like express my sincere appreciation to my dear parents, brothers and my sweet fiancée Celeste Amorim, for their unfailing patience, support, encouragement, affection and love, that made this experience to happen. I wish to dedicate this thesis to them all, with appreciation for patiently enduring and sharing these years of preparation with me.

This work is also dedicated to the memory of those who lost their lives and those that have been injured as a result of earthquakes.

## resumo

Sismos recentemente ocorridos em todo o mundo têm demonstrado de forma dramática que a investigação na engenharia sísmica deve ser direccionada para a avaliação da vulnerabilidade das construções existentes, desprovidas de adequadas características resistentes. O seu reforço deve ser realizado, reduzindo a sua vulnerabilidade e conseqüentemente risco para níveis aceitáveis. O estudo e desenvolvimento de novas técnicas de reforço tem um papel principal no sentido de evitar a perda de vidas humanas e económicas. Os principais objectivos desta tese são: a avaliação experimental de edifícios existentes de betão armado, o desenvolvimento de modelos numéricos refinados capazes de reproduzir rigorosamente a sua resposta estrutural, o desenvolvimento de metodologias simplificadas para a análise não-linear dinâmica de estruturas irregulares, e o desenvolvimento de ferramentas numéricas para a optimização de reforço para este tipo de estruturas. São apresentadas as mais comuns causas de dano ou colapso de estruturas existentes, bem como as técnicas de reparação e reforço adequadas. Em muitas cidades do sul da Europa, os edifícios existentes, dimensionados e construídos até finais dos anos 70, sem considerar a acção sísmica, constituem um elevado risco para as populações.

Dois pórticos de 4 pisos à escala real, representativos da prática de projecto e construção até finais dos anos 70 na maioria dos países do sul da Europa, foram dimensionados, construídos e testados para crescentes intensidades de acção. Os principais objectivos desta série de ensaios foram a avaliação da capacidade original destes edifícios, com e sem alvenaria, e ainda a validação experimental da eficiência de várias técnicas de reparação e reforço. Os ensaios realizados demonstraram que a vulnerabilidade destas construções, dimensionadas sem características sísmo-resistentes, que constituem uma parte importante dos edifícios existentes na Europa, são uma fonte de alto risco para as populações. Foi ainda comprovado que soluções de reforço adequadamente seleccionadas, podem reduzir consideravelmente este risco para níveis aceitáveis de acordo com a actual filosofia dos códigos de dimensionamento e avaliação da segurança estrutural.

Foram utilizados modelos numéricos refinados para o pórtico e para a alvenaria. Os modelos foram calibrados com os resultados dos ensaios à escala real. Especial atenção foi dedicada ao escorregamento das armaduras de aderência normal, dada a sua influência na resposta de estruturas existentes. Os modelos calibrados demonstraram ser adequados na determinação da resposta não-linear de estruturas existentes.

Adicionalmente é proposta uma metodologia simplificada para a análise dinâmica não-linear de edifícios baseada no cálculo espectral multi-modal da resposta sísmica. Esta metodologia apresenta a possibilidade de análise de estruturas irregulares e constitui-se como uma ferramenta essencial para a optimização do reforço de edifícios existentes que se desenvolveu no âmbito da presente tese.

## **abstract**

Recent major earthquakes around the world have evidenced that research in earthquake engineering must be directed to the assessment of vulnerability of existing constructions lacking appropriate seismic resisting characteristics. Their retrofit or replacement should be made in order to reduce vulnerability, and consequent risk, to currently accepted levels. The development of retrofitting techniques represents a key issue in order to avoid both human casualties and economic losses.

The aims of this thesis are to experimentally study the behaviour of existing reinforced concrete buildings, to calibrate a refined numerical model in order to reproduce rigorously their structural behaviour, to develop a simplified methodology for non-linear dynamic analysis of irregular buildings, and to propose a methodology for optimum strengthening.

As a background, a theoretical summary on the most common causes of damage and failure and on repair and strengthening techniques for existing reinforced concrete buildings is presented. Older buildings, designed and constructed until the late 1970's, without considering earthquake provisions, constitute a significant hazard in many cities of southern Europe.

Two full-scale four-storey frame models, representative of the common practice of construction until the late 1970's in most southern European countries, were designed, constructed and tested pseudo-dynamically. This experimental study aimed at assessing the original capacity of existing structures, with and without infill masonry, and to compare performances of different retrofitting solutions.

The tests have shown that the vulnerability of existing reinforced concrete frames designed without specific seismic resisting characteristics, which are an important part of the existing buildings in Europe, constitute a source of high risk for human life. Furthermore, it was demonstrated that advanced retrofitting methods, solutions and techniques substantially reduce that risk to levels currently considered in modern design.

Refined finite element models for the frame and infill masonry were calibrated with the results of the full-scale tests. Special attention was devoted to bond-slip phenomenon, which is likely to influence the behaviour of existing reinforced concrete structures with round smooth reinforcing. The improved models were found capable to analyse existing reinforced concrete structures, reproducing accurately their non-linear response.

Additionally, it is proposed a simplified methodology for non-linear dynamic analysis of buildings based on the multi-modal spectral seismic response. This methodology is a valuable tool to analyse irregular structures and constitutes an important tool for the optimum strengthening design of existing buildings, which was also developed in this thesis.

## **Keywords**

- Assessment, strengthening and repair of structures
- Existing reinforced concrete buildings
- Structural deficiencies
- Seismic retrofitting
- Pseudo-dynamic earthquake testing
- Global refined non-linear numerical modelling and analysis
- Masonry infilled frames
- Bond-slip
- Performance-based earthquake engineering
- Simplified assessment methods
- Optimum strengthening

## List of Abbreviations

Here are catalogued the abbreviations used in this thesis, which can be pronounced as whole words, abbreviations that do not form a word, as well as, codes which constituents do not derive from words. Generally speaking the database entries are retrieved from English language sources but the acronym itself does not necessarily need to be of English origin. Their meaning are listed in the following:

2D	two-dimensional
3D	three-dimensional
AASHTO	American Association of State Highway and Transportation Officials
ACI	American Concrete Institute
AIJ	Architectural Institute of Japan
AISC	American Institute of Steel Construction
ADRS	Acceleration-Displacement Response Spectra
ASCE	American Society of Civil Engineers
ASR	Assessment, Strengthening and Repair
ASTM	American Society for Testing Materials
ATC	Applied Technology Council
BF	Bare Frame
BS	Base-Shear
BS	British Standards
CALTRANS	California Department of Transportation (USA)
CBC	California Building Code
CEA	Commissariat à l'Energie Atomique (France) - (French Atomic Energy Commission)
CEB	Comité Euro-International du Béton (Euro-International Concrete Committee)
CEN	European Committee for Standardization
CFRP	Carbon Fibre Reinforced Polymers
CNS	Council of the National Seismic System (USA)
CONLIN	CONvex LINearization method
CPU	Central Processing Unit
CSM	Capacity Spectrum Method
CUREE	California Universities for Research in Earthquake Engineering (USA)
DBD	Displacement Based Design
DC	Ductility Class
DCM	Displacement Coefficient Method



DE	Design Earthquake
DI	Damage Index
DOF	Degree-Of-Freedom
EASY	Earthquake engineering slide information system
EC	European Commission
EC2	Eurocode 2
EC6	Eurocode 6
EC8	Eurocode 8
ECEE	European Conference on Earthquake Engineering
ECOEST	European Consortium of Earthquake Shaking Tables (Access to LSF research project)
EDD	Energy Dissipation Device
EDS	Energy Dissipation System
EE	Earthquake Engineering
EERC	Earthquake Engineering Research Center (USA)
EERI	Earthquake Engineering Research Institute (USA)
ELSA	European Laboratory for Structural Assessment
EN	Norme Européenne (European Standard)
ENV	Prénorme Européenne (European Prestandard)
EQ	Earthquake
EQGM	Earthquake Ground Motion
ERA	European Research Area
ESC	European Seismological Commission
ESD	European Strong-motion Database
FE	Finite Element
FEM	Finite Element Method
FEMA	Federal Emergency Management Agency
FEUP	Faculty of Engineering - University of Porto (Portugal)
FFT	Fast Fourier Transform
FIB	Fédération Internationale du Béton (International Federation for Structural Concrete)
FIP	Fédération Internationale de la Précontrainte (International Federation for Prestressing)
FP	Framework Program
FRP	Fibre Reinforced Polymers
GECORPA	Portuguese Society for Conservation and Rehabilitation of the Architectural Heritage
GIS	Geographic Information Systems
HCM	Human Capital and Mobility programme of the European Commission
IABSE	International Association for Bridge and Structural Engineering
IBC	International Building Code
ICONS	Innovative seismic design CONcepts for new and existing Structures (EC funded programme of research network)
ICT	Information and Communication Technology
ID	Inter-storey Drift

IN	Infilled frame
IPSC	Institute for the Protection and the Security of the Citizen (JRC)
IRIS	Incorporated Research Institutions for Seismology
ISIS	Institute for Systems, Informatics and Safety (JRC)
ISPMNH	International Society for the Prevention and Mitigation of Natural Hazards
IT	Information Technology
JBC	Japanese Building Code
JBDPA	Japan Building Disaster Prevention Association
JMA	Japanese Meteorological Agency
JRC	Joint Research Centre
JSCE	Japan Society of Civil Engineers
KB	K-Bracing
KOERI	Kandilli Observatory & Earthquake Research Institute (Turkey)
LNEC	Laboratório Nacional de Engenharia Civil (Portugal)
LSF	Large-Scale Facilities
MAE	Mid-America Earthquake Center
max	maximum
MCE	Maximum Capable Earthquake
MCEER	Multidisciplinary Center for Earthquake Engineering Research (USA)
MDOF	Multiple-Degree-of-Freedom system
ME	Maximum Earthquake
min	minimum
MMA	Method of Moving Asymptotes
NAHB	National Association of Home Builders
NEHRP	National Earthquake Hazard Reduction Program (USA)
NEIC	National Earthquake Information Center
NISEE	National Information Service for Earthquake Engineering - University of California, Berkeley (USA)
NIST	National Institute of Standards and Technology (USA)
NSF	National Science Foundation (USA)
NZ	New Zealand
NZCS	New Zealand Concrete Society
NZS	New Zealand Standard Code of Practice for General Structural Design and Design Loading for Buildings
NZNSEE	New Zealand National Society for Earthquake Engineering
OECD	Organisation for Economic Co-operation and Development
OSHA	Occupational Safety and Health Administration (USA)
PA	Park and Ang Damage Index
PBD	Performance Based Design
PBE	Performance Based Engineering
PBEE	Performance Based Earthquake Engineering

PBSD	Performance Based Seismic Design
PBSE	Performance Based Seismic Engineering
PC	Personal Computer
PEER	Pacific Earthquake Engineering Research Center (USA)
PGA	Peak Ground Acceleration
PGV	Peak Ground Velocity
PO	Performance Objective (or Performance design Objective)
PP	Performance Point
PREC8	Prenormative Research in support of Eurocode 8 project (preceded the ICONS project)
PSA	Pseudo Acceleration Spectrum
PsD	Pseudo-Dynamic
PSV	Pseudo Velocity Spectrum
RC	Reinforced Concrete
R&D	Research and Development
REBAP	Regulamento de Estruturas de Betão Armado e Pré-esforçado (Portuguese code for RC structures)
RILEM	International Union of Laboratories and Experts in Construction Materials, Systems and Structures
RSA	Regulamento de Segurança e Acções para estruturas de edifícios e pontes (Portuguese code for actions on structures)
SAFERR	Safety Assessment For Earthquake Risk Reduction (European Research Training Network)
SC	Infill strengthened frame ('Shotcrete')
SCP	Sequential Convex Programming
SDOF	Single-Degree-Of-Freedom system
SE	Serviceability Earthquake
SEAOC	Structural Engineers Association Of California
SI	Système International d'unités (International System of Units)
SLP	Sequential Linear Programming
SPES	Sociedade Portuguesa de Engenharia Sísmica (Portuguese Society for Earthquake Engineering)
SR	Selective Retrofitted frame
SRC	Steel Reinforced Concrete
TD	Top-Displacement
TMR	Training and Mobility of Researchers
UBC	Uniform Building Code
UK	United Kingdom
URM	Un-Reinforced Masonry
USA	United States of America
USGS	United States Geological Survey
WCEE	World Conference on Earthquake Engineering
yrp	Years Return Period

# TABLE OF CONTENTS

## CHAPTER 1 – INTRODUCTION, MAIN OBJECTIVES AND PLAN OF THE THESIS

1.1 – INTRODUCTION.....	1
1.2 – MAIN OBJECTIVES OF THE THESIS .....	10
1.3 – PLAN OF THE THESIS .....	11

## CHAPTER 2 – SEISMIC VULNERABILITY AND REHABILITATION OF EXISTING RC STRUCTURES

2.1 – INTRODUCTION.....	15
2.2 – STRUCTURAL ASSESSMENT AND RETROFITTING .....	16
2.2.1 – Structural assessment.....	16
2.2.2 – Structural retrofitting .....	18
2.2.3 – Seismic assessment and redesign criteria and codes: Overview .....	19
2.3 – METHODOLOGIES FOR ASSESSMENT AND REDESIGN .....	22
2.3.1 – Performance-based design and assessment .....	23
2.3.2 – Displacement coefficient method .....	25
2.3.3 – N2 method .....	25
2.3.4 – Capacity spectrum method .....	26
2.3.4.1 – Capacity curve .....	27
2.3.4.2 – Demand spectrum .....	27
2.3.4.3 – Performance point.....	28

2.3.4.4 – Performance objective .....	28
2.3.4.5 – Procedure to calculate the performance point.....	29
2.3.4.6 – Conversion of the capacity curve to the capacity spectrum.....	30
2.3.5 – Equivalent damping ratio.....	31
<b>2.4 – FIELD EVIDENCE: OBSERVED DAMAGE IN RC BUILDINGS AND CASUALTIES DURING RECENT EARTHQUAKES .....</b>	<b>34</b>
2.4.1 – The 24 <sup>th</sup> March 2001 Geiyo earthquake, southwest Japan .....	35
2.4.2 – The 20 <sup>th</sup> February 2001 Nisqually earthquake, Seattle-Olympia, US .....	36
2.4.3 – The 7 <sup>th</sup> September 1999 Athens earthquake, Greece.....	37
2.4.4 – The 17 <sup>th</sup> August 1999 Izmit earthquake, Kocaeli, Turkey.....	39
2.4.5 – The 25 <sup>th</sup> January 1999 Armenia earthquake, Colombia .....	43
2.4.6 – The 26 <sup>th</sup> January 1995 Great Hanshin-Awaji earthquake, Kobe, Japan .....	45
2.4.7 – The 17 <sup>th</sup> January 1994 Northridge earthquake, Los Angeles, US.....	49
2.4.8 – Conclusion and discussion.....	50
<b>2.5 – TYPICAL CAUSES OF DAMAGE AND FAILURE OF EXISTING NON- DUCTILE RC BUILDINGS .....</b>	<b>50</b>
2.5.1 – Stirrups/hoops, confinement and ductility .....	52
2.5.2 – Bond, anchorage, lap-splices and bond splitting .....	53
2.5.3 – Inadequate shear capacity and failure.....	56
2.5.4 – Inadequate flexural capacity and failure.....	59
2.5.5 – Inadequate shear strength of the joints .....	60
2.5.6 – Influence of the infill masonry on the seismic behaviour of frames.....	61
2.5.7 – Vertical and horizontal irregularities .....	63
2.5.8 – Higher modes effect.....	66
2.5.9 – Strong-beam weak-column mechanism.....	66
2.5.10 – Structural deficiencies due to architectural requirements.....	67
<b>2.6 – COMMON RETROFITTING STRATEGIES AND TECHNIQUES OF EXISTING RC BUILDINGS .....</b>	<b>68</b>
2.6.1 – Global structural system intervention techniques.....	69
2.6.1.1 – Addition of RC structural shear walls.....	71
2.6.1.2 – Addition of steel bracing or post-tensioned cable systems .....	73
2.6.1.3 – Base seismic isolation.....	74
2.6.1.4 – Passive energy dissipation systems.....	76

---

2.6.1.5 – Mass reduction.....	77
2.6.1.6 – Other techniques .....	77
2.6.2 – Member intervention techniques for RC elements .....	78
2.6.2.1 – Epoxy resin injection .....	78
2.6.2.2 – Jacketing of existing members.....	79
2.6.2.3 – Shotcrete .....	82
2.6.2.4 – Other techniques .....	83

### **CHAPTER 3 – DESCRIPTION OF THE EXPERIMENTAL TESTS**

3.1 – INTRODUCTION.....	85
3.2 – CHARACTERISATION OF THE RC FRAMES.....	89
3.2.1 – Reinforced concrete frame structure: geometry and section detailing .....	89
3.2.2 – Modern codes requirements for earthquake resisting structures .....	92
3.2.3 – Construction of the frames and loading devices.....	95
3.2.4 – Transportation of the frame models.....	97
3.2.5 – Materials properties .....	98
3.2.6 – Vertical loads.....	101
3.2.7 – Earthquake input.....	102
3.3 – SELECTIVE STRENGTHENING SOLUTION FOR THE BARE FRAME .....	104
3.4 – MASONRY INFILL WALLS AND MASONRY STRENGTHENING; CONSTRUCTION DETAILS AND MATERIALS .....	107
3.4.1 – Masonry infill walls.....	108
3.4.2 – Strengthening of the infill panels.....	110
3.4.3 – Material properties.....	113
3.4.3.1 – Mortar used in joints and plaster.....	113
3.4.3.2 – Compression tests on infill block units.....	114
3.4.3.3 – Compression tests on masonry wallets in the directions parallel and perpendicular to the bed joints .....	114
3.4.3.4 – Concrete used for the shotcrete of the infill walls .....	115
3.4.3.5 – Diagonal compression tests on masonry wallets .....	116

3.4.3.6 – Mechanical properties of the masonry walls obtained from diagonal compression tests.....	121
3.4.3.7 – Comparison of the results obtained for the masonry materials and masonry wallets.....	124
3.4.4 – Empirical estimation of the masonry strength.....	126
3.4.4.1 – Infilled frames without apertures .....	126
3.4.4.2 – Reduction of strength and stiffness of the panels due to the presence of apertures .....	129
3.4.4.3 – Drift limits for masonry infill walls .....	131
3.4.4.4 – Storey strength of the infilled frame .....	132
3.5 – K-BRACING WITH SHEAR-LINK .....	134
3.6 – REPAIR AND STRENGTHENING OF THE FRAMES .....	136
3.6.1 – Damage-state after the pseudo-dynamic tests.....	136
3.6.2 – Repair and retrofitting using composite carbon fibre materials.....	137
3.6.3 – Material properties.....	138
3.6.4 – Application to repair and strengthening of the frames .....	139
3.6.4.1 – Overview.....	139
3.6.4.2 – Concrete repair and crack injection .....	139
3.6.4.3 – Carbon fibre application .....	140
3.6.5 – Remarks .....	141
3.7 – TESTING PROGRAMME AND TEST SET-UP .....	142
3.7.1 – Additional masses.....	143
3.7.2 – Reaction-wall.....	145
3.7.3 – Pseudo-dynamic test method.....	146
3.7.4 – Horizontal loading system .....	147
3.7.5 – Instrumentation of the RC frames.....	149
3.7.5.1 – Rotations: inclinometers .....	150
3.7.5.2 – Beam deformation at first floor level.....	152
3.7.5.3 – Slab-participation.....	153
3.7.5.4 – Strong-column .....	154
3.7.6 – Instrumentation of the infilled frame .....	154
3.7.7 – Instrumentation for the K-bracing test.....	156
3.7.8 – Instrumentation for the final capacity tests.....	157

3.7.8.1 – Relative displacement transducers at the repaired joints .....	158
3.7.8.2 – Relative displacement transducers at the strong-column .....	158
3.7.8.3 – Storey displacement transducers (PSITRONIX) .....	159
3.7.9 – Data acquisition system and post-processing .....	159
3.8 – NON-DESTRUCTIVE TESTS: FREQUENCIES IDENTIFICATION .....	160
3.8.1 – Non-infilled frame .....	161
3.8.2 – Infilled frame .....	165
3.9 – REMARKS .....	165

## **CHAPTER 4 – ANALYSIS OF EXPERIMENTAL TEST RESULTS**

4.1 – INTRODUCTION.....	167
4.2 – RESULTS FROM THE TESTS ON THE BARE FRAME.....	170
4.2.1 – Storey displacement, drift and shear.....	170
4.2.2 – Observed damages.....	173
4.2.3 – Maximum absolute and relative rotations measured at the critical zones .....	175
4.2.4 – Strong-column: 3 <sup>rd</sup> storey .....	176
4.2.5 – Local ductility and damage indices .....	178
4.2.6 – Energy dissipation .....	180
4.2.7 – Damage index.....	182
4.2.7.1 – Park and Ang damage index .....	182
4.2.7.2 – Calculation of the PA damage index for the bare frame tests.....	185
4.2.8 – Deformation at the beam extremities.....	188
4.2.9 – Remarks.....	189
4.3 – RESULTS FROM THE TESTS ON THE SELECTIVE STRENGTHENED FRAME .....	189
4.3.1 – Storey displacement, drift and shear.....	190
4.3.2 – Observed damages.....	195
4.3.3 – Maximum absolute and relative rotations measured at the critical zones .....	196
4.3.4 – Energy dissipation .....	197
4.3.5 – Deformation at the beam extremities.....	199



4.4 – COMPARISON BETWEEN BF AND SR TESTS.....	200
4.4.1 – Storey displacement, drift and shear.....	200
4.4.2 – Maximum absolute and relative rotations measured at the critical zones .....	204
4.4.3 – Energy dissipation .....	206
4.4.4 – Deformation at the beam extremities.....	207
4.4.5 – Vulnerability analyses .....	209
4.4.5.1 – Maximum inter-storey drift and global drift.....	209
4.4.5.2 – Maximum rotation .....	210
4.4.5.3 – Energy dissipation.....	211
4.5 – RESULTS FROM THE TESTS ON THE INFILLED FRAME.....	212
4.5.1 – Storey displacement, drift and shear.....	213
4.5.2 – Observed damages .....	218
4.5.3 – Damage intensity classification for infill masonry panels.....	221
4.5.4 – Maximum absolute and relative rotations measured at the critical zones .....	222
4.5.5 – Energy dissipation .....	224
4.6 – COMPARISON BETWEEN BF AND IN TESTS .....	226
4.7 – RESULTS FROM THE TESTS ON INFILL STRENGTHENED FRAME .....	228
4.7.1 – Storey displacement, drift and shear.....	229
4.7.2 – Observed damages .....	232
4.7.3 – Maximum absolute and relative rotations measured at the critical zones .....	234
4.7.4 – Energy dissipation .....	235
4.8 – COMPARISON BETWEEN IN AND SC TESTS .....	238
4.9 – K-BRACING WITH SHEAR-LINK TEST .....	240
4.9.1 – Test program.....	240
4.9.2 – Test results.....	240
4.10 – FINAL CAPACITY CYCLIC TESTS.....	245
4.10.1 – Description of cyclic loading history.....	246
4.10.2 – Selective strengthened frame cyclic test results .....	248
4.10.2.1 – Maximum absolute and relative rotations measured at the instrumented points .....	251
4.10.2.2 – Analyses of the repaired top-columns.....	252

4.10.3 – Bare frame cyclic test results.....	253
4.10.4 – Remarks.....	256
4.11 – LOCAL MEASUREMENTS.....	257
4.11.1 – Plastic hinge length.....	257
4.11.2 – Shear cracks at the base of the 1 <sup>st</sup> storey's strong-column.....	258
4.11.3 – Slab-participation.....	260
4.11.4 – Diagonal deformation of the short external panel.....	264
4.12 – FINAL REMARKS AND CONCLUSIONS.....	272
4.12.1 – Bare and selective strengthened frames.....	273
4.12.2 – Infilled and infill strengthened frames.....	275
4.12.3 – K-bracing.....	278
4.12.4 – Final capacity cyclic tests.....	279
4.12.5 – Remarks.....	279

## **CHAPTER 5 – REFINED AND SIMPLIFIED MODELS FOR EARTHQUAKE SIMULATION, ASSESSMENT AND OPTIMAL REDESIGN OF EXISTING RC STRUCTURES**

5.1 – INTRODUCTION AND MAIN OBJECTIVES.....	281
5.2 – NUMERICAL TOOLS: CASTEM.....	284
5.3 – STRUCTURAL MODELLING ASPECTS.....	287
5.3.1 – Description of the building frame model.....	289
5.3.2 – Improved element model.....	291
5.3.3 – Plastic hinge length.....	293
5.3.4 – Non-linear behaviour of RC elements.....	295
5.3.4.1 – Concrete model.....	299
5.3.4.2 – Steel model.....	301
5.3.5 – Bond–slip modelling of the longitudinal reinforcing steel plain bars.....	302
5.3.6 – Slab–participation.....	309
5.3.7 – Infill masonry modelling.....	313
5.3.8 – Retrofitting solutions modelling.....	318
5.3.8.1 – X- and K-bracing with dissipator retrofitting.....	318

5.3.8.2 – Selective strengthening .....	322
5.3.9 – Vertical static loads, earthquake actions, masses and damping .....	324
5.3.10 – Shear strength verification for the bare frame .....	325
5.4 – NATURAL FREQUENCIES AND VIBRATION MODES .....	328
5.5 – NUMERICAL PREDICTIONS OF THE PSEUDO-DYNAMIC TESTS.....	329
5.6 – RESULTS OF THE NUMERICAL NON-LINEAR DYNAMIC ANALYSES.....	331
5.6.1 – Bare frame numerical results .....	332
5.6.2 – Strengthened frame numerical results .....	338
5.6.3 – Infilled frame numerical results.....	343
5.6.4 – Discussion of the numerical results with refined FE models.....	349
5.7 – STRUCTURAL RESPONSE AND ASSESSMENT USING SIMPLIFIED METHODS.....	351
5.7.1 – Equivalent viscous damping from the experimental hysteretic curves.....	352
5.7.2 – Capacity spectrum method .....	355
5.7.2.1 – Capacity curve and capacity spectra .....	355
5.7.2.2 – Verification of the earthquake tests .....	359
5.7.2.3 – Assessment of the bare and strengthened structures .....	361
5.7.2.4 – Final remarks .....	365
5.7.3 – Improved MDOF non-linear dynamic model for structural assessment.....	366
5.7.3.1 – Description of the implemented algorithm .....	368
5.7.3.2 – Verification of the earthquake tests .....	371
5.7.3.3 – Assessment of the bare frame structure .....	373
5.7.4 – Observed seismic performance in the earthquake tests .....	374
5.8 – STRUCTURAL OPTIMIZATION PROBLEM IN SUPPORT OF BUILDING RETROFITTING DECISION .....	377
5.8.1 – Introduction .....	377
5.8.2 – Theoretic mathematical background.....	378
5.8.3 – Structural strengthening optimization problems' formulation .....	381
5.8.3.1 – Problem I: storey yielding strength.....	383
5.8.3.2 – Problem II: storey yielding stiffness (initial stiffness).....	384
5.8.3.3 – Problem III: yielding strength of the energy dissipator devices .....	385
5.8.4 – Implementation of the optimization problems.....	387

---

5.8.5 – Illustrative examples.....	389
5.8.5.1 – Existing structure.....	390
5.8.5.2 – Optimum design of the existing structure.....	390
5.8.5.3 – Multiple optimum strengthening design.....	393
5.8.6 – Final remarks.....	397
<b>CHAPTER 6 – SUMMARY AND CONTRIBUTIONS, CONCLUSIONS, IMPLICATIONS AND FUTURE RESEARCH</b>	
6.1 – SUMMARY AND CONTRIBUTIONS .....	399
6.2 – CONCLUSIONS.....	401
6.3 – IMPLICATIONS FOR RESEARCHERS, POLICY MAKERS AND OWNERS .....	410
6.3.1 – Implications for academic community, practitioner engineers and code makers.....	411
6.3.2 – Implications for policy makers and government agencies .....	413
6.3.3 – Implications for building owners.....	414
6.4 – FUTURE RESEARCH LINES .....	415
<b>APPENDIX A – PHOTOGRAPHIC DOCUMENTATION AND STRENGTHENING DETAILS.....</b>	<b>421</b>
<b>APPENDIX B – TEST RESULTS AND PHYSICAL DAMAGE PATTERNS Visual inspection and photographic documentation.....</b>	<b>443</b>
<b>APPENDIX C – GLOSSARY .....</b>	<b>463</b>
<b>REFERENCES AND RECOMMENDED READING .....</b>	<b>477</b>

---

# TABLE OF FIGURES

## CHAPTER 2 – SEISMIC VULNERABILITY AND REHABILITATION OF EXISTING RC STRUCTURES

Figure 2.1 – Seismic performance design objective matrix (VISION-2000, SEAOC, 1995).....	24
Figure 2.2 – Capacity spectrum method (adapted from ATC-40, 1996) .....	27
Figure 2.3 – Modal participation factors and modal mass coefficients (ATC-40, 1996).....	30
Figure 2.4 – Equivalent viscous damping for reinforced concrete structures (adapted from Priestley, 1997).....	31
Figure 2.5 – Energy dissipated ED in a cycle of harmonic vibration determined from an experiment (Chopra, 2001).....	32
Figure 2.6 – Damping for an hysteretic cycle .....	33
Figure 2.7 – Partial collapse of a three-storey residential building in Imabari (EQE, 2001).....	35
Figure 2.8 – Chevron eccentrically braced steel frame used to seismically upgrade building (Filiatrault <i>et al.</i> , 2001).....	36
Figure 2.9 – Yielding of the chevron eccentrically braced frame in the east–west direction of the building (Filiatrault <i>et al.</i> , 2001) .....	36
Figure 2.10 – Extent of the damage (KOERI, 1999).....	39
Figure 2.11 – General buildings damage and collapse in Gölcük, Adapazari and Yalova (KOERI, 1999; EQE, 1999; Sucuoglu, 2000).....	40
Figure 2.12 – Damage in buildings due to inappropriate detailing (KOERI, 1999).....	42
Figure 2.13 – Damage in RC buildings under construction after the Izmit earthquake (EQE, 1999) .....	43
Figure 2.14 – Typical middle rise RC frame building with brick infill walls (Kagami, 1999) .....	44

---

Figure 2.15 – Damage in an ordinary RC moment-resistant infilled RC frame (Kagami, 1999) .....	44
Figure 2.16 – Poor reinforcing details in RC joints (Kagami, 1999).....	45
Figure 2.17 – RC frame structures with a mid-height collapse (KOBEnet, 1995): a) collapsed 6 <sup>th</sup> storey of an eight-storey high office building; b) intermediate storey damage of a moderately high building; c) 5 <sup>th</sup> storey collapse of hospital.....	46
Figure 2.18 – RC frame structures with a mid–height collapse (EQE, 1995; KOBEnet, 1995).....	47
Figure 2.19 – Soft-storey building' collapses (EQE, 1995; KOBEnet, 1995) .....	47
Figure 2.20 – Badly damaged irregular RC building in Sannomiya (EQE, 1995) .....	48
Figure 2.21 – Damages on buildings of different type in central Kobe (EQE, 1995) .....	48
Figure 2.22 – Damaged RC columns without transverse reinforcement (Saatcioglu <i>et al.</i> , 1999) .....	52
Figure 2.23 – Damaged RC columns with inadequate transverse reinforcement (Saatcioglu <i>et al.</i> , 1999) .....	52
Figure 2.24 – Inadequate lap–splice and lack of stirrups (Saatcioglu <i>et al.</i> , 1999).....	54
Figure 2.25 – Typical deficiencies in buildings: a) beam bars terminate with tight 180° hooks in the joint; b) yielding of the longitudinal steel adjacent to the floor slab (Aschheim, 2001) .....	54
Figure 2.26 – Column lap-splice details (Aschheim, 2001) .....	55
Figure 2.27 – Bar pullout-columns (Aschheim, 2001).....	55
Figure 2.28 – Column shear failure examples: a) 1979 Montenegro earthquake (EASY, 1997); b) 1999 Izmit earthquake (note the to lack of transverse reinforcement - Saatcioglu <i>et al.</i> , 1999).....	58
Figure 2.29 – Shear and bond failure at the mid-height of a RC column during the 1985 Mexico city earthquake (EASY, 1997) .....	58
Figure 2.30 – Damaged RC corner column at the 1 <sup>st</sup> storey (Bertero, 1997) .....	58
Figure 2.31 – Column shear failure (Aschheim, 2001) .....	58
Figure 2.32 – Shear cracks at the RC column of an old school building (Yamazaki, 1993).....	58
Figure 2.33 – Column shear failures (Aschheim, 2001): a) strong-axis behaviour; b) oblique column shear failure; c) captive column shear failure .....	59
Figure 2.34 – Typical flexural failure: column hinging (Aschheim, 2001).....	60

---

Figure 2.35 – Lack of proper design of beam-column connections (Saatcioglu <i>et al.</i> , 1999) .....	61
Figure 2.36 – Inadequate strength of joints (Aschheim, 2001): a) joint damages; b) joint failures .....	61
Figure 2.37 – Damages on masonry infill walls (Saatcioglu <i>et al.</i> , 1999): a) RC frame building with almost fully damaged masonry infills; b) diagonal tension failure of a masonry wall.....	62
Figure 2.38 – Short column effect caused by: window opening; masonry walls; and, landing slabs of staircases (Saatcioglu <i>et al.</i> , 1999; Aschheim, 2001) .....	63
Figure 2.39 – Partial masonry infill in concrete frame (Paulay and Priestley, 1992).....	63
Figure 2.40 – Damage on infill walls (Aschheim, 2001): a) infill cracking; b) in-plane infill failure .....	63
Figure 2.41 – Soft-storeys (Aschheim, 2001).....	64
Figure 2.42 – Building failure due to the higher modes effect during the 1985 Mexico city earthquake (EASY, 1997) .....	66
Figure 2.43 – Strong-beam weak-column mechanism (Aschheim, 2001; Saatcioglu <i>et al.</i> , 1999) .....	67
Figure 2.44 – Typical buildings in Turkey (Aschheim, 2001): a) view; b) typical beam details .....	68

### **CHAPTER 3 – DESCRIPTION OF THE EXPERIMENTAL TESTS**

Figure 3.1 – Plan and elevation views of concrete frame plus masonry infill building .....	90
Figure 3.2 – Beam reinforcement details .....	91
Figure 3.3 – Column reinforcement details.....	91
Figure 3.4 – Transverse reinforcement for lap-splice zones (EC2) .....	94
Figure 3.5 – Attachment system at floor level .....	96
Figure 3.6 – Best-fit of steel constitutive law (Carvalho <i>et al.</i> , 1999) .....	100
Figure 3.7 – Scheme of vertical static loads .....	101
Figure 3.8 – Ground motion acceleration time histories for 475, 975 and 2000-yrp.....	103
Figure 3.9 – Response linear-elastic spectra for 475, 975 and 2000-yrp (5% damping): a) displacement; b) pseudo-acceleration.....	103

---

Figure 3.10 – Selective strengthening of the RC frame: a) strength-only intervention in strong-column; and, b) ductility-only intervention in strong-column (Elnashai and Pinho, 1999) .....	105
Figure 3.11 – Selective strengthened RC frame .....	105
Figure 3.12 – Elevation view of the infilled concrete frame (frame A): infill openings (location and dimensions) .....	108
Figure 3.13 – Infill block units .....	108
Figure 3.14 – Detail of the infill walls construction.....	108
Figure 3.15 – Reconstruction of the 1 <sup>st</sup> storey infill panels and infill strengthening (shotcrete) of the short external bay at all storeys (elevation): a) south view; b) north view .....	110
Figure 3.16 – Constructive details (layout and dimensions) of the infill strengthening.....	111
Figure 3.17 – Infill strengthening: a) light connection between masonry and steel mesh (nine connection points); b) reinforcement detailing (lateral overlapping of 0.50 m) .....	112
Figure 3.18 – Diagonal compression tests: typology and nomenclature of the tested specimens .....	117
Figure 3.19 – Diagonal compression test: a) testing set-up; b) instrumentation and loading shoe detail.....	118
Figure 3.20 – Diagonal compression tests: generic scheme .....	118
Figure 3.21 – Diagonal compression tests on specimens without plaster.....	119
Figure 3.22 – Diagonal compression tests on specimens with plaster in both sides .....	120
Figure 3.23 – Diagonal compression tests on specimens with plaster in both sides and strengthened .....	120
Figure 3.24 – Diagonal compression tests: specimens without plaster (red), with plaster in both sides (blue) and with plaster in both sides and strengthened (black) .....	120
Figure 3.25 – Reference stress on diagonal compression tests: specimens without plaster (red), with plaster in both sides (blue) and with plaster in both sides and strengthened (black) .....	124
Figure 3.26 – Masonry model: a) simplified pattern of distribution of interactive forces between infill and frame; b) tri-linear non-symmetric envelope and hysteretic rules .....	126
Figure 3.27 – Nomenclature: a) aperture and panel dimensions; b) identification of four panel-types .....	131
Figure 3.28 – Empirical shear-drift curves for the 1 <sup>st</sup> storey confined masonry panels.....	133

---



---

Figure 3.29 – Simplified tensile behaviour curves for the concrete and masonry.....	133
Figure 3.30 – K-bracing with shear-link system: possible layouts.....	135
Figure 3.31 – K-bracing with shear-link system test assembly .....	136
Figure 3.32 – Failure (shear-out) of the column/joint interface .....	137
Figure 3.33 – Distribution of the additional loads.....	144
Figure 3.34 – Reaction wall/floor facility (dimensions in <i>m</i> ) at the ELSA laboratory (Pinto, 1998).....	145
Figure 3.35 – General layout of the pseudo-dynamic test: reaction-wall, structure, pistons and reference steel-frame .....	148
Figure 3.36 – General layout of the 2 <sup>nd</sup> storey cyclic test: reaction-wall, structure, pistons and reference steel-frame .....	149
Figure 3.37 – Location of the 64 inclinometers.....	151
Figure 3.38 – Inclinometers location scheme: a) strong-column; b) slender-column .....	151
Figure 3.39 – 1 <sup>st</sup> floor beam instrumentation: general layout, dimensions and detail of the zone nearest to the strong-column.....	152
Figure 3.40 – Instrumentation for the slab-participation monitoring .....	153
Figure 3.41 – Strong-column instrumentation: 1 <sup>st</sup> storey, joint and base of the 2 <sup>nd</sup> storey.....	154
Figure 3.42 – Infill masonry instrumentation (general layout): 1 <sup>st</sup> and 2 <sup>nd</sup> storeys .....	155
Figure 3.43 – Infill masonry instrumentation (numbering): 1 <sup>st</sup> and 2 <sup>nd</sup> storeys.....	156
Figure 3.44 – K-bracing test instrumentation: bracing and shear-link instrumentation .....	157
Figure 3.45 – K-bracing test instrumentation: location of the 22 inclinometers .....	157
Figure 3.46 – K-bracing test instrumentation: infill relative-displacement transducers.....	157
Figure 3.47 – Instrumentation at the repaired joints: a) frame A; b) frame B; c) detail.....	158
Figure 3.48 – Strong-column instrumentation for the final capacity cyclic test: frame A .....	159
Figure 3.49 – Evolution of the four eigenfrequencies .....	162
Figure 3.50 – Evolution of the four eigenfrequencies (relative values: measured frequencies divided by the initial frequency).....	163

**CHAPTER 4 – ANALYSIS OF EXPERIMENTAL TEST RESULTS**

Figure 4.1 – BF tests: storey displacement time histories.....	170
Figure 4.2 – BF tests: top-displacement evolution.....	171
Figure 4.3 – BF tests: storey shear versus inter-storey drift.....	171
Figure 4.4 – BF tests: base-shear versus top-displacement.....	172
Figure 4.5 – BF tests: envelope storey shear versus inter-storey drift .....	172
Figure 4.6 – BF tests: a) maximum inter-storey drift profiles; b) maximum storey shear profiles .....	172
Figure 4.7 – Damage observed on the 3 <sup>rd</sup> storey strong-column after BF tests: a) at the bar termination zone (note reinforcement detail); b) at the top of the column .....	174
Figure 4.8 – BF tests: maximum absolute and relative rotation demands.....	175
Figure 4.9 – Strong-column at the base of the 3 <sup>rd</sup> storey: lap-splice reinforcement detail (70 cm length) .....	176
Figure 4.10 – Evolution of the rotations at the 3 <sup>rd</sup> storey strong-column during the BF975 test .....	177
Figure 4.11 – 3 <sup>rd</sup> storey strong-column: a) scheme of reinforcement; b) moments distribution .....	178
Figure 4.12 – Local rotation ductility demand and damage for the bare frame tests .....	179
Figure 4.13 – BF tests: storey and total energy dissipation.....	181
Figure 4.14 – BF tests: relative energy dissipation profiles .....	181
Figure 4.15 – Calculated damage index versus observed damage (Park <i>et al.</i> , 1987).....	184
Figure 4.16 – BF tests: evolution of the storey damage index .....	187
Figure 4.17 – BF tests: influence of the energy dissipation on the evolution of the storey damage index .....	187
Figure 4.18 – BF tests: beam 1 <sup>st</sup> floor: a) maximum relative rotation; b) maximum uniform strain .....	188
Figure 4.19 – SR tests: storey displacement time histories .....	191
Figure 4.20 – SR tests: top-displacement evolution .....	192
Figure 4.21 – SR tests: base-shear versus top-displacement .....	192
Figure 4.22 – SR tests: storey shear versus inter-storey drift .....	193

Figure 4.23 – SR tests: envelope storey shear versus inter-storey drift.....	193
Figure 4.24 – SR tests: a) maximum inter-storey drift profiles; b) maximum storey shear profiles .....	194
Figure 4.25 – SR tests: maximum absolute and relative rotation demands.....	196
Figure 4.26 – SR tests: storey and total energy dissipation.....	198
Figure 4.27 – SR tests: relative energy dissipation profiles .....	199
Figure 4.28 – SR tests: beam 1 <sup>st</sup> floor: a) maximum relative rotation; b) maximum uniform strain.....	199
Figure 4.29 – BF and SR tests: maximum inter-storey drift profiles .....	202
Figure 4.30 – BF and SR tests: maximum inter-storey drift profiles .....	202
Figure 4.31 – BF and SR 975-yrp tests: storey shear versus inter-storey drift.....	203
Figure 4.32 – BF and SR tests: storey shear versus inter-storey drift .....	204
Figure 4.33 – BF and SR tests: maximum relative rotation demands for the 975-yrp tests .....	205
Figure 4.34 – BF and SR tests: relative energy dissipation profiles.....	206
Figure 4.35 – BF and SR tests: relative energy dissipation profiles (475-yrp and 975-yrp tests).....	207
Figure 4.36 – BF and SR 475-yrp tests (beam 1 <sup>st</sup> floor): a) maximum relative rotation; b) maximum uniform strain .....	207
Figure 4.37 – BF and SR 975-yrp tests (beam 1 <sup>st</sup> floor): a) maximum relative rotation; b) maximum uniform strain .....	208
Figure 4.38 – BF and SR tests: a) maximum inter-storey drift; b) maximum global drift.....	209
Figure 4.39 – BF and SR tests: local rotation maximum demands .....	211
Figure 4.40 – BF and SR tests: total energy dissipation.....	212
Figure 4.41 – IN tests: storey displacement time histories.....	214
Figure 4.42 – IN tests: top-displacement evolution.....	214
Figure 4.43 – IN tests: base-shear versus top-displacement.....	215
Figure 4.44 – IN tests: envelope storey shear versus inter-storey drift .....	215
Figure 4.45 – IN tests: storey shear versus inter-storey drift.....	216
Figure 4.46 – IN tests: a) maximum inter-storey drift profiles; b) maximum storey shear profiles .....	216

---

Figure 4.47 – Types of damage in masonry infill panels (Sortis <i>et al.</i> , 1999).....	221
Figure 4.48 – IN tests: maximum absolute and relative rotation demands.....	223
Figure 4.49 – IN tests: relative energy dissipation profiles .....	224
Figure 4.50 – IN tests: storey and total energy dissipation.....	225
Figure 4.51 – BF and IN tests: 1 <sup>st</sup> and 2 <sup>nd</sup> storey shear versus inter-storey drift and respective envelope curves.....	227
Figure 4.52 – BF and IN tests (475 and 975-yrp): maximum inter-storey drift profiles .....	228
Figure 4.53 – SC tests: storey displacement time histories .....	229
Figure 4.54 – SC tests: top-displacement evolution .....	230
Figure 4.55 – SC tests: base-shear versus top-displacement .....	230
Figure 4.56 – SC tests: storey shear versus inter-storey drift .....	231
Figure 4.57 – SC tests: envelope storey shear versus inter-storey drift.....	231
Figure 4.58 – SC tests: a) maximum inter-storey drift profiles; b) maximum storey shear profiles.....	232
Figure 4.59 – SC tests: maximum absolute and relative rotation demands .....	234
Figure 4.60 – SC tests: storey and total energy dissipation.....	236
Figure 4.61 – SC tests: relative energy dissipation profiles .....	237
Figure 4.62 – IN and SC tests: base-shear versus global drift.....	238
Figure 4.63 – IN and SC tests: base-shear versus global drift and respective envelope curves .....	238
Figure 4.64 – IN and SC tests: storey shear versus inter-storey drift and respective envelope curves.....	239
Figure 4.65 – IN and SC tests: maximum inter-storey drift profiles .....	239
Figure 4.66 – KB-cyclic test: total storey shear versus relative storey displacement.....	241
Figure 4.67 – KB-cyclic test: damage inspection.....	242
Figure 4.68 – KB-cyclic test: shear force versus relative lateral displacement at the shear- link .....	243
Figure 4.69 – KB-cyclic test: total lateral storey resistance and shear-link shear resistance .....	244
Figure 4.70 – KB-cyclic test: energy dissipation for retrofitted frame and shear-link.....	244

Figure 4.71 – KB-cyclic test: total storey shear versus relative storey displacement and shear force versus relative lateral displacement at the shear-link .....	245
Figure 4.72 – Controlled force pattern and top-displacement: a) schematic representation; b) history of imposed lateral displacements.....	246
Figure 4.73 – SR and SR-cyclic tests: storey shear versus inter-storey drift .....	249
Figure 4.74 – SR and SR-cyclic tests: base-shear versus top-displacement.....	250
Figure 4.75 – SR2000 and SR-cyclic tests (frame B): maximum absolute rotation demands .....	251
Figure 4.76 – SR2000 and SR-cyclic tests (frame B): maximum relative rotation demands .....	251
Figure 4.77 – Nomenclature of the repaired external top-column (1 <sup>st</sup> and 2 <sup>nd</sup> storeys).....	252
Figure 4.78 – Frame B (evolution of N2 and D2 top-columns dislocation): a) test L33 (before repair), b) test L38 (after repair).....	253
Figure 4.79 – Frame B (joints N2 and D2): top-columns dislocation versus inter-storey drift before repair (test L33) and after repair (test L38).....	253
Figure 4.80 – BF and BF-cyclic tests: storey shear versus inter-storey drift .....	255
Figure 4.81 – BF and BF-cyclic tests: base-shear versus top-displacement.....	256
Figure 4.82 – Maximum uniform strain for positive and negative bending at the plastic hinge zone for the BF and SR tests.....	258
Figure 4.83 – BF475 test (1 <sup>st</sup> storey strong-column): a) ID; b) elongation in transducer #105.....	259
Figure 4.84 – IN975 test (1 <sup>st</sup> storey strong-column): a) ID; b) elongation in transducer #105.....	259
Figure 4.85 – Scheme of the slab-participation.....	261
Figure 4.86 – Scheme of the slab-participation.....	261
Figure 4.87 – BF tests: maximum deformation distribution ( <i>mm</i> ) at the internal long-bay .....	262
Figure 4.88 – SR tests: maximum deformation distribution ( <i>mm</i> ) at the internal long-bay .....	262
Figure 4.89 – Nomenclature for diagonal deformation (six zones) in the short external panel.....	264
Figure 4.90 – IN tests: 1 <sup>st</sup> storey strain of the short external panel (total mean diagonal strain) .....	266
Figure 4.91 – IN tests: 2 <sup>nd</sup> storey strain of the short external panel (total mean diagonal strain) .....	266

---

Figure 4.92 – IN tests: 1 <sup>st</sup> storey strain of the short external panel (middle).....	266
Figure 4.93 – IN tests: 2 <sup>nd</sup> storey strain of the short external panel (middle).....	266
Figure 4.94 – IN tests: 1 <sup>st</sup> storey strain of the short external panel (diagonal ascendant /) .....	267
Figure 4.95 – IN tests: 1 <sup>st</sup> storey strain of the short external panel (diagonal descending \) .....	267
Figure 4.96 – IN tests: 2 <sup>nd</sup> storey strain of the short external panel (diagonal ascendant /) .....	267
Figure 4.97 – IN tests: 2 <sup>nd</sup> storey strain of the short external panel (diagonal descending \) .....	267
Figure 4.98 – SC tests: 1 <sup>st</sup> storey strain of the short external panel (total mean diagonal strain).....	269
Figure 4.99 – SC tests: 2 <sup>nd</sup> storey strain of the short external panel (total mean diagonal strain).....	269
Figure 4.100 – SC tests: 1 <sup>st</sup> storey strain of the short external panel (middle) .....	270
Figure 4.101 – SC tests: 2 <sup>nd</sup> storey strain of the short external panel (middle).....	270
Figure 4.102 – SC tests: 1 <sup>st</sup> storey strain of the short external panel (diagonal ascendant /) .....	270
Figure 4.103 – SC tests: 1 <sup>st</sup> storey strain of the short external panel (diagonal descending \).....	270
Figure 4.104 – SC tests: 2 <sup>nd</sup> storey strain of the short external panel (diagonal ascendant /) .....	271
Figure 4.105 – SC tests: 2 <sup>nd</sup> storey strain of the short external panel (diagonal descending \).....	271

## **CHAPTER 5 – REFINED AND SIMPLIFIED MODELS FOR EARTHQUAKE SIMULATION, ASSESSMENT AND OPTIMAL REDESIGN OF EXISTING RC STRUCTURES**

Figure 5.1 – Schematic flow chart of modelling procedures adopted for the RC frames .....	288
Figure 5.2 – Model of the plane bare frame .....	290
Figure 5.3 – Generic element model: association of sub-elements with elastic linear (joints and central elements) and non-linear behaviour (plastic hinge zones).....	292
Figure 5.4 – Length of the non-linear fibre element .....	295

Figure 5.5 – General fibre method: section, discrete elements and curvature (adapted from CEB-161, 1983).....	297
Figure 5.6 – Discrete elements for the fibre model.....	298
Figure 5.7 – Concrete axial stress-strain constitutive law: envelope monotonic curves for concrete under tension and compression with the effects of confinement and cyclic curves (Guedes, 1997).....	300
Figure 5.8 – Uniaxial constitutive model for steel (Guedes, 1997).....	301
Figure 5.9 – Bond-slip deformation of the constituent materials.....	303
Figure 5.10 – Correction of the steel reinforcing constitutive law.....	304
Figure 5.11 – Bond stress-slip relationship (CEB-217, 1993) .....	305
Figure 5.12 – Bond stress-slip relationship for smooth reinforcing steel.....	306
Figure 5.13 – Comparison of the bond stress-slip behaviour of plain and deformed bars (Rehm, 1961; CEB-217, 1993) .....	307
Figure 5.14 – Bond stress-slip behaviour of plain bars (Rehm studies, 1961; and, MC-90, 1990) .....	307
Figure 5.15 – Computed relative steel strain function of the total ('concrete') strain.....	307
Figure 5.16 – Computed steel strain function of the total ('concrete') strain.....	307
Figure 5.17 – Proposed bond stress-slip relationship for smooth reinforcing bars .....	309
Figure 5.18 – Variation of sectional properties along the span of a beam (Paulay and Priestley, 1992) .....	310
Figure 5.19 – Variation of sectional properties along the span of a beam (Paulay and Priestley, 1992) .....	311
Figure 5.20 – Effective flange width of T-beam.....	312
Figure 5.21 – Slab geometry and reinforcement details.....	313
Figure 5.22 – Equivalent bracing action of masonry infill in the frame behaviour (Paulay and Priestley, 1992) .....	314
Figure 5.23 – Equivalent strut for the infill masonry model: a) geometric support of the strut diagonals; b) envelope and cyclic curves of the uniaxial behaviour law (Combesure and Pegon, 1996) .....	316
Figure 5.24 – Model of the plane infilled frame .....	318
Figure 5.25 – Typical diagrams for a device: a) schematic, and b) typical diagram for a device tested at ELSA in the framework of the project REEDS (Molina <i>et al.</i> , 2000.a) .....	319

---

Figure 5.26 – Bracing system in the central bay: device details and general layout.....	320
Figure 5.27 – Bracing system in the shorter-external bay: device details and general layout.....	320
Figure 5.28 – Vulnerability functions: a) top-displacement; b) base-shear .....	321
Figure 5.29 – Evolution of energy dissipation .....	321
Figure 5.30 – Loading and modelling sequence for the SR numerical analyses .....	323
Figure 5.31 – Natural first four modal frequencies and mode shapes numerically evaluated for the BF and IN structures.....	329
Figure 5.32 – BF: storey displacement time histories (4 <sup>th</sup> , 3 <sup>rd</sup> , 2 <sup>nd</sup> and 1 <sup>st</sup> storeys) .....	333
Figure 5.33 – BF: inter-storey drift time histories (4 <sup>th</sup> , 3 <sup>rd</sup> , 2 <sup>nd</sup> and 1 <sup>st</sup> storeys).....	334
Figure 5.34 – BF: storey shear time histories (4 <sup>th</sup> , 3 <sup>rd</sup> , 2 <sup>nd</sup> and 1 <sup>st</sup> storeys).....	335
Figure 5.35 – BF: storey shear versus inter-storey drift (4 <sup>th</sup> , 3 <sup>rd</sup> , 2 <sup>nd</sup> and 1 <sup>st</sup> storeys).....	336
Figure 5.36 – BF: dissipated energy at storey level (4 <sup>th</sup> , 3 <sup>rd</sup> , 2 <sup>nd</sup> and 1 <sup>st</sup> storeys) .....	336
Figure 5.37 – BF: base-shear versus top-displacement.....	337
Figure 5.38 – BF: total dissipated energy.....	337
Figure 5.39 – BF: maximum drift profile.....	337
Figure 5.40 – BF: maximum shear profile .....	337
Figure 5.41 – SR: storey displacement time histories (4 <sup>th</sup> , 3 <sup>rd</sup> , 2 <sup>nd</sup> and 1 <sup>st</sup> storeys) .....	339
Figure 5.42 – SR: inter-storey drift time histories (4 <sup>th</sup> , 3 <sup>rd</sup> , 2 <sup>nd</sup> and 1 <sup>st</sup> storeys).....	340
Figure 5.43 – SR: storey shear time histories (4 <sup>th</sup> , 3 <sup>rd</sup> , 2 <sup>nd</sup> and 1 <sup>st</sup> storeys).....	341
Figure 5.44 – SR: storey shear versus inter-storey drift (4 <sup>th</sup> , 3 <sup>rd</sup> , 2 <sup>nd</sup> and 1 <sup>st</sup> storeys).....	342
Figure 5.45 – SR: dissipated energy at storey level (4 <sup>th</sup> , 3 <sup>rd</sup> , 2 <sup>nd</sup> and 1 <sup>st</sup> storeys) .....	342
Figure 5.46 – SR: base-shear versus top-displacement.....	343
Figure 5.47 – SR: total dissipated energy.....	343
Figure 5.48 – SR: maximum drift profile.....	343
Figure 5.49 – SR: maximum shear profile .....	343
Figure 5.50 – IN: storey displacement time histories (4 <sup>th</sup> , 3 <sup>rd</sup> , 2 <sup>nd</sup> and 1 <sup>st</sup> storeys).....	345
Figure 5.51 – IN: inter-storey drift time histories (4 <sup>th</sup> , 3 <sup>rd</sup> , 2 <sup>nd</sup> and 1 <sup>st</sup> storeys) .....	346



Figure 5.52 – IN: storey shear time histories (4 <sup>th</sup> , 3 <sup>rd</sup> , 2 <sup>nd</sup> and 1 <sup>st</sup> storeys) .....	347
Figure 5.53 – IN: storey shear versus inter-storey drift (4 <sup>th</sup> , 3 <sup>rd</sup> , 2 <sup>nd</sup> and 1 <sup>st</sup> storeys).....	348
Figure 5.54 – IN: dissipated energy at storey level (4 <sup>th</sup> , 3 <sup>rd</sup> , 2 <sup>nd</sup> and 1 <sup>st</sup> storeys).....	348
Figure 5.55 – IN: base-shear versus top-displacement.....	349
Figure 5.56 – IN: total dissipated energy .....	349
Figure 5.57 – IN: maximum drift profile .....	349
Figure 5.58 – IN: maximum shear profile.....	349
Figure 5.59 – Equivalent storey damping (%) for the earthquake and cyclic tests on the BF and SR structures.....	352
Figure 5.60 – Equivalent global damping (%) versus global drift for the earthquake and cyclic tests on the BF and SR structures .....	354
Figure 5.61 – Pushover capacity curves for the BF and SR structures .....	355
Figure 5.62 – BF structure: pushover capacity curve (blue), PsD tests (green), and cyclic test (red) .....	357
Figure 5.63 – BF storey shear-drift curves: pushover (blue), PsD tests (green), and cyclic test (red) .....	357
Figure 5.64 – SR structure: pushover capacity curve (blue) and PsD tests (green).....	358
Figure 5.65 – BF response estimation with the CSM.....	359
Figure 5.66 – SR response estimation with the CSM.....	360
Figure 5.67 – ADRS: for the earthquake input motions and EC8 (5% damping).....	362
Figure 5.68 – Assessment of the BF with the CSM (subsoil class A; response spectra type I) for input motions: a) $a_g = 2.180 \text{ m/s}^2$ ; b) $a_g = 2.884 \text{ m/s}^2$ .....	362
Figure 5.69 – Assessment of the SR with the CSM (subsoil class A; response spectra type I) for input motions: a) $a_g = 2.180 \text{ m/s}^2$ ; b) $a_g = 2.884 \text{ m/s}^2$ ; c) $a_g = 3.728 \text{ m/s}^2$ .....	363
Figure 5.71 – Assessment of the SR with the CSM (subsoil class A; response spectra type I) for input motions: $a_g = 2.180 \text{ m/s}^2$ , $a_g = 2.884 \text{ m/s}^2$ and $a_g = 3.728 \text{ m/s}^2$ .....	364
Figure 5.72 – MDOF structural simplified model with concentrated masses at storey levels being connected by shear beam elements: a) damping defined for each storey, b) global first mode structural damping .....	367
Figure 5.73 – Reduced spectral seismic demand .....	370
Figure 5.74 – Inter-storey drift profile computed and PsD test results for the BF structure.....	372

---

Figure 5.75 – Inter-storey drift profile computed and PsD test results for the SR structure .....	372
Figure 5.76 – Vulnerability functions of the top-displacement and storey drift for the BF structure calculated with the multi-mode model .....	374
Figure 5.77 – BF capacity curves: multi-mode method (black), pushover (blue), PsD tests (green) and cyclic test (red) .....	374
Figure 5.78 – Lateral storey shear versus inter-storey drift behaviour (exact and idealized bilinear behaviour) .....	382
Figure 5.79 – Control variable: strength (yielding shear force - $F_y$ ) .....	383
Figure 5.80 – Problem I: a) yielding displacement constant; b) yielding stiffness constant .....	384
Figure 5.81 – Control variable: pre-yielding stiffness ( $K_y$ ) .....	384
Figure 5.82 – Control variable: yielding force of the dissipator device .....	386
Figure 5.83 – Iterative optimization procedure .....	388
Figure 5.84 – First order derivatives - Numerical evaluation.....	389
Figure 5.85 – Storey Shear-drift curves adopted from the experimental tests .....	390
Figure 5.86 – Storey strength ( $N$ ).....	392
Figure 5.87 – Objective function ( $N$ ) .....	392
Figure 5.88 – Storey displacements ( $m$ ).....	392
Figure 5.89 – Inter-storey drift ( $m$ ).....	392
Figure 5.90 – Converged solution: shear-drift storey response.....	392
Figure 5.91 – Storey yielding strength of the existing structure and optimum strengthening distribution .....	393
Figure 5.92 – Total additional strength .....	394
Figure 5.93 – 1 <sup>st</sup> storey additional strength.....	395
Figure 5.94 – 2 <sup>nd</sup> storey additional strength .....	395
Figure 5.95 – 3 <sup>rd</sup> storey additional strength.....	396
Figure 5.96 – Vulnerability function of the structure designed for 2% drift and 2500-yrp .....	396

## APPENDIX A – PHOTOGRAPHIC DOCUMENTATION AND STRENGTHENING DETAILS

Figure A.1 – Base foundation reinforcement (general view) and reinforcement of the columns (lap-splice at the columns base).....	423
Figure A.2 – Base foundation (detail): slender-column reinforcement and tubes to apply the vertical jacks (for structure uplift).....	423
Figure A.3 – General view of the base foundation (concrete casting) .....	423
Figure A.4 – Base foundation (concrete casting) and column longitudinal reinforcement at the base with 180° bends .....	423
Figure A.5 – Slab reinforcement, reinforcement added in the attachment zone and plastic tubes for connection to the steel loading frame.....	423
Figure A.6 – Joint detail .....	423
Figure A.7 – Casting of the 1 <sup>st</sup> floor (general view).....	424
Figure A.8 – Casting of the 1 <sup>st</sup> floor (general view): the 1 <sup>st</sup> to 2 <sup>nd</sup> floor transition without lap-splice in the columns reinforcement.....	424
Figure A.9 – Joints and columns reinforcement details .....	424
Figure A.10 – Construction at various phases (general views).....	425
Figure A.11 – Transport: vertical jacks.....	425
Figure A.12 – Transport: general view of the frames at the external area of the ELSA laboratory .....	426
Figure A.13 – Frames transportation.....	426
Figure A.14 – Vertical connectors pre-stressing (to attach the actuators at the steel load frame).....	427
Figure A.15 – Steel frames: a) pinned bars connecting the two frames and fixings to the reaction-wall; b) frame to control out-of-plane deformation in the frame extremity opposite to the reaction-wall.....	427
Figure A.16 – Fixings to the reaction-wall, steel pinned bars connecting the two frames and actuators .....	427
Figure A.17 – Additional loads (2.7 ton concrete blocks and 1.2 ton steel plates) and floor attachment steel bars system with pre-stressed connectors .....	428
Figure A.18 – Actuators (double acting servo-hydraulic actuator linked at the extremity to piezoresistive load cell).....	428
Figure A.19 – Displacement controllers (HEIDENHEIN optical transducers).....	428

---

Figure A.20 – Acquisition, control and monitoring system .....	428
Figure A.21 – Instrumentation: strong-column at 1 <sup>st</sup> storey .....	429
Figure A.22 – Instrumentation: slab (below).....	429
Figure A.23 – Instrumentation: inclinometers.....	429
Figure A.24 – 1 <sup>st</sup> storey strong-column: selective retrofitting (ductility and shear resistance improvement) and instrumentation (strong-column, slab, joint and beam deformation).....	429
Figure A.25 – Strength improvement: connection of the steel bars to columns.....	429
Figure A.26 – Construction of the infill masonry walls: sequential phases and detail.....	430
Figure A.27 – Four-storey full-scale reinforced concrete infilled frame: a) construction of the masonry infill walls; b) general views of the structure .....	430
Figure A.28 – Infill strengthening construction: sequential operations and details of the reinforcing steel mesh .....	431
Figure A.29 – Infills instrumentation installed for the IN and SC tests: panels and local instrumentation at the panel corners of the short external panel .....	431
Figure A.30 – Concrete specimens extraction from the frame structure .....	432
Figure A.31 – Additional masses (water reservoirs) .....	432
Figure A.32 – Instrumentation in repaired external joints (relative displacement transducer).....	432
Figure A.33 – Instrumentation at the 1 <sup>st</sup> storey strong-column for the final capacity cyclic test .....	432
Figure A.34 – Storey displacement measurement systems: HEIDENHEIN and PSITRONIX displacement transducers.....	432
Figure A.35 – K-bracing and shear-link: summary table .....	433
Figure A.36 – K-bracing and shear-link: general layout .....	433
Figure A.37 – K-bracing and shear-link: shear-link details .....	434
Figure A.38 – K-bracing and shear-link: details of shear-link and adjacent connections .....	434
Figure A.39 – K-bracing and shear-link: detail of braces .....	434
Figure A.40 – K-bracing and shear-link: detail of the bottom braces connection.....	434
Figure A.41 – K-bracing and shear-link: detail of Pos. 8.....	435
Figure A.42 – K-bracing and shear-link: detail of Pos. 14.....	435

---

Figure A.43 – K-bracing and shear-link: detail of Pos. 15.....	435
Figure A.44 – K-bracing and shear-link: detail of Pos. 16.....	435
Figure A.45 – K-bracing and shear-link: detail of Pos. 17 and Pos. 2 .....	435
Figure A.46 – Columns drilling: strong-column (left) and weak column (right).....	436
Figure A.47 – Anchoring of the top-beam to the existing RC frame .....	437
Figure A.48 – Bottom-beams: drilling .....	438
Figure A.49 – Shear-link with the surrounding beam and braces .....	438
Figure A.50 – Bracing instrumentation (strain-gauges).....	438
Figure A.51 – Instrumentation: relative displacement transducer (detail of the zone nearest to the shear-link).....	439
Figure A.52 – Repair operations (steps): 4 – remove concrete at the top of the damaged column; 5 – relocation of the column; 6 – concreting of the column/joint; 7 – strengthening with carbon fibre .....	439
Figure A.53 – Repair intervention: frame B.....	440
Figure A.54 – Repair intervention: frame A .....	440
Figure A.55 – Damages on the first storey strong-column: frame A .....	440
Figure A.56 – Column repaired with carbon fibre materials.....	440
Figure A.57 – Strong-column (frame B) repair intervention (schematic sequential operations): 1– longitudinal fibres; 2 – confinement of the column upper- part; 3 – confinement of the column low part (including bar termination zone).....	441
Figure A.58 – Joints repair intervention: schematic sequential operations.....	441
Figure A.59 – Sequential operation phases for the joints intervention .....	442

## **APPENDIX B – TESTS RESULTS AND PHYSICAL DAMAGE PATTERNS:**

### **Visual inspection and photographic documentation**

Figure B.1 – Plots of the time-domain identified frequency and damping ratio for the first two vibration modes of BF475 (L05), BF975 (L06), SR475 (L10), SR975 (L11) and SR2000 (L12).....	445
Figure B.2 – Equivalent modal frequency and damping for the virgin bare frame (10% intensity of 475-yrp earthquake) .....	446

---

Figure B.3 – Equivalent modal frequency and damping for the BF 475-yrp test .....	447
Figure B.4 – Equivalent modal frequency and damping for the BF 975-yrp test .....	448
Figure B.5 – Equivalent modal frequency and damping for the BF after 975-yrp earthquake test (5% intensity of 475-yrp earthquake).....	449
Figure B.6 – Equivalent modal frequency and damping for the SR - 5% intensity of 475-yrp earthquake (before full-intensity earthquake tests).....	450
Figure B.7 – Equivalent modal frequency and damping for the SR 475-yrp test .....	451
Figure B.8 – Equivalent modal frequency and damping for the SR 975-yrp test .....	452
Figure B.9 – Equivalent modal frequency and damping for the SR 2000-yrp test .....	453
Figure B.10 – Equivalent modal frequency and damping for the SR after 2000-yrp earthquake test (5% intensity of 475-yrp earthquake).....	454
Figure B.11 – Damage pattern after the bare frame tests (general layout).....	455
Figure B.12 – Slab damage pattern after the bare frame tests.....	455
Figure B.13 – BF975: the horizontal storey displacement is evidenced (comparing the relative position of the transversal beams of the two frames).....	456
Figure B.14 – BF975: Damage (spalling) at the top of the 3 <sup>rd</sup> storey strong-column (beginning) .....	456
Figure B.15 – BF975: damage (spalling) at the bar termination zone of the 3 <sup>rd</sup> storey strong-column .....	456
Figure B.16 – BF975: damage (spalling) at the top of the 3 <sup>rd</sup> storey strong-column.....	456
Figure B.17 – BF975: damage (spalling) at the bar termination zone of the 3 <sup>rd</sup> storey strong-column .....	456
Figure B.18 – Damage pattern after the selective strengthened frame tests (general layout) .....	457
Figure B.19 – Damage pattern after the infill frame tests (general layout).....	457
Figure B.20 – Slab damage pattern after the infill frame tests.....	458
Figure B.21 – IN975: damages at the 1 <sup>st</sup> storey infill panels and RC strong-column at the base.....	458
Figure B.22 – Damage pattern after the infill strengthened frame tests (general layout) .....	459
Figure B.23 – Damage on the reinforced concrete frame, infill and infill strengthened panels after the SC earthquake tests.....	459
Figure B.24 – KB-cyclic test: damage pattern in the shear-link .....	460

---

---

Figure B.25 – KB-cyclic test: damaged external columns ('shear-out').....	460
Figure B.26 – KB-cyclic test: details of the damaged external columns ('shear-out') .....	460
Figure B.27 – Frame A (brick infilled frame): damaged joints after the PsD tests.....	461
Figure B.28 – Frame B (brick infilled 2 <sup>nd</sup> storey and K-bracing with shear-link in the internal bay): damaged joints after cyclic tests .....	461

# TABLE OF TABLES

## CHAPTER 2 – SEISMIC VULNERABILITY AND REHABILITATION OF EXISTING RC STRUCTURES

Table 2.1 – Earthquake hazard level (according to SEAOC, 1995) .....	24
Table 2.2 – Earthquake hazard level (according to ATC-40, 1996) .....	24
Table 2.3 – Definition of a performance objective (according to ATC-40, 1996) .....	29

## CHAPTER 3 – DESCRIPTION OF THE EXPERIMENTAL TESTS

Table 3.1 – Testing programme .....	87
Table 3.2 – EC8 and EC2 requirements in terms of transversal reinforcement spacing (in mm) .....	93
Table 3.3 – Volumetric ratio of the columns transversal reinforcement (%) .....	93
Table 3.4 – Volumetric ratio of the columns longitudinal reinforcement (%) .....	95
Table 3.5 – C16/20 (nominal strength values).....	98
Table 3.6 – Tests on concrete specimens (average compressive strength).....	98
Table 3.7 – Fe B22k (nominal properties).....	99
Table 3.8 – Test on steel specimens (mean mechanical properties).....	100
Table 3.9 – Hazard curves for the moderate-high European scenario .....	102
Table 3.10 – Quantities used in masonry construction by meter square of wall (reference values) .....	109
Table 3.11 – Mortar used in the joints and plaster (proportioning).....	109



Table 3.12 – Flexural and compressive strength of the mortar .....	113
Table 3.13 – Compressive strength test on the block units .....	114
Table 3.14 – Compression strength test on the infill specimens (loading perpendicular to the bed joints) .....	115
Table 3.15 – Compression strength test on the infill specimens (loading parallel to the bed joints).....	115
Table 3.16 – Concrete used in the strengthening (proportioning) .....	116
Table 3.17 – Concrete compressive strength (average and characteristic values) .....	116
Table 3.18 – Diagonal compression tests: shear strength ( $S_u$ ) and shear modulus ( $G$ ) .....	122
Table 3.19 – Diagonal compression tests (average values): shear strength ( $S_u$ ) and shear modulus ( $G$ ).....	122
Table 3.20 – Diagonal compression tests: vertical ( $\varepsilon_v$ ) and horizontal ( $\varepsilon_k$ ) deformation at collapse.....	124
Table 3.21 – Summary table of materials (brick units and plaster) and masonry specimens test results.....	125
Table 3.22 – Reduction strength and stiffness coefficient for the panels.....	131
Table 3.23 – Repair operations (general steps) .....	138
Table 3.24 – Repair and strengthening (works timetable) .....	139
Table 3.25 – PsD testing programme of RC frames (bare and infilled).....	142
Table 3.26 – Final capacity cyclic testing programme of RC frames .....	143
Table 3.27 – Characteristics of the ELSA reaction-wall (adapted from Pinto, 1998).....	145
Table 3.28 – Evolution of the four modal frequencies of RC frame (frame B) .....	162
Table 3.29 – Natural frequencies of frame B evaluated with an impact hammer .....	164
Table 3.30 – Modal frequencies of the original infilled frame (frame A).....	165

## **CHAPTER 4 – ANALYSIS OF EXPERIMENTAL TEST RESULTS**

Table 4.1 – BF tests: response maximum values (summary table).....	173
Table 4.2 – BF tests: damage inspection and damage states (ATC-40, 1996).....	174
Table 4.3 – Calculated damage index versus observed damage .....	185

---

Table 4.4 – Parameters estimated for the PA damage index for the RC columns .....	185
Table 4.5 – BF tests: Park & Ang damage indicator .....	186
Table 4.6 – SR tests: response maximum values (summary table).....	194
Table 4.7 – SR tests: damage inspection and damage states (ATC-40, 1996) .....	195
Table 4.8 – IN tests: response maximum values (summary table) .....	217
Table 4.9 – IN tests: damage inspection .....	218
Table 4.10 – Damage severity evaluation in masonry infill panels (Sortis <i>et al.</i> , 1999).....	222
Table 4.11 – Damage severity evaluation in the IN earthquake tests .....	222
Table 4.12 – SC tests: response maximum values (summary table).....	232
Table 4.13 – SC tests: damage inspection.....	233
Table 4.14 – Peak horizontal top–displacement imposed in the BF-cyclic and SR-cyclic tests.....	247
Table 4.15 – Imposed shear profile.....	247
Table 4.16 – Shear profiles (obtained from the earthquake tests and imposed in the cyclic tests) .....	248
Table 4.17 – SR–cyclic test: response maximum values (summary table).....	250
Table 4.18 – BF–cyclic test: response maximum values (summary table).....	254
Table 4.19 – BF and SR tests: evaluation of the slab-participation for the internal long-bay .....	263
Table 4.20 – Estimation of the slab-participation according to EC8 provisions.....	263
Table 4.21 – IN tests: maximum positive (elongation) and negative (shortenning) strain (%) in the short external panel at the 1 <sup>st</sup> storey .....	265
Table 4.22 – IN tests: maximum positive (elongation) and negative (shortenning) strain (%) in the short external panel at the 2 <sup>nd</sup> storey.....	265
Table 4.23 – SC tests: maximum positive (elongation) and negative (shortenning) strain (%) in the short external panel at the 1 <sup>st</sup> storey.....	271
Table 4.24 – SC tests: maximum positive (elongation) and negative (shortenning) strain (%) in the short external panel at the 2 <sup>nd</sup> storey.....	272

**CHAPTER 5 – REFINED AND SIMPLIFIED MODELS FOR EARTHQUAKE  
SIMULATION, ASSESSMENT AND OPTIMAL REDESIGN OF  
EXISTING RC STRUCTURES**

Table 5.1 – Columns cross-sections ( $m \times m$ ) and reinforcement detailing .....	291
Table 5.2 – Beams cross-sections ( $m \times m$ ) and reinforcement detailing.....	291
Table 5.3 – Concrete: parameters to the numerical model.....	300
Table 5.4 – Steel: parameters to the numerical model .....	301
Table 5.5 – Parameters for defining the bond stress–slip relationship of smooth bars (CEB-217, 1993).....	306
Table 5.6 – Parameters for the Zarnic and Gostic numerical model .....	317
Table 5.7 – Properties of the energy dissipation devices .....	319
Table 5.8 – Maximum calculated shear forces ( $kN$ ) in columns (BF calculations).....	326
Table 5.9 – Maximum estimated shear strength ( $kN$ ) of the columns.....	328
Table 5.10 – Non-linear dynamic analyses of the BF, SR and IN structures.....	331
Table 5.11 – Maximum equivalent global damping (%) for the earthquake tests.....	354
Table 5.12 – Modal parameters for assessment of the BF and SR with the CSM .....	358
Table 5.13 – Summary table of the response point (estimated with the CSM and PsD experimental results) .....	361
Table 5.14 – Summary table of the assessment response point (estimated with the CSM) .....	365
Table 5.15 – Representative damage descriptions for elements in non-ductile RC frame buildings (adapted from ATC-40, 1996).....	375
Table 5.16 – Storey deformation limits (adapted from ATC-40, 1996).....	376
Table 5.17 – Matrix of the observed seismic performance for the BF and SR tests .....	376
Table 5.18 – Bi-linear storey shear-drift curves adopted .....	390
Table 5.19 – Converged solution: optimum distribution of the additional yielding strength (3 $cm$ drift limit and earthquake 975-yrp) .....	393

# CHAPTER 1

## INTRODUCTION, MAIN OBJECTIVES AND PLAN OF THE THESIS

*'Thousands of people live in older homes that can and should be seismically strengthened... An earthquake can throw an entire frame off the foundation and turn a house into a heap of rubble. The good news is that this is probably preventable.'* (Los Angeles Times editorial, 21<sup>st</sup> March 1994)

### 1.1 - INTRODUCTION

The magnitude of the damage caused by all natural disasters is infinite. But it is earthquakes which demonstrate the greatest power of destruction and, at the same time, take the heaviest toll in human life (Pichard, 1984), as evidenced in the 1<sup>st</sup> November 1755 Lisbon earthquake, in Portugal, where more than half of the constructions in town were destroyed or heavily damaged, and 10% of the population was killed (SPES, 2001). Earthquakes in 1950 and 1971 seriously damaged the beautiful old towns of Cuzco and Trujillo respectively, both in Peru. The 1975 earthquake in Burma devastated Pagan, an ancient city of 2000 Buddhist pagodas. Antigua Guatemala and Friuli, in Italy, were rocked by earthquakes in 1976. The Algerian town of El-Asnam has been struck by strong earthquakes three times in forty-six years. The last, in 1980, damaged archaeological sites in the surrounding region. The Republic of Montenegro was ravaged in 1979 by one of the most violent earthquakes occurred in the last few years. The Popayan earthquake of 1983 razed to the ground this historic town, jewel of Colombian colonial architecture. These are but a few dated examples of the terrible destructive power of earthquakes.

When the 1989 Loma Prieta earthquake struck the San Francisco bay area, it revealed the vulnerability of a major metropolitan area to the damage and death that can result from a major earthquake. Unfortunately, Loma Prieta did not reduce the chances for future large earthquakes and even more devastation in the bay area, as demonstrated in 1994 by the Northridge earthquake.

More recently, earthquakes occurring in highly populated zones have shown that existing buildings constructed without appropriate seismic resisting characteristics constitute the main source of risk and are the cause of most of the casualties. The tragedy in Kobe, Japan (17<sup>th</sup> January 1995), one year after the Northridge earthquake (17<sup>th</sup> January 1994), painfully warned us that the best building codes in the world do nothing for buildings built before the codes were enforced.

The very recent earthquakes in Europe (e.g. Bucharest, Romania, 1977; Montenegro, Yugoslavia, 1979; Azores, Portugal, 1980; Campania, Italy, 1980; Kalamata, Greece, 1986; Umbria/Marche, Italy, 1997; Azores, Portugal, 1998; Kocaeli, Turkey, 1999; Athens, Greece, 1999; Molise, Italy, 2002) confirm and highlight that also Europe may suffer from the vulnerability of the existing building stock.

Firstly, the vast majority of buildings in earthquake prone areas in Europe constructed before the 1980's are seismic deficient. In fact, until the 1960's no specific seismic design provisions were included in the codes and, from that period on, only seismic equivalent lateral loading has been considered in their design. Provisions for design and detailing of members and structures resembling those of modern codes only appeared in Europe in the 1980's in the national codes (e.g.: Portuguese design code - RSA, 1983) (Fardis, 1998).

Secondly, worldwide experience from past and present seismic activity shows that by far non-ductile reinforced concrete (RC) frame buildings are one of the most vulnerable structures and, therefore, represent overall the largest threat to human life and property in future earthquakes. Furthermore, RC is the most common construction material in southern Europe. For example, a survey on the Portuguese residential park recently conducted by LNEC (2000) based on the 1991 CENSUS results, reveals the predominance of RC buildings. First, the study shows that 56% of the total residential buildings had been constructed between 1961 and 1991. Moreover, it reveals that 62% of the family

households by 1991 had been constructed in the period 1961-1991, and 75% was less than 50 years old. Second, it clearly highlights that RC buildings gained increasing relevance since their introduction in 1935-1940, being the predominant type of residential construction in the 1990's. By 1991, 45% of the family residences were RC buildings. If one considers constructions after 1960 only, the share increases to more than 50%. It also shows that 97% of the family residences constructed in RC were less than 50 years old, and 88% were constructed after 1961. Silva-Araya *et al.* (1997), for example, also highlight that RC is the most common construction material in buildings in the Americas. Consequently, this predominant type of existing buildings constitute a major source of risk to human life and property loss, as demonstrated in the studies conducted at LNEC (LNEC, 2000; Carvalho *et al.*, 2000-b).

While the threat of severe earthquake ground motions is approximately the same today as it was 100 years ago, the potential for a major earthquake catastrophe has grown alarmingly over this period as a result of an uncontrolled increase in population and urbanisation in seismically active regions (Bertero *et al.*, 1991).

Nevertheless, the presence of an advanced building code, in earthquake prone zones does not guarantee adequate performance of buildings and their contents (EQE, 1999). Field inspection and analyses of the performance of structures during recent earthquake shakings have clearly shown that a building design that blindly follows seismic code regulations does not guarantee safety against collapse or serious damage. The reasons are discussed in detail in Bertero (1979; 1982) and can be summarized as follows. First, there are large uncertainties in many of the aspects involved in the numerical design of structures, particularly in establishing the design earthquake shaking and in estimating the demands and predicting the supplies of the real three-dimensional soil-foundation-building system. Second, the performance of the system depends on its state when the earthquake strikes. Thus construction and maintenance, which includes repair, retrofitting and/or modifications, must also be considered in addition to the design aspects (Bertero, 1979; 1982). Take for example Turkey. It has a modern building code for earthquake design, very similar to that used in California. The 1975 Turkish code includes detailing requirements for seismic resistant structures as (Aschheim, 2001): *a*) closer spacing of transverse steel near beam-column joints; *b*) transverse steel within joints; *c*) 135° hooks

with cross-ties; *d*) joint shear calculations; *e*) strong-column weak-beam provisions; etc. Therefore, modern buildings should have had moderate-to-light damage during the 1999 Kocaeli earthquake, given that the intensities of shaking in this earthquake were moderate. In fact, new buildings performed very poorly because they were not properly designed, not properly constructed, or located on ground that failed from shaking or faulting. This is a fact that building owners around the world need to clearly understand.

Even if the building's vulnerability is diminishing, with the evolution of codes and strengthening measures for existing constructions, pushing the risk to values that prevent human losses, we have to deal with the crescent society complexity, which makes the capital losses increase. The so-called knowledge-based economy (OECD, 2001), based on growth of high technology industries, crescent sophistication of the phone communication, Internet, electronic networks, among others, makes our economies and cities increasingly fragile and complex. Consequently, the economic consequences associated with a hypothetical earthquake also grow exponentially. Take, for example: loss of information in banks, hospitals, companies, research institutes, costs of the inoperative factories and companies, schools and universities closed, etc.

From the discussion above, it follows that the two most effective ways to mitigate the human, social and economical losses due to earthquakes are the improvement of current methods and development of new methods of designing, constructing and maintaining new structures, and of seismic upgrading of existing hazardous facilities (Anderson *et al.*, 1991). Engineers are confronted with the continuous challenge of developing new methods to build, repair, replace or rehabilitate existing structures (Silva-Araya *et al.*, 1997). According to USGS (1995), odds are 2-in-3 that at least one disastrous earthquake will strike the San Francisco bay area before 2020. Faced with this threat, corporations, government and other agencies have, in the last years, stepped up notable efforts intending to reduce future human, social and economical losses. In the US, considerable effort and millions of dollars are being spent now to save lives and billions later (USGS, 1995).

Summarising, recent major earthquakes around the world have dramatically evidenced that research in earthquake engineering (EE) must be directed to the assessment of seismic vulnerability of existing constructions lacking appropriate seismic resisting characteristics. The development of retrofitting techniques represent also a key issue in order to mitigate

the effects of future earthquakes and avoid both human casualties and economic losses. Their retrofit or replacement should be made in order to reduce vulnerability and consequently risk to currently accepted levels. The issue of retrofitting existing constructions is complex and difficult and involves many factors, namely, at political, decision-making, economical, scientific and technical levels. The increasing interest in the structural seismic redesign, to reach optimum structural behaviour, under earthquake actions, has led to the development of new retrofitting techniques, such as base isolation, eccentric steel bracing coupled with energy dissipators concepts, controlled behaviour mechanisms, passive damped systems, and composite solutions, reaching innovative and, for certain cases, economically attractive retrofitting solutions. However, providing new buildings with seismic resisting characteristics is presently easy and inexpensive, whereas the seismic rehabilitation of existing buildings involves considerable costs, including those of disruption of use, and poses several specific problems (Pinto *et al.*, 2001-*b*). Both the scientific and technical community should play a key role in the process of developing and assessing effective solutions and techniques for the seismic retrofitting of those existing vulnerable constructions. Transport infrastructures, such as bridges, should also be taken into account, as well as the priceless architectural heritage, which may suffer very heavy and/or irreversible damages from earthquakes.

Considering the devastating effects of past recent earthquakes, particularly evidenced in non-ductile RC structures and the predominance of that kind of structures in Europe, the study developed in this thesis concentrates on the seismic assessment and rehabilitation of RC constructions.

The relevance of the topic has been clearly acknowledged by policy makers, researchers and academics, as one can understand from the development and number of studies on seismic engineering. In the past few years much attention has been focussed on the structures assessment and strengthening design. The current growing number of national and international conferences and workshops (SPES, 2001; Geradin and Pinto, 2000; among others), bilateral cooperative research programmes and the emergent number of research papers published and specialized publications dedicated to the assessment, strengthening and repair of existing buildings, as well as application of new materials and innovative construction techniques, proves the actuality and vital importance of the topic.



Several state-of-the-art reviews on repair and strengthening have been published confirming the importance of the topic. Nevertheless, this literature presents a number of shortcomings, which need to be addressed.

First, a considerable amount of research work has been carried-out on the behaviour of new (designed and constructed according to recent seismic resistant codes) RC structures subjected to static and earthquake dynamic loads. However, there is a need of experimental results and numerical analyses dedicated to the study of old (designed without any specific seismic resistant rule) RC structures. As largely recognised by several authors (e.g. Fardis, 1998; Pinto *et al.*, 2001-*b*), the challenge to the scientific EE community is to define appropriate criteria to retrofit existing structures, to develop rational redesign methods and to investigate and assess innovative cost-effective strengthening solutions and techniques. Particular attention should be devoted to RC buildings because most of public critical facilities (schools, hospitals and local or state administrative services, among other essential facilities), as well as buildings with high rates and duration of occupancy (commercial and office buildings, hotels, etc.) belong to this class of buildings. Different approaches are followed for assessment and retrofit existing buildings in different countries, with different degrees of success. Still, much research is needed to evaluate the performance, response and reliability of existing and rehabilitated structures. Our knowledge of the capacities of rehabilitation schemes and procedures for retrofitting structures must be improved, as expressed by Silva-Araya *et al.* (1997). The work developed and presented in this thesis emerges as consequence of these identified needs, and adding to the theoretical and empirical literature by addressing old RC structures.

Second, there is still a lack of experimental research on seismic performance of existing RC buildings. The scarce experimental studies focus on isolated elements or in reduced scale structures. Data on the real characteristics of buildings that have been subjected to earthquakes are in general difficult to obtain. This thesis attempts to push research a step further by conducting experimental tests on full-scale structure models. The work conducted in this thesis benefits from being part of the ICONS network project financed by the TMR (Training and Mobility of Researchers) programme (access to Large-Scale Facilities, LSF) of the European Commission (EC), which focuses on Innovative seismic design CONcepts for new and existing Structures (see ICONS WebPages, 1999, for

details). Two full-scale RC frames representative of the building's design and construction practice until the late 1970's in most of south European countries, and currently needing seismic retrofit, were constructed and tested pseudo-dynamically, at the ELSA laboratory (European Laboratory for Structural Assessment). The test frames had been designed without specifically considering seismic action (non-seismic resistant constructions). Furthermore, an extensive testing campaign, comprised of several pseudo-dynamic (PsD) tests on bare, infilled and retrofitted frames for several earthquake intensity levels, was performed. A detailed description of the test frames, materials and test campaign will be presented in Chapter 3, while Chapter 4 will deeply analyse the test results.

Third, much of the past research follows either a numerical or experimental work. The research approach followed in this thesis combines numerical and experimental work. The experimental tests on full-scale structure models assisted the calibration of those numerical models and sustain in the assessment of proportioning and detailing rules for the different structural sub-assemblages. This complementary numerical and experimental approach emphasise the important role of the research for the mitigation of the seismic risk.

Forth, and concerning scientific aspects, there is a need for more rational assessment methods able to predict seismic response and to identify local deficiencies leading to failure, as well as to find effective and economic retrofitting solutions and techniques. Considering this weakness in existing knowledge, the main objective of the theoretical, experimental and analytical work conducted in the thesis is to achieve a reliable numerical methodology, experimentally calibrated, able to reproduce with rigour the structural behaviour of existing RC buildings, which can be used for subsequent verification of simplified assessment-methods.

Finally, as far as technical issues are concerned, in Europe, there is still a lack of codified criteria for redesign, as well as, a specific code for assessment and redesign of seismic vulnerable buildings. Hence, the work developed in this thesis, in the framework of the ICONS project, intends to contribute to the calibration and development of the European seismic codes, as well as, development of innovative assessment, design and redesign methods. Results from this study may help building owners, research teams, government and other agencies involved in design codes and policy action start with action plans in order to avoid human and economical losses in future earthquakes. Recall that in 1977 it

was published in Japan the first document on assessment and retrofit of structures, later revised in 1990 (see Pinto, 2000), developed by the Japan Building Disaster Prevention Association (JBDPA, 1977). In the United States, Japan and New Zealand, several dedicated research programmes have been set-up and a series of documents on this matter were issued recently (e.g. FEMA-274, FEMA-273, 1997; FEMA-310, 1998; ATC-40, 1996; CALTRANS, 1998; JSCE, 1996; NZNSEE, 1996, etc.). In Europe, there is still a lack of appropriate codes for the retrofitting of existing structures in particular for RC structures. Most European national codes neglect the subject. Eurocode 8 (EC8, 1994) comprises a dedicated chapter drafted recently (EC8 Part 1-3, 2003) but there are difficulties in obtaining agreement on several aspects of the code. In fact, it involves several actors namely the EE community, policy makers and building owners who must work together for a successful end. To the EE community the following tasks should be assigned: development of effective retrofitting solutions and techniques and development of codified redesign methods and rules allowing their widespread application by the technical community.

As mentioned above, this thesis is conducted within the framework of the ICONS network project. Details on this research programme of relevance to this thesis are presented next.

### ***ICONS Research Programme***

The ICONS cooperative research program was contracted by LNEC, and coordinated at the Joint Research Centre (JRC, in Ispra, Italy), with the participation of a Working Group, involving researchers from several European Universities, the JRC and Industry. A total of twelve partners from eight countries with complementary expertise were engaged in the project. The ICONS network project extends the seismic research into new concepts and subjects in EE, which should be developed further to convert EC8 into a truly state-of-the-art standard, for the safe and economic design of earthquake resistant new structures and for the seismic upgrading of existing ones. Therefore, ICONS contributes indirectly to the development of the European construction industry and to the realisation of the European engineering and construction industry open market. The project constitutes an important contribution to the calibration and development of the European seismic design codes, as well as, development of innovative assessment and design and redesign methods.

ICONS extended across the main pillars of seismic design, covering five research topics, namely: 1) the design seismic action; 2) methodologies for the assessment of the seismic vulnerability of existing structures and development of strengthening and repair techniques; 3) innovative design concepts and methods (this task comprises: base isolation and energy dissipation in structures, uplifting/rocking as base isolation and displacement-based-design); 4) steel/concrete composite structures and sub-assemblages; and, 5) shear-wall structures.

The work developed in this thesis was concentrated in the topic 2 of the ICONS project (methodologies for the assessment of the seismic vulnerability of existing structures and development of strengthening and repair techniques; in short: Assessment, Strengthening and Repair - ASR). Structures built prior to the introduction of seismic design codes were commonly designed for gravity loads only, not possessing specific earthquake resistant provisions, and thus constitute a considerable earthquake risk source. The vast PsD testing campaign of the topic ASR aims at: *a*) the seismic assessment of the original capacity of existing RC buildings, with and without infill masonry panels, representative of buildings design and construction until the late 1970's; *b*) the investigation of the effectiveness of current assessment methods (including those proposed in EC8 Part 1-3) to predict seismic vulnerability/performance of buildings; and, *c*) investigating and comparing performances of different common seismic retrofitting (repair and strengthening) solutions and techniques, for the seismic upgrading of existing RC buildings, namely: a selective retrofitting scheme, which provides either strength, or ductility, or stiffness; shotcrete of infill walls; and, k-bracing with dissipative devices. The ASR topic addresses also the development of rapid screening methods and refined analytical methods and procedures for the assessment of existing structures. For test purposes, in order to study several retrofit concepts, and to provide optimum test conditions, two identical parallel full-scale RC frame structures, four storey height and with three bays, with an overall length of 12.50 *m* and a height of 10.80 *m*, had been constructed at the ELSA facility (one as a bare frame and one as a frame with hollow brick-masonry infill walls), representative of the 'non-seismic' design practice until the late 1970's. It must be highlighted that the research work presented in this thesis, as well as the ICONS network project, took advantage of the co-operation between ICONS and the ECOEST II (European Consortium of Earthquake Shaking Tables) large-scale facilities consortium in EE (shaking-tables laboratories and

ELSA reaction wall laboratory of the JRC, see for example Carvalho and Bairrão, 2000; Severn, 2000), in defining and following the necessary experimental programme to reach the project objectives.

## **1.2 - MAIN OBJECTIVES OF THE THESIS**

The main objective of the theoretical, experimental and analytical work subject of this thesis is to achieve a numerical methodology, which is experimentally calibrated and able to reproduce rigorously the structural behaviour of existing reinforced concrete buildings. Therefore, it can be used in the systematic vulnerability assessment of this kind of structures. The experimental work consists on assessing the original capacity of frames, with and without infill masonry, and to compare performances of different retrofitting solutions.

In order to achieve the main objectives, the work is organised in three main blocks. First, a summary of the most common causes of damage and failure and of repair and strengthening techniques for existing RC buildings is described in Chapter 2. Second, a vast experimental programme to obtain the local and global vulnerabilities of this kind of structures was developed. In this regard, the author and a team of researchers involved in the ICONS research programme conducted a series of PsD tests on two four storey full-scale planar frames, which are described in Chapters 3 and 4. And, finally, evaluation of the available refined models in analysing the seismic performance of existing buildings, proposing improvements to reach a reliable numerical methodology to predict their seismic response.

Initial calculations were performed based on the available refined models commonly used to model the new structures. Due to the unsatisfactory results, parametric analyses were performed, and confirmed with the experimental full-scale test results to identify the discrepancies. The detailed parametric analyses reveal inadequacies of the current models when applied to the existing structures. This effort led to fine-tuning of the model parameters' (as plastic hinge length, slab-participation, etc.), as well as to the inclusion of the bond-slip effect, which is presented in Chapter 5.

Various analysis methods, either linear elastic or non-linear, static or dynamic, are available for the performance analysis of existing reinforced concrete buildings. Despite its advantages, it must be admitted that non-linear time history analysis can frequently become overly complex and impractical for general use as a first assessment. Simplified non-linear static methods, as the Capacity Spectrum Method (CSM), are unable to accurately assess irregular structures, as will be presented in Section 5.7.2. Considering these limitations, in this thesis it is proposed a simplified MDOF non-linear dynamic model for the assessment of structures. For structural redesign, it is judged appropriate to have a methodology that generates optimal distribution of the strengthening in the structure components. Therefore are proposed optimization algorithms to achieve optimum storey strengthening levels of existing vulnerable structures.

### **1.3 - PLAN OF THE THESIS**

This thesis is structured into six chapters. Following the introduction, the seismic vulnerability of existing RC structures and the common retrofitting techniques for this kind of structures are presented in Chapter 2. Chapters 3 and 4 are devoted to the experimental work performed in the framework of this thesis. Chapter 5 deals with the numerical analyses performed. Finally, Chapter 6 draws the main contributions and conclusions of the research work, derives implications for agents with an interest on the topic and identifies possible future research directions.

Chapter 2 reviews the current state of knowledge in the assessment of seismic vulnerability of existing RC structures, discussing further the motivation and the current problems with retrofitting of these buildings. Various methodologies for the assessment and redesign of existing structures are reviewed. Lessons from significant recent earthquakes are also presented. In this regard, are emphasised the common causes of seismic damage and failure modes of existing RC buildings designed and/or constructed without specific seismic capacity. Finally, the strengthening techniques adequate to improve the seismic performance of the existing RC structures are summarised.

Chapter 3 describes all aspects related to the test campaign, namely details on the structure, on the construction of the RC frame and materials' mechanical properties, testing

programme, loading system, additional loads, instrumentation and data acquisition system, as well as on the construction of the infill masonry walls and infill strengthening technique applied. The extensive test campaign performed to evaluate the mechanical properties of the materials is also discussed in this chapter. The retrofitting techniques applied are reviewed, namely: selective retrofitting, K-bracing with shear-link, and a retrofitting technique based on carbon fibre materials. Finally, based on non-destructive tests, the dynamic characterisation of the frames is presented and discussed.

Chapter 4 provides an analysis of a series of pseudo-dynamic and cyclic tests on the two frames. It starts by presenting the test results from the first testing model, bare frame, and on the strengthened frame using selective retrofitting techniques. It follows results on the second frame model, a masonry infilled frame, which was subjected to a series of PsD earthquake tests in order to assess its seismic performance and ultimate capacity. The effects of the masonry on the global response of the structure are also evaluated, comparing the test results of the infilled frame with the previous campaign of tests carried out on the bare frame structure. Then, the most damaged infill panels were replaced, one bay of the frame was strengthened using 'shotcrete' and the structure was subsequently tested up to collapse. Results of the strengthened infilled frame are analysed and compared to the non-strengthened infilled frame. Results of the K-bracing with shear-link cyclic tests, as well as, on the frames repaired with carbon fibre materials are commented. The principal aspects on the local behaviour such as slab-participation, plastic hinge length and joint deformation are also addressed in this chapter.

In Chapter 5, the refined non-linear numerical modelling of the structures is described. First, the computer software used in these analyses (CASTEM) is briefly presented. Then, the most significant results of a series of non-linear dynamic numerical studies conducted to reproduce the seismic response of the four-storey RC planar frame are shown. In this chapter, the numerical models adopted, as well as the material and model parameters involved are explained. The numerical results are compared to the previous PsD earthquake experimental ones. With this procedure, it was possible to calibrate and confirm the accuracy of the analytical models. The efficiency of the selective retrofitting solution, outlined in previous chapters, is numerically evaluated with inelastic structural models. Inelastic models were developed for the strengthened structure, and implemented in

CASTEM. Both original and strengthened configurations are modelled independently. Masonry infill walls, which play an important role especially in the original (non-strengthened) frame, are modelled as diagonal struts. In Section 5.7 the tested structure is assessed with the capacity spectrum method reviewed in Section 2.3.4. It is also proposed and tested a MDOF non-linear dynamic displacement-based assessment method. Finally, in Section 5.8, it is proposed a methodology to estimate the optimum distribution of strengthening needs in existing buildings.

The last chapter of the thesis collects and further discusses the main contributions from the research work and identifies key results, which can be considered relevant for the seismic assessment and retrofitting of existing RC frame structures. Possible research directions are also suggested.

Finally, Appendices A and B, report on the instrumentation details, test results, damage observed during the tests and include a photographic documentation of the tests. Definitions of certain terms related with the subjects herein studied and used in the thesis are given in Appendix C.



## **CHAPTER 2**

### **SEISMIC VULNERABILITY AND REHABILITATION OF EXISTING RC STRUCTURES**

*'If we lose our origin, we will lose our identity.'* (UNESCO, 1968)

#### **2.1 - INTRODUCTION**

There has been an increasing attention to the topic of seismic retrofit of existing buildings in recent years. Griffith (1999-*a*), for example, highlighted the growing number of research papers published in this field. Pinho (2000) also recalls the extensive literature on repair and strengthening methods for RC structures. Several state-of-the-art reviews on repair and strengthening published confirm the importance of the topic (e.g. Pinho, 2000; Griffith, 1999-*a*; Dyngeland, 1998; Fardis, 1998; Sugano, 1996; Varum and Oliveira, 1994; Bertero, 1992; Jirsa and Kreger, 1989). The current growing number of national and international conferences and workshops, multi-partner and bilateral cooperative research programmes and specialized publications dedicated to the assessment, strengthening and repair of existing buildings, prove the actuality and vital importance of the issue (see, for example, SPES, 2003; SPES, 2001; Geradin and Pinto, 2000; Karadogan, 1998; EERI, 1996; Hanson, 1981).

The interest in the topic does not come as a surprise considering that past and recent seismic activity show that, by far, the major damages and collapses of structures and human life losses come from deficiencies in existing buildings. Recall the widespread damage to older buildings and bridge structures in the relatively recent Loma Prieta,

Northridge, Kobe and Izmit earthquakes. As a result, in the US and Japan, in particular, owners have begun to take action to prevent similar damage to existing structures in future earthquakes. Similar actions should be encouraged in Europe.

This chapter overviews the current state of knowledge in the assessment and retrofitting of seismically vulnerable existing RC structures (Section 2.2). Section 2.3 reviews the methodologies for the assessment and redesign of existing structures. Lessons from recent earthquakes are reviewed in Section 2.4. The analysis reveals the enormous amount of life and property losses, which were mainly caused by the collapse or heavily damaged multi-storey RC buildings. The seismic risk in urban areas is still worth considering, specially in Europe where this type of building structures are so widespread. Section 2.5 identifies the main causes of seismic damage and failure of existing RC buildings designed and/or constructed without specific seismic capacity. Finally, strengthening techniques for the existing RC structures are summarised in Section 2.6.

## **2.2 - STRUCTURAL ASSESSMENT AND RETROFITTING**

As already stated in Chapter 1, seismic assessment and retrofit of existing constructions is a complex and difficult issue evolving political, social, economic, technical and scientific aspects. In particular, it was stated that the challenge to the scientific earthquake engineering community is: *a)* to develop rational assessment and redesign methods; *b)* to define appropriate decision criteria for retrofit of existing structures; and, *c)* to investigate and assess innovative cost-effective strengthening solutions and techniques.

### **2.2.1 - Structural assessment**

Seismic assessment of an existing structure can be defined as the detailed investigation to determine the characteristics of the structure as it stands. It tries to identify the particular structural weakness and deficiencies. Ersoy (1998) recalls that data collected at the assessment stage is used to evaluate the seismic performance of the structure. As a result of this evaluation, the structural engineer decides whether to repair or strengthen.

The engineer should try to estimate the structural characteristics as accurately as possible. However, as stated by Ersoy (1998), no matter how detailed the collected data is, the structural characteristics estimated are not exact values. It involves numerous uncertainties, such as the strength of the materials, reinforcement detailing of members, reduction of stiffness due to time effect and cracking. In the seismic assessment of an existing structure, the engineer should consider the possible variations of the estimated structural characteristics. Since the construction type and quality are not the same in different countries, such criteria should be calibrated using the data obtained for each country. The effect of non-structural elements, such as infill walls, should also be taken into consideration.

The structural assessment is highly relevant not only for old structures. As pointed out in Bertero *et al.* (1991) and Anderson *et al.* (1991), most of the human injury and economic loss due to moderate or severe earthquake ground motions are caused by failures of civil engineering facilities, particularly buildings, many of which presumably were designed and constructed to provide protection against such natural hazards. This has been confirmed dramatically during recent earthquakes around the world (the 1985 Mexico, the 1988 Armenia, the 1989 Loma Prieta, the 1990 Iran, and the 1990 Philippines earthquakes).

The current available methods for evaluating the structural characteristics are quite primitive and time consuming. When the building stock to be evaluated is very large, the classical comprehensive evaluation methods become unfeasible. Also, the rehabilitation of a large group of buildings may require investments beyond the budget. In such cases, it is necessary to prioritize buildings by their vulnerability. Obtaining detailed data for a comprehensive evaluation is highly time consuming and expensive. Furthermore, decisions related to vulnerability can only be taken by the judgement of experienced engineers. Therefore, the need for simple criteria and methods to select buildings with high vulnerability (screening) and assign rehabilitation priorities of the building inventory is obvious (Ersoy, 1998). Research leading to more accurate and faster evaluation tools and rapid screening methods, such for example, the displacement-based method proposed by Varum and Pinto (2001-*b*), Abrams (2000), Fajfar (2000), Taucer (2000), Calvi (1999), Priestley (1998), Calvi and Pavese (1997), Kowalsky *et al.* (1994), as well as, the development of instrumentation for assessment of old structures should be encouraged.

### 2.2.2 - Structural retrofitting

Structural retrofitting can be defined as the operation to bring the structural system or some of the structural members to a specified performance level. Depending on the state of the structure and on the purpose, rehabilitation can simply be classified as: *a*) repair; or *b*) strengthening. Structural repair is the rehabilitation of a damaged structure, or of a structural member with the objective of regaining the capacity back to the pre-damage state. Structural strengthening is increasing the existing capacity (in strength, ductility or stiffness) of an undamaged structure or of a structural member to a specified higher performance level (Ersoy, 1998).

Before making any retrofitting intervention (repair or strengthening), a detailed assessment should be made (as discussed in previous Section 2.2.1). Using the data obtained from the assessment, the engineer decides whether repair or strengthening is needed or not. As referred by Ersoy (1998), in the redesign for repair or strengthening, the engineer should first define the performance level expected from the structure. Then, he should decide, using design codes and data obtained from the assessment, what to use as design loads and/or deformation limits, load factors, material strength and material factors. The retrofitting strategy depends on the degree of the deficiencies identified in the assessment analysis (Fardis, 1998):

- If the structural deficiencies are found just in a few scattered components, then the strategy of local modification of these components can be sufficient to guaranty the structural performance objectives.
- When the deficiencies are concentrated in one part of the structure (may be due to an irregularity of the structural configuration as a weak-storey or a torsionally unbalanced structure), then it is required to strengthen some vertical elements (those of the weak-storey or of the weak and flexible side of the building), to add some new elements which are strong and stiff enough to remove or overshadow the irregularity, or to remove material to weaken some elements. For strongly 3D irregular structural configuration, vertical joints could be introduced at selected locations in plan, cutting the building into a set of structurally independent but regular units.

- But, if the preliminary evaluation reveals a generalised deficiency in the building, a more radical intervention may be necessary (addition of shear walls or bracing systems, upgrading most existing elements, especially vertical elements).

Although repair and strengthening are made to provide satisfactory performance of the structure under different load effects, seismic action becomes the main concern of the engineer at the redesign stage in countries located in seismic regions. Nevertheless, since the costs of seismic repair are quite high, seismic strengthening of existing buildings to reduce hazards of probable future earthquakes is finding support in many countries (Ersoy, 1998).

### **2.2.3 - Seismic assessment and redesign criteria and codes: Overview**

Seismic design of buildings has slowly evolved over the time by a trial and error process. The trend in the early 1900's was to use conventional building technology methods with minor modifications to account for earthquakes, in response to previous observed damage. In recent decades, the primary focus has been the study and enhancement of conventional systems and element connections performed in structural laboratories and institutes (Elsesser, 2002).

Fardis (2000) recalls that worldwide experience from past earthquakes shows that non-ductile RC frame buildings are one of the most vulnerable and represent, overall, the largest threat to human life and property in future earthquakes (as illustrated in Section 2.4).

As recalled by Fardis (1998), the design of new buildings for earthquake actions is relatively recent in Europe. Until the 1950's in the US and until the 1960's in Europe, there were essentially no formal seismic design provisions in design codes. It was only in the mid-1970's that provisions for design and detailing of members and structures came out in the US standards. Yet, it was not before the mid-1980's that these provisions were included in the European national codes.

Since the 1926 code, Japan's seismic codes have typically been as advanced as any in the world. The regulations have been reviewed and amended several times over the years as

the result of damage during strong-motion earthquakes (EQE, 1995). Japan applies since 1977 a very practical three-level seismic assessment procedure. The first level screens out strong buildings. Application of the two higher levels to the questionable buildings is easy and fast and gives fairly realistic assessment results. The higher level assessment procedure is enforced since 1996 as a law for the promotion of strengthening of private vulnerable buildings (Fardis, 2000).

After a well coordinated effort during at least one decade, the US Federal Management Emergency Agency (FEMA) came up since 1996 with seismic assessment and rehabilitation guidelines (ATC-40, 1996; FEMA-273, 1997; FEMA-274, 1997; FEMA-310, 1998) that produce more economic and rational results than earlier ad-hoc procedures based on adaptation of design codes for new buildings. These guidelines are essentially displacement-based. They employ linear or equivalent static or multimodal analysis, or non-linear static (pushover) or dynamic (time-history) analysis, depending on the (strength and stiffness) regularity of the structure and the choice of the engineer between the opposite extremes of sophistication on one hand and conservatism on the other. Instead of a global behaviour factor ( $q$ ) they use demand-supply comparisons for the deformation capacities of individual elements, existing, retrofitted or new (Fardis, 2000).

The Eurocodes, originally aiming at the unification of the European codes in the field of constructions, nowadays introduce innovations and improvements in the quality of design of new structures. Regarding safety, they point at ductile buildings in order to provide strength even under heavy but localised loading. The ductility demand is particularly important under seismic loading and the competent EC8 is wholly innovative in relation to the codes in force in the European Community.

Reinforced concrete and masonry are, by far, the most common structural materials in the seismic regions of Europe. The average size and occupancy of individual RC buildings exceed by far those of masonry buildings. Moreover, facilities that are crucial in the post-earthquake emergency period (police station, fire station, hospitals, schools, banks, hotels, administrative and government centres, power and telecommunication facilities) are typically RC buildings. For these reasons, it is argued that European pre-normative and normative research in seismic assessment and rehabilitation of existing buildings should

primarily focus on these two structural materials, with some priority to RC buildings (Fardis, 2000).

Policy- and code-makers in Europe recognised the seriousness of the problem and decided to address strengthening of existing structures within the system of Eurocodes for the seismic action alone. Eurocode 8 Part 1-3, strengthening and repair of buildings, was one of the first seismic assessment and rehabilitation standards in the world to be applied. To encourage its use by practitioners familiar with codified seismic design, and in particular with the parts of EC8 applicable to new structures, EC8 Part 1-3 tries to bring the problem of seismic assessment and rehabilitation as close as possible to that of new designs. To this end, the engineer is asked to determine first the value of the global behaviour factor, which is compatible with the available ductility of the structure. Members are then assessed by comparing their design resistance to seismic internal forces, determined from linear analysis, and the design spectrum entered with the above global  $q$ -factor. Strengthening should be such that this verification is fulfilled throughout the existing structure and should employ a  $q$ -factor consistent with the global configuration and strength hierarchy in the modified system and the local ductility of all its members: new, modified and old ones (Fardis, 2000).

The current state of practice in Europe makes difficult to introduce some of the current scientific knowledge into the EN for 'Strengthening and Repair'. Moreover, there are many open questions on several issues, such as those regarding the performance of members and structures of existing buildings designed only for gravity loads (Fardis, 2000).

To resolve some of these questions, further research is required at the European level. Moreover, the development of rational, simple and practical seismic assessment procedures is required for low-to-medium-rise regular buildings. Such procedures should be influenced by the spirit of the recent US documents (FEMA, ATC) and by the displacement-based philosophy (see Varum and Pinto, 2001-*b*, for example), but should entail less sophistication and engineering effort than required by ATC-40 (1996) and FEMA-274 (1997). Last but not least, complete and clear provisions for the design and detailing of the strengthening of existing elements need to be developed for EC8, including simple procedures for designing of the retrofitting for the most common and effective strengthening techniques (Fardis, 2000).

## 2.3 - METHODOLOGIES FOR ASSESSMENT AND REDESIGN

The seismic vulnerability of a building or other structure may be defined as its susceptibility to damage during an earthquake having a specified level of ground shaking. This damage may result in physical injury or death to occupants, temporary or permanent loss of function of the building, and associated economic impact. The degree of seismic vulnerability of a building will depend upon its general configuration, load transfer system, design specifics, and the quality of materials and construction. By carefully examining these factors, it is possible to estimate the level of vulnerability of a class of buildings or a specific building structure (Imanbekov *et al.*, 1999).

Various analysis methods, either linear elastic or non-linear are available for the performance analysis of existing reinforced concrete buildings. Elastic analysis methods include code static lateral force procedures, code dynamic lateral force procedures and elastic procedures using demand capacity ratios (ATC-40, 1996). The most popular non-linear analysis methods are the non-linear time history analysis and simplified non-linear static analysis.

The non-linear time history analysis method, with recorded or simulated ground motion records, provides the most accurate means for predicting seismic demands (Fajfar, 1998). This inelastic dynamic method is widely used to model specimens tested in laboratory and real structures with a reduced number of elements. Despite its advantages, it must be admitted that non-linear time history analysis can frequently become overly complex and impractical for general use as a first assessment. An alternative is to use simplified non-linear static analysis methods.

In Section 2.3.1 are recalled some concepts on performance-based design, performance design objective matrix, and earthquake hazard levels according to the VISION-2000 committee (SEAOC, 1995) and ATC-40 (1996). In the following Sections 2.3.2 to 2.3.4 are described three of the most popular simplified non-linear static procedures, namely: *a*) the displacement coefficient method, which uses pushover analysis and a modified version of the equal displacement approximation; *b*) the N2 method, that uses non-linear analysis and two mathematical models; and, *c*) the capacity spectrum method. The capacity spectrum method (CSM) is described in more detail, because it is used in Chapter 5 to



---

assess the structural response. Finally, in Section 2.3.5 it is described the procedure adopted to estimate the damping from the experimental tests, as will be presented in Chapter 5.

### **2.3.1 - Performance-based design and assessment**

Performance-based design (PBD) procedures intend to design and redesign structures to perform at appropriate levels for all earthquakes. In Europe, the concept is usually called Limit State Design (Fajfar, 1998). PBD involves the design of structures that will resist earthquakes of different severities within specified limiting levels of damage.

A performance level is a damage state or a limit state. It is a measure of the maximum desired extent of damage to a facility given that a specific earthquake design level affects it (Fajfar, 1998). Each performance level is defined for the structural system (structural performance level), the non-structural system (non-structural performance level) and facility content (content performance level).

The VISION-2000 committee (SEAOC, 1995) has selected and defined four individual performance levels (see also Figure 2.1), namely:

- 'Fully Operational' or 'Serviceable' (facility continues in operation with negligible damage);
- 'Operational' or 'Functional' (facility continues in operation with minor damage and minor disruption in non-essential services);
- 'Life Safety' (life safety is substantially protected, damage is moderate to extensive);  
and,
- 'Near Collapse' or 'Impending Collapse' (life safety is at risk, damage is severe, and structural collapse is prevented).

In ATC-40 (1996) are also proposed four performance levels, namely: 'Operational', 'Immediate Occupancy', 'Life Safety', and 'Structural Stability'.

The seismic hazard at a given site is represented as a set of earthquake ground motions and associated hazards with specified probabilities of occurrence. The VISION-2000

committee has proposed four levels of probabilistic events (SEAOC, 1995), as presented in Table 2.1 (see also Figure 2.1).

Table 2.1 - Earthquake hazard level (according to SEAOC, 1995)

Event	Recurrence interval	Probability of exceedance
Frequent	43 years	50% in 30 years
Occasional	72 years	50% in 50 years
Rare	475 years	10% in 50 years
Very Rare	970 years	10% in 100 years

In Table 2.2 are presented the three hazard levels of earthquake ground motion defined at ATC-40 (1996), namely: the 'Serviceability Earthquake' (SE), the 'Design Earthquake' (DE), and the 'Maximum Earthquake' (ME).

Table 2.2 - Earthquake hazard level (according to ATC-40, 1996)

Event	Recurrence interval	Probability of exceedance
SE	75 years	50% in 50 years
DE	500 years	10% in 50 years
ME	1000 years	5% in 50 years

In Figure 2.1 is presented the matrix of seismic performance objectives for buildings recommended by the VISION-2000 committee (SEAOC, 1995).

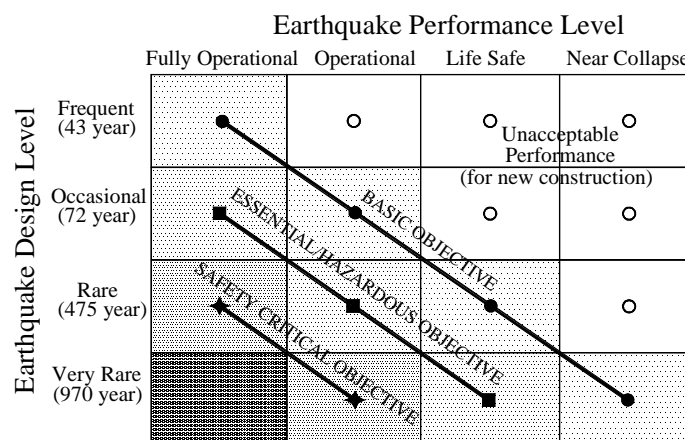


Figure 2.1 - Seismic performance design objective matrix (VISION-2000, SEAOC, 1995)

### 2.3.2 - Displacement coefficient method

The displacement coefficient method (DCM), proposed in FEMA-273 (1997), estimates the structural performance point in terms of maximum expected top-displacement ( $\delta_t$ ) of a building. It combines the pushover analysis with a modified version of the equal displacement approximation. The linear elastic spectral displacement,  $S_d$ , or spectral acceleration,  $S_a$ , corresponding to the effective fundamental period  $T_{eff}$  and damping of the linear equivalent SDOF system, is corrected by some factors as follows (Albanesi *et al.*, 2002)

$$\delta_t = C_0 \cdot C_1 \cdot C_2 \cdot C_3 \cdot S_d = C_0 \cdot C_1 \cdot C_2 \cdot C_3 \cdot S_a \frac{T_{eff}^2}{4\pi^2} \quad (2.1)$$

where:  $C_0$  is the modification factor to relate spectral displacement and likely building expected maximum top-displacement,  $C_1$  is the modification factor to relate expected maximum inelastic top-displacement to the displacement calculated for linear elastic response,  $C_2$  is the modification factor to represent the effect of hysteresis shape on the maximum displacement response, and  $C_3$  is the modification factor to represent increased displacements due to second order effects (FEMA-273, 1997). These corrective factors were obtained for regular frame buildings. The determination of these factors for structures with irregularities in terms of mass distribution, stiffness and strength is under investigation, as referred by Albanesi *et al.* (2002). The DCM provides a direct numerical procedure to define displacement demand and does not need conversion into spectral format, by contrast to the capacity spectrum method.

### 2.3.3 - N2 method

The N2 method was initially influenced by the Q-model developed by Saiidi and Sozen (1981). From the original version, Fajfar (2002, 2000, 1998), Fajfar *et al.* (1997) developed the method, which is adopted in the most recent draft of the Eurocode 8.

The N2 method combines pushover analysis with response spectrum approach and provides tools for a rational and practical evaluation procedure for multiple performance objectives (Fajfar, 1998). This performance evaluation method, described in detail by

Fajfar and Gaspersic (1996), can be summarised as follows. Firstly, a non-linear pushover analysis of a MDOF system is performed. The distribution of lateral loads corresponds to the distribution of inertia forces due to the assumed displacement shape. Secondly, an equivalent SDOF system with a bi-linear behaviour force-displacement curve is approximated from the computed force-displacement curve of the MDOF system. In the next step, seismic demand for the equivalent SDOF system in terms of displacement and energy is obtained by using inelastic spectra. The local seismic demand is determined by pushing the MDOF system to the maximum displacement determined in the previous step (Fajfar, 1998; Fajfar *et al.* 1997). Finally, local and global damage indices are computed by using the Park & Ang damage model (Park *et al.*, 1984).

#### **2.3.4 - Capacity spectrum method**

The capacity spectrum method (CSM), originally proposed by Freeman (1978), and now adopted in the ATC-40 (1996), is a simplified non-linear static analytical procedure for the assessment of existing reinforced concrete buildings. The graphical representation of the global force-displacement provides a clear picture on how a building responds to earthquake ground motion, and how various retrofitting strategies, such as adding stiffness, strength or damping will impact on the building's response to earthquake demands (ATC-40, 1996).

The CSM uses the intersection of the capacity curve in spectral coordinates (determined, for example, analytically by a pushover analysis) and a reduced response spectrum, to estimate maximum displacement (performance point), as schematically represented in Figure 2.2. It provides a particularly accurate treatment of the reduction of seismic demand for increasing displacement.

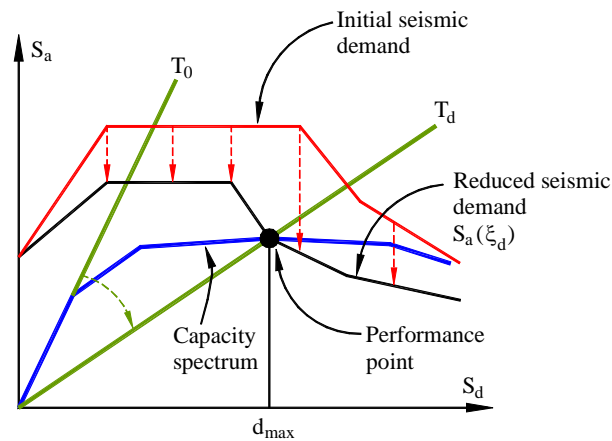


Figure 2.2 - Capacity spectrum method (adapted from ATC-40, 1996)

#### 2.3.4.1 - Capacity curve

The central focus of the simplified non-linear procedure is the generation of the capacity curve, which represents the structure's capacity to resist the seismic demand. The capacity curve is a plot of the building's base-shear versus top-displacement (GSREB, 2001). The capacity curve depends on the strength and deformation capacity of the individual components of the structure. The capacity curve shall be determined by performing a series of sequential analyses with increasing lateral load (pushover), using a model that accounts for non-linear behaviour of the building components. Some non-linear computer programs are able to perform a pushover analysis directly, for example PORANL (Varum and Costa, 1997), DRAIN-2DX (Prakash *et al.*, 1993). The analysis should include the effect of gravity and other non-seismic loads on the building's response to lateral loads. Development of a capacity curve for an existing building in itself is extremely useful to the engineer, and will yield insights into the building's performance characteristics as well as methods of retrofit (ATC-40, 1996).

#### 2.3.4.2 - Demand spectrum

The displacement based evaluation procedure requires reliable knowledge of the seismic displacement demand, which is the representation of the earthquake ground motion. The displacement response spectrum is an estimation of the maximum displacement response,

during the ground motion, as a function of the fundamental period of the building. The seismic displacement demand is site-dependent, therefore investigations of the dynamic soil behaviour are important in many cases.

The demand spectrum is a plot of the spectral acceleration and spectral displacement of the earthquake ground motion in the Acceleration-Displacement Response Spectra (ADRS) format (GSREB, 2001), for a given damping ratio. For any point of the acceleration response spectrum, the corresponding spectral displacement can be computed as follows

$$S_d = \frac{1}{4\pi^2} \cdot S_a \cdot T^2 \quad (2.2)$$

where:  $T$  represents the period,  $S_a$  and  $S_d$  are the spectral acceleration and the spectral displacement, respectively.

#### *2.3.4.3 - Performance point*

The performance point (PP) represents the maximum top-displacement expected for the demand earthquake ground motion. When the displacement corresponding to the intersection of the capacity spectrum and the demand spectrum are of the same damping value, this intersection point is considered the performance point.

#### *2.3.4.4 - Performance objective*

A seismic performance objective (PO) is defined by selecting a desired building performance level for a given level of earthquake ground motion, as represented in Table 2.3. According to ATC-40 (1996), three levels of earthquake hazard are used to define ground shaking, namely: the 'Serviceability Earthquake' (SE), the 'Design Earthquake' (DE), and the 'Maximum Earthquake' (ME). They are defined probabilistically as the level of ground shaking that has respectively a 50%, 10% and 5%, probability of exceedance in 50-years.

A dual- or multiple-level performance objective can be created by selecting two or more different desired performances, each for a different level of ground motion.

Table 2.3 - Definition of a performance objective (according to ATC-40, 1996)

Defining a performance objective				
Earthquake ground motion	Building performance level			
	Operational	Immediate Occupancy	Life Safety	Structural Stability
SE				
DE				
ME				

The variety of building performance levels can be combined with various levels of ground motion to form many possible performance objectives. Performance objectives for any building may be assigned using functional, preservation, or cost considerations (ATC-40, 1996).

The ATC-40 (1996) presents the 'Basic Safety Objective', which is a dual-level performance objective defined as: *a*) the building performance level 'Life Safety', for the 'Design Earthquake' level of ground motion; and, *b*) the building performance level 'Structural Stability', for the 'Maximum Earthquake' level of ground motion. Other performance levels and performance objectives have been defined or described in other documents, such as, FEMA-273 (1997) and SEAOC (1995).

#### 2.3.4.5 - Procedure to calculate the performance point

To determine the location of the performance point, a displacement along the capacity curve, consistent with the seismic demand, must be determined. Therefore, the performance point must lie on: *a*) the capacity spectrum curve in order to represent the structure at a given displacement; and *b*) on a spectral demand curve, reduced from the elastic spectrum, that represents the non-linear demand at the same structural displacement (ATC-40, 1996). For this methodology, spectral reduction factors are given in terms of effective damping. In the general case, determination of the performance point requires trial and error search for satisfaction of the two criterion of the performance point.

### 2.3.4.6 - Conversion of the capacity curve to the capacity spectrum

In order to use the capacity spectrum method, it is necessary to convert the capacity curve, which is in terms of base-shear versus top-displacement, to a capacity spectrum. The capacity spectrum is a representation of the capacity curve in the Acceleration-Displacement Response Spectra (ADRS) format.

In order to calculate the capacity spectrum from the capacity curve, it is necessary to do a point-by-point conversion to spectral coordinates. Any point of the curve base-shear ( $V$ ) versus top-displacement ( $\Delta_{roof}$ ) on the capacity curve is converted to the corresponding point ( $S_a$  ;  $S_d$ ) in the capacity spectrum using the following equations (ATC-40, 1996)

$$S_a = \frac{V}{W} \cdot \frac{1}{\alpha} \quad S_d = \frac{\Delta_{roof}}{PF_1 \cdot \phi_{roof,1}} \quad (2.3, 2.4)$$

where,  $S_a$  and  $S_d$  are respectively the spectral acceleration and the spectral displacement,  $\alpha$  and  $PF_1$  are respectively the modal mass coefficient and the modal participation factor, for the first natural mode of the structure, and  $\phi_{roof,1}$  is the roof level amplitude of the first mode (see Figure 2.3).  $W$  represents the building dead load weight plus likely live loads.

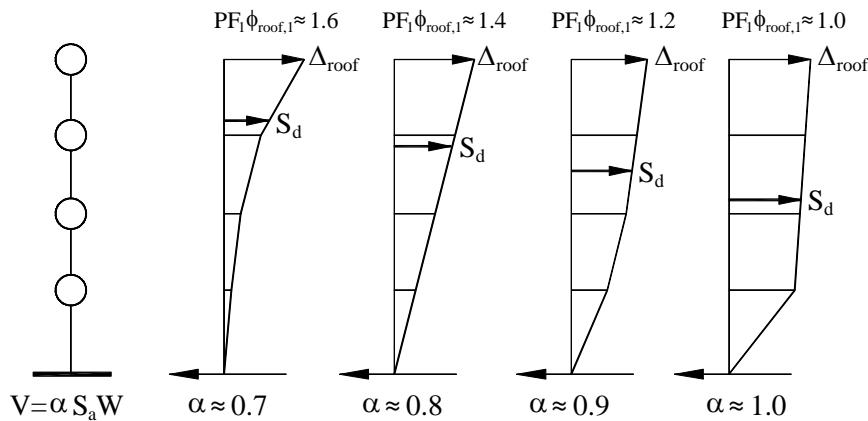


Figure 2.3 - Modal participation factors and modal mass coefficients (ATC-40, 1996)

To convert the capacity curve to the capacity spectrum, that is, converting the capacity curve into the ADRS format, the following expressions are used to calculate the modal participation factor and the modal mass coefficient



$$PF_1 = \frac{\sum_{i=1}^N (w_i \cdot \phi_{i1})/g}{\sum_{i=1}^N (w_i \cdot \phi_{i1}^2)/g} \quad \alpha_1 = \frac{\left( \sum_{i=1}^N (w_i \cdot \phi_{i1})/g \right)^2}{\left( \sum_{i=1}^N w_i/g \right) \cdot \left( \sum_{i=1}^N (w_i \cdot \phi_{i1}^2)/g \right)} \quad (2.5, 2.6)$$

where:  $w_i/g$  represents the mass assign to the level  $i$ ,  $\phi_{i1}$  is the amplitude of mode 1 at level  $i$ , and  $N$  is the uppermost level of the structure.

### 2.3.5 - Equivalent damping ratio

As stated by Priestley (1997), the equivalent damping, for concrete structures, depends on the structural displacement ductility demand ( $\mu_\Delta = \Delta_d / \Delta_y$ , as the ratio between maximum displacement,  $\Delta_d$ , and the displacement corresponding to the yielding,  $\Delta_y$ ) and the predominant location (in beams or columns) of plastic hinging developed in the structure, as shown in Figure 2.4. The energy dissipated in beam plastic hinges is typically larger than in column plastic hinges, and this should be recognized in the estimation of equivalent viscous damping.

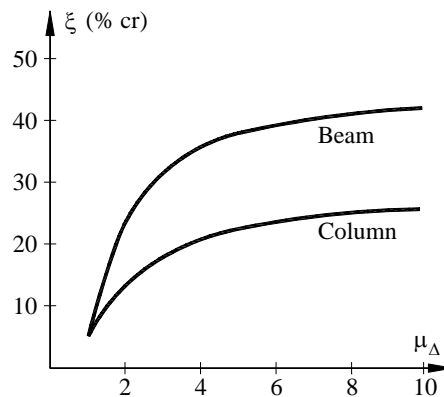


Figure 2.4 - Equivalent viscous damping for reinforced concrete structures (adapted from Priestley, 1997)

The simplest definition of equivalent viscous damping is based on the measured response of a system to harmonic force at exciting frequency ( $\omega$ ) equal to the natural frequency ( $\omega_n$ ) of the system. This is the equivalent viscous damping since it accounts for all the energy-dissipating mechanisms (Chopra, 2001).

The most common method for defining equivalent viscous damping is to equate the energy dissipated in a vibration cycle of the actual structure and an equivalent viscous system. For an actual structure the force-displacement relation obtained from an experiment under cyclic loading with displacement amplitude  $u_0$  is determined; such a relation of arbitrary shape is shown schematically in Figure 2.5.

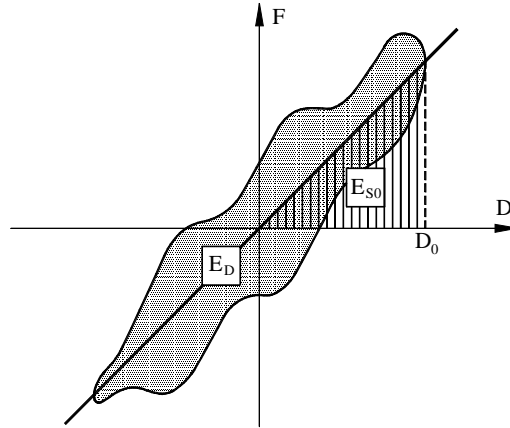


Figure 2.5 - Energy dissipated  $E_D$  in a cycle of harmonic vibration determined from an experiment (Chopra, 2001)

The energy dissipated in the structure is given by the area  $E_D$  enclosed by the hysteresis loop. Equating this to the energy dissipated in viscous damping leads to

$$\xi_{eq} = \frac{1}{4\pi} \cdot \frac{1}{\omega/\omega_n} \cdot \frac{E_D}{E_{S0}} \quad (2.7)$$

where the strain energy,  $E_{S0} = k \cdot u_0^2/2$ , is calculated from the stiffness ( $k$ ) determined by experiment.

The experiment leading to the force-deformation curve of Figure 2.5, and hence  $E_D$ , should be conducted at  $\omega = \omega_n$ , where the response of the system is most sensitive to damping. Under these conditions Equation (2.7) gives

$$\xi_{eq} = \frac{1}{4\pi} \cdot \frac{E_D}{E_{S0}} \quad (2.8)$$

The equivalent damping ratio ( $\xi_{eq}$ ) of a general structural system determined from a test at  $\omega = \omega_n$  would not be correct at any other exciting frequency, but it would be a satisfactory

approximation (Chopra, 2001). Iwan and Gates (1979) present a summary of equivalent damping ratios for different behaviour models.

To estimate the equivalent damping from experimental PsD tests, first it is calculated the damping at storey level, and subsequently it is computed the global damping for the structural system, as explained next.

For each storey, the equivalent damping is evaluated for each half-cycle of the curves force-displacement, as represented in Figure 2.6. The damping is calculated for each degree of freedom, considered at storey level. From the force-displacement half-cycle the equivalent linear viscoelastic damping is identified as described in the following steps:

- i) The absorbed energy ( $E_D$ ) is computed by performing the integral of the force-displacement curve (by the differential displacement);
- ii) From each force-displacement half-cycle is evaluated the maximum generalised force ( $F_{\max}$ ) and the maximum generalised displacement ( $D_{\max}$ ), which allows to calculate the strain energy ( $E_{S0}$ ); and,
- iii) Finally, the equivalent linear viscous damping ratio ( $\xi_{eq}$ ) is computed with the Expression (2.9), for each half-cycle, characterised by it displacement amplitude ( $D_{\max}$ ).

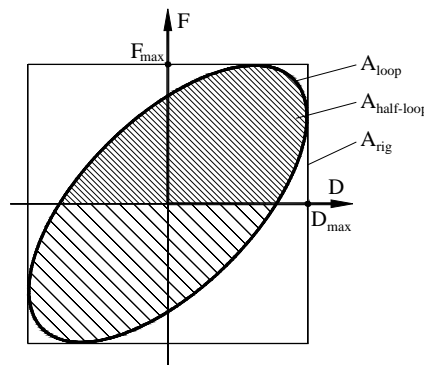


Figure 2.6 - Damping for an hysteretic cycle

$$\xi_{eq} = \frac{1}{4\pi} \cdot \frac{E_D}{E_{S0}} = \frac{1}{8\pi} \cdot \frac{A_{half-loop}}{F_{\max} \cdot D_{\max}} \quad (2.9)$$

For a MDOF system, the global structural equivalent damping can be computed, as stated by Priestley (1997), as a function of the effective damping estimated for each component (storey the case of buildings) weighted with the storey potential energy, given by

$$\xi_G = \frac{\sum_{i=1}^{ns} \xi_i \times E_i}{\sum_{i=1}^{ns} E_i} \quad (2.10)$$

where:  $\xi_G$  is the equivalent damping of the global system;  $\xi_i$  is the equivalent damping of the component  $i$  of the system (column, beam or storey);  $E_i$  is the potential energy in the component  $i$  and for the level of damping  $\xi_i$ ;  $ns$  is the number of components of the system.

This methodology will be used to estimate the structural equivalent damping from the results of the pseudo-dynamic tests in Section 5.7.1.

## **2.4 - FIELD EVIDENCE: OBSERVED DAMAGE IN RC BUILDINGS AND CASUALTIES DURING RECENT EARTHQUAKES**

*'Buildings were toppled, houses were in rubbles, infernos swallowed entire towns, elevated highways and railways collapsed and crumbled cliffs buried houses. Everywhere people died...'* (Asahi Evening News, 18<sup>th</sup> January 1995, on the day after the Kobe earthquake)

Observations on the performance of structures during strong earthquakes have served as a mean of teaching builders and engineers on proper and improper construction of earthquake load resisting systems. In regions that have long been inhabited, and that are subjected to relatively frequent strong ground shaking, design procedures have evolved, resulting in relatively good performance of engineered structures (Moehle and Mahin, 1991). Although such design procedures are not universally applicable because of regional differences in construction materials and techniques, structural engineers can learn much by studying such procedures.

Next, the disastrous consequences resulting from recent seismic activity are reviewed, based on reconnaissance documentation, and drawing on examples from the March 2001 Geiyo earthquake in southwest Japan, to the 1994 Northridge earthquake in Los Angeles. Particular attention is drawn to the 17<sup>th</sup> August 1999 Izmit earthquake, in Turkey, because the affected structures are representative of the construction practice in southern Europe until the late 1970's. The analysis highlights the vulnerability of RC buildings, the type of structures investigated in the studies conducted in this thesis. The devastation, human casualties and economic losses resulting from seismic activity in a recent past around the world confirm that research on repair and strengthening of RC structures is urgently needed.

#### **2.4.1 - The 24<sup>th</sup> March 2001 Geiyo earthquake, southwest Japan**

An earthquake of magnitude 6.9 struck Hiroshima, 580 *km* southwest of Tokyo, in Japan, on Saturday, 24<sup>th</sup> March 2001. The earthquake occurred on the Philippine Sea Plate, close to the subduction zone interface with the Eurasian Plate. While ground shaking was intense in certain localized areas, the magnitude reflects a moderate earthquake. The epicentre is estimated offshore in Hiroshima Bay, some 51 *km* deep. There were no reports of tsunami. Two people were reported dead, and nearly 200 injured. The most severe damage in Imabari City was the partial collapse of a RC three-storey residential building, in which the first-storey columns failed, as shown in Figure 2.7. The damage was indicative of soft-storey effects and non-ductile detailing of reinforced concrete (EQE, 2001).



Figure 2.7 - Partial collapse of a three-storey residential building in Imabari (EQE, 2001)

#### 2.4.2 - The 20<sup>th</sup> February 2001 Nisqually earthquake, Seattle-Olympia, US

On 20<sup>th</sup> February 2001 an earthquake of magnitude 6.8 struck the Puget Sound, in the western region of Washington State. The epicentre of the earthquake was located in the Nisqually Valley, about 20 km northeast of Olympia and 60 km southwest of Seattle.

In this section it is only presented the structural behaviour of a nine-storey building, incorporating a steel lateral load-resisting system, located in the Starbucks headquarter on Utah Street in downtown Seattle. The original structural system of this building consisted of a RC flat slab-columns framing system with masonry walls. Parking and retail structures were later added next to the north and south sides of the building, respectively. Significant movement between the adjacent parts of the building occurred during the earthquake, as evidenced by the distortion of the vertical expansion joint between the original building and the north parking structure. The building was seismically upgraded circa 1995 by adding two lines of chevron eccentrically braced steel frames in both perpendicular directions (Filiatrault *et al.*, 2001). A general view of the bracing element on the sixth floor of the building is shown in Figure 2.8.

According to Filiatrault *et al.* (2001), the eccentric braced frames in the north-south direction did not show any evidence of inelastic deformation while the central shear-link of each bracing element in the east-west direction yielded, as shown in Figure 2.9. This observation indicates that despite its fairly square floor plan, the dynamic response of the building was significantly larger in the east-west direction than in the north-south direction.



Figure 2.8 - Chevron eccentrically braced steel frame used to seismically upgrade building (Filiatrault *et al.*, 2001)



Figure 2.9 - Yielding of the chevron eccentrically braced frame in the east-west direction of the building (Filiatrault *et al.*, 2001)

### 2.4.3 - The 7<sup>th</sup> September 1999 Athens earthquake, Greece

Greece, a country of about 10 million people located at the African and Eurasian plate boundary, has the highest seismicity in Europe (Anagnostopoulos, 2000). In its long history, it has suffered from many devastating earthquakes, which continue to threaten the lives of its people and to burden its economy till today. In recent years, it is estimated that the direct average annual cost of earthquake damages in Greece reaches 150 to 200 million US dollars (Anagnostopoulos, 2000).

Based on data for the period of 1950-2000 (Anagnostopoulos, 2000), it is estimated that the mean annual number of buildings totally destroyed by earthquakes in Greece to be about 2200. This number, however, has been estimated without any qualification, e.g. as to size of the building, construction material, engineered or non-engineered type. Hence, it cannot be used for reliable predictions of annual economic losses. We must also note that Greek earthquakes have often their epicentres at sea and hence they do not cause much damage.

The worst known earthquake in terms of human losses is most probably the earthquake that levelled the ancient city of Sparta in 464 B.C. killing over 20000 people. In the last two centuries, the worst event was an earthquake of magnitude 6.4 on 3<sup>rd</sup> April 1881 destroying most of the island of Chios in the eastern Aegean sea, killing 3650 people and injuring about 7000. During the last century, the most catastrophic sequence of earthquakes was a series of shocks with magnitudes 6.4, 6.8, 7.2 and 6.3 that destroyed almost completely the Ionian islands of Cephalonia, Zakynthos and Ithaca on 9<sup>th</sup>, 11<sup>th</sup> and 12<sup>th</sup> August 1953, killing 476 people and injuring about 2400. In the last 2 decades, strong earthquakes hit modern Greek cities causing extensive damage and loss of life. The most damaging were (by chronological order): *i*) the Thessaloniki earthquake of 1978 (magnitude 6.5) that killed 48 people, most of them in one major collapse; *ii*) the Alkyonides sequence of 1981 (magnitudes 6.7, 6.4 and 6.3) that killed 20 people and caused widespread damage in towns around the gulf of Corinth and in Athens; *iii*) the Kalamata earthquake of 1986 (magnitude 6.2) that killed 20 people and destroyed many of the old houses in the city of Kalamata; *iv*) the Aigion earthquake of 1995 (magnitude 6.2) that killed 26 people; and, *v*) the most recent Athens earthquake of 1999 (magnitude 5.9) that killed 143 people, and caused many collapses and widespread damage.

According to the editors of the special issue of the Journal of the International Society for the Prevention and Mitigation of Natural Hazards (ISPMNH, 2002), the earthquake of 7<sup>th</sup> September 1999 was the first strong (magnitude 5.9) earthquake ever reported to occur so close to the historical centre of Athens. Recall that Athens hosts nearly half of the country's over 10 million people, the administrative function, and roughly two-thirds of the economic activity (Dimitriu *et al.*, 2000). Apart from its social and economic consequences, the earthquake revealed a previously unidentified seismic source (Papadopoulos *et al.*, 2002).

A modern earthquake resistant design code was introduced in Greece in 1992, becoming mandatory in 1995, right after the Aigion earthquake. It replaced the old 1959 code, which had been hastily modified in 1984, following the Alkyonides earthquake of 1981. Unfortunately, the great majority of engineered Greek buildings by 1999 had been built with the old code, which was outdated and inadequate for multi-storey buildings. Furthermore, non-awareness of seismic hazard in the period of intensive construction, i.e. from the early 1950's up to the 1978 Thessalonica earthquake, combined with lack of quality control under intensive competition, resulted in gross abuses in design and construction practices (Anagnostopoulos, 2000).

According to Dimitriu *et al.* (2000), with the exception of some extreme cases attributable to adverse site conditions, to design deficiencies or to poor construction, the majority of the structures responded reasonably well to the admittedly very severe 1999 Athens earthquake, which exceeded the provisions of the seismic codes. The Athens earthquake thus reconfirmed the well-known fact that the existing building stock possesses a substantial amount of strength reserves due to the redundancy and over-strength of individual structural elements, as well as additional energy-dissipation mechanisms usually not taken into account in the design stage. Experience gathered from this and previous events points out the key role of several vulnerability-reducing factors, such as the rational use of infill walls and the regular configuration of structural systems, along with good material and workmanship quality.

Anagnostopoulos (2000) recalls that in addition to the code revision, several other measures have been taken in Greece, especially after each new damaging earthquake. Yet, in spite of these efforts, some very basic actions, quite essential for mitigating seismic risk



and which can produce tangible results at insignificant costs have been, unfortunately, overlooked.

#### 2.4.4 - The 17<sup>th</sup> August 1999 Izmit earthquake, Kocaeli, Turkey

A 45-second earthquake of 7.4 Richter magnitude struck the north-west of Turkey on 17<sup>th</sup> August 1999. The epicentre occurred approximately 11 km southeast of Izmit, the capital of the province of Kocaeli, an industrial city approximately 90 km east of Istanbul. The epicentral region was directly under Gölçük, with a focal depth of 17 km (Aschheim, 2001; USGS, 2000; EQE, 1999; Saatcioglu *et al.*, 1999; KOERI, 1999).

The most heavily damaged area was around the gulf of Izmit and the city of Adapazari. The towns of Gölçük and Yalova along the south shore of the gulf, the harbor city of Izmit at the eastern end of the gulf, the town of Sapanca about 50 km east of Izmit, and the city of Adapazari 60 km east of Izmit were sites of massive structural destruction and extensive ground failures. There was also extensive damage in the Avcilar district of Istanbul, which is located approximately 100 km north-west of the epicentre (Saatcioglu *et al.*, 1999). Figure 2.10 illustrates the location of the epicentre and the areas that sustained heavier damage.



Figure 2.10 - Extent of the damage (KOERI, 1999)

According to Aschheim (2001), it were confirmed 15135 deaths, more than 24000 injured and approximately 500000 homeless. A large number of buildings either collapsed or sustained heavy damage, leaving an estimated 750 thousand people in need of housing. Saatcioglu *et al.* (1999) estimate 77000 severely damaged or collapsed buildings. An

estimated 80000 buildings registered moderate damage, and 90000 were lightly damaged. Furthermore, the earthquake affected approximately 35% of the industrial base in Turkey, creating a total financial loss of approximately 15000 to 20000 million US dollars. The downtown of Adaparazi area was severely affected, with up to 3/4 of the buildings damaged beyond repair (Aschheim, 2001).

The enormous amount of life and property losses during the Kocaeli earthquake was mainly caused by the collapse or heavily damage observed in multi-storey RC buildings, typically four- to eight-storey height, either under construction or built within the last few years (EQE, 1999; KOERI, 1999; Saatcioglu *et al.*, 1999), as shown in Figure 2.11.

The predominant buildings in Turkey are typically multi-storey RC commercial and residential structures with non-structural masonry infill walls (EQE, 1999). Aschheim (2001) highlights that much of the larger apartment buildings were built in the 1990's.

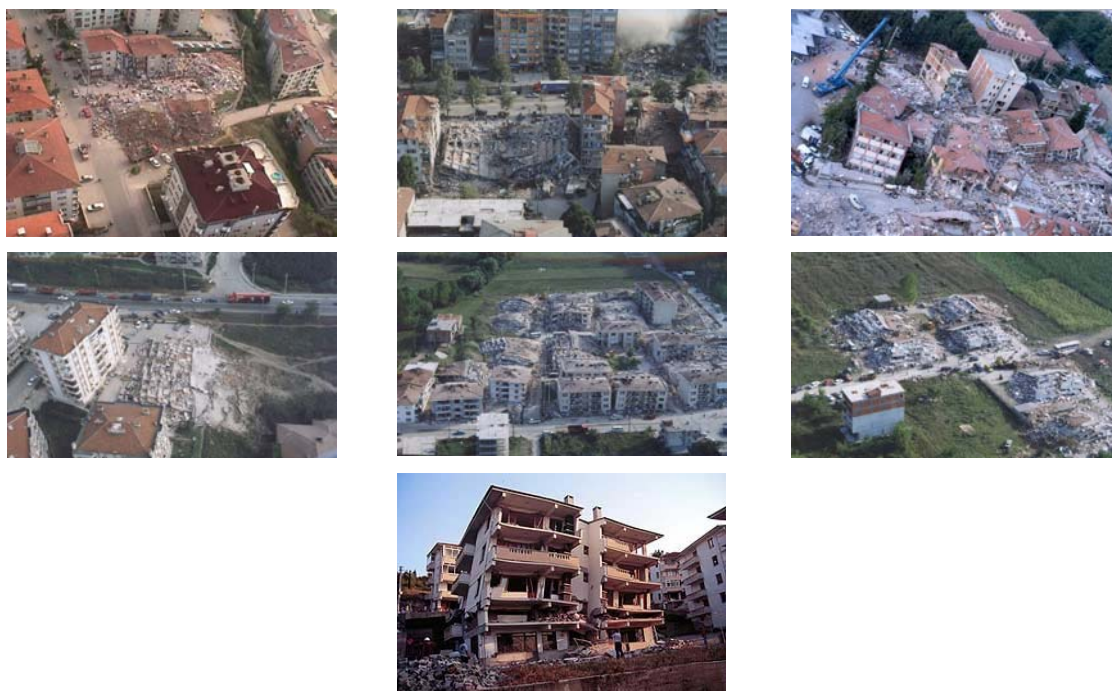


Figure 2.11 - General buildings damage and collapse in Gölcük, Adapazari and Yalova (KOERI, 1999; EQE, 1999; Sucuoglu, 2000)

The inspection of collapsed and damaged buildings indicates that, proportionally, the newest buildings suffered the most collapses. This is surprising considering that these buildings are supposed to be designed and built in accordance to a modern code that

incorporates sophisticated earthquake-resistant provisions (EQE, 1999). The Turkish code includes detailing requirements for seismic resistant structures as (Aschheim, 2001): *a*) closer spacing of transverse steel near beam-column joints; *b*) transverse steel within joints; *c*) 135° hooks with cross-ties; *d*) joint shear calculations; *e*) strong-column weak-beam provisions; etc. Therefore, modern buildings should have had moderate-to-light damage, given that the intensities of shaking in this earthquake were moderate. However, as observed by Sucuoglu (2000) and Saatcioglu *et al.* (1999), new buildings performed very poorly, mostly due to the repetition of well-known mistakes of the past in the design, detailing and construction of RC buildings, as well as location on ground that failed from shaking or faulting. Although most of them were relatively new, less than 10 years old, none of them satisfy the minimum seismic safety requirements, prescribed by the seismic design codes, and therefore the inelastic deformation capacity needed to save the structures was inadequate. Post-earthquake reports, by several researchers in the field, highlight the following main causes for the observed damages or collapses in buildings (see Figures 2.12 and 2.13):

- Improper construction site (buildings constructed on active faults, in areas of high liquefaction potential, or on soft soils which amplifies the seismic demands to critical values).
- Typically, the structural design engineer, who is an employee of the contractor, does not inspect the on-going construction to verify that the contractor has built the building according to the intent of the design drawings. This lack of construction oversight by the design engineer allows for on-the-spot field design modifications, which compromises the earthquake resistance of the buildings. Many of the buildings were built with poor and inappropriate construction materials (poor concrete quality) and used poor workmanship.
- Structural alterations (added floor, long cantilevers with heavy load).
- Inadequate longitudinal and transversal reinforcement detailing in beams, columns and joints, widespread use of smooth reinforcing steel, lack of concrete confinement, and, inadequate lap-splice length. Beam-column connections in many buildings did not contain any transverse reinforcement, as showed in Figure 2.12. The transverse reinforcement in columns consisted, typically, of 8.0 mm diameter

smooth reinforcement, generally placed at 300 mm spacing (or even some hoops were omitted, see Figure 2.12), and limited to perimeter hoops with 90° hooks, which are insufficient. This resulted in widespread column shear failures.

- Strong-beam weak-column mechanism.
- No employment of desirable shear walls or bracing elements.
- Undesirable short column mechanism created around window and similar openings, or produced by the landing slabs of staircases connected to columns (see Figure 2.12).
- In-plane irregularities (although most floor plans had symmetric layouts, there were cases where torsional effects were created by asymmetry in structural elements).
- Extensive use of soft-storeys was verified (brittle behaviour of the masonry infill walls in structures, or open space at the first floors to accommodate commercial spaces), typically formed at the bottom storey or in the bottom two storeys, placing excessive deformation demands on the highly critical first storeys' columns.



Figure 2.12 - Damage in buildings due to inappropriate detailing (KOERI, 1999)

The Izmit earthquake has wide-ranging lessons for the earthquake engineering, building code development and application in earthquake regions, construction quality, risk management, and insurance. Almost all of the damage caused by the earthquake, and most of the deaths were caused by the collapse of inadequately designed and constructed buildings. However, as stated in EQE (1999), some buildings in the most heavily damaged areas survived without significant damage. Typically, these buildings were properly designed with earthquake-resistant features, were well-constructed with obviously good quality materials, and were on firm ground or rock, which sustains the idea that loss of life and building' collapse were avoidable.



Figure 2.13 - Damage in RC buildings under construction after the Izmit earthquake (EQE, 1999)

#### 2.4.5 - The 25<sup>th</sup> January 1999 Armenia earthquake, Colombia

An earthquake occurred in 25<sup>th</sup> January 1999 in the Colombian town of Córdoba, in the Quindio Prefecture. The earthquake caused severe damages in buildings and casualties in the cities of Armenia, the capital of Quindio, and Pereira. The focal depth was as shallow as 10 *km*. In spite of its rather small magnitude of 6.2, it caused severe disaster in Armenia, the central capital city of quarter million people. This earthquake caused 1171 dead and 4795 injured. Collapsed and heavily damaged buildings exceeded 45000 and the total amount of monetary loss reached up to 2000 million US dollars. In the north zone of Armenia, where new buildings predominate, damage was limited, while in the central zone nearly 10% of the buildings collapsed. In the south, dwelling houses of low-income people are concentrated. Here the collapse reached 95% (Kagami, 1999; Jaramillo and Campos, 2000).

Typical structures in Armenia and Pereira city are of bamboo (or timber) frame wall structures, unreinforced masonry (URM) wall structures, and confined masonry wall

structures (Kagami, 1999). Figure 2.14 depicts a middle rise RC frame building with brick infill walls, illustrating a typical building in Pereira.

During the earthquake, not only low-rise popular traditional buildings but also medium-rise or relatively high-rise buildings in Armenia city were structurally damaged. Among these, there are important buildings such as the police station (five-storey RC), fire station, telecommunications office (six-storey RC), hospitals, schools, banks, churches and hotels.

Figure 2.15 shows the damages of a building of ordinary RC moment-resistant frame in Armenia. The extensive damage observed is mainly due to an inadequate structural design resulting, in many cases, in extremely irregular frame structures (Kagami, 1999).



Figure 2.14 - Typical middle rise RC frame building with brick infill walls (Kagami, 1999)



Figure 2.15 - Damage in an ordinary RC moment-resistant infilled RC frame (Kagami, 1999)

In addition, extensive structural and non-structural damage was observed in buildings with inadequate structural design (e.g. Figure 2.16, buildings in Armenia), such as, extremely irregular structures configuration, buildings with abrupt changes in lateral resistance and/or lateral stiffness, buildings with unusual size and shape, buildings constructed on steep hillsides or constructed on soft soils (Kagami, 1999).

Regarding masonry filled RC frame structures in particular, Kagami (1999) observed that most of the walls were separated from the surrounding RC column, beam or slab members, and that some masonry walls completely collapsed. As a result, RC columns became independent from the walls, and, consequently, some of them buckled or failed, losing their gravity load-carrying capacity that results in partial or total collapse of the buildings.

Typically, the columns lost their vertical and lateral load-carrying capacity due to the relatively small section of the RC columns and to the inadequate reinforcing provided. Other structural damage to RC columns, beams and beam-to-columns connections of the masonry filled RC frame structures were due to the lack of concrete sections or the discontinuity of concrete at and around the beam-to-column connections. This is due to frequent use of improper formwork materials. Furthermore, poor reinforcement details were also observed especially in RC beam-to-column connections (see Figure 2.16).



Figure 2.16 - Poor reinforcing details in RC joints (Kagami, 1999)

#### 2.4.6 - The 26<sup>th</sup> January 1995 Great Hanshin-Awaji earthquake, Kobe, Japan

Considering the development of the Japanese Building Code, and the Japanese advance in earthquake engineering research and technology at the time, it was hard to imagine structures collapsing in such miserable manners as during the 26<sup>th</sup> January 1995 Great Hanshin-Awaji (Hyogoken-Nanbu, Kobe) earthquake (Katayama, 1996). In the EQE report (1995) it is referred that age of construction, soil and foundation condition, proximity to the fault, and type of structural system were major determinant factors in the performance of structures in the Kobe earthquake.

The number of buildings destroyed by the earthquake exceeded 100000, that is, approximately 20% of buildings in the strongly shaken area, and further 80000 buildings were badly damaged. In a portion of the Kobe city centre 22% of office buildings were unusable, while an additional 66% need more than six months for complete restoration. After the earthquake, approximately 50% of the multifamily dwellings in Kobe were

unsafe to enter or unfit for habitation, leaving more than 300000 people homeless (EQE, 1995).

Damage was worst in the areas bordering the port or streams and rivers, where soils were poorly consolidated alluvial deposits. The fires following the earthquake also destroyed several thousand buildings. The older mid-rise buildings in Kobe are commonly non-ductile RC frame structures. Very narrow multi-storey buildings with open storefronts are also very common (EQE, 1995), as is also frequently found in urban areas in Europe.

The highest concentration of damaged and collapsed RC mid-rise buildings, typically of six to twelve storeys height, was observed in the Sannomiya area of Kobe's central business district. These RC buildings partially or completely collapsed at one or more storey levels. The failure, or concentration of damage, often occurred within the middle third of the building height (EQE, 1995; KOBEnet, 1995). Figures 2.17 and 2.18 show examples of mid-height RC frame buildings collapsed in Kobe. Figure 2.17-c it shows the collapse of the 5<sup>th</sup> floor of the eight-storey Kobe-west citizens hospital burying about fifty people.

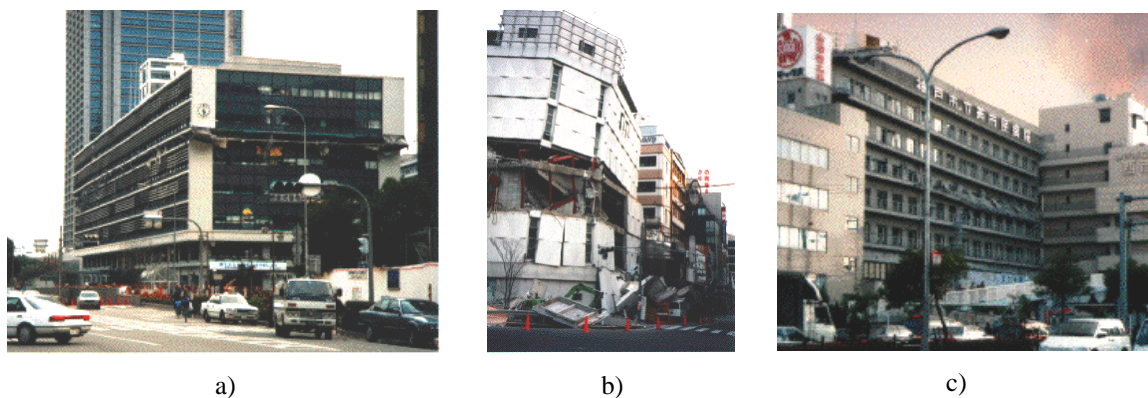


Figure 2.17 - RC frame structures with a mid-height collapse (KOBEnet, 1995): a) collapsed 6<sup>th</sup> storey of an eight-storey high office building; b) intermediate storey damage of a moderately high building; c) 5<sup>th</sup> storey collapse of hospital





Figure 2.18 - RC frame structures with a mid-height collapse (EQE, 1995; KOBEnet, 1995)

As stated in KOBEnet report (1995), possible reasons for the high incident of damages at intermediate floors are: strong vertical ground motion, extremely high intensity of the impact due to the closeness of the hypocenter, reduced density of walls in a particular floor due to office space use, changes in building strength or stiffness at these floor levels. A badly damaged RC building is represented in Figure 2.20, where the irregular structural configuration induces the concentration of serious damage at structural discontinuity.

A common type of RC buildings collapse in Kobe city was due to the failure of the lower storeys, as shown in Figure 2.19 (EQE, 1995; KOBEnet, 1995). These failures typically resulted from soft or weak storeys created for garages and from the desire to have numerous large open windows for storefronts at the bottom floor. The high land costs and general congestion in Japan exacerbated this problem. In many cases, an irregular distribution of shear walls or concrete frames resulted in substantial torsion, causing the structure to twist as well as sway due to earthquake loading (EQE, 1995).

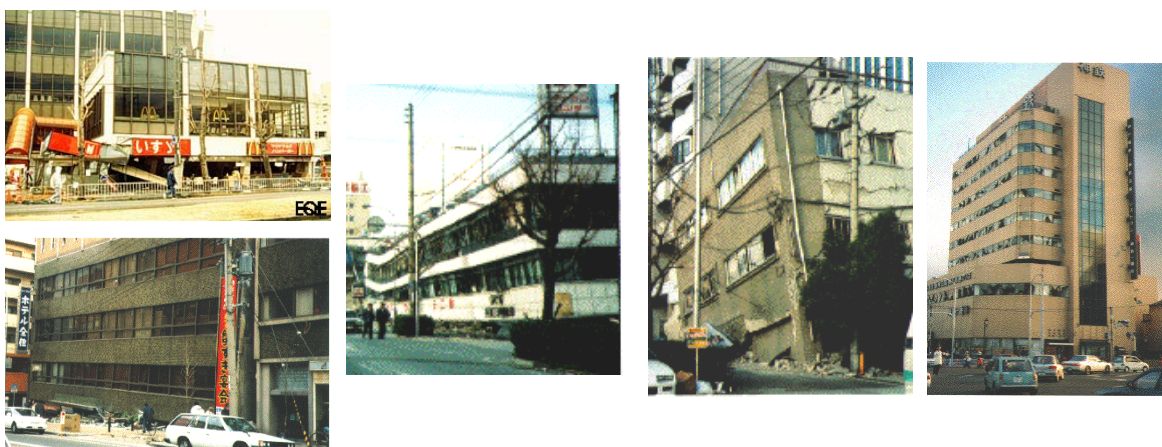


Figure 2.19 - Soft-storey building' collapses (EQE, 1995; KOBEnet, 1995)

The damage mode most commonly observed was a brittle shear failure of concrete column elements in old buildings, leading to a pancake collapse of the floor level above. These brittle failures resulted from inadequate reinforcing details. In general, damaged columns were observed to have transversal reinforcing with relatively large spacing. These hoops typically had hooks at their ends, which were bent only  $90^\circ$ . Many of the damaged buildings in Kobe were also constructed with undeformed reinforcing bars. Current Japanese code requirements include closer and larger hoops of deformed steel,  $135^\circ$  hooks that extend into the confined concrete, and cross-ties to supplement the rectangular hoops around the perimeter bars. In addition, according to recent codes, hoops must be closely spaced and extend through the joint created by the beams and columns (EQE, 1995).

The developments in engineering in Japan and the evolution of seismic design methods and codes for buildings contributed to reduce the effects of the earthquakes on structures. Figure 2.21 reports damages on different types of buildings. At the bottom of the picture is a two- or three-storey traditional Japanese wood-frame building with a heavy tile roof completely collapsed. On the right hand side of the picture is a six- or seven-storey office building of the 1960's or 1970's. This RC building is a typical example of a mid-height storey collapse. The high rise to the left is a post-1981 office building that has no apparent damage.



Figure 2.20 - Badly damaged irregular RC building in Sannomiya (EQE, 1995)



Figure 2.21 - Damages on buildings of different type in central Kobe (EQE, 1995)

The most severely damaged buildings generally appeared to be of older construction, dating from about 1950 to 1980. In general, newer buildings constructed using the current code provisions with not too irregular configurations performed relatively well and ensured

---

life safety. Many older houses, smaller commercial buildings of both concrete and steel, and mid-rise concrete structures designed and constructed prior to the early 1980's behaved poorly (EQE, 1995). Millions of RC buildings had been designed and constructed using the same non-ductile details that had been employed in high-seismic regions around the world up until the early 1970's, which are an enormous potential source of casualties and economic losses in the future.

#### **2.4.7 - The 17<sup>th</sup> January 1994 Northridge earthquake, Los Angeles, US**

As the population of the US continues to expand in areas of high seismic activity, the increasing exposure to personal injury and property damage from earthquakes demands our attention. The destruction caused by California's 1994 Northridge earthquake remind this concern. The destruction reached far beyond physical damage, leaving lasting emotional and economic changes for people and communities during a long and difficult reconstruction process (NAHB, 1994).

The Northridge earthquake occurred on 17<sup>th</sup> January 1994. Its epicentre was located in a densely populated area of Los Angeles county near the community of Northridge. Over 30 deaths were reported as a direct result of the tremor, and a total death toll of 58 was attributed to both direct and indirect causes (NIST, 1994). Current estimates of the severity of this earthquake place it at a magnitude of 6.4 on the Richter scale (Hall, 1994). Uncorrected peak horizontal ground accelerations were recorded at 0.9g near the epicentre. In terms of the effective peak horizontal ground accelerations, the 475 years return period (475-yrp) design estimate of 0.4g was exceeded by a factor of 1.5 to 2 at several locations (Naeim, 1994). A large 'pulse' of ground movement produced during the 15 and 20 second duration by this earthquake is among the worst recorded in the US history (Naeim, 1994). Large ground movements from the earthquake were felt as far as Las Vegas (NAHB, 1994).

In US earthquakes (e.g. southern California's 1971 San Fernando and 1994 Northridge earthquakes) non-ductile RC construction has been the source of collapse of buildings, elevated highways and overpasses. In the recent Northridge earthquake, office and residential buildings as well as hotels had generally a satisfactory behaviour. Yet, a

considerable number of buildings, particularly the ones designed before the recent codes in force, suffered significant damage. Many were demolished or extensively repaired (Oliveira *et al.*, 1995). The soft-storey mechanism, insufficient transverse reinforcement in columns, excessive concrete cover, short columns and other deficiencies of reinforcement detailing were the most frequent causes of building's collapse. As stated by Oliveira *et al.* (1995), deficient connection to the surrounding frame elements caused unsatisfactory behaviour of the external infill walls in many cases.

#### **2.4.8 - Conclusion and discussion**

The review above indicates that seismic risk in urban areas is still high and worth considering. The disastrous consequences, in terms of damages on RC buildings, and consequent human casualties, resulting from seismic activity in a recent past all around the world reveal that research on assessment and retrofitting of existing structures is urgently needed. Next, the typical causes of damage and failure of existing non-ductile construction are reviewed.

### **2.5 - TYPICAL CAUSES OF DAMAGE AND FAILURE OF EXISTING NON-DUCTILE RC BUILDINGS**

*'A chain breaks at its weakest link.'* (Anonym)

Structures should be provided with balanced stiffness, strength and ductility between its members, connections and supports (Bertero, 1997). As already stated, frame type RC structures were the most commonly structural system used until the late 1970's in the southern European countries, especially in buildings. Consequently, the seismic rehabilitation practice for constructions of that period is concentrated on that kind of structures. In spite of the current rather strict seismic code requirements (see Section 2.2.3), serious deficiencies/weaknesses still take place in the design and construction of most buildings. Tankut and Ersoy (1998) and Sasani *et al.*'s (1999) work, for example, point out major sources of seismic weakness in buildings, which can be grouped in four main categories, as follow:

- 
- Design deficiencies, such as: insufficient lateral stiffness and strength, horizontal and vertical irregularities, soft-storeys, short columns, weak-column strong-beam mechanism, critical torsional response, not adequate spacing between adjacent structures, etc.
  - Detailing deficiencies, such as: insufficient confinement, insufficient and improper anchorage of the longitudinal reinforcement at the joints and footings, inexistence or inadequate beam-column joint reinforcement, lack of adequate amount and detailing of the longitudinal and transverse reinforcement along the beams and columns, inadequate lap-splice in column longitudinal reinforcement, etc.
  - Construction deficiencies, such as: poor workmanship, poor quality concrete, construction of the structures not following the design and detailing prescriptions, etc.
  - Deterioration and structural modifications. As stated by Souza and Ripper (1998), 'a lie that we tell for ourselves for willing to believe that all of which we make, build, or in which creation we take part, is meant to glow forever in the infinity'.

However, it should be noted that these categories couldn't be looked at separately. In fact, design, detailing and construction of a structure are intimately related, and the achievement of good workmanship depends, to a large degree, on the simplicity of the detailing of the members, and of their connections and supports. As referred by Bertero (1982), in the case of a RC structure, it is possible to detail complex reinforcement on paper and even to realize it in laboratory specimens so that seismic behaviour is improved. Nevertheless, such design details may not be economically feasible in the field. Bertero (1982) defends that a design is only effective if it can be constructed and maintained.

Next the most common causes of failure or damage of RC buildings are overviewed: *i*) stirrups/hoops, confinement and ductility; *ii*) bond, anchorage, lap-splices and bond splitting; *iii*) inadequate shear capacity and failure; *iv*) inadequate flexural capacity and failure; *v*) inadequate shear strength of the joints; *vi*) influence of the infill masonry on the seismic behaviour of frames; *vii*) vertical and horizontal irregularities: abrupt change in structural and/or element properties; *viii*) higher modes effect; *ix*) strong-beam weak-

column mechanism; and, finally, x) structural deficiencies due to architectural requirements. Emphasis is placed on effectively integrating the description of each cause of damage with photographic documentation.

### 2.5.1 - Stirrups/hoops, confinement and ductility

As mentioned in EASY (1997), the philosophy behind confining seems nowadays very simple and self-understood. Concrete in compression crushes in a very brittle manner perpendicular to the direction of the principal compression stresses (the particles are simply pushed out of the stressed zone in the perpendicular direction). Yet, confining this concrete region with stirrups precludes or at least postpones the push-out. In this way, the strength and ductility of concrete is enhanced considerably. The confinement effect depends on the stirrup diameter, on the spacing between the stirrups and longitudinal bars, on the steel quality, and on the shape of the cross-section and stirrups.

This simple principle was not fully understood until a few decades ago, and, even now, it has not been applied to all designs. Therefore, many deficient structures with respect to confinement exist. And some of them are not old at all. An illustrative example is the better behaviour of buildings in Kobe earthquake. Those designed after 1981, when Japanese engineers had started to use much stronger confinement, behaved better in comparison to those designed prior to this year (EASY, 1997). Figures 2.22 and 2.23 shows examples of earthquake damaged RC columns without adequate transverse reinforcement.

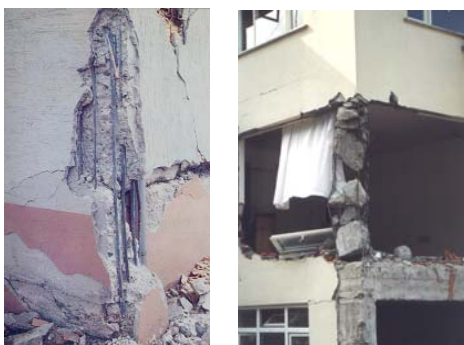


Figure 2.22 - Damaged RC columns without transverse reinforcement (Saatcioglu *et al.*, 1999)



Figure 2.23 - Damaged RC columns with inadequate transverse reinforcement (Saatcioglu *et al.*, 1999)

In the columns' plastic hinging region the concrete core must be adequately confined to prevent deterioration of the shear and flexural strength of these columns. This confinement requirement is more severe because of the high axial load and shear that typically needs to be carried through the plastic hinging region (FEMA-274, 1997).

During earthquake, failures of beams and beam-to-column connections are most commonly related to inadequate use of transverse reinforcement for shear strength and confinement. These are typically local beam failures and will not necessarily lead to collapse of the building (FEMA-274, 1997). A common structural problem in buildings is inadequate transverse confinement reinforcement in the beam plastic hinging zones.

Ductility is defined in EASY (1997) as the ability of a certain material, of a structural element or of a structure as a whole to sustain inelastic deformations without collapse, having a decisive effect on the energy dissipation capacity of a building (see also the Glossary, in Appendix C). Shear behaviour (see inadequate shear capacity and failure, in Section 2.5.3) is typically non-ductile and flexural behaviour (see inadequate flexural capacity and failure, in Section 2.5.4) can be made ductile. In general, designers are much more concerned about strength than ductility. In fact, strength appears to be more important to static vertical loading in everyday design. But, as earthquakes happen from time to time, we have been gradually realizing the importance of ductility in preventing structural collapse in such events. Unfortunately, this development has been rather slow, and the principle of ductility in earthquake engineering was understood only a few decades ago. Therefore, a large number of older buildings and their structural elements are non-ductile, which represents a serious risk.

### **2.5.2 - Bond, anchorage, lap-splices and bond splitting**

When efficiently developed, bond enables the concrete and reinforcement to form a composite structure. Thus, the attainment of satisfactory performance in bond is the most important aim of the detailing of reinforcement in structural components (Park and Paulay, 1975). As stated in EASY (1997), bond is even more vital problem in the case of dynamic loading and when plain reinforcement bars are used. Bond is developed by friction, wedging action of small-dislodged sand particles between the bar and the

surrounding concrete, and with bearing stresses against the faces of ribs. It is important to realize that when a bar is tried to pull out of the concrete it tends to push the surrounding concrete apart, developing the so-called circumferential stresses. If the area of concrete surrounding the bar is small, splitting is the common mode of failure.

There are some basic rules in detailing of anchorage and lap-splices: *a)* lap-splices and anchorage at the location where the surrounding concrete is extensively cracked (plastic hinges for example) should be avoided; *b)* concrete with embedded anchors and lap-splices should be well confined preventing the concrete to be pushed apart; *c)* compression in the direction perpendicular to the lap-splice has a beneficial effect also preventing the concrete to be pushed apart; and, *d)* if large diameter bars are used, it is very difficult to ensure the required anchorage length because the force in the bar increases proportionally to the square of the diameter and the bond force is linearly related to the bar diameter (EASY, 1997).

The columns in Figure 2.24 collapsed during the 1999 Izmit, Turkey, earthquake due to inadequate lap-splice and to lack of transverse reinforcement. As shown in Figure 2.25-*a*, in typical buildings in Turkey, beam bars terminate with tight 180° hooks in the beam-column joint. In Figure 2.25-*b* lap-splices are made just above the floor slabs.



Figure 2.24 - Inadequate lap-splice and lack of stirrups (Saatcioglu *et al.*, 1999)



Figure 2.25 - Typical deficiencies in buildings: a) beam bars terminate with tight 180° hooks in the joint; b) yielding of the longitudinal steel adjacent to the floor slab (Aschheim, 2001)

Typically, the bottom bars extend straight up, the bars from above terminate in hooks just above the floor slab, which according to Aschheim (2001) focuses yielding of the longitudinal steel in a narrow region adjacent to the floor slab. At the particular joints in



Figure 2.26 two of the vertical bars terminated in a hook, but there was no space for a third to do so, and it terminated straight. In Figure 2.27, anchorage problems for longitudinal column bars terminated in a roof beam.



Figure 2.26 - Column lap-splice details  
(Aschheim, 2001)

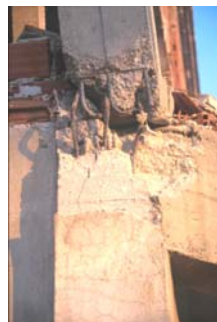


Figure 2.27 - Bar pullout-columns  
(Aschheim, 2001)

In recent years there has been increasing emphasis in many countries on seismic assessment and retrofit of existing RC structures designed to the pre-1970's codes (Aoyama, 1981; ATC-21, 1989; Park, 1992). A large number of tests on as-built and retrofitted RC columns and beam-column joint assemblies using simulated seismic loading have been conducted. Most of these previous studies used ribbed longitudinal bars. Yet, very few were conducted on as-built RC components reinforced by plain round bars. Liu and Park (2001; 2000) highlighted that the information on the effect of the use of plain round longitudinal bars on seismic behaviour of existing RC structures is scarce and is urgently needed. Liu and Park's (2001; 2000) and Takiguchi *et al.*'s (1988) studies are indeed an exception in this regard.

Takiguchi *et al.* (1988) tested cyclically a series of RC columns designed according to the 1962 AIJ (Architectural Institute of Japan) Japanese Building Code (JBC). In the specimens, both longitudinal and transversal reinforcement were designed with plain round bars, as typically used in Japan. Recall that the Japanese RC Building Code was revised in 1971, just after the 1968 Tokachi-Oki earthquake (see Section 2.4.8). In their study, Takiguchi *et al.* (1988) also investigated the influence of the repair and strengthening techniques in columns' behaviour.

Liu and Park (2001; 2000) tested the response of full-scale beam-column joints with plain round reinforcement bars, designed according to the pre-1970's codes. In the studies conducted by Liu and Park (2001) the main test variables were the manner the longitudinal beam bars were hooked in the joint core, and the level of the axial load applied to the columns. The amount of transverse reinforcement used in the beams, columns and joint cores was very small, as was typical of the pre-1970's. Similar units using deformed bars were also tested. Comparing the experimental results obtained on the units with plain round reinforcement bars with those with deformed bars, the former have shown less joint shear distortion but high opening of beam bar hooks in tension, and column bar buckling. As a result, premature concrete tension cracking failure along the outer layer of column bars adjacent to the beam bar hooks was enhanced. The attained stiffness, in particular, and the strength were significantly lower, especially the stiffness.

Concerning the beam and column behaviour, Liu and Park (2001) observed that the measured steel strains along the longitudinal reinforcement of the members (beams and columns) were generally larger than the values estimated by conventional flexural theory at the beam-column interfaces. Hence, conventional flexural theory overestimates the member moments, because severe bond degradation along the longitudinal reinforcement greatly violated the assumption of plane sections. The observed beam and column performance was dominated by degrading flexural behaviour for all units, and the steel strains measured on the transverse reinforcement were well below the steel yield strain. This suggests that the code approach and the procedure in the current seismic assessment method for shear strength greatly underestimate the available member shear resistance when plain bars are used. The measured member flexural deformations concentrated mainly in the member fixed-end regions, and were similar to that observed for tests on interior beam-column joint units with plain bar reinforcement.

### **2.5.3 - Inadequate shear capacity and failure**

Typical gravity and wind load designs normally result in a design shear force significantly lower than the shear force that could be developed in a column during seismic loading. Moreover, recent seismic design procedures for structures rely on ductility. Therefore,

---

shear limit states should be avoided in seismic resistant structures. For this goal, the shear demand should be limited or shear capacity should be enhanced.

Shear demand is better controlled by capacity design procedures. Since capacity design has been introduced in the last 25 years or so, and is still not adopted by all designers, there are many structures in the field which are deficient in shear. Consequently, shear failure is one of the most frequent during earthquakes. What actually happens is that designers have used a global seismic force reduction factor affecting equally flexural (ductile behaviour) and shear (brittle behaviour) forces. Hence, the shear capacity is reached soon after yielding starts, and, therefore, energy dissipation is precluded (EASY, 1997).

To enhance shear capacity: *a)* use suitable amount of stirrups and ties to enhance truss mechanism; *b)* use enough stirrups to ensure concrete integrity and enhance aggregate interlock mechanism; *c)* avoid the combination of shear and tension; *d)* use better quality of concrete; and, *e)* use diagonal reinforcement to prevent sliding shear in deep elements (EASY, 1997).

The problem of shear strength and confinement is commonly more severe in corner columns, especially if the building has significant eccentricity between the centre of mass and the centre of resistance. Corner columns need to have a higher degree of confinement (FEMA-274, 1997). Figure 2.30 shows the first storey RC columns of the Medical Treatment and Care Unit of the Olive View Hospital after the 1971 (9<sup>th</sup> February) San Fernando earthquake ( $M = 6.5$ ). As can be observed in the figure, while the spirally confined central columns remained structurally sound, the unconfined concrete at the corner columns disintegrated (Bertero, 1997).

Column transverse steel in existing buildings typically consists of hoops with 90° hooks at 20 to 25 *cm* spacing and no cross-ties. Figures 2.28 to 2.33 show examples of damaged RC columns in shear due to insufficient transversal reinforcement.



a)



b)

Figure 2.28 - Column shear failure examples: a) 1979 Montenegro earthquake (EASY, 1997); b) 1999 Izmit earthquake (note the to lack of transverse reinforcement - Saatcioglu *et al.*, 1999)



Figure 2.29 - Shear and bond failure at the mid-height of a RC column during the 1985 Mexico city earthquake (EASY, 1997)



Figure 2.30 - Damaged RC corner column at the 1<sup>st</sup> storey (Bertero, 1997)



Figure 2.31 - Column shear failure (Aschheim, 2001)



Figure 2.32 - Shear cracks at the RC column of an old school building (Yamazaki, 1993)

During the 1993 (15<sup>th</sup> January) earthquake at Hokkaido, Japan, the Kushiro Technical High School, a 30-year old building, developed extensive shear cracks on the RC columns, as shown in Figure 2.32.

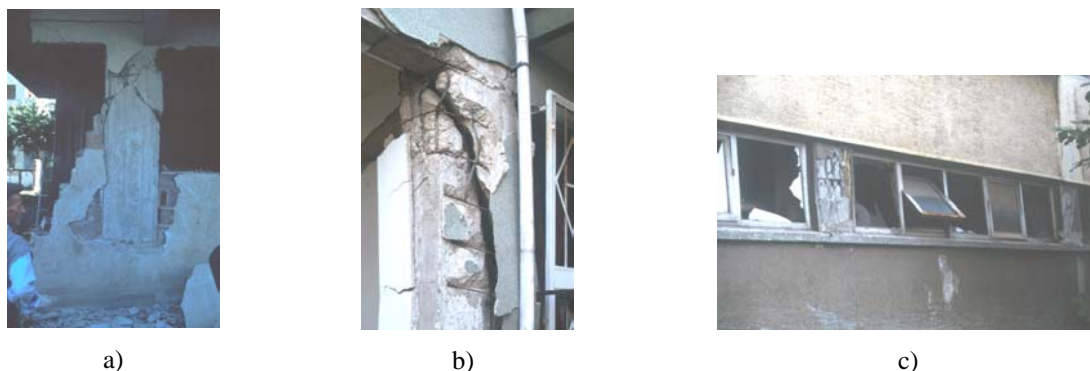


Figure 2.33 - Column shear failures (Aschheim, 2001): a) strong-axis behaviour; b) oblique column shear failure; c) captive column shear failure

When loaded in the strong axis direction, columns often fail in shear, as illustrated in Figure 2.33-*a*. As shown at the image in the centre, in this isolated case, the shear failure was oblique, extending down the length of the column, fracturing the transverse steel in various places. Another common problem is to artificially shorten a column, provoking stiffer ones, attracting much higher shear forces than they were designed to carry, as discussed in Section 2.5.6. Short columns are vulnerable to shear failure as shown in Figure 2.33-*c*, where a column shear failure induced by the partial infill walls is shown.

#### 2.5.4 - Inadequate flexural capacity and failure

As recalled by Bertero (1997), the proper amount and correct detailing of the reinforcing steel plays an important role in the seismic response of a RC structure. Therefore, for regions of moderate to high seismic risk it is necessary to reinforce the concrete structural members adequately.

Seismic design nowadays relies on ductile behaviour of flexural elements, i.e. beams and columns. As recalled in EASY (1997), flexural behaviour can be made ductile if some basic rules are followed. The designer's goal is to prevent the brittle crushing of concrete in compression prior to the stage when substantial yielding in tension reinforcement occurs. This can be done if the demand on the compression zone is lowered and/or the capacity of this zone is enhanced. To this end, one can: *a*) limit the compression axial forces or increase the area of the cross-section; *b*) limit the area of the tensile reinforcement. The force in this reinforcement should be namely in equilibrium with the force in the

compression (and the external axial force). The larger area of the tensile reinforcement and the higher yield stress are, larger demand is imposed on the compression zone; and, *c*) the compression zone capacity can be enhanced with better quality of concrete, compression reinforcement and with adequate confinement (see also stirrups/hoops and confinement, in Section 2.5.1). Since traditionally the designers were concerned with strength and seldom with ductility, some of these principles have been not understood and followed. Thus, also many brittle failures are also observed in flexure (in particular in older buildings) after an earthquake. In Figure 2.34 examples of RC column flexural failures are shown.



Figure 2.34 - Typical flexural failure: column hinging (Aschheim, 2001)

### 2.5.5 - Inadequate shear strength of the joints

It is not worthwhile using strong, stiff and ductile structural members if they are not properly connected (Bertero, 1997). Beam-to-column connections can suffer a significant loss of stiffness due to inadequate shear strength and anchorage capacity in the connection. Both of these failure modes are related to inadequate use of confinement reinforcement in the connection, and improper detailing of main reinforcement anchored in or passing through the connection (FEMA-274, 1997). Collapse and severe damage of buildings due to lack of good connections is common during earthquakes. In the Izmit earthquake, joint failures were catastrophic in many cases (see, e.g. Saatcioglu *et al.*, 1999; Aschheim, 2001). Figures 2.35 and 2.36 illustrate cases of such damage, where no adequate transverse reinforcement (inexistent in many cases) was apparent in any of the joints, resulting in many cases in building collapse.



Figure 2.35 - Lack of proper design of beam-column connections (Saatcioglu *et al.*, 1999)



Figure 2.36 - Inadequate strength of joints (Aschheim, 2001): a) joint damages; b) joint failures

### 2.5.6 - Influence of the infill masonry on the seismic behaviour of frames

It is a common misconception that masonry infill in structural RC frames can only increase the overall lateral load capacity, and that, therefore, must always be beneficial to seismic performance. In fact, Section 2.4 shows numerous examples of earthquake damages that can be traced to structural modification of the basic frame by the so-called non-structural masonry partitions and infill panels. Even if they are relatively weak, masonry infill can drastically modify the intended structural response, attracting forces to parts of the structure that have not been designed to resist them (Paulay and Priestley, 1992). The examples provided below illustrate the relevant influence of the infill masonry in the behaviour of the frames.

Masonry infill panels can increase substantially the global stiffness of the structure. Consequently, the natural period of the structure will decrease and, depending on the

spectrum shape at the natural period of the bare structure, the seismic forces will correspondingly increase. The higher shear forces generated in the infilled frames are transmitted primarily by shear stresses in the panels. Shear failure commonly results, with shedding of masonry into streets below, or into stairwells, with great hazard to life (see Figure 2.37).



Figure 2.37 - Damages on masonry infill walls (Saatcioglu *et al.*, 1999): a) RC frame building with almost fully damaged masonry infills; b) diagonal tension failure of a masonry wall

Situations in which masonry walls extend only to part of the storey height (short columns), leaving a relatively short portion of the columns exposed, may also induce vulnerable behaviour. Frequently, a column is shortened by elements which have not been taken into account in design. For example, infills, window openings or landing slabs of staircases.

In some cases, when the earthquake occurs only portions of the infill fail and fall out, and the remained infill can cause the shortened column effect (as shown in Figure 2.38). If the frame is designed for ductile response to the design-level earthquake, without consideration of the infill effects, plastic hinges can be expected at the top and bottom of the columns, or preferably, in beams at the column faces. The influence of the infill will be to inhibit beam hinges, to stiffen the centre and one face of the column (depending on the direction of the lateral load), causing plastic hinges to form at top of the column and top of the infill, as schematically shown in Figure 2.39. If the design has not considered this effect of the infill, the consequence will be a dramatic increase in column shears and, consequently, shear failure of the columns will appear. Complete collapse of the column and, consequently, of the building can occur if such column is not well furnished with transverse reinforcement. However, as referred in EASY (1997), for strong earthquakes, even if very strong stirrups are used, it is difficult to save such short columns. Therefore, such collapses have been very frequent in past earthquakes (see examples in Figures 2.38



and 2.40). The only solution is to use different structural concepts. As shown in Figure 2.40-*a*, diagonal cracking seemed to precede out-of-plane failure in many cases. In Figure 2.40-*b* is represented an in-plane infill failure at the Sakarya telephone building.



Figure 2.38 - Short column effect caused by: window opening; masonry walls; and, landing slabs of staircases (Saatcioglu *et al.*, 1999; Aschheim, 2001)

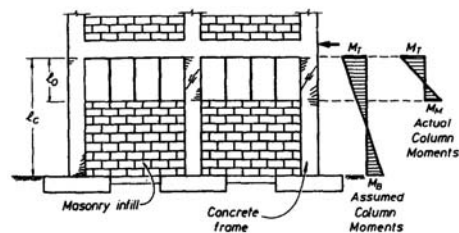


Figure 2.39 - Partial masonry infill in concrete frame (Paulay and Priestley, 1992)

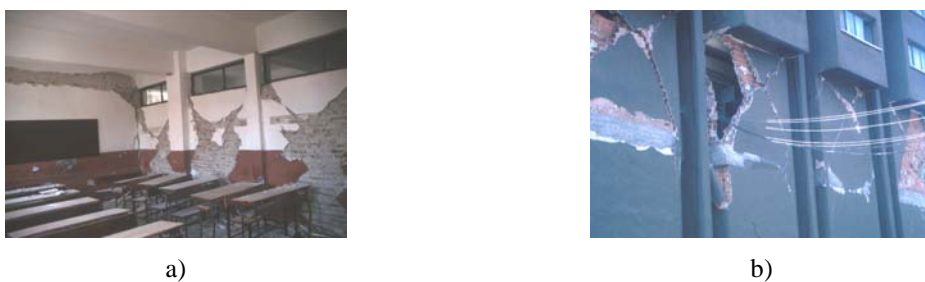


Figure 2.40 - Damage on infill walls (Aschheim, 2001): a) infill cracking; b) in-plane infill failure

### 2.5.7 - Vertical and horizontal irregularities

Abrupt changes in stiffness, strength or mass in structural and/or element properties of a building, either in plan or in elevation, can result in distributions of lateral loads and

deformations very different from those that are anticipated for uniform structures (Moehle and Mahin, 1991). As evidenced by several recent earthquakes, structural configuration plays an important role in the building behaviour. Several authors (e.g. Costa, 1989; Bento and Azevedo, 2000, among others) argue that a large number of the structural collapses are to some extent related to configuration problems or wrong conceptual design (see Figure 2.41, for example).

Common equivalent elastic procedures rely on the supposition that inelastic behaviour (damage) is uniformly distributed to all ductile elements of the structure. If structural characteristics (geometry, mass, stiffness or strength) are not uniform or they are not continuously changing (e.g. setbacks, abrupt diminishing of cross-section column dimensions, change in the storey height, change in materials, sudden change on the column's cross sections, interruption of a shear wall at certain storey, change of structural system at a particular storey, sudden change of non-structural partition walls, etc.) it is very difficult to avoid damage concentrations at the locations of these abrupt changes. In some situations, there is even a combination of these negative aspects. Since damage tends to concentrate in a limited number of locations, around the discontinuities, it follows that it is difficult to provide enough capacity to these elements. To make the situation worse, usual elastic design procedures are often unable to predict locations of damage concentration. The most serious problem of this type in earthquake engineering is the problem of soft-storey (EASY, 1997).

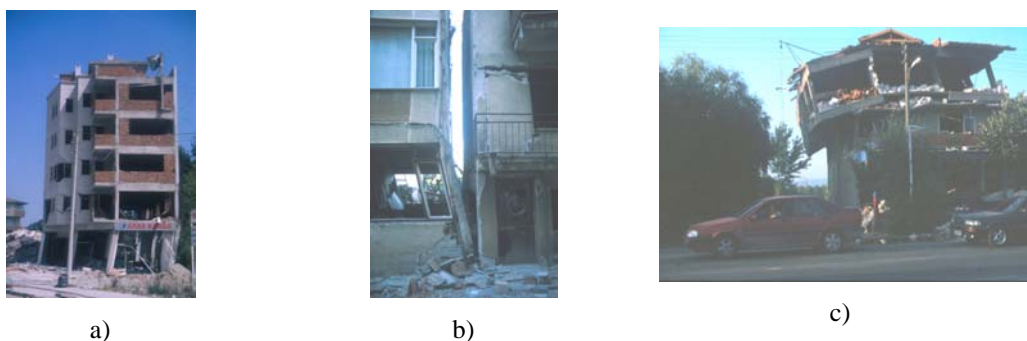


Figure 2.41 - Soft-storeys (Aschheim, 2001)

Many examples where discontinuity apparently resulted in severe damage or collapse are frequent in the earthquake reconnaissance literature. A very common irregularity in buildings appears at the lower storey levels, resulting from the absence of infills, contrary

---

to the other upper storeys with the common larger height of the columns at this storey level. Buildings with mixed-use occupancies (commercial at the lowest storeys and offices or residential above) have typically large clear spaces in order to accommodate stores, for example. Thus, the resulting structural frame system is irregular and, if not accurately designed, inadequate to resist earthquakes.

As stated by Moehle and Mahin (1991), another common form of vertical discontinuity arises from unintended effects of non-structural elements. The problem is more severe in structures having relatively flexible lateral load resisting systems because in that case the non-structural component can compose a significant portion of the total stiffness. A common cause of failure occurs in infilled frames. Soft-storeys can result if infills are omitted in a single storey (often the first storey), as has occurred in several earthquakes (e.g. 1985 Mexico, 1999 Kocaeli). Even if placed continuously and symmetrically throughout the structure, a soft-storey mechanism can form if one or more infill panels fail (Rosenblueth and Meli, 1986).

In the 1999 Izmit, Turkey, earthquake soft-storeys were apparent in many collapsed buildings. The photos in Figures 2.41-*a* and 2.41-*b* illustrate the effect of column orientation. Weak axis orientations (to maximize storefront glazing) led to soft-storey mechanisms. Strong axis orientations (Figure 2.41-*b*, see the building on the right hand) appeared to do better. In Figure 2.41-*c* weak axis bending, again, appears to be the problem.

Apparent vertical irregularities can also occur due to the interaction between adjacent structures having inadequate separation. A tall building adjacent to a shorter building may experience irregular response due to effects of impact between the two structures. The effect can be exacerbated by local column damage due to pounding of the roof of the small building against the columns of the taller one (Moehle and Mahin, 1991). Rosenblueth and Meli (1986) refer examples of distress due to this phenomenon during the 1985 Mexico earthquake.

Another relevant aspect is the possible seismic torsional response because of the shift in the centre of rigidity due to the presence of a non-symmetric distribution of the infill panels. A consequent increase of shear forces can appear, especially in the external frames.

Even if it is a well-known undesirable structural misconception, soft-storey in buildings tends to appear, most of the times due to architectural reasons (see also Section 2.5.10). Bento and Azevedo (2000) investigated the behaviour coefficients for soft-storey structures, and confirm the high vulnerability of this kind of irregular structural systems. The excessive inter-storey drift at a soft-storey level conduces a concentration of damage at this level, resulting in a less safe structure. The study also calls the attention to the importance of a correct consideration of the geometric non-linearity due to the high level of deformation expected at the soft-storey level.

### **2.5.8 - Higher modes effect**

Many structures have been designed using simplified procedures based on the equivalent single mode representations. In certain cases these procedures work fine. Nevertheless, frequently they fail. In Mexico city, for example, many buildings collapsed in upper storeys (see Figure 2.42). Partly, this fact can be attributed to the higher modes effect. These buildings, being very soft, were further weakened by the very long earthquake excitation (infills fell out of frames for example). In some cases, the second mode of vibration was in resonance with the predominant frequency of the earthquake. And this was true even for apparently regular structures where equivalent single mode methods were allowed by the majority of the existing seismic codes (EASY, 1997).



Figure 2.42 - Building failure due to the higher modes effect during the 1985 Mexico city earthquake (EASY, 1997)

### **2.5.9 - Strong-beam weak-column mechanism**

Modern codes include capacity design procedures in order to create structures with enhanced earthquake performance, and which are economical to build and to repair after an

earthquake. In order to create the most desirable and stable energy dissipating mechanism, a hierarchic formation of plastic hinges should be enforced by design, as recalled by Bento and Lopes (2000). It is widely recognised that the most desirable location for plastic hinges in moment resisting frames is the beams' extremities. Thus, modern codes recommend, to obtain ductile moment frames and to ensure inelastic action in the beams, thereby localizing damage and controlling drift, the preference for the weak-beam strong-column mechanism. Accordingly, the strength of the column at any joint must be greater than those of the beams.

Existing RC frame structures were designed without having this concept in attention, as they were constructed before the current codes enter into force. Furthermore, even today, it is often difficult to adopt some code prescriptions due to architectural requirements.

In recent earthquakes, many RC structures have collapsed or were severely damaged due to the development of the strong-beam weak-column mechanism, confirming the importance of this code prescription. Figure 2.43 illustrates examples of buildings' collapses during earthquakes, and where the strong-beam weak-column behaviour mechanism is evident.



Figure 2.43 - Strong-beam weak-column mechanism (Aschheim, 2001; Saatcioglu *et al.*, 1999)

### 2.5.10 - Structural deficiencies due to architectural requirements

As observed by Moehle and Mahin (1991), past earthquakes have repeatedly proved that proper selection of the load carrying system is essential to good structural performance under any loading. They also recall that a properly selected structural system tends to be relatively forgiving of lapses in analysis, detail and construction. But, extra attention to

analysis and detail is not likely to improve significantly the performance of a poorly conceived structural system. More caution should be put on structures that can be subjected to earthquake actions, since the intensity and orientation of loading are highly uncertain. Thus, architecture makes sometimes much more difficult (and expensive) to properly design the structural system for earthquakes.

Figure 2.44-*a* shows a typical building in Turkey (Aschheim, 2001), with columns oriented to satisfy architectural requirements. The column sections have large aspect ratios (typically 25 cm by 60 cm) with infill built up to the narrow sides of the columns. Thus, the columns are located and oriented to fit within the partition walls. In Figure 2.44-*b* are shown beams eccentric to joints as consequence of a more convenient architectural solution.

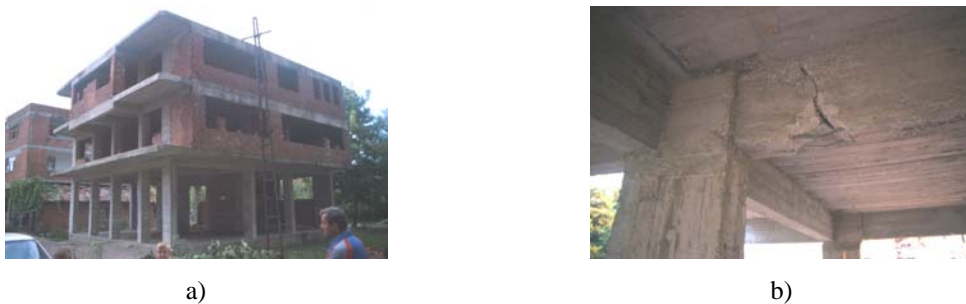


Figure 2.44 - Typical buildings in Turkey (Aschheim, 2001): a) view; b) typical beam details

Recapitulating, citing Moehle and Mahin (1991), buildings having simple, regular and compact layouts incorporating a continuous and redundant lateral force resisting system tend to perform well. Complex structural systems that introduce uncertainties in the analysis and detailing or that rely on effectively non-redundant load paths can lead to unanticipated and potentially undesirable structural behaviour.

## **2.6 - COMMON RETROFITTING STRATEGIES AND TECHNIQUES OF EXISTING RC BUILDINGS**

Efficient seismic-resistant behaviour of buildings can be achieved by a proper selection of the building configuration and its structural layout and by the proper proportioning and detailing of the structural and non-structural components (Bertero, 1997).

The selection of the retrofitting strategy and its implementation should be guided by results of a detailed assessment or evaluation of the structure. As recalled by Ersoy (1998), the seismic rehabilitation of structures is based on two general approaches: *a*) system rehabilitation or improvement; and, *b*) member rehabilitation or strengthening. The former approach is sufficient when individual members are not too weak and they are expected to perform satisfactorily under the reduced seismic effects as a result of the improvement in the system behaviour. Very rarely the later approach may be suitable if the seismic weakness is local and can be eliminated by strengthening a limited number of individual members. However, in the majority of cases, both approaches need to be combined.

Fardis (1998) advocates that, 'any retrofitting intervention should not prejudice the safety or the capacity of any part of the building in any aspect'. Therefore, the designer should make sure that: *a*) upgrading the flexural capacity of an element does not make it critical in shear; *b*) strengthening of a beam does not shift plastic hinging to columns; and, *c*) consequences of discontinuing the retrofitting (i.e. the new shear walls or bracing, or upgrading of existing columns, at a certain storey can concentrate the damage in the storey just above the retrofitted level). As recalled by Fardis (1998), the designer should guaranty the 'continuity of the load path(s)'. Indeed, regardless of the particular rehabilitation strategy chosen, the designer should check carefully the existing and the retrofitted structure in terms of safe transfer of inertia forces, from the masses (where they originate) to the elements of the lateral-load-resisting system and from there to the foundation. Therefore, the safety of connections within the floor system, between the floors and the lateral-load-resisting elements, and, between existing and new components should be verified.

In the next sections the most common techniques of rehabilitation of structures are presented. One should bear in mind that rehabilitation of buildings may use more than one strategy in order to avoid failures in the system.

### **2.6.1 - Global structural system intervention techniques**

Global intervention methods may represent a more cost-effective strategy than universal upgrading of the existing components, especially if the disruption of occupancy and the

demolition and replacement of partitions, architectural finishes and other non-structural components are considered (Fardis, 1998). This is particularly true for structures where no horizontal load-path is available, or when all structural members are extremely flexible. In such cases the methods described below may indeed provide an optimum solution (Pinho, 2000).

Stiffness, mass, and strength irregularities, such as soft or weak-storeys and torsional irregularities, are common causes of undesirable earthquake performance (FEMA-273, 1997). Effective corrective measures for removal or reduction of these irregularities and discontinuities include: *a*) partial demolition (this measure obviously has significant impact on the appearance and utility of the building); *b*) addition of moment frames, braced frames or shear walls within the soft/weak storey or to balance the distribution of stiffness and mass within a storey; and, *c*) creation of expansion joints (a single irregular building can be transformed into multiple regular structures, however, care must be taken to avoid the potential problems associated with pounding).

Some flexible structures behave poorly in earthquakes because critical components and elements do not have adequate ductility to resist the large lateral deformations that ground shaking induces in the structure. Global structural stiffening can be realised with the construction of new braced frames or shear walls within an existing structure. As recalled by Ersoy (1998), inadequate lateral stiffness has been found to be the major cause of damage in buildings in recent earthquakes.

Some existing buildings have inadequate strength to resist lateral forces. To provide supplemental strength to such a building's lateral-force resisting system new shear walls or braced frames can be constructed. A major drawback of these retrofitting measures is that usually they may be significantly stiffer than the structure to which they are added, requiring to be designed to provide nearly all of the structure's lateral resistance.

In the 1990's the development and use of seismic energy dissipation mechanisms, such as link devices, dampers and base isolation, have gained widespread interest, and are increasingly being used to protect buildings from earthquakes (Elsesser, 2002). These seismic retrofitting techniques are viable design strategies for seismic rehabilitation of buildings. Other special seismic protective systems, including active control, hybrid



combinations of active and passive energy devices, tuned mass and liquid dampers, may also provide practical solutions in the near future. These retrofitting systems enhance the structural performance during an earthquake by modifying the building's response characteristics.

Each of the most common global structural system improvement techniques are exposed in detail in the next section.

#### *2.6.1.1 - Addition of RC structural shear walls*

As recalled by Ersoy (1998), Fardis (1998) and Pinho (2000), one of the most common methods of improving the behaviour of buildings where unsatisfactory seismic behaviour is inherent in the system is to provide adequate number of structural RC shear walls. The new structural walls protect the existing elements by controlling the global lateral drift. Such shear walls not only increase the lateral stiffness significantly, but also relieve the existing frames from the lateral loads. Adding shear walls to complete the load path can also correct discontinuities. The new elements provide most of the resistance to lateral loads. If the walls have adequate stiffness and strength to take the total lateral load, the weaknesses in frames (such as soft-storey, short column, etc.) usually do not lead to undesirable behaviour. However, it should also be pointed out that adding infill shear walls will decrease the natural period, which can increase the demand considerably.

If interventions at the perimeter of the building are feasible, addition of shear walls or bracing (see Sections 2.6.1.1 and 2.6.1.2) at the façades is favoured over general upgrading of (vertical) elements throughout the building (especially if occupancy needs to be continued during retrofitting) (Fardis, 1998).

As referred by Pinho (2000), several studies (e.g. Higashi *et al.*, 1984; Aoyama *et al.*, 1984; Frosh *et al.*, 1996) on variations of this popular retrofitting technique have been carried out. Full continuity between different levels increases strength, whilst proper anchorage or re-bars to delimiting beams and closely spaced mesh provides high deformation abilities. By contrast, poor detailing and lack of proper load-paths between old and new members may lead to global ductility reduction or brittle failure of infill panels.

In rehabilitating existing non-ductile framed structures, this technique usually involves partial or total infilling of one of the bays of the existing framed buildings. If the wall takes up the full width of the bay, it incorporates the beams and the two columns (that acting as its boundary elements). Then, only the web of the new wall needs to be added, normally by shotcreting against a light formwork or a partition wall. Sometimes, the use of precast panels as infills becomes very convenient (recent examples applied after the 1995 Kobe earthquake are given by Sugano, 2000), reducing construction period and cost of the intervention, provided that adequate connection is made between the precast panels and the frame members (Pinho, 2000; Ersoy, 1998; Fardis, 1998).

This retrofitting technique becomes very feasible when: *a*) framed structure does not have adequate lateral stiffness; *b*) structural system has important weaknesses, such as soft-storey, short column, etc.; and, *c*) the number of frame members to be rehabilitated is beyond feasible limits (Ersoy, 1998). To ensure proper wall behaviour, the infill should be connected to the surrounding frame, so as to fasten the new web to the frame members. The most effective way of connecting the infill to the frame members is placing dowel bars into the drilled holes in the members. Bonding of dowel bars is usually accomplished by using epoxy-based adhesives. However, as stated by Ersoy (1998), such technique can be questioned when fire resistance is considered. Also, anchorage of dowels in beams and columns with poor concrete may cause problems. Alternatively, the new wall may be thick enough to encapsulate the existing beams and columns. In this case, holes should be drilled through the slab so that the vertical bars pass from one storey to the next.

A major drawback of this retrofitting method relies on the fact that sometimes it may require strengthening of the foundation system so as to resist the increased overturning moment and the larger weight structure. This type of work is usually costly, quite disruptive, and a technically challenging operation, rendering the application of this retrofitting technique unsuitable sometimes, particularly for buildings without an adequate foundation system. Another disadvantage is the disruptive characteristic of the procedure. Indeed, the use of shotcrete may require building evacuation.

Since the lateral stiffness of infilled frames is high as compared to bare frames, significant floor torsion can be induced if such retrofitting infill shear walls are placed without considering this effect (Ersoy, 1998). Application of this technique as a repairing measure

to a single previously damaged storey can cause hazardous vertical strength irregularities. Nakano (1995), for example, reports how a three-storey building repaired with shear walls at the first storey only, after the 1968 Tokachi-oki earthquake, suffered heavy damage at the second storey during a subsequent event in 1994 (Pinho, 2000).

Infilled frames were commonly used in Turkey for rehabilitation of buildings located in seismic zones. From the 1970's, this retrofitting technique was used to strengthen buildings showing several weaknesses, such as, inadequate lateral stiffness, inadequate confinement, or inadequate anchorage length of reinforcing bars. Infilled frames were preferentially used to repair and strengthen the damaged framed buildings after 1992 Erzincan earthquake (Ersoy, 1998).

#### *2.6.1.2 - Addition of steel bracing or post-tensioned cable systems*

Global structural behaviour improvement can also be made by placing bracing consisting of steel structural shapes, or it can be accomplished by post-tensioned cables. Ersoy (1998) defends that bracing is not as effective as the infill in upgrading the lateral stiffness. Moreover, since bracing is traditionally made from steel, fire resistance has to be considered. As stated by Fardis (1998), the global stiffening effect of the bracing is rather limited and it is likely that significant lateral displacements may need to develop before full mobilisation of the bracing.

However, Fardis (1998) and Pinho (2000) also advocate that this global strengthening method can be very effective. Concentric or eccentric steel bracing schemes may be used in selected bays of an RC frame to provide a significant increase in horizontal capacity of the structure. Diagonal bracing is normally completed with horizontal and vertical steel members continuously fastened to the existing beams and columns around the braced bays. These additional members transfer the lateral loads from the floors to the diagonal bracing and are proportioned to play the role of the vertical chords and the horizontal ties of the vertical cantilever truss. The shear connectors between the horizontal or vertical steel members and the existing beams or columns should be proportioned conservatively as force-controlled components.

Normally, no intervention to foundations is required and its installation is not as disruptive as that of shear walls. Nevertheless, connection between existing concrete elements and bracing system may be laborious and expensive. Bracing is usually placed for convenience at the façades, causing the installation minimal disruption. Also, architectural constraints are likely to condition the positioning of the bracers due to the effects that these have on existing openings.

Several researchers have reported successful results on the use of steel bracing to upgrading RC structures (Jara *et al.*, 2001; Higashi *et al.*, 1984). Register also the series of RC buildings retrofitted with steel bracing have been reported to withstand the 1985 Michoacán earthquake with practically no structural damage (Calderón, 1980; Foutch *et al.*, 1988; Jara *et al.*, 2000).

Passive energy dissipation devices or shear-links may also be used in conjunction with the bracing to efficiently increase dynamic damping (Martinez-Romero, 1993; Okada *et al.*, 1992). However, if the bracing system increases the stiffness of the frame considerably, the efficiency of the damping mechanism is compromised. This follows because the damping mechanisms, normally, require large levels of displacement to be cost-effective (Fardis, 1998). A thorough review of passive devices installed within steel bracing systems can be found in the work of Martinez-Rueda (1997), and referred by Pinho (2000).

Post-tensioned steel bracing has also been successfully used to upgrade the response of low-rise school buildings in Mexico (Miranda and Bertero, 1990). This system involves the addition of post-tensioned rods that will yield for small levels of deformation, allowing energy dissipation at an early stage of a large event. However, the initial brace pre-stressing induces additional forces in the structure modifying the internal force distribution. This needs to be considered, especially for serviceability limit states (Pinho, 2000).

#### 2.6.1.3 - Base seismic isolation

One promising retrofitting method is the use of base isolation techniques including energy absorbing devices in the system (Kelly *et al.*, 1979). The conceptual idea is to control the input to the structure' foundation, suppressing the interaction between soil and the superstructure. Thus, vibration of the superstructure and consequent damage is reduced.

This technique consists on providing the structure with a double foundation system, separated by an isolation layer that grants discontinuity between the superstructure and the foundation of the entire structure. In this way, the structure is decoupled from the input motion and the majority of the seismic energy is absorbed by the isolation device, which may consist on a thin sliding surface, rubber bearings or flexible members (Pinho, 2000; Fardis, 1998; EQE, 1995). These bearings are designed to limit forces transferred from the foundation to the building. The three basic properties of an isolation system are (FEMA-274, 1997): *a*) horizontal flexibility to increase structural period and reduce spectral demands; *b*) energy dissipation (damping) to reduce displacements; and, *c*) sufficient stiffness at small displacements to provide adequate rigidity for service-level environmental loadings.

Typical isolation reduces forces transmitted to the superstructure by lengthening the period of the building and adding some amount of damping. Under favourable conditions, the isolation system reduces drift in the superstructure by a factor of at least two (sometimes by as much as a factor of five) from that which would occur if the building was not isolated. Accelerations are also reduced in the structure, although the amount of reduction depends on the force-deflection characteristics of the isolators and may not be as significant as the reduction of drift. Reduction of drift in the superstructure protects structural components and elements, as well as non-structural components sensitive to drift-induced damage. Reduction of acceleration protects non-structural components that are sensitive to acceleration-induced damage (FEMA-274, 1997).

The philosophy or purpose of seismic rehabilitation using isolation is directly dependent on the owner's motivation to upgrade the building, and expectations of upgraded building's performance during and following an earthquake (FEMA-274, 1997). As referred by Pinho (2000) and Fardis (1998), seismic isolation is gaining wide acceptance as an attractive and alternative means of upgrading structures with minimal disturbance to architectural significant features, such as in historic monuments. Its application to upgrading of RC structures is also feasible, particularly in the case of critical buildings that need to remain open and operational or to be available for immediate occupancy after seismic events. Take for example, hospitals, museums and other buildings in which important contents must be protected against damage due to earthquake shaking.

Seismic isolation is very effective for retrofitting stiff buildings with low profiles and large mass. It can offer safety to the buildings and occupants (under very strong earthquakes), but also protection to buildings' contents (under any earthquake). Such methods are extremely efficient in reducing response acceleration and inter-storey drift thus minimising structural and non-structural damage. Examples of successful applications can be found in Allen and Bailey's (1988) and Mokha *et al.*'s (1996) work. However, it is also an extremely expensive solution and its application to general purpose buildings is non-cost effective (Pinho, 2000). As stated in FEMA-274 (1997), owners that are only interested in collapse prevention should probably consider other more economical design strategies than seismic isolation.

Seismic isolation and energy dissipation systems will not be appropriate design strategies for most buildings, particularly for buildings that have only limited rehabilitation objectives. In general, these systems will be most applicable to the rehabilitation of buildings whose owners desire superior earthquake performance and can afford the special costs associated to the design, fabrication, and installation of seismic isolators and/or energy dissipation devices. These costs are typically offset by the reduced need for stiffening and strengthening measures that would otherwise be required to meet rehabilitation objectives (FEMA-274, 1997).

Furthermore, seismic isolation and energy dissipation systems are relatively new and sophisticated concepts that require more extensive design and detailed analysis than do most conventional rehabilitation schemes. Similarly, design (peer) review is required for all rehabilitation schemes that use either seismic isolation or energy dissipation systems (FEMA-274, 1997).

#### *2.6.1.4 - Passive energy dissipation systems*

Passive energy dissipation is an emerging technology that enhances the performance of the building by adding damping (and in some cases stiffness) to the building. Fardis (1998) refers that energy dissipation systems can be used combined with base-isolation, or can be inserted in the braces of a steel bracing system added to the existing structure for strengthening. The primary use of energy dissipation devices is to reduce earthquake

displacement of the structure, provided the structure is responding elastically. Special devices dissipate energy in a controlled manner, generally through frictional, hysteretic, or viscoelastic processes. Under favourable conditions, passive energy dissipation devices reduce drift of the structure by a factor of two or three if no stiffness is added, and by larger factors if the devices also add stiffness to the structure. Energy dissipation devices will also reduce force in the structure, but would not be expected to reduce force in structures that are responding beyond yield (FEMA-274, 1997).

This solution is effective in structures that are relatively flexible and that have some inelastic deformation capacity because it requires the development of significant lateral displacements. The dissipative systems are commonly installed in structures as components of braced frames. In some cases, the forces induced in the structure can actually be increased. Sugano (2000) refers to examples of buildings in Japan retrofitted with supplemental damping systems. The energy dissipating devices used were steel elasto-plastic dampers and were installed on the top of braces or wall panels.

#### *2.6.1.5 - Mass reduction*

Stiffness and mass control the amount of force and deformation induced in a structure by a ground motion (FEMA-273, 1997). Therefore, mass reduction of the building can be considered as an efficient retrofitting technique, namely through: *a)* demolition of upper storeys and penthouses; *b)* replacement of heavy cladding interior partitions and finishes; and, *c)* removal of heavy storage and equipment loads.

#### *2.6.1.6 - Other techniques*

Methods and techniques to reduce the seismic inertia forces on building caused by earthquake actions are being developed (response control methods). Other special seismic protective systems, including active control, hybrid combinations of active and passive energy dissipation devices, tuned mass and liquid dampers, may also provide practical solutions for the seismic retrofitting of existing structures in the near future. These systems enhance the performance during an earthquake by modifying the buildings' response characteristics (FEMA-274, 1997). As argued by Ersoy (1998), these techniques were used

in the past just in new constructions in seismic areas, but they are emerging for retrofitting applications.

### **2.6.2 - Member intervention techniques for RC elements**

Some existing buildings have substantial strength and stiffness. However, some of their components do not have adequate strength, stiffness, or deformation capacity to satisfy the rehabilitation objectives (FEMA-273, 1997). Members without adequate strength, stiffness and/or ductility can be rehabilitated using various techniques. These member intervention techniques play an important role in the repair and strengthening of structures where only a reduced number of members present structural deficiencies or have suffered damage due to previous earthquakes (Pinho, 2000). Local modifications of those components that are inadequate can be performed while retaining the basic configuration of the building's lateral force resisting system. This member intervention strategy tends to be the most economical approach to rehabilitation when only a few of the building's components are inadequate. Some of the most popular member intervention techniques are reviewed next.

#### *2.6.2.1 - Epoxy resin injection*

This is the most widely used repair method for minor to medium size cracks in RC structures. As referred by Iglesias and Aguilar (1996), this technique was largely applied to repair the damaged buildings after the 1985 Mexico earthquake. This technique is quite effective provided that the travel path inside the crack is clear. The strength is usually reinstated, especially for under-reinforced members. Tests in low viscosity epoxies have confirmed the feasibility of this technique especially with regard to bond reinstatement (Cowell *et al.*, 1980). More recently, tests on RC beam-column joints also yielded good results with regard to strength reinstatement (Karayannis *et al.*, 1998), as referred by Pinho (2000).

However, tests carried out on RC walls by Salama (1993) and Pinho *et al.* (1999) did not confirm such efficiency. This outcome is most certainly related to the particular characteristics of RC walls where complex crack-patterns are formed due to the large width of the members, thus reducing the level of epoxy resin penetration. Hence, it is



difficult to guarantee the degree of penetration of the resin, and the level of reinstatement of stiffness remains equally ambiguous. Moreover, the displacement at which the repaired parts of the structural member start 'pickhng-up' lead is uncertain due to the impossibility of injecting cracks smaller than 0.5 mm (Pinho, 2000).

#### 2.6.2.2 - Jacketing of existing members

The most commonly used technique to improve the performance of existing RC elements (columns, walls, beams or joints) is jacketing. Jacketing is effective in correcting specific deficiencies in strength and/or deformation capacity, to improve longitudinal reinforcement development or lap-splices, identified during the detailed evaluation (Fardis, 1998). It is normally not a cost-effective strategy for global strengthening and stiffening, because it may entail intervention to practically all vertical elements of the structure increasing not only direct costs but also occupancy disruption. Jacketing can be made either using steel structural shapes or fibre wrap overlays, or by enlarging the cross-section of the existing member with a new RC shell. The new materials shall be designed and constructed to act compositely with the existing concrete.

When the objective is the flexural capacity improvement of columns and beams, the jacket should extend into the beam-column joint region and hoops should be placed there through horizontal holes drilled in the beams so that the enhanced strength can be transferred to adjacent framing components. However, past experience has shown that interior joints with all four faces confined by beams are much less vulnerable than exterior ones, even when unreinforced. So the laborious task of placing hoops in such joints is not absolutely necessary (Fardis, 1998). Appropriate measures should be implemented to provide shear transfer between new and existing materials. If the jacket's only aim is to improve shear strength, confinement, ductility and lap-splices (but not the flexural strength), it does not need to be continuous through the slab. The longitudinal reinforcement in concrete jackets, and steel in steel jackets should be discontinued at a short distance from the connection with adjacent components (FEMA-274, 1997).

To increase the shear strength, steel, concrete, or other types of jackets can be added to the deficient sections. When proper connections between old and new materials are achieved,

it is usually appropriate to calculate the nominal shear strength as if the section were composite (FEMA-274, 1997).

The interventions using thin jackets employ steel or composite (fibre reinforced polymers) jackets to the column. Hence, no significant change to the original flexural capacity of the member is introduced. Similarly, using thin steel plates or high-strength composite materials also prevents significant modifications of the columns stiffness. The later will induce changes in pre-yielding stiffness of up to a maximum of 5%, as opposed to a 75% change if conventional concrete jacketing is used (Priestley *et al.*, 1996; Pinho, 2000; Ersoy, 1998).

When the member is heavily damaged or considered to be of insufficient strength, a RC jacket may be used to enhance stiffness, strength and ductility. This is one of the most commonly applied methods of repair and strengthening of RC members and, apart from the welding of the links between the new and existing reinforcement bars, it does not require specialist knowledge. Concrete jackets can accommodate longitudinal and transverse reinforcement to increase the flexural and shear strength, enhance the deformation capacity (through confinement and anti-buckling action) and improve the strength of deficient lap-splices. Being one of the objectives of the concrete jacket to increase flexural strength, the surface of the existing concrete has to be roughened prior to concrete placement, and the shear connection using dowels to improve shear transfer between the old and the new concrete should be assured. Good results have been observed by Rodriguez and Park (1991) in terms of upgrading all three design parameters of the member (Pinho, 2000; Fardis, 1998).

*a) Steel jacketing:* Steel jacket can be used to improve the confinement. Normally, a non-shrink grout is used to effectively bond the materials, filling the gap between the steel jacket and the old concrete column. The effectiveness of thin rectangular steel jackets for seismic retrofit (to enhance shear and flexural performance) of large rectangular and circular non-ductile RC columns was investigated by Aboutaha *et al.* (1996), Priestley *et al.* (1994), Chai *et al.* (1991), for example. The major feature of the work conducted by Aboutaha *et al.* (1996) is the use of anchor bolts to provide extra confinement to lap-splices in the centre of the column. This is an essential issue since in wide columns the steel collars can only provide confinement to the lap-splices close to the corners of the

member. Aboutaha *et al.* (1996) results indicate significant increase in the ductility and strength of the RC members, whilst minimum change in their stiffness was observed. Moreover, the tests revealed that the use of long jackets increases ductility supply by providing better lap-splice confinement. Aviles *et al.*'s (1996) experiments on nineteen column specimens have shown that retrofitting with thick steel plate wrapping combined with anchor bolts increased deformation capacity of the specimens, whilst no change in stiffness or strength was evident (Pinho, 2000).

It should be pointed out that one of the weaknesses of the rehabilitation carried out by bonding steel strips to the members is its poor fire resistance. Also the long-term performance of the bonding material (epoxy) is not well known (Ersoy, 1998).

*b) Fibre Reinforced Polymers (FRP) jacketing:* Strengthening of RC structures using FRP's has found numerous field applications around the world (Triantafillou, 1998; Meier, 1992). These applications include wrapping of columns in seismic zones and flexural strengthening of beams and slabs.

Saadatmanesh *et al.* (1997) carried out experimental work on the application of high-strength FRP composite straps to retrofit rectangular columns. Both oval and rectangular shapes were used, and active confinement was applied in the specimens by means of pressure injection of epoxy resin. The increase in the level of ductility of the upgraded models was evidenced in their work. Saadatmanesh *et al.* (1994) summarise the benefits of the strengthening concrete columns with FRP's, namely, the capability to increase the ductility (depending on the degree of confinement, significant increases in ductility can be achieved) and the strength. The lateral pressure exerted by the straps increases the compressive strength of the concrete in both the core and shell regions, resulting in higher load-carrying capacity. The lateral confinement provided by the straps also provides additional support against buckling of the longitudinal bars. The flexibility of the straps allows wrapping around circular as well as rectangular columns. The low density of composites (typically one-fifth that of steel) simplifies the construction procedure and reduces cost. The proposed method will cause no disturbance to the integrity of the existing structure, i.e. no anchor bolts, dowels, etc., will be required. The straps are very thin, therefore, they will not alter the appearance of the structure. Because of their resistance to electrochemical deterioration, FRP's do not corrode and they are not affected

by salt spray and other aggressive environmental factors. Ultraviolet light, however, can adversely affect some FRP's. Providing a protective coating for the straps during or after the manufacturing process can eliminate this problem.

Seible *et al.* (1997; 1995) also performed a series of tests on large-scale bridge columns, for the three modes of failure: shear, plastic-hinge confinement and lap-splice de-bonding. Circular and rectangular columns geometries and different levels of column reinforcement ratios were investigated. From the large-scale tests, they conclude that column retrofit jacket with advanced composite materials can be just as effective structurally as conventional steel jacketing, in improving the seismic response characteristics of substandard reinforced concrete columns.

The basic concept of the most commonly used technique of jacketing is simple, but the actual behaviour involves many uncertainties, as recalled by Ersoy (1998). First of all, there is the uncertainty regarding load sharing between the original existing member and the jacket. As also pointed out by Pinho (2000), if jacking-up of the slab is not undertaken prior to the construction of the jacket, load sharing does not take place until after some measurable seismic displacement has occurred. Experimental research at the 1990's has improved our knowledge on the behaviour of jacketed members. However, further research is needed to clarify the behaviour of jacketed columns, especially for jacketing made under load (Ersoy, 1998).

#### 2.6.2.3 - Shotcrete

Not only is this method used in its own right, but is also often applied as part of repair by a RC jacket. It comprises the spraying of a high cement content and fine aggregate concrete mix onto the surface of the affected member. Warner (1996) carried out a thorough review of the features of this method, as referred by Pinho (2000).

The strength of the applied layer of concrete is usually very high, and the technique may be applied in situations where the use of formwork is not possible (such as for a beam-column connection). It is also often applied to masonry structures. However, there are several drawbacks. For example, considerable waste in materials is inevitable due to rebound, and

---

wire mesh is required to avoid shrinkage cracks of the high cement concrete mix (Pinho, 2000).

#### 2.6.2.4 - Other techniques

Apart from the techniques previously presented, the following member retrofitting solutions can be also envisaged (FEMA-274, 1997):

- Post-tensioning existing beams, columns, or joints using external post-tensioned reinforcement. Lateral deformations of slender walls may result in significant tension force requirements for boundary columns, which may lead to unacceptable behaviour of reinforcement lap-splices. Post-tensioning can be considered as an option for pre-compressing columns to avoid excessive tension forces. When this approach is adopted, the design needs also to consider the possible negative effects on column behaviour when the lateral forces reverse and the column becomes loaded in compression. Anchorages shall be located away from regions where inelastic action is anticipated, and shall be designed considering possible force variations due to earthquake loading.
- Modification of the element by selective material removal from the existing element. This is a primary method of rehabilitating existing infilled frames. Either the infill can be completely removed from the frame, or gaps can be provided between the frame and the infill. In general, removal of existing infills should not result in vertical or plan irregularities in the structural system.
- Improvement of deficient existing reinforcement details. This approach involves removal of cover concrete, modification of existing reinforcement details, and casting of new cover concrete. This approach may also be useful for improving tension lap strength of existing columns lap-splices. When this option is selected, chipping of concrete cover may be required. Care should be exercised to ensure that core concrete, and bond with existing transverse reinforcement, are not damaged excessively. New cover concrete shall be designed and constructed to achieve fully composite action with the existing materials.

# CHAPTER 3

## DESCRIPTION OF THE EXPERIMENTAL TESTS

*'If you want a description of scientific method in three syllables, I propose: guess and test'* (George Pólya, Mathematical Discovery, Vol. II)

### 3.1 - INTRODUCTION

As previously referred in Chapter 1, the vast majority of buildings in earthquake prone areas in Europe constructed before the 1980's are seismic deficient in light of our current knowledge. In fact, until the 1960's no specific seismic design provisions were included in the codes and, from that period on, only seismic equivalent lateral loading has been considered in their design. Provisions for design and detailing of members and structures resembling those of modern codes only appeared in European national codes in the 1980's (e.g. Portuguese design code – RSA, 1983). Consequently, most of the existing buildings constitute a major source of risk to human life and property loss. Therefore, their retrofitting or replacement should be made in order to reduce vulnerability and consequently risk to current accepted levels.

The research programme of research network ICONS (presented in Chapter 1), topic 2 – Assessment, Strengthening and Repair, addresses the issues of seismic assessment and retrofitting of existing structures covering several aspects of the problem (see Section 1.1 for details). In particular, the assessment of reinforced concrete buildings with and without infill panels and several strengthening solutions and techniques are investigated through numerical and experimental work. The experimental research work includes several studies carried out at the ELSA reaction-wall laboratory, at the JRC. In order to evaluate the

efficiency of different retrofitting solutions and to investigate bare and infilled frame test conditions, two representative identical full-scale four-storey, three-bay reinforced concrete frames (one as a bare frame and one as a frame with brick infilled walls), were designed, constructed and placed parallel to each other and were tested in sequence using pseudo-dynamic testing procedures.

For the experimental model, one degree-of-freedom (DOF), corresponding to a longitudinal horizontal displacement, was considered per floor. The experimental seismic response was obtained by means of application of the continuous PsD test method.

The main objectives of the test campaign were: *a)* calibration of numerical models capable of predicting the non-linear behaviour of existing RC structures; *b)* experimental evaluation of seismic vulnerability of existing RC structures; *c)* experimental verification of the infill walls influence on the global structural response; and *d)* experimental evaluation of retrofitting solutions.

The test program was divided into four phases. In the first phase, the frames were subjected separately to pseudo-dynamic tests to assess the earthquake performance of both, the bare concrete frame and the frame structure with infilled walls.

In the second phase of the research program, the tests were repeated, now to evaluate retrofitting techniques. The non-infilled frame had been retrofitted, with selective retrofitting techniques, which balance strength, stiffness and ductility according to the requirements for increased seismic performance. For the infilled frame, the infills were strengthened with a grouted mesh reinforcement ('shotcrete').



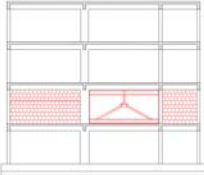

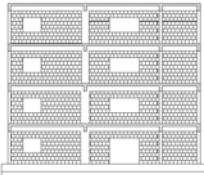
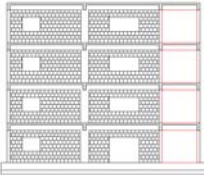
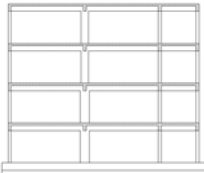
The third study dealt with the design and assessment of a retrofitting solution involving the introduction of a ductile eccentrically steel braced frame (K-bracing with a vertical shear-link). This retrofitting was applied just to one storey and a cyclic test was performed to evaluate the efficiency of this retrofitting technique.

The local damages inflicted to the structures, after the PsD tests, inhibited the final capacity tests (fourth phase), which were required to assess their ultimate global capacity. Therefore, in order to assess the ultimate capacity of the bare frame and of the selective repaired frame, after their repair and strengthening using composite carbon fibre materials,

final capacity cyclic tests were performed. The repair and strengthening operations allowed the frames to recover their vertical load carrying capacity, as well as most of their seismic resistance.

The complete set of tests performed on the two RC frames is given in Table 3.1.

Table 3.1 - Testing programme

		Test series		Label
Frame B	PsD	Bare frame		BF
		Strengthened frame (selective retrofit techniques)		SR
	Cyclic	K-bracing with steel shear-link dissipator at the 2 <sup>nd</sup> storey		KB-cyclic
		Final capacity on strengthened frame		SR-cyclic
Frame A	PsD	Infilled frame		IN
		Shotcrete infilled frame (infill strengthened frame)		SC
	Cyclic	Final capacity on bare frame (recovered from the infilled frame, removing the infill walls)		BF-cyclic



The author, involved in the team of the ICONS research programme, followed the experimental tests on the four storey full-scale frames. In this study full-scale models are used, representative of existing RC buildings, and there is a full knowledge of the materials' properties and structural topology. Normally, these details are not fully known in current assessment engineering practice. Instead, when the engineer has to evaluate the vulnerability of an existing structure he faces a major barrier that is the inexistence of the original drawings. Moreover, in many cases, those drawings exist but changes to the original design during the construction phase or during the subsequent interventions are not inventoried. Therefore, in the majority of the cases, the engineer has to investigate the structure carefully so as to verify its topology and eventual degradation degree, as well as to take material samples (steel and concrete) to estimate their mechanical properties.

To achieve the experimental purposes, two full-scale four-storey reinforced concrete frames were constructed and tested for several earthquake intensities. The efficiency of various repair and retrofitting techniques were also experimentally evaluated. The tests carried out within the research programme are presented in two chapters, namely 3 and 4. Chapter 3 provides the background to Chapter 4 by detailing the experimental research work carried out at the ELSA laboratory. Chapter 4 presents and discusses the experimental results from all the pseudo-dynamic and cyclic tests performed. Appendices A and B gather all the instrumentation details, test results, damage observed during the tests and a photographic documentation.

This chapter is organised as follows. First it provides details on the structure, on the construction of the RC frame, materials' mechanical properties and loads. Next, it presents the properties of the masonry infill and of the masonry strengthening. Then, it reviews the retrofitting solutions tested, namely the selective retrofitting technique, the K-bracing with shear-link system and the retrofitting using composite carbon fibre materials. All the aspects related to the test campaign and test set-up are discussed. Section 3.8 focuses on the non-destructive tests aimed at the dynamic characterisation of the frames, and discuss the related aspects. Finally, this chapter closes with final remarks.

## 3.2 - CHARACTERISATION OF THE RC FRAMES

### 3.2.1 - Reinforced concrete frame structure: geometry and section detailing

The two reinforced concrete frames tested at ELSA laboratory can be considered representative of the design and construction common practice until the late 1970's in southern European countries such as Italy, Portugal and Greece. They were designed to withstand vertical loads only. Previous numerical analyses of the designed frames found that they have a resistance to horizontal loads, in terms of ultimate limit state, of approximately 8% of their weight. Similar analysis in terms of allowable stresses, as was common practice at the time, would lead to a lateral resistance of 5% of the frame weight (Carvalho *et al.*, 1999). The reinforcement details were specified in accordance to the normative available and to the construction practice at that time. Thus, no specific seismic detailing provisions were considered, preferential inelastic dissipation mechanisms were not assumed and no specific ductility or strength provisions were provided.

Figure 3.1 shows the general layout of the structure. It is a reinforced concrete four-storey frame with three bays: two of 5.0 m span and one of 2.5 m span. The inter-storey height is 2.7 m and a 0.15 m thick slab of 2.0 m on each side is cast together with the beams. Equal beams (geometry and reinforcement) were considered on all floors. All but the wider interior column (column 2) have equal geometric characteristics along the height of the structure. It should be noted that only column 2 is working in its stronger axis. Therefore, this column plays a dominant role in the structural response of the frame and is hereafter referred as 'strong-column'. The other columns (1, 3 and 4) are referred as 'slender-columns'. The strong-column is characterized by a rectangular cross-section with dimensions of 0.60 m × 0.25 m on the first and second storeys and 0.50 m × 0.25 m on the third and fourth storeys.

Geometric characteristics of the beams and reinforcement details are shown in Figure 3.2. It should be noted that smooth round bars, which were commonly used some years ago, constitute the longitudinal reinforcing steel. All beams in the direction of loading are 250 mm wide and 500 mm deep, while transverse beams are 200 mm wide and 500 mm deep. Figure 3.3 shows the columns reinforcement details and their geometric dimensions.

The column reinforcement splicing, joints and stirrup detailing should be noted in particular, as they are representative of the lack of confinement common in non-ductile reinforced concrete structures constructed until the late 1970's.

The longitudinal reinforcement of all (four) columns has a lap-splice (70 cm) at the base of the 1<sup>st</sup> storey and another at the base of the 3<sup>rd</sup> storey. Therefore, at the base of the 1<sup>st</sup> storey's column, duplication of the reinforcement occurs. A superposition of the nominal reinforcement exists also at the base of the 3<sup>rd</sup> storey.

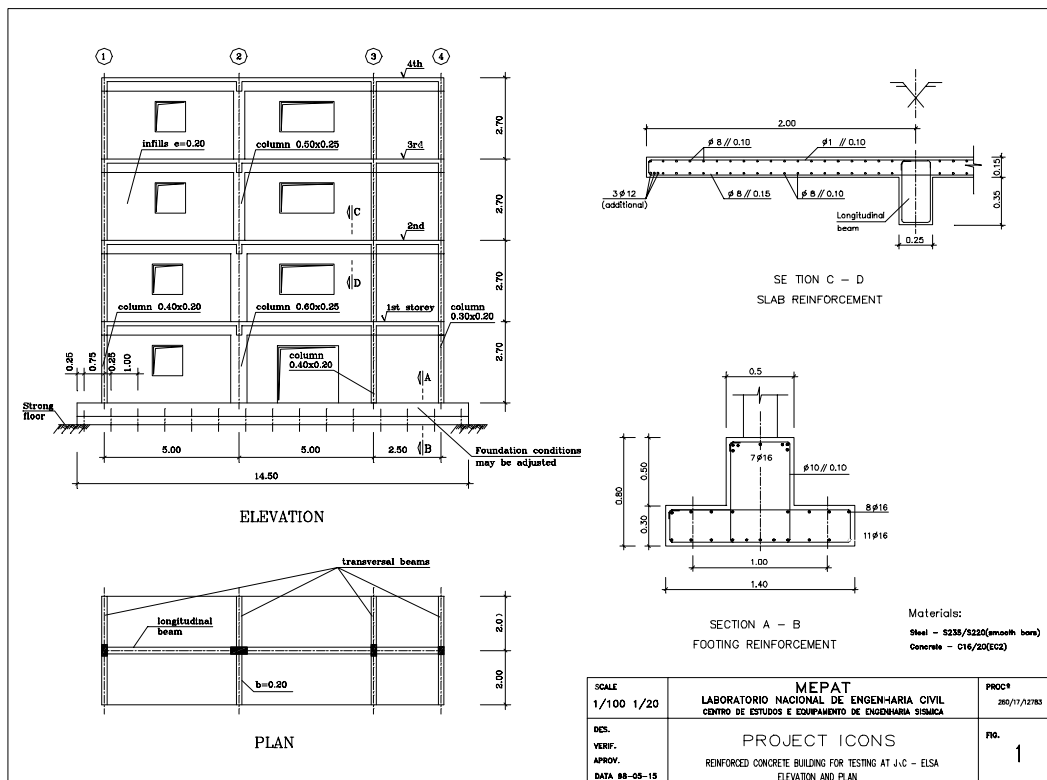


Figure 3.1 - Plan and elevation views of concrete frame plus masonry infill building

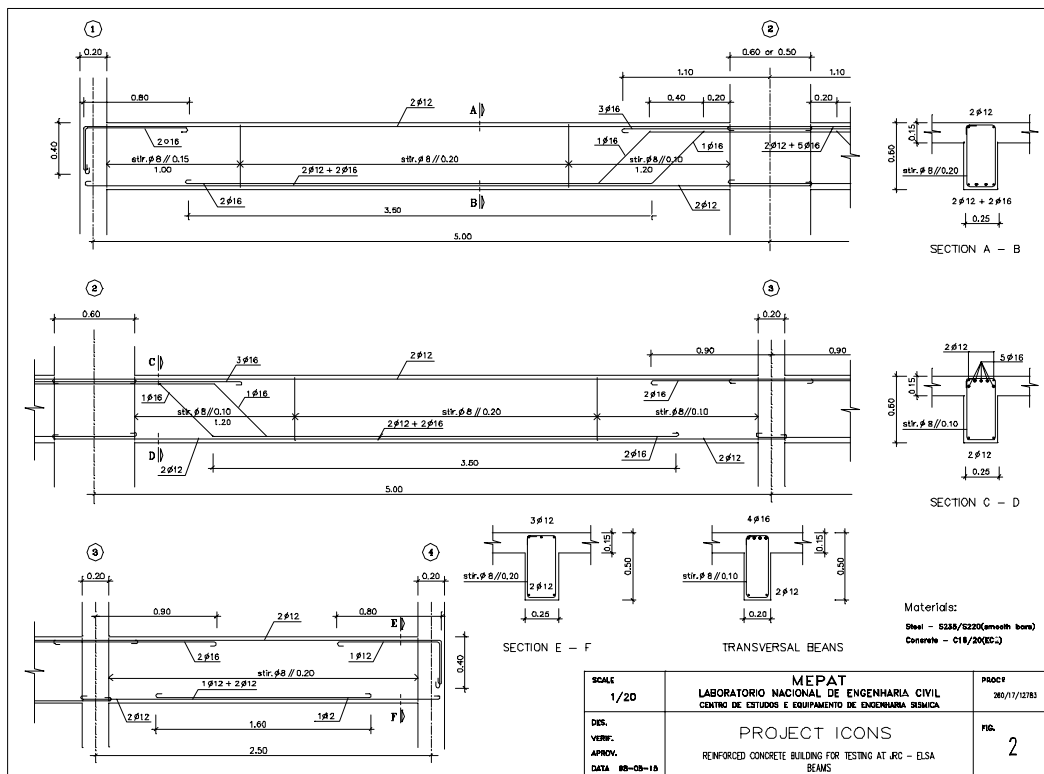


Figure 3.2 - Beam reinforcement details

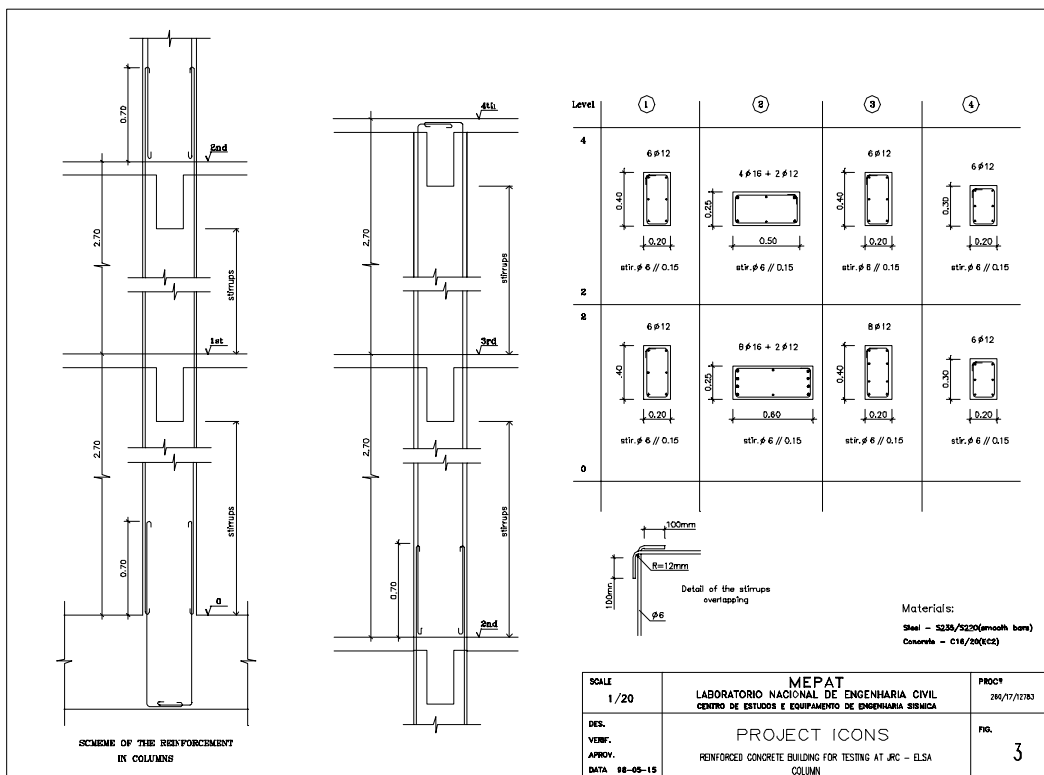


Figure 3.3 - Column reinforcement details

### 3.2.2 - Modern codes requirements for earthquake resisting structures

As already stated, the frames investigated here do not meet the modern code seismic design requirements. Similarly, a number of seismic design deficiencies and problems were identified, such as: inadequate transversal reinforcement, maximum distance between longitudinal bars, inexistence of transversal reinforcement in the joints, inadequate bends of the stirrups, and no specific mechanism for energy dissipation (see also the preliminary analytical assessment of the frame capacity made by Griffith, 1999-*a*).

Concerning the issue of transversal reinforcement, it will be compared the minimum reinforcement requirements of modern codes with the shear reinforcement provided to the structure designed essentially for the vertical loads. For instance, Eurocode 8 (EC8, 1994) states that: within the critical regions, hoops and cross-ties of not less than 6 *mm* in diameter shall be provided at a spacing such that a minimum ductility is ensured and local buckling of longitudinal bars is prevented. Further the hoop pattern is such that the cross-section of the column benefits from the triaxial stress conditions produced thereby. The minimal conditions to be satisfied in terms of hoops spacing, *s*, proposed in EC8, for buildings designed for ductility class (DC) 'L' (low) and DC 'E' (enhanced), should satisfy the following conditions

$$s = \min \left\{ \begin{array}{l} b_0 / 2 \\ 200mm \\ 9 \cdot d_{bL} \end{array} \right\} \quad s = \min \left\{ \begin{array}{l} b_0 / 3 \\ 150mm \\ 7 \cdot d_{bL} \end{array} \right\} \quad (3.1, 3.2)$$

respectively for DC 'L' and DC 'E'; where:  $b_0$  stands for minimum dimension of the concrete core; and,  $d_{bL}$  is the minimum diameter of longitudinal bars.

According to the Eurocode 2 (EC2, 1991), the minimum spacing, *s*, of transversal reinforcement in the vicinity of the joints, critical zones in seismic design, should not exceed

$$s = 0.6 \cdot \min \left\{ \begin{array}{l} b_{\min} \\ 400mm \\ 20 \cdot d_{bL} \end{array} \right\} \quad (3.3)$$

where:  $b_{\min}$  stands for the minimum dimension of the column cross-section.

Applying the stirrups spacing requirements to the frame, the values shown in Table 3.2 for the strong-column (column 2 in Figure 3.3) and for the slender-columns (columns 1, 3 and 4 in Figure 3.3) were obtained. These results should be compared with the 150 mm stirrup spacing provided.

Table 3.2 - EC8 and EC2 requirements in terms of transversal reinforcement spacing (in mm)

Columns	EC8		EC2	Used in the tested frame
	DC 'L'	DC 'E'		
Strong-column (all storeys)	100	67	144	150
Slender-columns (all storeys)	75	50	120	150

Therefore, it can be concluded that the transversal reinforcement does not satisfy the EC8 requirements for any of the columns. Furthermore, not even the EC2 requirements are fulfilled in terms of hoops spacing.

Table 3.3 summarises the volumetric ratio of the transversal reinforcement used for the columns. It was calculated as the ratio of the transversal reinforcement volume to the volume of the concrete core. The hoops volumetric ratio is less than 0.1% for all the columns, being 0.06% for the strong-column at the first storey.

Table 3.3 - Volumetric ratio of the columns transversal reinforcement (%)

Storeys	Column (according to the nomenclature in Figure 3.3)			
	1	2	3	4
3 <sup>rd</sup> and 4 <sup>th</sup>	0.09	0.07	0.09	0.10
1 <sup>st</sup> and 2 <sup>nd</sup>	0.09	0.06	0.09	0.10

According to EC8, the distance between consecutive longitudinal bars restrained by hoop bends or cross-ties, should not exceed 250 mm for the DC 'L' and 200 mm for the DC 'E'. In the frame tested, only the external slender-column with dimensions 0.30 m × 0.20 m satisfies the Eurocode requirements.

The frame is not provided with transversal reinforcement in the joints. It should be noted that the EC8 for the DC 'L' states that: *a)* the horizontal confinement reinforcement in the beam column joints shall not be less than that provided along the column critical regions; and, *b)* at least one intermediate (between column corner bars) vertical bar shall be provided on each side of the joint.

EC8 also states that hoops should be made as closed stirrups with  $135^\circ$  bends, and  $10d_{bw}$  long bends should be used, whereby  $d_{bw}$  represents the hoop diameter. However, stirrups with  $90^\circ$  bend were used in the frame under investigation.

The anchorage of longitudinal reinforcing bars is achieved by hooks with  $180^\circ$  bends, and no supplementary transverse reinforcement is provided in the lap-splice zone. EC2 requires that the reinforcing bars shall be anchored so that the internal forces imposed on them are transmitted to the concrete, and that longitudinal cracking or spalling of the concrete is avoided. Transverse reinforcement should also be provided, according to the rules presented in Figure 3.4. Furthermore, it is considered that bends and hooks do not contribute to compression anchorages.

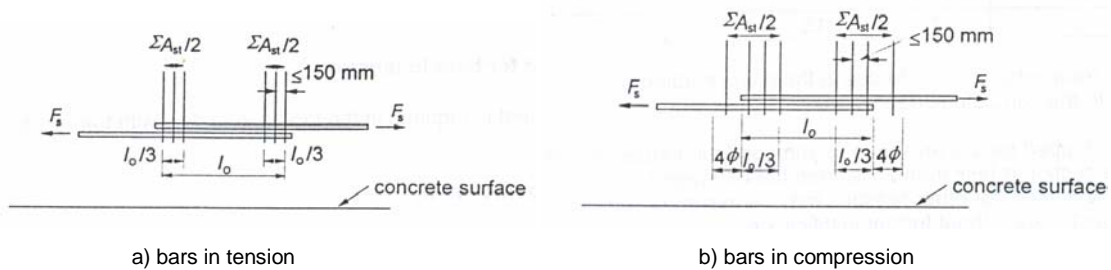


Figure 3.4 - Transverse reinforcement for lap-splice zones (EC2)

Concerning longitudinal reinforcement, EC2 refers that bars should have a diameter not smaller than  $8 \text{ mm}$ , and that the minimum amount of total longitudinal reinforcement ( $A_{s,min}$ ) should be derived from the following conditions

$$A_{s,min} = \max \left\{ \begin{array}{l} (0.10 \cdot N_{sd}) / f_{yd} \\ 0.002 \cdot A_c \end{array} \right\} \quad (3.4)$$

where:  $N_{sd}$  is the design axial compression force;  $f_{yd}$  is the design yield strength of the reinforcement; and,  $A_c$  is the total cross-sectional area of the column. As shown in

Table 3.4, the percentage of longitudinal reinforcement in relation to the total cross-section of the columns (longitudinal reinforcement volumetric ratio) complies with the minimum requirements of 0.2%, which prevails in equation (3.4).

Table 3.4 - Volumetric ratio of the columns longitudinal reinforcement (%)

Storeys	Column (according to the nomenclature in Figure 3.3)			
	1	2	3	4
3 <sup>rd</sup> and 4 <sup>th</sup>	0.85	0.82	0.85	1.13
1 <sup>st</sup> and 2 <sup>nd</sup>	0.85	1.22	1.13	1.13

Another important aspect considered in modern codes is the global dissipation mechanism for which capacity design provisions are required. The frame is not provided with any of those requirements, and then premature storey mechanisms are highly probable to develop.

As a result, the studied frame does not satisfy most of the current requirements in terms of detailing and global deformation mechanisms, therefore poor seismic performance is expected.

### 3.2.3 - Construction of the frames and loading devices

As previously mentioned, the design of the two four-storey full-scale reinforced concrete frames was carried out at LNEC (Carvalho *et al.*, 1999) within the framework of the ICONS project. The design of the RC frames was dictated by several objectives and constraints. The frames are completely disconnected, allowing for testing one on one, independently. They have a common base foundation, and are braced with lateral steel pinned bars in order to avoid out-of-plane deformation during transportation and testing, as showed in Figures A.15 and A.16. A strong foundation, consisting of a thick continuous slab and high foundation beams, was provided with the aim of fixing the structure to the laboratory strong floor (with prestressed Diwidag steel bars). This procedure would avoid sliding and overturning during testing and damage during the transportation and lift of the frames from the construction area to the testing floor.



The final design also included provisions for the attachment of the transducers and for the load application fixtures. In particular, the connections for the attachment of the actuators were located at each floor level on the slab at the mid-span central bay, through a V-loading steel frame. Figure 3.5 represents, in plan view, the attachment system employed at each floor. In order to ensure better distribution of the applied horizontal forces, additional reinforcement was provided in the slab zone where the V-loading frame were attached to the structure.

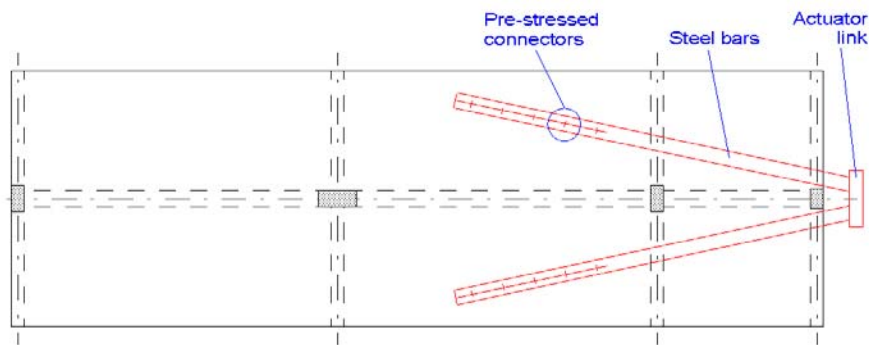


Figure 3.5 - Attachment system at floor level

The steel square-hollow bars transfer the loads to the slab by friction, which is guaranteed by the vertical pre-stressing applied to the five connectors on each bar (see Figure A.17). Figure A.14 shows the pre-stressing intervention. The hollow steel bars have a square cross-section with 200 mm side and 10 mm thickness, and were filled with concrete to avoid local deformations during pre-stressing. The actuators, or rather the actuators and corresponding load cells (in series), are directly connected to the thick steel plates, labelled in Figure 3.5 as 'actuator-link', on one side and to the reaction wall on the other.

The frames were constructed in the east-side working area, outside of the ELSA laboratory. By doing so, it was possible to carry out other tests in the laboratory simultaneously, and to better reproduce the real curing conditions. Traditional wood formwork and workmanship were adopted to reproduce the common practice construction more accurately. The concrete was ready-mixed and vibrated with a vibrating needle. The total weight of the specimens is 277 tons, which includes 75 tons for the foundation and 101 tons for each frame.

The construction was supervised in order to achieve the design specifications in terms of materials, structural geometry and reinforcement detailing. Therefore, the common uncertainties that occur in real existing structures are reduced. Indeed, aspects such as variance in material properties and reinforcement detailing relatively to the designed structure, non-documented structural modifications, difficulties to find the original drawings and materials degradation make the assessment of existing structures difficult. Hence, in this particular case, the constructed frames reproduce well the designed structure.

In Appendix A, Figures A.1 to A.10 show pictures with relevant details of the different phases of the construction of frame models, namely: foundation reinforcement and casting, slab, columns and joint reinforcement details, casting of the first floor and general views of the construction at various phases.

### **3.2.4 - Transportation of the frame models**

As stated earlier, provisions for the transportation of the frames were defined and designed at the Joint Research Centre, namely: the slab, the base foundation and the attachment location of the vertical jacks necessary for lifting the frames. The procedure used to move the structure into the laboratory in front of the ELSA reaction-wall was already used in previous test campaigns to transport other test specimens (Negro *et al.*, 1994), which is summarized herewith.

The frame specimens' foundation was raised 120 *mm* by means of 16 hydraulic jacks (see Figure A.11) acting at equal oil flux in order to avoid deformation at the base. A set of polythene plastic tubes connected to form a sort of roller 'ladder' was then placed underneath the foundation, and then pulled to its final destination, in front of the reaction wall. The plastic tube system was designed in order that the material of the tubes is stressed at a level close to its apparent elastic limit, so that the irregularities of the floor could have been compensated by plastic deformation of the tubes, without transmitting any significant deformation to the upper part of the structure. The transportation and positioning of the frames took two days, and due care was taken to assure the integrity of

the structure. Figures A.11 to A.13 illustrate the transportation into the ELSA laboratory, namely: vertical jacks and general views.

### 3.2.5 - Materials properties

The materials considered at the design phase (Carvalho *et al.*, 2000-*a*; 1999) were a normal weight low strength concrete, class C16/20 (EC2), and round smooth reinforcing steel of class Fe B22k (Italian standards). The aim was to be as similar as possible to the properties of the materials used in construction practice until the late 1970's in southern European countries. Tests on samples of the materials used in the construction (steel reinforcement and concrete) of the structure have been carried out and the results obtained are presented next.

The nominal properties of the concrete adopted in the design are given in Table 3.5. Compressive strength tests on concrete reference specimens, cubes with 150 mm side, have been performed (four cubes for each casting phase). The average values obtained from these tests are given in Table 3.6. It is noteworthy that these values were confirmed by extensive rebound tests (with the sclerometer) on the structure.

Table 3.5 - C16/20 (nominal strength values)

Compressive ultimate strength (characteristic values - MPa)	
Cylindrical strength $f_{ck,cylind}$	Cubic strength $f_{ck,cubic}$
16	20

Table 3.6 - Tests on concrete specimens (average compressive strength)

Specimen group (casting phase)	Date of casting (1999)	Compressive cubic ultimate strength <sup>a</sup> (MPa)	Compressive cylindrical ultimate strength <sup>b</sup> (MPa)
columns 1 <sup>st</sup> storey	24/02	16.66	13.90
slab/beams 1 <sup>st</sup> floor	17/03	13.24	16.45
columns 2 <sup>nd</sup> storey	22/03	13.78	13.80
slab/beams 2 <sup>nd</sup> floor	06/04	18.10	17.40
columns 3 <sup>rd</sup> storey	08/04	16.50	9.20
slab/beams 3 <sup>rd</sup> floor	20/04	21.63	17.30
columns 4 <sup>th</sup> storey	22/04	13.58	11.00
slab/beams 4 <sup>th</sup> floor	06/05	16.98	20.17

a) Compressive tests on cube specimens carried out on 30/07/1999.

b) Compressive tests on cylindrical core specimens taken in the structure (after the test campaign) on 01/03/2001.

The concrete compression tests on twenty-eight cubes cast during construction led to a mean strength of 16 MPa, thus indicating that the concrete is of rather poor quality. In order to confirm the real properties of the concrete, further tests were performed by an external company using concrete core specimens (carrots) after the test campaign has been completed. The carrots were taken from both columns and slab/beams elements, located at no damaged zones. The picture in Figure A.30 shows the operation of specimens' extraction in the frame structure. Results of the compressive tests on the cylindrical specimens taken from the structure are also listed in Table 3.6. A good relation was found between the test results of the cubes specimens and of the cylindrical specimens.

A small variance was found for each casting phase, whilst large differences corresponded to the various casting phases. This variability shall be taken into account in the refined non-linear numerical analyses.

Table 3.7 presents the nominal (mean and characteristic) values for the mechanical properties of the steel adopted in the frame's construction. The steel is Fe B22k, smooth bars (Italian standards: Gazzetta Ufficiale, n. 176; Decreto del 28 Giugno 1980; 'Acciai in barre tonde lisce').

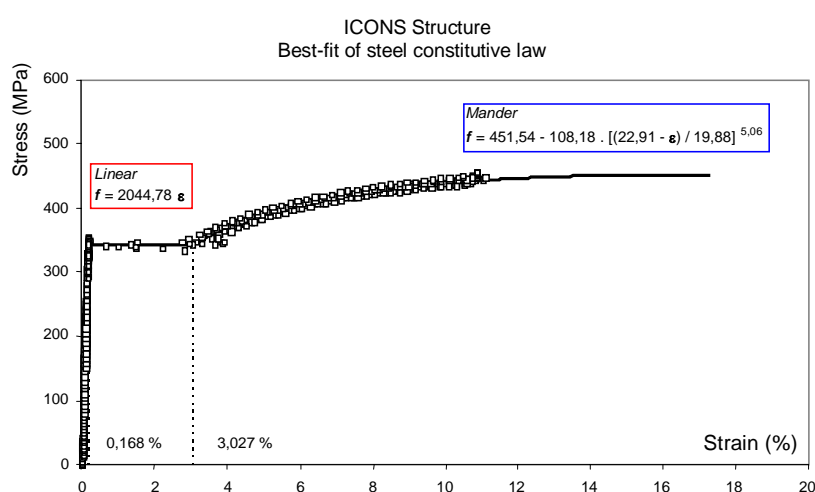
Table 3.7 - Fe B22k (nominal properties)

Relevant properties	Characteristic values
Yield stress	$f_{syk} = 215 \text{ MPa}$
Ultimate strength	$f_{suk} = 335 \text{ MPa}$
Ultimate strain	$\varepsilon_{suk} = 24.0 \%$

Tensile strength tests on steel bar specimens have been carried out at LNEC, in Lisbon (Carvalho *et al.*, 2000-*a*; 1999). The variance found was very small. From a best-fit of experimental diagrams for the reinforcing bars, the mean mechanical properties were estimated. The values obtained are summarised in Table 3.8. The best-fit was based on a linear regression for the elastic initial branch and on a non-linear regression using the Mander model for the hardening branch (scheme of the stress-strain curve in Figure 3.6). The LNEC test results are in line with the results obtained in other series of tests (see Pinto *et al.*, 1999-*c*).

Table 3.8 - Test on steel specimens (mean mechanical properties)

Mechanical properties	Value
Young modulus – $E_m$	204.5 GPa
Yield stress – $f_{sym}$	343.6 MPa
Hardening strain – $\varepsilon_{shm}$	3.03 %
Tangent modulus at beginning of hardening – $E_{sh}$	2.8 GPa
Ultimate strength – $f_{sum}$	451.5 MPa
Ultimate strain – $\varepsilon_{sum}$	22.9 %

Figure 3.6 - Best-fit of steel constitutive law (Carvalho *et al.*, 1999)

As shown in Table 3.8, the mechanical properties of steel obtained from tests on specimen bars differ considerably from the nominal values (see Table 3.7). The strength of steel is significantly higher than expected from the minimum values established in the Italian standards for the Fe B22k steel. In fact, the steel tested and used in the construction of the frame has significantly higher strength. The values of yield stress and ultimate strength found are 45% and 25%, respectively, higher than the nominal values. It should be noted that only minimum strength requirements were included in the old codes, which may lead to steel strength much higher than the nominal values. Systematic tests of reinforcement steel in existing buildings would be appropriate in order to get a more realistic estimation of its strength.

### 3.2.6 - Vertical loads

The vertical loads, represented in Figure 3.7, were defined in order to simulate the dead load other than the self-weight of the frame, considering that parallel frames have a distance of 5.0 m (Carvalho *et al.*, 1999). The frame model includes a 4.0 m wide slab, which requires additional vertical load accounting for such a slab portion missing. Vertical distributed loads on beams and concentrated loads on the column were considered in order to simulate the dead load of the frame other than the weight of partitions, finishings and live load. These correspond to the following vertical loads:

- Weight of slab:  $25 \times 0.15 = 3.75 \text{ kN/m}^2$
- Weight of finishings:  $0.75 \text{ kN/m}^2$
- Weight of transverse beams:  $2.5 \text{ kN/m}$
- Weight of masonry infills:  $1.1 \text{ kN/m}^2$  of wall area (it is considered that these walls exist both over longitudinal and transverse beams)
- Live load:  $1.0 \text{ kN/m}^2$  (quasi-permanent value)

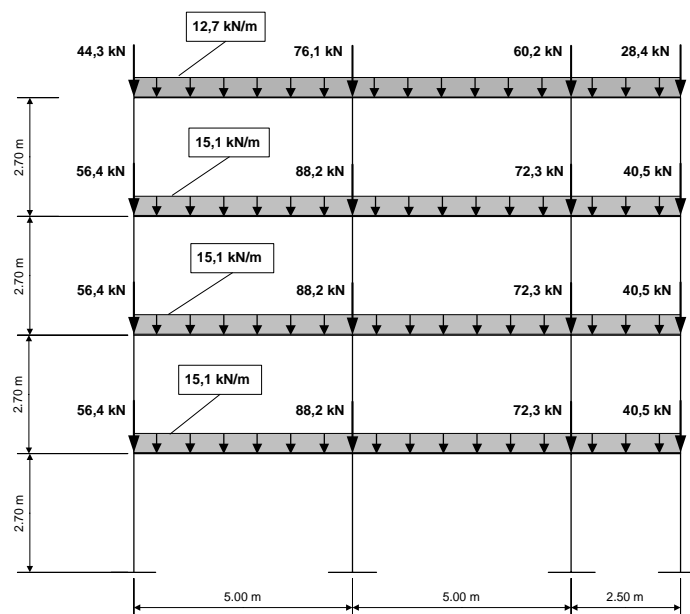


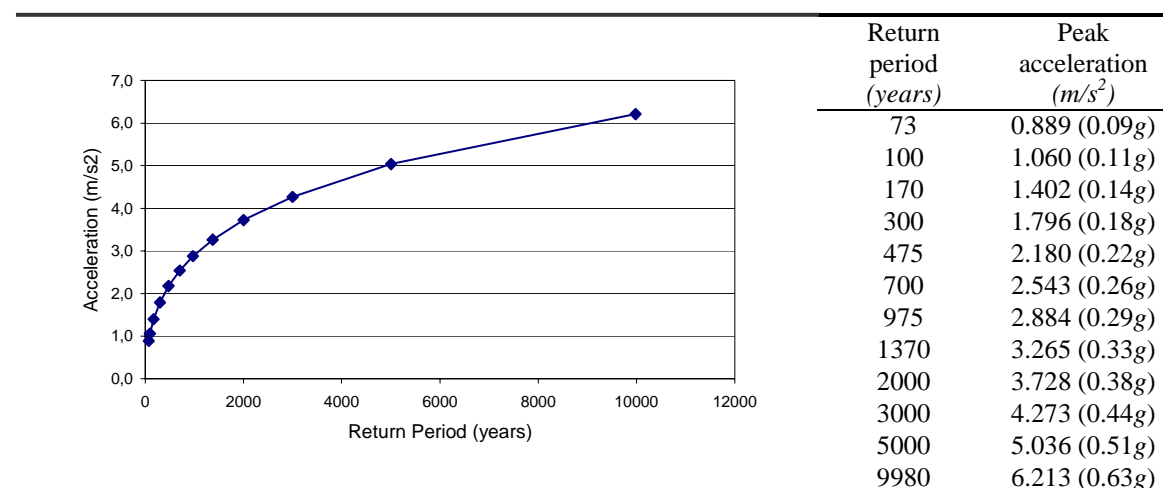
Figure 3.7 - Scheme of vertical static loads

The distribution of vertical loads applied to the infilled frame to simulate the dead load other than the self-weight of the frame was identical to the one used for the bare frame, and imposing the same load distribution for all the tests. The scheme of the loads considered can be found in Pinto *et al.* (1999-c).

### 3.2.7 - Earthquake input

The input seismic motions were defined in order to be representative of a moderate-high European seismic hazard scenario (Campos-Costa and Pinto, 1999; Carvalho *et al.*, 1999). Hazard consistent time series of acceleration (with 15 seconds duration) were artificially generated yielding a set of twelve uniform hazard response spectra for increasing return periods. The time increment considered to generate the records was 0.01 seconds, giving input accelerograms with 1500 points. The return periods considered, and the corresponding values of peak acceleration are given in Table 3.9. The acceleration time histories (accelerograms) considered for the PsD tests correspond to the 475, 975 and 2000-yrp, which are depicted in Figure 3.8. In Figure 3.9, the 5% damping displacement and pseudo-acceleration linear-elastic response spectra for 475, 975 and 2000-yrp are plotted.

Table 3.9 - Hazard curves for the moderate-high European scenario



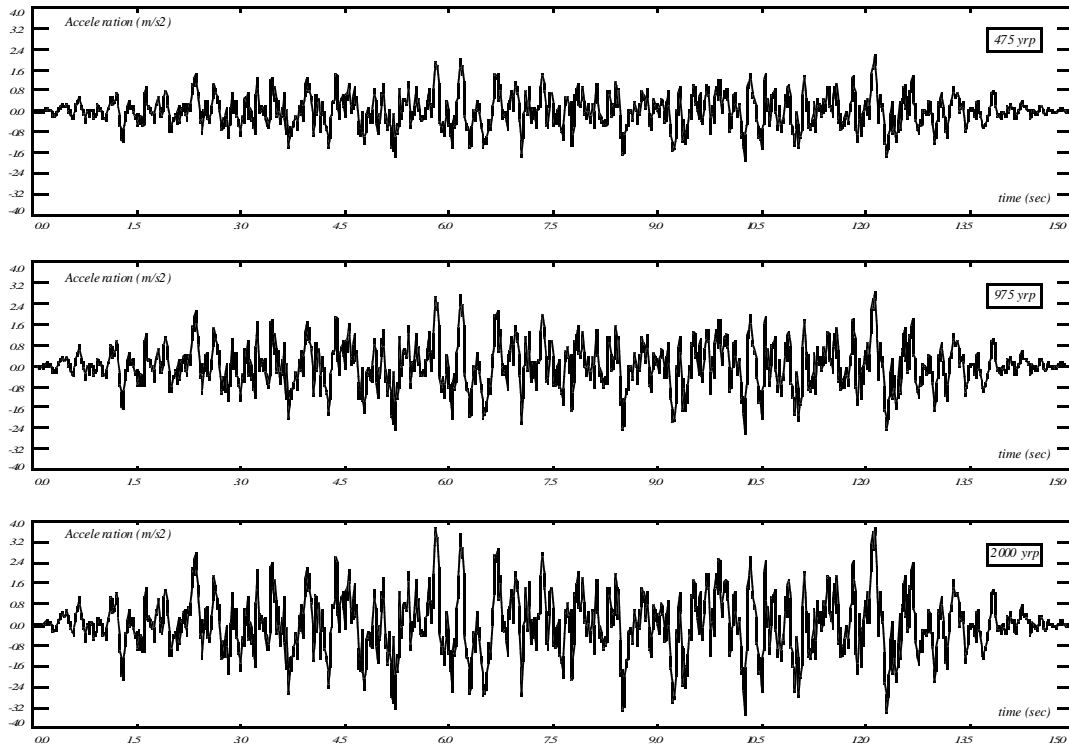


Figure 3.8 - Ground motion acceleration time histories for 475, 975 and 2000-yrp

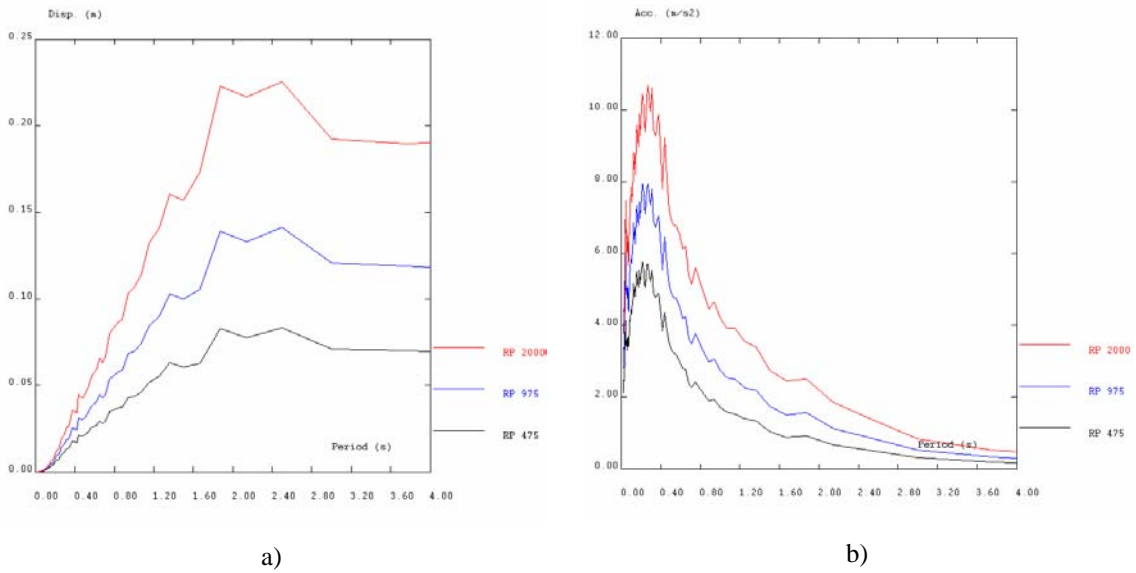


Figure 3.9 - Response linear-elastic spectra for 475, 975 and 2000-yrp (5% damping): a) displacement; b) pseudo-acceleration



### 3.3 - SELECTIVE STRENGTHENING SOLUTION FOR THE BARE FRAME

It is expected that the four-storey RC bare frame (frame B) will not perform satisfactorily. This was confirmed during the assessment tests (475 followed by 975-yrp earthquake motions). In order to improve the seismic performance of such a structure, a selective strengthening intervention was designed at Imperial College of London. The selective intervention scheme used was defined on the basis of the observed experimental behaviour for the structure tested without retrofit, and covered different design strategies within the same structure, namely strength-only and ductility-only solutions. These solutions were applied to different elements and regions of the structure aiming at improving its global and local seismic behaviour. Details of the selective intervention are given in Elnashai and Pinho (1999) and Pinho (2000). The retrofitting scheme was slightly revised after completion of the first series of tests (bare frame tests) because important damage was observed in the 3<sup>rd</sup> storey strong-column.

The damaged parts of frame B were repaired in the first phase. The repair consisted of the roughening of cracked surfaces and the sealing of cracks, the injection of epoxy resin in the opened cracks and the reinstatement of the spalled concrete using concrete similar to the original one.

Afterwards, the selective retrofitting solution involved two types of interventions in the internal strong-column. A strength-only intervention was implemented in the strong-column at the 3<sup>rd</sup> and 4<sup>th</sup> storeys to reduce the large flexural capacity differential verified at level 3. This intervention scheme is illustrated in Figure 3.10-*a* and consisted of using external re-bars embedded in a non-structural concrete (for protection purposes). Moreover, a ductility-only intervention was accomplished at the first three storeys in the strong-column, where large inelastic deformation demand is expected. This intervention is also depicted in Figure 3.10-*b* and was achieved by adding external confining steel plates at the critical zones, i.e. at the base and at the top of the member. Furthermore, additional plates were also added at mid-height of the columns in order to minimize the risk of shear failure. The final configuration of the RC strengthened frame is represented in Figure 3.11. Figure A.24 shows the strong-column repaired and strengthened, at the first storey level, according to the scheme described.

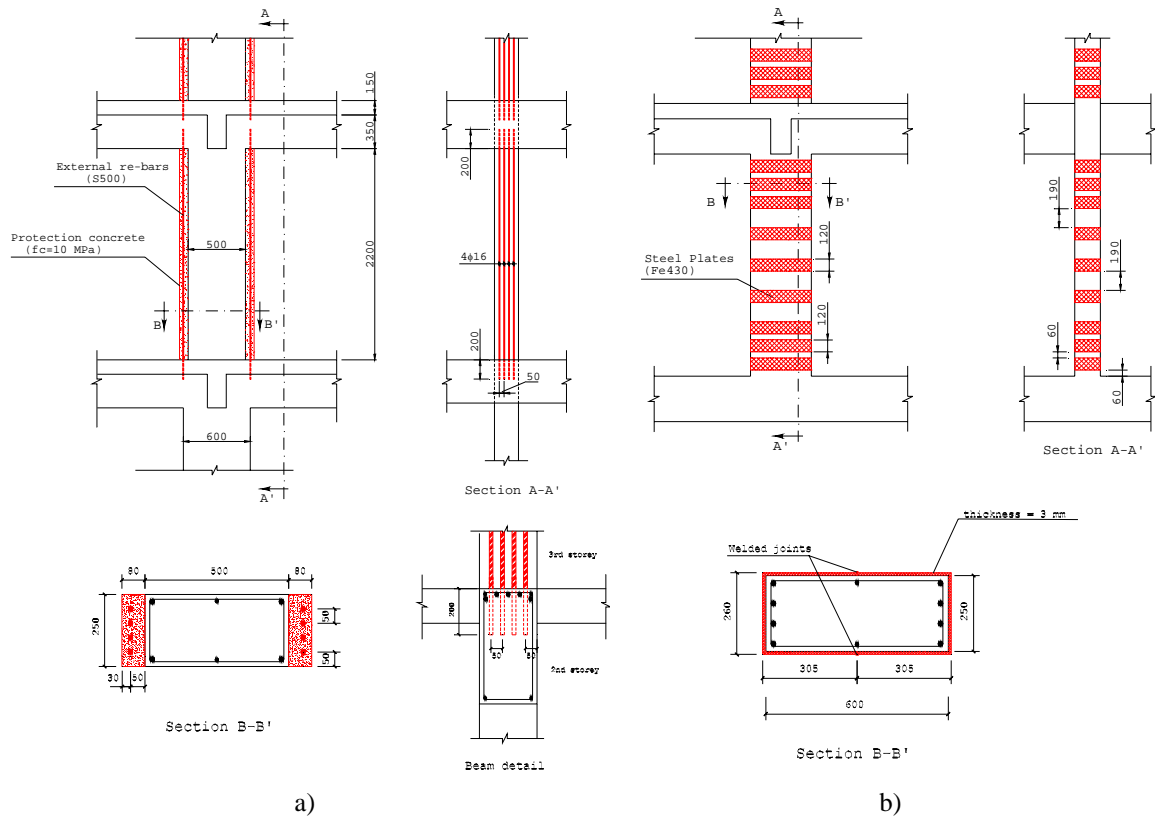


Figure 3.10 - Selective strengthening of the RC frame: a) strength-only intervention in strong-column; and, b) ductility-only intervention in strong-column (Elnashai and Pinho, 1999)

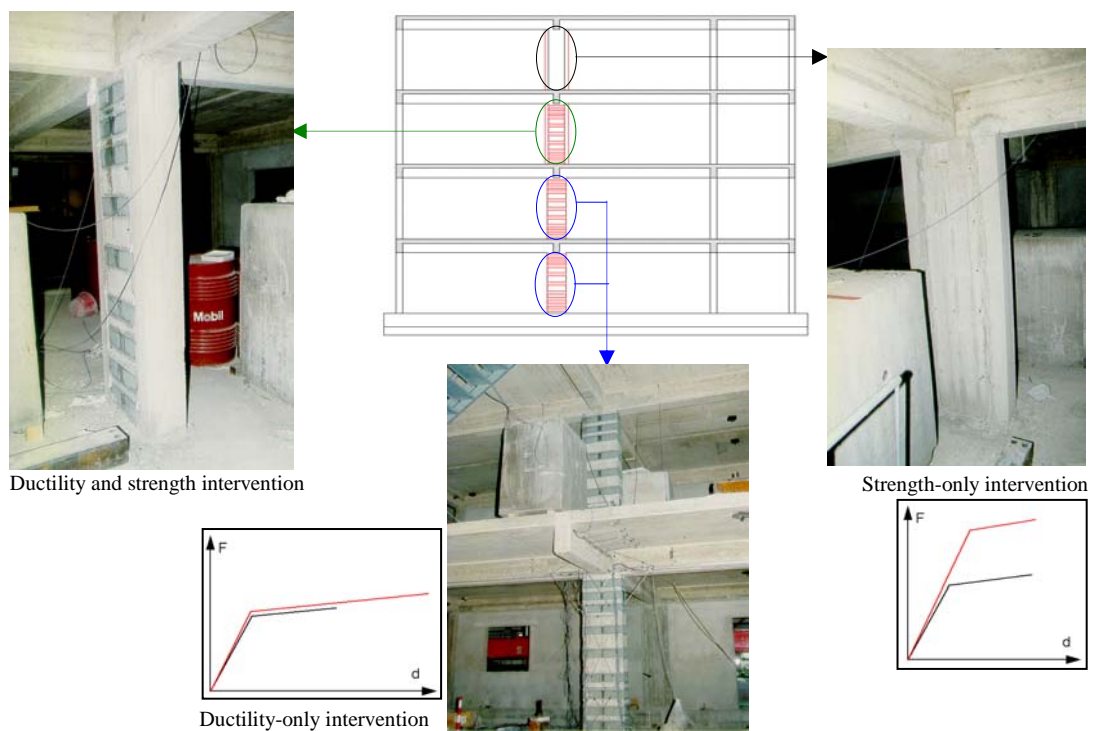


Figure 3.11 - Selective strengthened RC frame

To summarize, the selective intervention targeted the strong-column only, i.e. ductility-only on the first three storeys and strength-only on the upper two. In the particular case of the third storey, where both interventions were applied, the work had the following sequence: *i*) roughening of cracked surfaces and sealing of cracks; *ii*) injection of epoxy resin in opened cracks; *iii*) reinstate spalled concrete using concrete similar to the existing one; *iv*) apply ductility-only intervention; and, *v*) apply strength-only intervention.

Regarding practical application of the techniques, the following is observed:

*a*) Strength-only intervention:

- On the two top-levels (storeys three and four), the beams were drilled throughout their height so as to allow for introduction of the re-bars (from the top level downwards). At level four, the opening was executed from the top and is only 200 *mm* deep.
- Following insertion of the bars in the respective openings, the full-height holes at the two top beams were sealed at the base using fast-hardening paste. Epoxy resin was then injected from the top, fixing the bars to the beams.
- To allow the new re-bars to work mutually with the existing reinforced concrete section, at three different levels, steel connectors were bolted on to the existing column concrete and welded on these new external longitudinal re-bars (see Figure A.25).
- The re-bars were coated with grease to minimize adherence to the protective concrete.
- Formwork was placed at a distance of 80 *mm* from the column, leaving an opening at the top from which the weak concrete ( $f_c = 10 \text{ MPa}$ ) was poured in. Manual finishing of the surface was applied, though this is not crucial to the outcome of the intervention.

*b*) Ductility-only intervention:

- Mechanical chiselling was applied to roughen the surfaces where plates are to be applied.

- The steel plates were temporarily fixed to the wall using metallic clamps. The confinement plates, initially split into pairs of U-shape plates, were welded together.
- A quick-hardening paste was applied to seal the plates, leaving only a limited number of openings for the introduction of plastic hoses, required for the injection of the resin. This sealing cement was then brushed with acetone to ensure the closure of all pores.
- Injection of the resin started at the lowest hose, progressed upwards as the hoses started leaking. Adequate pressure (ideal values fluctuate according to equipment characteristics, dimension of plates and number of hoses) was required to ensure uniform contact between plates and retrofitted members.
- Where large gaps between plates and concrete element (greater than 3-5 mm) was detected, micro-silica was used for filling the cavities, optimising the behaviour of the epoxy-resin.
- A minimum period of 24 hours was allowed for curing of the resin.

### **3.4 - MASONRY INFILL WALLS AND MASONRY STRENGTHENING; CONSTRUCTION DETAILS AND MATERIALS**

The masonry infilled reinforced concrete frame was constructed with the same detailing and materials as for the bare frame. Figure 3.12 shows the general layout of the infilled structure, where the locations and dimensions of the infill openings are shown. The infill walls (non-load bearing) were constructed after the reinforced concrete frame. The long external bay infill contains a window opening ( $1.2\text{ m} \times 1.0\text{ m}$ ) at each of the four levels. The central bay contains a doorway ( $2.0\text{ m} \times 1.75\text{ m}$ ) at ground level and window openings ( $2.0\text{ m} \times 1.0\text{ m}$ ) in each of the upper three levels of the building. The external short ( $2.5\text{ m}$  span) bay contains solid infill panels, i.e. without openings (Pinto *et al.*, 2001-c; 2000-a).

The construction of the infill walls was carried out inside the ELSA laboratory in order to avoid damage of the infills due to even small inter-storey deformation during the structure transport into the laboratory.

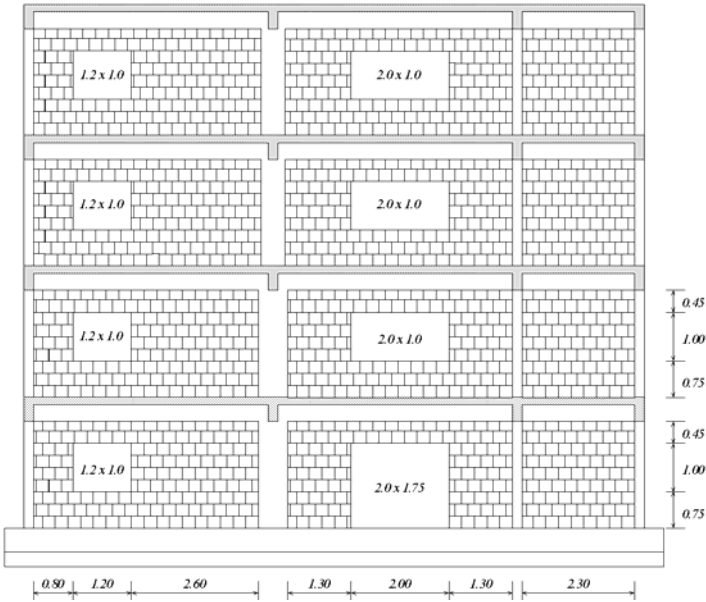


Figure 3.12 - Elevation view of the infilled concrete frame (frame A): infill openings (location and dimensions)

**3.4.1 - Masonry infill walls**

In order to be representative of the construction techniques and materials commonly used in Mediterranean countries, hollow blocks were chosen for the construction of infill walls. These blocks are horizontally perforated, and have the following dimensions: 0.12 m thick, 0.245 m base-length and 0.245 m height (see Figure 3.13).



Figure 3.13 - Infill block units

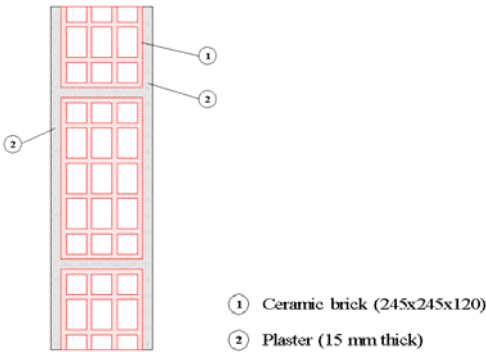


Figure 3.14 - Detail of the infill walls construction

According to the classification of masonry units presented in Eurocode 6 (EC6, 1995), the hollow blocks are included in Group 3, because they have 62% of voids (less than 70%) by

volume, holes are horizontal (relatively to the bed face units), pass right through the units and satisfy the following requirements:

- There are several holes and the area of any one hole does not exceed  $2800 \text{ mm}^2$ .
- The height to thickness ratio of any web does not exceed 7.5.
- The height to thickness ratio of any shell does not exceed 6.

The infill walls were constructed with the block units bedded on the  $0.120 \text{ m} \times 0.245 \text{ m}$  face and the hollows in the horizontal direction ( $0.120 \text{ m}$  thick). The weight of each unit is  $42.2 \text{ N}$  and the resulting specific weight, by meter square of wall, is  $0.785 \text{ kN/m}^2$ . The reference values of quantities in construction by square meters for the walls are presented in Table 3.10.

Table 3.10 - Quantities used in masonry construction by meter square of wall (reference values)

Unit	Number of units	Bedding mortar	Weight
$120 \times 245 \times 245$	15 blocks/ $\text{m}^2$	9 $\text{l/m}^2$	0.785 $\text{kN/m}^2$

The mortar used in the joints and plaster was manually prepared as current construction practice until the late 1970's. The aim was to reproduce the construction conditions at that time. The mortar joints are approximately  $1.5 \text{ cm}$  thick for both vertical and horizontal joints, so-called perpend and bed joints, respectively. A  $1.5 \text{ cm}$  thick plaster was applied on both sides of the walls. The same mortar proportioning was used for joints and plaster (see Table 3.11 for volume proportions of the components in the mortar). In comprehensive terms the proportion by volume used was 1:4.5 (Hydraulic binder : Sand).

Table 3.11 - Mortar used in the joints and plaster (proportioning)

Component	Proportion (by volume)
Sand (0-2 $\text{mm}$ )	45
Cement	1
Hydraulic lime	9

In short, the infill panels consist of ceramic hollow blocks with external plaster  $15 \text{ mm}$  thick on both sides, as schematically shown in Figure 3.14. Illustrative pictures of the infill walls construction are shown in Figures A.26 and A.27.

### 3.4.2 - Strengthening of the infill panels

The retrofitting solution applied to the walls in the infilled frame (see Figure 3.1) was proposed by Carvalho *et al.* (1999) and consists of a concrete layer with an embedded reinforced steel mesh, which is deemed to improve the post-peak behaviour of the walls. Shotcrete (SC) of the walls was initially foreseen. However, due to difficulties in finding a company to carry out the shotcrete works (namely: non-existing local company with appropriate tools, a job too small for a company with the appropriate tools) it was decided to apply the concrete manually (traditional method). The label 'shotcrete' (SC) is retained because it expresses better the strengthening operation.

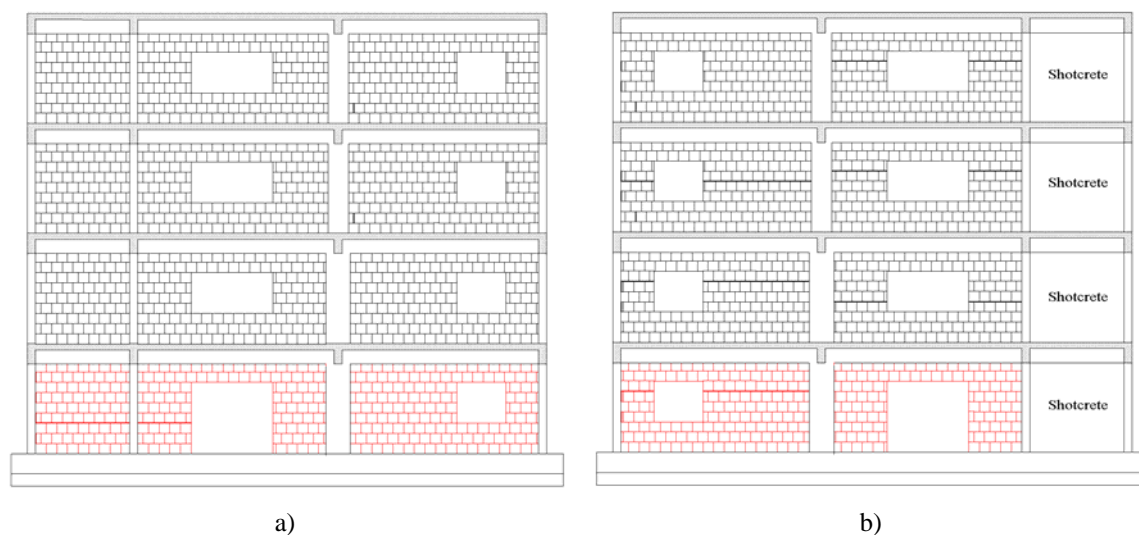


Figure 3.15 - Reconstruction of the 1<sup>st</sup> storey infill panels and infill strengthening (shotcrete) of the short external bay at all storeys (elevation): a) south view; b) north view

The general layout of the frame with the strengthened infills is shown in Figure 3.15, and comprises:

- At the 1<sup>st</sup> storey: *a*) a short panel with a new infill wall (with plaster in both sides) and a shotcrete layer (with 26 mm thickness and a steel mesh embedded); *b*) a central long-panel with a new infill wall (with a door opening, with plaster at both sides); and, *c*) an external long-panel with a new infill wall (with a window opening, with plaster at both sides).

At the 2<sup>nd</sup>, 3<sup>rd</sup> and 4<sup>th</sup> storeys: *a*) a short panel with an existing infill wall (with plaster in both sides) and a new shotcrete layer (with 26 mm thickness and a steel mesh embedded); *b*) a central long-panel with an existing infill wall (with a centred window opening, with plaster at both sides); and, *c*) an external long-panel with an existing infill wall (with a window opening, with plaster at both sides). It is noted that the existing infills at the 2<sup>nd</sup>, 3<sup>rd</sup> and 4<sup>th</sup> storeys were already subjected to the previous earthquake tests, suffering minor damage.

The shotcrete applied to the shorter external panels (one side/face only) at all storey levels consists of a 26 mm thick concrete layer, with an embedded welded steel mesh (S500, ribbed, grade 500 MPa), with 5 mm wire diameter and 10×10 cm spacing (#  $\phi$ 5 // 0.10), as shown in Figures 3.16 and 3.17. No specific connection (e.g. dowels) was provided between the shotcrete layer and the existing surrounding RC frame. A light connection (clamps) between the shotcrete layer and the masonry walls was provided in nine points, as shown in Figure 3.17. It is noted that these clamps were not specifically designed for that purpose, but they were used to keep in place the steel reinforcing mesh for the shotcrete works. It is believed that these 'connectors' will have a beneficial effect on the behaviour of the final wall-shotcrete system, avoiding premature buckling of the shotcrete layer.

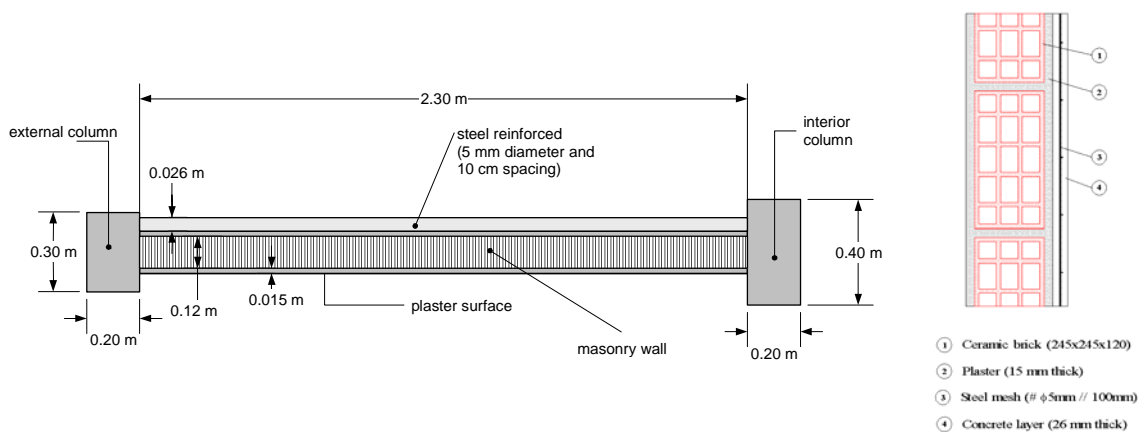


Figure 3.16 - Constructive details (layout and dimensions) of the infill strengthening



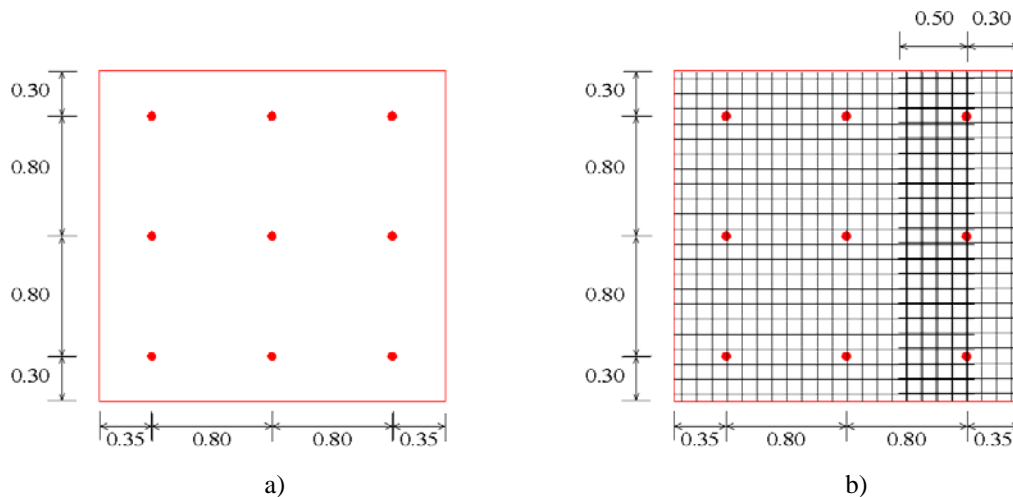


Figure 3.17 - Infill strengthening: a) light connection between masonry and steel mesh (nine connection points); b) reinforcement detailing (lateral overlapping of 0.50 m)

Regarding the shotcreting work, the following requirements were fulfilled:

- The surface was properly prepared for the shotcrete application, removing of all spalled, loose and deteriorated material from the existing wall surface. The masonry cracks were superficially filled with a conventional sand/cement mortar. The repair surface was cleaned and adequate pre-wetting was done prior to shotcreting.
- A wet-mix process was used and the specified maximum grain size for the aggregate was 8 mm. The nominal compressive strength of the shotcrete corresponds to a C25/30 concrete (according to ENV 206, 1993). The shotcrete had adequate cohesion in order to be applied with 26 mm thickness with the incorporation of a steel mesh. A wet curing process was provided. Just as shotcrete begins to stick, it was kept wet continuously. The final textured appearance of the shotcrete surface was flash coated.
- Adequate quality control procedures were followed, especially concerning the strength of the shotcrete. Also during execution, the control of the material properties was made in order to comply with quality assurance requirements (e.g. ACI 506R-90, 1995; ACI 506.2-95, 1995).

Figure A.28 illustrates the infill strengthening construction and shows details of the reinforcing steel mesh.

### 3.4.3 - Material properties

Tests on mortar specimens and block units were carried out in order to characterize the masonry infill wall components. Wallets representative of the masonry infill walls were constructed and tested in compression, in the horizontal, vertical and diagonal directions. In this section, results of the tests on specimens of block units, mortar and infill wallets are presented. A more detailed description of the infill' properties can be found elsewhere (Pinto *et al.*, 2001-c).

#### 3.4.3.1 - Mortar used in joints and plaster

The same materials and respective proportioning were used for the mortar employed in the joints and plaster of the infill masonry walls construction. Representative samples of mortar (prisms with dimensions  $4\text{ cm} \times 4\text{ cm} \times 16\text{ cm}$ ) were prepared and subsequently tested. Flexural and compressive tests, according to the procedures and specifications in EN-196-1 (1987), were performed on the mortar specimens at the University of Pavia laboratory.

A low value was found for the mortar strength. A flexural (indirect tensile) strength of  $0.59\text{ MPa}$  and a compressive strength of  $1.33\text{ MPa}$  were obtained from the tests (see Table 3.12), which is deemed to represent a typical mortar used in masonry infill walls of existing buildings. The standard deviation values are 38% for flexural strength and 36% for the compressive strength, which are typical values for these materials. According to EC6 the mechanical properties of the mortar fall into the range of characteristics of a mortar type M1 and type M2. The standard deviations found for the flexural and compressive strength for each group of specimens are also presented in Table 3.12.

Table 3.12 - Flexural and compressive strength of the mortar

Ultimate strength	Average values ( <i>MPa</i> )	Standard deviation (%)
Flexural	0.59	38%
Compressive	1.33	36%

### 3.4.3.2 - Compression tests on infill block units

Tests on infill block units were performed at the University of Pavia. Thirty units were tested in each direction (parallel and perpendicular to the bed joints). Table 3.13, summarises the compressive resistance test results for the block units. The gross area considered to determine the compressive stress (strength) is  $29400 \text{ mm}^2$ , which corresponds to the total surface area ( $0.245 \text{ m}$  height or base  $\times$   $0.120 \text{ m}$  thickness). For the direction parallel to the bed joints, a predictably higher strength was found, with a mean value of  $15.36 \text{ MPa}$  and a corresponding characteristic value of  $12.35 \text{ MPa}$ . In the compression tests perpendicular to the bed joints, the mean and characteristic values evaluated were  $2.80 \text{ MPa}$  and  $2.05 \text{ MPa}$ , respectively.

Table 3.13 - Compressive strength test on the block units

Collapse stress ( $MPa$ )	Parallel to the bed joints (30 specimens)	Perpendicular to the bed joints (30 specimens)
Minimum value	12.00	2.06
Maximum value	19.30	3.48
Average ( $f_m$ )	15.36	2.80
<i>s.q.m.</i>	1.84	0.46
Characteristic value ( $f_k$ )	12.35	2.05

### 3.4.3.3 - Compression tests on masonry wallets in the directions parallel and perpendicular to the bed joints

Five infill masonry specimens ( $1.00 \text{ m} \times 1.00 \text{ m}$  wallets without plaster) were constructed and tested in compression for each direction (perpendicular and parallel to the bed joints) at the University of Pavia. The specimens were constructed using the same materials (block units and mortar) and with the same geometry (joints thickness, fabric) as the ones used for the infill walls.

A detailed description of the series of tests performed in Pavia can be found in Pinto *et al.* (2001-c). Next, the test results are summarised in Tables 3.14 and 3.15, in terms of strength, Young modulus and Poisson ratio for each tested specimen and the resulting average and characteristic values.

Due to the substantially higher strength of the block units in the direction of the bed joints, a higher strength of the wallet in this direction would be expected. However, the strength of the wallets in this direction was found to be extremely low. This is justified by the fact that the specimens were constructed placing the blocks horizontally and filling the vertical joints. This construction process leads to poor vertical joints and, consequently, dictates poor strength of the masonry walls in the direction parallel to the bed joints. Obviously, this also implies poor shear strength of the masonry.

Table 3.14 - Compression strength test on the infill specimens (loading perpendicular to the bed joints)

Test No.	Area ( $mm^2$ )	Max. force ( $kN$ )	$\sigma_{max}$ ( $MPa$ )	$E_{\perp,sec}$ ( $MPa$ )	$\nu$
1	86825	-136.50	-1.57	2540	0.070
2	86825	-97.00	-1.12	2341	-
3	86825	-81.60	-0.94	950	0.076
4	86825	-122.00	-1.41	2490	-
5	86825	-42.00	-0.48	1042	0.046
Average		-95.82	-1.10	1873	0.064
<i>s.q.m.</i>		36.88	0.42	804	0.02
C.V. (%)		38	38	43	25

Table 3.15 - Compression strength test on the infill specimens (loading parallel to the bed joints)

Test No.	Area ( $mm^2$ )	Max. force ( $kN$ )	$\sigma_{max}$ ( $MPa$ )	$E_{//,sec}$ ( $MPa$ )	$\nu$
1	86825	-93.00	-1.07	1340	-
2	86825	-105.00	-1.21	1170	-
3	86825	-87.00	-1.00	266	-
4	86825	-84.00	-0.97	947	-
5	86825	-112.00	-1.29	1230	-
Average		-96.20	-1.11	991	-
<i>s.q.m.</i>		11.95	0.14	430	-
C.V. (%)		12	12	43	-

#### 3.4.3.4 - Concrete used for the shotcrete of the infill walls

The concrete considered in the design phase (Carvalho *et al.*, 1999) was a C25/30 concrete (EC2; ENV 206, 1993), which corresponds to a characteristic cubic strength of 30  $MPa$ .

Table 3.16 presents the proportioning of the components adopted for the concrete. Tests on the concrete samples of the shotcrete have been carried out and the results are presented in Table 3.17. For the 1<sup>st</sup>, 3<sup>rd</sup> and 4<sup>th</sup> casting phases, the required characteristic compressive cubic ultimate strength (30 *MPa*) is guaranteed. The strength achieved in the test specimens for the 2<sup>nd</sup> casting phase is lower than the nominal value, but the difference is very small (5.5%).

Table 3.16 - Concrete used in the strengthening (proportioning)

Component	Proportion (by volume)
Cement	1
Sand (0-3 <i>mm</i> )	2

Table 3.17 - Concrete compressive strength (average and characteristic values)

Specimen group (casting phase)	Compressive cubic ultimate strength ( <i>MPa</i> )	
	Average value	Characteristic value
1 <sup>st</sup> storey	40.55	39.57
2 <sup>nd</sup> storey	28.75	28.34
3 <sup>rd</sup> storey	37.35	35.38
4 <sup>th</sup> storey	32.20	31.50

#### 3.4.3.5 - Diagonal compression tests on masonry wallets

Diagonal compression tests on masonry wallets aim at evaluating the conventional tensile strength, which can be related to the shear strength of the masonry walls. The standard diagonal tension (shear) test was performed in several wallets according to the RILEM recommendations (1992) and ASTM standards (1997). Using these standards the shear strength in the centre of the panel and the respective shear modulus (modulus of elasticity in shear) were determined, for each specimen tested. According to the standards, such tensile strength is typically evaluated from the load at failure of the specimen assuming that the material is elastic, isotropic and homogeneous.

A square masonry panel is subjected to a compressive force applied at two opposite corners along a diagonal until the panel cracks. The shear strength is inferred from the measured diagonal compressive force based on a theoretical distribution of shear and

normal stresses for a homogeneous and elastic continuum. Using the same concept, shear modulus is inferred from measured diagonal compressive stress and strain.

The wallets were constructed at the same time, using the same materials (block units and mortar) and with the same geometrical requirements in terms of joint and plaster thickness as the infill walls. The specimens were constructed at the ELSA laboratory and tested at the laboratory of University of Pavia.

Twelve masonry wallets with nominal dimensions of  $1.00\text{ m} \times 1.00\text{ m}$  were tested in diagonal compression, namely: five specimens without plaster, four with plaster in both faces and three with plaster in both faces which were strengthened (see Figure 3.18).

The specimens were instrumented according to the scheme given in Figure 3.18 and illustrated in Figure 3.19. Four relative displacement transducers were used to measure the deformation, two in each direction (vertical and horizontal).

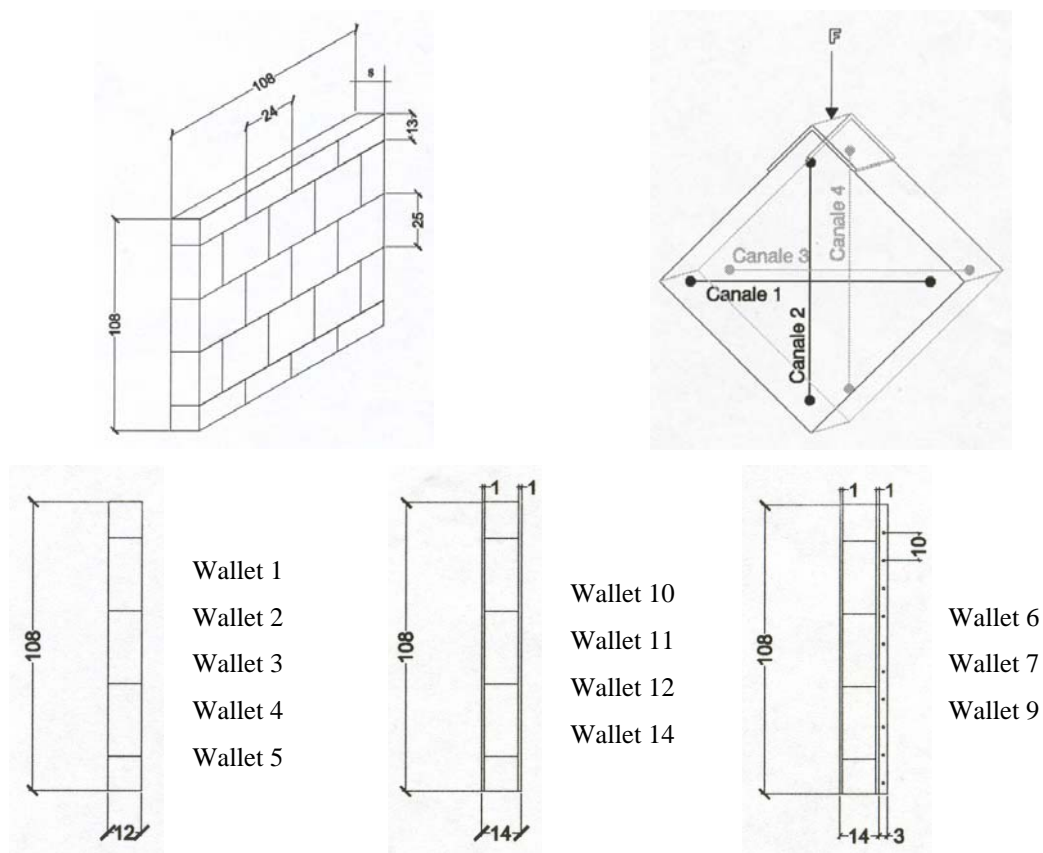


Figure 3.18 - Diagonal compression tests: typology and nomenclature of the tested specimens

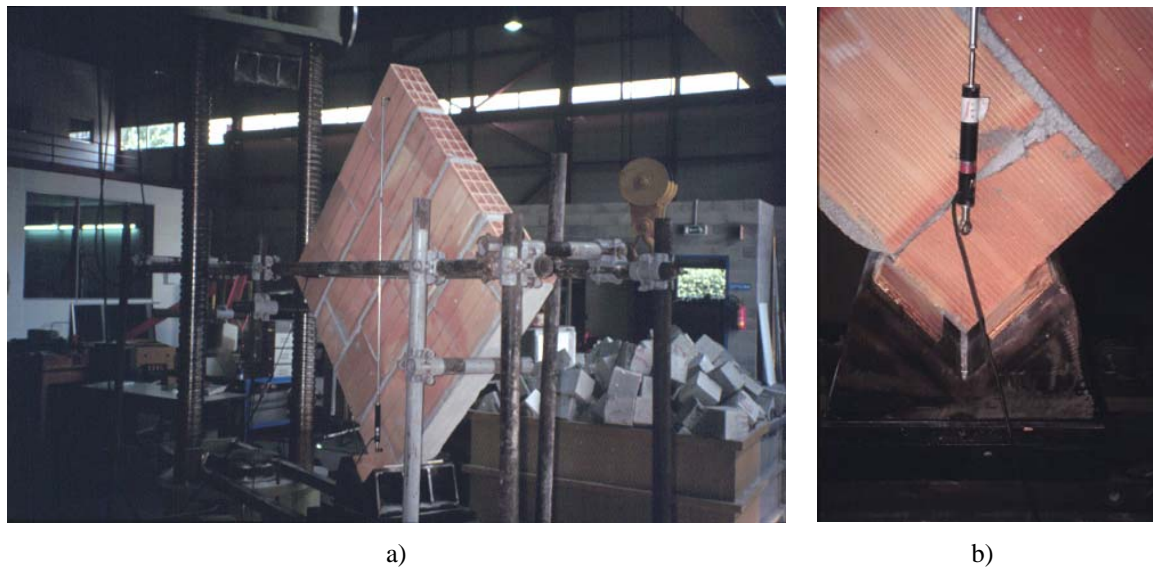


Figure 3.19 - Diagonal compression test: a) testing set-up; b) instrumentation and loading shoe detail

The results from the diagonal compression tests are represented by two curves, one with the vertical force versus vertical deformation (left) and the other versus the horizontal deformation (right), as schematically shown in Figure 3.20. The deformations correspond to the average of the two signals recorded in the associated directions.

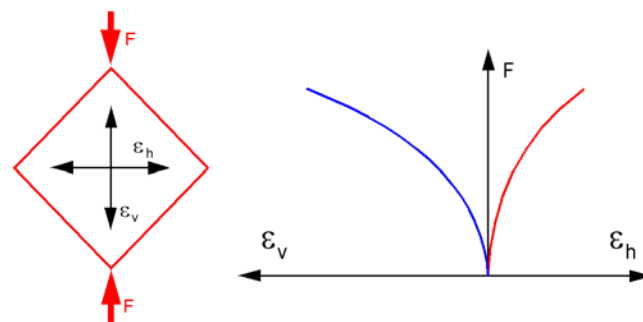


Figure 3.20 - Diagonal compression tests: generic scheme

Test results for the specimens without plaster, with plaster in the two faces and with plaster and strengthening layer are plotted in Figures 3.21, 3.22 and 3.23, respectively. Figure 3.24 represents the test results obtained for all test specimens grouped (and represented by colour) by each test series. From the results, the following features are underlined:

- There is an evident increasing of stiffness due to the plaster, as well as an increase in strength. The load capacity of the specimens with plaster is 2.2 times higher than the specimens without plaster.
- The shotcrete increases the strength by about 17%, if compared with the specimens without strengthening (with plaster in both sides).
- The transversal deformation in the strengthened specimens was always lower than the one obtained for the non-strengthened specimens. This confirms the beneficial effect of the shotcrete, which restrains the development of the cracks in the direction orthogonal to the loading and consequently leading to lower transversal deformation. However, the results in terms of force-deformation, in the loading direction, show unexpected low stiffness and strength (only one specimen has shown higher strength, comparing to the non-strengthened specimens). It is believed that the tested strengthened wallets are not representative of the real effect of the shotcrete on the infill walls, because of the difficulties in reproducing real conditions on small specimens, as well as in conceiving an adequate test set-up (uniform distribution of the load to the brick-wall and strengthening layer assemblage). Therefore, it is considered that the results for the strengthened specimens are not reliable enough to predict the mechanical properties of the strengthened walls.

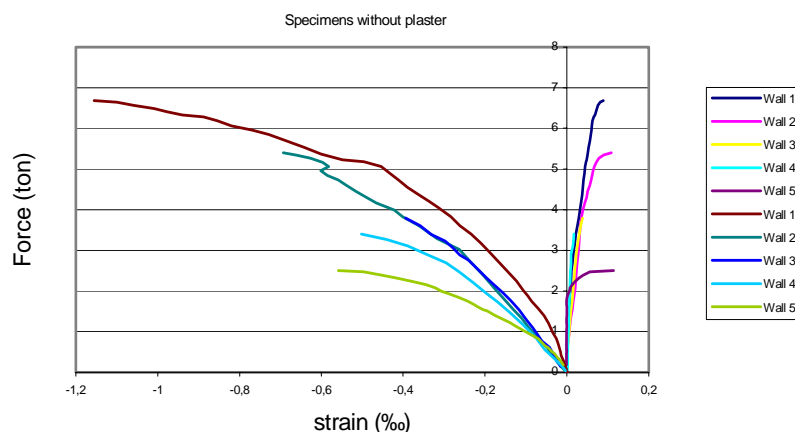


Figure 3.21 - Diagonal compression tests on specimens without plaster



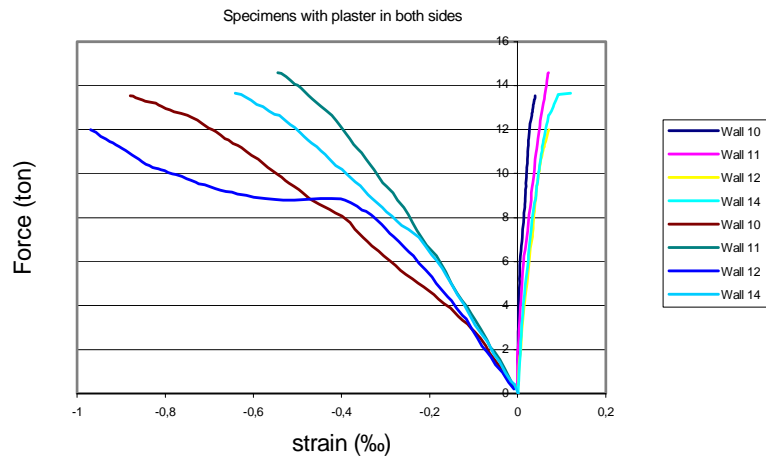


Figure 3.22 - Diagonal compression tests on specimens with plaster in both sides

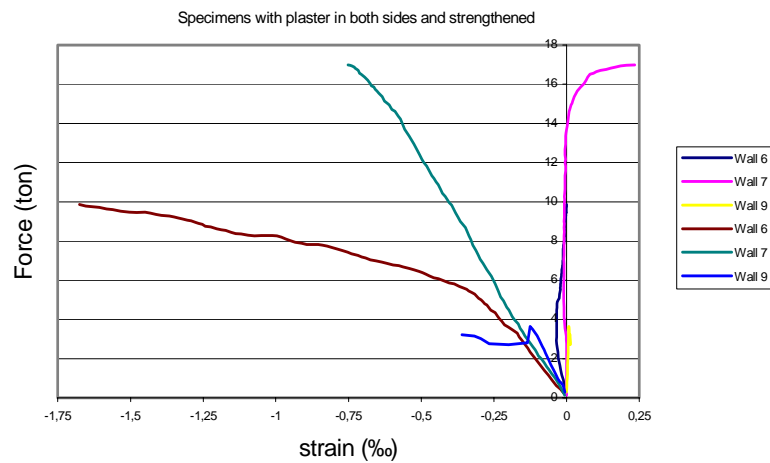


Figure 3.23 - Diagonal compression tests on specimens with plaster in both sides and strengthened

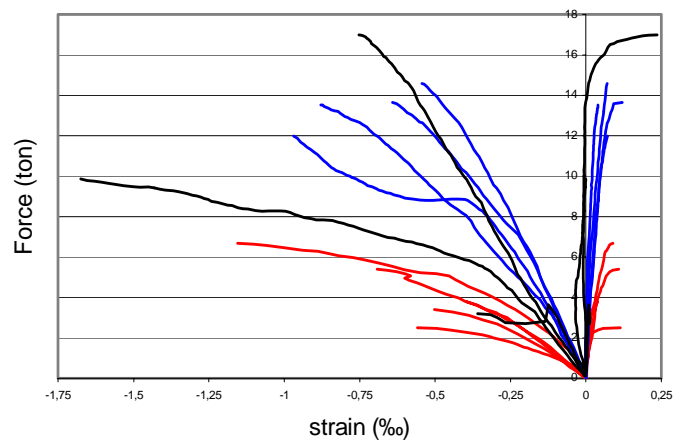


Figure 3.24 - Diagonal compression tests: specimens without plaster (red), with plaster in both sides (blue) and with plaster in both sides and strengthened (black)

### 3.4.3.6 - Mechanical properties of the masonry walls obtained from diagonal compression tests

From the force-deformation curves obtained in the diagonal tests, and presented in the previous section, the mechanical properties of the infills are calculated, according to the applicable normative. The shear stress ( $S_s$ ), which corresponds to the principal tensile stress, is calculated for specimens on the basis of net area ( $A_n$ ), by

$$S_s = \frac{0.707 \cdot P}{A_n} \quad (3.5)$$

where:  $P$  represents the load at failure and the net area ( $A_n$ ) is calculated by

$$A_n = \frac{l + h}{2} \cdot t \cdot n \quad (3.6)$$

where:  $l$ , stands for the width of the specimen;  $h$  is the height of the specimen;  $t$  is the total thickness of the specimen; and,  $n$  is the fraction of the gross area of the solid part of the specimen.

The shear strain ( $\gamma$ ) is obtained from

$$\gamma = \frac{\Delta V + \Delta H}{g} \quad (3.7)$$

where:  $\Delta V$  represents the vertical shortening;  $\Delta H$  is the horizontal extension; and,  $g$  is the vertical gage length assumed equal to the horizontal gage length (as required in the ASTM standards, 1997).

The shear modulus ( $G$ ) is calculated as the quotient between the shear stress and the shear strain as follows

$$G = \frac{S_s}{\gamma} \quad (3.8)$$

The shear stress and rigidity (initial stiffness) for each tested specimen were calculated with the net area and with the nominal area (with the total thickness of the specimen).

Table 3.18 gives, for each test, the values of shear strength ( $S_u$ ) and shear modulus ( $G$ ), calculated with the net and nominal area. The shear strength is calculated for the ultimate force and the shear modulus is calculated for one third of the ultimate force, as required in the ASTM standards (1997).

Table 3.18 - Diagonal compression tests: shear strength ( $S_u$ ) and shear modulus ( $G$ )

Specimen	Total thickness (mm)	$n$ (%)	using nominal area		using net area		
			$S_u$ (MPa)	$G$ (GPa)	$S_u$ (MPa)	$G$ (GPa)	
Specimens without plaster							
wallet 1	120	38.00	0.358	0.900	0.941	2.368	
wallet 2	120	38.00	0.289	0.569	0.760	1.497	
wallet 3	120	38.00	0.203	0.646	0.534	1.700	
wallet 4	120	38.00	0.182	0.560	0.479	1.475	
wallet 5	120	38.00	0.134	0.611	0.352	1.607	
Specimens with plaster in both sides							
wallet 10	150	50.40	0.579	0.991	1.149	1.967	
wallet 11	150	50.40	0.625	1.341	1.239	2.661	
wallet 12	150	50.40	0.513	1.085	1.018	2.152	
wallet 14	150	50.40	0.584	1.268	1.159	2.515	
Specimens with plaster in both sides and strengthening							
wallet 6	176	57.73	0.360	0.589	0.623	1.021	
wallet 7	176	57.73	0.620	0.826	1.074	1.431	
wallet 9	176	57.73	0.117	1.103	0.203	1.911	

Table 3.19 - Diagonal compression tests (average values): shear strength ( $S_u$ ) and shear modulus ( $G$ )

Group specimen	Number	using nominal area		using net area		C.V. (%)	
		$S_u$ (MPa)	$G$ (GPa)	$S_u$ (MPa)	$G$ (GPa)	$S_u$	$G$
without plaster	5	0.233	0.657	0.613	1.729	38.4	21.3
with plaster	4	0.575	1.171	1.141	2.324	8.0	13.8
with plaster and strengthened	2 <sup>a</sup>	0.490	0.708	0.849 (3.316)	1.226 (4.792)	37.5	23.7

a) The wallet 9 was not considered, because the test results are not of adequate quality.

Table 3.19 gives, for each test series, the average values of shear strength and shear modulus, considering the total nominal area and the net area. The values of the tensile

---

strength and shear modulus, for the strengthened specimens, considering the net area as just the strengthening thickness (assuming that only the strengthening layer is carrying the load applied during the test) are also presented in Table 3.19 (values in brackets). From the analyses of the Table 3.19, the following comments can be made:

- The plaster increases substantially the strength. In fact, comparing the shear strength obtained in the specimens without plaster with the ones with plaster in both sides, an increase of about 2.5 times was verified considering the total reference area (1.9 times for the net area). In terms of shear modulus the increase is of 1.8 times and 1.4 times, considering the total and net area, respectively.
- For the tests on the strengthened specimens, a lightly decrease of the strength and a considerable decrease of the shear modulus were observed. However, it should be noted that the test conditions (inadequate test set-up for uniform share of forces between the wall and strengthening layer) and due to the large stiffness difference between wall and shotcrete concrete, it can be assumed that just the shotcrete is carrying the load. Therefore, the smaller strength and stiffness can be justified, as well as the premature rupture of the shotcrete layer and subsequently of the strengthened wallet.

In Figure 3.25 new stress-strain curves are plotted for the diagonal compression tests and for each specimen, using as reference area the one corresponding to their net thickness. The net thickness is  $0.0456\text{ m}$ ,  $0.0756\text{ m}$  and  $0.026\text{ m}$ , for the specimens without plaster, with plaster and strengthened, respectively. It is underlined that for the strengthened specimens, a net thickness of  $0.026\text{ m}$  was used, which corresponds to the shotcrete thickness. In fact, the results in terms of reference stress (see Figure 3.25) show, for all the strengthened specimens, a higher strength than the strength obtained for the non-strengthened specimens. It is concluded, therefore, that the results from strengthened specimens, calculated with the total net area, are not reliable.

It is interesting to look at the Figure 3.25, where the stress-strain curve, for one of the strengthened specimens, shows that after premature failure or separation of the concrete strengthening layer, the curve tends to the ones obtained for the specimens without strengthening.

The average, minimum and maximum values of horizontal and vertical measured deformation at the failure point (ultimate deformation) are given in Table 3.20, for all the test series.

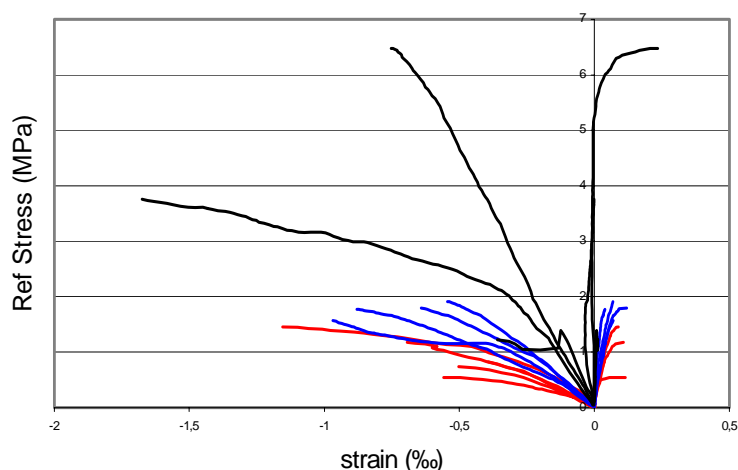


Figure 3.25 - Reference stress on diagonal compression tests: specimens without plaster (red), with plaster in both sides (blue) and with plaster in both sides and strengthened (black)

Table 3.20 - Diagonal compression tests: vertical ( $\varepsilon_v$ ) and horizontal ( $\varepsilon_h$ ) deformation at collapse

Group specimen	Number	$\varepsilon_v$ (‰)			$\varepsilon_h$ (‰)		
		average	min.	max.	average	min.	max.
without plaster	5	0.661	0.395	1.156	0.073	0.017	0.114
with plaster	4	0.759	0.544	0.969	0.075	0.039	0.120
with plaster and strengthened	3	0.929	0.359	1.676	0.082	-0.001	0.235

### 3.4.3.7 - Comparison of the results obtained for the masonry materials and masonry wallets

Table 3.21 summarises the results obtained for the tests on brick units, mortar and masonry panels (parallel and perpendicular to the bed joints and diagonal compression tests, for the nominal areas).

Table 3.21 - Summary table of materials (brick units and plaster) and masonry specimens test results

Element tested	Test	Symbol	Units	Value
Brick units	Compressive strength (parallel to the bed joints)	$\sigma_c^{\parallel}$	<i>MPa</i>	15.36
	Compressive strength (perpendicular to the bed joints)	$\sigma_c^{\perp}$	<i>MPa</i>	2.80
Mortar (joints and plaster)	Tensile strength	$\sigma_t$	<i>MPa</i>	0.59
	Compressive strength	$\sigma_c$	<i>MPa</i>	1.33
Masonry wallets Vertical and horizontal compressive tests (without plaster)	Compressive strength (parallel to the bed joints)	$\sigma_c^{\parallel}$	<i>MPa</i>	1.11
	Compressive strength (perpendicular to the bed joints)	$\sigma_c^{\perp}$	<i>MPa</i>	1.10
	Young modulus (parallel to the bed joints)	$E^{\parallel}$	<i>GPa</i>	0.991
	Young modulus (perpendicular to the bed joints)	$E^{\perp}$	<i>GPa</i>	1.873
Masonry wallets Diagonal compressive tests (without plaster)	Tensile strength	$\sigma_t$	<i>MPa</i>	0.233
	Shear modulus	<i>G</i>	<i>GPa</i>	0.657
Masonry wallets Diagonal compressive tests (with plaster in both sides)	Tensile strength	$\sigma_t$	<i>MPa</i>	0.575
	Shear modulus	<i>G</i>	<i>GPa</i>	1.171

The values presented in Table 3.21 show that:

- The compressive strength of the bricks in the direction perpendicular to the bed joints is 2.1 times higher than the compressive strength of the mortar, and for the direction parallel to the bed joints is 11.5 times higher.
- The tensile and compressive strength of the mortar is higher than the associated strength evaluated in the wall specimens (without plaster). It is noted that the collapse mechanisms, and consequently the strength, depends very much on the interface bricks/joints behaviour. The debility of the interface causes a masonry strength value lower than the strength of the components (mortar and bricks).
- For wall specimens without plaster, the compressive strength is approximately 5 times higher than the tensile strength.

- The shear modulus, for the specimens without plaster, is 0.45 times the elasticity modulus value obtained for the masonry specimens (considering the average value for the direction perpendicular and parallel to the bed joints). In EC6 it is considered that, in the absence of a more precise value, it may be assumed that the shear modulus,  $G$ , is 40% of the elastic modulus,  $E$ . The value obtained in the experimental tests is in accordance with this standard assumption.
- The tensile strength, in terms of nominal area, for the specimens with plaster, is 2.5 times higher than the one for the specimens without plaster, which confirms the strong influence of the plaster on the panels strength.

### 3.4.4 - Empirical estimation of the masonry strength

#### 3.4.4.1 - Infilled frames without apertures

There are several empirical models to estimate the strength of masonry infill panels. One of them has been recently proposed by Zarnic and Gostic (1998, 1997) and was calibrated against experimental results of masonry infilled reinforced concrete frames similar to the frames under testing in this study. Therefore, aiming to estimate the infill panels strength of the testing frame (presented in Section 3.4.4.4), the empirical expressions suggested by Zarnic and Gostic (1998, 1997) are used (see Figure 3.26).

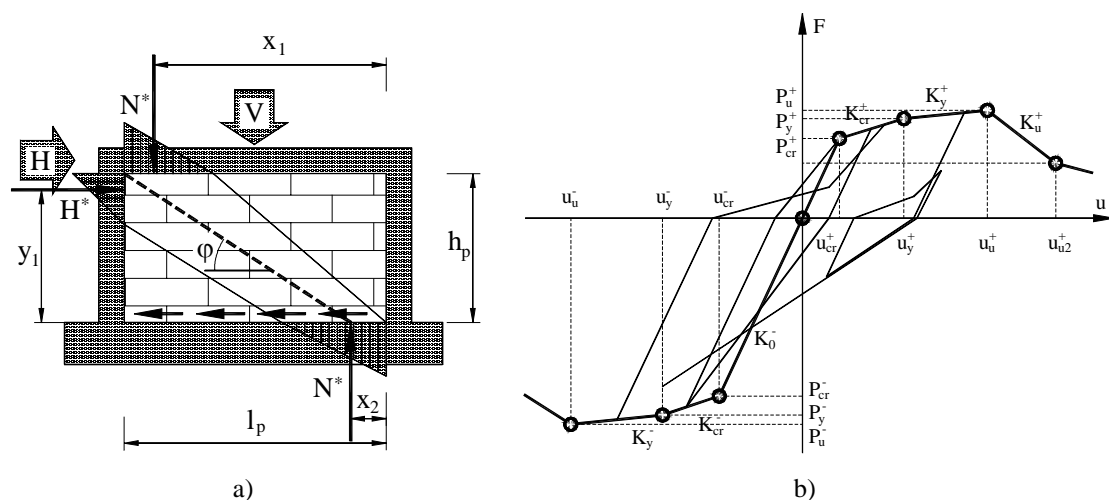


Figure 3.26 - Masonry model: a) simplified pattern of distribution of interactive forces between infill and frame; b) tri-linear non-symmetric envelope and hysteretic rules

For a confined infill masonry panel, the shear strength ( $H_{sp}$ ) can be evaluated by the following expression

$$H_{sp} = C_R \cdot \frac{A_p \cdot f_{tp}}{C_I \cdot b} \cdot \left( 1 + \sqrt{C_I^2 \cdot \left( 1 + \frac{\sigma_{oz}}{f_{tp}} \right) + 1} \right) \quad (3.9)$$

where

$$C_I = 2 \cdot \alpha \cdot b \cdot \frac{l_p}{h_p} \quad \alpha = \frac{(x_1 - x_2) \cdot h_p}{y_1 \cdot l_p} \quad (3.10, 3.11)$$

$$K_e = \frac{1}{\frac{h_p^3}{C_F \cdot E_p \cdot I_e} + \frac{1.2 \cdot h_p}{G_p \cdot A_e}} \quad A_e = A_p + 2 \cdot C_E \cdot A_f \cdot \frac{G_f}{G_p} \quad (3.12, 3.13)$$

$$I_e = I_p + 2 \cdot C_E \cdot \frac{E_f}{E_p} \cdot \left( I_f + A_f \cdot \frac{(h_c + l_p)^2}{4} \right) \quad (3.14)$$

$$H_{cr} = \frac{1}{3} \cdot H_y \quad \delta_{cr} = \frac{H_{cr}}{K_e} \quad (3.15, 3.16)$$

$$H_y = H_{sp} \quad \delta_y = 1.1 \cdot \frac{H_y}{K_e} \quad (3.17, 3.18)$$

$$H_u = H_y \cdot (1 - \nu \cdot (1 - \mu)) \quad \delta_u = \mu \cdot \delta_y \quad (3.19, 3.20)$$

the parameters appearing in equations (3.9) to (3.20) represent:

- For the dimensions and elastic parameters of the panel:  $l_p$  is the length,  $h_p$  the height and  $e_p$  the thickness of the infill panel;  $E_p$  is the Young modulus and  $G_p$  is the shear modulus of the masonry;  $A_p$  is the horizontal cross sectional area and  $I_p$  is the moment of inertia of the horizontal cross-section of the infill panel;  $\varphi_d$  is the inclination of the equivalent strut (used in numerical simulations of infill panels by diagonal struts).



- For the dimensions and elastic parameters of the frame:  $A_f$  is the horizontal cross-sectional area and  $I_f$  is the moment of inertia of horizontal cross-section of frame columns;  $E_f$  is the Young modulus and  $G_f$  is the shear modulus of the frame elements.
- For the homogenised mechanical properties and effective stiffness:  $A_e$  is the effective cross-sectional area and  $I_e$  is the effective moment of inertia of the horizontal cross-section of infilled frame;  $K_e$  is the effective stiffness.
- For the masonry strength:  $f_{tp}$  is the reference tensile strength;  $C_R$  is the quality factor of masonry construction works;  $C_I$  is the factor of interaction between infill and surrounding frame;  $\sigma_{oz}$  is the compressive stress acting on the horizontal cross-section of the infill panel;  $H_{sp}$  is the shear strength of masonry infill.
- For the ultimate strength of the equivalent strut:  $\nu$  is the post-yield slope of envelope curve;  $\mu$  is the ductility of the panel.

For numerical modelling using an equivalent strut model, the behaviour laws are defined for the axial direction of each strut on the basis of the three characteristic points (cracking –  $cr$ , yielding –  $y$  and ultimate –  $u$ ), for which force ( $P$ ) and displacement ( $\delta$ ) values are calculated from

$$P_{cr} = \frac{1}{3} \cdot P_y \quad \delta_{cr} = \frac{P_{cr}}{K_e} \quad (3.21, 3.22)$$

$$P_y = \frac{H_{sp}}{\cos \varphi_d} \quad \delta_y = 1,1 \cdot \frac{P_y}{K_e} \quad (3.23, 3.24)$$

$$P_u = P_y \cdot (1 - \nu \cdot (1 - \mu)) \quad \delta_u = \mu \cdot \delta_y \quad (3.25, 3.26)$$

### 3.4.4.2 - Reduction of strength and stiffness of the panels due to the presence of apertures

The presence of apertures (windows or doors) in the infill masonry panels modify their structural behaviour, having the following implications (Sortis *et al.*, 1999):

- Ultimate strength reduction.
- Stiffness reduction for the different deformation stages.
- Reduction of the loading corresponding to the initial cracking stage, with premature development of cracks due to the stress concentration in the aperture corners.
- Acceleration of the damage and loss of panel integrity, when no adequate strengthening of the aperture contour is provided.
- Reduction of the energy dissipation capacity.

The parameters characterizing the strength and stiffness reduction of the infill masonry due to the apertures are: *a*) ratio between aperture area and panel area ( $A_a$ ); *b*) ratio between the aperture width and panel width ( $A_c$ ); and, *c*) existence and type of strengthening in the aperture.

The ratio between aperture area and panel area ( $A_a$ ) and the ratio between the aperture width and panel width ( $A_c$ ) are given by

$$A_a (\%) = \frac{a \cdot b}{l \cdot h} \cdot 100 \qquad A_c (\%) = \frac{a}{l} \cdot 100 \qquad (3.27, 3.28)$$

where  $l$  and  $h$  are the width and height of the panel, and  $a$  and  $b$  represent the width and height of the aperture, respectively (see Figure 3.27-a).

Three classes of strengthening at the aperture (opening) sides are considered, namely:

- NS – non-strengthened aperture – when elements of reinforced concrete or steel profiles do not exist in any side of the aperture.
- SS – semi-strengthened aperture – when elements of reinforced concrete or steel profiles exist in the upper side of the aperture.

- AS – strengthened aperture – when elements of reinforced concrete, steel profiles or steel reinforcement exist at least at two opposite aperture sides.

An infill panel with aperture can be considered effective in terms of the influence in the structural behaviour, if the following conditions are verified (Sortis *et al.*, 1999)

$$A_a \leq 25\% \quad A_c \leq 40\% \quad (3.29, 3.30)$$

For numerical applications, the following reduction coefficient ( $r_{ac}$ ) for strength and stiffness can be computed (Sortis *et al.*, 1999)

$$\text{NS case} \quad r_{ac} = 0.78 \cdot e^{-0.322 \ln A_a} + 0.93 \cdot e^{-0.762 \ln A_c} \quad (3.31)$$

$$\text{SS case} \quad r_{ac} = 1.04 \cdot e^{-0.322 \ln A_a} + 1.51 \cdot e^{-0.762 \ln A_c} \quad (3.32)$$

$$\text{AS case} \quad r_{ac} = 1.25 \cdot e^{-0.322 \ln A_a} + 1.97 \cdot e^{-0.762 \ln A_c} \quad (3.33)$$

The previous expressions are applicable if all the following conditions are verified

$$r_{ac} \leq 1 \quad A_a \leq 25\% \quad A_c \leq 40\% \quad (3.34, 3.35, 3.36)$$

The infilled frame under study has four different infill panels, three of them with apertures. Figure 3.27-*b* represents schematically the different types of panels, identified according to the presence and type of aperture. Table 3.22 contains the calculations of the reduction strength and stiffness coefficient for the different panels with aperture. All the panels with aperture are of non-strengthened (NS) type, because no special strengthening was provided in any side of the apertures. From the results in Table 3.22, it can be concluded that:

- The applicability restrictions of the reduction factor approach are generally satisfied, with the exception of the parameter  $A_a$  for the panel type 2.
- Even the apparent small aperture in panel type 4 induces a drop of 57% in terms of strength and stiffness.
- The presence of apertures in panel types 2 and 3 causes a reduction of approximately 2/3 of the stiffness and strength, when compared with the solid panel.

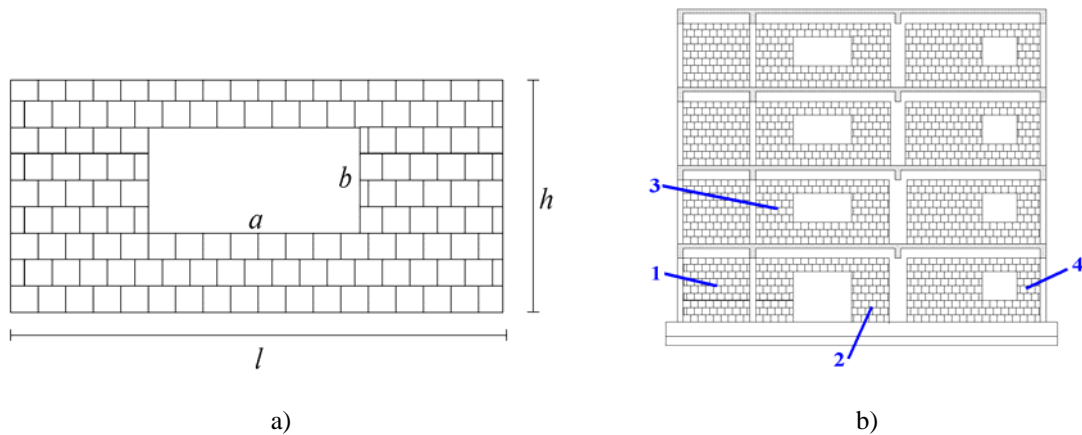
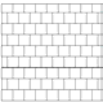
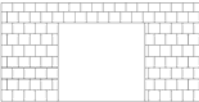
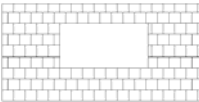
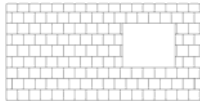


Figure 3.27 - Nomenclature: a) aperture and panel dimensions; b) identification of four panel-types

Table 3.22 - Reduction strength and stiffness coefficient for the panels

	1	2	3	4
Panel type				
$A_a$ (%)	---	34.6	19.8	11.9
$A_c$ (%)	---	43.5	43.5	26.1
$r_{ac}$	1.00	0.30	0.35	0.43

#### 3.4.4.3 - Drift limits for masonry infill walls

Experimental results from tests on confined masonry walls (Pinto, 1998) indicate that the infill panels can accommodate inter-storey drifts up to 0.1% without any significant damage and assume full collapse for inter-storey drifts higher than 0.4%.

Zarnic and Gostic (1998) obtained in a series of cyclic tests performed on a two-storey infilled reinforced concrete frame, constructed in 1:4 reduced scale, the peak lateral load resistance for a drift of about 0.15%.

Recently, Lafuente *et al.* (2000) on a basis of a series of tests on half-scale masonry infilled reinforced concrete frames subject to in-plane cyclic loads, suggested a lateral drift limit ( $\Delta$ ), in order to limit the damage in confined masonry walls, without important loss of strength. This limit is calculated from

$$\frac{\Delta}{H} < \frac{e}{700} \quad (3.37)$$

where:  $H$  represents the wall height and  $e$  the panel aspect ratio ( $e = H / L$ ), being  $L$  the length of the infill panel.

For the frame under study, and considering that the storey behaviour strongly depends on the behaviour of the short external panel (without openings), the limit in terms of drift, using the expression proposed by Lafuente *et al.* (2000) is 3 mm (0.11%).

#### 3.4.4.4 - Storey strength of the infilled frame

Using the empirical expressions to estimate the masonry strength given in Section 3.4.4.1, the correction due to the presence of openings (according to the methodology exposed in Section 3.4.4.2) and the average mechanical properties obtained from the infill masonry test specimens (Section 3.4.3.7), the strength of the first storey infill panels was computed. The procedure was conducted for each panel and for the complete storey. The curves have been derived assuming that the infill behaviour is represented by a multi-linear curve defined by four characteristic points, namely: cracking, yielding, collapse and ultimate. The cracking and yielding points are calculated by the empirical expressions given in Section 3.4.4.1 (expressions 3.22 to 3.25). The collapse point was assumed for an inter-storey drift of 1.2 times the yielding drift and with a post-yielding slope of 5% of the initial slope. The ultimate point corresponds to a drift 10 times higher than the collapse and the ultimate strength is 7% of the peak strength (collapse strength).

The resulting curves are given in Figure 3.28. They show that the short infill panel controls the storey stiffness and strength. The apertures reduce the initial stiffness and strength, as well as increase the inter-storey drift corresponding to the peak strength of the panel. The resulting storey shear-drift curve has a peak strength of approximately 750 kN, for a inter-storey drift of 0.11%, which is in line with the proposed value by Lafuente *et al.* (2000).

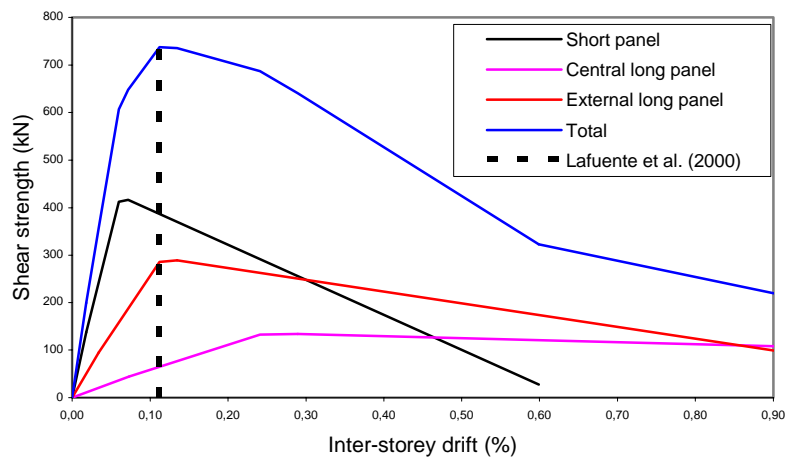


Figure 3.28 - Empirical shear-drift curves for the 1<sup>st</sup> storey confined masonry panels

The diagonal compression test results on the shotcrete wallets cannot be used to derive the empirical curves of the strengthened panel, because they are not reliable as discussed in Section 3.4.3.6. An alternative solution to estimate the mechanical properties and characteristics of the behaviour curve of the strengthened panel is to assume that there is deformation compatibility between the infill panel and the shotcrete layer. Assuming the simplified (bi-linear) tensile stress-strain curves (for the concrete and for the masonry wall), given in Figure 3.29-*a*, and weighting each component with its effective area, the resulting curves, in terms of reference strength, are represented in Figure 3.29-*b*. They show that the concrete tensile strength does not increase the peak strength of the strengthened wall, but increases the initial stiffness.

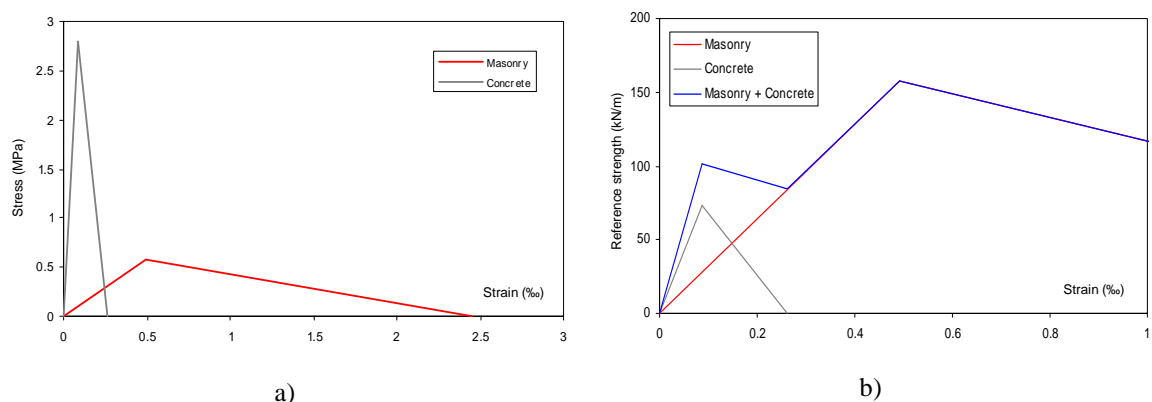


Figure 3.29 - Simplified tensile behaviour curves for the concrete and masonry

Therefore, it is concluded that the maximum strength of the strengthened frame is not increased by the application of the shotcrete. Nevertheless, an improved ductility capacity is expected due to the presence of the steel wire mesh, as well as lower stress levels for the same drift, due to the mobilization of a wider panel strut.

According to the behaviour curves of each infill panel, reflected in Figure 3.28, the resulting shear strength of the first storey infilled frame is approximately 750 kN. Assuming that the strength of the first storey of the bare frame is 200 kN and that it develops for an inter-storey drift of 0.55% (which is confirmed by the bare frame test results, see Section 4.2.1), the additional frame strength for a storey drift of 0.11% is 40 kN. Therefore, the maximum first storey shear capacity of the infilled frame is calculated by the sum of the infills strength (750 kN) and the bare frame strength (40 kN) for 0.11% drifts, which leads to a strength value of 790 kN.

The first storey shear capacity of shotcrete infilled frame should be similar to the infilled frame, as expressed in Figure 3.29.

### **3.5 - K-BRACING WITH SHEAR-LINK**

Retrofitting of buildings often leads to a significant increase in the lateral load resistance. Consequently, such solutions increase foundation loads under future earthquakes. Also, considerable disturbance for the occupants may occur. In comparison, the installation of a K-bracing with shear-link system causes relatively little disturbance and results in a design with a lateral load resistance similar to the initial resistance but with a significantly increased energy dissipating capacity. Hence, the risk of overloading the foundation can be significantly reduced (Bouwkamp *et al.*, 2000).

In fact, the retrofit work at each floor would be limited to only one bay, namely calling for: *i*) the removal of the brick infill wall in a single bay; *ii*) the installation of the specially designed pre-fabricated K-bracing system; and, *iii*) the placement of partition walls to cover the steel work (timber or metal studs with plasterboard sheeting). The proposed retrofit procedure may require strengthening of the columns of the bay in which the K-bracing is being placed, particularly at lower floor levels. However, such strengthening

can be incorporated in the K-bracing design and does not need strengthening of the column itself.

Specifically, the K-bracing with shear-link system consists of an eccentrically braced steel assembly with a vertical shear-link located at mid-span of either the upper or bottom floor beam (see Figure 3.30). The brace assembly consists of a set of diagonal braces, arranged in a V or inverted-V like fashion, and two horizontal steel beams, one of which with a short steel beam stub in the middle of the beam serving as vertical shear-link. In addition, vertical steel straps or actual steel sections connected to the adjacent columns are part of the assembly. The steel beams and straps are installed first in the open bay and anchored, respectively, to the beams, floor slab and columns. Subsequently, the vertical steel straps are welded to the ends of the steel beams to provide a closed force resisting system. Finally, the braces are installed and welded to the gusset plates (one at the end of the shear-link and one on each end of the opposite beam).

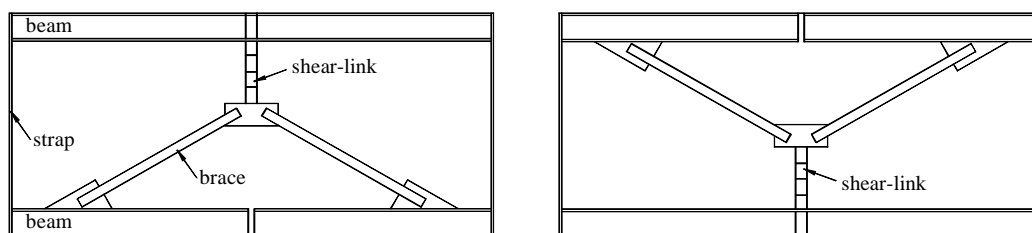


Figure 3.30 - K-bracing with shear-link system: possible layouts

The K-bracing with shear-link retrofit design concept, summarised above, was applied to the full-scale structure at the second storey of the masonry-brick infilled test frame shown in Figure 3.31. A detailed description of the design process can be found in Bouwkamp *et al.* (2000). The effectiveness of the retrofitting system will be assessed subsequently by studying the response of the retrofitted second floor frame/wall system under increasing cyclic displacement-controlled loads (holding the lateral displacement of the second floor constant throughout the test and imposing identical displacements at the third and upper floor levels, see Figure 3.36). In order to maintain structurally a symmetric layout, it was decided to retrofit the second storey frame by replacing the infilled wall of the 5.00 m wide middle bay by the k-bracing with shear-link (see Figure 3.31). In order to allow a fundamental assessment of the proposed retrofitting procedure the outer 2.50 m and 5.00 m



wide bays were filled completely with hollow-brick masonry of the type used in the other test series (see Section 3.4.3).

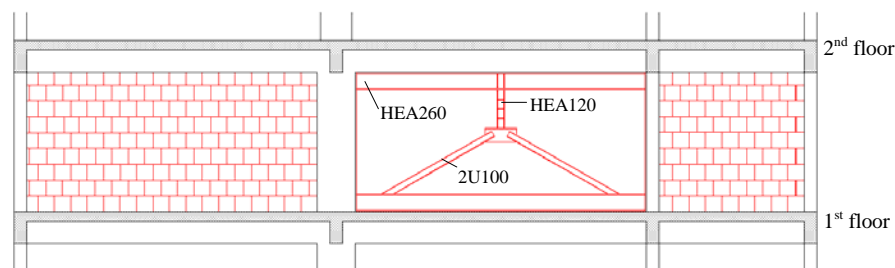


Figure 3.31 - K-bracing with shear-link system test assembly

Details of the bracing, shear-link, beams, straps and templates are given in Appendix A (Figures A.35 to A.45). The shear-link is shown in Figure A.49. For anchoring the steel beams and metal side straps to the surrounding concrete, new chemical HVZ M16 anchors from HILTI, placed in pairs, one on each side of the beam webs and centrelines of the metal straps were used (see Figures A.46, A.47 and A.48, for details on anchoring the steel beams and straps to the concrete columns, top and bottom beams, respectively).

### 3.6 - REPAIR AND STRENGTHENING OF THE FRAMES

#### 3.6.1 - Damage-state after the pseudo-dynamic tests

The testing campaign comprised several pseudo-dynamic earthquake tests on the bare, infilled and retrofitted frames for several earthquake intensity levels. In order to assess the ultimate capacity of the bare frame (BF) and of the selective repaired frame (SR), a final capacity cyclic test was foreseen. However, the local damages inflicted on the structures inhibited these final capacity tests, which required repair of the local damages as well as strengthening using carbon reinforced composites.

The tests performed on the frames with masonry infill walls led to several local damage (shear-out) of a few columns (top part) with lateral dislocations of the external columns of 50 mm, approximately 25% of the column cross-section characteristic height (see

Figures 3.32, B.27 and B.28). Relocation, repair and strengthening of the column/joint parts were required to carry out the final capacity tests.

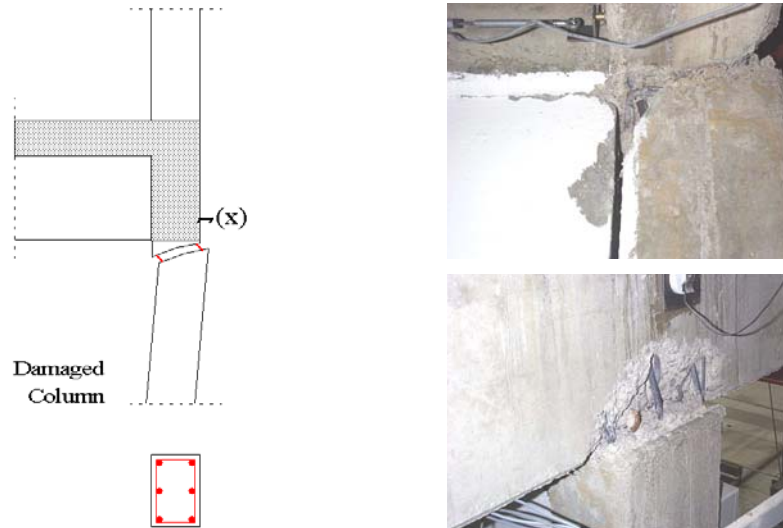


Figure 3.32 - Failure (shear-out) of the column/joint interface

A detailed description of the repair and strengthening of the two frames for the final capacity tests, including photographic documentation, materials used and their properties can be found elsewhere in Pinto and Varum (2000). Next, a summary of the materials used in the repair works is presented, as well as a photographic documentation and further relevant details of repair strengthening operation.

### 3.6.2 - Repair and retrofitting using composite carbon fibre materials

In order to recover the vertical load carrying capacity of the external dislocated columns, repair of these columns/joints was carried-out following the steps listed in Table 3.23. Figure A.52 shows the schemes and pictures of the intervention at different phases of the repair work as defined in Table 3.23.

Table 3.23 - Repair operations (general steps)

Step	Repair operation
1	Unload frame (remove additional vertical loads in the external bays)
2	Remove infill walls and bracing system
3	Up-lift floors (1 <sup>st</sup> and 2 <sup>nd</sup> ) near to the external column
4	Remove concrete at the top of the damaged column (20 cm)
5	Positioning/Relocation of the columns <sup>a</sup> to its original vertical position
6	Concreting of the columns/joints
7	Apply, in each column/joint, external carbon fibre repair system (column upper part and joint)

a) Marked in Figures A.53 and A.54.

### 3.6.3 - Material properties

The repair and strengthening materials were special concrete (to replace existing crushed concrete and the parts destroyed to allow relocation of the columns) and carbon fibre composites to reinforce and confine the new concrete and weak parts of the existing structure (e.g. joints and columns heavily damaged). The repair works were carried out by the ELSA laboratory and an external company using SIKA products.

To repair the joints and other damaged zones (spalling in the columns) a mortar type *Sika MonoTop-622* was used, which nominal technical properties are given in Pinto and Varum (2000).

The carbon fibre strengthening composite material used is a registered trademark of SIKA, with commercial mark: *SikaWrap Hex-230C/Sikadur-330 LVP*. This composite material is appropriate for strengthening/repair of the structural members composed of reinforced concrete and is an externally applied technique. The composite components are: carbon fibre fabric *SikaWrap Hex-230C* with the epoxy based impregnation resin *Sikadur-330 LVP*. A technical description of the materials used in the repair of the heavy damaged elements is given in Pinto and Varum (2000).

### 3.6.4 - Application to repair and strengthening of the frames

#### 3.6.4.1 - Overview

The preparation and execution of the repair and strengthening works (see Figure A.52 to A.59) for the six external top-columns/joints and for one internal strong-column at the first storey (in shear) were carried-out in four working days. The time elapsed being a period of two weeks between the application of the first repair products and when the final operation was carried out. Detailed information on the progress is given in Table 3.24.

Table 3.24 - Repair and strengthening (works timetable)

Dates (2000)	Repair work	Executed by
11/7	Remove concrete at the top of the damaged column (20 cm). Positioning of columns <sup>a</sup> to its original vertical position	ELSA laboratory
18/7	Concreting of the external heavy damaged joints and column (1 <sup>st</sup> storey, strong-column, frame A). Lightly cover reconstruction (columns 1 <sup>st</sup> storey). Injection of cracks on beams (with resin)	External company <sup>b</sup>
31/7	Roughening of the external superficies (column and joints) for application of carbon fibre system. External carbon fibre repair system of the strong-column	External company <sup>b</sup>
1/8	External carbon fibre repair system of the heavy damaged joints	External company <sup>b</sup>

a) Marked in Figures A.53 and A.54.

b) External company with large experience in the employment of composite materials.

#### 3.6.4.2 - Concrete repair and crack injection

Most of the large cracks in critical zones were injected with epoxy resin (*Sikafix 50 E*). The parts of spalled concrete were removed and new concrete was used to replace it. Figures A.53 and A.54 schematically show the location of the interventions and also specify the type of these interventions. It should be underlined that many other zones would require light interventions (mainly crack injections), but they were considered not particularly relevant for the tests to be carried out (the final capacity tests).

### 3.6.4.3 - Carbon fibre application

A single layer of carbon fibre was used in all strengthening interventions. Furthermore, the carbon fibre fabrics used are unidirectional, which requires control during their application. In fact, they must be oriented along the direction requiring strengthening. For required bi-directional strengthening two superposed carbon orthogonal oriented fibre fabrics must be used and, for shear-controlled situation, inclined carbon fibre fabrics are required, unless multi-oriented fabrics are used. Figures A.57 and A.58 schematically represent the direction of the fibres per use, for the strengthening of the columns and joints, respectively.

#### *Column:*

As shown in Figure A.55, the first floor strong-column suffered heavy damage at the base and top extremities. Shear failure at the bars termination zone (0.70 m from the column base) was particularly evident. Therefore, it was necessary to increase strength and to provide sufficient confinement in the critical zones, including the bars termination zone. According to these requirements, confinement was continuously provided from the base up to 0.90 m, and the top column confinement was limited to the last 0.30 m. The strong-column was wrapped at these critical regions. The carbon fibre fabric was only available in 0.60 m width pieces. At the base of the strong-column, the fabric was used on the first level up to a height of 0.60 m and on the second level, at a height of 0.30 m, without any lateral superposition. Figure A.56, show pictures of the column repaired.

#### *Joints:*

As already explained, a few joints were seriously damaged and some columns were dislocated from their original positions due to the shear-out effect caused by the infill panels. They were forced back to their original position and partially reconstructed. However, it is known that reconstruction processes do not provide lateral resistance for horizontal or even vertical loads. It was therefore necessary to provide confinement to the joint and anchoring top-columns to the adjacent beams, which was provided by means of a carbon fibre fabric layout schematically represented in Figure A.58. Fabric 1 in this figure provides resistance to the joint, top of the column and column/joint interface. Fabric 2 provides resistance of the joint in the orthogonal direction and increases adherence of fabric 1. Fabric 3 increases adherence of fabric 2. Fabric 4 provides confinement to the upper part of the column. Anchoring of the column to the internal beam is somewhat

disregarded, but it is too difficult to perform (due to the geometry of the joint) and it is believed that such a carbon fibre layout is sufficiently strong for a bare frame configuration (sufficient to avoid the dislocation of the columns during the final capacity tests). For the phase 4, illustrated in Figure A.58 (upper part of the column), the carbon fibre was applied with a longitudinal superposition of 10-12 cm. Figure A.59, show pictures with the operation phases of the joint retrofitting.

### **3.6.5 - Remarks**

The use of fibre reinforced polymers in seismic repair and retrofit seems to be an economical alternative to traditional materials and technologies allowing addressing most of the deficiencies commonly found in non-seismic resisting structures. However, there is a lack of experimental evidence on the performance of structures and elements repaired or retrofitted with FRP's. Moreover, there is a lack of specific codified rules for design (redesign), which represents a major drawback and delays a much wider use and application of FRP's in seismic retrofit.

It should be noted that specialized companies, producers of composite materials or their associates carried out most of the repair and strengthening works using fibre composite materials. Technical characteristics of the products, including nominal values for 'adherence' between fabrics and concrete are not systematically made available, which could be a commercial strategy or a consequence of lacking of fundamental reliable data for civil engineering applications. This fact creates serious problems for the widespread use of these materials in repair and strengthening of existing structures. Urgent actions should be taken by universities and technical communities to teach and update technical background in the field. Furthermore, appropriate norms and design guidelines for strengthening of existing structures with FRP's should be developed (Pinto *et al.*, 2001-*b*; Pinto and Varum, 2000).

### 3.7 - TESTING PROGRAMME AND TEST SET-UP

The complete testing programme (see Table 3.1) for the two RC frames intended to determine the original capacity of the frames with and without infill panels and to assess and compare performances of different retrofitting solutions.

For each test series (bare, selective strengthened, infill and infill strengthened frames), the frame was subjected to increasing earthquake intensities (from moderate to high intensities, as given in Table 3.25), in order to reach different damage levels. The return periods for the input motions were chosen so as to test the structure under the different seismic hazard levels specified in the VISION-2000 (SEAOC, 1995). These correspond to the 'Rare' (475-yrp) and 'Very Rare' (975 and 2000-yrp) events, under which a structure has to meet the 'Life Safety' and 'Collapse Prevention' performance levels, according to the minimum acceptable performance objectives for buildings of normal occupancy and use.

Table 3.25 - PsD testing programme of RC frames (bare and infilled)

Frame	Test	Input motion <sup>a</sup>	Testing date (1999)	Label
A and B	Dynamic characterisation (frequencies and modal shapes)	---	10-11/06	---
	0 – Very low seismic test <sup>b</sup>	<sup>b</sup>	5-9/07	---
	1 – Bare	475-yrp	13/07	BF475
	2 – Bare	975-yrp <sup>c</sup>	14/07	BF975
B	3 – Bare + Selective <sup>d</sup>	475-yrp	16/09	SR475
	4 – Bare + Selective <sup>d</sup>	975-yrp	16/09	SR975
	5 – Bare + Selective <sup>d</sup>	2000-yrp	17/09	SR2000
	0 – Very low seismic test <sup>b</sup>	<sup>b</sup>	28/09-5/10	---
	1 – Infilled	475-yrp	6/10	IN475
	2 – Infilled	975-yrp	7/10	IN975
A	3 – Infilled	2000-yrp <sup>e</sup>	8/10	IN2000
	4 – Infilled + Infill strengthened <sup>f</sup>	475-yrp	16/12	SC475
	5 – Infilled + Infill strengthened <sup>f</sup>	975-yrp	17/12	SC975
	6 – Infilled + Infill strengthened <sup>f</sup>	2000-yrp	21/12	SC2000

a) Duration of the input motions is 15 seconds, for the earthquake PsD tests.

b) Very low seismic test for checking testing system (loading and measuring systems) – 5% intensity of the 475-yrp.

c) Test performed up to 7.5 seconds because imminent collapse was attained.

d) Repair of damaged parts + strengthening only for strong-column.

e) Test performed up to 5.0 seconds because imminent collapse was attained.

f) Shotcrete over the infills 25 mm – light steel mesh – one face – one bay – no connection.

The pseudo-dynamic tests on the bare frame and on the strengthened frame using selective methods are deeply described in Pinto *et al.* (2001-*a*; 1999-*a*; 1999-*c*), and on the infill frame and infill strengthened frame in Pinto *et al.* (2002; 2001-*c*).

The cyclic test on the RC infilled retrofitted frame, with the K-bracing with shear-link dissipative device, was labelled as KB-cyclic test. The final capacity cyclic tests programme performed on the bare and selective strengthened frames is summarised in Table 3.26 (see also Table 3.1).

Table 3.26 - Final capacity cyclic testing programme of RC frames

Frame	Test	Testing date (2000)	Label
A	Bare <sup>a</sup>	7/11	BF-cyclic
B	Bare + Selective	10/10	SR-cyclic

a) The bare frame was recovered from the infilled frame, removing the infills.

### 3.7.1 - Additional masses

The masses used in the PsD algorithm are introduced numerically, and were considered 44.6 *ton* for the first three storeys and 40.0 *ton* for the fourth storey (in accordance to the load distribution, see Section 3.2.6). These masses are assumed to be concentrated at each DOF (storey). For the PsD test algorithm, it is enough to consider numerically this distribution of masses. However, in order to correctly consider the internal forces in the frame, corresponding to the idealised force distribution, it was necessary to use additional masses in the tested structures.

Hence, additional masses were placed in each floor by means of concrete blocks, steel plates, big sandbags and large water containers. These additional masses simulate live loads, finishings, partitions and other self-weights. Their distribution, shown in Figure 3.33, is such as to represent as closely as possible a real scenario (in terms of load distribution in the floors and in terms of distribution between columns and beams). In the figure, additional masses are represented in *tons*.

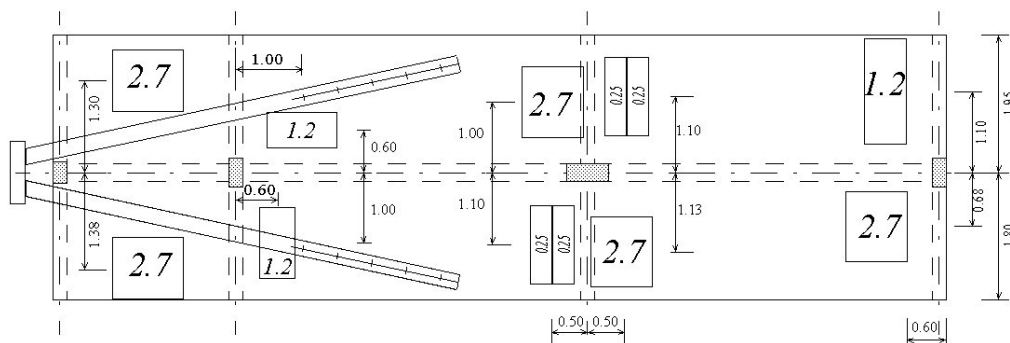
The additional vertical loads used in the tests were obtained by subtracting the weight of the specimen (including provisory stairs, jacks and respective attachment system) from the loads represented in the scheme shown in Figure 3.7. Also the lateral equilibrium of the



frames was assured with the adopted distribution of additional masses (it should be underlined that the slab is not symmetric: 1.80 m on one side, versus 1.95 m on the other). Other constraints were the additional loads available in the laboratory and the distribution of the testing equipment, as well as, all the instrumentation installed in the frames. Examples of the additional loads used are shown in Figure A.17.

The same distribution of additional loads was considered for the bare frame and for the infilled frame, meaning that the weight of the infill panels was neglected.

1<sup>st</sup>, 2<sup>nd</sup> and 3<sup>rd</sup> floors



4<sup>th</sup> floor

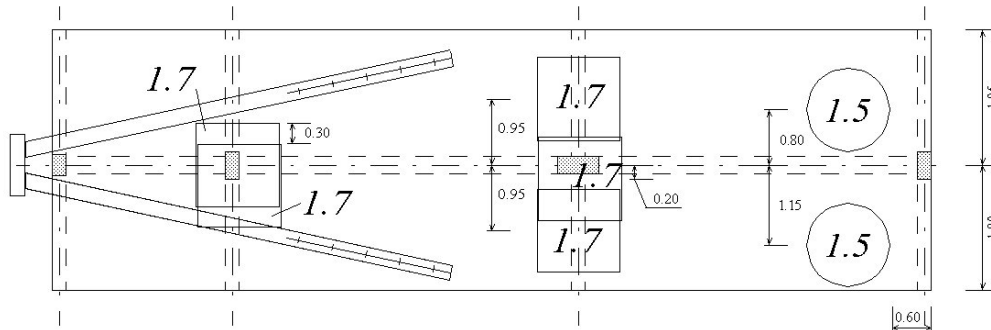


Figure 3.33 - Distribution of the additional loads

To perform the final capacity cyclic tests, removal of the masonry walls and removal of the K-bracing system required dislocation and/or removal of great part of the additional loads from the three first floors. Using the water reservoirs acquired in the meantime by the ELSA laboratory, which allow for faster and safer operations, a slightly different scheme for the floor distribution of the additional masses was adopted, but the initial distribution of the axial loads in columns was guaranteed. Figure A.31 illustrates the additional water reservoirs system adopted.

### 3.7.2 - Reaction-wall

The European Laboratory for Structural Assessment (ELSA) is a large-scale facility of the Joint Research Centre of the European Commission. It consists of a 16 m high, 21 m wide reaction-wall hollow core with a total thickness of 4 m, and it is designed to resist the forces, which are necessary to deform and seriously damage full-scale models of structures (see technical data summarized in Figure 3.34 and Table 3.27). In addition to static and cyclic testing capabilities, the facility is equipped to perform tests utilizing the pseudo-dynamic (PsD) testing method which enables, for instance, the simulation of earthquake loading of full-scale buildings.

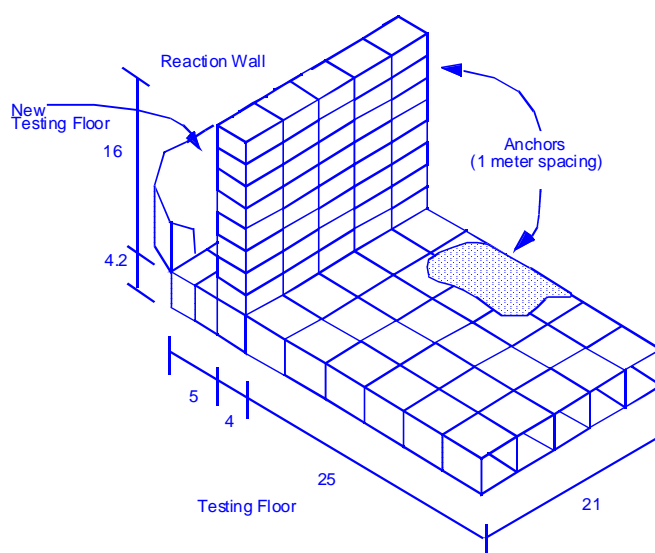


Figure 3.34 - Reaction wall/floor facility (dimensions in *m*) at the ELSA laboratory (Pinto, 1998)

Table 3.27 - Characteristics of the ELSA reaction-wall (adapted from Pinto, 1998)

Load capacity	Reaction wall	Bending moment	200 <i>MN·m</i>
		Base-shear	20 <i>MN</i>
	Reaction floor	Bending moment	240 <i>MN·m</i>
	Anchor load	Axial force	500 <i>kN</i>
Hydraulic characteristics	Flow		1500 <i>l/min.</i>
	Pressure		210 <i>bar</i>
	Actuators	Load	0.5 to 1.0 <i>MN</i>
		Stroke	± 0.25 to ± 1.0 <i>m</i>

Many of the advantages of the PsD implementation at ELSA laboratory are due to the fully digital, in-house designed, system architecture. The system is based on distributed control units, connected via optical fibre to the master PsD computer. Measurements are done by optical digital transducers, interfaced to the control units without the need of analog conversion (Pinto, 1998).

### 3.7.3 - Pseudo-dynamic test method

The PsD testing technique is based on the modelling of a system by a discrete equation of motion

$$M \cdot a + C \cdot v + r(d) = p(t) \quad (3.38)$$

where:  $M$  is the mass matrix,  $C$  is the viscous damping matrix,  $a$ ,  $v$ ,  $d$  and  $p$  are the vectors of acceleration, velocity, displacement and external load, respectively, which are functions of time  $t$ , and  $r$  is the vector of restoring forces, which is a non-linear function of the displacements. Within this model,  $M$ ,  $C$  and  $p(t)$  are known data, while  $r(d)$  is directly measured on line (Donea *et al.*, 1996; Molina *et al.*, 1999-b).

In PsD testing, the inertia and viscous damping forces are simulated numerically and the corresponding matrices may be calculated from the preliminary dynamic identification tests performed on the structure (e.g. free vibration and stiffness tests). Alternatively, these matrices are computed by the static condensation of the matrices corresponding to the complete structure to the degrees of freedom of interest. The numerically modelled inertia and viscous damping forces are a relatively straightforward matter compared to the non-linear structural restoring forces, which are measured experimentally because of the difficulty in modelling them accurately. The process automatically accounts for the hysteretic damping due to inelastic deformation and damage of the structural materials, which is the major source of energy dissipation. Typically, the viscous damping matrix  $C$  is considered null in a PsD test (Pinto *et al.*, 1996).

Usually, an explicit integration scheme is used by means of which, at every step, the computed displacement is quasi-statically imposed to the specimen and the required forces are simultaneously measured. By using many actuators of the required capacity, the

---

method can be applied to test large structures with clear advantages with respect to a shaking table test (Donea *et al.*, 1996; Molina *et al.*, 1999-*b*).

To simulate the earthquake response of a structure, a record of an actual or artificially generated earthquake ground acceleration history is given as input data to the computer running the pseudo-dynamic algorithm. The displacements of the controlled horizontal degrees of freedom (where the mass of the structure can be considered concentrated) are calculated for a small time step using a suitable time integration algorithm. These displacements are then applied to the structure by servo-controlled hydraulic actuators fixed to the reaction wall. Load cells mounted in series with the actuators measure the forces necessary to achieve the required displacements and these structural restoring forces are returned to the computer for use in the next time-step calculation (Pinto *et al.*, 1996).

In a classic PsD test, every integration time step typically takes at least one second of time, which allows for the imposing of the ramp of incremental displacements, followed by the stabilisation of the system, before the forces are measured, after which the next displacement is computed. However, in an 'accelerated' continuous PsD test, as currently implemented at the ELSA laboratory (Magonette *et al.*, 1998), every integration time step takes just 2 *ms*, which is also the sampling period of the closed-loop controllers of the actuators. Within that time-lapse, the same CPU, which is in charge of the control algorithm, reads the force, integrates one step in the equation of motion and corrects the target according to the new computed displacement. The accelerogram history is subdivided into very small time increments (0.02 *ms*, for example) so that the displacement increments can appropriately be followed by the pistons in just 2 *ms*. Thus, for a real size specimen with several DOF's, a typical test time scale of  $\lambda = 2 / 0.02 = 100$  can be reached, which mean being around ten times faster and still rendering results much more accurate than those obtained by means of a classic PsD test performed using the same hardware.

#### **3.7.4 - Horizontal loading system**

In the PsD test of a building, one horizontal displacement (one DOF) is considered per floor. Displacements are applied to the structure, at each floor-level, by means of an actuator, as shown in Figure 3.35, which is, in the present case, a double-acting servo-

hydraulic actuator with 500 kN maximum load capacity. Actuators are connected by cylindrical joints to the reaction wall, on one side, and on the opposite side attached to the V-loading frame, which transmits the forces to the floor, at the middle of the central span of the structure, at each floor level (see Figure 3.5). The pictures depicted in Figures A.16 and A.18 show the four actuators linked to the load cells.

The evolution of forces is measured by piezoresistive load cells mounted at the end of the piston. The structural displacements were measured with respect to an external steel unloaded reference frame, mounted on the reaction-floor.

The structural displacements are measured, at storey level, using HEIDENHEIN optical transducers with 2  $\mu\text{m}$  resolution, which provide a digital output of very high precision. These displacements are the ones used in the PsD algorithm, instead of the displacements measured at the actuator levels. The storey displacements measured relatively to the external reference frame should correspond to the global structural deformation. On the other hand, the displacements measured on the jacks include not only the structural deformation, but also the deformation of the attachment system and a slight deformation of the reaction-wall. Figure A.19 contains a picture showing the HEIDENHEIN optical transducers and their external fixing support (steel frame).

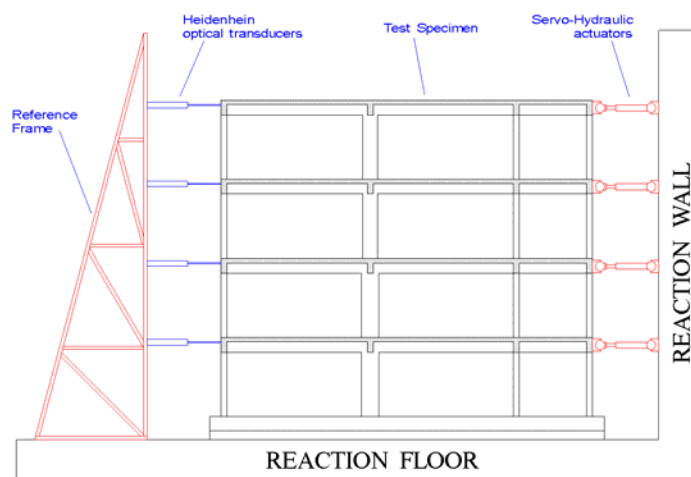


Figure 3.35 - General layout of the pseudo-dynamic test: reaction-wall, structure, pistons and reference steel-frame

To perform the cyclic test at the 2<sup>nd</sup> storey level (K-bracing test), actuators were placed at the 1<sup>st</sup> and 2<sup>nd</sup> storey levels, as represented in Figure 3.36. Displacements are applied to the

structure at the 2<sup>nd</sup> floor-level, imposing constant zero displacement at the 1<sup>st</sup> storey. The double-acting servo-hydraulic actuators used in this test can develop 1000 kN maximum load.

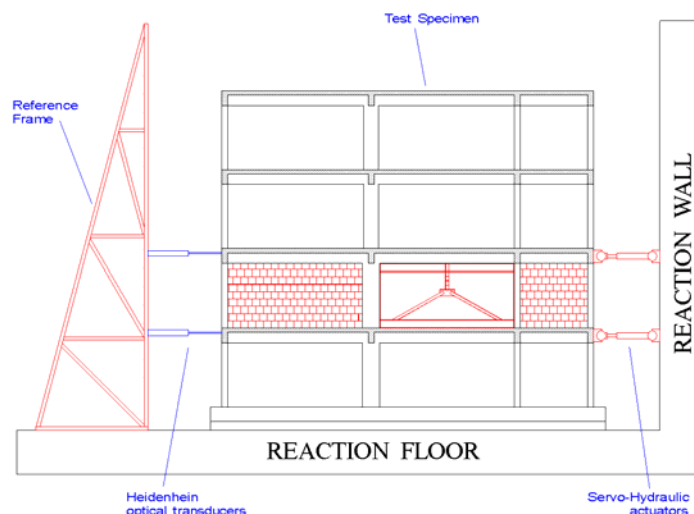


Figure 3.36 - General layout of the 2<sup>nd</sup> storey cyclic test: reaction-wall, structure, pistons and reference steel-frame

The plane frames have a very low strength in their orthogonal direction. But, out-of-plane deformation is controlled through a system of hinged steel members which connect, at each floor, the frame being tested, to the other frame. The frame that is not being tested is fixed to the reaction-wall (at one end) and to an out-of-plane steel frame (at the other end), as shown in Figures A.15 and A.16.

### 3.7.5 - Instrumentation of the RC frames

The instrumentation used in the ELSA laboratory tests is usually divided into two groups. The first group is reserved to measurements related to the pseudo-dynamic algorithm and comprises storey displacements and forces. All the other measurements (labelled standard acquisition), constituting the second group, are treated and recorded separately.

For the tests on the bare and selective strengthened frame, a total of 151 acquisition channels were used. Eight of the 151 channels were used for the PsD algorithm measurements, which include four optical transducers used to measure displacements at each storey level, with the corresponding four restoring forces measured by calibrated load

cells mounted in series with the actuators. The remaining 143 channels are reserved for the standard acquisition.

Standard measurements include the acquisition of the rotation at several points (sections) in the structure and other three groups of relative displacements. These three relative displacement groups were defined having in mind the purpose of the measurements. The relative displacements are measured using a set of displacement transducers (potentiometers) with measuring capacities of 25, 50 and 100 *mm*, depending on the maximum deformation expected at each measuring point. The sensitivity of these potentiometers is 2.66, 5.14 and 10.14 *mm/V* for the 25, 50 and 100 *mm*, respectively when powered at 5 *Volts*.

All transducers are connected in groups of 16 channels to the data acquisition system, where data from all channels are sampled and averaged for each step. Each relative displacement transducer, inclinometer and strain-gauge is associated with two reference numbers (see figures with instrumentation), namely: *i*) the file number where the test results are recorded; and, *ii*) in brackets, the board channel in the data acquisition system. The positive signal is associated to elongation of the transducers, to clock-wise rotation at inclinometers, and to tension at strain-gauges.

In what follows, each group of instrumentation used is presented individually, including the respective location schemes and the conventions adopted. The pictures in Figures A.18 and A.19 show the actuators and displacement controllers at floor levels, whilst Figures A.21, A.22 and A.23 show the instrumentation, namely: instrumentation on the strong-column (1<sup>st</sup> storey), instrumentation on the slab and inclinometers.

#### *3.7.5.1 - Rotations: inclinometers*

The distribution of inclinometers was maintained for all the PsD tests. Rotations are measured at columns, beams and joints and are achieved by means of sixty-four digital inclinometers. Inclinometers with five-degrees measurement capacity were used for the columns and joints/beams in the strong-column vicinity (forty-six inclinometers) and one-degree capacity for the remaining inclinometers (located at the other beams and joints). The definition of the inclinometers capacity was prescribed according to the expected

maximum rotation at each point on the structure. In Figure 3.37 is represented the location and numbering of the inclinometers used in the testing campaign. Such configuration provides important information regarding the response of structural members, such as global rotation at the beam and column ends, relative rotation between sections, deformation along the strong-column line and joint deformation. Figure 3.38 gives location details of the inclinometers layout at two of the structure zones. Figure A.23 depicts examples of inclinometers.

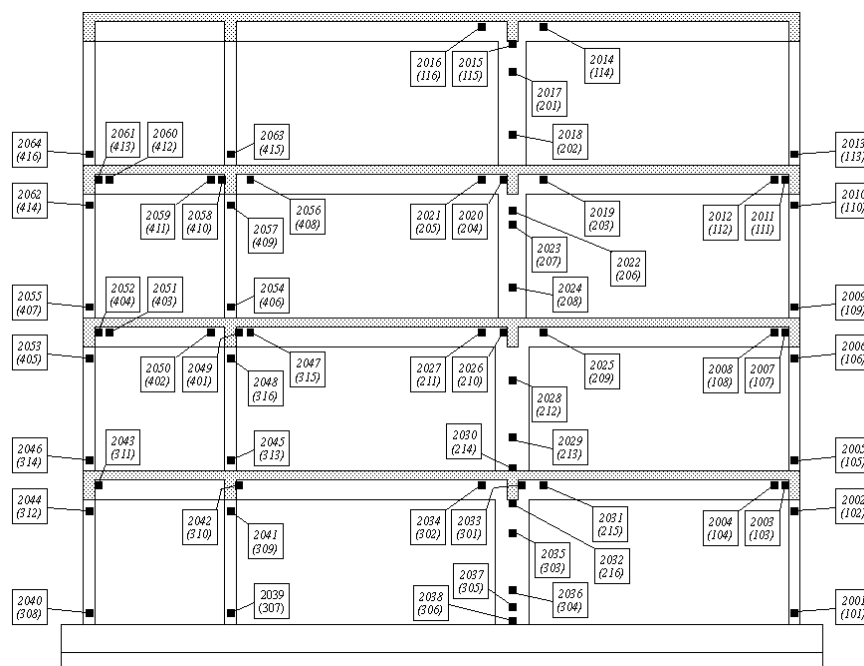


Figure 3.37 - Location of the 64 inclinometers

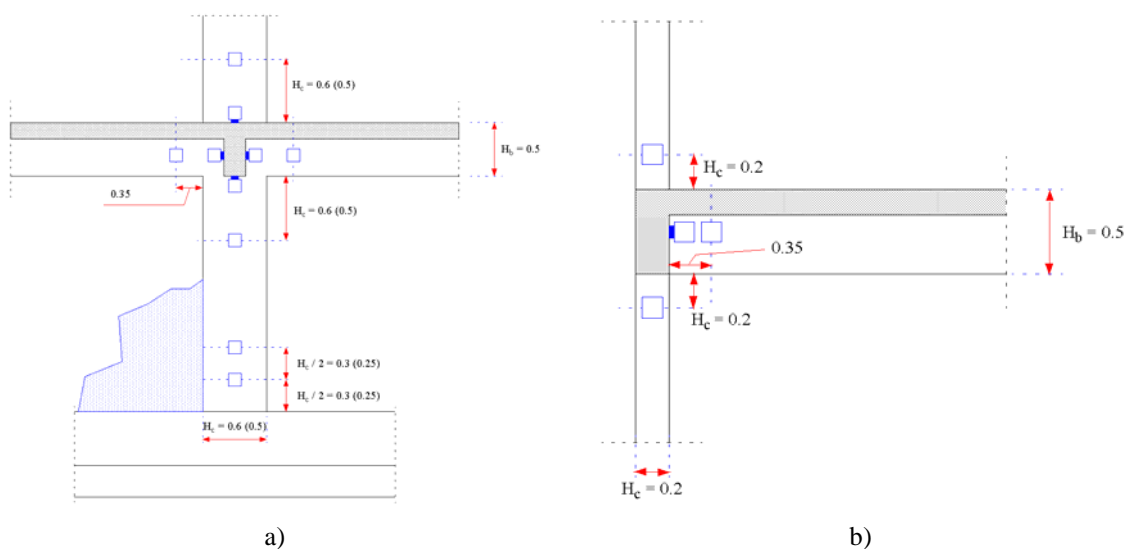


Figure 3.38 - Inclinometers location scheme: a) strong-column; b) slender-column



### 3.7.5.2 - Beam deformation at first floor level

A series of thirteen pairs of potentiometer displacement transducers (13 top and 13 bottom) were used to measure longitudinal deformation at the first floor beam. Figure 3.39 represents the instrumentation used to measure the beam deformation. With this instrumentation, it is possible to capture the rotation of all the sections monitored and the axial deformation of the beam can also be investigated. The base length for the plastic hinge was assumed with  $350\text{ mm}$  (which corresponds to approximately  $2/3$  of the beam depth,  $H$ ). In order to study the plastic hinge length, the distribution of the instrumentation in the zones nearest to the strong-column was increased.

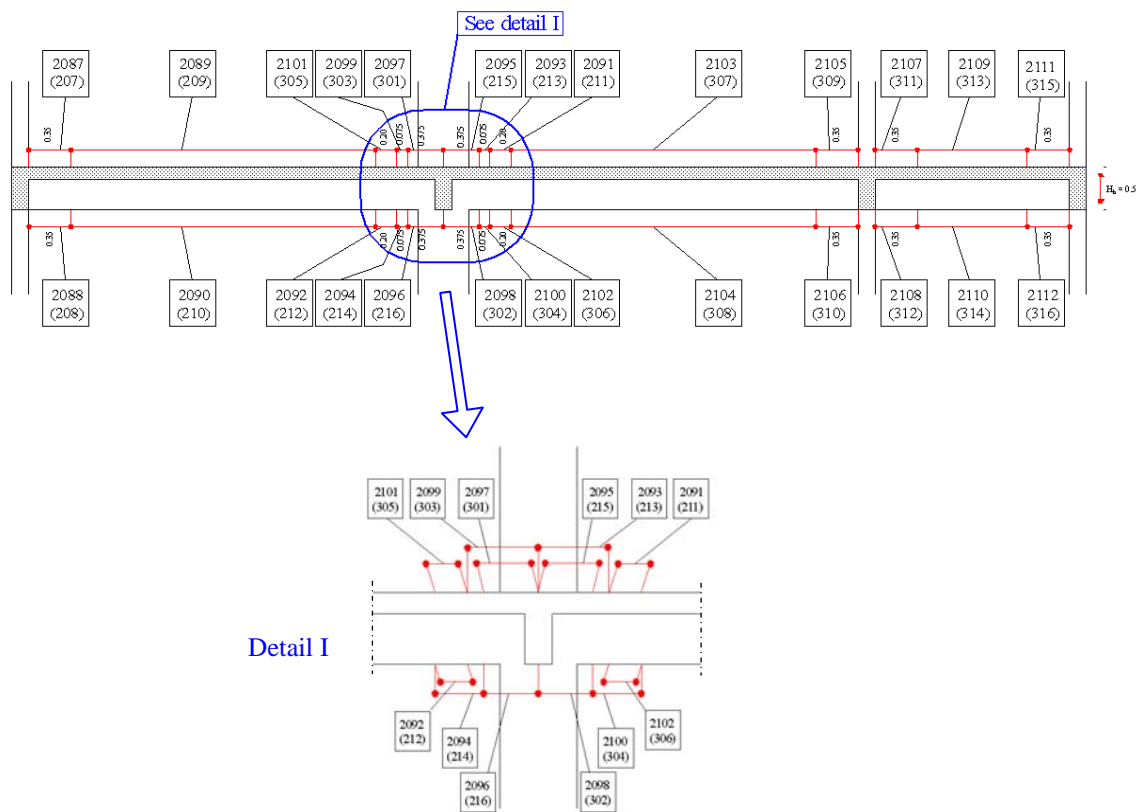


Figure 3.39 - 1<sup>st</sup> floor beam instrumentation: general layout, dimensions and detail of the zone nearest to the strong-column

### 3.7.5.3 - Slab-participation

In order to measure the contribution of the slab (slab-participation), twenty-six transducers were placed at the top and bottom of the first floor slab, in critical zones, with a base length of 350 mm from the column face, as shown in Figure 3.40. Figure A.22 shows a picture with the transducers arrangement in the slab. With the selected locations for the instrumented slab zones it is possible to contrast the slab-participation in a long span-bay versus a short span-bay, as well as, between interior and exterior joint zones. Two of the foreseen transducers on the top slab (#112 and #119) were not used, because the respective positions coincide with the attachment system used to impose the storey displacement.

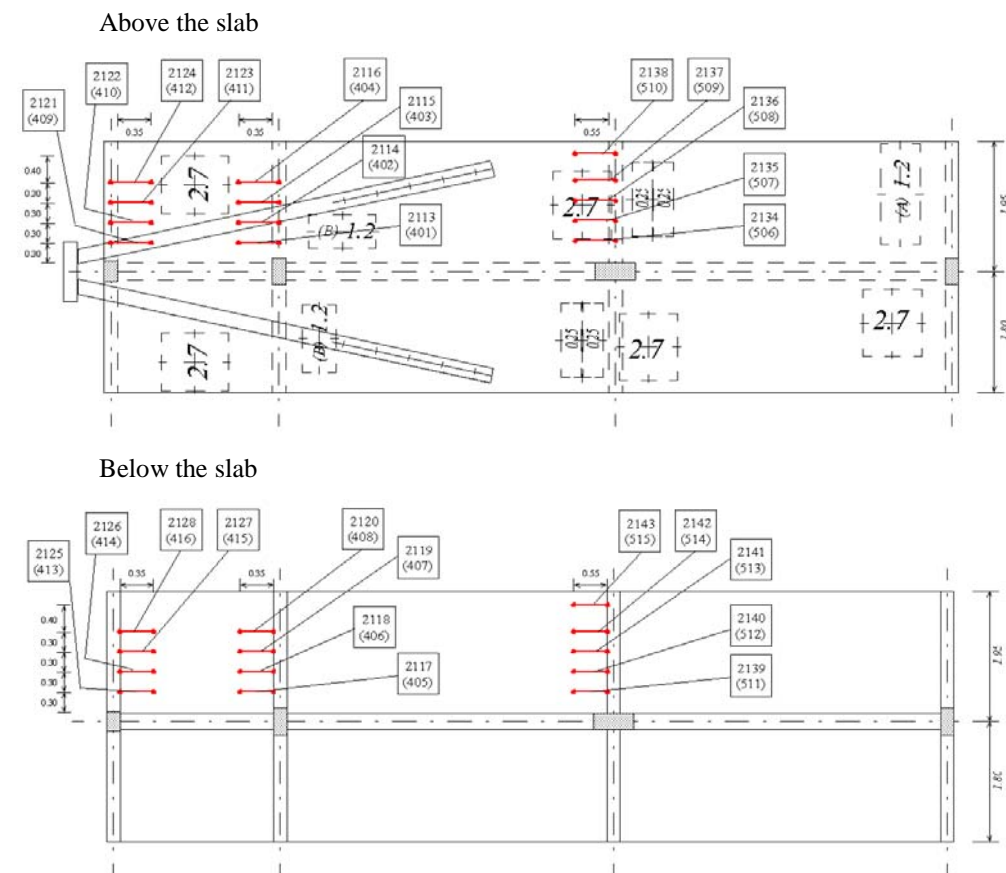


Figure 3.40 - Instrumentation for the slab-participation monitoring

### 3.7.5.4 - Strong-column

For the tests, twenty-seven channels (22 in the 1<sup>st</sup> storey and 5 in the 2<sup>nd</sup> storey) with relative displacement transducers were used on the 1<sup>st</sup> storey strong-column and at the base of the 2<sup>nd</sup> storey, where high levels of deformation were expected (particularly after retrofitting). Their distribution is illustrated in Figure 3.41, and aims at measuring both flexural and shear components of deformation in the column, as well as the behaviour of the joint and connected beam ends. The axial deformation can also be analysed with this instrumentation arrangement. Figures A.21 and A.24 show the instrumentation on the strong-column (1<sup>st</sup> storey).

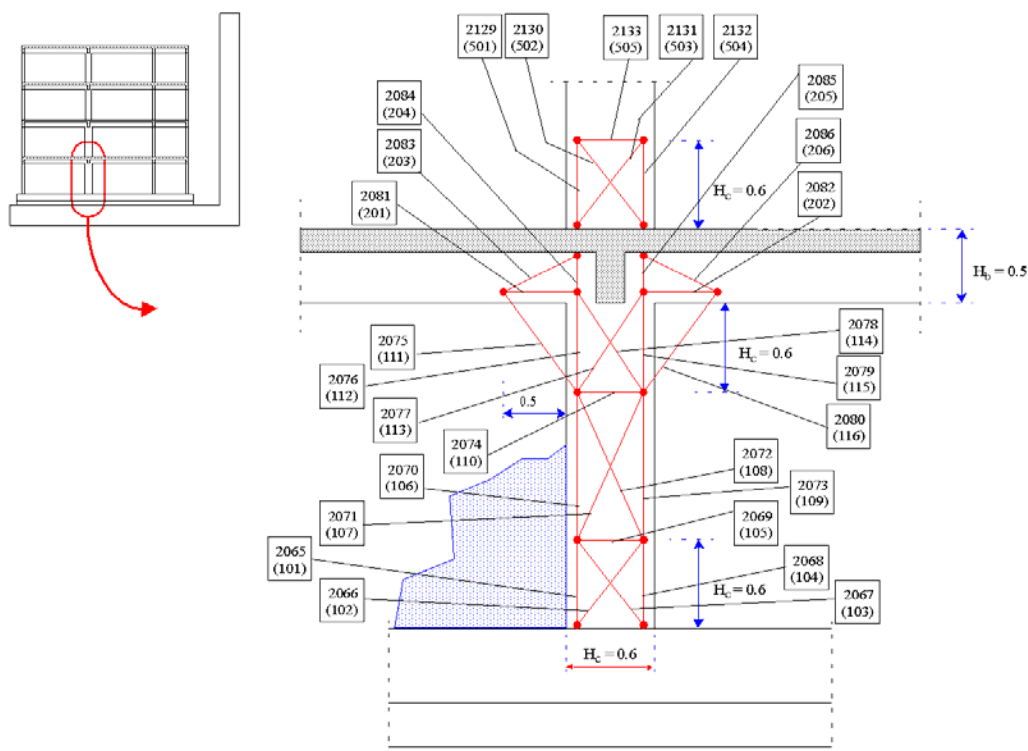


Figure 3.41 - Strong-column instrumentation: 1<sup>st</sup> storey, joint and base of the 2<sup>nd</sup> storey

### 3.7.6 - Instrumentation of the infilled frame

The instrumentation used in the bare frame and strengthened frame tests was also used for the tests on the infilled frame structure. A detailed description of the instrumentation set-up used for the tests on the frame without infills can be found in the previous section, namely

rotations (inclinometers), beam deformation at first floor level, slab-participation and strong-column deformation. For the tests on the infilled frame additional instrumentation (32 additional measurement channels) was used to record specific information on deformation of masonry infill panels (see Figures 3.42 and 3.43, for arrangement and details). The larger storey deformation is essentially expected at the two lower storeys (mainly on the ground storey). Therefore, the infill instrumentation was applied at these two storeys.

Two groups of instrumentation were used for measurements related to the infill panels. They were defined on the basis of distinct objectives, namely to record the global panel deformation and to assess local deformations in the short-bay panel, specifically at the panel corners.

Global panel deformations are derived from a set of transducers in the vertical, horizontal and diagonal directions, as shown in Figure 3.42 and 3.43. At the base of the 1<sup>st</sup> storey panels no relative deformation is expected, so no transducers were located there. For the panels-top at 1<sup>st</sup> storey, and bottom at the 2<sup>nd</sup> storey, horizontal transducers were not installed, because the instrumentation used in the frame (namely, the group dedicated to the beam deformation) gave the desired deformation measurements. Also, the instrumentation used to record the strong-column deformation on the first storey is adequate to determine the vertical deformation of the adjacent panels at that location.

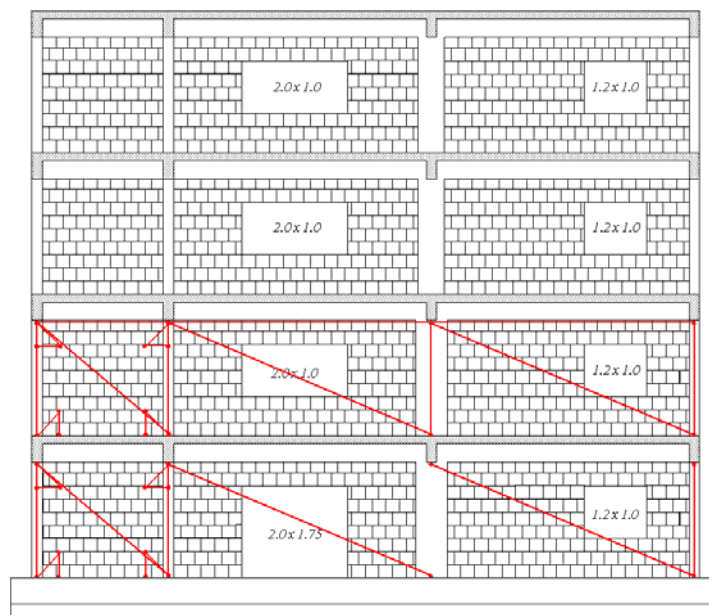


Figure 3.42 - Infill masonry instrumentation (general layout): 1<sup>st</sup> and 2<sup>nd</sup> storeys

The second group of instrumentation (to capture local deformation) is composed of two transducers at each corner of the external short-bay panel, and are placed to measure local deformation of the infill masonry corners and relative deformation between masonry and surrounding concrete frame (see Figures 3.42 and 3.43).

The instrumentation used for the infilled frame tests was maintained for the strengthened infill tests. Photographic documentation of the instrumentation of the infill panels is shown in Figure A.29.

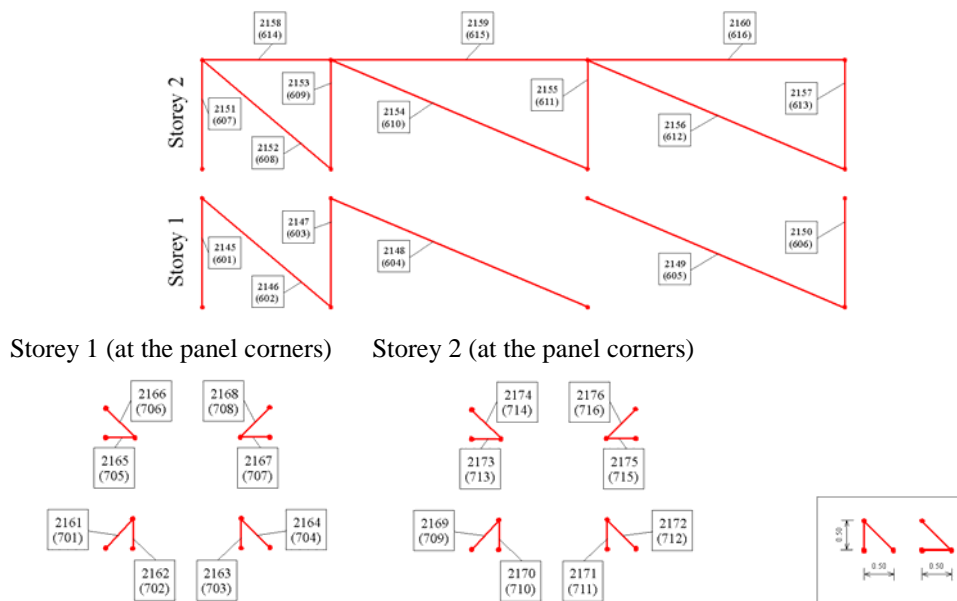


Figure 3.43 - Infill masonry instrumentation (numbering): 1<sup>st</sup> and 2<sup>nd</sup> storeys

### 3.7.7 - Instrumentation for the K-bracing test

The instrumentation used in the previous PsD tests at the second storey was maintained for this cyclic test, namely: rotations at columns, beams and joints (Figure 3.45) and relative displacement transducers used to record the deformation of the masonry infill panels (Figure 3.46). In Figure 3.44 is represented the bracing and shear-link instrumentation. The relative displacement transducer #190 was set-up to measure the distortion of the shear-link, and one strain-gauge was set-up for each steel profile in the bracing (#185 to #188). Figures A.50 and A.51 show the instrumentation adopted for the bracing system.

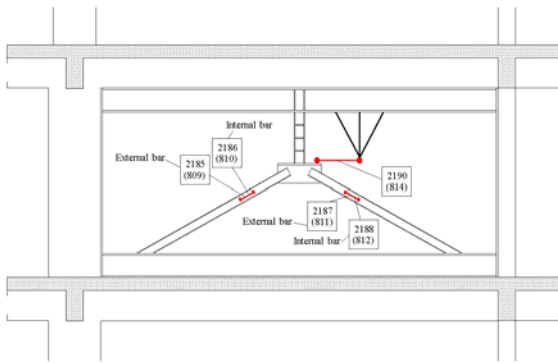


Figure 3.44 - K-bracing test instrumentation: bracing and shear-link instrumentation

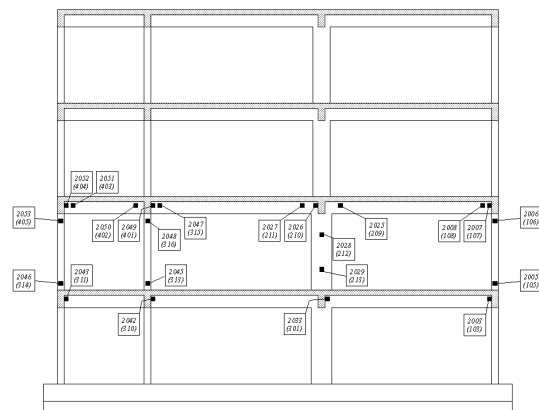


Figure 3.45 - K-bracing test instrumentation: location of the 22 inclinometers

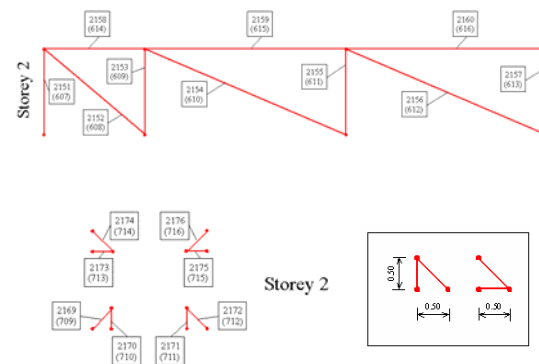
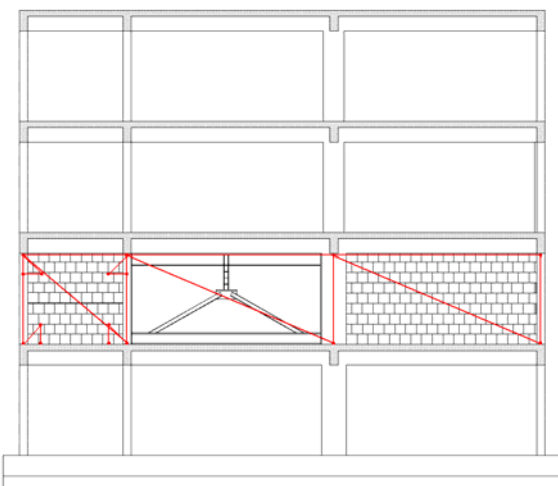


Figure 3.46 - K-bracing test instrumentation: infill relative-displacement transducers

### 3.7.8 - Instrumentation for the final capacity tests

The inclinometers distribution adopted in the PsD tests was also employed in the final capacity cyclic tests. In addition, one relative displacement transducer at each repaired joint was set-up in order to measure their deformation during the final capacity tests. Regarding the final capacity test on frame A, where the 1<sup>st</sup> storey strong-column was repaired, the relative displacement instrumentation scheme already adopted in the precedent earthquake PsD tests was applied.

Having in mind the on-line control of storey displacement, in the final capacity tests, one additional transducer type PSITRONIX was adopted at each floor level.

### 3.7.8.1 - Relative displacement transducers at the repaired joints

One transducer was used at each repaired joint, to measure their deformation during the final capacity tests. Specifically, it was intended to record the possible relative horizontal dislocation between the joint and the top of the external repaired column (see Figure 3.47-c and picture in Figure A.32). Therefore, for the bare frame final capacity cyclic test (frame A), four transducers were used and for the selective repaired frame (frame B), two transducers were used, as shown in Figure 3.47. The relative displacements at the repaired joints were measured using a potentiometer (displacement transducers) with measuring capacity of 50 mm.

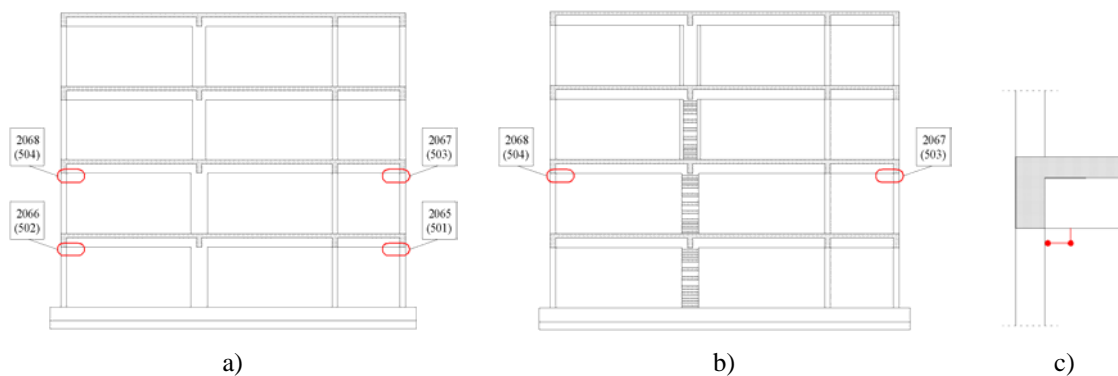


Figure 3.47 - Instrumentation at the repaired joints: a) frame A; b) frame B; c) detail

### 3.7.8.2 - Relative displacement transducers at the strong-column

The transducers arrangement adopted for the strong-column at the base (tests on frame A) and their numeration is represented in Figure 3.48. Figure A.33 shows the instrumentation used.

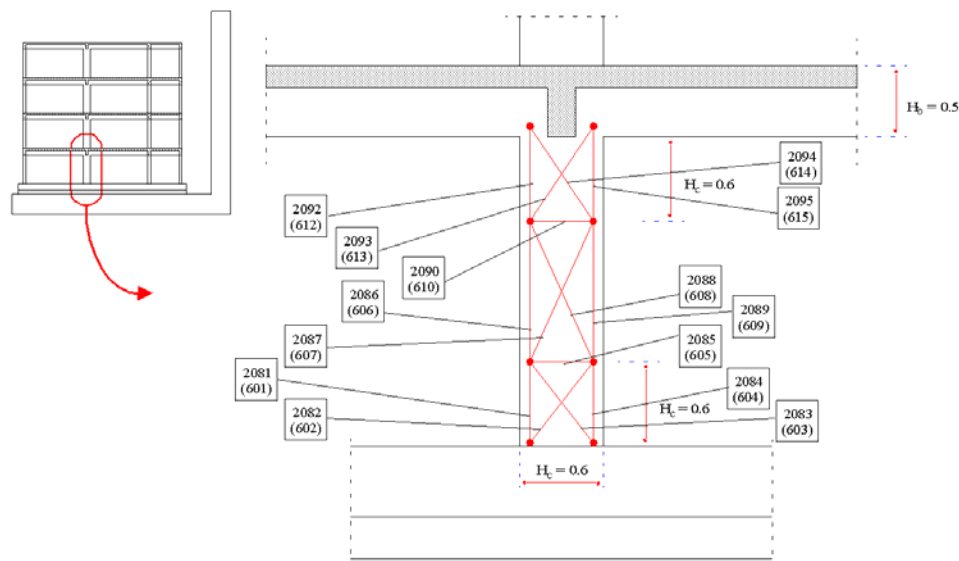


Figure 3.48 - Strong-column instrumentation for the final capacity cyclic test: frame A

### 3.7.8.3 - Storey displacement transducers (PSITRONIX)

For the final capacity cyclic tests it was important to control on-line the storey behaviour, especially for the cyclic tests performed at storey level. For this purpose four additional displacement transducers were installed at storey levels, type PSITRONIX with 500 mm measurement capacity, allowing during the test for the on-line visualisation of the storey shear versus inter-storey drift curves. With these transducers it was possible to follow the storey response and consequently control the damage and decide about levels of drift to be imposed. Another reason to adopt this additional storey displacement measurement system was the need to control and prevent the eventual full collapse of the structure. Figure A.34 shows simultaneously the HEIDENHEIN transducers used in all the tests and the additional PSITRONIX transducers adopted in the final capacity tests. The transducer numeration adopted was #2073 until #2076 for the 1<sup>st</sup> until 4<sup>th</sup> storey, respectively.

### 3.7.9 - Data acquisition system and post-processing

Finally, input data, acquisition control and monitoring of the tests were accomplished by means of a cluster of 10 PC's, shown in Figure A.20. This allows for real-time monitoring the frame response during each test, and the control system allows for halting at any time,



especially at the point of peak deformation for close damage inspection, or to prevent full collapse.

All the data is saved in Voltage units. The post-processing begins with the conversion from Voltage units to physical units (in terms of force and displacement). Following conversion, all measurements are kept in a database for later use. Within the ELSA laboratory work environment, two groups of measurements are taken and recorded. As already mentioned, one group of measurements is related to the pseudo-dynamic algorithm and the other is related to standard measurements. Consequently, two result data files are created for each test.

### 3.8 - NON-DESTRUCTIVE TESTS: FREQUENCIES IDENTIFICATION

In order to provide data for modal identification of the structure before and after each test series, a very low intensity earthquake (non-destructive test) was applied to the structure allowing exciting all the modes. This input corresponds to 5% intensity referring to the 475-yrp earthquake ( $0.109 \text{ m/s}^2$  peak acceleration) employed in the previous pseudo-dynamic tests. The frequency and viscous-equivalent damping ratio were obtained by applying an identification method to the experimental response. These methods, based on time-domain linear models (Molina *et al.*, 1999-a), are extensively applied to the results of PsD tests at the ELSA laboratory. The simplest and more robust of those models is a spatial model, which is described here next. Within this model, the measured restoring forces  $r(n)$  and the corresponding displacements  $d(n)$  and velocities  $v(n)$  are assumed to be linked as

$$r(n) = K \cdot d(n) + C \cdot v(n) \quad (3.39)$$

for every discrete time  $n$ .  $K$  and  $C$  are the stiffness and damping matrixes, respectively. More precisely, the model can be formulated as

$$\begin{bmatrix} d^T(n) & v^T(n) & 1 \end{bmatrix} \begin{bmatrix} K^T \\ C^T \\ 0^T \end{bmatrix} = r^T(n) \quad (3.40)$$

where a constant force offset term  $\theta$  has been added. Here, if  $NDOF$  is the number of DOF's in the structure,  $K$ ,  $C$  and  $\theta$  contain  $2 \cdot NDOF^2 + NDOF$  unknowns and the number of available equations is  $N \cdot NDOF$ , so that, the required number of discrete-time data sets is

$$N \geq 2 \cdot NDOF + 1 \quad (3.41)$$

Once  $K$  and  $C$  have been estimated by a least squares solution, the complex eigen-frequencies and mode shapes can be obtained by solving the generalised eigen-value problem

$$s \begin{bmatrix} C & M \\ M & 0 \end{bmatrix} \varpi + \begin{bmatrix} K & 0 \\ 0 & -M \end{bmatrix} \varpi = 0 \quad (3.42)$$

where  $M$  is the theoretical mass matrix. The conjugate couples of eigen-values can be written as

$$s_n, s_n^* = \omega_n (-\zeta_n \pm j\sqrt{1 - \zeta_n^2}) \quad (3.43)$$

where:  $\omega_n$  is the natural frequency and  $\zeta_n$  the damping ratio. The corresponding mode shape is also given by the first  $NDOF$  rows of the associated eigen-vector  $\varpi_n$ .

Since this model assumes an invariant system, at any selected time instant, the identification may be done based on a data time window of duration roughly the period of the first mode, centred on that instant. The adopted time window has to be narrow enough so that the system does not change too much inside of it, but, at the same time, it has to contain enough data to allow the compensation of different existing data noises and nonlinearities. The selection of the most appropriate window length is done by trial and error. Working like that, it is possible to obtain the eigen-frequencies and damping ratios of all the modes at any time instant (Molina *et al.*, 1999-a).

### 3.8.1 - Non-infilled frame

From the analyses of the non-destructive tests, the modal parameters listed in Table 3.28 were obtained for the non-infilled frame (frame B) using the procedure described before. A more detailed analysis of these results can be found in Molina *et al.* (2001; 2000-b).

Table 3.28 - Evolution of the four modal frequencies of RC frame (frame B)

State	Test label	$f_1$ (Hz)	$f_2$ (Hz)	$f_3$ (Hz)	$f_4$ (Hz)
original structure	L03	1.57	4.60	7.58	11.14
after BF tests	L08	1.19	3.65	5.63	9.06
after repair	L09	1.41	5.07	9.95	14.80
after SR tests	L13	0.93	3.31	6.46	8.87
after K-bracing tests and carbon fibre repair	L35	1.08	3.60	6.45	8.84
after final capacity cyclic tests	L39	0.92	3.21	5.93	8.27

In Figure 3.49, the four eigenfrequencies evaluated are plotted (in Hz) at each stage (original structure, after the earthquake tests on the bare frame, after the selective strengthening interventions, after the earthquake tests on the strengthened structure, after the repair with carbon fibre materials, and after the final capacity tests). Figure 3.50 presents the evolution of each of the four eigenfrequencies, relatively to the corresponding measured initial eigenfrequency.

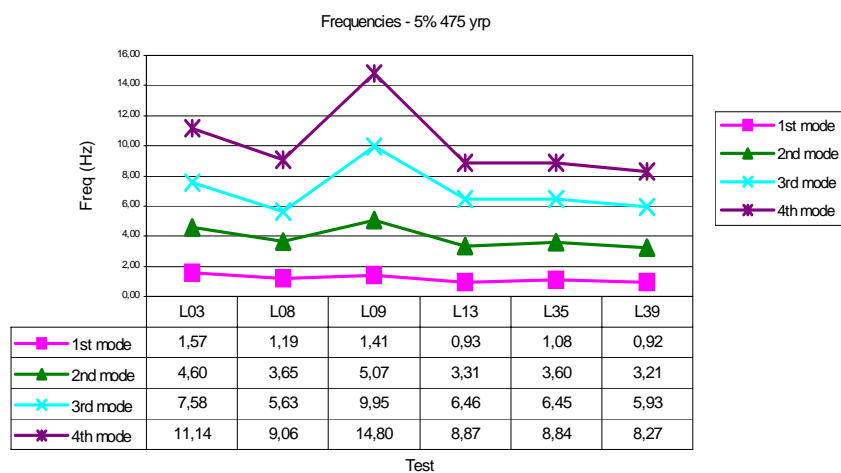


Figure 3.49 - Evolution of the four eigenfrequencies

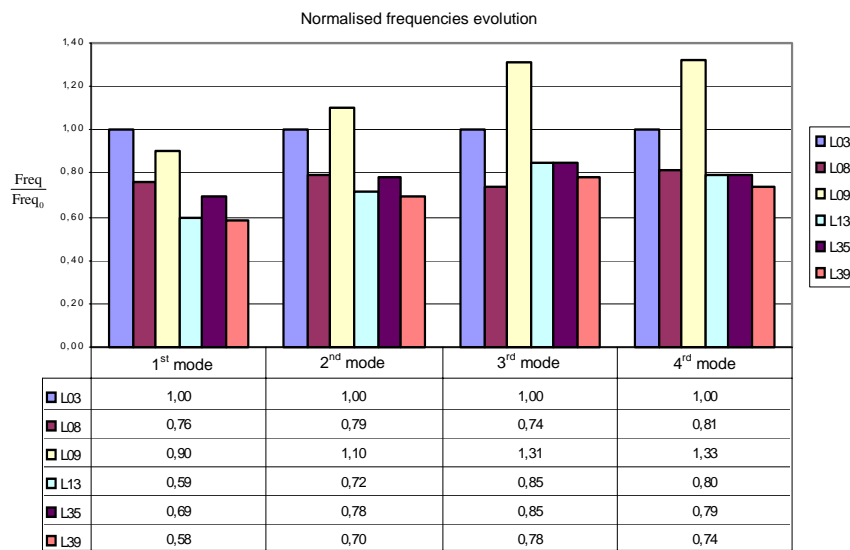


Figure 3.50 - Evolution of the four eigenfrequencies (relative values: measured frequencies divided by the initial frequency)

From the analyses of the results listed in Table 3.28 and Figures 3.49 and 3.50, the following is noted:

- The tests on the bare frame (475 and 975-yrp) caused an eigenfrequency drop of about 20-25%, for the four modes, as a consequence of structural damage.
- With the selective strengthening intervention, the frequencies increase substantially. The first, second, third and fourth eigenfrequencies increased at about 18%, 39%, 77% and 64% respectively, compared with the frequencies of the damaged structure (after BF tests). It is noted that after the repair interventions, the initial first frequency was almost achieved (90% of the original structure) and the second, third and fourth original eigenfrequencies were increased by about 10%, 31% and 33%. This large increase of the frequencies, particularly for the highest modes was mainly due to the stiffening intervention in the 3<sup>rd</sup> and 4<sup>th</sup> floors.
- The tests on the selective repaired structure (475, 975 and 2000-yrp) caused serious damage in the repaired structure (the four frequencies drop at about 35-40%, in contrast to the repaired structure). It should be underlined that after the tests on the selective repaired structure the second, third and fourth eigenfrequencies reached a value comparable to the frequencies identified before

repair operations. But the first mode dropped 35% after this series of tests (41% in contrast to the first eigenfrequency of the original structure).

- The repair interventions carried out before the final capacity tests slightly increase the first and second eigenfrequencies (17% and 8%, respectively). The third and fourth were maintained. This small variation was expected and desirable, because the intervention was essentially motivated to avoid the premature collapse of the structure due to the vertical loads, without increasing the stiffness of the structure.
- After the final capacity cyclic tests (when the maximum imposed displacement was similar to the values attained in the previous PsD tests) the frequencies evaluated did not vary too much, when compared to the values obtained before the repair. The first two eigenfrequencies are similar to the ones evaluated before repair intervention (2% variation), and the third and fourth decreased at about 8%, in contrast to the value before repair with carbon fibre materials.

In Appendix B, Figures B.2 to B.10 give the equivalent modal frequency and corresponding damping for the entire test campaign for the bare original and strengthened structures, including also the tests carried out for very low intensity earthquake input (5% of the 475-yrp earthquake). In Figure B.1 the equivalent modal frequency and damping for the two first modes and for the main PsD tests performed are shown, namely: BF475, BF975, SR475, SR975 and SR2000.

Previously to the PsD tests, modal dynamic tests were carried out in order to assess the natural frequencies of the bare frame. The tests were conducted by exciting the structure with an instrumented (with load cell) Impact Hammer of 5 kg mass. The three first frequencies obtained are summarised in Table 3.29. A good agreement was verified between the natural frequencies estimated with the non-destructive tests (Table 3.28) and those experimentally measured (Table 3.29).

Table 3.29 - Natural frequencies of frame B evaluated with an impact hammer

$f_1$ (Hz)	$f_2$ (Hz)	$f_3$ (Hz)	$f_4$ (Hz)
1.57	4.69	7.83	---

### 3.8.2 - Infilled frame

From the analyses of the non-destructive tests on the infilled frame (frame A), the modal parameters listed in Table 3.30 were obtained.

Unfortunately it was not possible to make the frequency identification test after the IN tests (and before the strengthening with shotcrete technique). Therefore, here are just presented the eigenfrequencies of the original (uncracked stiffness) infilled RC frames. Comparing the frequencies of the original bare frame (L03, frame B) with the infilled frame (L15) it is observed that masonry infill panels increased the frequencies about four times.

Table 3.30 - Modal frequencies of the original infilled frame (frame A)

State	Test label	$f_1$ (Hz)	$f_2$ (Hz)	$f_3$ (Hz)	$f_4$ (Hz)
original structure (frame with infill masonry walls)	L15	7.22	20.83	24.93	45.35

### 3.9 - REMARKS

This chapter provides the background for the test result's analysis in the next chapter. It details the experimental research work carried out at the ELSA laboratory, including analyses of the material properties. It is noted that a small variance was found for the concrete properties for each casting phase, and a large variance was noted between the various casting phases. This variability will be taken into account in the refined non-linear numerical analyses to be conducted in Chapter 5. Otherwise, the analysis of the steel reveals that the steel used in the construction of the frames has significantly higher strength than the nominal values. From these preliminary analyses of the specimens, one moves into Chapter 4, which presents the pseudo-dynamic (PsD) and cyclic tests in order to assess the vulnerability of this kind of structures and to evaluate the efficiency of the different retrofit solutions.

# CHAPTER 4

## ANALYSIS OF EXPERIMENTAL TEST RESULTS

### 4.1 - INTRODUCTION

In the previous chapter were presented the characteristics of the test frames, infill masonry, vertical static loads, earthquake input motions, repair and strengthening techniques and materials properties. This chapter presents and discusses all the results of the earthquake PsD and cyclic tests. Figure 3.1 summarised schematically the complete set of tests performed in this study. Next it is presented an overview on the general experimental results as a preliminary step to guide into the posterior extensive analysis of the test results.

The first part of the test campaign focussed on the bare frame (BF) and on the selective strengthened frame (SR) tests. Two PsD test series were carried out. In the first test series, the frame was subjected to two earthquake input signals, represented by two artificial 15-second duration accelerograms. The earthquakes of 475-yrp ( $PGA = 2.180 \text{ m/s}^2$ ) and 975-yrp ( $PGA = 2.884 \text{ m/s}^2$ ) were generated for a moderately high-risk scenario in Europe (see input signals in Figure 3.8 and Table 3.9). As predicted by the numerical pre-test analysis, the frame did not perform satisfactorily and the strong-column suffered severe damage at the third level. In fact, the 975-yrp earthquake was applied only for the first 7.5 seconds in order to avoid collapse. During the 975-yrp test of the BF series, the third storey (strong-column) experienced severe deformations and reached eminent collapse. Hinging occurring at the top, bottom and at the bars termination zone (lap-splice). However, only spalling and yielding took place. Neither buckling nor rupture of the rebars occurred. Also,

no stirrups disclosure or rupture occurred, except at the bars termination zone where slight yielding/disclosure of stirrups occurred. Therefore, repair of the column was feasible. In order to improve the seismic performance of such structure, selective repair and strengthening interventions were applied to the frame. Afterwards, the retrofitted structure was submitted again to the 475, 975 and additionally to the 2000-yrp accelerograms ( $PGA = 3.728 \text{ m/s}^2$ ). After this second series of earthquakes, the frame had developed larger global displacements and some limited damages, but its stability was not compromised thanks to the applied retrofitting. The results from the SR tests have shown a clear benefit from the strengthening intervention.

Frame A (infilled frame) was also object of two series of tests. First, the original infilled frame (IN) was subjected to the same three earthquake input motions as the previous campaign on frame B (labelled 475, 975 and 2000-yrp earthquake input motions). During the 2000-yrp test the infilled frame reached imminent collapse. The infills at the first storey reached collapse, and the soft-storey mechanism was nearly to appear. After reconstruction of the infills on this storey, and strengthening on the external short panel at the four storeys, the frame was subjected to the same three earthquake inputs. This test series was labelled SC (shotcrete). Infills reconstruction and strengthening was applied to the frame, following good practice techniques. The repaired and strengthened structure (SC) was also subjected to three PsD tests (475, 975 and 2000-yrp), which revealed some benefit from the strengthening operation.

Prior to the K-bracing with shear-link test, infill hollow brick-masonry walls with two-sided plaster were constructed in the outer bays of the second floor. Subsequently, the K-bracing with shear-link assembly was inserted into the middle bay of the second floor and anchored to the beams and columns of this bay. The second storey was subjected to quasi-static cyclic tests with imposed increasing amplitude displacements. The test results in terms of total lateral-load (storey shear) versus storey-displacement, confirmed that the maximum shear capacity was about  $600 \text{ kN}$ . The actual limiting cause was not a failure of the infilled walls, but rather the premature development of a shearing failure in the outer frame column of the short external bay. In fact, the failure resulted from the transverse slip of a joint between the top of the column and the bottom of the beam. The cyclic response of the vertical shear-link, as reflected by the lateral displacement of the link and the link



---

shear force, shows a typical ductile stable behaviour with the resistance steadily increasing under repeated displacement cycles. The results clearly show that under increasing number of displacement cycles (and associated progressive failure) the participation of the shear-link in resisting the total lateral load becomes more pronounced. The progressively increasing energy absorbing capacity of the shear-link and the continually deteriorating energy dissipation of the infilled concrete frame was observed.

Final capacity cyclic tests on the four-storey frames were performed to estimate the ultimate structural displacement and to investigate the post-peak structural behaviour, which are important parameters, for example to define damage indices, and to verify numerical simulations. The collapse test campaign on the four-storey concrete frames includes two cyclic tests series. The first part of this test campaign was carried out on the selective strengthened frame (frame B). The second series of cyclic tests was performed on the bare frame that was recovered from the infilled frame tests (frame A), removing the infill masonry walls. Cycles with increasing amplitude, up to the capacity of the structure were imposed to the frames. These cyclic tests were performed with imposed displacements on the fourth floor, being the three lower floors force-controlled, according to a constant-pattern, inverted-triangular storey-wise force distribution.

This chapter presents and discusses the results from the tests above summarized and is organised as follows. The test results are presented and discussed, first for the bare frame (BF) test series (Section 4.2) and subsequently for the strengthened frame (SR) (Section 4.3). Comparison between the most relevant results from BF and SR tests is made in a separate subsequent section (Section 4.4). In Section 4.5 are presented and discussed the test results for the original infilled frame (IN) and for the strengthened infilled frame (SC) (Section 4.7). One section is dedicated to compare the most relevant results between IN and the previous BF test series (Section 4.6). Results for the IN and SC test series are compared in Section 4.8 and results of the K-bracing with shear-link cyclic tests appear in Section 4.9. Final capacity cyclic tests are analysed in Section 4.10. The main results and issues concerned with shear and flexural deformations/failure of the strong-column, slab-participation, plastic hinge length and joint deformation are dealt in Section 4.11. A summary of the most relevant experimental results is collected in Section 4.12.

## 4.2 - RESULTS FROM THE TESTS ON THE BARE FRAME

The bare frame (BF) was subjected to one earthquake corresponding to 475-yrp and subsequently to a 975-yrp input motion.

### 4.2.1 - Storey displacement, drift and shear

In Figure 4.1, the time histories of storey displacement are plotted for the two earthquake pseudo-dynamic tests performed on the bare frame structure, namely for 475 and 975-yrp. Figure 4.2 shows the top-displacement curves for the two tests and Figure 4.4 presents the curves base-shear versus top-displacement. In Figure 4.3, the storey shear-drift curves are presented (for the four storey levels) and the respective envelope curves are plotted in Figure 4.5. Figure 4.6 represents the maximum inter-storey drift profile and the maximum storey shear profile. Table 4.1 collects the maximum values of the characteristic response variables for the BF tests.

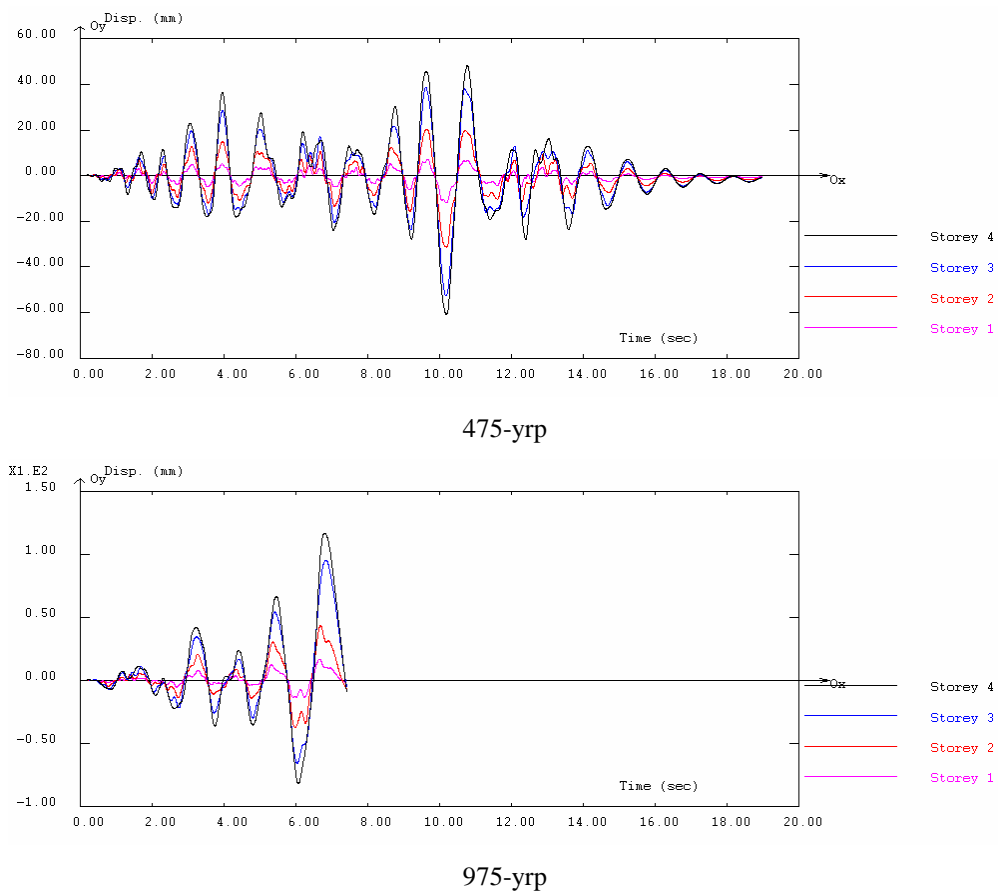


Figure 4.1 - BF tests: storey displacement time histories

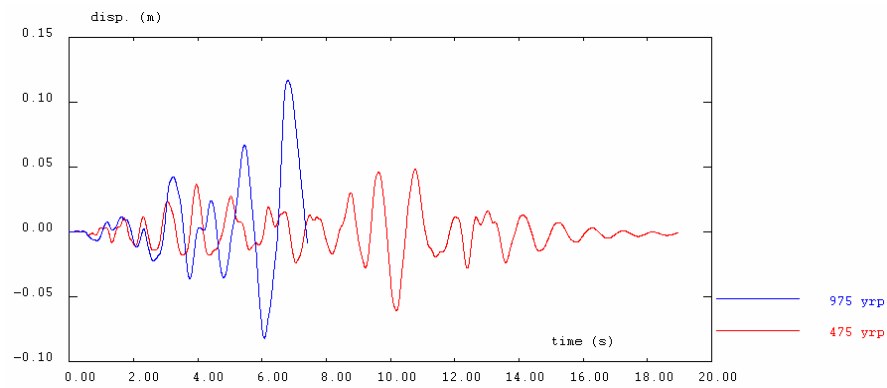


Figure 4.2 - BF tests: top-displacement evolution

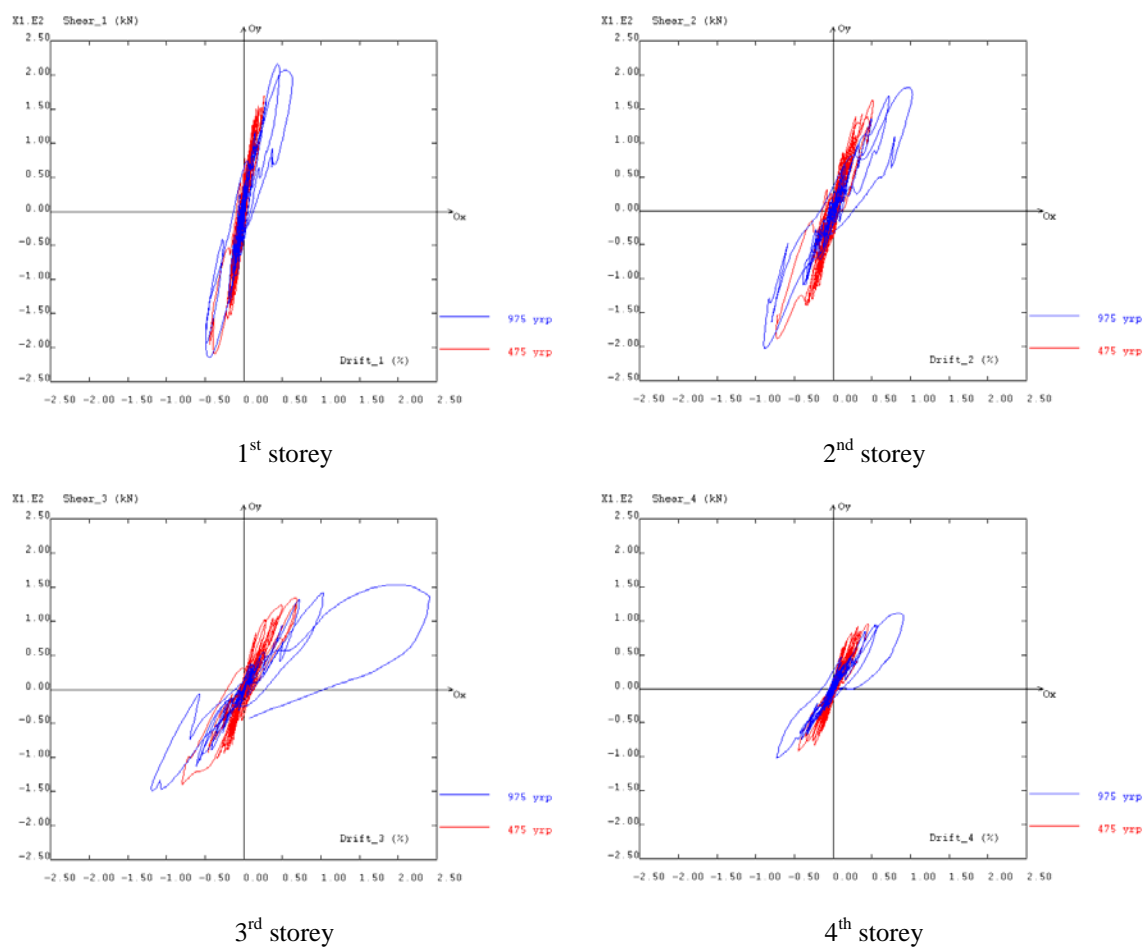


Figure 4.3 - BF tests: storey shear versus inter-storey drift

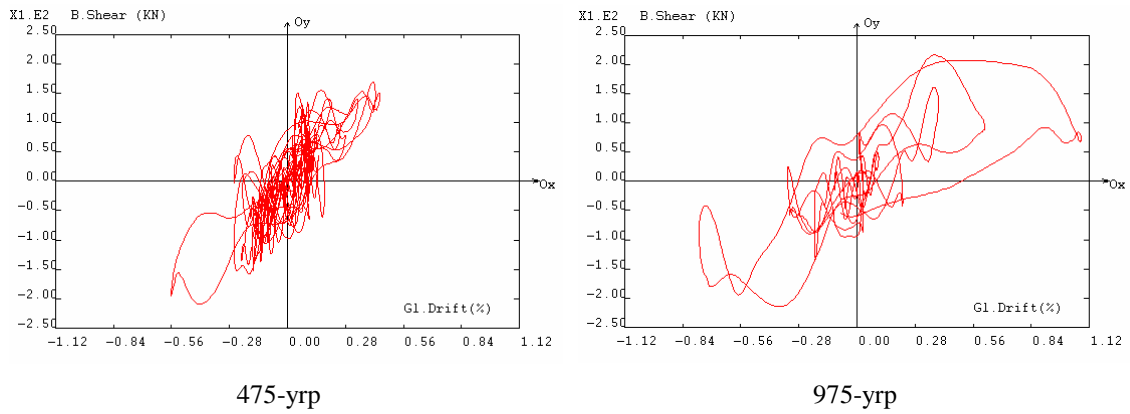


Figure 4.4 - BF tests: base-shear versus top-displacement

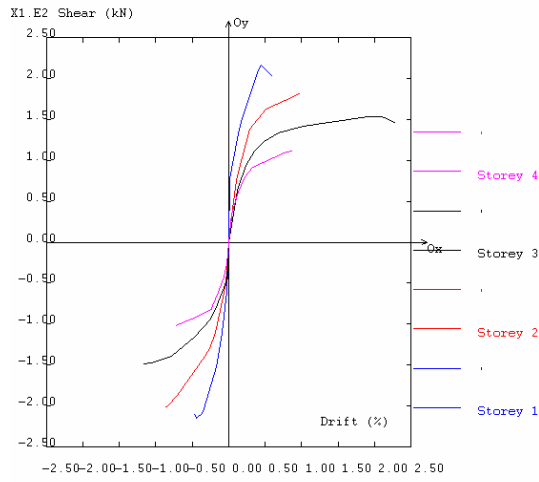


Figure 4.5 - BF tests: envelope storey shear versus inter-storey drift

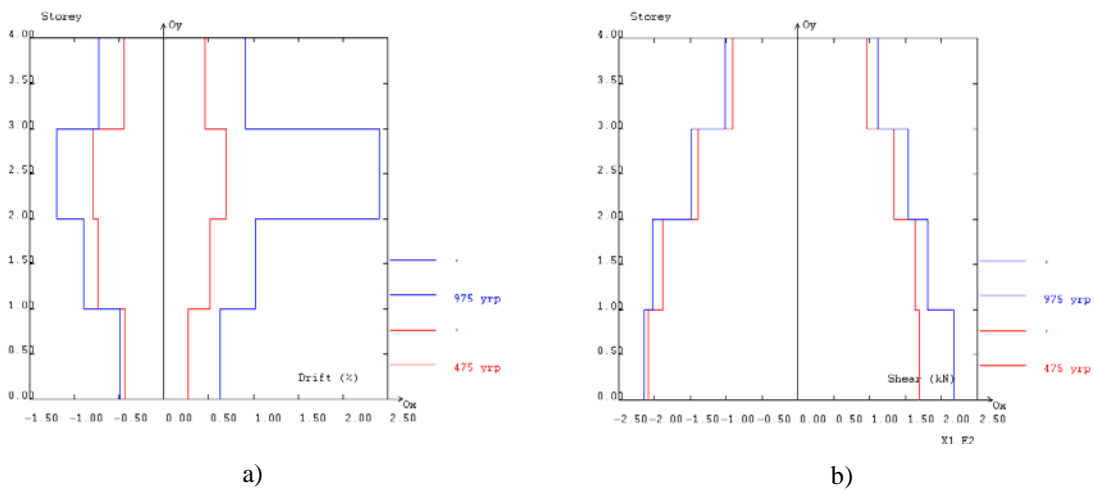


Figure 4.6 - BF tests: a) maximum inter-storey drift profiles; b) maximum storey shear profiles

Table 4.1 - BF tests: response maximum values (summary table)

Test <sup>a</sup>	Top-displacement ( <i>mm</i> )		Global drift (%)	
BF475	60.8		0.56	
BF975 <sup>b</sup>	116.7		1.08	
	Inter-storey drift (%)			
	storey 1	storey 2	storey 3	storey 4
BF475	0.44	0.74	0.80	0.46
BF975 <sup>b</sup>	0.63	1.03	2.41	0.91
	Storey shear ( <i>kN</i> )			
	storey 1	storey 2	storey 3	storey 4
BF475	209.0	188.2	139.0	95.8
BF975 <sup>b</sup>	216.7	202.7	153.9	111.1
	Max. hinge rotation ( <i>mRad</i> )			
	<i>(mRad)</i>		Location	
BF475	10.0		strong-column 3 <sup>rd</sup> storey	
BF975 <sup>b</sup>	31.0		strong-column 3 <sup>rd</sup> storey	

a) Duration of the input motions is 15 seconds for the earthquake tests.

b) Test performed up to 7.5 seconds because imminent collapse was attained.

It is apparent that the deformation demands tend to concentrate in the 3<sup>rd</sup> storey for the 475-yrp earthquake test and for the 975-yrp earthquake test the 3<sup>rd</sup> storey almost collapsed. This test was stopped after 7.5 seconds in order to allow for repair and subsequent strengthening.

#### 4.2.2 - Observed damages

A detailed description of the visual damage for each test and an attempt at categorising it according to the ATC-40 (1996) damage states are included in Table 4.2. Figure 4.7 shows the damage observed on the strong-column at the 3<sup>rd</sup> storey after the earthquake pseudo-dynamic tests. It shows the concrete cover spalling at the top of the column and the bar termination zone (70 *cm* from the base). Figure B.11 shows a general layout of the damage observed at the end of the bare frame tests and in Figure B.12 the damage in the slabs is schematically represented. More pictures can be found in Appendix B (Figures B.13 to B.17).

Table 4.2 - BF tests: damage inspection (see damage patterns in Figures B.11 and B.12) and damage states (ATC-40, 1996)

Test	Damages	Damage state	Repair required?
BF475	<ul style="list-style-type: none"> <li>• Cracking (not clearly visible at the end of the test)</li> </ul>	Slight	No
BF975	<ul style="list-style-type: none"> <li>• Cracking: Top and bottom of the columns</li> <li>• Failure at the 3<sup>rd</sup> storey (spalling and crushing of the strong-column at top, bottom and bars termination zone (700 mm from the base).</li> <li>• Flexural and shear cracking at top and bars termination zone</li> <li>• Shear cracking (slight) at the bars termination zone of the 1<sup>st</sup> storey strong-column</li> <li>• Cracking of the beams at 1<sup>st</sup> and 2<sup>nd</sup> floors for negative moments</li> </ul>	Heavy	Yes

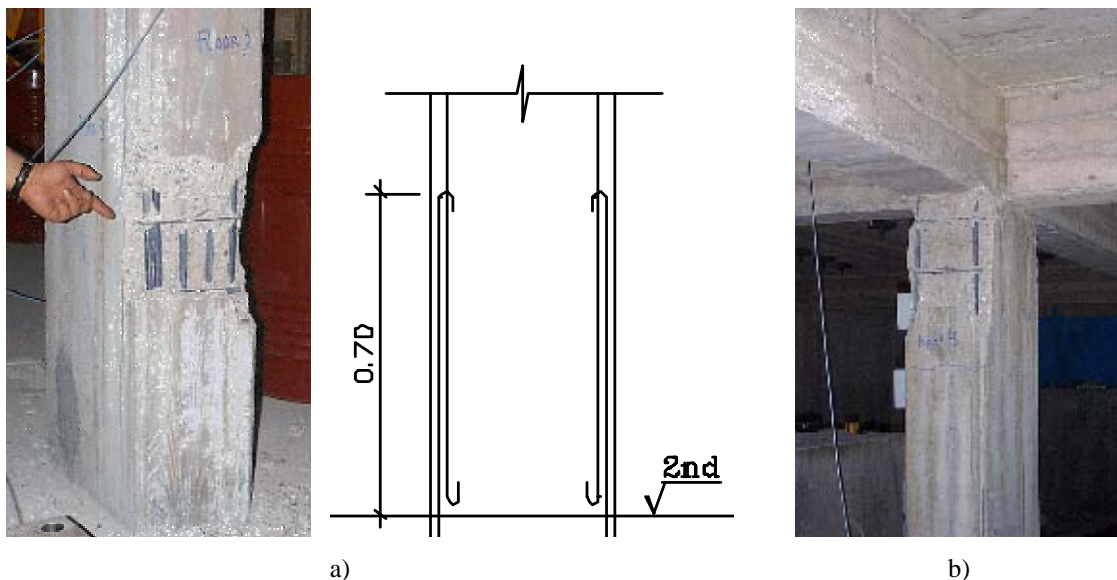
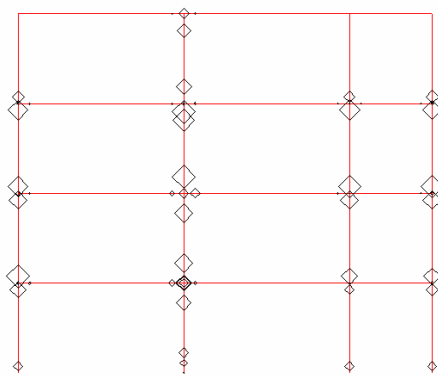


Figure 4.7 - Damage observed on the 3<sup>rd</sup> storey strong-column after BF tests: a) at the bar termination zone (note reinforcement detail); b) at the top of the column

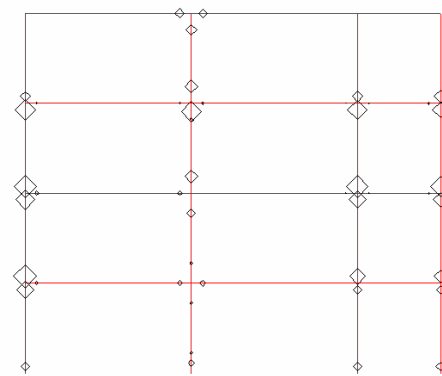
The spalling observed on the bar's termination zone at the third storey (see Figure 4.7) indicates the loss of the anchorage of such reinforcing bars. Recall that, based on tests on column specimens with anchorage made by hooks, Hassan and Hawkins (1977) concluded that in buildings surviving an earthquake, the loss of cover from behind the hook should be interpreted as a possible loss of the anchorage for such reinforcing bars. This phenomenon was frequently observed in reinforced concrete buildings damaged by earthquakes (see for example Figures 2.24 to 2.27).

### 4.2.3 - Maximum absolute and relative rotations measured at the critical zones

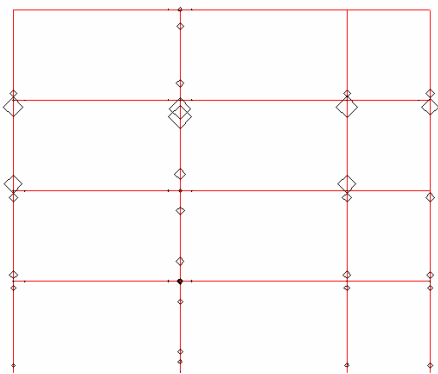
Figure 4.8 presents the maximum absolute and relative rotations measured during the tests performed on the bare frame structure. Note that absolute rotations stands for the values obtained directly from the inclinometers, while relative rotations stands for the values calculated from the difference of two adjacent inclinometers (the effective relative section rotation). Results for the two earthquake pseudo-dynamic tests carried out (475 and 975 years return periods) are presented.



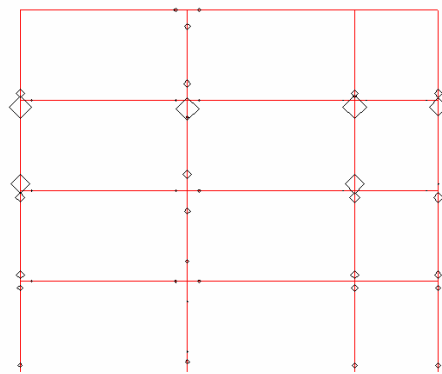
BF475 – max. abs. rotation = 9.6 *mRad*



BF475 – max. relat. rotation = 10.0 *mRad*



BF975 – max. abs. rotation = 34.2 *mRad*



BF975 – max. relat. rotation = 31.0 *mRad*

Figure 4.8 - BF tests: maximum absolute and relative rotation demands

From the analyses of Figure 4.8, it can be concluded that:

- Comparing the absolute and relative rotations for the slender-columns, it is clear that the relative rotations are similar to the absolute ones. This is justified by the low ratio between stiffness of these columns and those beams (much larger for the

beam). Therefore, in the vicinity of the slender-columns, the beam practically does not rotate and the storey deformation is concentrated in the columns.

- From visual inspections, confirmed by the results, it was perceived that in the columns the deformation is mainly concentrated at their extremities (top and bottom).
- It was in the vicinity of the strong-column that the beams reached their maximum rotation, due to the large stiffness and strength of the strong-column, when compared with the other columns.
- The strong-column reaches its maximum relative rotation at the 3<sup>rd</sup> storey, where severe damage was detected.

#### 4.2.4 - Strong-column: 3<sup>rd</sup> storey

As mentioned previously, the 975-yrp test performed after the 475-yrp test was stopped at 7.5 seconds because failure of the 3<sup>rd</sup> storey was imminent (see damages in Figure 4.7, Section 4.2.2). In fact, clear hinging of the strong-column at the 3<sup>rd</sup> storey at the base, top and also at the bar's termination zone (700 mm from the base of the column) developed with severe damage (yielding, spalling and yielding of the stirrups at the bars termination zone). Disclosure of the 90 degrees bent stirrups was not observed but it would certainly have occurred if the test had been continued. Figure 4.9 contains a picture illustrative of the reinforcing details at the 3<sup>rd</sup> storey strong-column.



Figure 4.9 - Strong-column at the base of the 3<sup>rd</sup> storey: lap-splice reinforcement detail (70 cm length)



Figure 4.10 shows the evolution of the relative rotation between two consecutive sections at the 3<sup>rd</sup> storey strong column during the 975-yrp test.

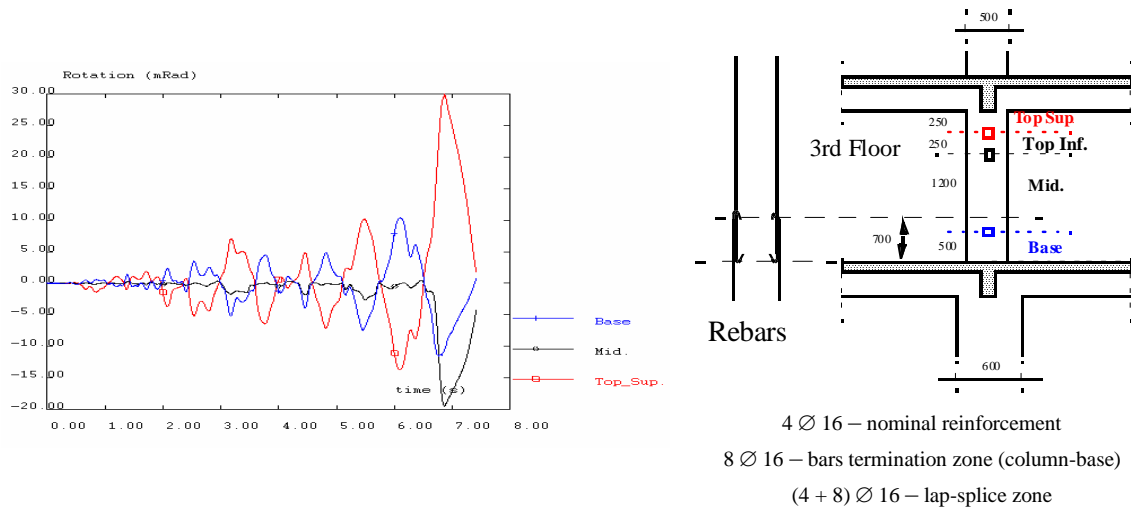


Figure 4.10 - Evolution of the rotations at the 3<sup>rd</sup> storey strong-column during the BF975 test

Looking at Figure 4.10, four slices can be identified: *a*) Top-Sup (0.25 m length), corresponding to the critical zone at the top of the column; *b*) Top-Inf (0.25 m length), adjacent to Top-Sup; *c*) Base (0.50 m length), corresponding to the critical zone at the bottom of the column; and, *d*) Mid (1.20 m length), corresponding to the column middle part, where a plastic hinge developed at the final part of the 975-yrp earthquake test.

Figure 4.11-*b* schematically represents the following: *a*) the distribution of moments in the column at two stages, i.e. stage 1, in blue, before yielding of the mid-section, and stage 2, in red, when yielding of the mid-section occurs; *b*) the moment-curvature diagrams for the three sections, i.e. one at the column base which has higher strength due to higher longitudinal reinforcement, and at the top and mid-section of the column with the same moment-curvature diagrams. From measurements and visual observation of the column during test, the following can be concluded. First, plastic hinging develops at the top and bottom of the column, without yielding of the mid-section. At a certain demand stage (red in Figure 4.11-*b*), softening starts at the top-section. From that stage forward, moments increase at the bottom and mid-section, being constant at the top-section. At a particular point, a hinge develops at the mid-section, which would lead to failure of the 3<sup>rd</sup> storey if the test had continued.

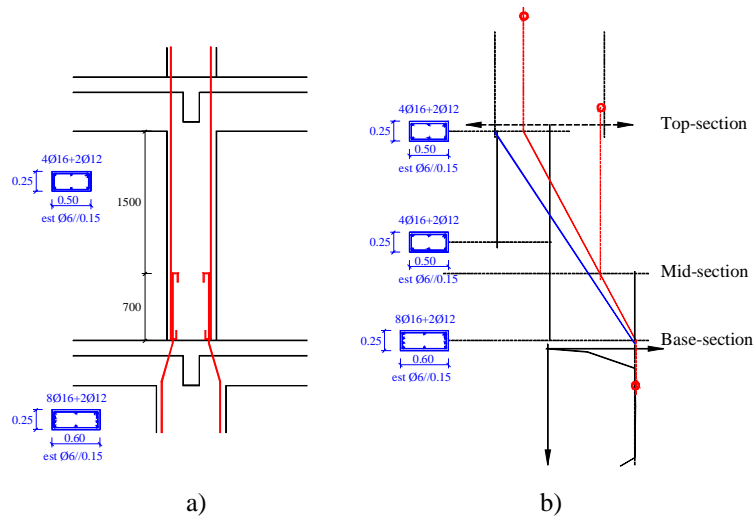


Figure 4.11 - 3<sup>rd</sup> storey strong-column: a) scheme of reinforcement; b) moments distribution

Figure 4.10 shows the evolution of rotations at the strong-column of the 3<sup>rd</sup> storey during the BF975 test. It is apparent that in the first part of the test the storey drift essentially arises from the 'plastic' rotations at both extremities of the column. At 6.5 seconds a hinge opens at the bars termination zone, leading to the imminent collapse of this storey (see shear-drift diagram at the 3<sup>rd</sup> storey in Figure 4.3).

#### 4.2.5 - Local ductility and damage indices

In order to quantify the earthquake demands and the remaining capacity of the structural elements, yielding and ultimate rotations were estimated for the columns and then compared with the demands for the BF tests. Specifically, the ultimate rotation capacity was obtained from the product of the plastic hinge length,  $l_p$  (empirical expression by Paulay and Priestley, 1992) and the ultimate curvature. The ultimate curvature was estimated from the moment-curvature diagrams, at the cross-section level, and corresponds to the concrete ultimate compression strain ( $\varepsilon_{cu}$ ) as in the following equation (given by Paulay and Priestley, 1992)

$$\varepsilon_{cu} = 0.004 + 1.4 \rho_s f_{yh} \varepsilon_{sm} / f_{cc} \quad (4.1)$$

where:  $\rho_s$  is the volumetric ratio of the confining steel,  $f_{yh}$  is the steel yield strength,  $\varepsilon_{sm}$  is the steel strain at maximum tensile stress, and  $f_{cc}$  is the compression concrete strength

of the confined sections. According to Paulay and Priestley (1992), typical values for  $\varepsilon_{cu}$  range from 0.012 to 0.05, a 4- to 16-fold increase over the traditionally assumed value for unconfined concrete.

In this analysis, the plastic hinge length,  $l_p$ , was estimated based on the empirical expression given by Paulay and Priestley (1992)

$$l_p = 0.08 \cdot l + 0.022 \cdot \phi_l \cdot f_{sy} \quad (4.2)$$

where:  $l_p$  stands for the equivalent plastic hinge length;  $l$  for the length of the element;  $\phi_l$  for the diameter of the main longitudinal reinforcing bars; and  $f_{sy}$  for the yielding strength of reinforcement (in *MPa*).

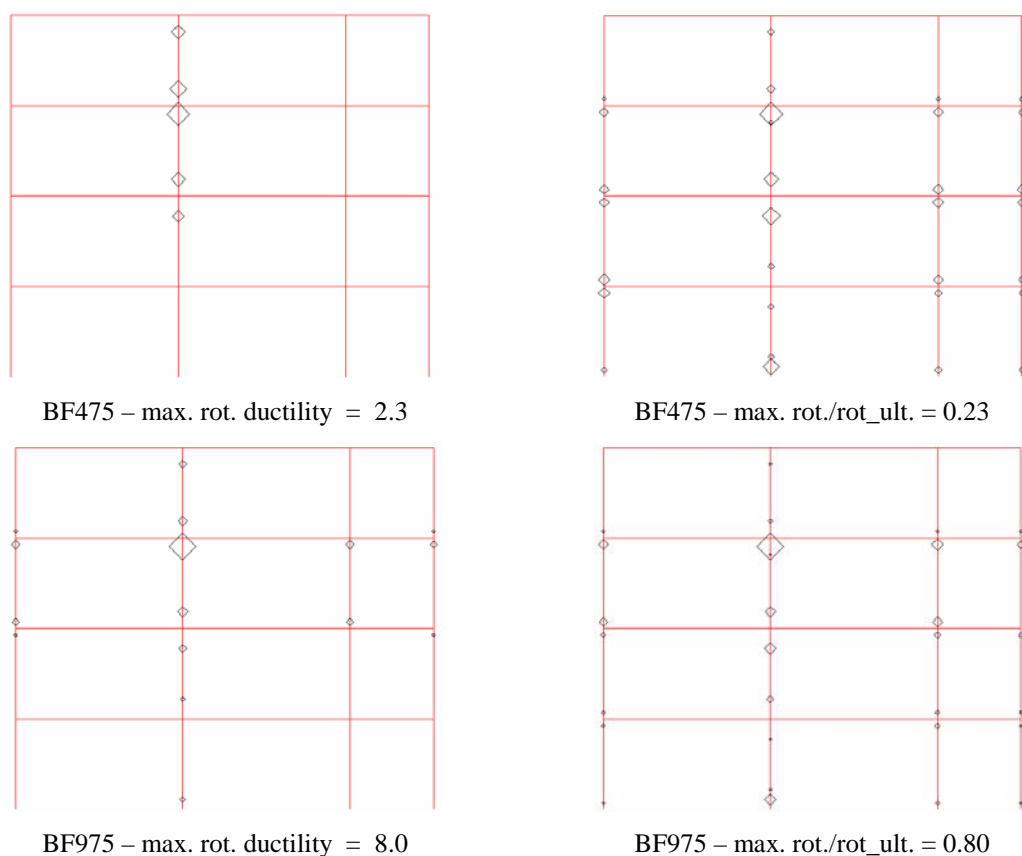


Figure 4.12 - Local rotation ductility demand and damage for the bare frame tests

Figure 4.12 shows the local rotation ductility demands in columns as well as the damage indices estimated as the ratio between the rotation demand and the ultimate rotation

capacity. The maximum ductility values found at the top of the 3<sup>rd</sup> storey strong-column (ductility = 8) is in line with the values implied by the shear-drift diagrams of the 3<sup>rd</sup> storey (see Figure 4.3). In fact, ductility 8 should imply a high damage level, which is confirmed by the apparent strength degradation in the 3<sup>rd</sup> storey shear-drift diagram. Furthermore, the maximum damage index is also in line with the damage, which occurred at the end of each test. The BF475 test with a maximum damage index (DI) of about 0.2 indicates slight damage and a DI of 0.8 (no energy contribution was included) would correspond to the imminent collapse attained during the BF975 test.

#### **4.2.6 - Energy dissipation**

Figure 4.13 plots the evolution of energy dissipation at the storey levels and the evolution of the total energy dissipated in the structure, for the earthquake tests on the bare frame. The total dissipated energy for each test, at the storey level, is represented in the schematic storey profile in Figure 4.14.

From the analyses of the energy dissipation plots, it can be concluded that:

- For the 475-yrp test, the contribution of the three first storeys to the total energy dissipated, is similar. But for the subsequent 975-yrp test, a considerable increase of the 3<sup>rd</sup> storey contribution is verified, associated with the extensive damage induced in the strong-column on this storey. Consequently, the ratio of energy dissipated at the other storeys decreases significantly.
- The low percentage of energy dissipated at the 4<sup>th</sup> storey (15% for the 475-yrp test), justified by the low non-linearity verified on this storey. This value drops to 12% in the 975-yrp test.
- Regarding the evolution of the energy dissipated, a quasi-linear variation in time was observed for the 475-yrp test. Yet, for the 975-yrp test, an exponential-like variation is verified, which is related to rapid damage increase.

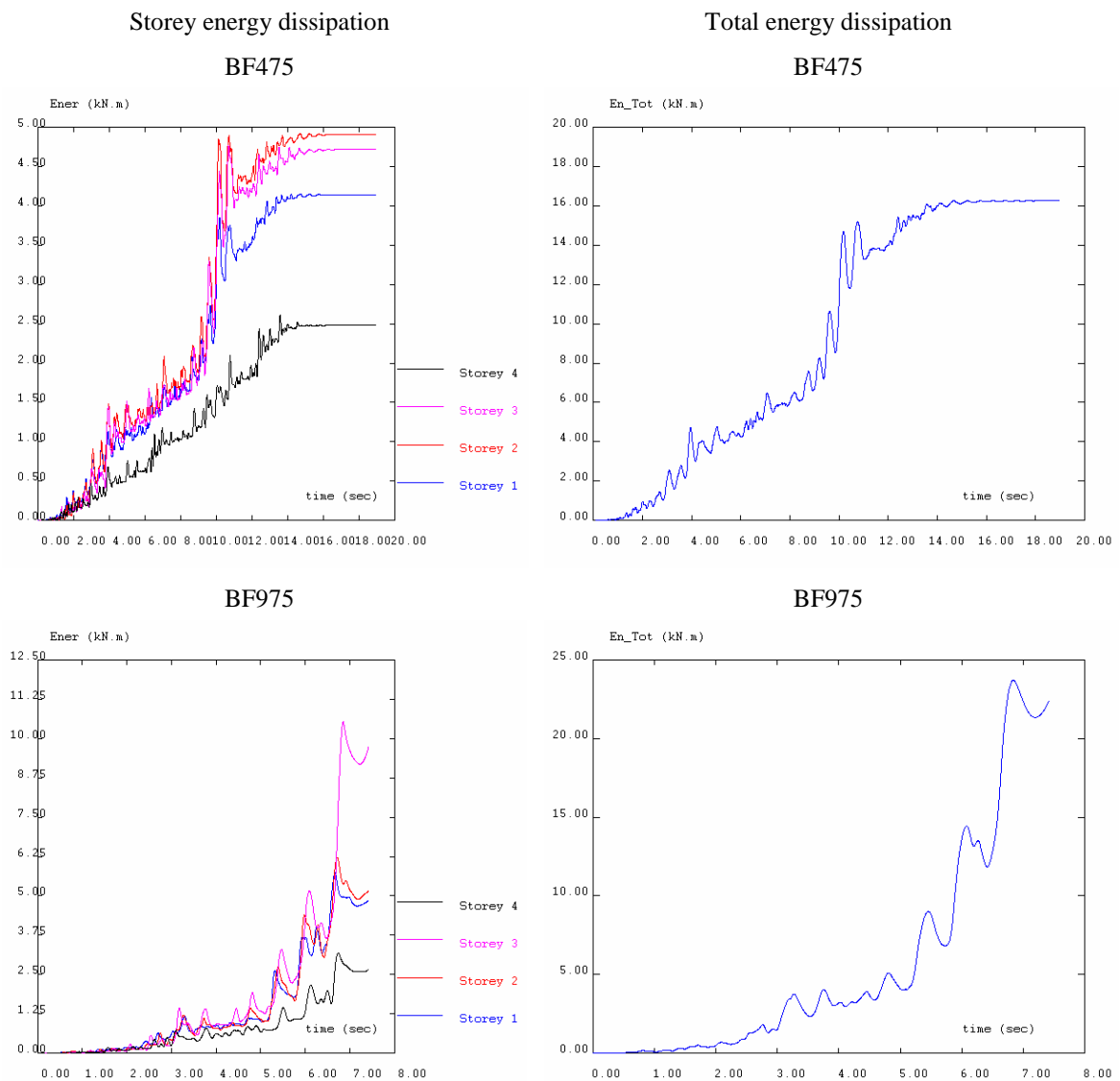


Figure 4.13 - BF tests: storey and total energy dissipation

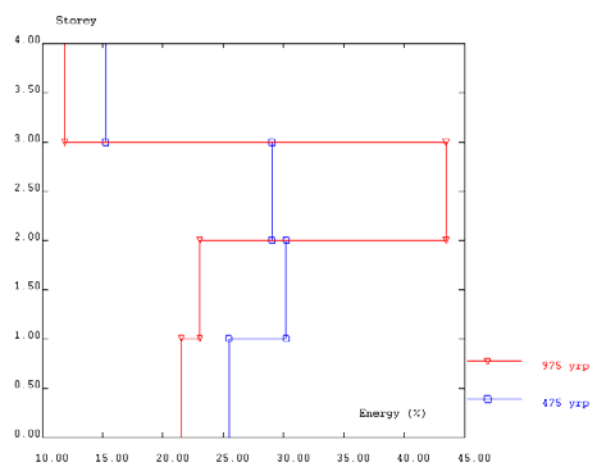


Figure 4.14 - BF tests: relative energy dissipation profiles

### 4.2.7 - Damage index

The requirements for a good damage assessment method can be formulated, for example, as advocated by Stephens and Yao (1987): *a*) the index should have general applicability, i.e. it should be valid for a variety of structural systems; *b*) it should be based on a simple formulation and be easy to use; and, *c*) it should generate easily interpretable results. Commonly, damage evaluation methods are devised for assessment of storey damage or global damage in a framed structure. The formulation presented here for the damage index is based on the methodology proposed by Park and Ang (1985). Next we present this index and apply it to our case.

#### 4.2.7.1 - Park and Ang damage index

Park and Ang damage index (PA) combine the contributions from maximum deformation damage and from dissipated energy as

$$PA_i = \frac{u_{\max,i}}{u_{u,i}} + \frac{\beta}{P_{y,i} \cdot u_{u,i}} \cdot \int dE_i \quad (4.3)$$

where:  $PA_i$  is the Park and Ang damage index for the storey  $i$ ;  $u_{\max,i}$  is the maximum inter-storey displacement of storey  $i$ ;  $u_{u,i}$  is the ultimate inter-storey deformation (under monotonic loading);  $\beta$  is the strength deterioration parameter (non-negative);  $P_{y,i}$  is the yielding strength; and  $\int dE_i$  is the incremental hysteretic dissipated energy.

The seismic structural damage index proposed by Park and Ang (1985) is expressed as a linear combination of the damages caused: by excessive deformation; and, by repeated cyclic loading effect. Theoretically, the value of PA should be zero under elastic response. Concerning the damage index, a value larger than 1.0 correspond to complete collapse or to total damage.

The literature based on a great amount of experimental test results suggest numerous empirical expressions for the strength deterioration parameter ( $\beta$ ). Typical average value

of  $\beta$  is 0.05 (Kunnath *et al.*, 1990). One of the most used expression to estimate  $\beta$  is the one proposed by Kunnath *et al.* (1990) and adapted by Arêde (1997)

$$\beta = 0.9^{100\rho_w} \left( 0.37 \cdot \max\{\nu; 0.05\} + 0.5 \cdot (\omega_t - 0.17)^2 \right) \quad (4.4)$$

where:  $\rho_w$  is the volumetric confinement ratio (volume of closed stirrups divided by the volume of confined concrete core);  $\nu$  is the normalised axial force (taken positive if compressive); and  $\omega_t$  is the mechanical ratio of tension reinforcement.

Also, from several experimental tests until failure carried out on beams and columns, Park *et al.* (1987) suggest an expression to estimate the ultimate displacement, that adapted to the SI units system ( $kN$ ,  $m$ ) can be written as follows

$$R_u (\%) = 1.958 \cdot (l/d)^{0.93} \cdot \rho^{-0.27} \cdot \rho_w^{0.48} \cdot n_0^{-0.48} \cdot f_c^{-0.15} \quad (4.5)$$

where

$$R_u = \delta_u / l \quad \rho = p_t \cdot f_y / f_c \quad n_0 = P / (b \cdot d \cdot f_c) \quad (4.6, 4.7, 4.8)$$

$R_u (\%)$  is the ultimate rotational capacity (in percent);  $\delta_u$  the ultimate horizontal displacement capacity;  $l/d$  the shear span ratio;  $\rho$  the normalized steel ratio;  $p_t$  the volumetric ratio of longitudinal steel;  $\rho_w$  the confinement ratio (in percent; replaced by 0.4%, if  $\rho_w < 0.4\%$ );  $n_0$  the normalized axial stress (replaced by 0.05, if  $n_0 < 0.05$ );  $P$  the axial load (in  $kN$ );  $b$  the width of the cross section;  $d$  the effective depth of the cross section;  $f_c$  the concrete strength (in  $kN$ ); and  $f_y$  the yield strength of steel reinforcement (in  $kN$ ).

The PA damage index may be applied at different levels, namely at mechanism, storey and global levels, and as a combination of the local damage indices. The global damage index ( $PA_G$ ) can be computed as a weighted function of the local damage indices, using the total local energy (hysteretic dissipated plus potential) with the weighing function

$$PA_G = \sum_i \alpha_i \cdot PA_i \quad \text{with} \quad \alpha_i = E_i / \sum_k E_k \quad (4.9, 4.10)$$

The application of this 'combination rule', or of another similar one, for seismic reliability analyses has to be done carefully. Shortcomings of these global indices are presented in Pinto (1998), for example.

The damage calculated using the model proposed by Park *et al.* (1987) was calibrated with respect to observed damage of nine reinforced concrete buildings moderately or severely damaged during the 1971 San Fernando earthquake and the 1978 Miyagiken-Oki earthquake in Japan. Based on this calibration, a damage criterion was developed for specifying the tolerable damage state as well as the extreme damage state that corresponds to collapse (Park *et al.*, 1984). From the calibration work, authors categorised damages into 5 damage states according to physical appearance in buildings. These are: slight, minor, moderate, severe and collapse. Results of the analyses of the nine buildings are plotted in Figure 4.15.

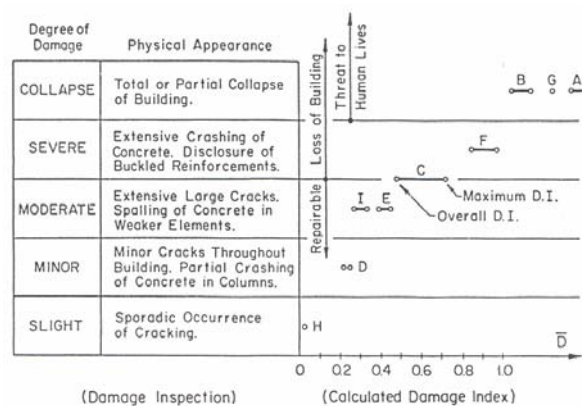


Figure 4.15 - Calculated damage index versus observed damage (Park *et al.*, 1987)

In light of the calibration results and the subsequent decisions on the respective buildings after the earthquake, it was concluded that an overall damage index of  $PA_G \leq 0.4$  may be considered to be repairable, whereas  $PA_G > 0.4$  represents damage beyond repair, and  $PA_G > 1$  represents total collapse. Based on the results of the work carried out by Park *et al.* (1987), damage indices boundaries for each degree of damage observed after an earthquake event are proposed in Table 4.3. In the table are also included proposals for local (*L*) and global (*G*) damage indices limits for each state.



Table 4.3 - Calculated damage index versus observed damage

Damage inspection		Calculated damage index	
Degree of damage	Physical appearance	Local	Global
Collapse	Total or partial collapse of building	>1.0	>1.0
Severe	Extensive crushing of concrete. Disclosure of buckled reinforcements	0.75-1.0	0.50-1.0
Moderate	Extensive large cracks. Spalling of concrete in weaker elements	0.35-0.75	0.30-0.50
Minor	Minor cracks throughout building. Partial crushing of concrete columns	0.10-0.35	0.10-0.30
Slight	Sporadic occurrence of cracking	0.0-0.10	0.0-0.10

#### 4.2.7.2 - Calculation of the PA damage index for the bare frame tests

The damage indices presented in Section 4.2.7.1 were computed and analysed for the pseudo-dynamic tests on the four-storey full-scale reinforced concrete frame tested at the ELSA laboratory. Expressions (4.4) and (4.5) were applied to the RC bare frame to estimate  $\beta$  and  $\delta_u$  parameters. A detailed description of the frame characteristics and loads was provided in Chapter 3. The results obtained for the sixteen RC columns are listed in Table 4.4.

Table 4.4 - Parameters estimated for the PA damage index for the RC columns

Storey	Parameter	Alignment			
		1	2 (strong-column)	3	4
4	$\beta$	0.029	0.028	0.039	0.025
	$\delta_u (m)$	0.300	0.117	0.258	0.340
3	$\beta$	0.060	0.060	0.084	0.054
	$\delta_u (m)$	0.207	0.081	0.177	0.214
2	$\beta$	0.092	0.080	0.135	0.085
	$\delta_u (m)$	0.168	0.055	0.133	0.168
1	$\beta$	0.124	0.106	0.179	0.115
	$\delta_u (m)$	0.146	0.047	0.115	0.144

For the frame under analysis, the behaviour of each storey is dominated by the characteristics of the column in the second alignment (strong-column). Therefore, to

evaluate the damage index at storey level, the parameters corresponding to the strong-column are considered.

In fact, looking at the results of the test BF975, it is clear that the collapse of the 3<sup>rd</sup> storey was imminent the ultimate inter-storey deformation (under monotonic loading),  $\delta_u$ , was estimated by: assuming that at the end of the test the damage index for the 3<sup>rd</sup> storey reached 1.0; using the value of parameter  $\beta$  estimated (0.06); computing the hysteretic energy dissipated (14500 *kN·m*) and the maximum inter-storey displacement of the 3<sup>rd</sup> storey (0.065 *m*); and, by using the value of lateral yielding storey strength observed during the tests (90 *kN*). Substituting in expression (4.3) the damage index for 1.0, the ultimate inter-storey displacement can be obtained as indicated in the following equation

$$u_{u,i} = u_{\max,i} + \frac{\beta}{P_{y,i}} \cdot \int dE_i \quad (4.11)$$

Regarding the 3<sup>rd</sup> storey of the frame analysed, the value 0.075 *m* for  $\delta_u$  was computed. Comparing to the value in Table 4.4 (0.081 *m*), it can be concluded that the parameters  $\beta$  and  $\delta_u$  estimated with the empirical expressions (4.4) and (4.5), respectively, give reasonable values. The evolution of the damage index with the parameters estimated for each storey (Table 4.4) was also computed. The results obtained are plotted in Figure 4.16. Table 4.5 summarises the PA damage index for each storey at the end of each PsD test on the bare frame.

Table 4.5 - BF tests: Park & Ang damage indicator

Earthquake (yrp)	storey			
	1	2	3	4
475	0.316	0.416	0.304	0.115
975 <sup>a</sup>	0.511	0.629	0.928	0.230

a) Test performed up to 7.5 seconds because imminent collapse was attained.

Figure 4.17 represents the influence of the energy dissipation on the damage index. The red curves represent the damage index considering the complete definition. Curves in green represent the index considering only the contribution of the maximum deformation.

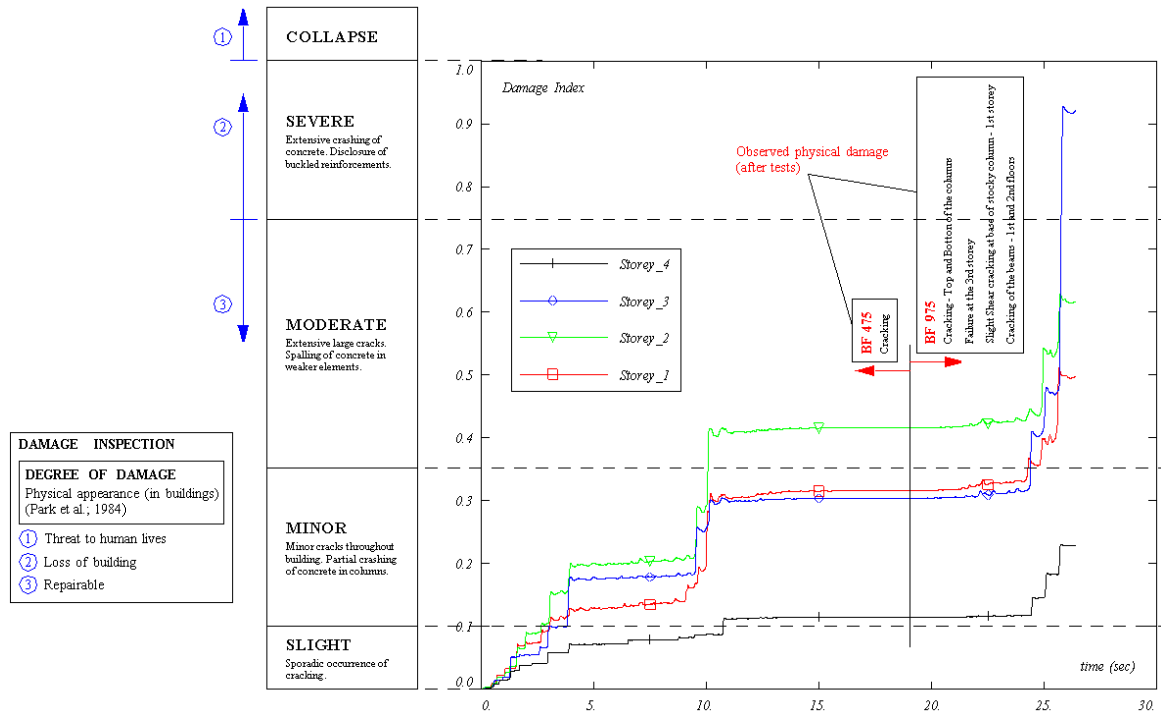


Figure 4.16 - BF tests: evolution of the storey damage index

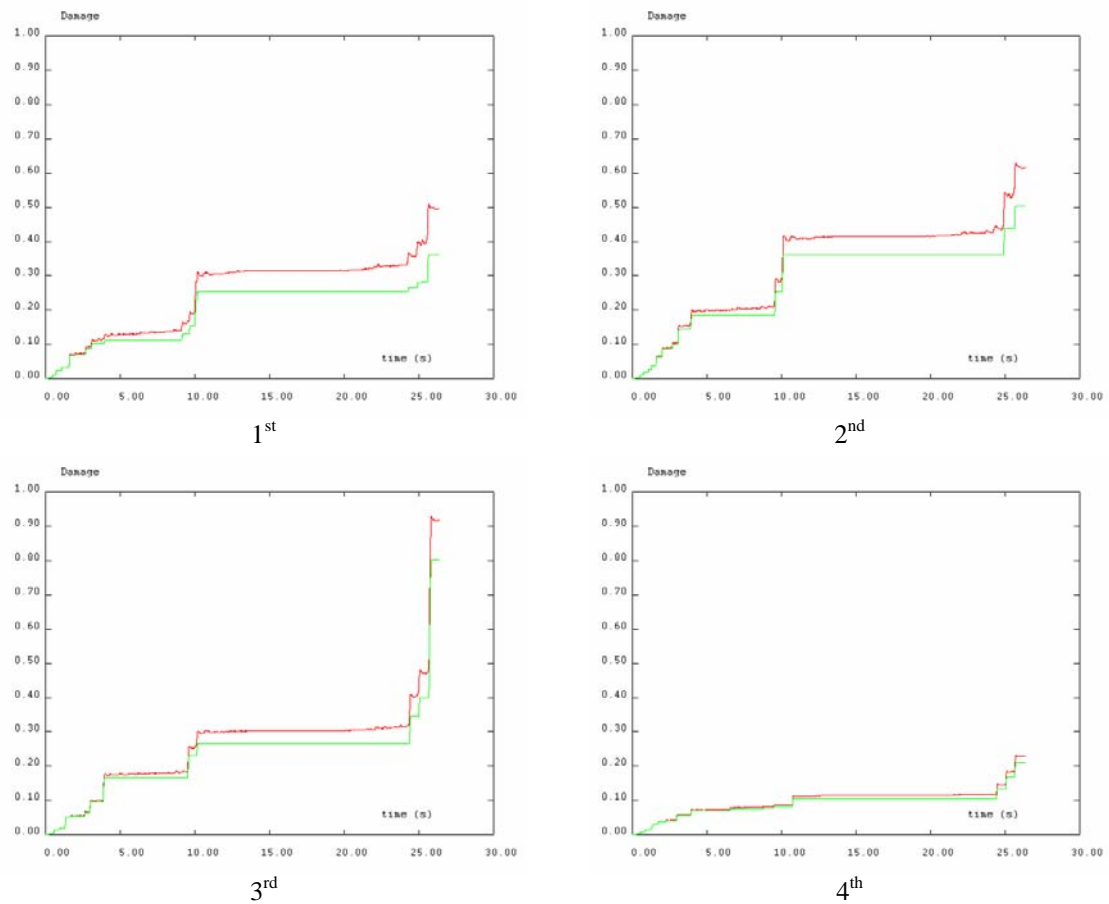


Figure 4.17 - BF tests: influence of the energy dissipation on the evolution of the storey damage index

From the analyses of Figure 4.17, it can be concluded that the influence of the energy dissipation on the damage index is not negligible, but it is of minor importance when compared to the maximum deformation contribution.

#### 4.2.8 - Deformation at the beam extremities

Figure 4.18-*a* plots the envelope of maximum relative rotation for the bare frame tests, measured at the 1<sup>st</sup> storey beam adjacent to the strong-column's joint. In the figure, beam length stands for distance from the column face. The relative rotation is computed as the maximum relative value measured between two consecutive inclinometers. In Figure 4.18-*b*, the maximum uniform strain at the top and bottom beam fibres measured during the tests are represented. It is apparent that most of the rotation and deformation concentrate in a very narrow beam slice (75 mm length) adjacent to the beam/column interface. Moreover, the uniform strain values indicate that no rebar yielding takes place out-side of this beam slice and the reinforcement only experienced deformation lower than the hardening strain (maximum of about 1.5%).

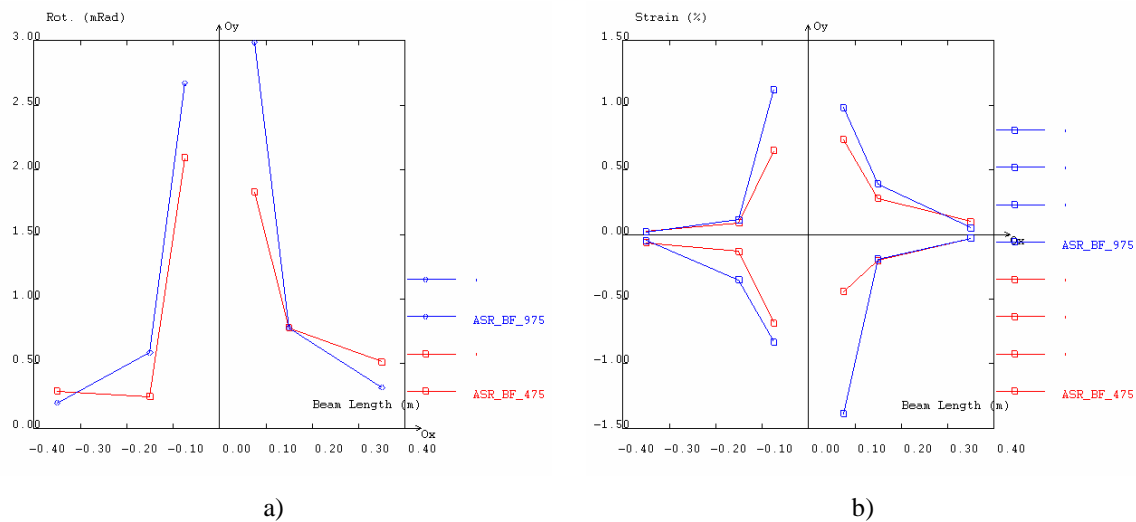


Figure 4.18 - BF tests: beam 1<sup>st</sup> floor: a) maximum relative rotation; b) maximum uniform strain

#### 4.2.9 - Remarks

From the tests carried out on the bare frame, it is possible to confirm the storey mechanism, which were expected to develop during the earthquake response due to the vertical irregularity induced by the sudden change in the cross-section of the strong-column at the 3<sup>rd</sup> storey. In fact, the structure represents design that was common practice until the late 1970's, when seismic loading was only roughly considered or even not taken into account. Consequently, this structural misconception induces commonly the collapse of buildings when an earthquake occurs, as reviewed in Section 2.5.7. From the shear-drift diagrams for the 475-yrp test, it is apparent that a rather limited non-linear behaviour (storey ductility of about 2 at the 3<sup>rd</sup> storey) and quite limited damage occurred during the test. Slight cracking at column extremities, as well as in the girders (at the slabs – for negative moments) could be observed and no spalling of cover concrete occurred.

However, it was possible to confirm the high vulnerability of these structures. In fact, in spite of the very limited damages for the 475-yrp earthquake, it was demonstrated that, the demands for a slightly higher intensity earthquake (1.3 times the maximum acceleration of the 475-yrp input motion) led to an imminent storey failure, and to consequent collapse of the structure. Therefore, development and validation of effective (and also economic) retrofitting solutions and techniques for this type of structures urges.

### 4.3 - RESULTS FROM THE TESTS ON THE SELECTIVE STRENGTHENED FRAME

Following the two tests on the bare frame, the damaged parts of the structure were repaired (strong-column of the 3<sup>rd</sup> storey). The spalled concrete was removed and the cracks were injected with epoxy, the surfaces were cleaned and the selective retrofitting scheme (described in Section 3.3) proposed by the research group at the Imperial College of London (Elnashai and Pinho, 1999) was applied. Figure 3.11 shows the strong-column strengthened according to the scheme proposed.

The initial testing programme for the selective strengthened frame (SR) was similar to the BF programme. However, considering that the SR975 test led to rather small demands and

damage, it was decided to perform an additional test with higher intensity. This test was expected to inflict more significant damage on the structure but it was also necessary to guarantee structural integrity for the next strengthening solution foreseen for this frame (K-bracing with shear-link test). A 2000-yrp earthquake was adopted for this high-level test. In the next sections is given a compilation of the results from these tests in terms of storey displacement, maximum inter-storey drift profiles for positive and negative deformations, energy dissipation, and shear-drift diagrams.

#### **4.3.1 - Storey displacement, drift and shear**

In Figure 4.19 the time histories of storey displacement are plotted for the three earthquake pseudo-dynamic tests performed on the selective strengthened structure, namely 475, 975 and 2000-yrp. Figure 4.20 shows the top-displacement curves for the three earthquake tests, and Figure 4.21 plots the curves base-shear versus top-displacement for the SR tests. In Figure 4.22 the curves storey shear versus inter-storey drift are presented, and in Figure 4.23 the respective envelope curves of these storey shear-drift diagrams are plotted. Figure 4.24 represents the maximum inter-storey drift profile and the maximum storey shear profile. Table 4.6 presents the maximum values for characteristic response variables for the SR tests.

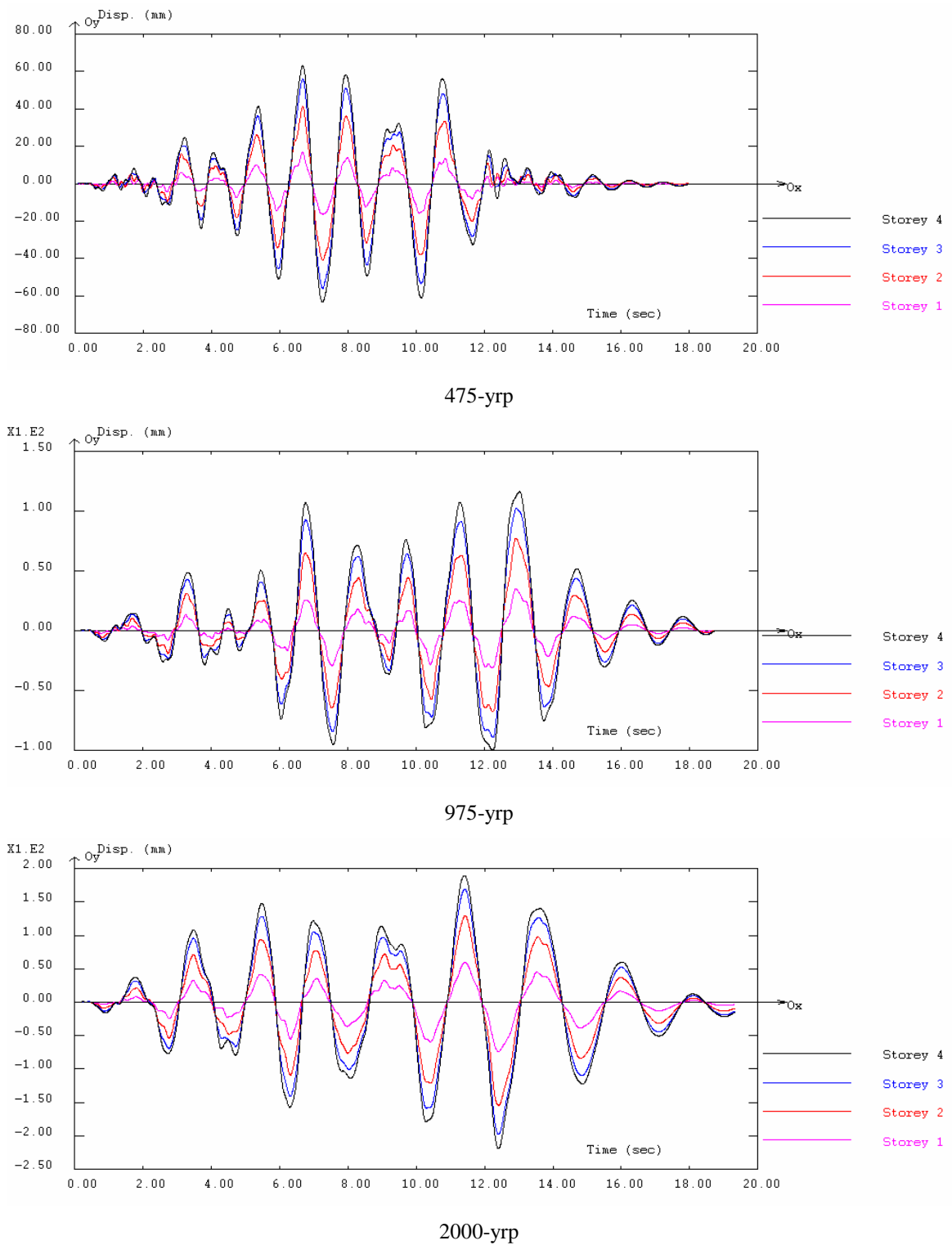


Figure 4.19 - SR tests: storey displacement time histories

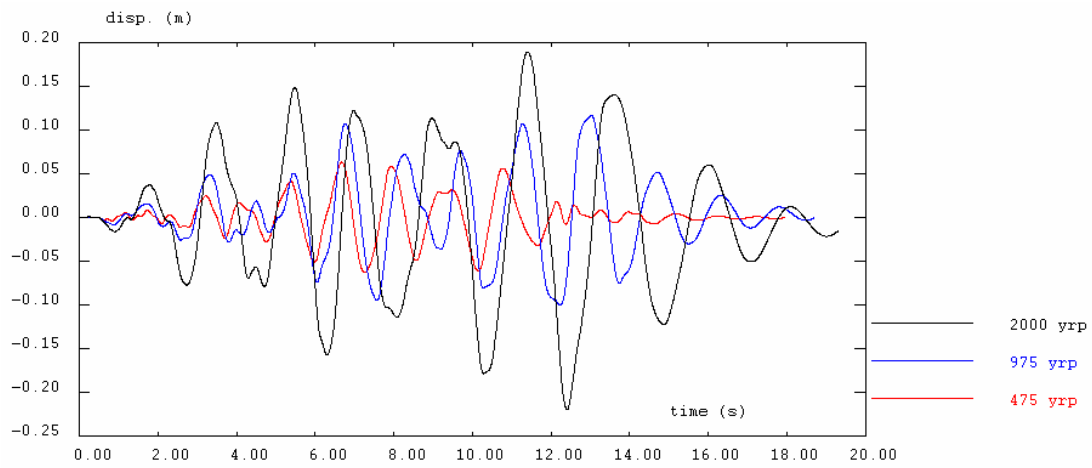


Figure 4.20 - SR tests: top-displacement evolution

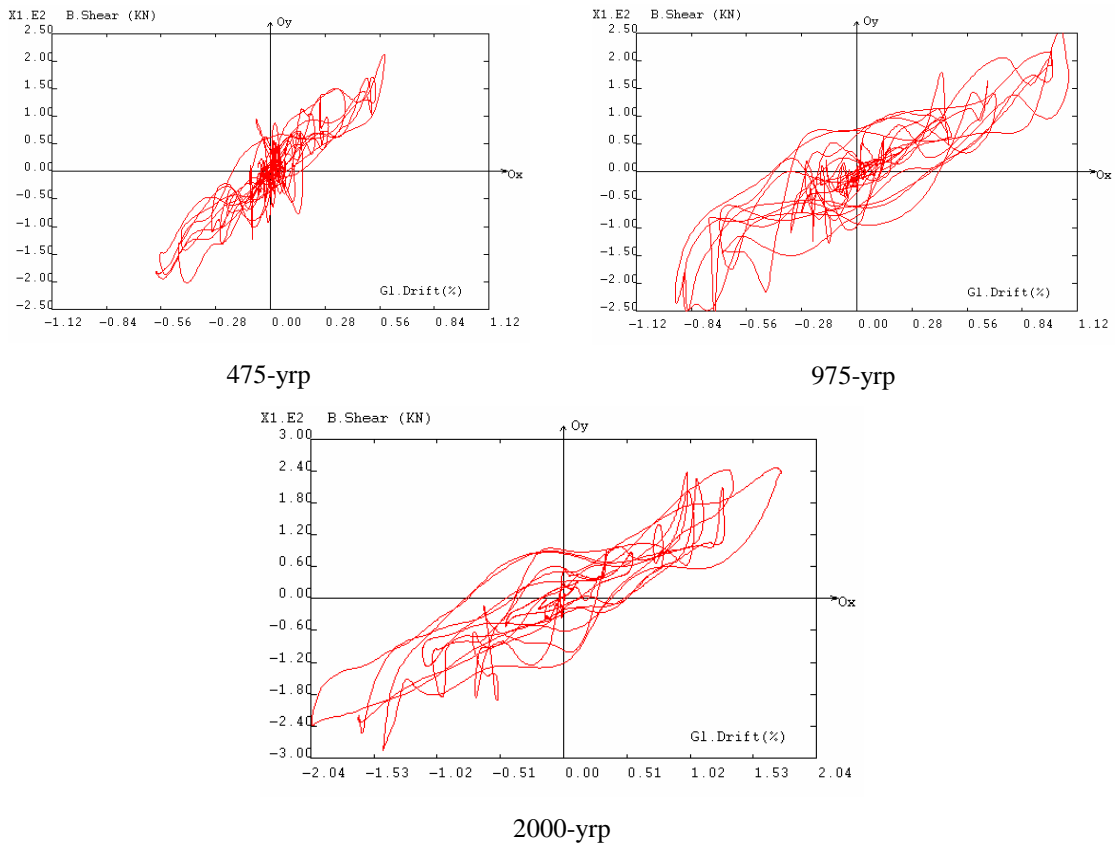


Figure 4.21 - SR tests: base-shear versus top-displacement



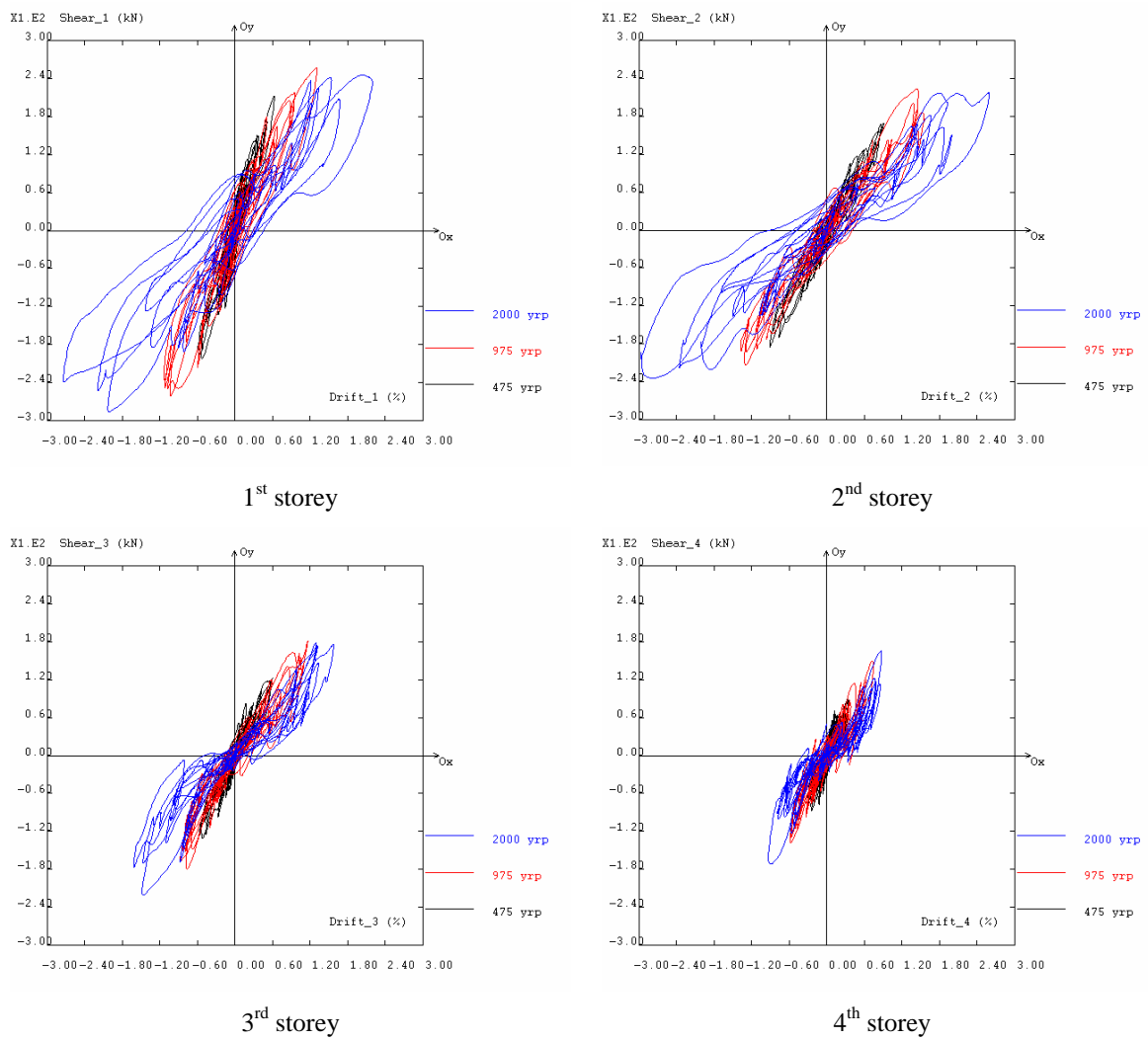


Figure 4.22 - SR tests: storey shear versus inter-storey drift

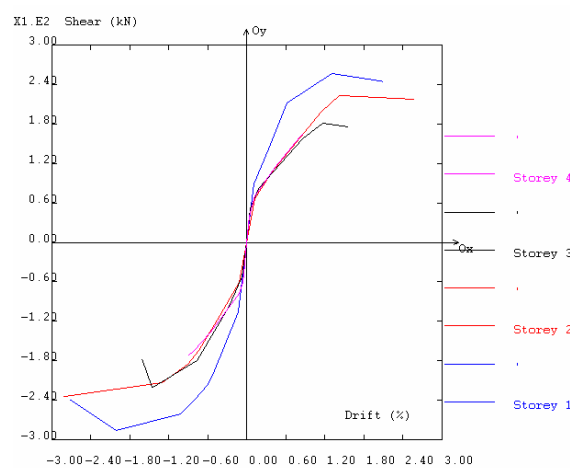


Figure 4.23 - SR tests: envelope storey shear versus inter-storey drift

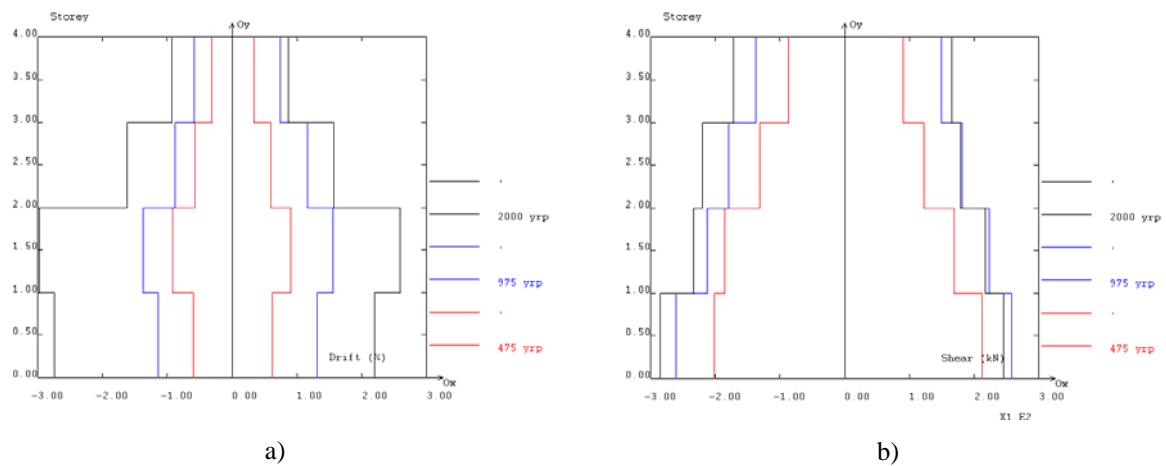


Figure 4.24 - SR tests: a) maximum inter-storey drift profiles; b) maximum storey shear profiles

Table 4.6 - SR tests: response maximum values (summary table)

Test <sup>a</sup>	Top-displacement (mm)		Global drift (%)	
SR475	63.2		0.59	
SR975	116.3		1.08	
SR2000	219.5		2.03	
	Inter-storey drift (%)			
	storey 1	storey 2	storey 3	storey 4
SR475	0.63	0.92	0.60	0.34
SR975	1.31	1.56	1.16	0.74
SR2000	2.75	2.98	1.62	0.94
	Storey shear (kN)			
	storey 1	storey 2	storey 3	storey 4
SR475	212.2	185.5	130.8	90.1
SR975	261.1	223.3	181.6	149.2
SR2000	285.9	234.1	220.4	171.9
	Max. hinge rotation (mRad)			
	(mRad)	Location		
SR475	12.0	slender-column 2 <sup>nd</sup> storey		
SR975	21.1	slender-col. 1 <sup>st</sup> and 2 <sup>nd</sup> storey		
SR2000	38.7	slender-col. 1 <sup>st</sup> and 2 <sup>nd</sup> storey		

a) Duration of the input motions is 15 seconds for the earthquake PsD tests.

Regarding top-displacements, the demands for the SR475 and SR975 tests are similar to the corresponding ones for the bare frame. However, the behaviour of the structure was

significantly improved by the strengthening scheme. As shown in Figure 4.24, the strengthened structure became rather regular, and the storey drift demands were quite uniformly shared by the three lower storeys. Moreover, this regular drift profile pattern was maintained for the higher intensity test (SR2000).

### 4.3.2 - Observed damages

A detailed description of the damage on the strengthened frame (visual damage inspection) for each test is included in Table 4.7. It also attempts at categorising them according to the ATC-40 (1996) damage states. Figure B.18 shows a general layout of the damage observed on the strengthened frame at the end of the tests.

Table 4.7 - SR tests: damage inspection (see damage patterns in Figure B.18) and damage states (ATC-40, 1996)

Test	Damages	Damage state	Repair required?
SR475	<ul style="list-style-type: none"> <li>• Cracking – Strong-column – base of 1<sup>st</sup> storey, base and top of 2<sup>nd</sup> storey</li> <li>• Slight cracking of the beams at 1<sup>st</sup> and 2<sup>nd</sup> floors for positive moments</li> </ul>	Slight	No
SR975	<ul style="list-style-type: none"> <li>• Cracking – Strong-column – 1<sup>st</sup> storey – Between the first and the second confining plates and at the bars termination zone (between the 3<sup>rd</sup> and 4<sup>th</sup> confining plates)</li> <li>• Cracking of the beams (near the strong-column joint – only one side) at all floors for positive moments</li> </ul>	Light	No
SR2000	<ul style="list-style-type: none"> <li>• Cracking at the strong-column – 1<sup>st</sup> storey – Additional cracking between confining plates; Crushing at the base; Crushing (slight) at the bars termination zone</li> <li>• Additional cracking of the beams (near the strong-column joint – Both sides) at 1<sup>st</sup> and 2<sup>nd</sup> floors for positive moments</li> <li>• Spalling of cover (beams of the 1<sup>st</sup> and 2<sup>nd</sup> floors)</li> <li>• Spalling of cover at the ends of the slender-columns (1<sup>st</sup>, 2<sup>nd</sup> and 3<sup>rd</sup> storeys)</li> <li>• Confining plates peeling from concrete (plastic deformation of the plates) at all storeys: 1<sup>st</sup> storey – 1<sup>st</sup> and 4<sup>th</sup> plate; 2<sup>nd</sup> storey – upper plate; 3<sup>rd</sup> storey – 6<sup>th</sup> and last (upper) plates</li> </ul>	Moderate	Yes

### 4.3.3 - Maximum absolute and relative rotations measured at the critical zones

Figure 4.25 presents the maximum absolute and relative rotations measured during the tests performed on the strengthened structure. Results are presented for the three pseudo-dynamic tests. Concerning the relative deformation of the beams and columns, it is apparent from Figure 4.25 that similar comments to the ones for the BF can be made. However, the SR frame shows a much uniform distribution of demands in the frame height. In addition, the slight strong-column retrofit leads to higher demands in the beams.

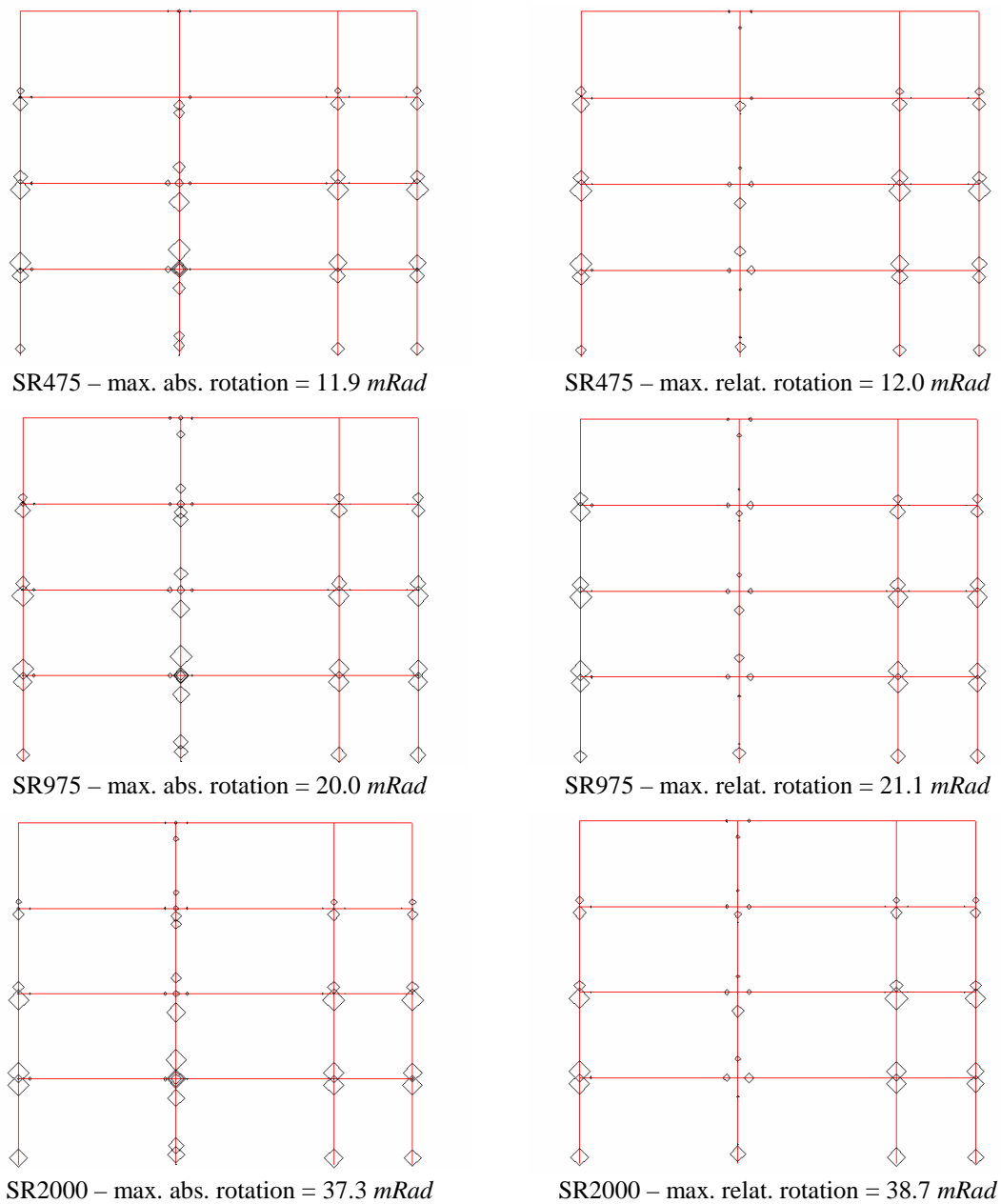


Figure 4.25 - SR tests: maximum absolute and relative rotation demands

---

From the analyses of the Figure 4.25, the following can be observed:

- Comparing the absolute and relative rotations for the weak-columns, it is clear that the relative rotations are similar to the absolute ones. This is justified with the stiffness difference between these columns and the beam (greater for the beam). Therefore, in the vicinity of the weak-columns, the beam practically does not rotate and the storey deformation is concentrated in the columns.
- From the results analysis and test observations it was perceived that, in the weak-columns, all the deformation is concentrated in the column extremities. Contrarily, for the strong-column the deformation is spread along its height.
- Looking at the results for the strong-column it can be observed that its greater stiffness, compared with the beam, force the beam to deform. In fact, it is in the vicinity of this column that the beams reached their maximum relative rotation.
- The strong-column reaches its maximum relative rotation at the first two storeys, namely: base of the first and top of the second storeys.

#### **4.3.4 - Energy dissipation**

Figure 4.26 plots the evolution of energy dissipation at the storey levels and the evolution of the total energy dissipated in the structure for the PsD tests on the strengthened frame. The total dissipated energy storey profiles are represented in Figure 4.27.

From the analyses of the energy dissipation plots, it can be concluded:

- The total dissipated energy at the 2000-yrp test is approximately the double than at the 975-yrp test, and six times the dissipated at the 475-yrp test.
- As observed in the dissipated energy profiles in Figure 4.27, the relative energy dissipated between storeys is roughly equal for the three earthquake tests.
- For all earthquake tests, the two first storeys dissipate about the same amount of energy, contributing each storey to approximately 40% of the total energy dissipated by the structure.

- The fourth storey dissipates only 8% of the total dissipated energy for the first two PsD tests, and just 5% for the more intense earthquake test (2000-yrp).

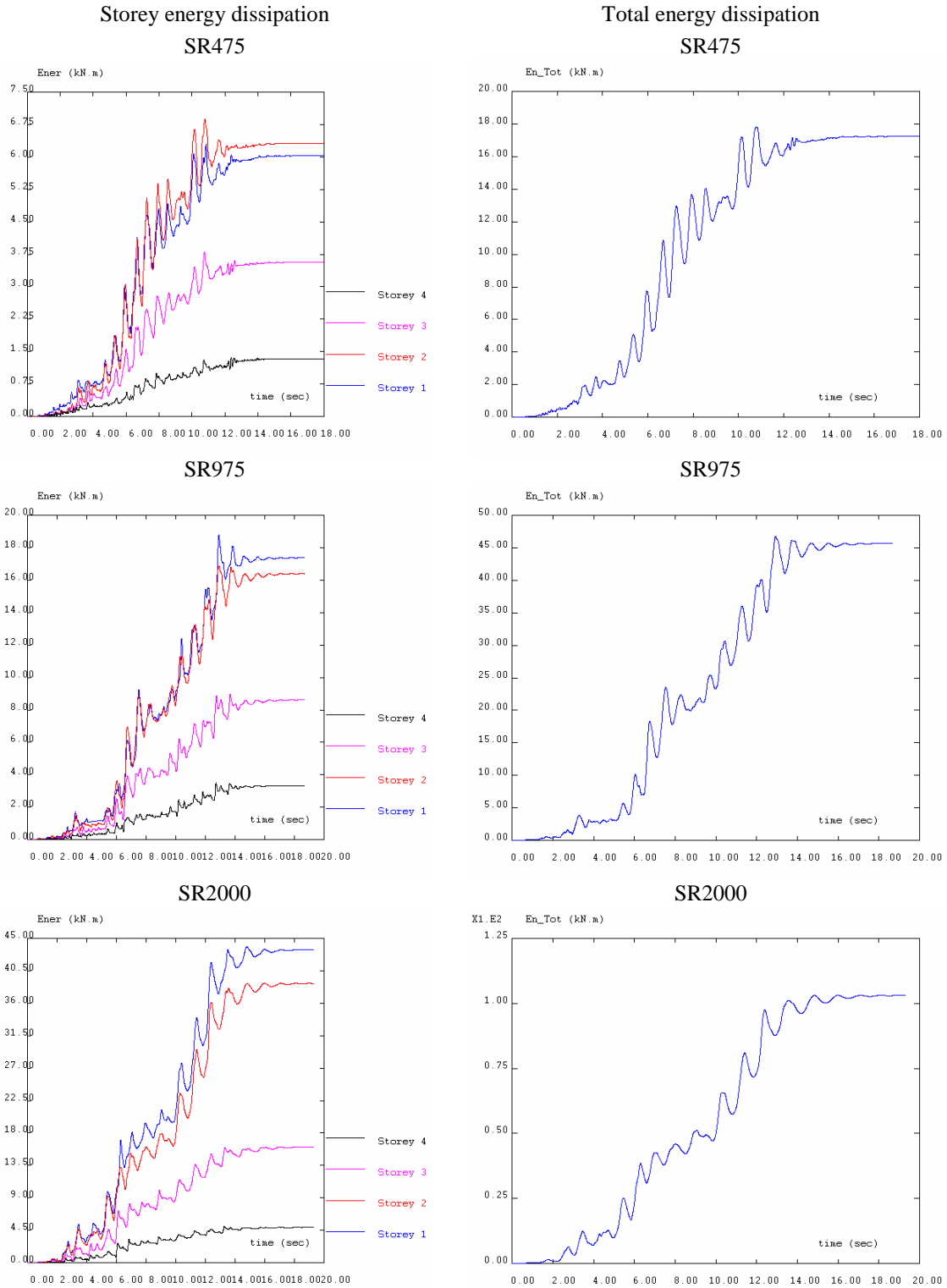


Figure 4.26 - SR tests: storey and total energy dissipation

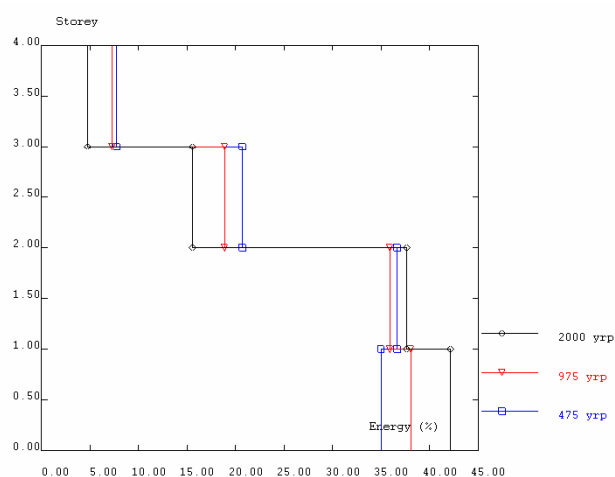
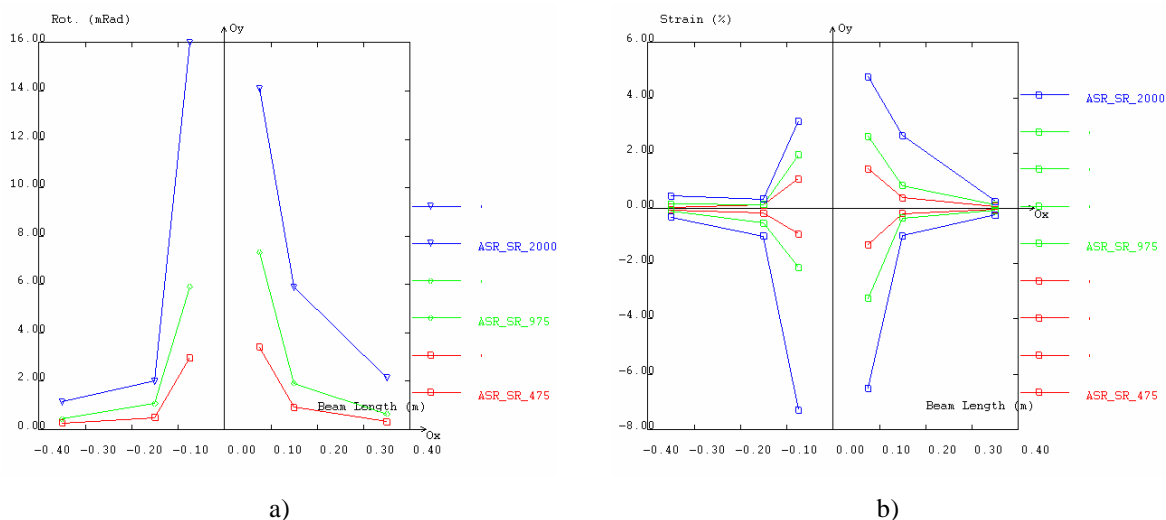


Figure 4.27 - SR tests: relative energy dissipation profiles

#### 4.3.5 - Deformation at the beam extremities

Figure 4.28-a plots the envelope of relative rotation for the SR tests, measured at the 1<sup>st</sup> storey beam adjacent to the strong-column's joint. The relative rotation is computed as the maximum relative value measured between two consecutive inclinometers. In Figure 4.28-b, the maximum uniform strain at the top and bottom beam fibres measured during the tests are represented.

Figure 4.28 - SR tests: beam 1<sup>st</sup> floor: a) maximum relative rotation; b) maximum uniform strain

The comments for the BF case are extendable to this strengthened frame case because no intervention was made in the beam. Thus, it is apparent that most of the rotation and deformation concentrate in a very narrow beam slice (75 mm length) adjacent to the beam/column face. Moreover, the uniform strain values indicate that no rebars yielding takes place outside of this beam slice and the reinforcement only experienced deformation (maximum of about 7%) lower than the hardening strain. However, for the 975-yrp test, the uniform strain values are approximately twice the values for the bare frame. Section 4.4.4 further discusses and compares the results obtained for the BF and SR tests.

#### **4.4 - COMPARISON BETWEEN BF AND SR TESTS**

The results from the BF and SR tests were presented in the previous sections without direct comparison between them. It is important to quantify both the BF and SR demands and ultimate capacities, but it is also very useful to highlight the effectiveness of the retrofit provided to the frame. This section aims at a direct comparison between the performances of the two frames underlining the potential benefits of such a selective retrofitting intervention.

##### **4.4.1 - Storey displacement, drift and shear**

Although a building with an irregular configuration may be designed to meet all code requirements, irregular buildings generally do not perform as well as regular buildings under similar earthquake loading. Typical building configuration deficiencies include irregular geometry, weakness in a given storey, soft-storey phenomenon in a given storey, a concentration of mass, discontinuity in the lateral force resisting system, or torsion effect due to the irregularities in the plan. Horizontal irregularities involve the horizontal distribution of lateral forces to the resisting frames or shear walls. Vertical irregularities are defined in terms of strength, stiffness, geometry and mass.

After recent earthquakes, important level of damage was observed in a considerable number of buildings that suffered mid-height collapses. The reduction in strength and/or



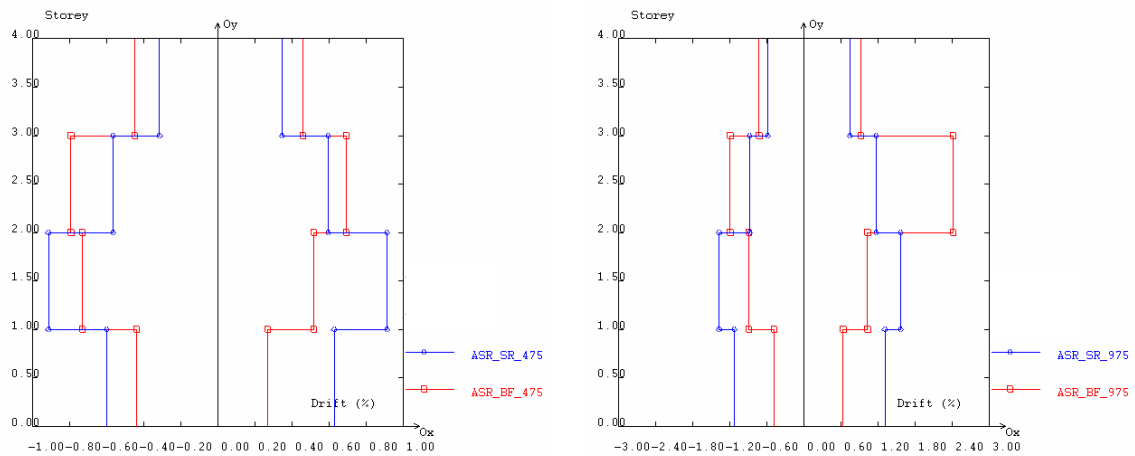
---

stiffness coupled with unexpected higher mode effects may have the potential to cause such mid-height collapses (FEMA-310, 1998).

In the structure tested at ELSA laboratory, the change in cross-section size and reinforcement of the strong central column (from 60 to 50 *cm* cross-section height) at the 3<sup>rd</sup> storey level strongly affect its strength and stiffness, making the original non-strengthened frame an irregular structure in elevation. The selective strengthening solution, applied at the 3<sup>rd</sup> storey, intended to correct these deficiencies, increasing storey stiffness and strength at appropriate levels.

The tests performed on the bare frame show a concentration of inter-storey drift demand, and consequently damage in the 3<sup>rd</sup> storey. The mechanism developed in the structure was due to its vertical irregularity in terms of stiffness and strength. The selective strengthening addressed and solved the irregularity problem of the structure. The maximum storey drift profiles plotted in Figures 4.29 and 4.30 confirm the effectiveness of the strengthening.

For the 475-yrp test, no substantial differences exist between the BF and SR drift demands. For the 975-yrp earthquake test on the SR frame, the drift profile is considerably more uniform. The retrofit intervention vanishes the structural irregularity at the 3<sup>rd</sup> storey, which has caused large drift demand of this storey for the bare frame 975-yrp test. Recall that for the 975-yrp tests, similar value of top-displacement was observed for BF and SR, but more uniform distribution of drift demands was found for the SR frame. Furthermore, the strengthened frame is able to withstand an input motion intensity twice as much as the nominal one without collapse and with reparable damages, while the bare frame collapsed for an input motion 1.3 times the nominal intensity. For the strengthened structure, it should also be noted the uniformity of the inter-storey drift profile pattern for different input motion intensities. In fact, as shown in Figure 4.30 (on the right), the drift demands increase proportionally to the input motion maintaining the drift pattern. This confirms that the selective strengthening prevented the storey mechanism. In addition, the drift demands are rather uniformly shared between the three lower storeys.



475-yrp tests

975-yrp tests

Figure 4.29 - BF and SR tests: maximum inter-storey drift profiles

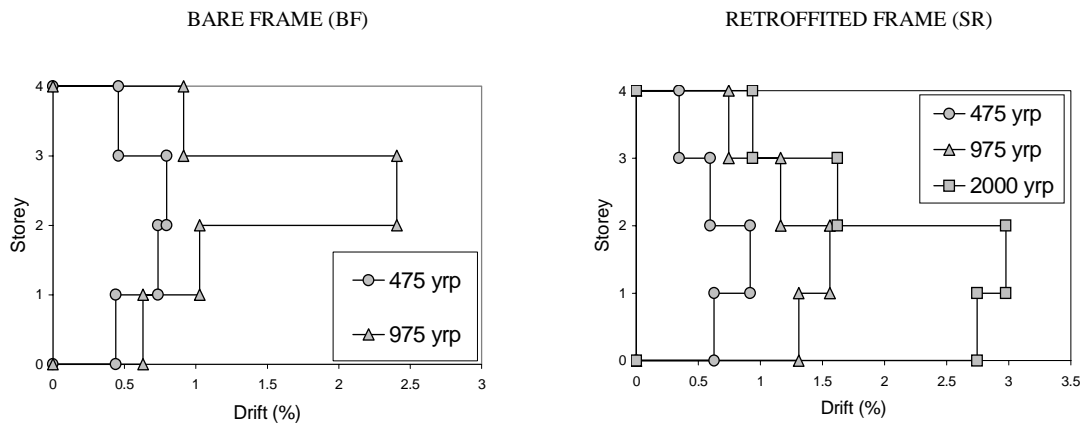


Figure 4.30 - BF and SR tests: maximum inter-storey drift profiles

The series of diagrams (shear-drift) given in Figure 4.31 include the diagrams for the BF and SR test for the 975-yrp earthquake, reflecting the effects of the strengthening operation. There was an increase of the stiffness and strength (see for peak drifts) at the 3<sup>rd</sup> and 4<sup>th</sup> storeys, and an increase of strength at the 1<sup>st</sup> and 2<sup>nd</sup> storeys (substantially higher confinement and shear resistance).

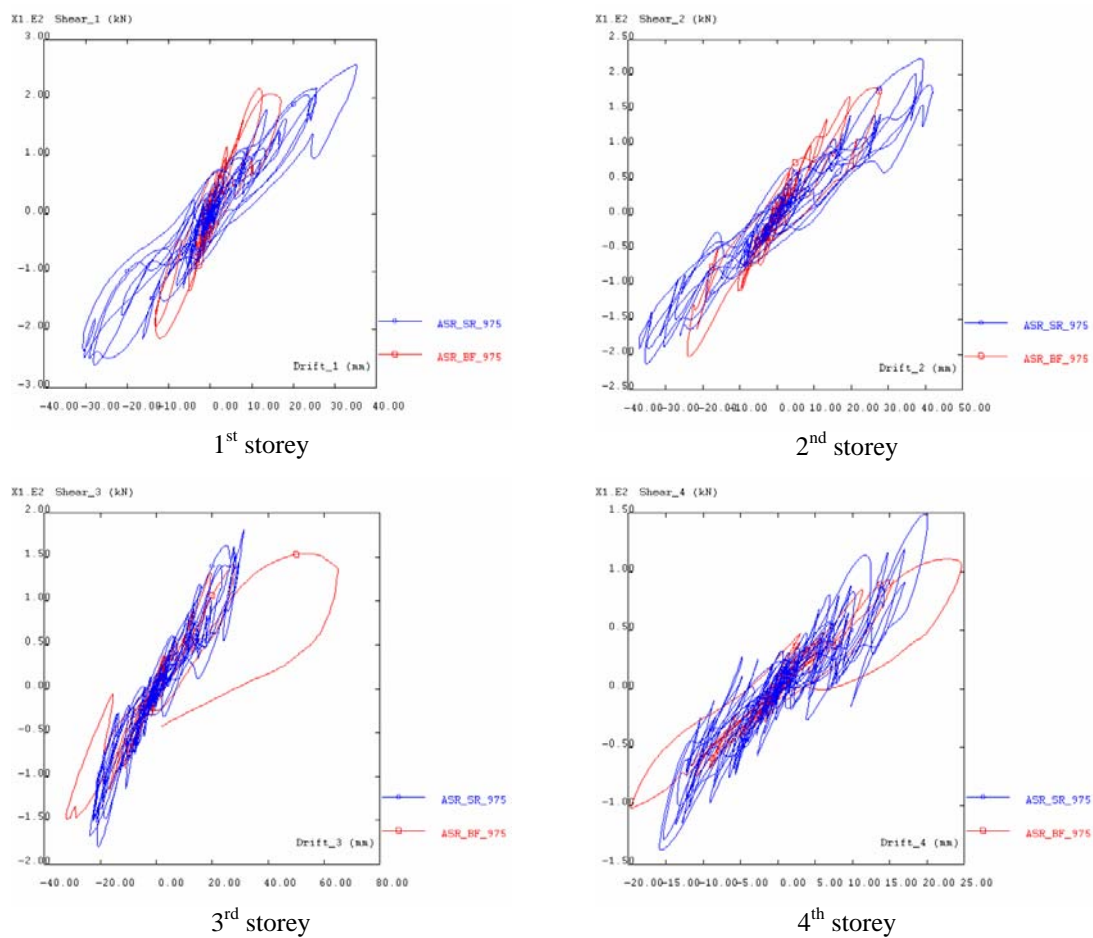


Figure 4.31 - BF and SR 975-yrp tests: storey shear versus inter-storey drift

The series of diagrams (shear-drift) given in Figure 4.32 cover all tests and give a good idea of the envelope curves for each storey as well as the storey ductility reached during the SR2000 test. It is also apparent from these diagrams the strength degradation, i.e. crushing of concrete in the strong-column, spalling of cover in the slender-columns, and in the beams, and a very pronounced pinching effect due to slippage of rebars in the central beam-column joints occurred.

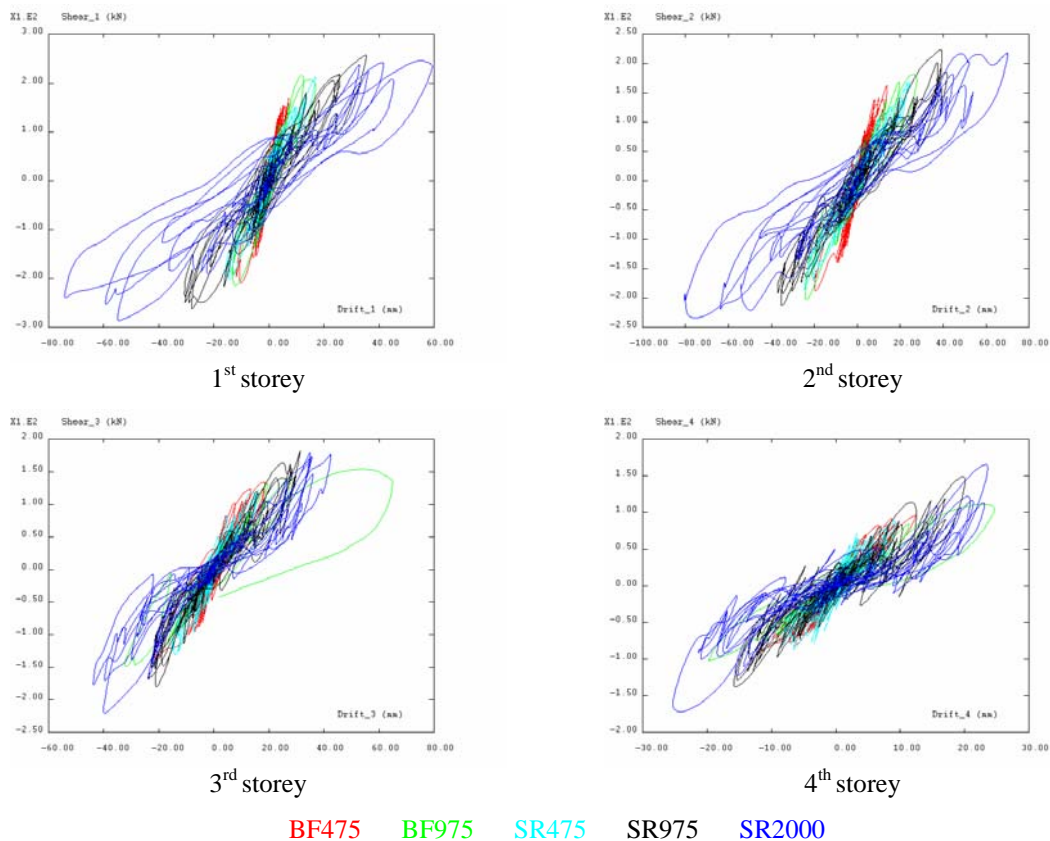


Figure 4.32 - BF and SR tests: storey shear versus inter-storey drift

#### 4.4.2 - Maximum absolute and relative rotations measured at the critical zones

Modern codes support the strong-column weak-beam concept (EC8; FEMA-310, 1998), presupposing that beams will develop hinges before the columns at locations distributed throughout the structure. It is expected that the combined action of gravity loads and seismic forces will cause the formation of plastic hinges first in the beams, distributing the yielding, and further dispersing the ductility demand throughout the structure.

Existing structures not designed for earthquake loads do not have the performance required by modern codes. A concentration of plastic hinge formation at undesirable locations can severely undermine the stability of the structure. For example, in a weak-column situation, hinges can form at the tops and bottoms of all the columns in a particular storey, and a storey mechanism develops. This results in a concentration of ductility demand and displacement in a single storey, which can lead to collapse.

Figure 4.33 shows for the same earthquake intensity (975-yrp) the response of BF and SR frames in terms of relative rotations. Yet, recall that the BF structure was just subjected to 7.5 seconds earthquake ground motion.

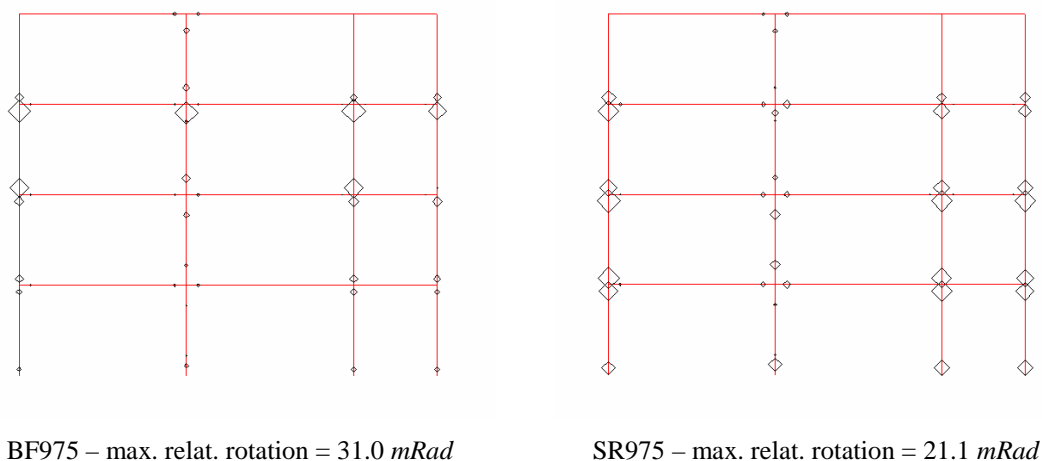


Figure 4.33 - BF and SR tests: maximum relative rotation demands for the 975-yrp tests

Analysing the Figure 4.33, the improved performance of the strengthened structure can be perceived. Again, only the strong-column will be analysed, because the slender ones are not preponderant to the structure response. Comparing the behaviour of the strong-column and the beam in its vicinity, the beams of the BF practically do not deform, being the deformation demand concentrated in the strong-column. For the retrofitted structure, a larger deformation demand develops in the beams, protecting the columns and, consequently, improving the structure performance.

From the rotation patterns for the 975-yrp tests given in Figure 4.33, it can be observed a much more uniform distribution of the rotation demands at the member end-sides (potential plastic hinge zones) for the retrofitted frame. Furthermore, it is also apparent that the demands are higher in the girders compared to the BF frame tests. This is a very important result. It confirms that a slight increase on the column strength can increase its performance. This kind of strong-beam weak-column structures designed without appropriate seismic provisions (for example: capacity design), can be significantly protected if a rational strengthening operation is carried out.

### 4.4.3 - Energy dissipation

The dissipated energy profiles given in Figures 4.34 and 4.35 confirm the benefits gained from the SR operation:

- For the low level test on the bare frame (BF475), the significant and balanced contribution of the first three storeys to the energy dissipation is evident.
- For the BF975 test, the higher contribution of the 3<sup>rd</sup> storey for the energy dissipation is evident. This is due to the high concentration of damage in the strong-column at this storey.
- All the tests on the selective strengthened frame produced an energy dissipation profile with almost the same configuration. Yet, it was clearly shown in Section 4.3.4 for the case of SR tests that the amount of energy dissipated in each test is very different.

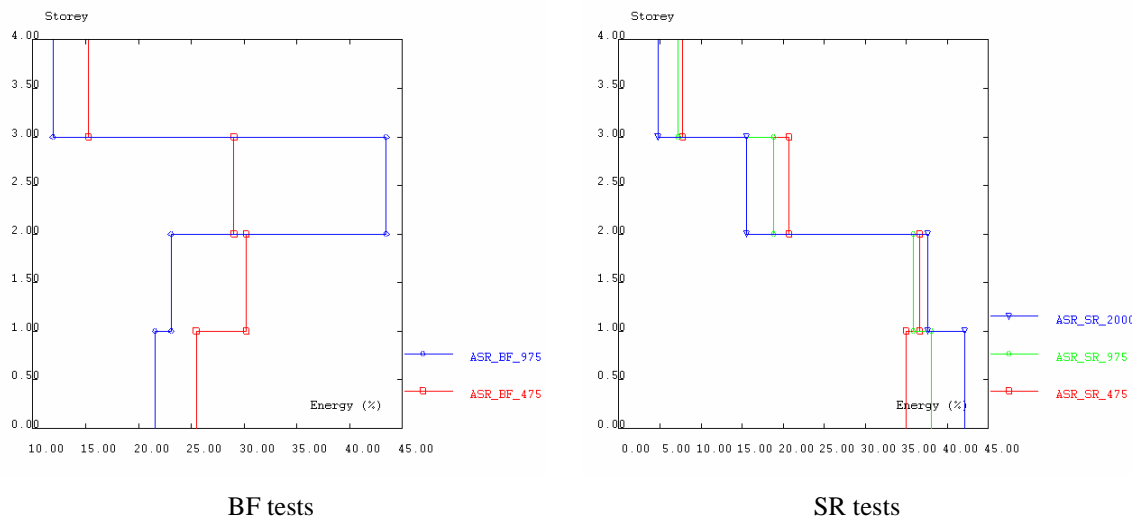


Figure 4.34 - BF and SR tests: relative energy dissipation profiles

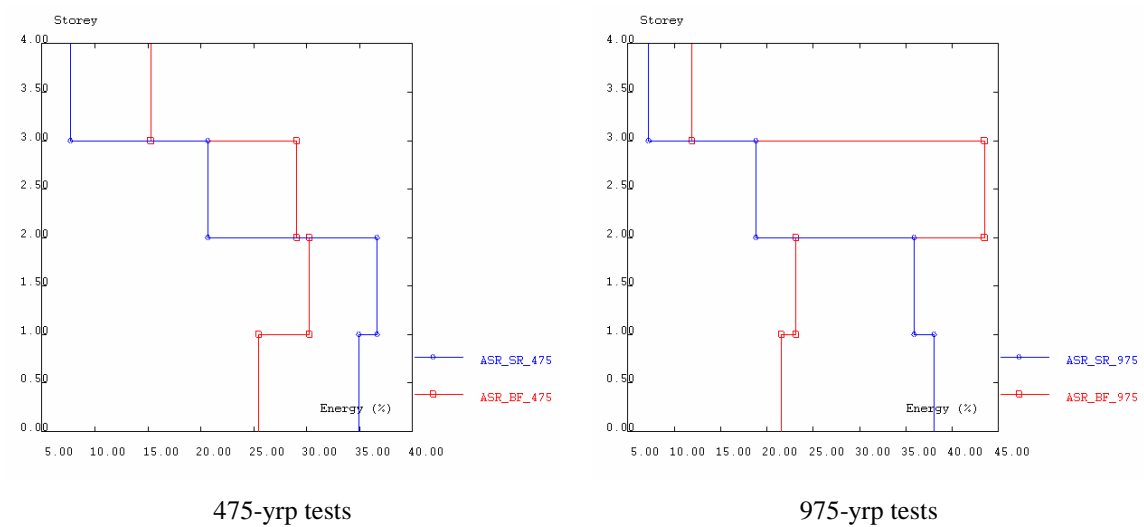


Figure 4.35 - BF and SR tests: relative energy dissipation profiles (475-yrp and 975-yrp tests)

#### 4.4.4 - Deformation at the beam extremities

Figures 4.36 and 4.37 show the envelope of relative rotation and the maximum uniform strain at the top and bottom beam fibres for the bare and strengthened frames for the 475-yrp and 975-yrp tests.

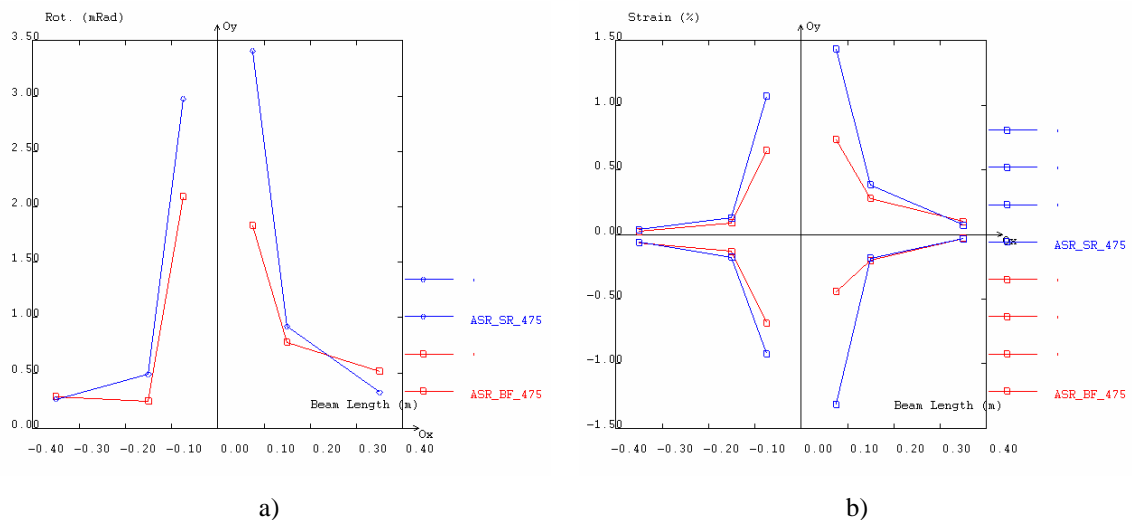


Figure 4.36 - BF and SR 475-yrp tests (beam 1<sup>st</sup> floor): a) maximum relative rotation; b) maximum uniform strain

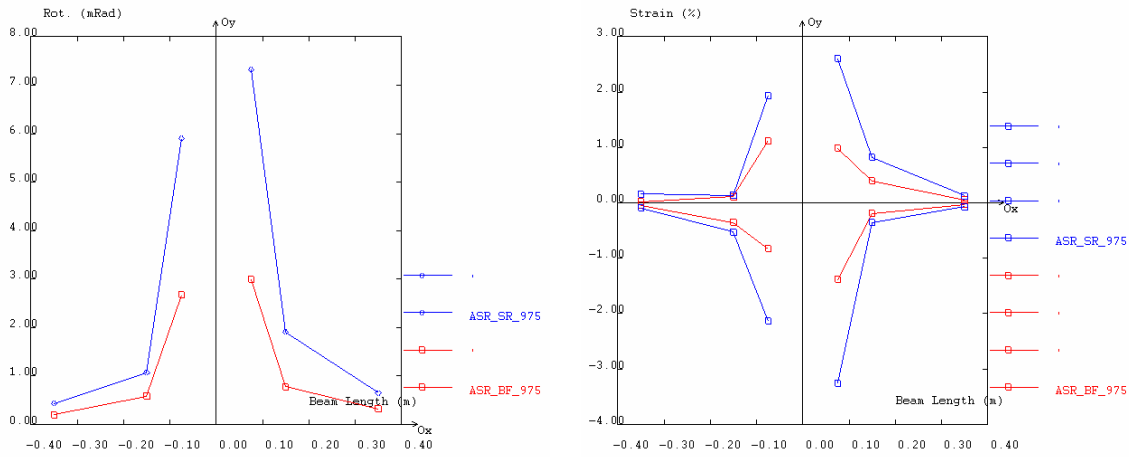


Figure 4.37 - BF and SR 975-yrp tests (beam 1<sup>st</sup> floor): a) maximum relative rotation;  
b) maximum uniform strain

Relative rotations measured at 75 mm, 150 mm and 350 mm from the column faces (left and right column faces) are plotted in Figures 4.36 and 4.37 (on the left), for the 475-yrp and the 975-yrp tests, respectively. On the right-hand side of these figures, the maximum uniform strains for the beam slices 0-75, 75-150 and 150-350 mm for the bare and strengthened frames are compared.

The deformation pattern along the beam is similar for the bare and strengthened frames for all tests. However, it is noted that the beam rotational deformation demands for the strengthened frames is much higher. In fact, the earthquake drift demand at the respective 1<sup>st</sup> storey has also increased. The ratios between the first inter-storey drifts (SR compared with BF tests) are

$$ID_{ratio,475} = \frac{ID_{SR,475}}{ID_{BF,475}} = \frac{0.63}{0.44} = 1.43 \quad ID_{ratio,975} = \frac{ID_{SR,975}}{ID_{BF,975}} = \frac{1.31}{0.63} = 2.07 \quad (4.12, 4.13)$$

And the maximum relative rotation ratios (SR compared with BF tests) are

$$Rot_{ratio,475} = \frac{Max Rot_{SR,475}}{Max Rot_{BF,475}} \approx 1.6 \quad Rot_{ratio,975} = \frac{Max Rot_{SR,975}}{Max Rot_{BF,975}} \approx 2.2 \quad (4.14, 4.15)$$

This shows that the beam rotation demands are almost proportional to the inter-storey drift demands, and, therefore, the dissipation and deformation mechanisms for the BF and SR frames are similar, with a slight increase in the beam demands for the SR case. Once more



it can be observed that the additional strength given by the confinement steel hoop plates should have contributed to increased beam demands.

#### 4.4.5 - Vulnerability analyses

##### 4.4.5.1 - Maximum inter-storey drift and global drift

Figure 4.38-*a* shows the vulnerability function in terms of maximum inter-storey drift, and Figure 4.38-*b* represents the maximum global drift, for the tests carried out on the bare and strengthened frames.

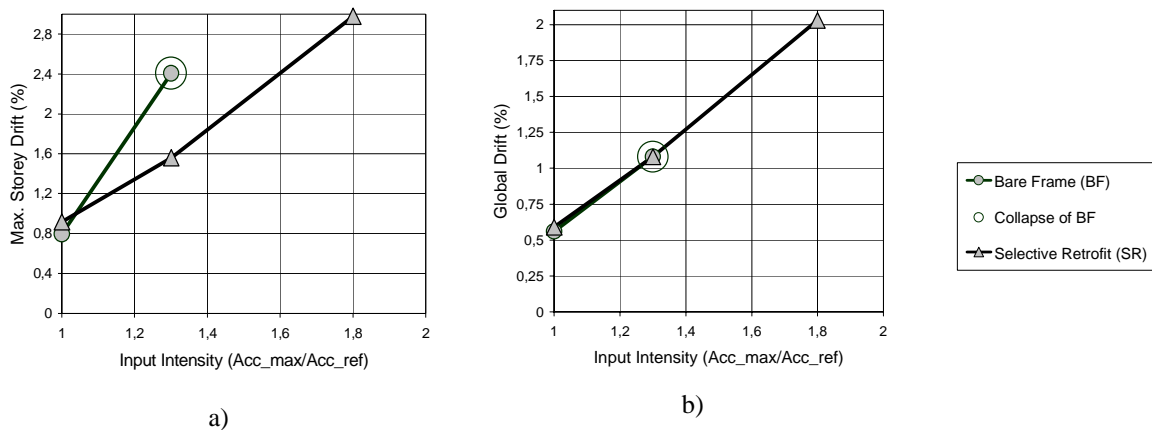


Figure 4.38 - BF and SR tests: a) maximum inter-storey drift; b) maximum global drift

As illustrated in the Figure 4.38-*a*, regarding maximum inter-storey drift, the demands for the SR structure are less than those for the original BF structure. This was due to the retrofitting intervention, carried out to correct the irregularity at the third storey. In addition, the strengthened structure was able to withstand much higher input intensity (1.8 times the nominal one) without collapsing and maintaining its load carrying capacity. Therefore, the benefits gained from the retrofitting operation were clearly demonstrated.

Looking in depth at the vulnerability functions, the following can be observed:

- For both, bare and strengthened frames, the 475-yrp earthquake test induces a similar magnitude of maximum inter-storey drift (ID) in the frames. However, it is

noted that the maximum ID reached occurs at different storeys: on the 3<sup>rd</sup> for the bare frame and on the 2<sup>nd</sup> for the strengthened one.

- For the 975-yrp earthquake tests, the strengthened frame stands for the complete 15 seconds earthquake input motion without structure collapse, reaching maximum ID of 1.56% at the 2<sup>nd</sup> storey. At 7.5 seconds of the 975-yrp input motion, the bare frame reached its maximum ID of 2.41% at the 3<sup>rd</sup> storey. This made imminent the storey collapse and, consequently, the test was interrupted.
- For the 2000-yrp test, the strengthened frame reached a maximum ID of 2.98% at the 2<sup>nd</sup> storey and 2.75% at the 1<sup>st</sup> storey, both greater than 2.41%, which corresponds to the ID at imminent collapse of the 3<sup>rd</sup> storey in the 975-yrp test on the bare frame.
- BF and SR tests reached a very similar global drift for each earthquake intensity. Consequently, the influence of the retrofit in the global drift is not evident. However, recall that the previous tests carried out on the bare frame induced considerable damage in the structure, and that test on the BF for the 975-yrp earthquake stopped at 7.5 seconds.

An important conclusion is the noticeable non-influence of the retrofitting in the global drift vulnerability function. It seems that global measurements, such as global drift, for example, can be no sensitive to local large damage/deformation. Therefore, caution is recommended when analysing structures based on one global parameter only (like the displacement based design, DBD). This is particularly so for structures with high irregularity.

#### *4.4.5.2 - Maximum rotation*

Figure 4.39 shows the vulnerability functions in terms of maximum local relative rotation for the tests on the BF and on the SR frame. The beneficial effects of the strengthening regarding local demands are visible.

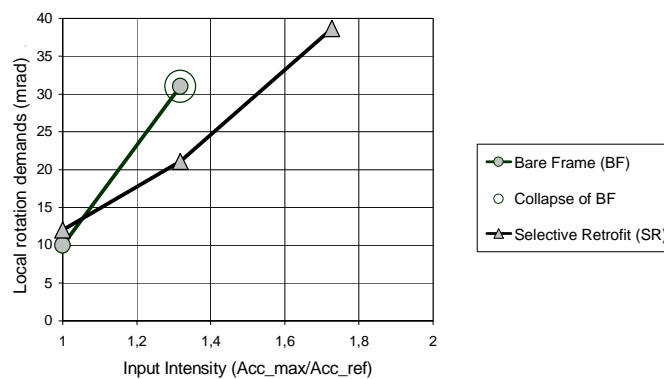


Figure 4.39 - BF and SR tests: local rotation maximum demands

From the analysis of Figure 4.39, the following can be observed:

- The maximum rotation demands for the bare frame for the two earthquake tests were measured in the strong-column at the 3<sup>rd</sup> storey. For the three earthquake tests on the strengthened frame, the maximum rotation demands were found in the slender-columns on the two first storeys. Therefore, it is concluded that for the storeys 1 and 2, the additional strength provided by the confining plates moves part of the deformation demands from the strong-column to the adjacent beams.
- The vulnerability function in terms of maximum relative rotation (local deformation measurement), is similar to the maximum inter-storey drift vulnerability function. This shows the obvious correlation between local and semi-local (inter-storey) demands when the same mechanism is activated. In fact, there was no intervention on the slender-columns, and the same deformation mechanism should develop for the bare and strengthened frames.

#### 4.4.5.3 - Energy dissipation

Figure 4.40 presents the evolution of the total dissipated energy with the maximum earthquake acceleration (intensity), for the pseudo-dynamic tests on the original bare and strengthened structures. The peak ground acceleration of the 475-yrp earthquake ground motion was used as reference.

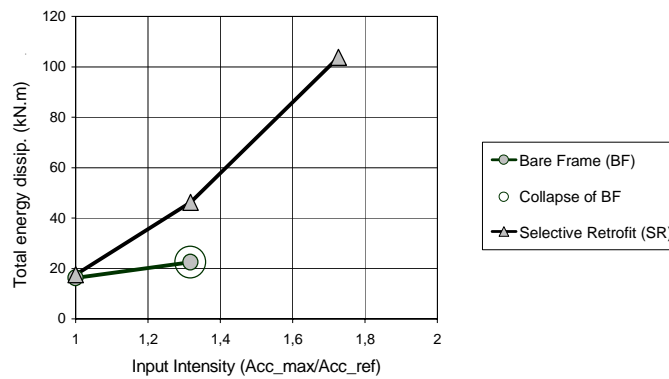


Figure 4.40 - BF and SR tests: total energy dissipation

Analysing the Figure 4.40, it can be concluded that:

- For the 475-yrp earthquake, the original bare frame and the strengthened frame structures dissipated approximately the same amount of energy.
- For the 975-yrp earthquake test, the SR frame dissipated twice as much as the energy dissipated by the BF structure. It should be highlighted that the BF structure was subjected to 7.5 seconds of the input motion only, because imminent collapse was attained at the 3<sup>rd</sup> storey. Collapse would imply no further significant dissipation capacity. Thus, it can be stated that retrofitting interventions were very effective also in terms of energy dissipation capacity. In fact, this results from a much more uniform dissipation of energy throughout the structure, which is confirmed by the amount of energy dissipated in the 2000-yrp earthquake test.

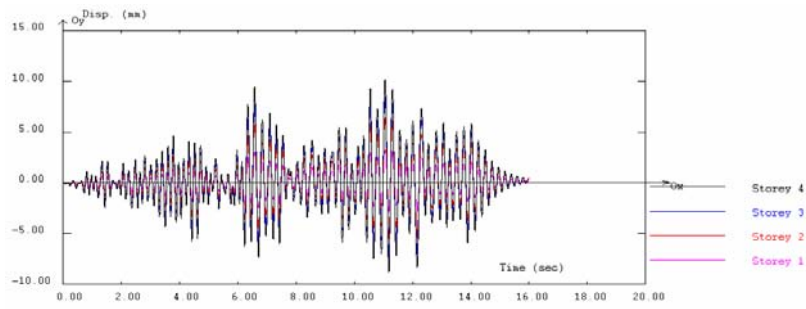
#### 4.5 - RESULTS FROM THE TESTS ON THE INFILLED FRAME

The original full-scale four-storey infilled frame (IN) was subjected to three consecutive earthquake tests corresponding to 475, 975 and 2000-yrp. During the 2000-yrp test, the masonry infills at the first storey collapsed, stopping the test at 5 seconds. In the next are provided results from these tests in terms of storey displacement, maximum inter-storey drift profiles for positive and negative deformations, energy dissipation, storey shear-drift curves and base-shear versus top-displacement.

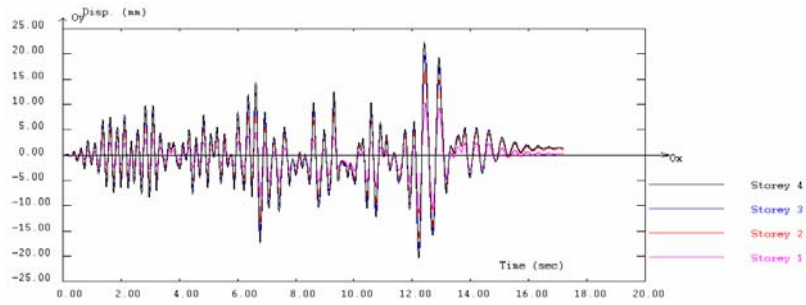
#### 4.5.1 - Storey displacement, drift and shear

Time histories of storey displacement for the three earthquake pseudo-dynamic tests performed on the IN structure are given in Figure 4.41. Figure 4.42 collects the top-displacement time histories for the three tests performed on the infilled frame. Analysing the Figure 4.41, it is apparent the soft-storey mechanism. In fact, storey displacements for 2000-yrp test are similar for the four floors, which leads to inter-storey drifts at the 1<sup>st</sup> storey much higher than ones for the three upper storeys. The soft-storey mechanism develops from the failure of the infill panels at the first storey and is a direct consequence of the storey softening behaviour characteristics of these infills after failure. This will be also emphasized in the drift profiles in Figure 4.46.

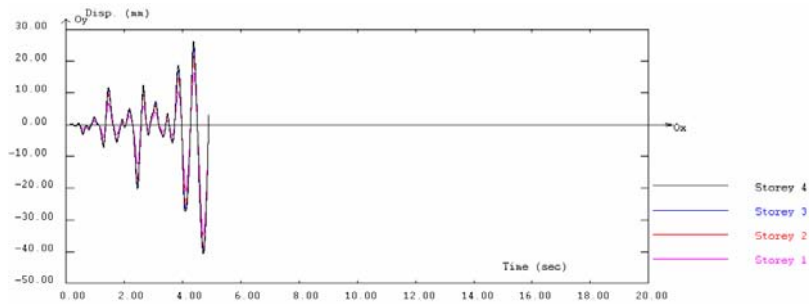
The curves base-shear-top-displacement for the three earthquake tests are given in Figure 4.43 and show that quasi-linear elastic behaviour was exhibited during the 475-yrp test. The 975-yrp test inflicted severe damage to the infills which reached deformation beyond its peak strength with considerable loss of strength. The short test, with the first part of the 2000-yrp earthquake (5 seconds) only, prompted the infill panels to failure. In Figure 4.44 are plotted the respective envelope curves of these storey shear-drift diagrams. The curves storey shear versus storey drift presented in Figure 4.45, are also indicative of the infilled frame behaviour during the three consecutive earthquake tests. Moreover, these curves give a clear idea of the damage distribution and intensity. In fact, most of demands and consequently damage, concentrate in the first storey. The second storey also shows relatively high demands. The third and fourth storeys show typical quasi-linear behaviour for all tests. Figure 4.46 represents the maximum inter-storey drift profile and the maximum storey shear profile.



475-yrp



975-yrp



2000-yrp

Figure 4.41 - IN tests: storey displacement time histories

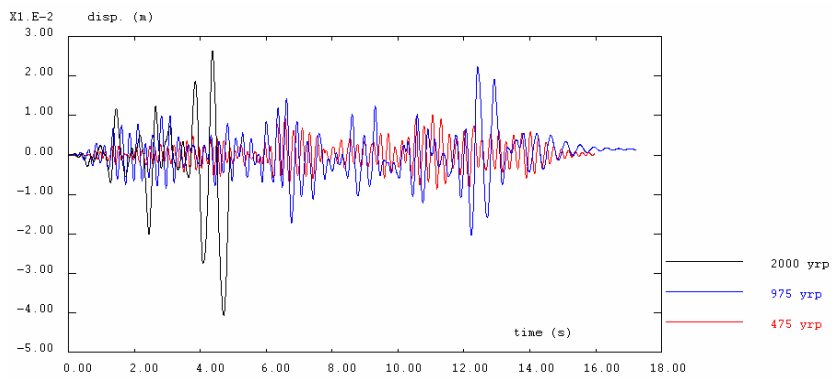


Figure 4.42 - IN tests: top-displacement evolution

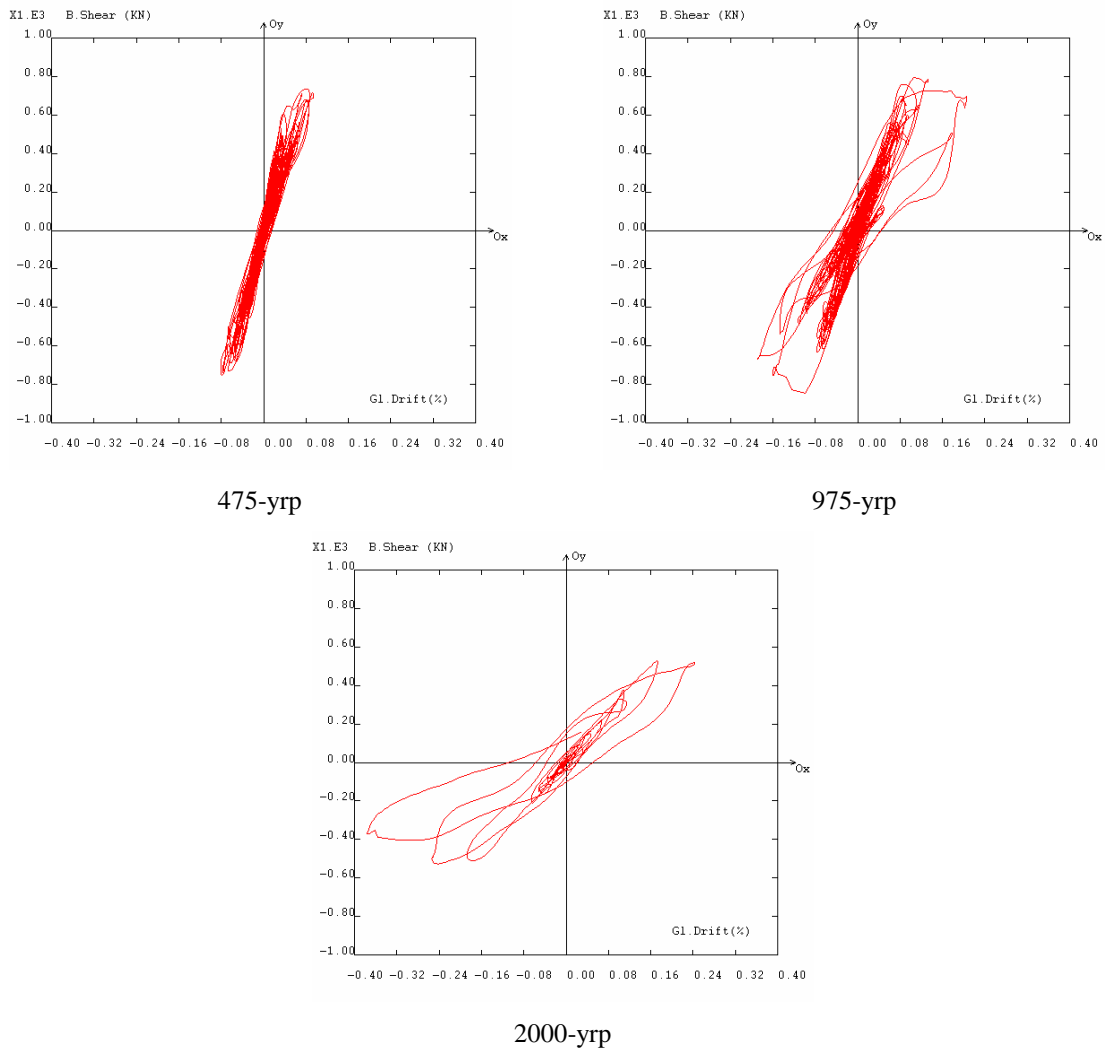


Figure 4.43 - IN tests: base-shear versus top-displacement

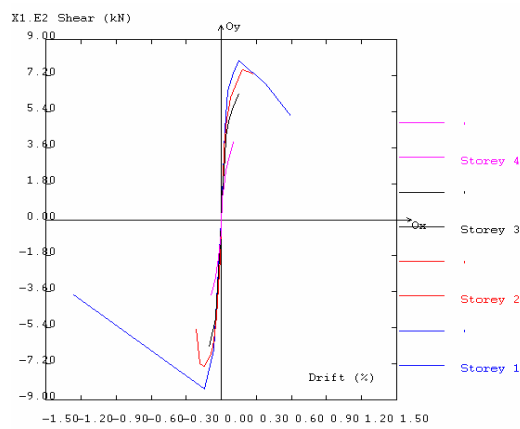


Figure 4.44 - IN tests: envelope storey shear versus inter-storey drift

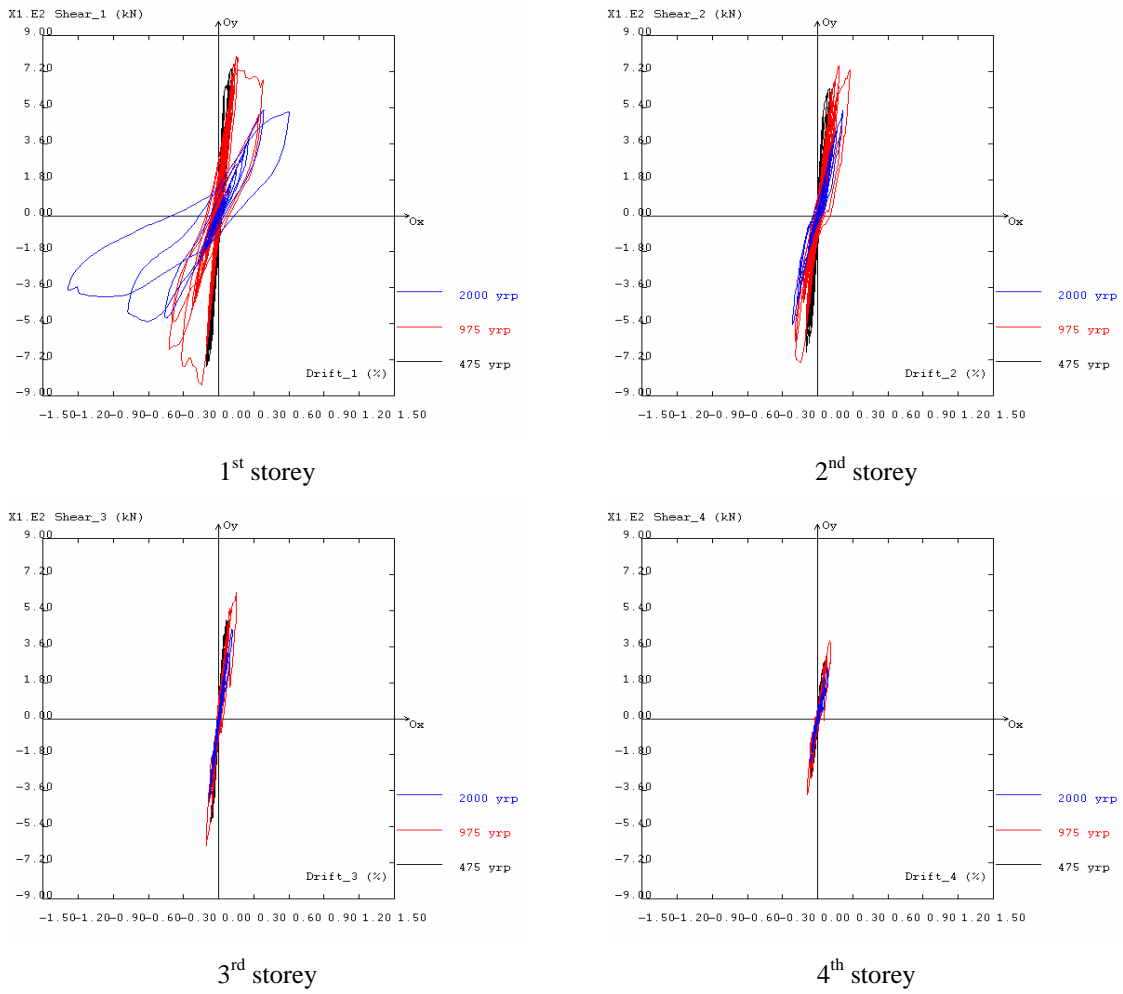


Figure 4.45 - IN tests: storey shear versus inter-storey drift

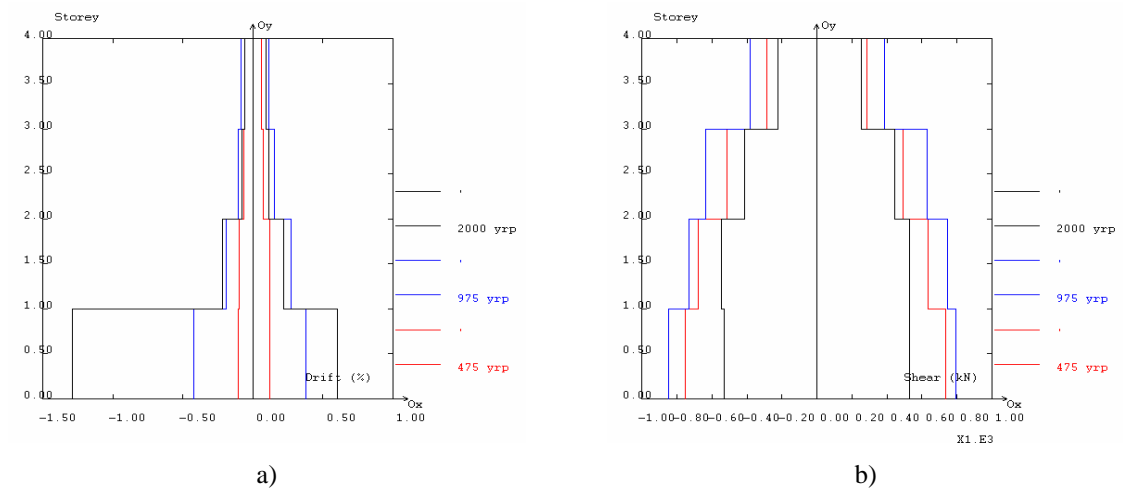


Figure 4.46 - IN tests: a) maximum inter-storey drift profiles; b) maximum storey shear profiles



The storey shear-drift envelope curves (Figure 4.44), illustrative of the storey demands and behaviour, show that the first storey residual strength tends to approach the strength of the bare frame (approximately 200 kN). The drift profiles presented in Figure 4.46-a show that the storey demands for the 475-yrp test are fairly uniform along the height of the structure, and for the 975-yrp test demands concentrate in the first two storeys with predominance of the first storey. The 2000-yrp test showed a clear soft-storey mechanism with demands strongly concentrated in the first storey which is not capable to develop further strength. In fact, the storey shear profiles presented in Figure 4.46-b show that the maximum base-shear for the 2000-yrp is practically equal to the second storey shear.

Table 4.8 - IN tests: response maximum values (summary table)

Test <sup>a</sup>	Top-displacement (mm)		Global drift (%)	
IN475	10.2		0.09	
IN975	22.3		0.21	
IN2000 <sup>b</sup>	40.6		0.38	
	Inter-storey drift (%)			
	storey 1	storey 2	storey 3	storey 4
IN475	0.12	0.12	0.08	0.06
IN975	0.43	0.27	0.15	0.11
IN2000 <sup>b</sup>	1.29	0.22	0.12	0.09
	Storey shear (kN)			
	storey 1	storey 2	storey 3	storey 4
IN475	754.0	680.8	512.4	288.4
IN975	846.5	749.1	635.5	388.1
IN2000 <sup>b</sup>	529.2	543.2	446.2	256.5

a) Duration of the input motions is 15 seconds for the earthquake PsD tests.

b) Test performed up to 5.0 seconds in order to reach full collapse of the 1<sup>st</sup> storey infill panels.

Maximum values of the response for the three earthquake tests on the infilled frame are collected in Table 4.8 in terms of top-displacement, global drift, storey drift and storey shear. Results in terms of maximum storey deformation show that:

- For the 475-yrp earthquake test, the deformation demands in the first and second storeys are similar.
- For the 975-yrp test beginning of concentration of deformation is verified at the first storey.

- For the 2000-yrp test, the soft-storey mechanism at the 1<sup>st</sup> storey level is evident, being the storey drift maximum demand at the upper storeys slightly increased relatively to the values observed for the 475-yrp test.

The maximum values for the inter-storey drift are indicative of the behaviour and damage state after each test. In fact, the 0.12% drift reached during the 475-yrp test in the first two storeys indicates that the infill panels in this storey should be reaching the peak strength deformation (see also the predictions of storey behaviour, Figure 3.28). Furthermore, the 0.47% drift reached in the first storey during the 975-yrp test shows that the infills should have been severely damaged. Also the maximum drift at the second storey (0.27%) indicates serious damage in the infills. The maximum values of the storey shear also decrease with the earthquake intensity (from 975-yrp to 2000-yrp), which indicates degradation of stiffness and strength properties.

#### 4.5.2 - Observed damages

A detailed description of the damage (visual damage inspection) for each test on the infilled RC frame is included in Table 4.9.

Table 4.9 - IN tests: damage inspection (see damage patterns in Figures B.19 and B.20)

Test	Damages
IN475	<ul style="list-style-type: none"> <li>• Minor cracking around openings (1<sup>st</sup> and 2<sup>nd</sup> storey)</li> <li>• Separation between infill panels and surrounding frames</li> <li>• No cracking was observed in the concrete frame</li> </ul>
IN975	<ul style="list-style-type: none"> <li>• <i>1<sup>st</sup> storey</i>: Diagonal cracking of the short panel; Severe cracking of the other panels; Plaster spalling in all panels</li> <li>• <i>2<sup>nd</sup> storey</i>: Additional cracking of the panels with openings; Separation of the short panel</li> <li>• <i>Concrete frame</i>: Cracking of the external columns (1<sup>st</sup> and 2<sup>nd</sup> storeys); Shear-cracking of the internal strong-column at the base</li> <li>• At the conclusion of this test it was found that the concrete frame was in good condition at all 4 levels as was the infill in the upper 3 storeys. The ground storey infill was severely damaged – too much to be retrofit without replacement</li> </ul>
IN2000	<ul style="list-style-type: none"> <li>• Concentration of the deformation demands in the 1<sup>st</sup> storey (inter-storey drift of about 1.5%)</li> <li>• Complete failure of the 1<sup>st</sup> storey infills</li> <li>• Additional shear cracking of the strong-column at the base</li> </ul>

---

Griffith's (1999-*b*) detailed damage description for each test performed on the block masonry infilled frame is presented below.

#### *475-yrp test*

Overall, the infilled frame structure behaved very well. A maximum base-shear force of about 700 *kN* occurred at a lateral drift of 0.08% global drift only (roof-displacement divided by frame height). The maximum inter-storey drift occurred at the 1<sup>st</sup> storey (0.12%). It decreased with increasing storey level up to a value of about 0.07% at the 4<sup>th</sup> storey.

As could be expected, the level of damage corresponding to these levels of drift was minor. Some cracking was visible in the masonry infill around the door and window openings in the 1<sup>st</sup> and 2<sup>nd</sup> storey, with most occurring in the 1<sup>st</sup> storey. The 1<sup>st</sup> storey hysteresis loops (shear force versus drift) suggest that significant damage had just started to occur, and that the maximum storey shear strength was nearly attained in this test. For the lower two storeys, the maximum storey shear force recorded was about 600 *kN* in the positive direction and nearly 800 *kN* in the negative direction.

In the concrete frame, the small shear cracks were also observed in the bottom metre of 1<sup>st</sup> storey's column 2 (strong-column). Small flexural cracking was noted in column 1, over the height of the window opening, and in column 4 at the 1<sup>st</sup> storey. Small cracks also developed in the exterior beam-column joints for columns 1 and 4 at the 1<sup>st</sup> floor level.

Even though the observable damage was slight, there was a substantial amount of noise coming from the masonry walls as they were sheared back and forth. Primarily, the bond between the infill panels and the surrounded concrete frame was 'broken' at the bottom of the two storeys during this test. The majority of energy dissipation in the brickwork probably occurred along these interfaces.

#### *975-yrp test*

This level of earthquake input caused a significant amount of damage to the block infill in the bottom storey of the concrete frame with some minor damage to the concrete beam-column joints and several columns at this level. Smaller amounts of damage in similar locations were noted in the 2<sup>nd</sup> storey. No significant damage was observable in the upper

two stories. For example, the small cracks in the exterior beam-column joints in the bottom two stories developed further but not severely. A small flexural crack also appeared in the 1<sup>st</sup> floor beam at the end of the door opening closest to column 2. A crack also appeared in the 1<sup>st</sup> floor slab, running parallel to the transverse beam on the side opposite to the loading arm, penetrating to about 1/3 of the slab depth from the top. Shear cracking at the base of column 2 in the first storey also developed further. The main difference, however, was observed in the infill panels. During the 975-yrp test, shear cracking became significant in all three of the first storey infill panels. This is also evident in the storey shear force versus drift hysteresis loops. The first storey shear strength of approximately 800 kN was reached at a storey drift of 0.15% and had reduced to approximately 650 kN at a drift of 0.4%. The second storey hysteresis loops also indicate that the ultimate storey shear strength was reached (approximately 800 kN) but little softening was observed since the storey drifts at this level never exceeded 0.2% in the negative direction and 0.3% in the positive direction. Storey drifts in the upper two stories essentially never exceeded 0.1% drift, hence there was no significant inelastic behaviour exhibited in the storey hysteresis loops which is consistent with the lack of observable damage in those two storeys at the conclusion of testing.

In summary, at the end of this test, the concrete frame was found in good condition at all four levels, as was the infill in the upper three storeys. The ground storey infill was severely damaged, too much to be retrofit without replacement.

#### *2000-yrp test*

It was recognised that the infill frame had become a soft-storey infill frame structure. Nevertheless, it was subjected to the 2000-yrp earthquake signal in order to study how gradually the lateral strength dropped off with increasing drift. To protect the frame and ensure that subsequent tests on retrofit techniques could be performed on the structure, the 2000-yrp test was stopped once the structure reached a first storey drift of approximately 1%. Consequently the test terminated at 5 seconds earthquake duration, and once the ground storey drift reached approximately 1.5%. The storey shear versus drift hysteresis loops illustrate clearly that the load deflection characteristics approach those of the bare frame as the drifts increase to values over 1%.

The damage patterns at the end of this test were essentially more severe versions of what had been observed in the 975-yrp test. On one hand, significant shear cracks of approximately 4 mm wide developed in the bottom metre of the 1<sup>st</sup> storey's of column 2. Spalling of cover concrete also occurred in column 2 at this location. However, the previous cracking patterns in the other frame elements showed no significant change. On the other hand, what remained from the 1<sup>st</sup> storey infill after the 975-yrp test was severely damaged during this test. Wide diagonal cracks developed in the solid infill panel. The infill panels with openings also cracked badly. When this test was terminated, the 1<sup>st</sup> storey shear strength had dropped by more than 50% to less than 400 kN. The maximum inter-storey drift was nearly 35 mm (or, roughly, 1.5% drift). The overall structural behaviour was definitely that of a soft-storey structure. The maximum drift at the top of the structure was 40 mm, and, as mention above, almost all of it (35 mm) occurred at the 1<sup>st</sup> storey. Most of the remaining 5 mm of drift occurred at the 2<sup>nd</sup> storey. Consequently, very little new damage occurred in the upper three storeys of the structure.

Figures B.19 and B.20 show the damage observed on the RC frame structure, slabs and in the masonry infills after the earthquake pseudo-dynamic tests. Pictures of the damage observed in the infills and in the RC structure also appear in Figure B.21.

#### 4.5.3 - Damage intensity classification for infill masonry panels

Sortis *et al.* (1999) proposed a methodology of damage intensity evaluation. As shown in Figure 4.47, five types of damage are considered. For each type of damage, the damage level is defined on the basis of the amplitude of the damage, namely the crack opening and crushing (see Table 4.10).

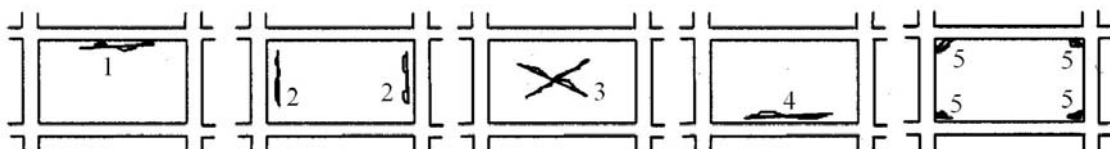


Figure 4.47 - Types of damage in masonry infill panels (Sortis *et al.*, 1999)

Table 4.10 - Damage severity evaluation in masonry infill panels (Sortis *et al.*, 1999)

Damage level	Amplitude of the observed damage ( <i>mm</i> )				
	Type 1	Type 2	Type 3	Type 4	Type 5
A = no damage	0	0	0	0	0
B = slight	$\leq 2$	$\leq 2$	$\leq 1$	0	0
C = medium	$\leq 5$	$\leq 5$	$\leq 2$	$\leq 1$	crushing indications
D = heavy	$\leq 10$	$\leq 10$	$\leq 5$	$\leq 2$	crushing
E = very heavy	$> 10$	$> 10$	$> 5$	$> 2$	significant crushing
F = total	total damage	destruction	partial collapse	extensive	

Following the classification proposed by Sortis *et al.* (1999), for each storey, the damages observed in the infill walls and at the end of each earthquake test are classified in Table 4.11.

Table 4.11 - Damage severity evaluation in the IN earthquake tests

Earthquake (yrp)	storey			
	1	2	3	4
475	slight	slight	no damage	no damage
975	very heavy	slight	slight	slight
2000	total	medium	slight	slight

#### 4.5.4 - Maximum absolute and relative rotations measured at the critical zones

Figure 4.48 presents the maximum (absolute and relative) rotations measured during the tests performed on the infilled frame structure. Results are presented relatively to the three earthquake pseudo-dynamic tests carried out (475, 975 and 2000-yrp). For these series of tests with infill masonry walls rotations at the concrete elements are very sensible to local force effects induced by the infill to the columns and beams.

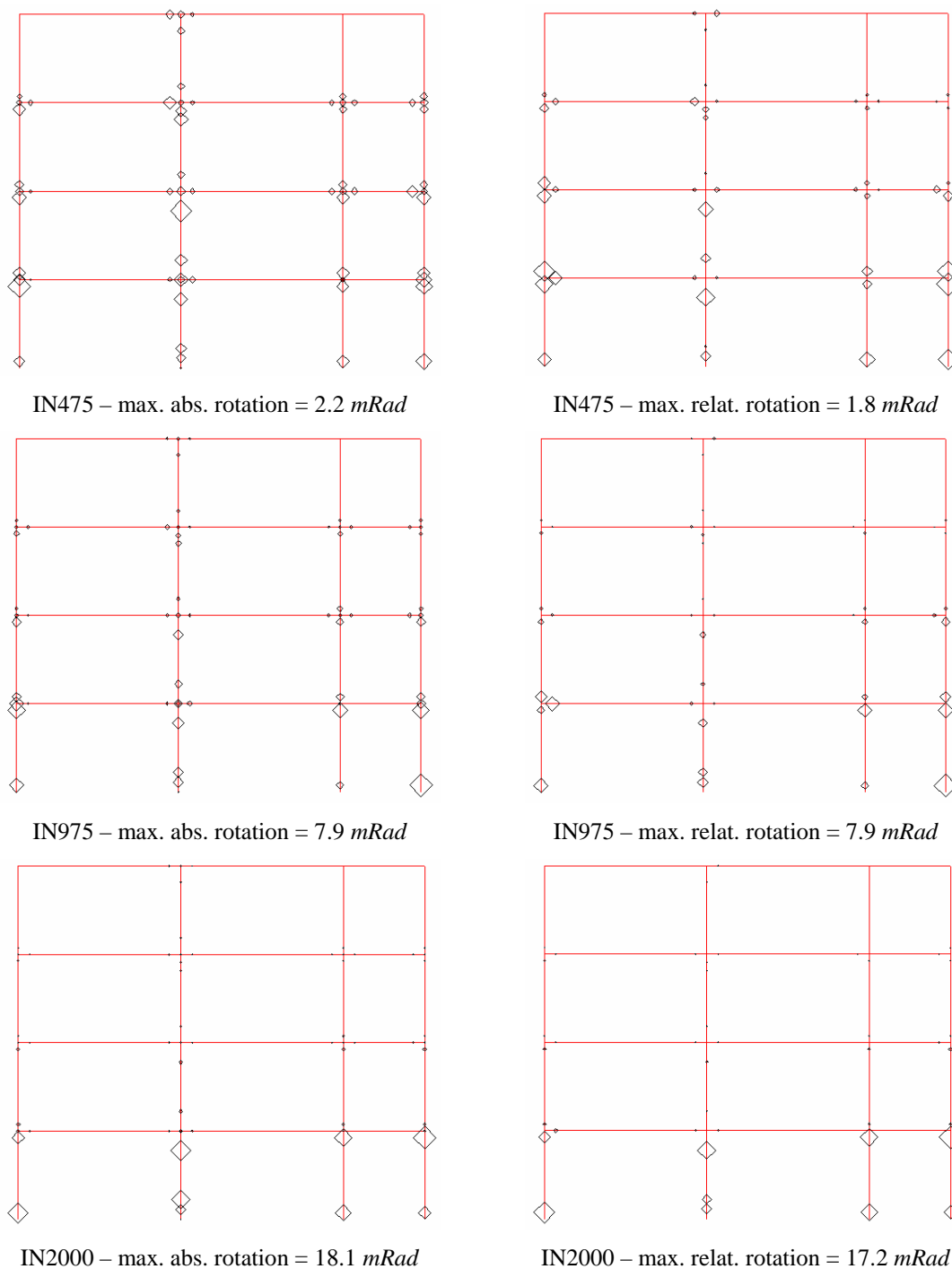


Figure 4.48 - IN tests: maximum absolute and relative rotation demands

From the analyses of the Figure 4.48, it can be concluded that:

- As observed earlier on the bare frame tests, it is clear that relative rotations are similar to the absolute ones for the weak-columns, specially for the tests with

stronger earthquake excitation (2000-yrp). This was also visually observed during the tests.

- For the high intensity earthquake, the 1<sup>st</sup> storey strong-column does not rotate at the top, which is contrary to what was observed for the tests on the bare frame. This effect is due to the high stiffness and strength of the second storey. In fact, for the 2000-yrp test, it was confirmed the soft-storey mechanism at the ground storey, being the second storey much stronger, which does not allow the top columns to rotate.
- The soft-storey mechanism for the 2000-yrp test, already noticed in the analysis of the storey displacements, is confirmed in the rotations plots.

#### 4.5.5 - Energy dissipation

The total dissipated energy at the storey level for each test is represented in the schematic storey profile in Figure 4.49. Figure 4.50 plots the evolution of energy dissipation at the storey levels and the evolution of the total energy dissipated in the infilled structure.

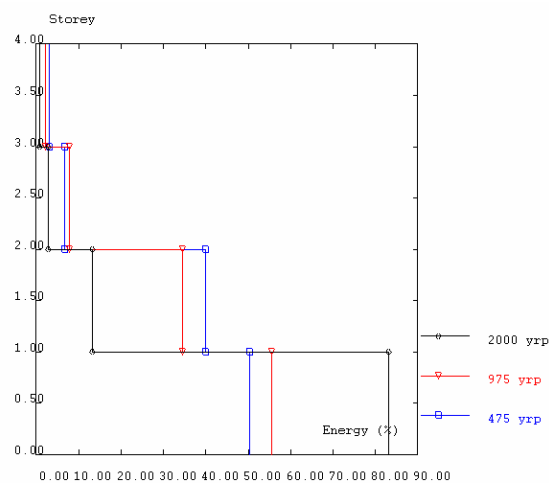


Figure 4.49 - IN tests: relative energy dissipation profiles



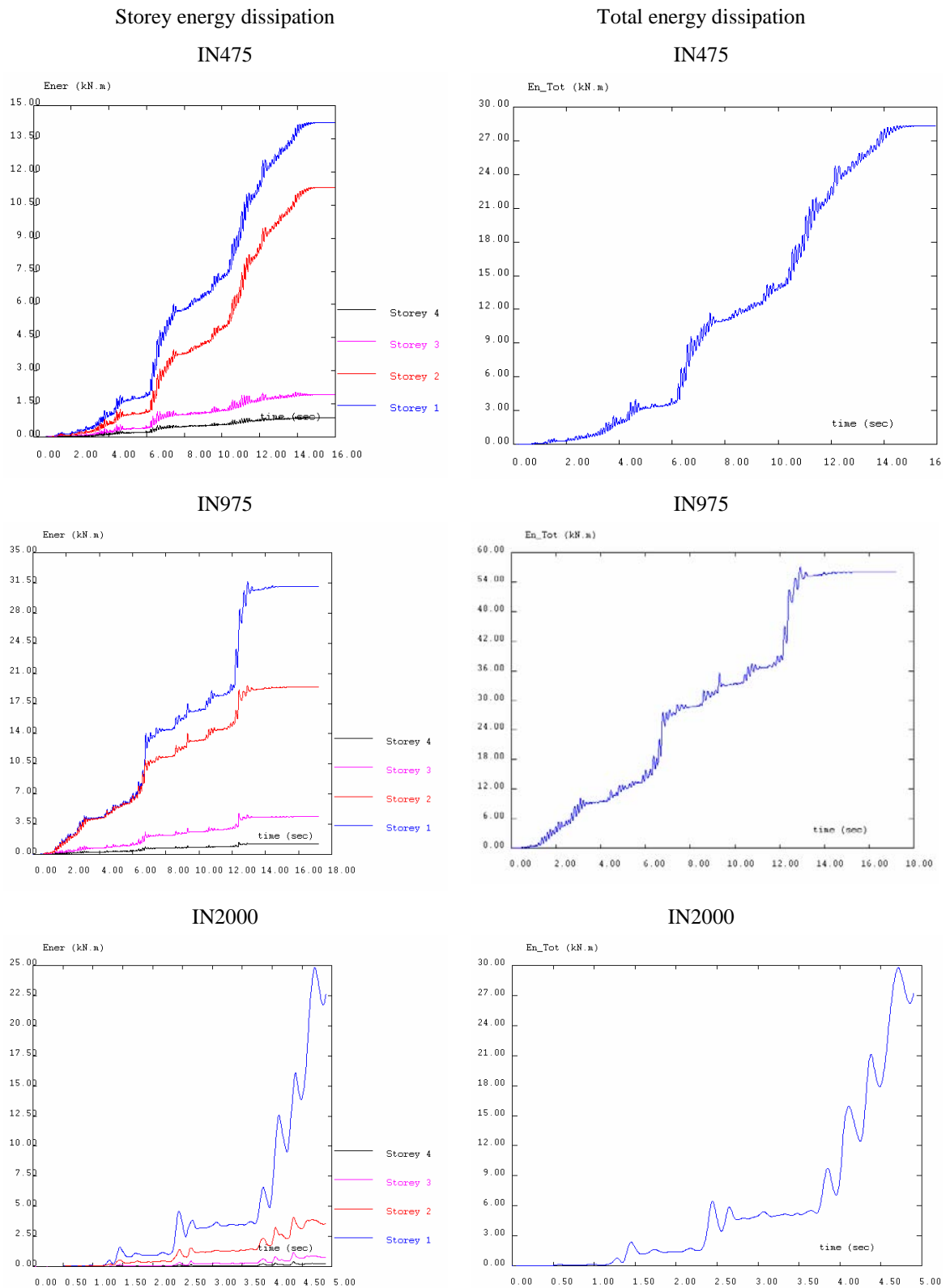


Figure 4.50 - IN tests: storey and total energy dissipation

From the analysis of the energy dissipation graphics, it can be observed:

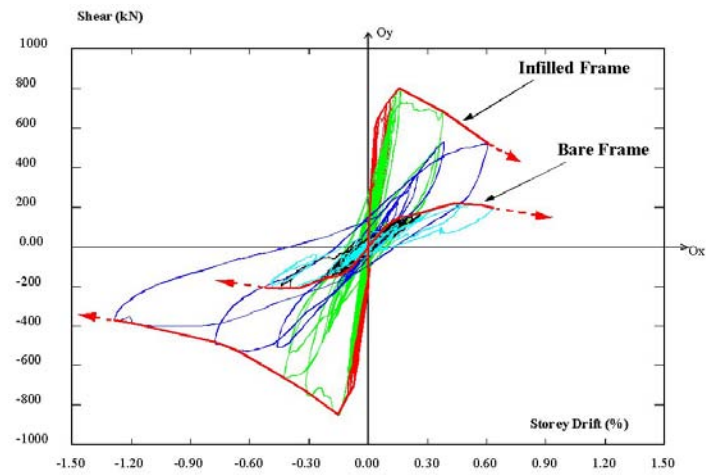
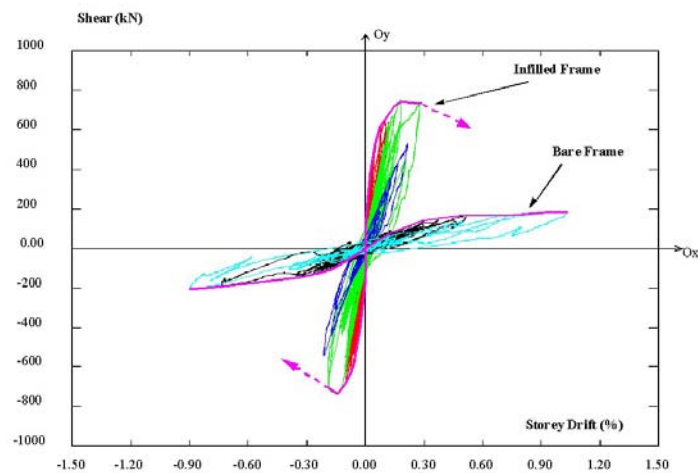
- The fourth storey practically does not dissipate energy: 3% for the 475-yrp test, reducing to 2% in the 975-yrp, and to 1% in the 2000-yrp test.
- The third storey has also low energy dissipation: 7-8% for the first two tests, reducing its participation in the energy dissipation to 3% for the stronger earthquake.
- For every earthquake test, the first storey is the most dissipative, increasing its relative quota with the accumulation of damage. The first storey is responsible for 50%, 55% and 83% of the total dissipated energy for the 475, 975 and 2000-yrp test, respectively. The soft-storey at the ground storey level explains the high dissipation of energy at this storey.
- In the second storey, the quantity of energy dissipated in the first five seconds for the 975-yrp test is superior to the energy dissipated, for the same period, in the 2000-yrp test. This fact follows from the demand concentration at the first storey, and can be observed in Figure 4.50.

#### **4.6 - COMPARISON BETWEEN BF AND IN TESTS**

This section emphasizes the effects of infill masonry walls in response of the structure.

The series of diagrams (1<sup>st</sup> and 2<sup>nd</sup> storey shear-drift) given in Figure 4.51 include the diagrams for the tests, for the BF and IN, and reflect the effects of the infill panels in the structural response. The infill panels increase substantially the initial stiffness and strength at the storey level, and, consequently, the global stiffness and strength of the structure. The maximum strength reached for the 1<sup>st</sup> storey infilled frame is about four times the value for the bare structure. The infills also increased significantly the initial stiffness. It is also outlined the brittleness of the infilled structure after reaching the maximum strength. In fact, the 1<sup>st</sup> storey shear-drift diagram for the infilled structure shows a rapid decrease of the strength after reaching its maximum value.

The tests performed on the bare frame showed a concentration of damage, and consequently a large amount of inter-storey drift, in the 3<sup>rd</sup> storey. Figures 4.52 compare the inter-storey drift profile for the BF and IN tests. The presence of infills changed entirely the structural response. The concentration of damage at the third storey in the irregular RC frame observed for the BF tests was not verified in the IN earthquake tests. In this particular case, the infill panels prevent the development of an irregular response.

1<sup>st</sup> storey2<sup>nd</sup> storey

BF475    BF975    IN475    IN975    IN2000

Figure 4.51 - BF and IN tests: 1<sup>st</sup> and 2<sup>nd</sup> storey shear versus inter-storey drift and respective envelope curves

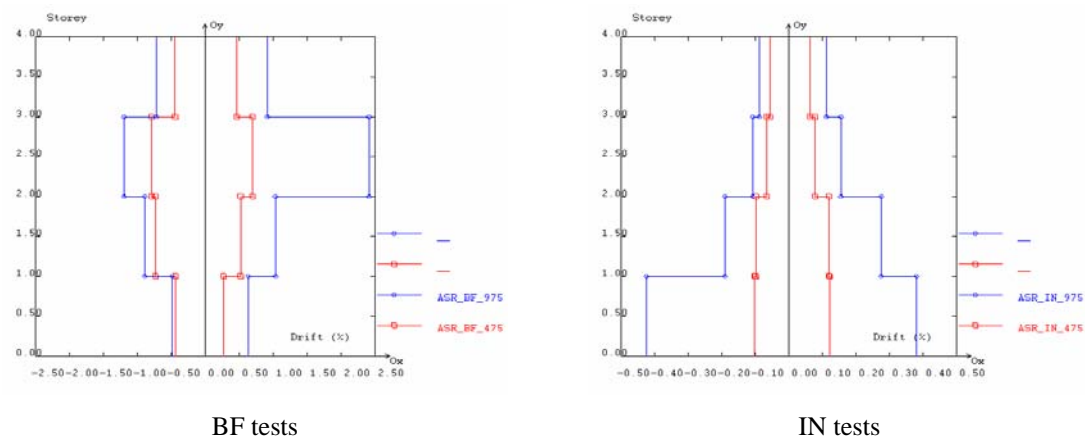


Figure 4.52 - BF and IN tests (475 and 975-yrp): maximum inter-storey drift profiles

#### 4.7 - RESULTS FROM THE TESTS ON INFILL STRENGTHENED FRAME

The original RC infilled frame was subjected to three consecutive earthquake tests. These tests induced severe damage to the infill panels. During the 2000-yrp test on the infilled frame, the infills at the first storey reached collapse. Maximum inter-storey drifts of 1.29%, 0.27%, 0.15% and 0.11% were experienced at 1<sup>st</sup>, 2<sup>nd</sup>, 3<sup>rd</sup> and 4<sup>th</sup> storeys respectively. This drift demand led to complete failure of the 1<sup>st</sup> storey walls and inflicted some (supposing minor) damage to the 2<sup>nd</sup> storey panels. Based on the test results and on visual inspection, it was decided to reconstruct the infill walls at the 1<sup>st</sup> storey and to apply the strengthening (shotcrete) just in the external short infill panels of each storey level. The new infill panels were rebuilt with the same geometry and materials as the original walls. Details on the infills strengthening were presented in Section 3.4.3.

After replacement of the infills at the 1<sup>st</sup> storey and strengthening in the external short panel of each storey, the infill strengthened frame (SC) was subjected to the three earthquake input motions (475, 975 and 2000-yrp earthquakes), as for the infilled frame. Next are compiled the results in terms of storey displacement, maximum inter-storey drift profiles for positive and negative deformations, energy dissipation and shear-drift diagrams (at storey and global levels).

### 4.7.1 - Storey displacement, drift and shear

In Figure 4.53 are plotted the time histories of storey displacement for the three earthquake pseudo-dynamic tests (475, 975 and 2000-yrp) performed on the SC structure. Figure 4.54 shows the top-displacement curves for the tests performed on the infill strengthened frame. Figure 4.55 plots the curves base-shear versus top-displacement for the three earthquake tests performed on the SC frame. In Figure 4.56 are presented the curves storey shear versus inter-storey drift, and, in Figure 4.57 are plotted the respective envelope curves for these storey shear-drift diagrams. Figure 4.58 represents the maximum inter-storey drift profile and the maximum storey shear profile. Table 4.12 summarises the maximum values for characteristic response variables for the SC tests.

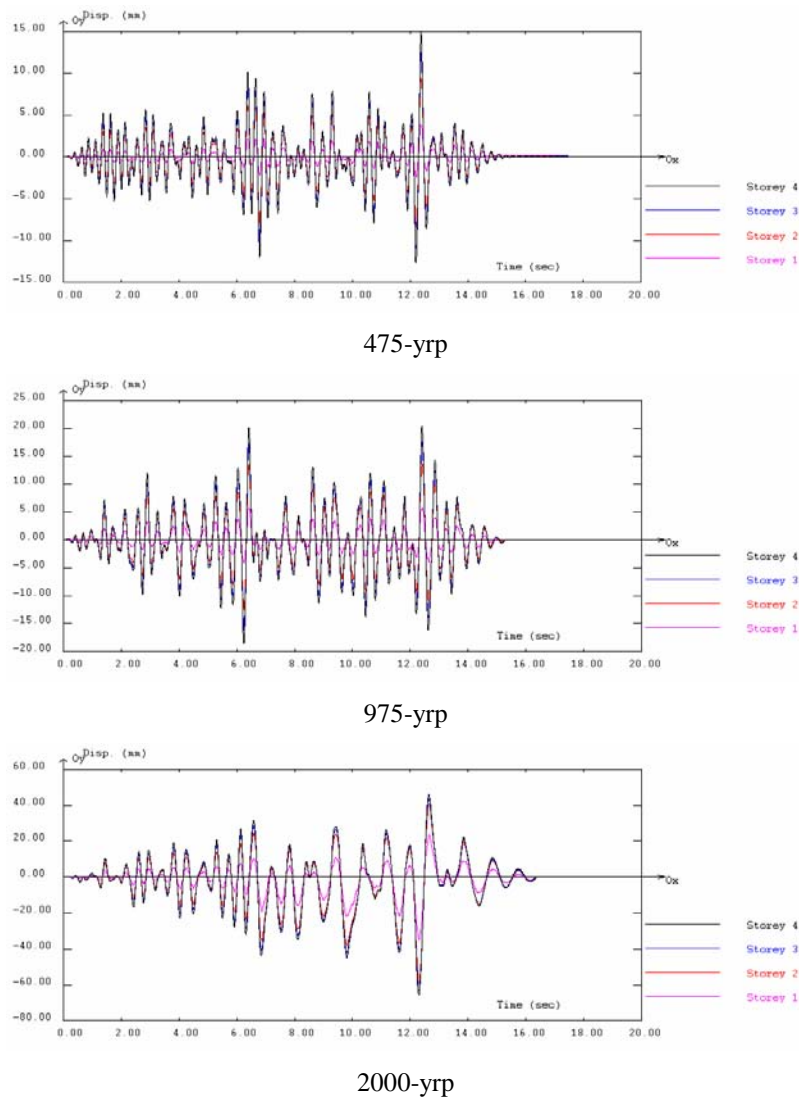


Figure 4.53 - SC tests: storey displacement time histories

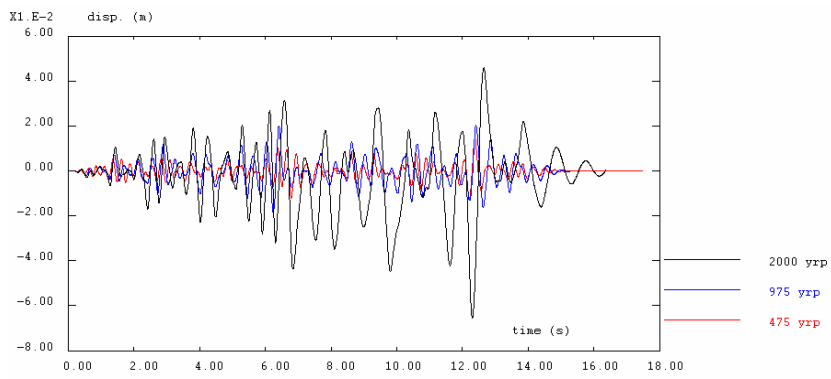


Figure 4.54 - SC tests: top-displacement evolution

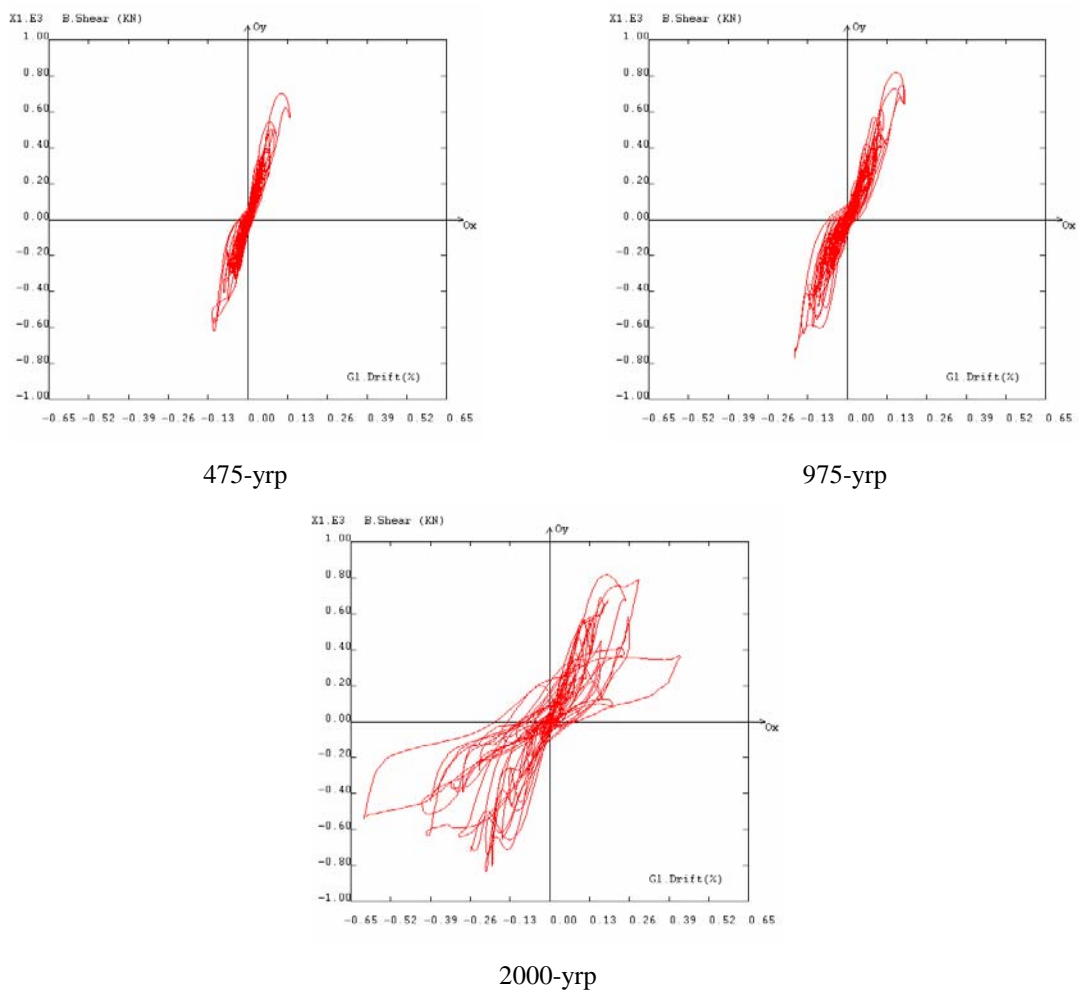


Figure 4.55 - SC tests: base-shear versus top-displacement

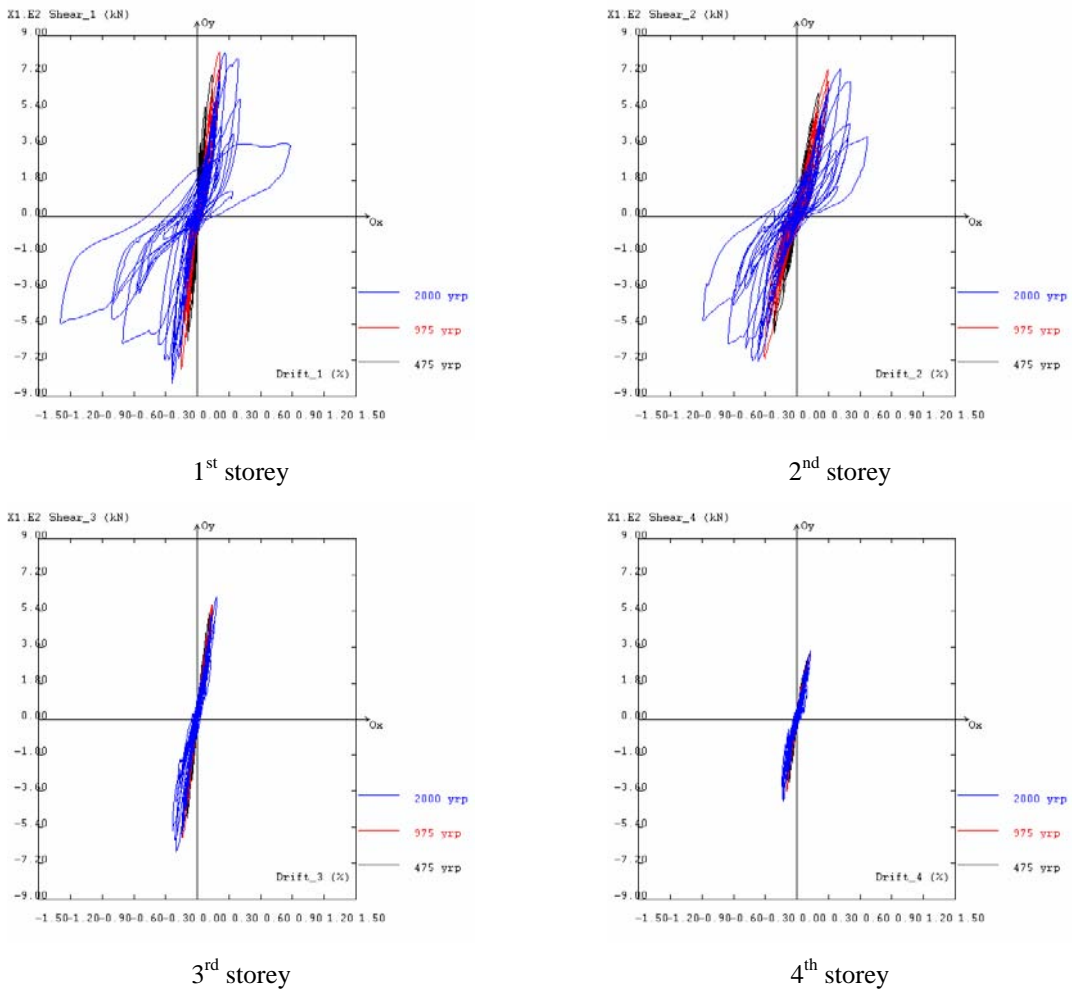


Figure 4.56 - SC tests: storey shear versus inter-storey drift

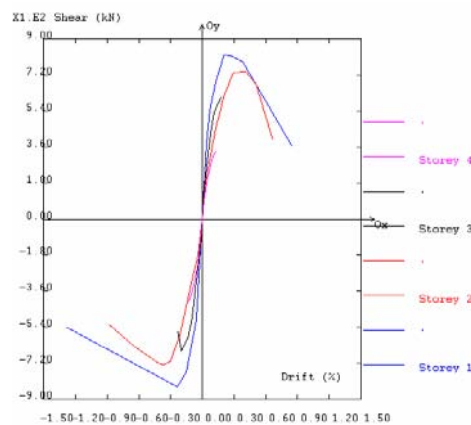


Figure 4.57 - SC tests: envelope storey shear versus inter-storey drift

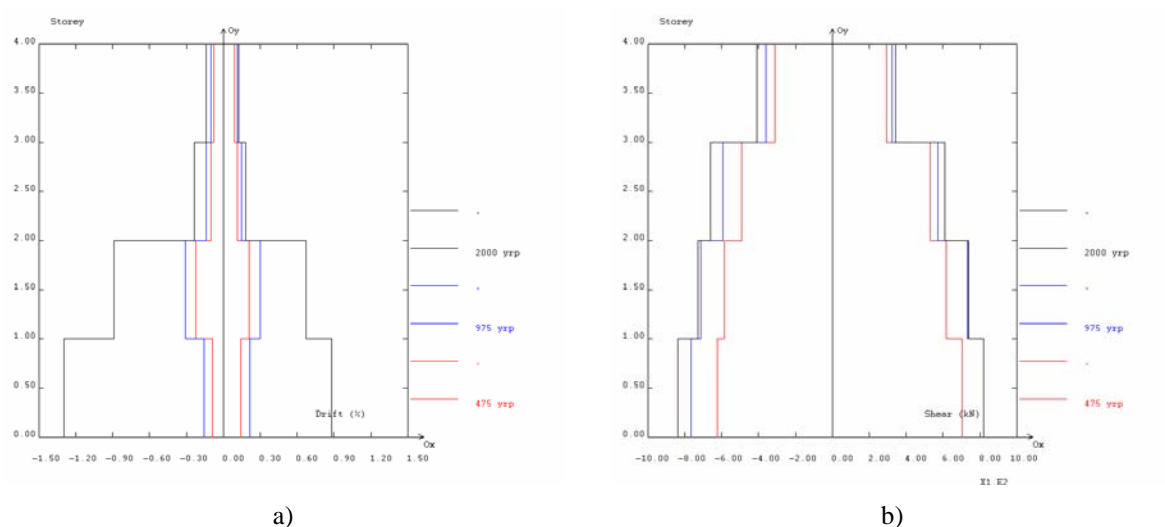


Figure 4.58 - SC tests: a) maximum inter-storey drift profiles; b) maximum storey shear profiles

Table 4.12 - SC tests: response maximum values (summary table)

Test <sup>a</sup>	Top-displacement ( <i>mm</i> )		Global drift (%)	
SC475	14.9		0.14	
SC975	20.4		0.19	
SC2000	65.4		0.61	
	Inter-storey drift (%)			
	storey 1	storey 2	storey 3	storey 4
SC475	0.14	0.22	0.11	0.09
SC975	0.22	0.31	0.15	0.11
SC2000	1.30	0.89	0.23	0.14
	Storey shear ( <i>kN</i> )			
	storey 1	storey 2	storey 3	storey 4
SC475	703.9	615.7	530.2	312.7
SC975	820.1	733.1	593.1	361.0
SC2000	838.6	738.5	659.1	407.6

a) Duration of the input motions is 15 seconds for the earthquake PsD tests.

### 4.7.2 - Observed damages

A detailed description of the damage at the end of each earthquake test is included in Table 4.13. Figure B.22 shows a general layout of the damage observed at the end of the tests on the infill strengthened frame. Pictures in Figure B.23 show the damage on the



reinforced concrete frame, on the infills and on the infills strengthened at the end of the tests.

Table 4.13 - SC tests: damage inspection (see damage patterns in Figure B.22)

Test	Damages
SC475	<ul style="list-style-type: none"> <li>• Separation of panels 2<sup>nd</sup> storey (short). The other panels were already separated</li> <li>• 1<sup>st</sup> storey – separation short panel, partial separation of the large panels. Slight cracking of the masonry in the corners of the openings</li> </ul>
SC975	<ul style="list-style-type: none"> <li>• Complete separation of the 1<sup>st</sup> storey panels</li> <li>• Increased cracking in the 1<sup>st</sup> storey opening (corners)</li> <li>• Crushing of concrete wall (short panel) in the bottom-left / top-right direction</li> <li>• 2<sup>nd</sup> storey: crushing short panel bottom-left / top-right (diagonal corners)</li> <li>• 2<sup>nd</sup> storey: increased crushing in the other panels (critical regions)</li> <li>• 3<sup>rd</sup> storey: slight cracking central zones of the panels with openings</li> </ul>
SC2000	<ul style="list-style-type: none"> <li>• 1<sup>st</sup> and 2<sup>nd</sup> storeys: failure of the non- strengthened panels</li> <li>• 1<sup>st</sup> storey – short panel: slight crushing in the corners. No additional cracking of the panel</li> <li>• Effects on the frame (<i>warning</i>): <ol style="list-style-type: none"> <li>1. Shear-out of the external columns (1<sup>st</sup> and 2<sup>nd</sup> storey) – (more pronounced in the external column adjacent to the strengthened panel)</li> <li>2. Spalling of the beam cover in the zone of the added 26 mm wall</li> </ol> </li> <li>• Short- strengthened infill panel (side opposite to the shotcrete): diagonal cracking of the wall</li> <li>• Slight crushing in the corners</li> </ul>

Two main aspects should be highlighted:

- The beneficial effects of the shotcrete on the behaviour of the infill panels were evident. Shotcrete avoided premature cracking and crushing of the ceramic block infill walls (positive effect).
- The shear-out of the external columns in their upper part leading to local collapse (*warning* – negative dangerous effect). Shear-out resulted from a combination of shear forces developed in the infill panel and overturning moment effects (up-lift of the upper beam inhibits transmission of shear forces between the panel and the beam, leading to direct shear-out of the top of the column).

### 4.7.3 - Maximum absolute and relative rotations measured at the critical zones

Figure 4.59 presents the maximum (absolute and relative) rotations measured during the three tests.

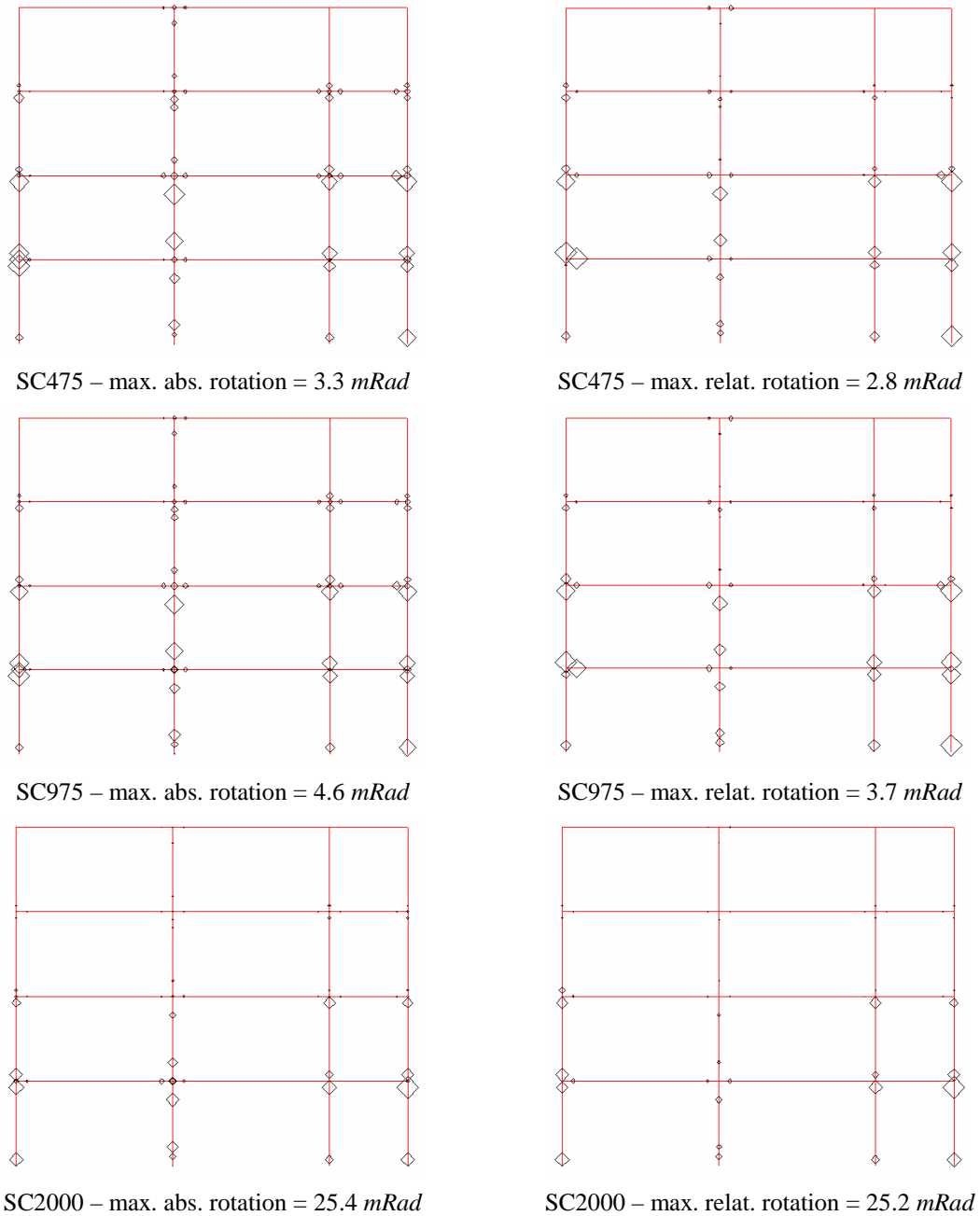


Figure 4.59 - SC tests: maximum absolute and relative rotation demands

---

From the analyses of the Figure 4.59, it can be concluded:

- For the two lower intensity earthquakes, the maximum deformation (relative rotation) for every column is observed at the second storey, which is in line with the maximum inter-storey drift at this storey. This happens because after the previous tests on the IN frame, the infill panels at the ground storey were replaced and the ones in the second storey were not. Therefore, the SC tests started with a considerable higher initial stiffness of the first storey when compared to the second storey.
- For the first two tests, the maximum deformation occurs in the outer columns of the first two storeys. This indicates the tendency for shear-out of these columns generated by the stresses induced by the adjacent masonry panels.
- For the stronger earthquake, the maximum deformation occurred at the external 1<sup>st</sup> storey' top-column adjacent to the short panel. This is in accordance to the verified shear-out of this external column, as shown in Table 4.13.
- In the two upper storeys, a very low deformation was recorded for all the earthquakes. For all the tests, the beams had little deformation.

#### **4.7.4 - Energy dissipation**

Figure 4.60 plots the evolution of energy dissipation at the storey levels and the evolution of the total energy dissipated in the structure for the earthquake tests on the SC frame. The total dissipated energy for each test, at the storey level, is represented in the schematic storey profile in Figure 4.61.

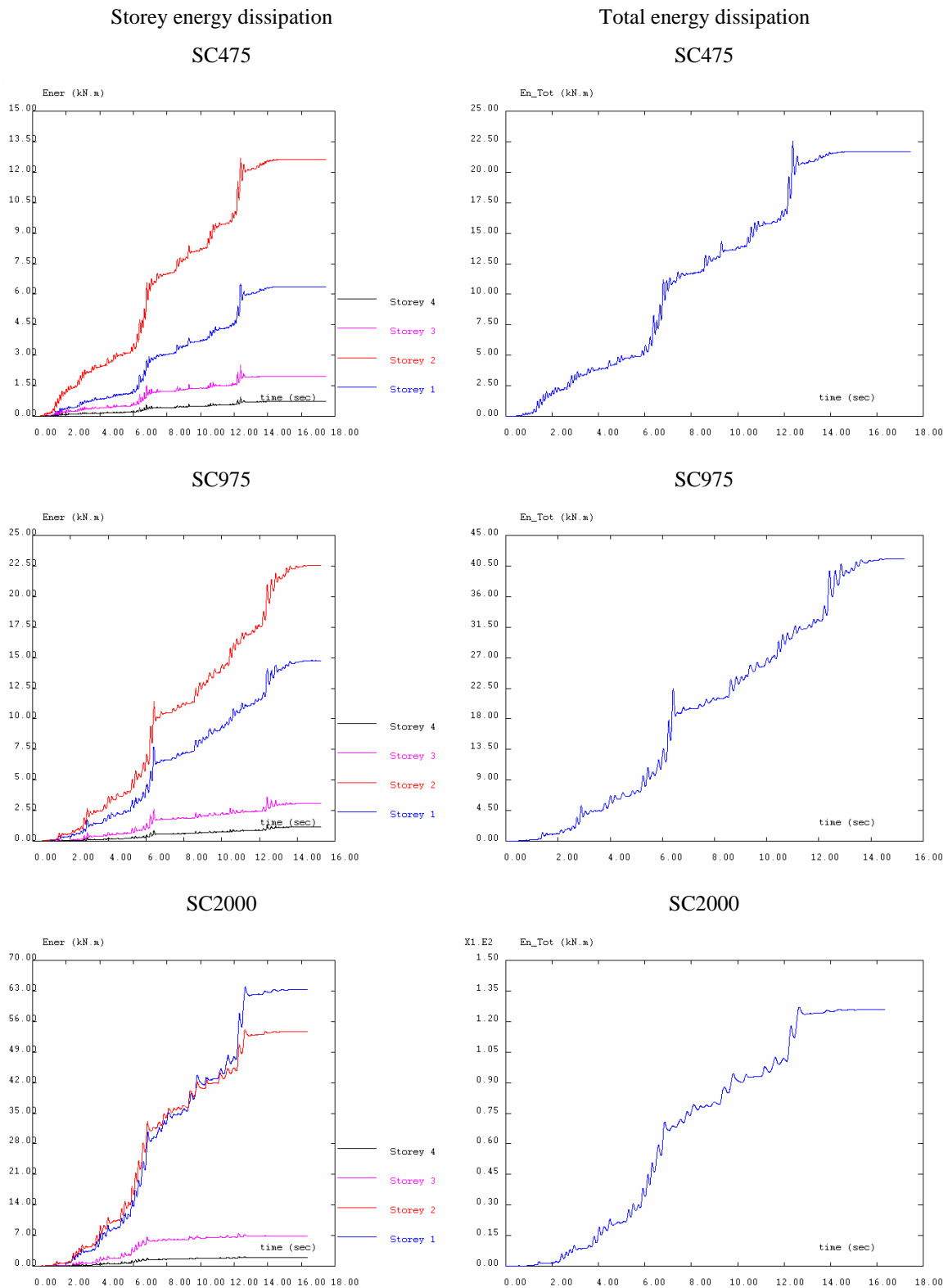


Figure 4.60 - SC tests: storey and total energy dissipation

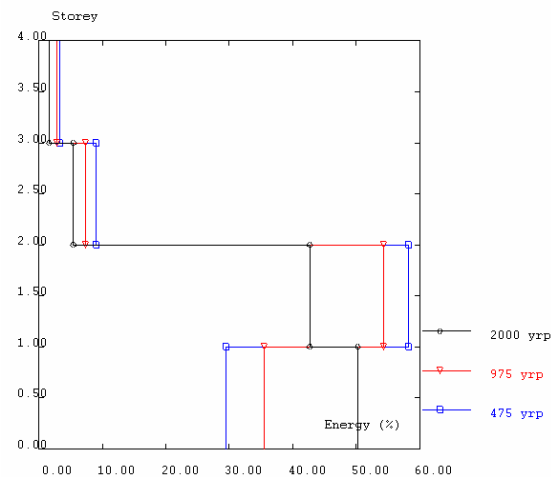


Figure 4.61 - SC tests: relative energy dissipation profiles

From the analysis of Figures 4.60 and 4.61, it can be concluded:

- For the SC tests, the fourth storey practically does not dissipate energy: 3%, 2.5% and 1.5% of the total dissipated energy, for the 475, 975 and 2000-yrp earthquake test, respectively. The third storey also dissipates a small amount of energy: 9%, 7% and 5%, for earthquake intensity corresponding to 475, 975 and 2000-yrp.
- For the first two earthquake intensities, the second storey is the one dissipating more energy. This tendency is dropped down as the earthquake intensity increases. For the most intense earthquake, it is the first storey the one which dissipates more energy.
- For every earthquake test (see Figure 4.61), the energy dissipation profile is in line with the inter-storey drift profile (Figure 4.58-*a*).
- The total dissipated energy at the 2000-yrp test is approximately three times the one dissipated for the 975-yrp test, and six times the dissipated for the 475-yrp test.

### 4.8 - COMPARISON BETWEEN IN AND SC TESTS

This section collects the principal structural effects of the infill strengthening in the response of the RC infilled frame, in terms of storey displacement, inter-storey drift and shear-drift behaviour curves. Figure 4.62 plots the curves base-shear versus top-displacement for the three earthquake tests performed on the IN and SC frame. Figure 4.63 collects all curves base-shear versus top-displacement for the IN and SC tests, and includes the envelope curves for the two series of tests.

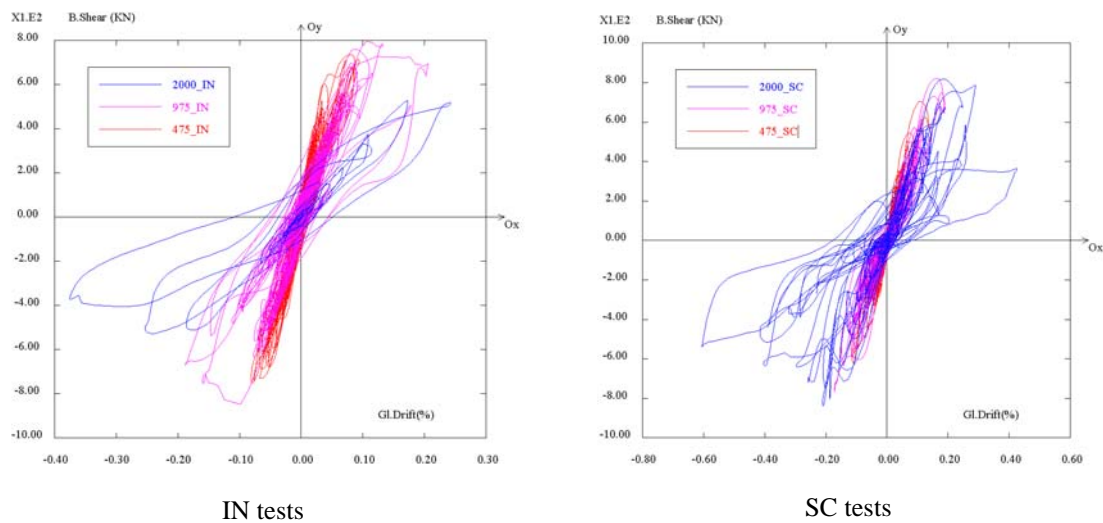


Figure 4.62 - IN and SC tests: base-shear versus global drift

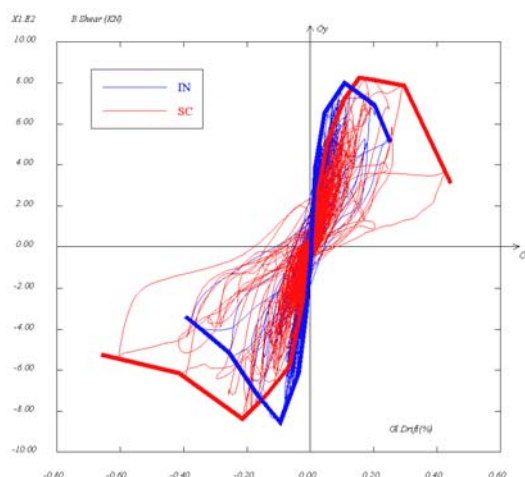


Figure 4.63 - IN and SC tests: base-shear versus global drift and respective envelope curves

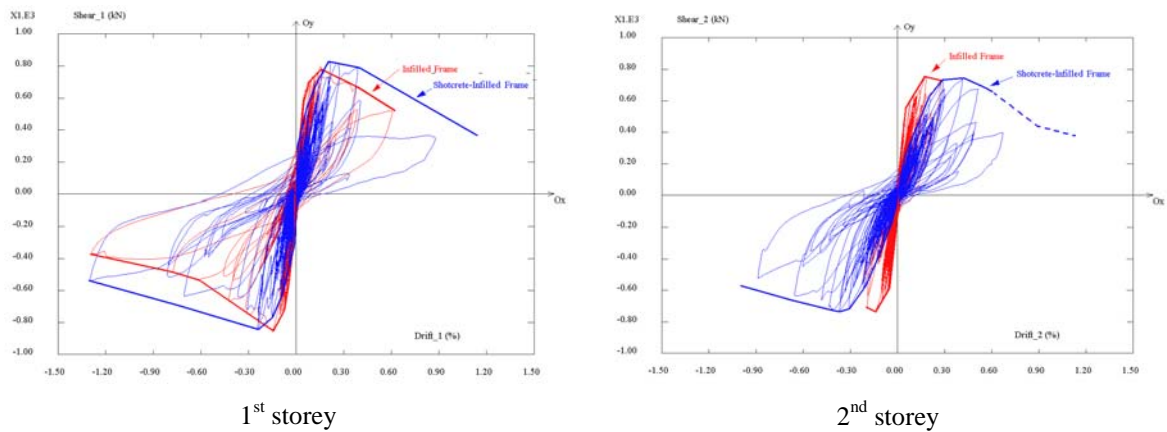


Figure 4.64 - IN and SC tests: storey shear versus inter-storey drift and respective envelope curves

It is apparent from the base-shear versus top-displacement (Figure 4.63) that an equivalent strength develops for the IN and SC frames, and the deformation capacity of the SC frame is moderately improved. Similar conclusions can be drawn from the diagrams storey shear versus storey drift shown in Figure 4.64 for the 1<sup>st</sup> and 2<sup>nd</sup> storeys, respectively.

The drift profiles for the IN and the SC frames for the different earthquake tests are given in Figure 4.65. Analysing the results, it is apparent that the 2<sup>nd</sup> storey drift demands are much higher for the shotcrete infilled frame tests. This relies on the fact that the infill panels at this storey have not been replaced after the previous tests (an inter-storey drift of 0.27% was experienced at this storey, which induced quite important damage in the infill panels).

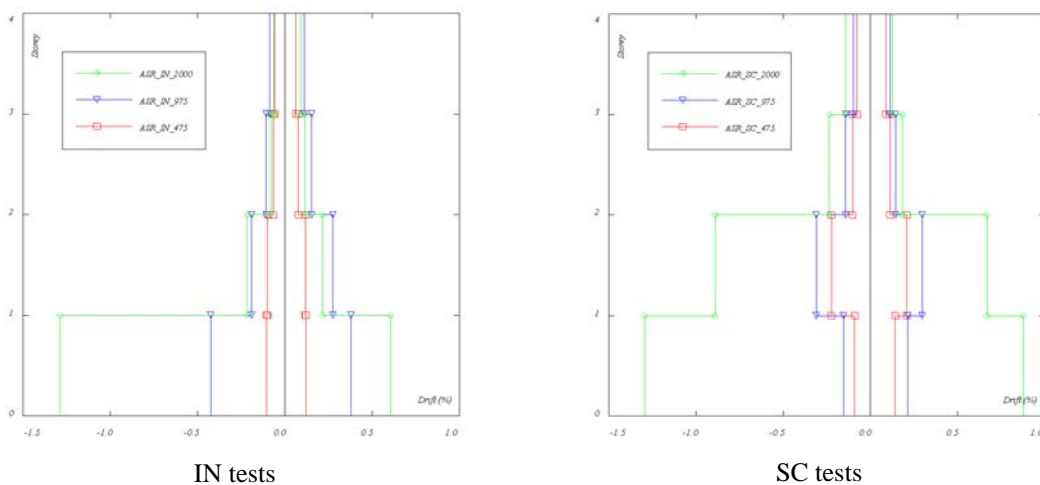


Figure 4.65 - IN and SC tests: maximum inter-storey drift profiles

Yet, several aspects should be further investigated in detail in order to conclude about the benefits and drawbacks of the shotcrete of existing RC infilled frames. It is however underlined that no substantial benefit arises from the strengthening of the infills if no appropriate dowels are provided between the infill and the adjacent girders.

## **4.9 - K-BRACING WITH SHEAR-LINK TEST**

### **4.9.1 - Test program**

Prior to the study of K-bracing with shear-link (frame B), the concrete frame columns were strengthened with selective retrofitting techniques and tested pseudo-dynamically. For the K-bracing study, hollow brick-masonry infill walls with two-sided plaster were constructed in the outer bays of the second floor. Subsequently, the K-bracing with shear-link assembly was inserted into the middle bay and anchored to the beams and columns of this bay (Bouwkamp *et al.*, 2000).

As noted in Section 3.5, the cyclic study was limited to the second floor. The quasi-static tests were carried out by introducing cyclic, displacement-controlled, actuator forces causing controlled shear deformations at the second storey only (labelled KB-cyclic test). The test control called for holding the first-floor actuator-displacement at zero, and at introducing at the second and higher floor levels identical cyclic, step-wise increasing, actuator displacements. Specifically, the test plan called for introducing a series of cyclic displacements reflecting storey drifts of 0.04, 0.08, 0.16, 0.24, 0.32, 0.48, 0.64 and 0.80% up to an expected maximum of 2%. In the tests, each displacement cycle was repeated 3 times.

### **4.9.2 - Test results**

The test results for the total cyclic lateral-load (storey shear) versus storey-displacement are presented in Figure 4.66. As can be observed in the figure, the maximum shear capacity was about 600 kN, versus the predicted value of about 520 kN. Considering the fact that the steel used in the shear-link was found to have a yield stress of 360 N/mm<sup>2</sup>, rather than



$300 \text{ N/mm}^2$  that was used in the pre-design considerations, the shear yield load would have been  $120 \text{ kN}$  (rather than  $100 \text{ kN}$ ). This would lead to a predicted maximum lateral resistance of  $540 \text{ kN}$ , at least (Bouwkamp *et al.*, 2000).

Figure 4.66 shows that at a drift of about 0.5% (displacement 12-13  $\text{mm}$ ) the lateral load did not increase further. Although this response was expected at that drift, the actual limiting cause was not a failure of the infilled walls, as had been assumed, but rather the premature development of a shearing failure in the outer frame column of the 2.5  $\text{m}$  bay. In fact, the failure resulted from the transverse slip of a joint between the top of the column and the bottom of the beam. A detailed description of the observed damages is shown in Figure 4.67 (see also Figures B.24 to B.26 and B.28).

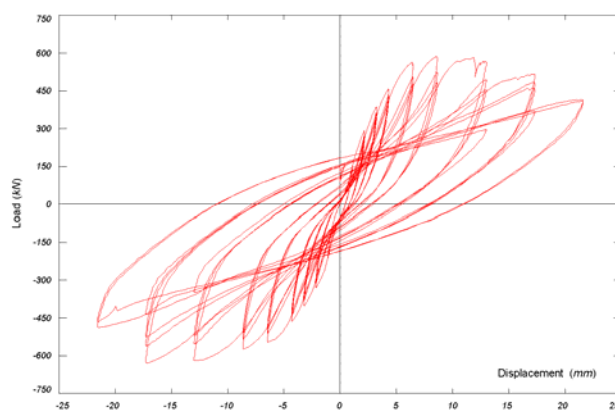


Figure 4.66 - KB-cyclic test: total storey shear versus relative storey displacement

Specifically, by a lateral displacement away from the reaction wall (see Figure 3.36), the resulting diagonal compressive force in the infilled panel caused tension in the outer column and an opening up of the cold joint (Figure 4.67, damage 5) of several millimetres. The behaviour was amplified by the fact that the column longitudinal bars distorted laterally causing a spalling of the concrete at the outer edge of the column-beam junction. This led to the development of an upward slanted crack towards the outside (see Figure 4.67, damage 8). Following a lateral displacement cycle of about 17  $\text{mm}$ , the progressive failure of the column exhibited a permanent horizontal offset of about 2 to 3  $\text{cm}$  between column and beam. It was recognized that an increasing offset could potentially endanger the column axial-load carrying capacity. Under increasing displacement cycles,

the above deterioration had been associated to a loss of resistance of about 15% (from about 600 kN to 500 kN).

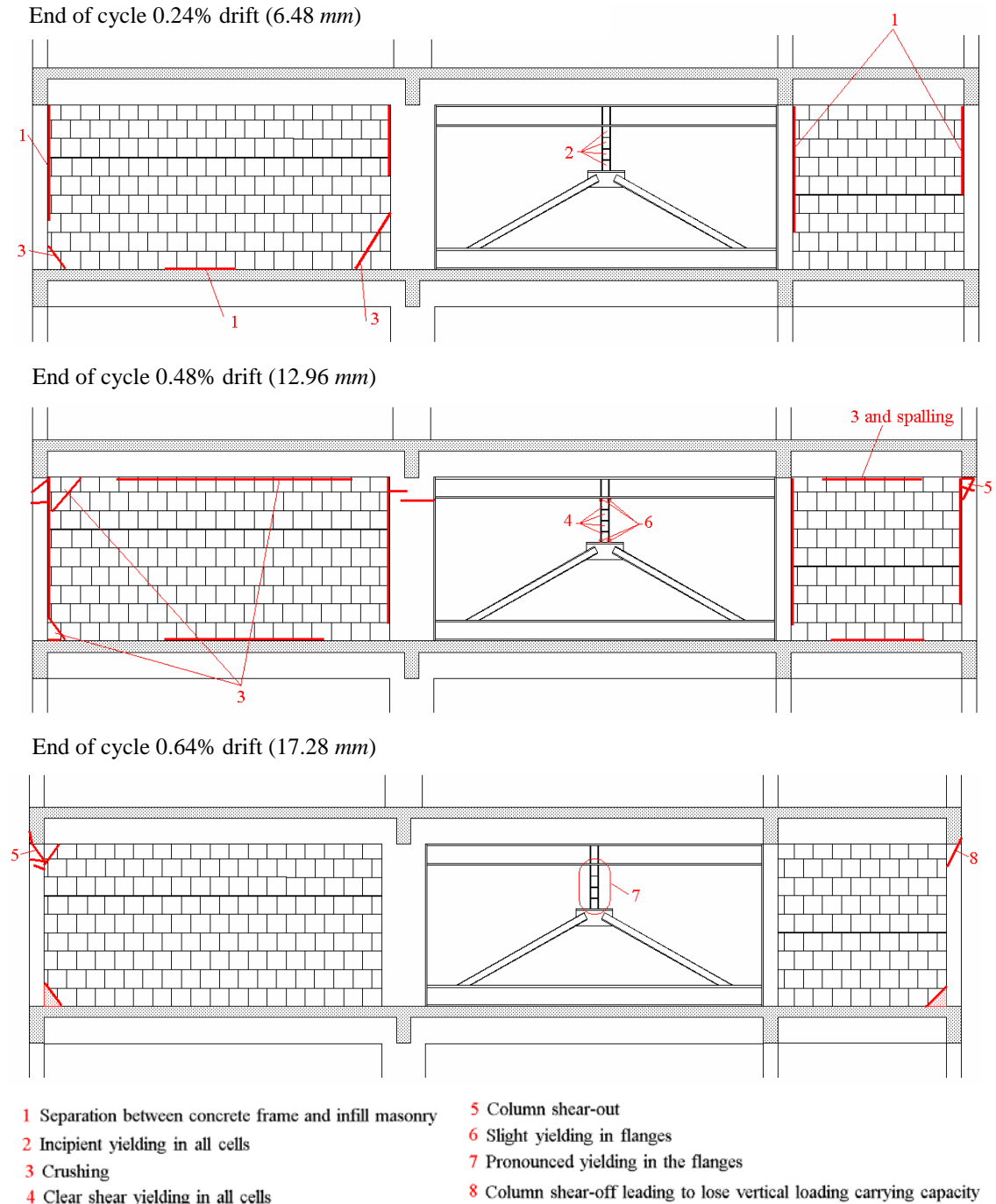


Figure 4.67 - KB-cyclic test: damage inspection

At that stage the test was stopped. Expecting that a separation between the infill wall and the column would prevent further deterioration, the brick infilled walls immediately

adjacent to the outer columns were removed leaving a gap of about 5 cm between walls and outer columns. The tests were then continued, repeating the last two previous steps, with single cycles of 13.5 mm (0.5% drift at a lateral load of only 330 kN) and 17.5 mm (0.65% drift at a lateral load of 400 kN). Subsequently, two cycles of 21.5 mm (0.8% drift at a lateral load of 420 kN) were introduced. Yet, the two repeated cycles at this displacement level showed little deterioration in the lateral load resistance. Unfortunately, the test had to be stopped prematurely as the outer column showed further outward slippage along the outwardly inclined crack, with an offset of almost 5 cm at the top of 2<sup>nd</sup> floor column, where failure of the joint and column was imminent. Wooden struts were introduced locally to secure the structure.

The cyclic response of the vertical shear-link, as reflected by the lateral displacement of the link and the link shear force, is shown in Figure 4.68. It derived from the sum of the horizontal components of the brace forces calculated from strain-gauge measurements on both brace members. The result shows a typical ductile stable behaviour with the resistance steadily increasing under repeated displacement cycles. As predicted, yielding was observed at a load of approximately 100 kN.

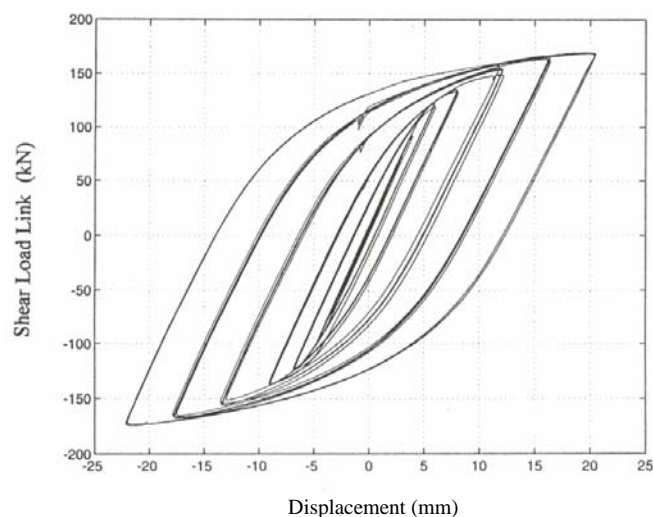


Figure 4.68 - KB-cyclic test: shear force versus relative lateral displacement at the shear-link

When the test had to be terminated prematurely, cyclic shear-strain hardening resulted in an increase of the lateral load resistance of the link to about 170 kN (at a link drift of 3.5% or only about 40% of the link design drift of 9%).

Both the cyclic resistance of the shear-link and the total-lateral load resistance of the retrofitted frame at the 2<sup>nd</sup> floor level are presented in Figure 4.69. On one hand, the results clearly show that under increasing number of displacement cycles and associated progressive failure, the participation of the shear-link in resisting the total lateral load becomes more pronounced. At the same time, a distinct drop in the overall shear resistance of the frame under repeated displacements is clearly illustrated. On the other hand, as a result of the cyclic shear-strain hardening in the link, both the gradual increase of the shear-link resistance within each series of repeated displacements as well as the increase of the resistance under progressively increasing displacements can be noted. The overall energy dissipating characteristics of both the retrofitted single-storey (including the shear-link) and the shear-link are illustrated by the results presented in Figure 4.70 (Varum and Pinto, 2001-*a*). The figure clearly shows the progressively increasing energy absorbing capacity of the shear-link, and the continually deteriorating energy dissipation of the infilled concrete frame. In fact, at the end of the tests, the link had dissipated 50% of the total energy absorbed. Figure 4.71 presents the test results in a load versus displacement format for both the shear-link and the overall retrofitted 2<sup>nd</sup> storey frame.

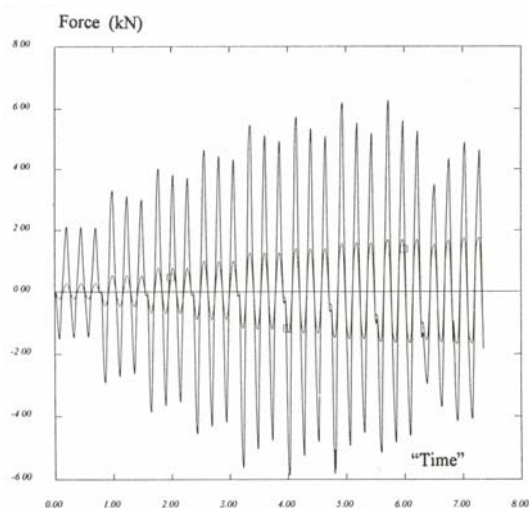


Figure 4.69 - KB-cyclic test: total lateral storey resistance and shear-link shear resistance

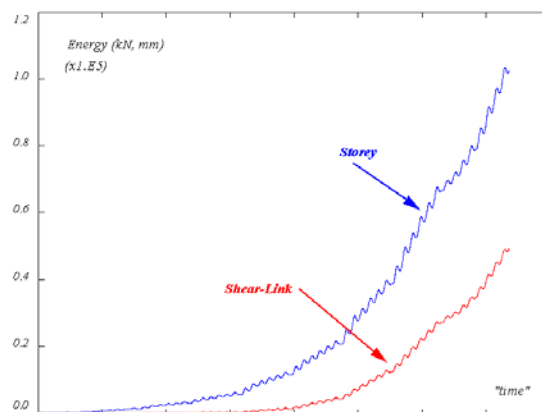


Figure 4.70 - KB-cyclic test: energy dissipation for retrofitted frame and shear-link

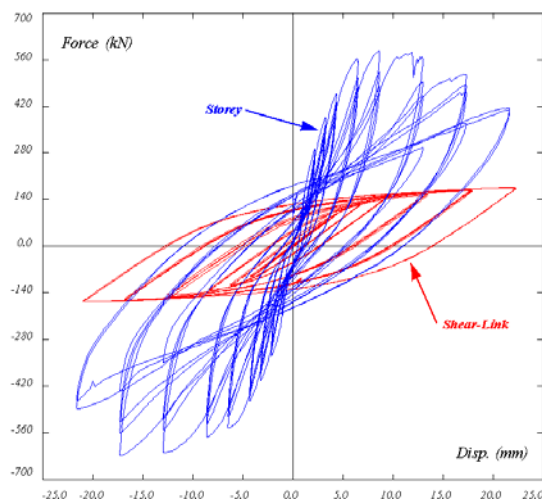


Figure 4.71 - KB-cyclic test: total storey shear versus relative storey displacement and shear force versus relative lateral displacement at the shear-link

Finally, the test results have clearly shown that the anchor bolts were effective and that slippage did not occur. Because of the basically rigid steel parts, it can be speculated that the anchor bolts forces in each part were fairly well distributed uniformly. Hence, in case that the deterioration of the frame would not have forced terminating the test prematurely, it could be expected that up to a (design) drift of 2%, which reflects a shear distortion of 9% of the 600 mm long link, the inter-welded braced frame assembly would have functioned well without showing distress in the bolted interface.

#### 4.10 - FINAL CAPACITY CYCLIC TESTS

Final capacity cyclic tests on the four-storey frames were performed to estimate the ultimate structural displacement and to investigate the post-peak structural behaviour. These are important parameters, for example, to define damage indices, and to verify numerical simulations (Pinto *et al.*, 2000-*b*).

The final capacity test campaign on the full-scale four-storey concrete frames includes two cyclic tests. The first part of the test campaign focuses on the selective repaired frame (SR-cyclic, frame B). The second cyclic test concentrates on the bare frame that was recovered from the infilled frame (BF-cyclic, frame A) removing the infill masonry walls.

#### 4.10.1 - Description of cyclic loading history

For the analyses of the cyclic inelastic behaviour of structures, controlled displacements instead of forces should be enforced. This follows because instability is associated with the descending strength branch (after maximum strength point) when the control is based on forces. The number of equal amplitude cycles for each level of imposed displacement is defined in order to characterize the hysteretic stability, i.e. the strength and stiffness degradation.

The last test series was decided to be cyclic with increasing amplitude up to the capacity of the structure. The cyclic tests were performed with imposed displacements on the top of the structure (fourth floor), being the three lower floors force-controlled, according to an inverted-triangular storey-wise distribution (see Figure 4.72). Such force distribution should result in a first-mode-like deformed shape.

The applied load cycles had symmetric and gradually increasing peak displacement, and were generally repeated once at each peak displacement in order to observe the hysteretic stability. The imposed lateral displacement time histories for both tests (frames A and B) are composed by two equal complete symmetric cycles for each displacement level, as shown in Figure 4.72. The displacement amplitudes (peak horizontal displacement) for each series of cycles were defined on the basis of the maximum top-displacement reached during the previous pseudo-dynamic test for each earthquake level. Figure 4.72 also shows a schematic representation of the force pattern.

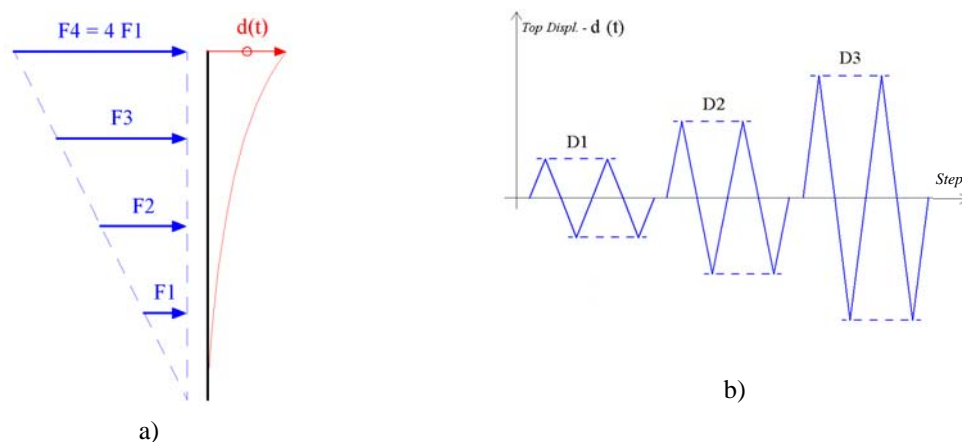


Figure 4.72 - Controlled force pattern and top-displacement: a) schematic representation; b) history of imposed lateral displacements

Table 4.14 gives the peak horizontal top-displacement imposed for each cycle and for each test (BF and SR). The maximum top-displacement obtained for each experimental earthquake test is displayed in brackets. Therefore, the displacement history imposed at the roof of the structure consisted on: two cycles of 60 *mm*, two cycles of 120 *mm*, and two cycles of 200 *mm*, as stated in Table 4.14.

Table 4.14 - Peak horizontal top-displacement imposed in the BF-cyclic and SR-cyclic tests

Test	Displacements ( <i>mm</i> )		
	D1	D2	D3
BF-cyclic	60 (60.8)	120 (116.7)	---
SR-cyclic	60 (63.2)	120 (116.3)	200 (219.5)

From the idealized conditions in terms of storey restoring forces, results an invariant relative storey shear profile, illustrated in Table 4.15.

Table 4.15 - Imposed shear profile

Storey	Shear force	Shear profile
4	4 F1	
3	7 F1	
2	9 F1	
1	10 F1	

Comparing the imposed shear profile with the profiles obtained in the earthquake tests performed on the bare frame and on the selective repaired frame, a good agreement is achieved with the proposed linear distribution of forces (triangular inverted), see Table 4.16. In the table, the relative shear profiles are defined as the maximum shear at each storey divided by the maximum base-shear. However, it should be noted that the shear profiles from the earthquake tests are the envelope of the developed storey shear forces. These storey shear maximum forces do not necessarily develop concomitantly.

Table 4.16 - Shear profiles (obtained from the earthquake tests and imposed in the cyclic tests)

Storey	Maximum storey shear / Maximum base-shear					
	BF475	BF975	SR475	SR975	SR2000	Cyclic test
4	0.46	0.51	0.42	0.57	0.60	0.4
3	0.67	0.71	0.62	0.70	0.77	0.7
2	0.90	0.94	0.87	0.86	0.82	0.9
1	1	1	1	1	1	1

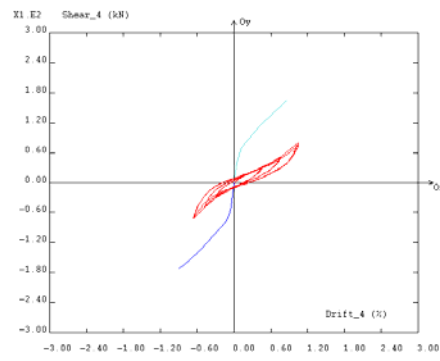
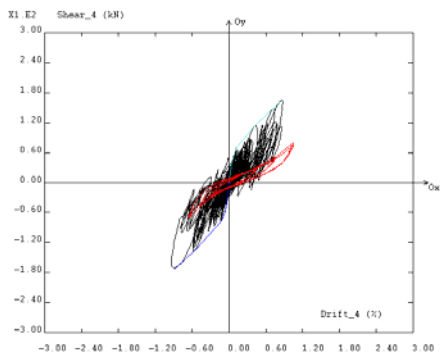
#### 4.10.2 - Selective strengthened frame cyclic test results

The results for the cyclic quasi-static test on the selective strengthened frame in terms of storey displacements, maximum drift profiles, maximum shear profiles, storey shear-drift, total energy dissipation, and base-shear versus top-displacement are given next.

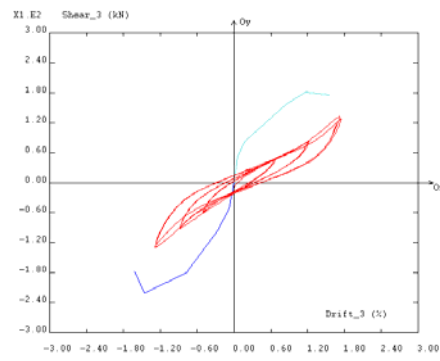
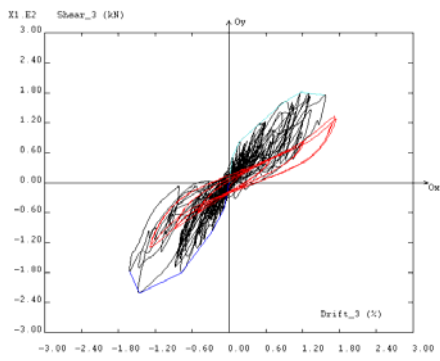
Table 4.17 summarizes the maximum values for characteristic response variables, i.e. top-displacement, global drift, inter-storey drift and storey shear, for the SR-cyclic test. The corresponding values for the SR frame earthquake tests were given in Table 4.6.

Figures 4.73 and 4.74 compare the responses obtained for the earthquake pseudo-dynamic tests with the final capacity quasi-static cyclic test. For each figure on the left, the curves shear-drift achieved for the PsD earthquake tests (black curve), the respective envelope curve (blue curves), and the corresponding shear-drift curve obtained for the cyclic quasi-static test (red curve) are represented. On the right, only the envelope earthquake test curve and the curve obtained for the cyclic quasi-static tests are represented.

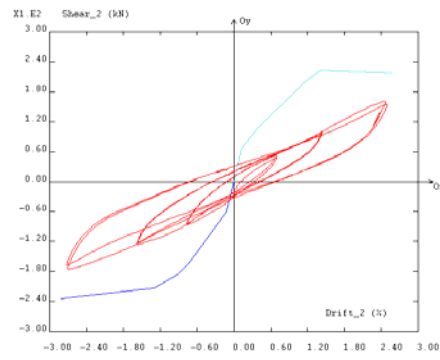
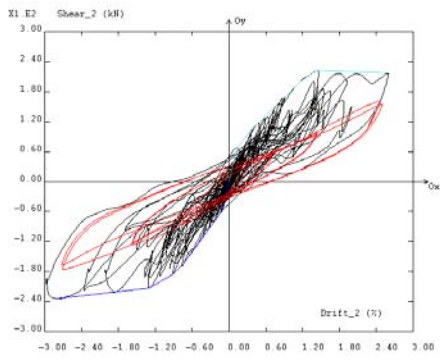




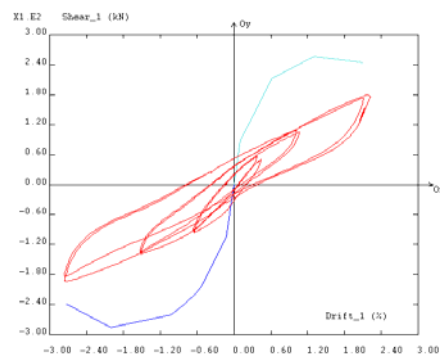
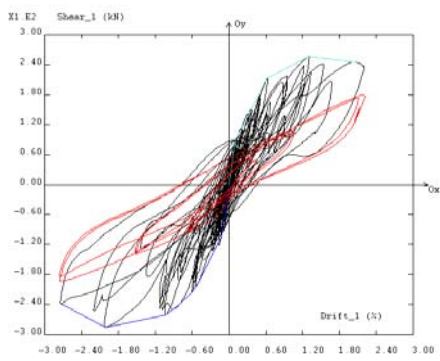
4<sup>th</sup> storey



3<sup>rd</sup> storey



2<sup>nd</sup> storey



1<sup>st</sup> storey

Figure 4.73 - SR and SR-cyclic tests: storey shear versus inter-storey drift

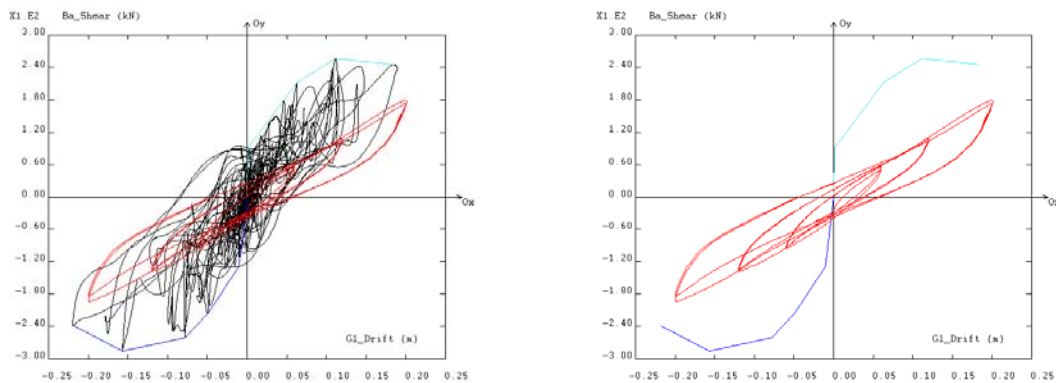


Figure 4.74 - SR and SR-cyclic tests: base-shear versus top-displacement

Table 4.17 - SR-cyclic test: response maximum values (summary table)

	Top-displacement ( <i>mm</i> )		Global drift (%)	
	storey 1	storey 2	storey 3	storey 4
	201.53		1.87	
Inter-storey drift (%)	2.77	2.72	1.75	1.05
Storey shear ( <i>kN</i> )	193.6	175.3	132.7	79.5

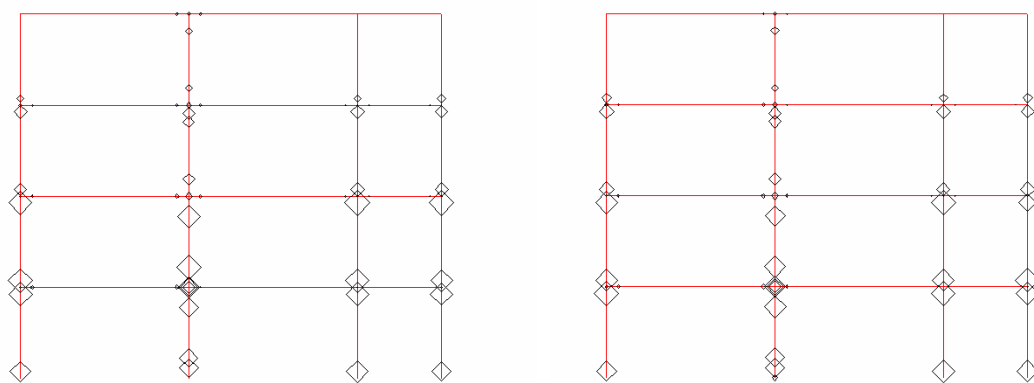
From the analyses of the storey shear-drift curves, it can be concluded that:

- For the 3<sup>rd</sup> and 4<sup>th</sup> storeys, it is observed an increase in stiffness ('hardening') after certain inter-storey drift level (of about 1% drift). The strengthening technique applied in these two storeys, consisted on the addition of external steel bars that work only after certain drift level, which explains this effect. Recall that this effect was already evident in the precedent earthquake pseudo-dynamic tests. The required level of drift at which this effect appears seems to increase with the accumulation of damage after each test.
- The maximum drift obtained at the first and second storeys was rather non-symmetric, but, nevertheless, this difference is very similar to the one observed in the previous earthquake tests.

#### 4.10.2.1 - Maximum absolute and relative rotations measured at the instrumented points

Figures 4.75 and 4.76 present the maximum (absolute and relative) rotations measured during the tests performed on the selective repaired structure (earthquake and cyclic tests). Only results for the 2000-yrp PsD test are presented because this is the test that achieved storey drift levels comparable with the final capacity cyclic test on this frame.

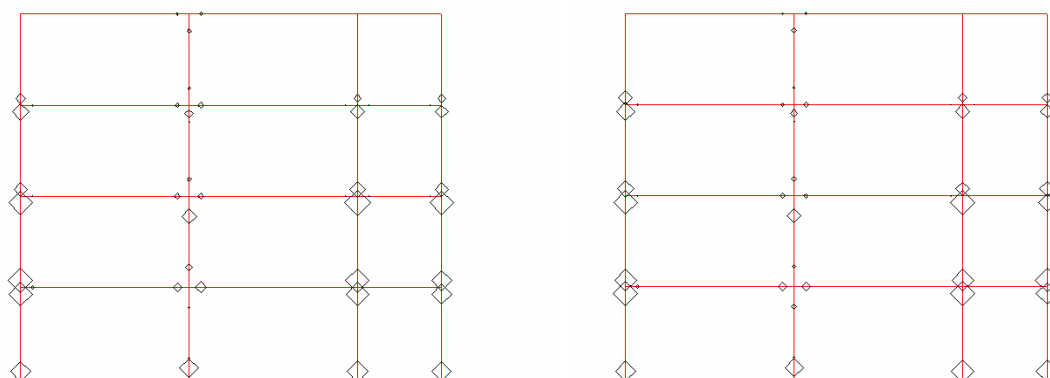
From the analysis of Figures 4.75 and 4.76, it can be observed that the rotations achieved in the dynamic and cyclic tests are identical. This similarity is verified in terms of maximum rotation values and distribution in the structure.



SR2000 – max. abs. rotation = 37.3 *mRad*

SR-cyclic – max. abs. rotation = 36.2 *mRad*

Figure 4.75 - SR2000 and SR-cyclic tests (frame B): maximum absolute rotation demands



SR2000 – max. relat. rotation = 38.7 *mRad*

SR-cyclic – max. relat. rotation = 37.0 *mRad*

Figure 4.76 - SR2000 and SR-cyclic tests (frame B): maximum relative rotation demands

#### 4.10.2.2 - Analyses of the repaired top-columns

This section is devoted to the analyses of the external top-columns of the 1<sup>st</sup> and 2<sup>nd</sup> storeys. As said in Section 3.7.8.1, a relative displacement transducer was arranged at each repaired joint intending to control the relative horizontal dislocation of the top-column during each test. To help the analyses and interpretation of the results, the top-columns studied were labelled as described in Figure 4.77.

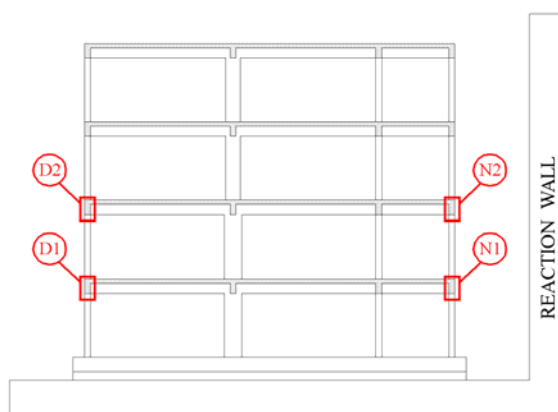


Figure 4.77 - Nomenclature of the repaired external top-column (1<sup>st</sup> and 2<sup>nd</sup> storeys)

Figure 4.78 shows the evolution of the relative displacements measured at the instrumented exterior top-columns, for the test on the original structure (PsD earthquake test, L33, before repair), and for the test on the repaired structure (cyclic test, L38, after repair). Figure 4.79 plots the relative displacement versus the correspondent inter-storey drift, for the earthquake and cyclic tests.

From the analyses of Figures 4.78 and 4.79, it can be concluded that:

- For the final capacity cyclic test it was observed deformation related just to the elastic behaviour of the structure, i.e., no permanent deformation was installed in the top-columns during the cyclic test.
- The maximum inter-storey drift reached at the 2<sup>nd</sup> storey during the test L33 was 3.4 times inferior to the value obtained in the L38 test. Even for this much larger value of drift obtained in L38 test, the lateral dislocation of the external columns was prevented with the repair technique adopted.

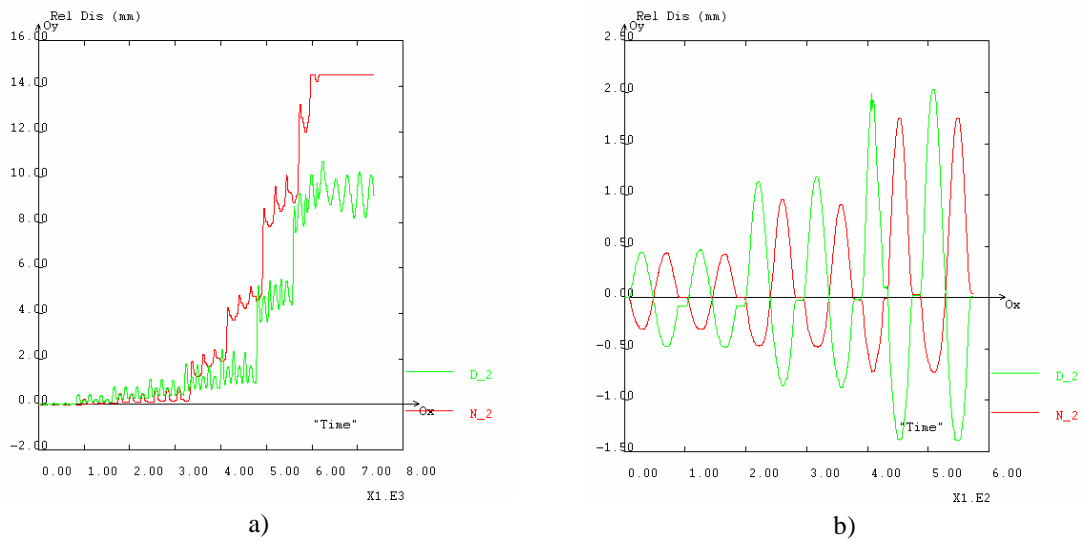


Figure 4.78 - Frame B (evolution of N2 and D2 top-columns dislocation): a) test L33 (before repair), b) test L38 (after repair)

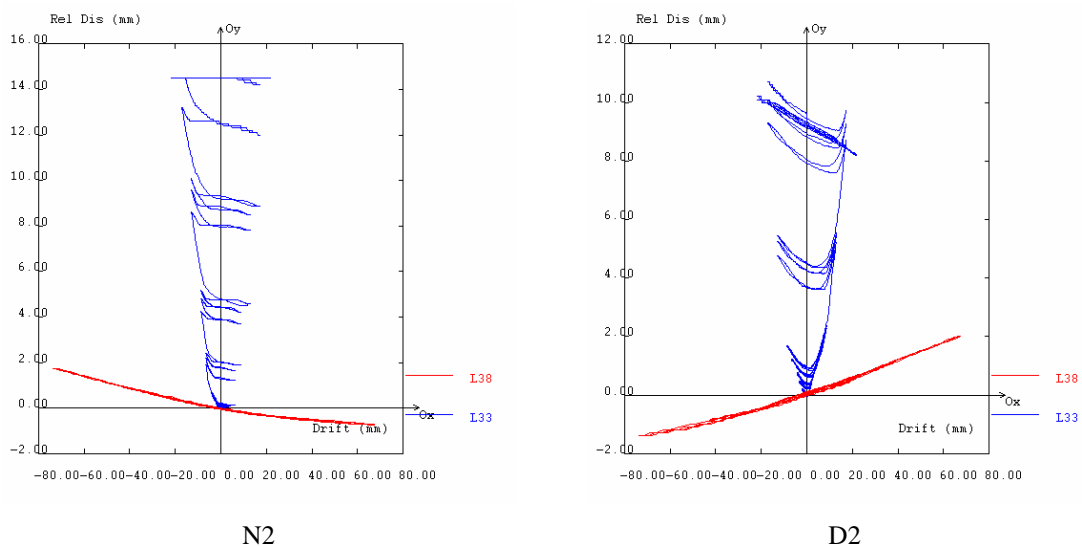


Figure 4.79 - Frame B (joints N2 and D2): top-columns dislocation versus inter-storey drift before repair (test L33) and after repair (test L38)

### 4.10.3 - Bare frame cyclic test results

The frame A had considerable damage induced by the previous earthquake tests (which was tested with infills). Due to the heavy damage inflicted during these previous tests, the strong-column on the 1<sup>st</sup> storey and the external top-columns on 1<sup>st</sup> and 2<sup>nd</sup> storeys had to be repaired. As already stated, the final capacity test on frame A was planned to be

performed with values of top-displacement listed in Table 4.14. However, the predicted collapse at the 3<sup>rd</sup> storey (reached in the bare frame earthquake test) for approximately 120 mm top-displacement was not reached in this cyclic test. The structure was slightly damaged at the first two storeys during precedent earthquake tests, and, consequently, the concentration of storey drift at the 3<sup>rd</sup> storey was not so pronounced.

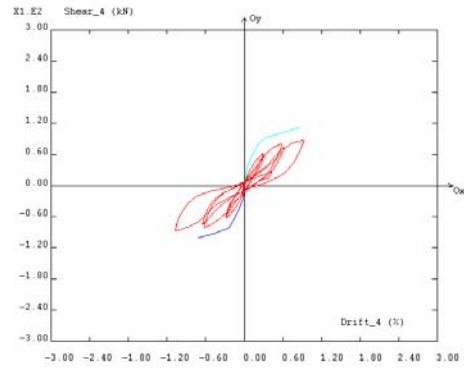
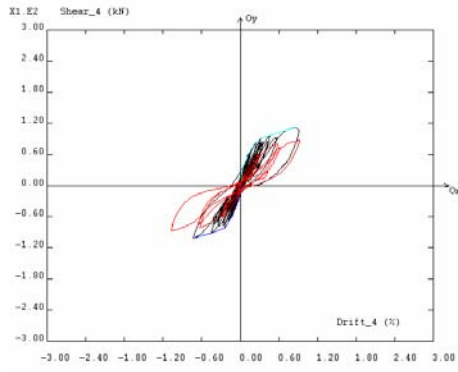
The results for the cyclic quasi-static test on the bare frame in terms of storey displacements, maximum drift profiles, maximum shear profiles, storey shear-drift, total energy dissipation, and base-shear versus top-displacement are given next.

Table 4.18 summarizes the maximum values for characteristic response variables, i.e. top-displacement, global drift, inter-storey drift and storey shear, for the BF-cyclic test. The corresponding values for the BF frame earthquake tests were given in Table 4.1.

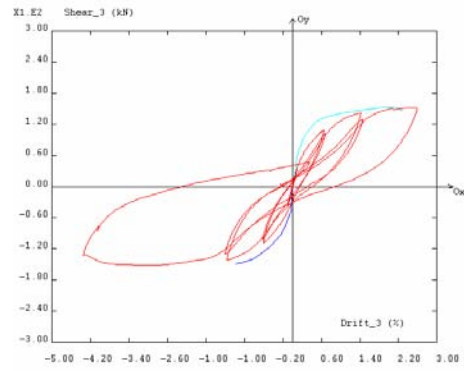
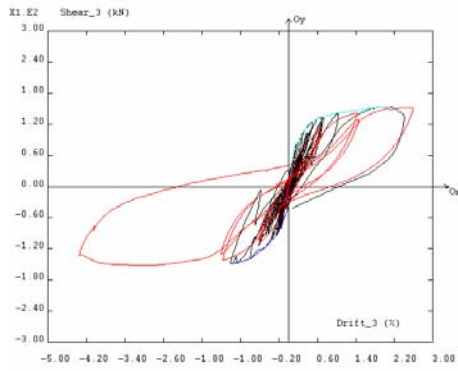
Figures 4.80 and 4.81 compare the response obtained for the earthquake tests (475, 975 and 2000-yrp) with the final cyclic test performed on the BF structure. For each figure, on the left, are represented the curves shear-drift achieved for the earthquake tests (black curve), the respective envelope curve (blue curves), and the corresponding shear-drift curve obtained for the cyclic quasi-static test (red curve). On the right are represented only the envelope earthquake tests curve and the curve obtained for the cyclic quasi-static tests.

Table 4.18 - BF-cyclic test: response maximum values (summary table)

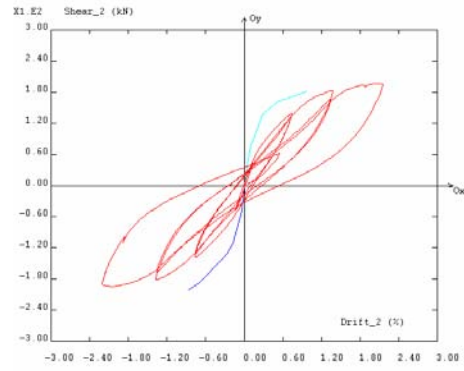
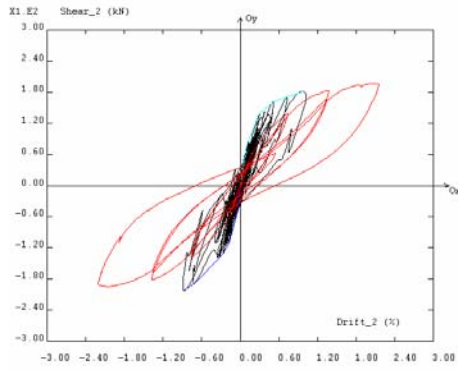
	Top-displacement ( <i>mm</i> )		Global drift (%)	
	249.7		2.31	
	storey 1	storey 2	storey 3	storey 4
Inter-storey drift (%)	1.75	2.21	4.35	1.07
Storey shear ( <i>kN</i> )	219.9	196.9	152.6	87.2



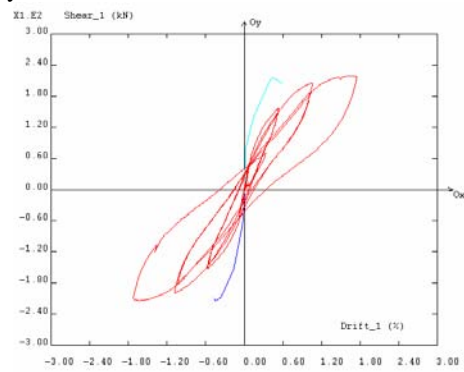
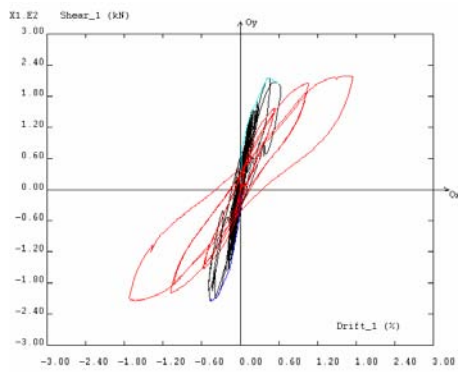
4<sup>th</sup> storey



3<sup>rd</sup> storey



2<sup>nd</sup> storey



1<sup>st</sup> storey

Figure 4.80 - BF and BF-cyclic tests: storey shear versus inter-storey drift

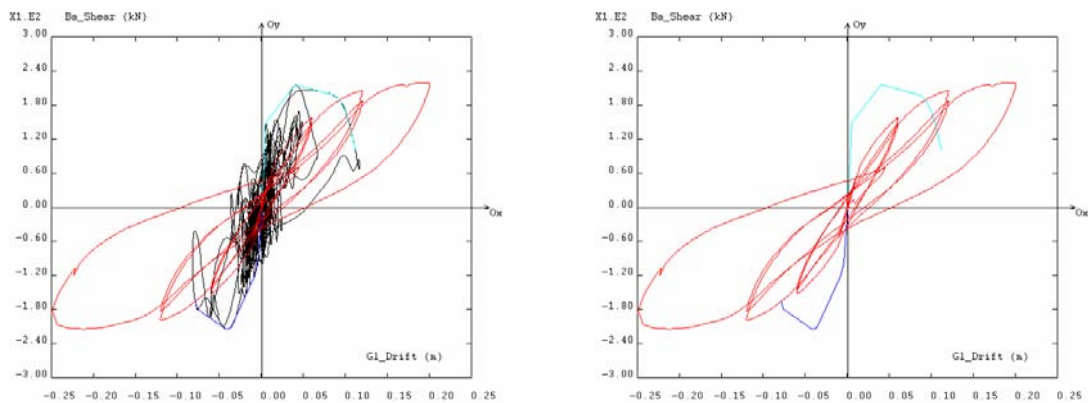


Figure 4.81 - BF and BF-cyclic tests: base-shear versus top-displacement

From the analysis of the storey shear-drift curves, it can be observed that the earthquake and cyclic test results are in conformity. For the bare frame and for all the storeys, the envelope of the shear-drift diagrams of the earthquake tests involves the diagrams of the cyclic tests. For the 3<sup>rd</sup> storey, the PsD envelope results are tangent to the response for the cyclic tests. For the other three storeys this correspondence is not observed. But, it has to be considered that the frame tested cyclically was already pseudo-dynamically tested with infills. Moreover, during these tests, the frame experienced considerable drifts and consequently damage, especially at the first and second storeys. The maximum inter-storey drift observed during PsD tests was of 1.30%, 0.89%, 0.23%, and 0.14%, for the 1<sup>st</sup>, 2<sup>nd</sup>, 3<sup>rd</sup> and 4<sup>th</sup> storey respectively. However, from the plots it can be observed that the cyclic curves tend to the PsD envelope curves.

#### 4.10.4 - Remarks

The results from the tests performed at ELSA laboratory on full-scale structures repaired with FRP's demonstrate that by using advanced composites it is possible to significantly improve the seismic behaviour/performance of vulnerable structures.

It is shown that a very effective (cost/benefit) repair or strengthening operation can be used to repair local heavy damages, like the ones resulting from the effects of infill panels on external columns and joints.



---

It has been shown that the application of carbon fibre wraps on the critical regions of damaged structural elements can recover an important part of the loss in stiffness and strength of those members. In addition, improvement in energy dissipation capacity and the global ductility of the structure can be achieved.

#### **4.11 - LOCAL MEASUREMENTS**

The measuring system designed for the tests presented in Chapter 3 includes several inclinometers and displacement transducers. It was aimed at complete instrumentation of the structure, to record both global and local responses. The rotations at potential plastic hinge zones were recorded by the inclinometers and the displacement transducers recorded slab-participation, total elongation of the girders, distribution of demands in the plastic hinge zone and deformation of the 1<sup>st</sup> storey strong-column and beam-column joint. Furthermore, it was possible to cross-check measurements from different systems placed at the same zones of the model.

A more detailed discussion on the aspects of shear and flexural deformations of the strong-column, slab-participation, plastic hinge length and joint deformation are dealt with in specific dedicated reports. However, the principal aspects and main results are briefly discussed herewith.

##### **4.11.1 - Plastic hinge length**

Displacement transducers were placed at the upper and lower parts of the girder in the central joint at distances of 75, 150 and 350 *mm* from the column face in both the left and the right column sides (see Figure 3.39). Figure 4.82 shows the results from these transducers, in terms of uniform strain, i.e. displacement divided by the measuring length, for the BF and SR tests. Figure 4.82-*a* compares the maximum strain envelopes, for the 975-yrp tests, between the bare frame and the strengthened frame, and Figure 4.82-*b* summarizes the maximum uniform strain reached during the tests on the strengthened frame.

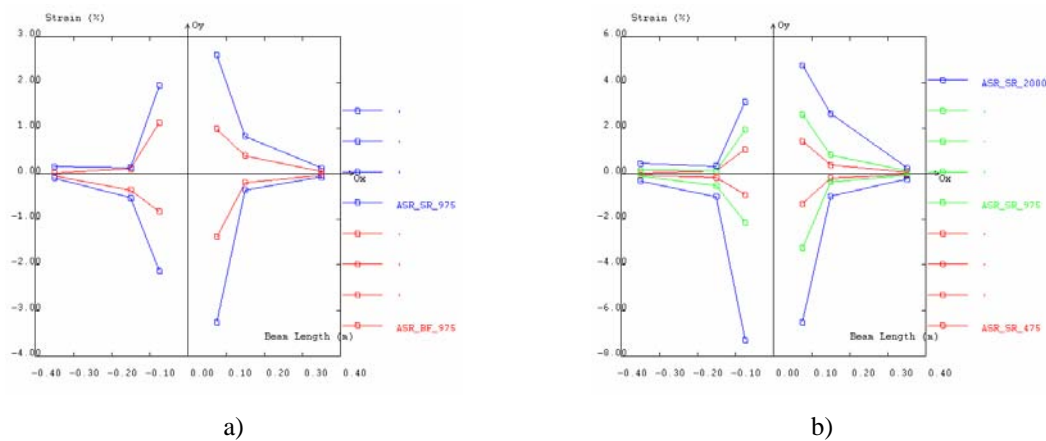


Figure 4.82 - Maximum uniform strain for positive and negative bending at the plastic hinge zone for the BF and SR tests

It is apparent that, as the response amplitude increases most of the deformation concentrates in the first instrumented slice 0-75 mm (80% for the SR2000 test for positive bending). Therefore, the plastic hinge length is very small compared to the values given by common empirical expressions.

The empirical expression (4.2) proposed by Paulay and Priestley (1992) for the plastic hinge length,  $l_p$ , gives, at the instrumented beam herein studied, a value of 0.52 m, which is higher than the values reached in the experimental tests (less than 0.20 m).

#### 4.11.2 - Shear cracks at the base of the 1<sup>st</sup> storey's strong-column

In the PsD test, the analyses of the deformation measured at the horizontal relative displacement transducer #105, in the strong-column at the base of the 1<sup>st</sup> storey, indicates that the first development of the shear crack in that region corresponds to an inter-storey drift of 0.4% (see Figures 4.83 and 4.84). In fact, the sudden change in the average deformation, i.e. at 10 seconds for the bare frame test (see Figure 4.83), and at 12 seconds for the infilled frame test (see Figure 4.84), corresponds to a permanent deformation due to the aperture of a shear crack. The visual observations of the damage in the column confirm this occurrence (see Figures B.19 and B.21).

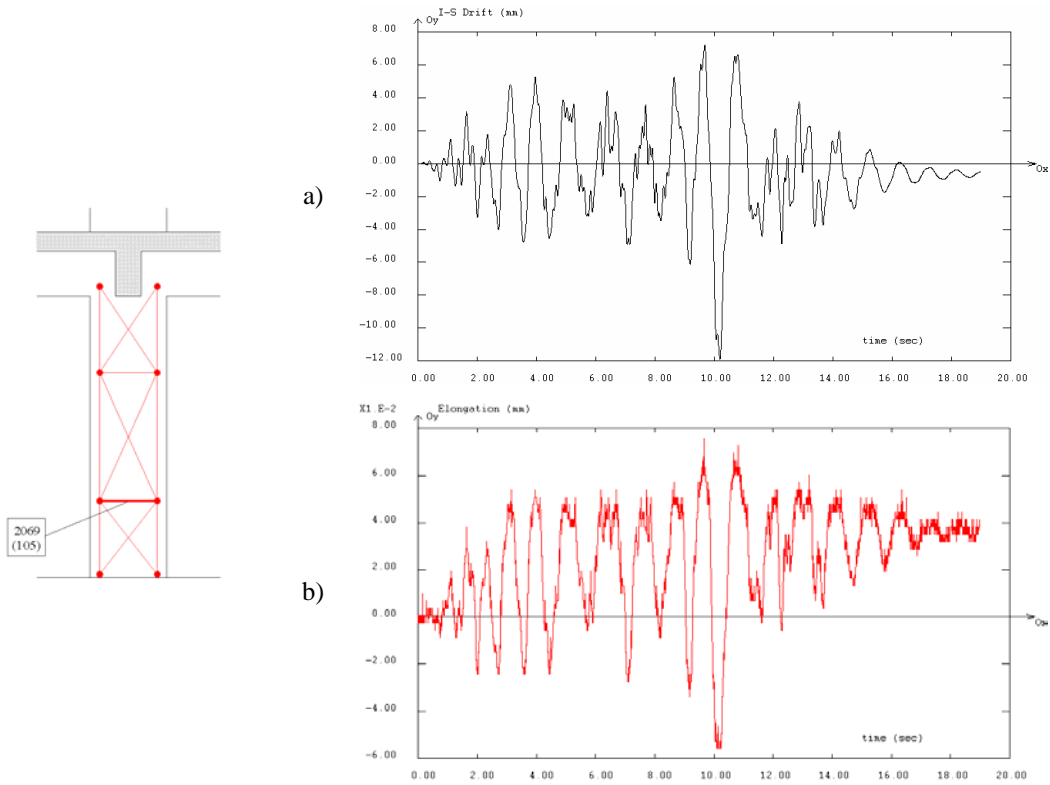


Figure 4.83 - BF475 test (1<sup>st</sup> storey strong-column): a) ID; b) elongation in transducer #105

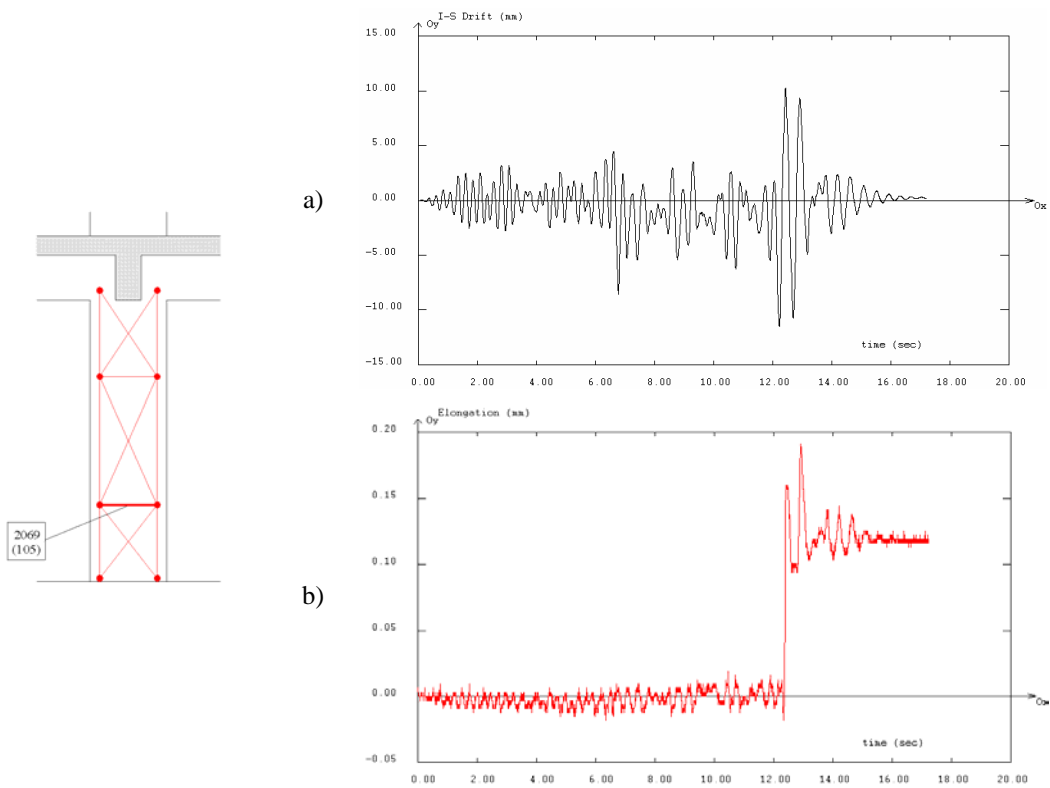


Figure 4.84 - IN975 test (1<sup>st</sup> storey strong-column): a) ID; b) elongation in transducer #105

### 4.11.3 - Slab-participation

In order to derive the contribution of the slab to the stiffness and strength of the girder (slab-participation), displacement transducers were arranged in three critical zones, as presented in Section 3.7.5.3 (see Figure 3.40). The three slab zones instrumented are: one external short-bay, one internal short-bay and one internal long-bay. With the selected locations for the instrumented slab zones, it is possible to compare the slab-participation in a long span-bay versus a short span-bay as well as between interior and exterior joint zones.

It is anticipated that, for tests where small deformations were reached, the results in terms of deformation profile and, consequently, the computation of the slab-participation, do not allow for sustainable detailed conclusions. Nevertheless, it was possible to find reasonable indications of the slab-participation for the higher intensity tests.

The slab-participation, during the time response,  $SP(t)$ , can be computed by the following equation (see also Figure 4.85)

$$SP(t) = \int_x \frac{\Delta(x,t)}{\Delta(x_0,t)} dx = \int_x \frac{\Delta_{static}(x) + \Delta'(x,t)}{\Delta_{static}(x_0) + \Delta'(x_0,t)} dx \quad (4.16)$$

where the variables involved represent:  $SP(t)$  slab-participation;  $\Delta(x,t)$  the deformation measured at a generic point / fibre ( $x$ ), function of time ( $t$ ); and,  $\Delta(x_0,t)$  the deformation measured at the beam level ( $x_0$ ), function of time ( $t$ ). The total deformation,  $\Delta(x,t)$ , involves two components, namely the deformation due to static loads  $\Delta_{static}(x,t)$  and the deformation due to the time varying response, as represented in Figure 4.85.

If the deformation due to the static loads is negligible, the slab-participation can be calculated as

$$SP(t) = \int_x \frac{\Delta'(x,t)}{\Delta'(x_0,t)} dx \quad (4.17)$$

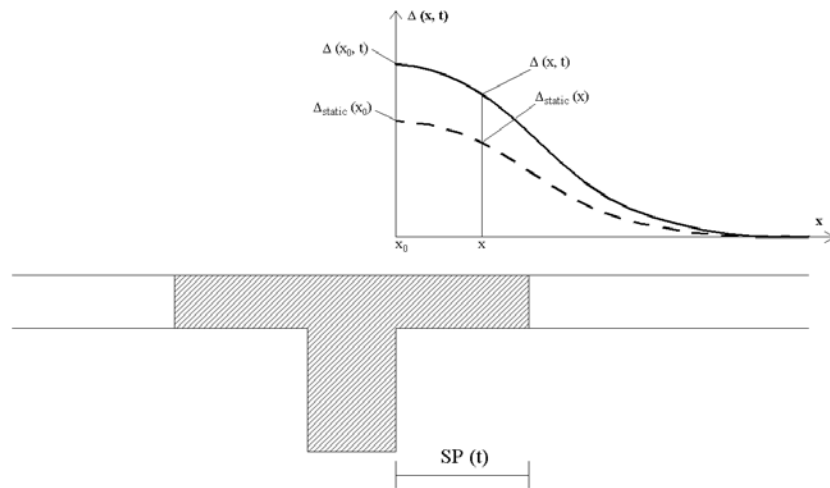


Figure 4.85 - Scheme of the slab-participation

For the discrete problem (see Figure 4.86), the slab-participation is computed as the coefficient between the sum of the product of each slice area by the corresponding average deformation and the maximum value of the deformation (deformation of the fibre closest to the longitudinal beam)

$$SP(t) = \sum_i A_i \cdot \frac{\Delta_i(t)}{\Delta_{beam}(t)} \quad (4.18)$$

where:  $A_i$  represents the characteristic length for slice  $i$ ;  $\Delta_i(t)$ , the deformation measured at point/fibre  $i$  of the slab; and,  $\Delta_{beam}(t)$ , the deformation measured at point/fibre  $i$  of the slab.

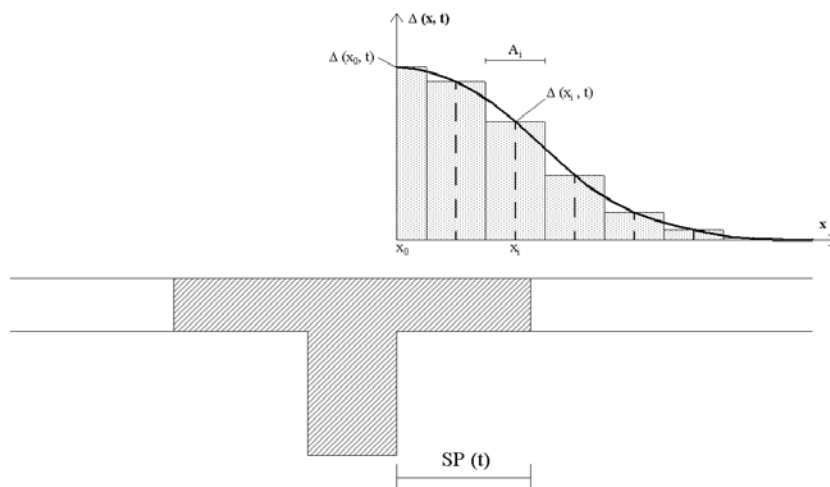


Figure 4.86 - Scheme of the slab-participation

Equation (4.18) was used to compute the slab-participation (including the beam width) for all PsD tests at the higher, lower and central fibre levels, and for the elongation and shortening states. Figures 4.87 and 4.88 give the peak values results in terms of elongation/shortening displacement ( $mm$ ) computed at the mid-thickness of the slab, for the internal long-bay, and for the BF and SR frames, respectively. They are indicative of the noticeable concentration of deformation in the vicinity of the longitudinal beam. Table 4.19 gives the calculated equivalent slab-participation width, at the medium fibre of the slab, for elongation and for the internal long-bay.

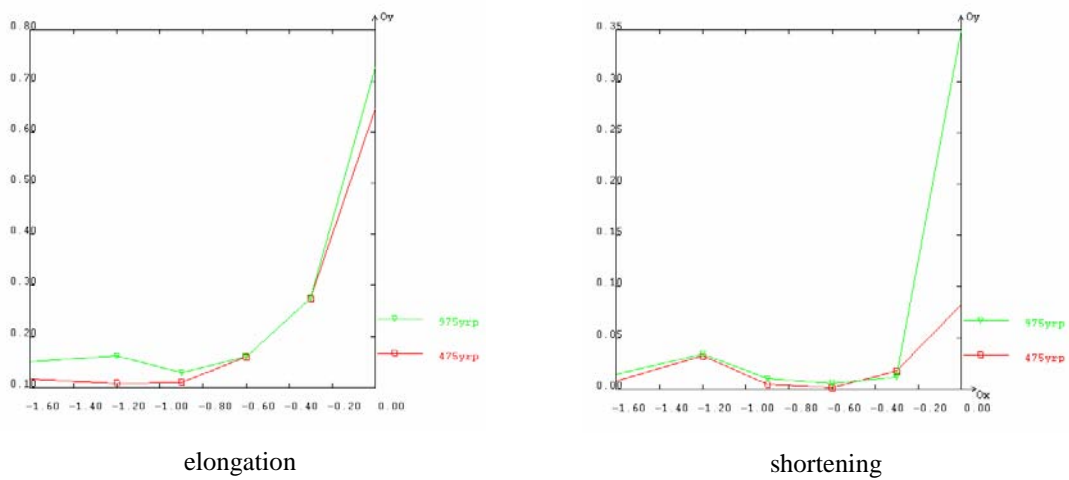


Figure 4.87 - BF tests: maximum deformation distribution ( $mm$ ) at the internal long-bay

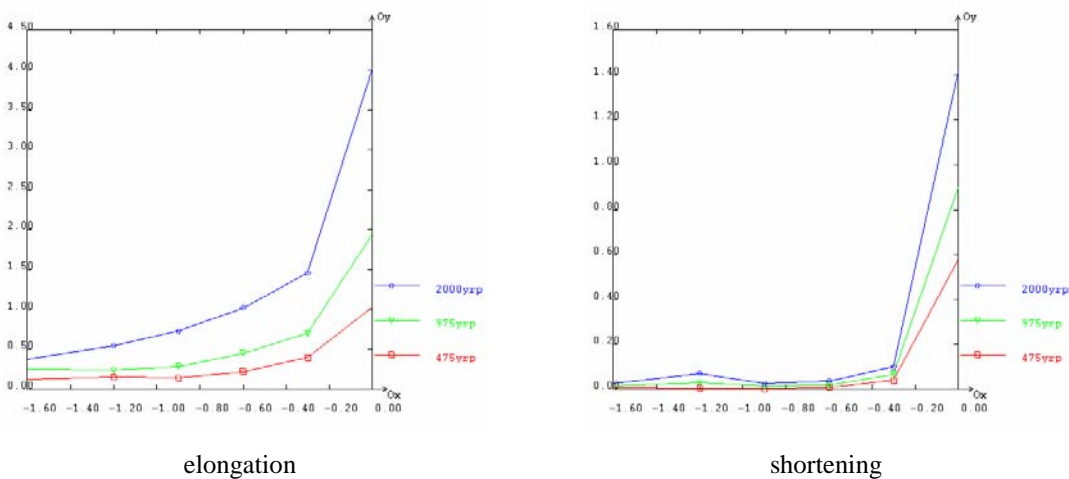


Figure 4.88 - SR tests: maximum deformation distribution ( $mm$ ) at the internal long-bay

Table 4.19 - BF and SR tests: evaluation of the slab-participation for the internal long-bay

Test	Slab-participation ( $m$ )
BF475	1.09
BF975	0.94
SR475	0.97
SR975	0.93
SR2000	1.08

It is important to refer to the values proposed in design codes, having in mind that those values are intended for design/analysis purposes. For example, EC8 proposes:

- For exterior columns: 'the slab-width considered should be within the column width, in the absence of a transversal beam. In the presence of a transversal beam with similar dimensions to the longitudinal beam, the slab-width with a length twice that of the slab thickness, on each side of beam should be considered'.
- For interior columns: 'the slab-width may be increased by twice the slab thickness'.

Applying these code provisions to our case, where the slab thickness is  $0.15\ m$ , the beam-width is  $0.25\ m$ , and column-widths are  $0.30$ ,  $0.40$  and  $0.25\ m$ , for joints 1, 2 and 3, respectively, the slab-participation, for each zone, was calculated and is given in Table 4.20.

Table 4.20 - Estimation of the slab-participation according to EC8 provisions

Joint / Bay	Slab-participation ( $m$ )
1 (external-short)	0.90
2 (internal-short)	1.60
3 (internal-long)	1.45

Comparing the values of slab-participation, estimated from the experimental PsD tests, with the values proposed in EC8, it can be observed that the value recommended for analyses in the EC8 for the interior long-bay studied is  $1.45\ m$ , which is 45% higher than the value obtained from experimental tests (approximately  $1.00\ m$ ). This might indicate that slab collaborating width, for structures with smooth round rebars, is quite smaller than

the values proposed in the design codes, and also smaller than the values estimated from other experimental tests on new structures constructed with improved-bond steel (e.g. Tjebbes, 1994).

#### 4.11.4 - Diagonal deformation of the short external panel

The short external panel was instrumented with transducers in order to catch the total deformation in the diagonal direction of the panels, and, short (0.50 m) transducers were setting-up in the corners, accordingly with schemes presented in Section 3.7.6, to capture the deformation in these corners. With the instrumentation in the corners it was intended to measure the deformation due to the separation between the infill panel and the frame (when in tension) and the crushing deformation (when in compression). As shown in Figure 4.89, three zones (central, inferior and superior) for each diagonal were identified (ascending and descending, considering from left to right). Subtracting the diagonal deformation measured in the corners to the total diagonal panel deformation, it is computed the diagonal deformation in the central zone of the panel. For the long diagonal non-instrumented, the deformation is calculated from the deformation in the transducer in the adjacent panel (mid-panel).

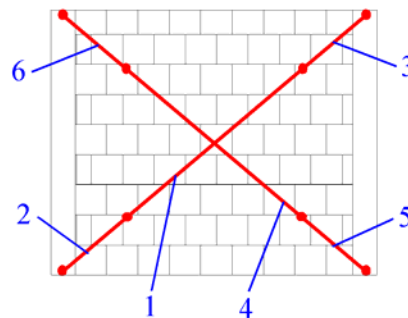


Figure 4.89 - Nomenclature for diagonal deformation (six zones) in the short external panel

In Figures 4.90 to 4.97, are plotted the average strain evolution measured during the earthquake tests on the infilled frame structure. In Tables 4.22 and 4.23 are listed the maximum (positive and negative) deformation measured at each zone, for the three zones (central, inferior and superior) for each diagonal (ascendant and descendent). It is also presented the mean deformation calculated for the total diagonal. The number in brackets corresponds to the zone label represented in schematic Figure 4.89.



Table 4.21 - IN tests: maximum positive (elongation) and negative (shortening) strain (%) in the short external panel at the 1<sup>st</sup> storey

Test	ascendant				descending				
	total (2+1+3)	central (1)	inf. (2)	sup. (3)	total (5+4+6)	central (4)	inf. (5)	sup. (6)	
IN 475	+	0.660	0.158	1.410	1.497	0.727	0.139	1.291	1.045
	-	-0.815	-0.368	-1.135	-0.908	-0.328	-0.111	-0.321	-0.597
IN 975	+	2.671	4.446	3.988	6.928	3.615	2.025	1.637	7.102
	-	-2.850	-0.457	-7.959 <sup>b</sup>	-3.404	-1.461	-0.577	-1.287	-3.150
IN 2000 <sup>a</sup>	+	5.387	3.199	9.423 <sup>c</sup>	3.791	2.906	1.713	0.521	5.629
	-	-2.792	-5.649	-0.002	-4.417	-5.311	-4.946	-0.687	-6.044

a) Due to the high level of deformation reached in the 2000-yrp test at the 1<sup>st</sup> storey, the instrumentation located in the masonry infill panels was removed, during the test (to 4.26 seconds), in order to avoid their deterioration.

b) It was verified the capacity saturation, in negative deformation, of the transducer located at the bottom of the ascendant diagonal.

c) The signal captured in the transducer located at the bottom of the ascendant diagonal, during the 2000-yrp test, is not of good quality, provably due to the damage of this transducer in the previous test.

Table 4.22 - IN tests: maximum positive (elongation) and negative (shortening) strain (%) in the short external panel at the 2<sup>nd</sup> storey

Test	ascendant				descending				
	total (2+1+3)	central (1)	inf. (2)	sup. (3)	total (5+4+6)	central (4)	inf. (5)	sup. (6)	
IN 475	+	0.615	0.273	1.234	0.603	0.753	0.621	0.618	0.511
	-	-0.670	-0.463	-0.868	-0.370	-0.514	-0.464	-0.253	-0.460
IN 975	+	1.226	0.218	1.866	2.905	2.818	2.134	2.370	2.327
	-	-1.679	-0.796	-2.761	-1.424	-1.205	-1.056	-0.453	-1.350
IN 2000 <sup>a</sup>	+	1.354	0.071	2.976	2.663	2.186	1.711	1.815	1.661
	-	-1.281	-0.467	-2.113	-1.407	-1.712	-1.586	-0.691	-1.409

Considering the maximum deformation at the 1<sup>st</sup> storey for the IN tests (Table 4.8) for the 475-yrp test, the relative deformation at the corners (zones 2, 3, 5 and 6) is 5 to 10 times higher than at the central part of the diagonal (zones 1 and 4). For earthquakes of higher intensity, the average strain observed at the corners and in the central part tends to be of comparable magnitude. This is the normal infilled masonry frames behaviour under horizontal loads. In fact, for smaller load intensities, the separation between the panels and the surrounding frame (deformation concentrated in the interface infill/frame) starts. For higher intensities, the mechanism of diagonal strut appears and the panel deformation pattern implies deformation also into the interior of the panel (central part, zones 1 and 4).

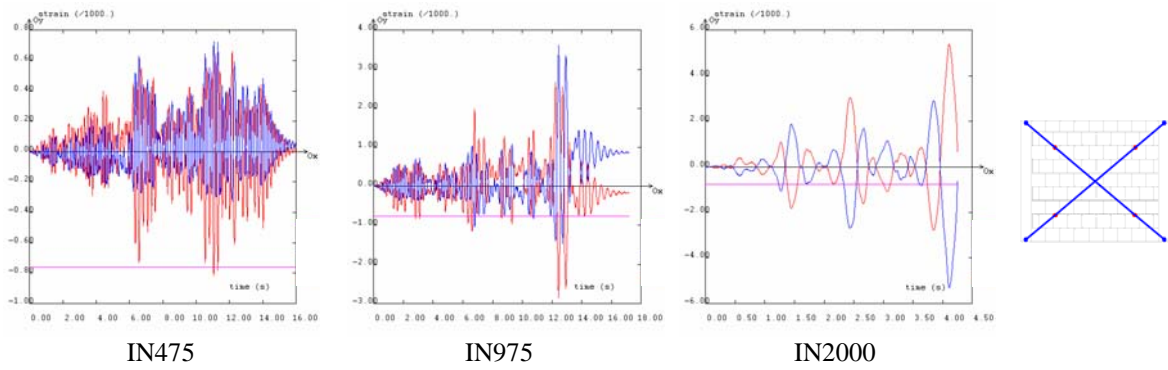


Figure 4.90 - IN tests: 1<sup>st</sup> storey strain of the short external panel (total mean diagonal strain)

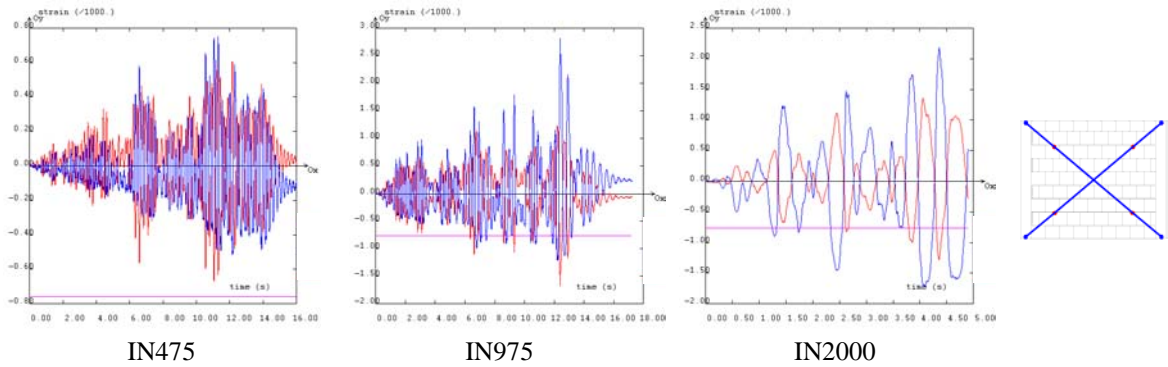


Figure 4.91 - IN tests: 2<sup>nd</sup> storey strain of the short external panel (total mean diagonal strain)

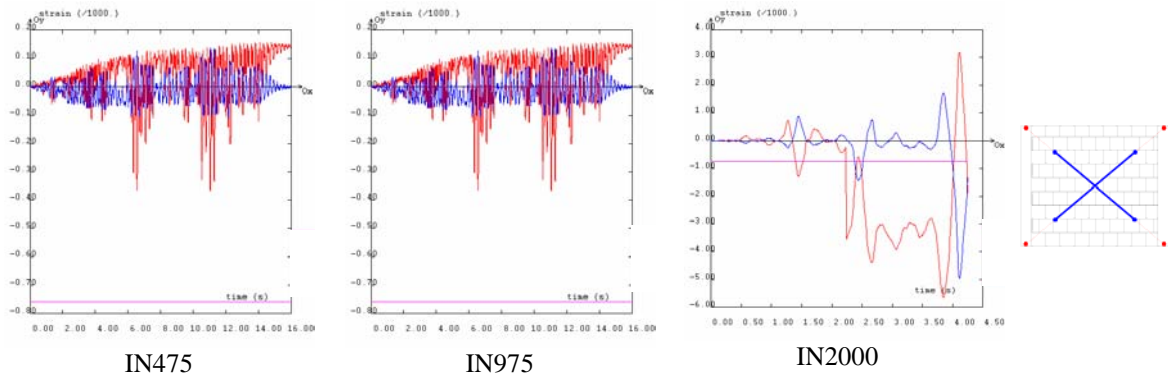


Figure 4.92 - IN tests: 1<sup>st</sup> storey strain of the short external panel (middle)

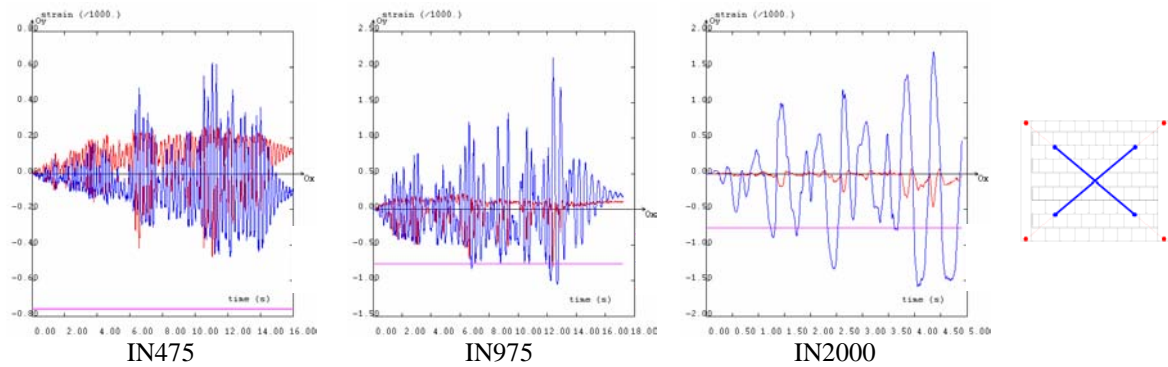


Figure 4.93 - IN tests: 2<sup>nd</sup> storey strain of the short external panel (middle)

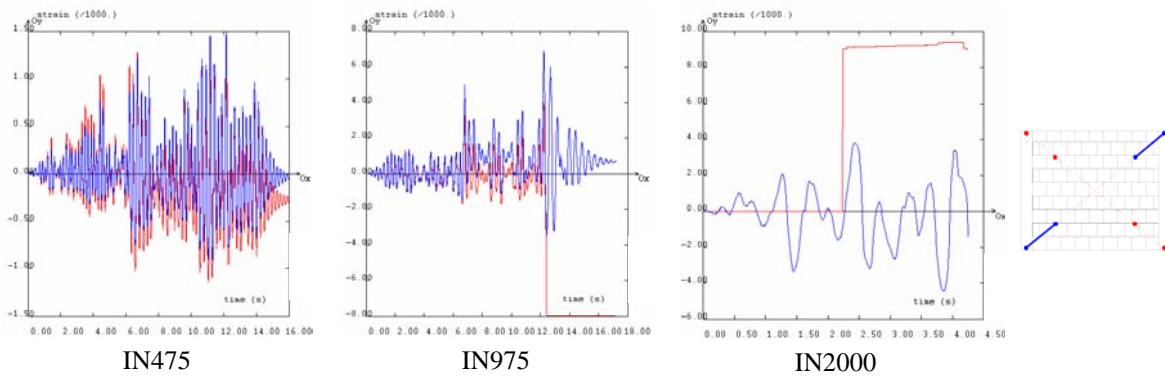


Figure 4.94 - IN tests: 1<sup>st</sup> storey strain of the short external panel (diagonal ascendant /)

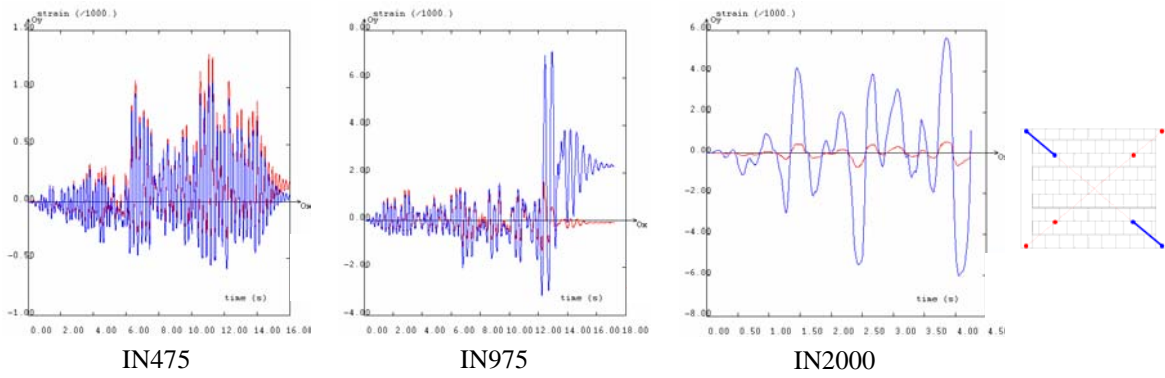


Figure 4.95 - IN tests: 1<sup>st</sup> storey strain of the short external panel (diagonal descending \)

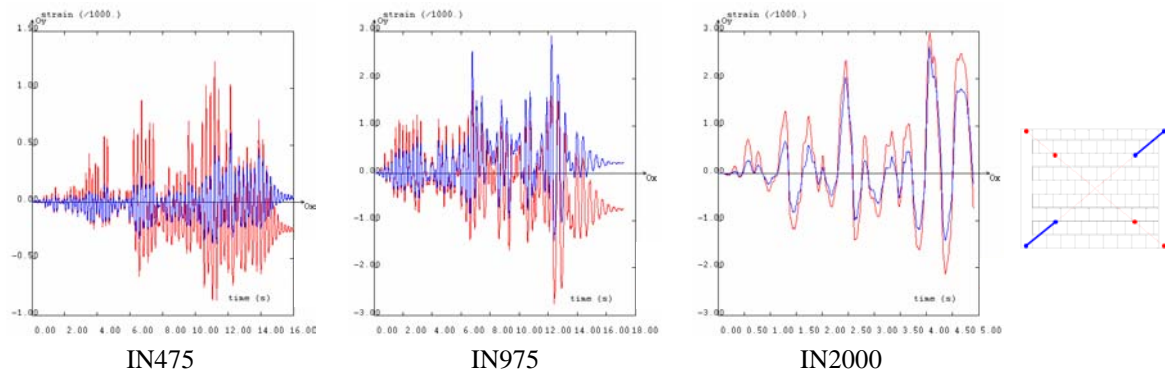


Figure 4.96 - IN tests: 2<sup>nd</sup> storey strain of the short external panel (diagonal ascendant /)

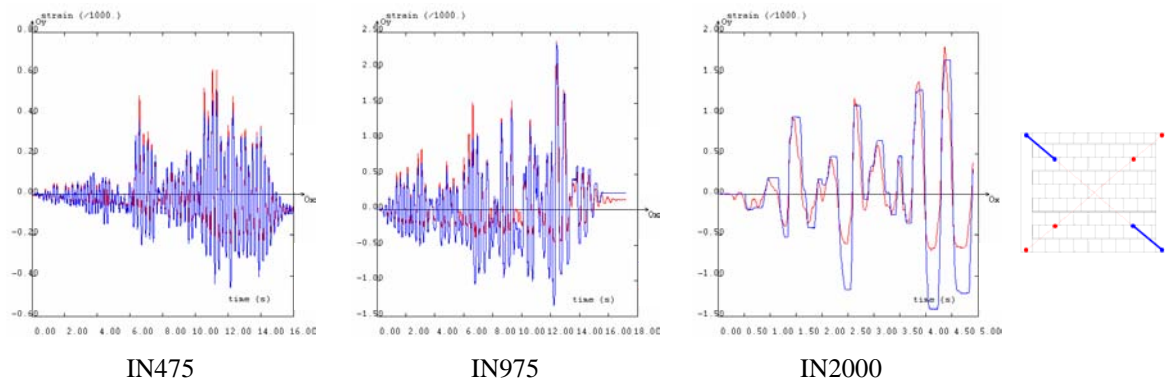


Figure 4.97 - IN tests: 2<sup>nd</sup> storey strain of the short external panel (diagonal descending \)

From the analyses of the previous figures, where the average strain in the external short infill panel for the PsD tests on the IN frame was depicted, the following should be noted:

- The analyses of the strain (deformation) in the total diagonal gives more information, particularly to the compression state, than the observed in the central and extremities zones of the diagonal, because it contains the deformation observed at the joint plus the panel deformation. It should be said that in compression direction, it is not expected high deformation in the joint, since these joints are closed. For the particular case of this external panel, pseudo-dynamic earthquake tests can be compared with the small wallets tested in diagonal compression.
- In Figure 4.95, for the 2000-yrp test, it is noted a quite large increase of the deformation at the 1<sup>st</sup> storey external top-corner, when compared with the opposite internal bottom-corner. This is due to the larger separation experienced between the masonry panel and the frame observed at the external top-corner. In fact, looking at the same results at the end of the 975-yrp test, it is noted a considerable residual deformation in this corner. This is the first indication of shear-out of the external 1<sup>st</sup> storey column at the top, as will be deeply analysed in the next test results analysis.
- The maximum diagonal average strain observed for the 475-yrp test is approximately equal to the ultimate value reached in the diagonal compression wallet tests. For the 975-yrp test this ultimate value is clearly over passed at around 6.5 seconds, which corresponds exactly to the first evident crack observed in the infill panel (see damage description in Section 4.5.2 during infill masonry frame tests). This crack appears in the direction corresponding to the compression in the strut ascendant, which is confirmed by the plots in Figure 4.90.
- In Figure 4.90 it is also observed at the first storey a tendency (475 and 975-yrp tests) to bigger development of compression deformation in the ascendant diagonal, when compared with the other diagonal. This is due to the higher rigidity of the bottom part of the external column, when compared with the top part. After 12 seconds of ground motion test, a much higher deformation was observed, which is in correlation with the considerable propagation of damage observed in the infill panel (see damage description in Section 4.5.2).

- For the second storey (Figure 4.91), it is observed a global diagonal compressive deformation bigger than the ultimate limit, which is in correlation with the observed initiation of crushing in the external top corner of the 2<sup>nd</sup> storey external infill panel. The maximum deformation observed during the 975-yrp test is not over-passed in the 2000-yrp test. It should be also said that this maximum deformation observed at the 2<sup>nd</sup> storey for the 2000-yrp test is almost half the maximum value reached at the first storey for the 975-yrp test.

In Figures 4.98 to 4.105 are plotted the average strain evolution measured during the PsD tests on the infill strengthened frame structure. In Tables 4.24 and 4.25 are listed the maximum (positive and negative) deformation measured at each zone, for the three zones (central, inferior and superior) for each diagonal (ascendant and descendent). It is also presented the mean deformation calculated for the total diagonal. The number in brackets corresponds to the zone label represented in the scheme of Figure 4.89.

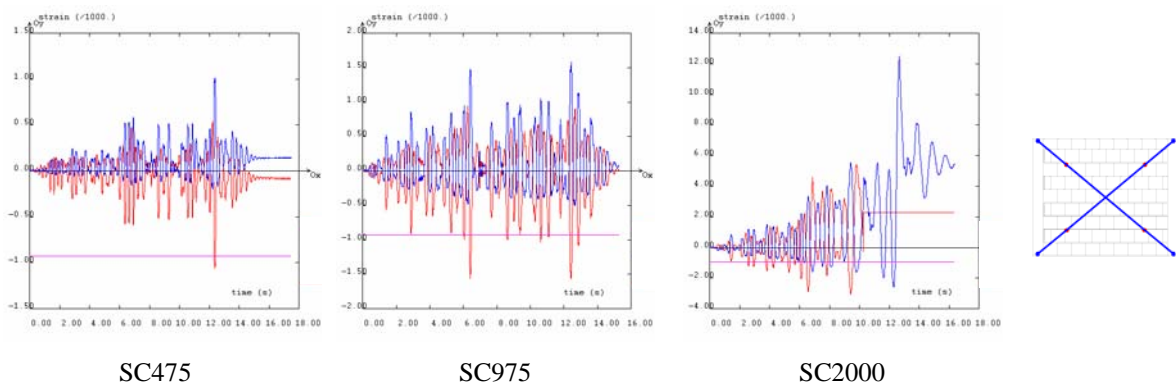


Figure 4.98 - SC tests: 1<sup>st</sup> storey strain of the short external panel (total mean diagonal strain)

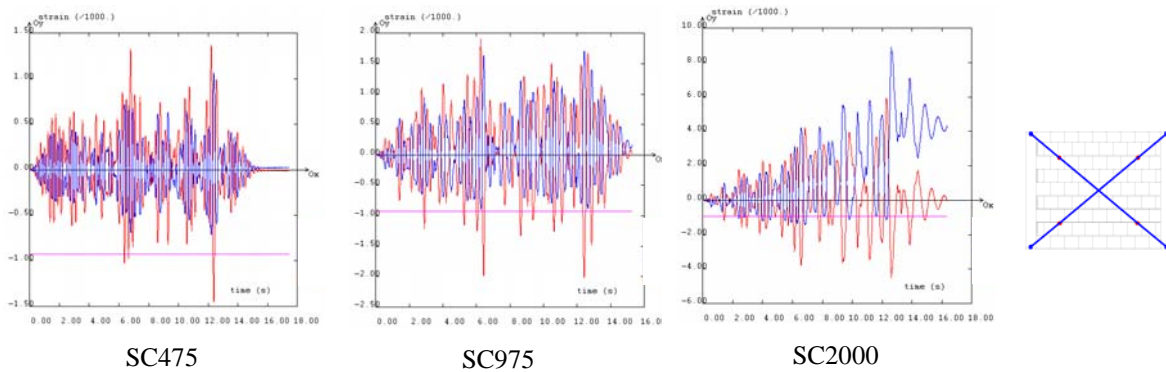


Figure 4.99 - SC tests: 2<sup>nd</sup> storey strain of the short external panel (total mean diagonal strain)

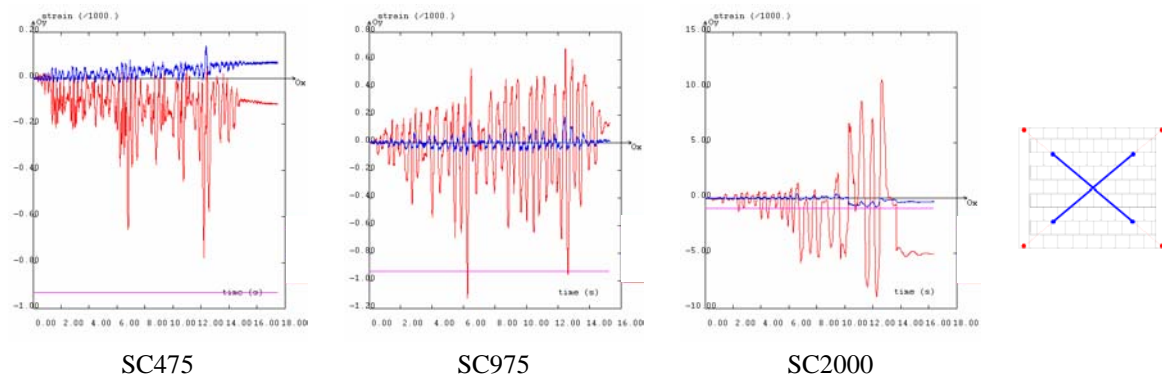


Figure 4.100 - SC tests: 1<sup>st</sup> storey strain of the short external panel (middle)

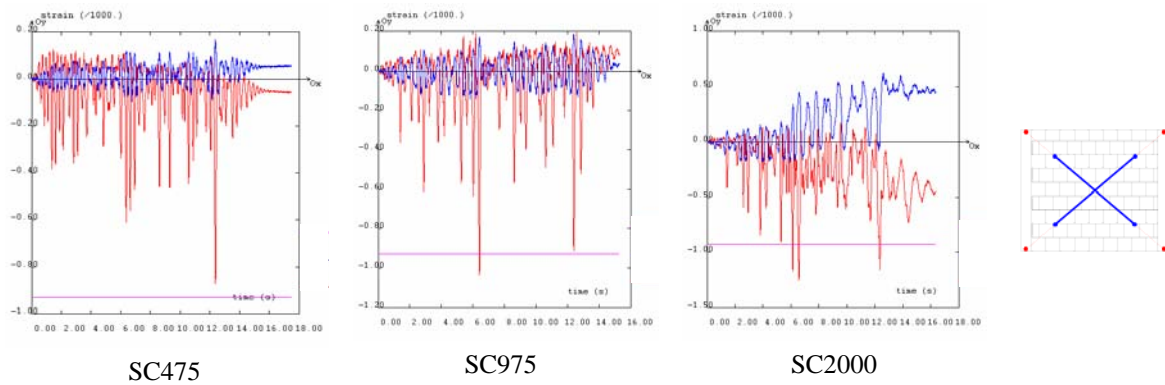


Figure 4.101 - SC tests: 2<sup>nd</sup> storey strain of the short external panel (middle)

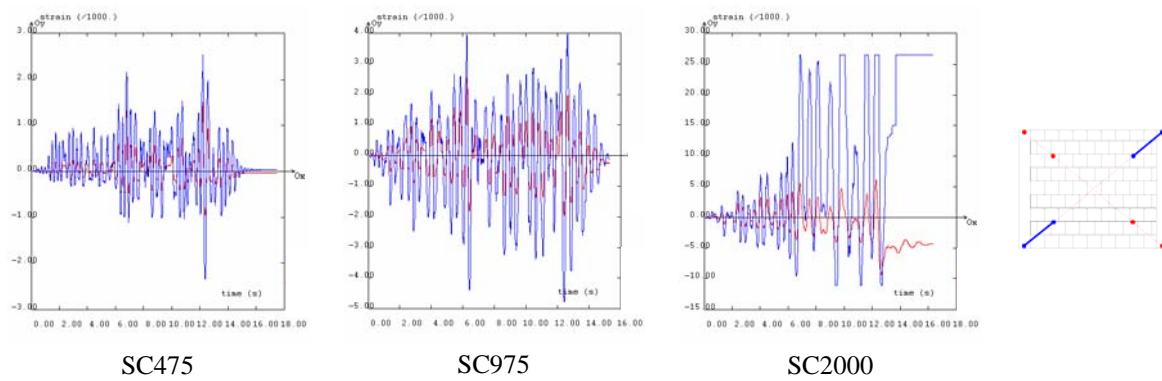


Figure 4.102 - SC tests: 1<sup>st</sup> storey strain of the short external panel (diagonal ascendant /)

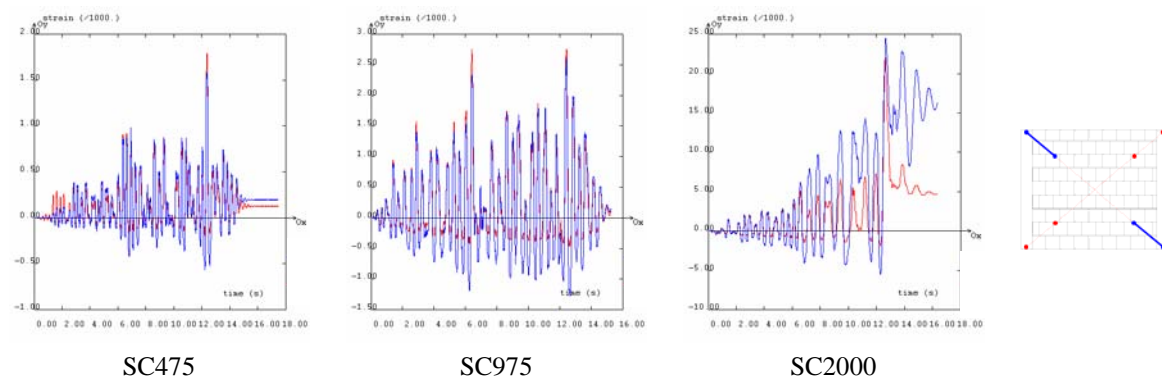
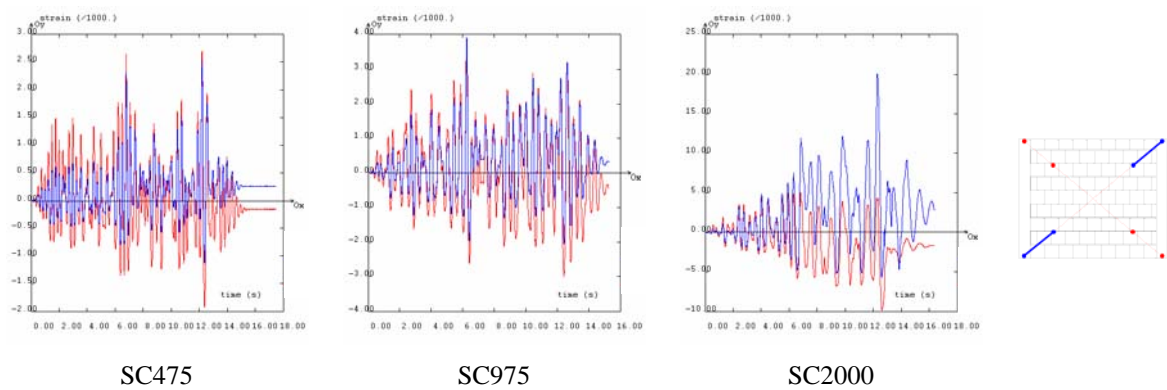
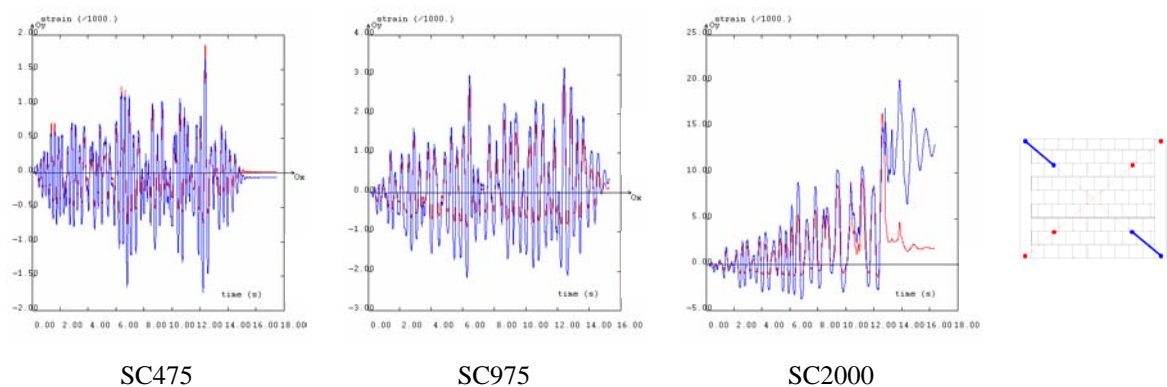


Figure 4.103 - SC tests: 1<sup>st</sup> storey strain of the short external panel (diagonal descending \)

Figure 4.104 - SC tests: 2<sup>nd</sup> storey strain of the short external panel (diagonal ascendant /)Figure 4.105 - SC tests: 2<sup>nd</sup> storey strain of the short external panel (diagonal descending /)Table 4.23 - SC tests: maximum positive (elongation) and negative (shortening) strain (%) in the short external panel at the 1<sup>st</sup> storey

Test	ascendant				descending				
	total (2+1+3)	central (1)	inf. (2)	sup. (3)	total (5+4+6)	central (4)	inf. (5)	sup. (6)	
SC475	+	0.538	0.102	1.501	2.531	1.010	0.142	1.793	1.589
	-	-1.057	-0.780	-0.947	-2.342	-0.200	-0.021	-0.196	-0.565
SC975	+	0.944	0.681	2.536	3.982	1.579	0.193	2.766	2.597
	-	-1.565	-1.128	-1.938	-4.770	-0.501	-0.093	-0.466	-1.278
SC2000	+	5.408	10.677	6.157	26.520 <sup>a</sup>	12.503	0.428	22.082	24.556
	-	-3.043	-8.889	-9.381	-11.104	-2.577	-0.811	-1.850	-5.526

a) It was verified the capacity saturation, in positive deformation, of the transducer located at the top of the ascendant diagonal.

Table 4.24 - SC tests: maximum positive (elongation) and negative (shortening) strain (%) in the short external panel at the 2<sup>nd</sup> storey

Test	ascendant				descending				
	total (2+1+3)	central (1)	inf. (2)	sup. (3)	total (5+4+6)	central (4)	inf. (5)	sup. (6)	
SC475	+	1.370	0.127	2.703	2.550	1.065	0.167	1.864	1.654
	-	-1.455	-0.871	-1.922	-1.124	-0.711	-0.095	-0.738	-1.736
SC975	+	1.906	0.194	3.463	3.909	1.711	0.184	2.728	3.172
	-	-2.023	-1.038	-3.013	-2.051	-0.900	-0.141	-0.861	-2.154
SC2000	+	5.946	0.175	5.008	20.076	8.898	0.625	16.486	20.136
	-	-4.499	-1.253	-9.812	-5.785	-1.425	-0.185	-1.291	-3.727

From the analyses of the previous figures, where the average strain in the external short infill panel for the earthquake tests on the SC frame was depicted, the following should be noted:

- In Figure 4.98 it is observed that the limit of compressive deformation in the strengthened masonry is reached. However, contrary to the immediate increase of the tension deformation in the orthogonal direction (due to the crack opening) observed in the previous infill tests, here in the SC tests, it is not verified. This is an important effect of the masonry strengthening that provides a significant increase of the tension strength, preventing the crack opening and propagation.

#### 4.12 - FINAL REMARKS AND CONCLUSIONS

The main findings from the experimental campaign are summarised here. These conclusions are presented for: *i*) the PsD tests on the bare and strengthened frames; *ii*) the PsD tests on the infilled and infill strengthened frames; *iii*) the cyclic tests performed at the 2<sup>nd</sup> storey of the frame retrofitted with the K-bracing technique; and finally, *iv*) the final capacity cyclic tests on the bare and strengthened frames. A conclusive section presents final remarks of the entire PsD and cyclic test campaigns.



#### 4.12.1 - Bare and selective strengthened frames

A series of pseudo-dynamic tests on a full-scale model of a four-storey RC frame representative of existing structures designed without specific seismic resisting characteristics were carried out at the ELSA laboratory.

Two testing campaigns were performed aiming at: *a*) a vulnerability assessment of the bare frame; and, *b*) assessment of the earthquake performance of the frame retrofitted using selective retrofit methods. The BF was subjected to two earthquakes of increasing intensity reaching imminent collapse at the 3<sup>rd</sup> storey during the second earthquake test. It was then repaired and strengthened using the selective techniques and subsequently was subjected to three earthquake input motions with increasing intensity.

The bare frame was tested first for an earthquake corresponding to a 475-yrp, when no significant damage was observed. Subsequently, the frame was subjected to an earthquake corresponding to a 975-yrp, and for this test a heavy level of damage was reached. In fact, imminent collapse was attained for 7.5 seconds of the accelerogram. The significant change in stiffness and strength from the 2<sup>nd</sup> to the 3<sup>rd</sup> storey, coupled with the inadequate lap-splice, induced the development of a soft-storey mechanism at the 3<sup>rd</sup> storey.

The analysis of the test results from the BF confirmed the high vulnerability of the original (non-strengthened) frame. In fact, in spite of 'a satisfactory performance' for the nominal input motion test corresponding to a return period of 475 years (BF475) (slight damage observed), the structure reached imminent collapse for an input intensity slightly higher than the nominal one (1.3 times, in terms of PGA and corresponding to a 975-yrp input motion).

The rather uniform distribution of demands for the BF475 test (maximum drifts of 0.4, 0.7, 0.8 and 0.5% were reached at the first, second, third and fourth storeys, respectively) was completely altered for the BF975 test (maximum drifts of 0.63, 1.0, 2.4 and 0.9% were reached at the first, second, third and fourth storeys respectively). From the shear-drift diagrams, it is apparent that the peak shear force at the 3<sup>rd</sup> storey is reached for a drift of 1.8% with subsequent important strength decreasing (imminent collapse). Furthermore, there was evidence of premature shear cracking in the strong-column at the 1<sup>st</sup> and 3<sup>rd</sup> storeys (where lap-splice exists) for storey drifts of approximately 0.4%. Tests on a similar

frame with infill panels have also shown shear crack initiation for 0.4% drift in the 1<sup>st</sup> storey, while severe (dangerous) shear cracking was apparent for storey drifts of 1.3%.

The results from the SR tests have shown a rather improved seismic performance. In fact, the SR frame was subjected to the same input motions as the BF with limited structural damage, and was able to withstand an input motion with intensity 1.8 times the nominal one (corresponding to a return period of 2000 years) maintaining its load carrying capacity with repairable damages. The retrofitting operation addressed and solved the irregularity problem and the confining steel plates definitively increased the limited deformation capacity of the central strong-column. In fact, drift demands were rather uniformly distributed in the first three storeys for the three earthquake tests and reached values much higher than the values of the bare frame tests. Inter-storey drifts of 2.8, 3.0, 1.6 and 0.9% were reached at the first, second, third and fourth storeys, respectively, without loss of load carrying capacity. It is noted that 2.8% drift in the first storey is twice the ultimate drift identified from the original (non-strengthened) frame. Therefore, it is concluded that the deformation capacity of the first storey is, at least, the double of the original structure.

There are other aspects that should be highlighted from the test campaigns on the original and strengthened frames, namely:

- As expected, the strong-beam weak-column deformation/dissipation mechanism (storey mechanism) is the only one activated for all tests. However, slight higher demands in the beams were apparent for the retrofitted frame.
- There is a strong concentration of the inelastic demands at the member ends, leading to equivalent plastic hinge lengths much lower than the empirical values proposed in the literature (calculated plastic hinge lengths are 40% of the empirical values). This is a direct consequence of the poor bond characteristics of the smooth round rebars, which leads to extremely high slippage with concentration of the deformation at the member (beam and column) extremities.
- The values calculated for the slab-participation are also much lower than the values proposed in the design codes and also lower than the values estimated from tests on building structures with improved bond steel (approximately 45% lower). This is also a direct consequence of the poor bond characteristics of the smooth round steel reinforcement also used in the slabs.

- The test results confirmed that lap-splice at the base of the columns, particularly in existing structures with smooth round rebars with extremity hooks and poor detailing and amount of shear/confinement reinforcement, develop premature shear cracks at the bar termination zones for inter-storey drifts of approximately 0.4%. These shear cracks dictate dangerous shear failure of the columns for inter-storey drifts in the range of 1.3-1.8%.

#### **4.12.2 - Infilled and infill strengthened frames**

The experimental pseudo-dynamic research programme on the infilled four-storey RC frame, performed at the ELSA laboratory, involved tests on the original infilled frame and on the same infilled frame with the infill panels uniformly strengthened at all the frame storeys using shotcrete. Previous tests on a similar (nominally equal) bare frame had been carried out with increasing intensity of the input earthquake motions bringing the structure to collapse.

The aims of these testing campaigns were to assess the seismic performance of the bare and infilled frames and to check the possible benefits from strengthening of the brittle infill masonry panels (ceramic bricks with horizontal hollows and plaster). In fact, it is well known that infill panels protect the frames for low/medium earthquake levels but its failure for medium/high levels of the input motions prompts soft-storey mechanisms and consequently premature failure of the entire structure. Therefore, strengthening of the infill panels, improving its deformation capacity maintaining its horizontal load carrying capacity would improve seismic performance of the entire structure also for severe levels of the input motions.

Qualitative and quantitative analysis of the test results and considerations on the behaviour of the frames were already made in the previous sections. However, a few important aspects should be now underlined:

- The bare frame structure was subjected to two earthquakes corresponding to return periods of 475 and 975 years (10% and 5% exceeding probability in 50 years). The first input motion caused slight damage to the frame (essentially

cracking) but the second earthquake (only 1.3 times higher than the first one) brought the frame to collapse. In fact, the second test was stopped at 7.5 seconds (15 seconds was the duration of the earthquake) because imminent collapse was reached at the 3<sup>rd</sup> storey. It was verified that the strong beam weak-column mechanism is the only one activated and it was demonstrated that this type of structures effectively represent a major source of risk for human life. It is recalled that structures designed according to new design codes are deemed to withstand earthquake input motions higher more than 2 times the design ones without collapse (see Pinto, 1998).

- The tests on the IN structure confirmed that infill panels protect the frame structure for low and medium intensity input motions. However, failure of the infills with consequent abrupt loss of resistance prompts a soft-storey mechanism. It however, underlined that the infilled frame was able to withstand part of the earthquake corresponding to 2000-yrp (1.8 times higher the nominal one in terms of PGA) while the bare frame failed during the 975-yrp earthquake test.
- Another important aspect that should be noted is the strong influence of the infills on the behaviour of the structure. In fact, the drift demands during the high level earthquake test on the bare frame concentrated in the 3<sup>rd</sup> storey where an important change on stiffness and strength exists (irregularity). Otherwise, the drift demands during the high level earthquake tests on the infilled frame concentrated in the first two storeys with predominance at the ground storey during the 2000-yrp earthquake test and without any excessive demands at the 3<sup>rd</sup> storey. It is confirmed that infills substantially alter the behaviour of frame structures and therefore, they must be taken into account in the assessment and redesign of existing structure as well as in the design of new ones.
- It is known that infills have a beneficial effect on frame structures but it is also recognized that its brittle failure (post-peak strength) with abrupt loss of loading carrying capacity (softening) prompts dangerous storey mechanisms and rapid collapse of the structure. Any strengthening of the infills panels 'preventing' failure of the walls or conferring additional deformation capacity without abrupt

loss of resistance would improve the earthquake behaviour of the infilled structures. In view of this, the wall at the shortest bay was uniformly strengthened at all storeys by a thin concrete layer with a steel mesh embedded in it. The steel mesh ( $\# \phi 5//100 \text{ mm}$ ) was positioned on one side of the walls and the wall was then shotcreted.

- The SC frame was then subjected to the same earthquake tests as the infilled frame. The results from these tests have shown the effectiveness of strengthening of the infills panels but only a slightly better performance was achieved for the structure. In fact, the infill walls have shown a much better behaviour (infill cracking was prevented and only slight crushing appeared in the corners). However, the higher strength of the panels led to premature failure of the external columns (shear-out of the columns in the interface column-joint) with dangerous loss of their vertical loading carrying capacity. This is a point that deserves special comments because it is common practice to apply these strengthening techniques in particular for repair and strengthening of infill structures after earthquakes. Strengthening of infill walls in frame structures should be made with appropriate doweling to the adjacent beams in order to transfer the shear forces gradually to the surrounding frame. In fact, for infill panels located at the frame extremities (external bays), the overturning moments result in decreasing of the vertical contact forces between the beam and the infill panel and most of the forces developed in the panels are directly transmitted to the external columns forcing its failure in the joint region. It is apparent that this phenomenon depends on the characteristics and detailing of the column as well as the joint region. However, it is known that existing frame structures are poorly detailed and that no transversal reinforcement was provided in the joint regions. Therefore, strengthening of infill panels in existing vulnerable frame structures should be avoided unless appropriate dowels are provided to transfer most of the forces developed in the walls directly to the surrounding beam or slab.
- It is also noted that after the tests on the original infilled frame there was also some evidence of column/joint dislocation (shear-out) caused by the same phenomenon observed for the SC frame tests. It is clear that column shear-out

depends on the relative strength of the infill panel and the surrounding columns/joints. But for existing structures, with poor column/joint detailing, this serious damage is likely to occur. Therefore, seismic assessment of this kind of structures shall take into account the possible negative effects of the infill in the resisting frame. Moreover, any strengthening intervention (even renewal of walls plaster may increase substantially the strength of the infill walls) should provide adequate doweling systems to transfer the forces developed in the walls directly from them to the surrounding beam/gird.

#### **4.12.3 - K-bracing**

A ductile steel eccentrically braced system has been presented for retrofitting brick-masonry infilled reinforced concrete frames. The K-bracing with shear-link system is formed by an assembly of steel beams, diagonal braces and a centrally located ductile vertical shear-link which is designed to replace the infilled masonry in a single bay of a concrete infilled frame. The assemblies are typically placed in one or more vertical arrays over the height of the building. Conceptually, the design aims at developing a retrofit system, which has a total storey shear resistance more or less equal to the lateral resistance of the original infilled system but with a substantially increased ductile energy absorbing capacity. The basically similar shear capacities prevent the development of a retrofitted system, which may otherwise introduce excessively increased foundation loads. Other significant characteristics of the K-bracing system are the extremely effective energy dissipating properties of the shear-link, with drift capacities of up to 9%, and the fundamental fact that cyclic shear-strain hardening of the web of the shear-link under earthquake loads, leads under increasing displacements to a cyclic plastic shear resistance of the link equal to about twice the initial lateral resistance at yield. This development allows the shear-links, under increasing cyclic displacements, to compensate for the progressive failure and loss of resistance of the non-retrofitted infilled walls.

The results of the tests on the retrofitted structure with a K-bracing with shear-link, in which the retrofitted storey was subjected to cyclic displacement-controlled deflections of increasing magnitude, showed the effectiveness of the solution. An excellent agreement between the predicted response and experimental results could be observed. Also, the

---

technology used to anchor a steel retrofit assemblage to the surrounding concrete elements (beams and columns) was proven to be effective.

#### **4.12.4 - Final capacity cyclic tests**

A series of cyclic tests on the four-storey RC frames (bare frame and strengthened frame with selective retrofitting techniques) were performed. The local failure of the external columns/joints at the 1<sup>st</sup> and 2<sup>nd</sup> storeys, reached in the previous earthquake tests, would not allow to perform a final capacity test on the frames to obtain their global ultimate capacity. After repair and strengthening, with carbon fibre techniques, the frames were subjected to the final capacity cyclic tests, consisting of imposed top-displacement cycles with increasing amplitude and assuming a triangular inverted force distribution. It is noted that the repaired frames were able to withstand storey deformations higher than the ones reached in the previous PsD tests, maintaining its load carrying capacity.

The results from the tests performed at ELSA laboratory on full-scale structures repaired and strengthened with FRP's demonstrate that by using advanced composites it is possible to significantly improve the seismic behaviour/performance of vulnerable structures.

It is shown that a very effective (cost/benefit) repair or strengthening operation can be used to repair local heavy damages, like the ones resulting from the effects on infill panels on external columns and joints.

It has been shown that the application of carbon fibre wraps on the critical regions of damaged structural elements can recover an important part of the loss in stiffness and strength of those members. In addition, improvement in energy dissipation capacity and the global ductility of the structure can be achieved. However, it is recognized that design of the retrofitting schemes with FRP's requires a more rigorous scientific and technical basis.

#### **4.12.5 - Remarks**

The tests have shown that the vulnerability of existing RC frames designed without specific seismic resisting characteristics, which are an important part of the existing

buildings in European earthquake prone regions, constitute a source of high risk for human life. Furthermore, it was demonstrated that advanced retrofitting methods, solutions and techniques substantially reduce that risk to levels currently considered in modern seismic design.

These tests produced a vast data set, which will be very useful as reference, and in setting-up guidelines for the assessment and redesign of structures in earthquake prone zones. In particular, these results serve as a basis for the calibration of EC8 Part 1-3. Moreover, several authors have used these experimental results to calibrate and to improve numerical models for various complexity levels (e.g. Pinho *et al.*, 2000; Dolsek and Fajfar, 2001; Delgado *et al.*, 2002).



# **CHAPTER 5**

## **REFINED AND SIMPLIFIED MODELS FOR EARTHQUAKE SIMULATION, ASSESSMENT AND OPTIMAL REDESIGN OF EXISTING RC STRUCTURES**

*'... it must be recognised that the results of any analysis will be only an approximation to the true condition...'* (Paulay and Priestley, 1992)

### **5.1 - INTRODUCTION AND MAIN OBJECTIVES**

The purpose of structural analysis is to determine the stresses, strains, reaction forces, and displacements of a given structure under given loading conditions. Based on the structural analysis results, engineers are able to check whether a proposed design meets the requirements regarding resistance to a combination of loading conditions, and, if necessary, to revise its design until all requirements are met. At the present time, linear elastic analysis remains the instrument of the design profession, for the calculation of forces and stresses, as well as for the proportioning of structural members.

Nevertheless, linear elastic analysis' inability to reflect the real behaviour of structures under abnormal or ultimate loading conditions has been pointed out. This follows because almost all structures behave in some non-linear manner prior to reaching their limit of resistance. As advocated by Yang and Kuo (1994), a more realistic evaluation of the strength of structures against the failure conditions, or the factor of safety, can only be achieved by analyses that take into account various non-linear effects. Also, from a review of numerous analytical and experimental studies, Borges and Ravara (1969) have drawn a general conclusion: the forces that develop in current buildings under the action of a

strong earthquake generally exceed the elastic limits. Thus, it becomes necessary to study the dynamic behaviour of buildings considering the non-linear properties of materials and structures. For this reason, most modern codes based on the ultimate strength design concept have incorporated certain provisions for structural engineers to consider the non-linear and/or second order effects using either exact or approximate analysis techniques (AISC, 1986; EC8).

In this regard, during the last decades, remarkable progress has been made towards a better understanding of the performance of reinforced concrete buildings when subjected to earthquake ground motions. Several authors, such as Umemura and Takizawa (1982), Costa (1989), Coelho (1992), Varum (1995) and Arêde (1997), among others, developed models and conducted studies on non-linear behaviour of RC buildings.

Two different classes of non-linearities can be identified. On the one hand, the geometric non-linearity standing for the second order effects produced by finite deformations coupled with change in stiffness of a structure under applied loading. On the other hand, the material non-linearity standing for the changes in the physical response of a material to stress or deformations, and appears in the form of path-dependent and non-unique constitutive laws. In brief, the essential computational task in the analysis of problems involving material non-linearity is that equations of equilibrium must be solved for the structure using material properties that depend on strains (Yang and Kuo, 1994).

The study of the non-linear behaviour of RC frame structures requires knowledge of the non-linear relationships between bending moments and curvatures at section level, based on a fibre model, for example. These relationships can be established by assuming that the transverse sections of the elements remain plane after deformation, and by adopting idealised stress-strain diagrams for both concrete and steel (Borges and Ravara, 1969). The monotonic stress-strain diagrams and hysteretic rules, for steel and concrete, are established from experimental tests on material specimens or from theoretical laws.

Furthermore, based on field evidence of existing RC structures' behaviour during earthquakes, and on experimental tests, it is known that those structures experience shear failure, failure at the beam-column joints, and phenomena such as slippage of rebars (specially when steel rounded rebars are used) and strain penetration. Therefore,

---

appropriate models that take into account most of the mentioned phenomena should be used.

Data on the real characteristics of buildings that have been subjected to earthquakes are in general difficult to obtain. Hence, the experimental pseudo-dynamic test results on the full-scale RC frame (presented in previous Chapters 3 and 4) generated an immense amount of records, that were used to corroborate the numerical models adopted and improved in this thesis. Therefore, the calibrated analytical models can be extensively used in reproducing the real behaviour of existing RC buildings.

The numerical analyses performed in this thesis and presented in this chapter are based in a non-linear fibre model, and take into account the material non-linearity according to the specific materials properties presented in Section 3.2.5. Towards a realistic description of the cyclic and the ultimate behaviour of existing RC structures, the studies conducted in this thesis proved to be necessary the inclusion of the bond-slip of reinforcing bars. Therefore, the bond-slip of smooth reinforcing bars was investigated, and the non-linear numerical models were enhanced by the introduction of a slippage factor to account for it.

This chapter is divided into eight sections. Section 5.2 presents the computer software CASTEM used in the non-linear numerical analyses of structures. Section 5.3 gives details on the structure, on the numerical models adopted, on the materials parameters, loads and retrofitting solutions' modelling. The description of the structural and materials models used, and the corresponding model parameters is also reviewed in Section 5.3. In addition, Section 5.3 describes the method of analysis used, as well as the fundamental assumptions and the general formulation of the models. Section 5.3.5 dedicates special attention to the improved representation of bond-slip for plain reinforcing steel bars, including a review of previous work. Section 5.4 presents the natural frequencies and mode shapes numerically evaluated. The experimental campaign, exposed in Chapters 3 and 4, was preceded by a set of numerical analyses. Section 5.5 provides a short discussion on the numerical analyses performed prior to the PsD earthquake tests.

Section 5.6 contains a description of the most significant numerical non-linear seismic analyses of the four-storey RC planar bare frame (BF). The selective strengthening solution applied to the central strong-column (selective strengthening based technique, SR)

is also numerically simulated. Both original BF and strengthened SR configurations are modelled independently. Masonry infill walls, which play an important role in the structural response of infilled frames (IN), are modelled with diagonal struts. A brief discussion of the results, for the BF, SR and IN frames, comparing with the correspondent experimental results is also performed. Comparisons of time-history response and maximum response envelopes are presented. Section 5.6.4 discusses the results obtained with the refined FE models. In Section 5.7 are performed numerical calculations with simplified numerical tools. It is also proposed and tested a MDOF non-linear dynamic displacement-based assessment method. Finally, in Section 5.8, it is proposed a methodology to estimate the optimum distribution of strengthening needs in existing buildings.

## **5.2 - NUMERICAL TOOLS: CASTEM**

The non-linear numerical analyses presented in this thesis were performed using the computer code CASTEM-2000, through the associated user-oriented development environment Visual CAST3M. A short description of these numerical tools is presented.

CASTEM (Millard, 1993) is a multi-purpose finite element based computer code for structural analysis, developed by the 'Commissariat à l'Énergie Atomique' (CEA), France, in the framework of structural mechanics research. The need of treating several types of problems based on different formulations (solid and fluid mechanics as well as thermal processes) stimulated the development of a high level tool of analysis based on a unified and powerful technique such as the finite element method (Arède, 1997).

Two main directions were followed to develop Visual CAST3M (Buchet *et al.*, 2000): first, to build a powerful NT user interface, including graphics; and, second, to have easy access to the documentation, including hyperlinks, ToolTips, etc.

Aiming at a unified way of handling different problems, the code has been structured following the object-oriented technique of programming, in the sense that the user creates, manipulates and destroys objects of different types (Buchet *et al.*, 2000). It is based on a specifically developed high level language GIBIANE (or simply GIBI) consisting on a

wide set of commands and operators used to control and to define the program flow by object manipulation in a specific environment or shell. The macrolanguage GIBI permits to define the usual operations characteristic of finite element analysis, by means of simple instruction involving commands or operators acting on input objects and, possibly, generating new output objects.

The object-oriented features of CASTEM (Millard, 1993) lead to a high level of versatility and flexibility in the sense that it can be adjusted to the particular problem to be solved. By contrast to classical codes designed for the analysis of certain well-defined type of problems, to which specific cases have to be adjusted, CASTEM allows the user to build-up the program flow by himself, to follow the analysis task-by-task, to modify the task sequence, to re-define tasks and to check their outputs. Summarising, CASTEM allows adapting it to user's own needs.

Objects are defined as pieces of information grouped according to specific well-defined rules characterising the object type. Arède (1997) refers a list of main object types. Commands and operators are used in the first case to perform operations on input objects allowing to manipulate them by modifying them or not, and to generate new objects in the second case. The available commands and operators in the GIBI language can cover a wide range of purposes. Commands and operators can be organised following a user-defined sequence of tasks in order to perform the desired analysis. Such sequence constitutes the so-called GIBI input for CASTEM running session, either in interactive or batch mode. Arède (1997) illustrates with a comprehensive example how CASTEM works. He also shows that for complex problems, the use of procedures becomes extremely advantageous; procedures are sequences of operators cast in independent GIBI segments and acting as higher-level operators to accomplish well-defined purposes. CASTEM provides a set of built-in procedures to accomplish some usual tasks in structural analysis, which cannot be handled by a single operator, but other procedures can be easily designed and implemented by the user. Thus, concerning tool implementation or improvement, Arède (1997) highlights that the code offers two ways, *viz*:

- Development of procedures, written in GIBI (thus, strictly relying upon existing operators) when the envisaged tasks do not involve new elements, models or formulations; in these conditions, this is a low cost option from the implementation

standpoint since it allows a very fast development and on-line testing, without the need of modifications at the basic CASTEM software level.

- Development of new operators, based on existing and new sub-routines constituting the code source software; new operators are required when not available elements. Models or formulations are to be incorporated, and may be appropriate for efficiency purposes when certain algorithms, despite also implementable at GIBI level, would lead to cumbersome and computationally heavy procedures; the implementation cost of operators is obviously higher than that of procedures, since it requires a more in-depth knowledge of the code data structure in order to provide the adequate operator interface.

In the present work, developments have been made at both procedure and operator levels. The main contribution consisted on new improvements on existing operators in order to incorporate the proposed Displacement-Based Assessment method and strengthening optimization tools, presented in Sections 5.7 and 5.8 (see also Varum and Pinto, 2001-*b*). In addition, several pre- and post-processing procedures for result analyses and visualisation were developed.

Concerning the programming feature, it is worth mentioning that the source code is written in an extended FORTRAN77 language, the so-called ESOPE language, which includes a few additional instructions for management and data structures. Basically, arrays of data are grouped into larger data segments, which are initialised, activated, de-activated or surpassed according to the code flows needs. The required data for subroutines to perform their tasks is made available by some of those extra instructions; once the data is no more needed, other instructions are used to make it unavailable again. Each operator is supported by a driver, i.e. a subroutine (written in ESOPE) where the input and output objects (fields, models, tables, etc.) are decoded into segment-based data structures managed by ESOPE instructions. The data is then transferred to lower level subroutines where the structural calculations are performed. Typically, the lowest level subroutines just handle data in traditional way of FORTRAN, which renders more transparent and easy the core of implementations where the basic structure-related operations are performed (Arêde, 1997).

### 5.3 - STRUCTURAL MODELLING ASPECTS

The building model used in this study is implemented through a CASTEM procedure, which performs a 'step-by-step' non-linear static or dynamic analysis (Millard, 1993). The adopted generic frame model is expected to have the degree of accuracy that can be achieved by frame models with member-by-member representation. The following assumptions, commonly adopted in many member-by-member frame models, were postulated: *a)* mass is lumped at floor levels; *b)* member plastification is represented by concentrated plastic hinges at member ends; *c)* the deformations (displacements, rotations and strains) are assumed to be small and, accordingly, the analysis uses the initial undeformed geometry of the structural system; and, *d)* the material properties are homogeneous within each sub-element.

The general procedure for the numerical modelling of the studied structures (bare, selective strengthened and infilled frames) is schematically represented in Figure 5.1. As can be observed in the flow chart, the preliminary numerical analyses are just based in experimentally measured material properties and empirical formulas to estimate the model parameters. Tests performed in the specimen' materials (concrete, steel and masonry) are used to define the material' properties for the RC elements (fibre models) and for the infill masonry elements. Recall that the preliminary numerical analyses of real structures are normally performed without knowing the real material' properties.

After the PsD full-scale tests, the parameters to model the slab-participation, plastic hinge length, the shear deformation of RC elements, the joint deformation, and the bond-slip effect are accurately estimated using the empirical formulas in combination with measurements on the full-scale tests allows (dashed line in the graph). To complete the global model of the structure, the geometry, supports, and viscous damping are also considered. After defining the mass distribution, the natural frequencies and the corresponding shape modes are calculated, which are then compared to the values obtained in the non-destructive tests. With the dead and live loads are calculated the initial stress and strain in the structure. For the numerical simulations on a structure previously subjected to another damageable earthquake input motions, which is the case of the strengthened frame, it were applied increasing imposed displacements in order to introduce in the numerical model a damage state corresponding to the one observed experimentally.

Finally, the earthquake input motions corresponding to the test series are applied. From the results of the non-linear numerical analysis, the time-histories of storey displacements, inter-storey drifts, storey shear, dissipated energies, etc. are obtained, which are subsequently compared to the results of the PsD tests performed in the corresponding full-scale frame structure.

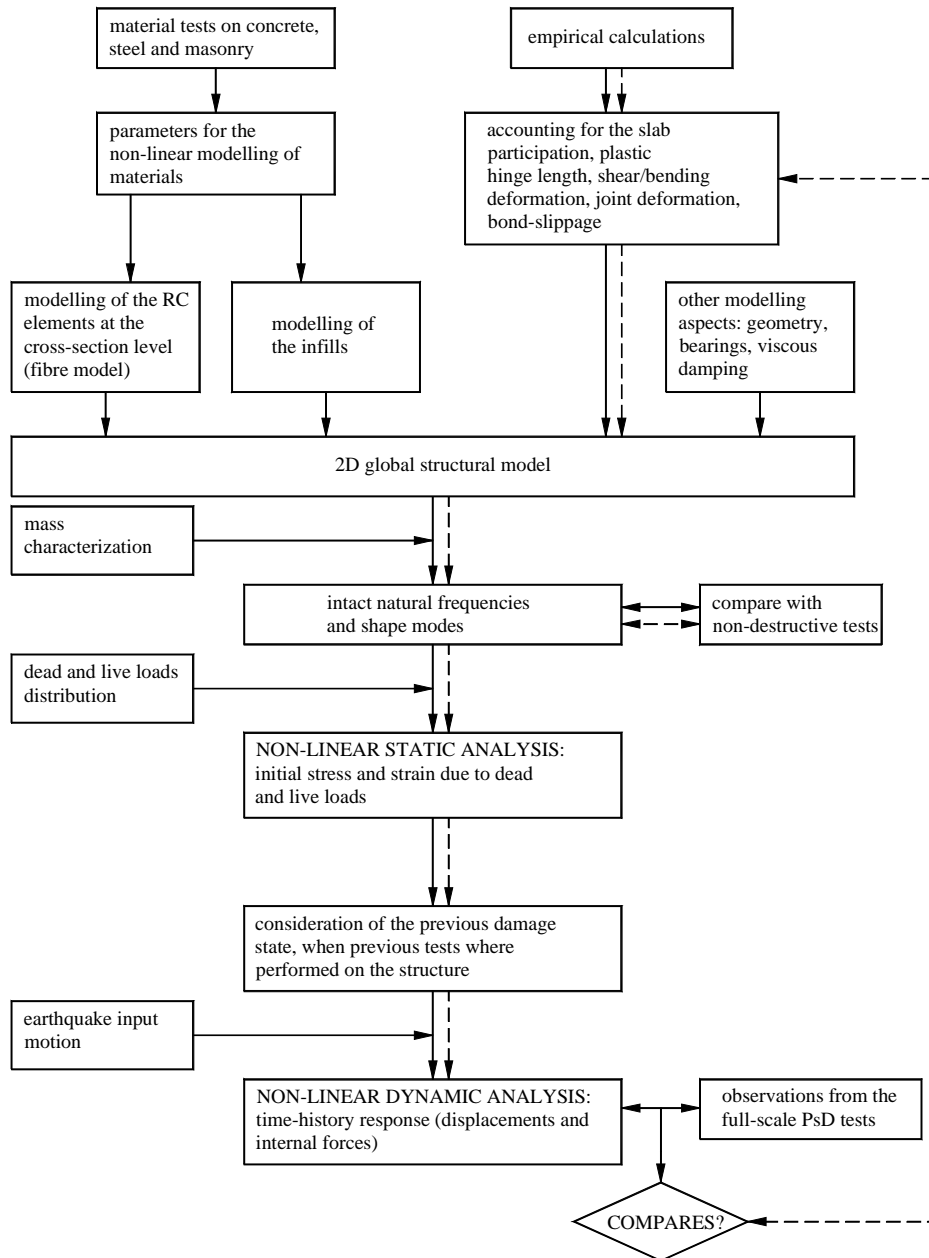


Figure 5.1 - Schematic flow chart of modelling procedures adopted for the RC frames



The non-linear numerical analysis is performed in two steps. Firstly, the static loads are imposed. Then, the displacements for pushover analyses or base acceleration for earthquake input motion analyses are imposed.

The analysis is currently performed by 'step-by-step' integration procedures, which comprise the following main phases: *i*) to divide the accelerogram in elementary short duration pulses (about 1/10 of the smaller structural period that contributes to the dynamic structural response); *ii*) to consider that while a certain pulse is acting the structural behaviour is linear; and, *iii*) to compute the successive increments of displacements, velocities and seismic forces due to the acceleration pulses, considering the actual stiffness of the structure. In this way, time series corresponding to displacements, velocities, accelerations and seismic forces defining the response of the structure are obtained.

The standard Newmark integration algorithm (currently one of the most widely accepted integration techniques) is used in the static and dynamic non-linear calculations by means of a common scheme. The non-linear dynamic problem is transformable into a pseudo-static problem (in each load step). The dynamic equilibrium equations are integrated 'step-by-step' using well-established algorithms, as presented in Arêde (1997).

### **5.3.1 - Description of the building frame model**

As stated in Chapter 1, one of the aims of this study is to investigate possible seismic retrofit schemes to use in the seismic upgrade of existing reinforced concrete frames, with and without brick masonry infill walls, and with and without openings. The concrete frame under study in this thesis was essentially designed for gravity loads only. The reinforcement details were specified in order to be representative of buildings constructed until the late 1970's in European Mediterranean countries, such as Italy, Portugal, Greece, Turkey, etc.

The general layout and dimensions of the investigated structure were given in Figure 3.1. It is a four-storey frame with three bays, two with a 5.00 *m* span and one external with a 2.50 *m* span. Inter-storey height is 2.70 *m* for all four storeys, and a concrete slab 2.00 *m* wide on each side and 0.15 *m* thick cast together with the beams. Equal beams (geometry and reinforcement details) were considered in all floors (see Figure 3.2). All beams in the

direction of loading are  $0.25\text{ m}$  wide and  $0.50\text{ m}$  deep. The columns have equal geometric characteristics, except for the stocky column, which develops on the 1<sup>st</sup> and 2<sup>nd</sup> storeys with dimensions of  $0.60\text{ m} \times 0.25\text{ m}$  and on the 3<sup>rd</sup> and 4<sup>th</sup> storeys with dimensions of  $0.50\text{ m} \times 0.25\text{ m}$  (see Figure 3.3 for reinforcement details). Further details on this plane frame were presented in Section 3.2.1.

For the infilled frame, brick masonry panels ( $0.20\text{ m}$  thick) were constructed according to the following specifications (see also Figure 3.12): *a*) the left-hand bay infill contains a window ( $1.20\text{ m} \times 1.10\text{ m}$ ) at each level; *b*) the central bay contains a doorway ( $2.00\text{ m} \times 1.90\text{ m}$ ) at ground level and at window openings ( $2.00\text{ m} \times 1.10\text{ m}$ ) at each of the upper three levels of the building; and, *c*) the right-hand ( $2.50\text{ m}$  span) bay contains solid infill, i.e., without openings.

The building studied in the present numerical analysis is represented by a plane frame model (considering three DOF's per node, i.e. two translations and one rotation) with four storeys and three bays, as represented in Figure 5.2. The cross-sections' geometrical characteristics and the reinforcement detailing of the columns and beams are summarised in Tables 5.1 and 5.2, respectively, while the reinforcement detailing were presented in Figures 3.2 and 3.3.

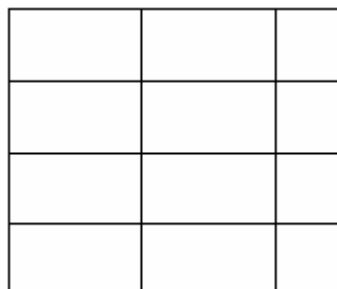


Figure 5.2 - Model of the plane bare frame

Table 5.1 - Columns cross-sections ( $m \times m$ ) and reinforcement detailing

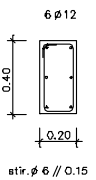
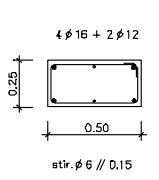
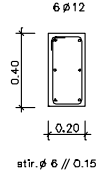
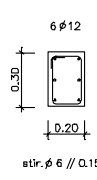
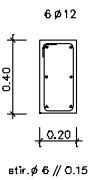
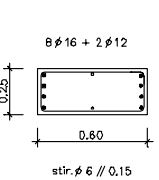
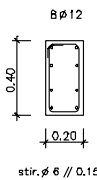
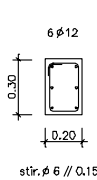
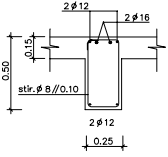
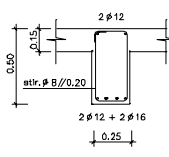
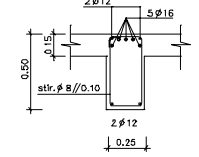
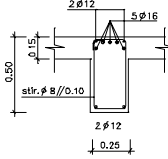
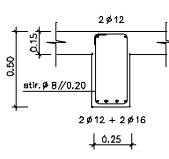
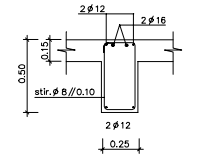
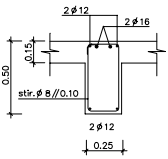
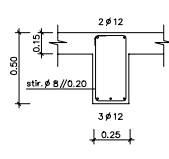
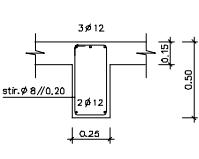
Columns	Column alignment			
	1	2 (strong-column)	3	4
3 <sup>rd</sup> and 4 <sup>th</sup> Storey	 <p>6 <math>\phi</math> 12 0.40 0.20 stir. <math>\phi</math> 6 // 0.15</p>	 <p>4 <math>\phi</math> 16 + 2 <math>\phi</math> 12 0.25 0.50 stir. <math>\phi</math> 6 // 0.15</p>	 <p>6 <math>\phi</math> 12 0.40 0.20 stir. <math>\phi</math> 6 // 0.15</p>	 <p>6 <math>\phi</math> 12 0.30 0.20 stir. <math>\phi</math> 6 // 0.15</p>
1 <sup>st</sup> and 2 <sup>nd</sup> Storey	 <p>6 <math>\phi</math> 12 0.40 0.20 stir. <math>\phi</math> 6 // 0.15</p>	 <p>8 <math>\phi</math> 16 + 2 <math>\phi</math> 12 0.25 0.80 stir. <math>\phi</math> 6 // 0.15</p>	 <p>8 <math>\phi</math> 12 0.40 0.20 stir. <math>\phi</math> 6 // 0.15</p>	 <p>6 <math>\phi</math> 12 0.30 0.20 stir. <math>\phi</math> 6 // 0.15</p>

Table 5.2 - Beams cross-sections ( $m \times m$ ) and reinforcement detailing

Bay (span length)	Left	Middle	Right
1 (5.00 m)	 <p>2 <math>\phi</math> 12 0.50 0.15 stir. <math>\phi</math> 8 // 0.10 2 <math>\phi</math> 16 0.25</p>	 <p>2 <math>\phi</math> 12 0.50 0.15 stir. <math>\phi</math> 8 // 0.20 2 <math>\phi</math> 12 + 2 <math>\phi</math> 16 0.25</p>	 <p>2 <math>\phi</math> 12 0.50 0.15 stir. <math>\phi</math> 8 // 0.10 5 <math>\phi</math> 16 2 <math>\phi</math> 12 0.25</p>
2 (5.00 m)	 <p>2 <math>\phi</math> 12 0.50 0.15 stir. <math>\phi</math> 8 // 0.10 5 <math>\phi</math> 16 2 <math>\phi</math> 12 0.25</p>	 <p>2 <math>\phi</math> 12 0.50 0.15 stir. <math>\phi</math> 8 // 0.20 2 <math>\phi</math> 12 + 2 <math>\phi</math> 16 0.25</p>	 <p>2 <math>\phi</math> 12 0.50 0.15 stir. <math>\phi</math> 8 // 0.10 2 <math>\phi</math> 16 2 <math>\phi</math> 12 0.25</p>
3 (2.50 m)	 <p>2 <math>\phi</math> 12 0.50 0.15 stir. <math>\phi</math> 8 // 0.10 2 <math>\phi</math> 16 2 <math>\phi</math> 12 0.25</p>	 <p>2 <math>\phi</math> 12 0.50 0.15 stir. <math>\phi</math> 8 // 0.20 3 <math>\phi</math> 12 0.25</p>	 <p>3 <math>\phi</math> 12 0.50 0.15 stir. <math>\phi</math> 8 // 0.20 2 <math>\phi</math> 12 0.25</p>

### 5.3.2 - Improved element model

From local to more global models, many analytical models have been proposed to simulate the behaviour of reinforced concrete structures.

The structure under study has been modelled as a planar frame, with Timoshenko finite elements, using the computer program CASTEM. The evident advantage of a member-by-member analysis lies in the quantitative assessment of overall structural safety with a direct

reference to the process of the damage sustained by each constituent element (Umemura and Takizawa, 1982).

Members of the planar-framed structure herein studied are slender elements and are conventionally represented by line elements in the finite element analysis. Columns and beams length are specified with centreline dimensions. The joints of planar frame are assumed to be rigidly connected.

In order to have a more realistic model of the reinforced concrete frame, each element (beam or column) has been modelled using five sub-elements, with one Gauss integration point. As shown in Figure 5.3, in addition to the end stiff zones (sub-elements 2 in Figure 5.3), which represent the joints, each beam/column is modelled by other three sub-elements. Therefore, the structure has been modelled by Timoshenko elements with non-linear behaviour at the potential plastic-hinge zones (vicinity of the frame joints), with length  $l_p$ , and elements with linear elastic behaviour in the internal sub-element of the structural elements. Furthermore, a stiff linear elastic element was also considered to simulate the joint rigidity. The non-linear elements are modelled by a fibre model with uniaxial non-linear behaviour constitutive laws for the constituent materials (concrete and steel).

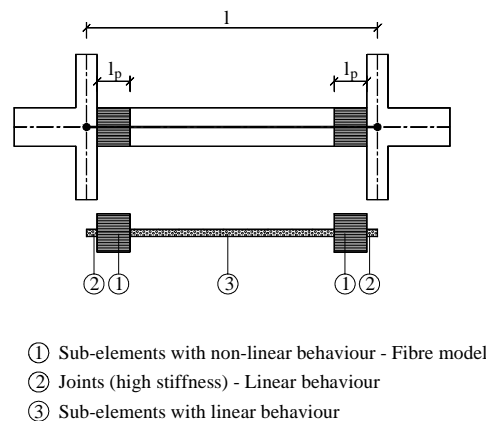


Figure 5.3 - Generic element model: association of sub-elements with elastic linear (joints and central elements) and non-linear behaviour (plastic hinge zones)

The non-linear sub-elements (zone 1 in Figure 5.3) are modelled using the fibre-model implemented by Guedes (1997). Each sub-element with non-linear behaviour is sub-

divided into longitudinal fibres and each fibre behaves according to the material law it represents.

In framed structures, joints are frequently modelled as an undeformable block of suitable dimensions. Models that take into consideration concentrated rotations at the beam to column interface provide flexural strength degradation. In the numerical analyses performed in this thesis, the joints were modelled with stiff linear elastic elements (zone 2 in Figure 5.3). To accurately simulate the higher strength and stiffness of the joint due to the confinement provided by the adjacent beams or columns, and by the transversal beams, a high value for the mechanical characteristics of the elements representative of the joints is considered. In the analyses, the Young modulus of each joint was considered to be three times its original value.

Fifty-seven type-sections with non-linear behaviour were considered for a refined modelling of the structure. Three type-sections were used for each of the sixteen columns of the structure, plus three type-sections for each of the three beam bays. Using this refinement, it is possible to define different material properties for each casting phase of the columns corresponding to each storey level. In fact, a considerable difference in strength was found for each casting phase of the columns. For the beams, it were considered similar type-sections for all storeys, because the beams have the same geometrical characteristics, as well as steel quantities and detailing, and, even though the beams were casting in different phases (one phase for each storey), an analogous concrete strength value was found for the four beams/slab casting phases (as presented in Section 3.2.5).

### 5.3.3 - Plastic hinge length

To estimate the equivalent plastic hinge length ( $l_p$ ), see Figure 5.3, many expressions based on experimental results have been suggested. One of the most commonly used expressions to estimate the plastic hinge length, already presented in Chapter 4, was proposed by Paulay and Priestley (1992)

$$l_p = 0.08 \cdot l + 0.022 \cdot \phi_l \cdot f_{sy} \quad (5.1)$$

where:  $l$  is the length of the RC element,  $\phi_l$  is the diameter of the main longitudinal reinforcing bars, and  $f_{sy}$  is the yielding strength of the reinforcement (in *MPa*). For typical beam and columns proportions, the expression (5.1) results in

$$l_p \cong 0.5 \cdot h \quad (5.2)$$

where  $h$  is the section depth.

In the preliminary numerical analyses, the length of the non-linear fibre element (plastic hinge length) was estimated based on the empirical formulae (5.1), the mean value of the yielding steel stress (see Table 3.8), the steel bar diameter corresponding to each reinforced concrete section, and considering that the used finite element is a Timoshenko element with constant curvature (one integration point only), through a correction factor, as justified in the next.

Assuming that the effective plastic hinge length can be estimated from the expression (5.1), and that the curvature in the plastic hinge zone has a parabolic distribution with extremity values given by  $\phi_m$  and  $\phi_y$ , the equivalent length hinge-element,  $l_p^*$ , calculated for the same chord rotation, depends on the ductility. The evolution of the ratio between the hinge element-length,  $l_p^*$ , and the plastic-hinge length,  $l_p$ , is plotted in Figure 5.4 as a function of the curvature and displacement ductilities. From the plots in Figure 5.4, it is apparent that this factor tends to an asymptotic value, which is 0.4 (Varum and Pinto, 1999). In the preliminary analyses, this factor was taken as equal to 0.5, which may be representative of an intermediate ductility demand level, as represented in the expression

$$l_p^* = 0.5 \cdot l_p \quad (5.3)$$

The plastic hinge lengths estimated from the PsD earthquake tests (less than 0.20 *m*, see Section 4.11.1) are much lower than the values obtained from the empirical expressions. In the earthquake tests, cracks opened at the extremity of the elements (base and top, for the columns) and controlled the structural flexibility. It was concluded that the empirical expressions do not properly evaluate the plastic hinge length for existing RC structures

with smooth rebars (poor bond conditions). The insufficient ability to properly model the real behaviour of the RC elements without considering a small value of the plastic hinge length was noted from the results of the preliminary analyses. Therefore, the final numerical analyses were performed considering a reduced length for the plastic hinges of the slender columns to better account for the concentration of the deformation at the elements' extremities in existing RC structures.

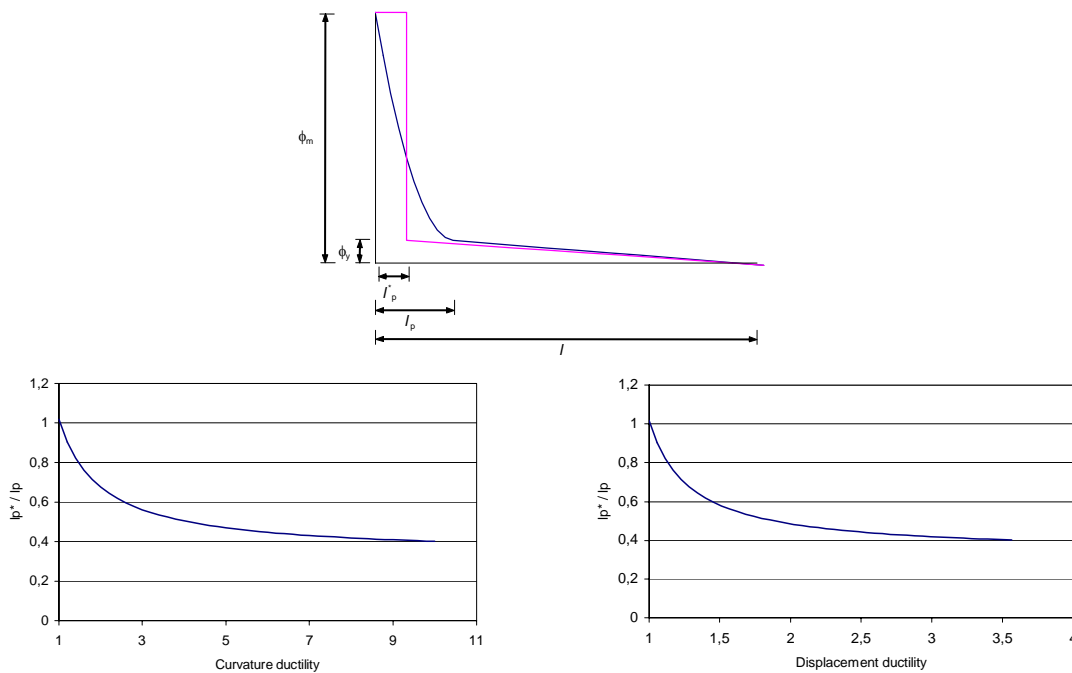


Figure 5.4 - Length of the non-linear fibre element

### 5.3.4 - Non-linear behaviour of RC elements

The numerical analyses were performed using a fibre model at section level, being the non-linearities concentrated at the element extremities. As recalled by Guedes (1997), the fibre model can be regarded as a step further in the refinement of standard beam models. In fact, it uses the same cinematic formulation to compute the deformation of the longitudinal axis of an element: two displacements and one rotation at each node. The difference to the standard beam models relies on the procedure that it follows to calculate the resisting forces: instead of considering a global constitutive law at the level of the transverse sections, the fibre model computes the deformation and the stress of a set of points

describing a mesh in the transverse section. The structure is thus divided not only in planar beam type elements, but each of these elements is also sub-divided into longitudinal fibres. One of the major limitations in this kind of model is the huge amount of computation required. However, it is considered that a refined model would provide more detailed results for a laboratory prototype.

A limitation that commonly appears in element models is the inability to consider the effect of variation of axial loads in the flexural behaviour. In fact, several models do not allow for considering the effects of varying axial forces (due to overturning). Instead, the fibre model explicitly considers the variation of the flexural inelastic properties of the columns according to the change of axial force. Axial load variation may lead to important changes in the flexural behaviour of the columns, especially in the external ones, where the axial load varies more significantly (overturning forces).

Fibre type models are in between the local and the global formulations. Although the algorithm computes the global deformations at the level of the Gauss points of the structural elements, the response is given by integration of the local forces calculated at different points representing different materials and locations in the transverse section. Fibre type models, such as the one used in this numerical analysis, are associated with axial stress versus strain constitutive laws of the constituent materials (concrete and steel). The shear and the axial stresses are uncoupled, and the Poisson effect is neglected or taken into account through simplified models that consider the confinement effect of the stirrups in the concrete core (Guedes, 1997). Nevertheless, fibre models are powerful tools in the analysis of the behaviour of structural elements. In particular, RC columns are composite elements particularly suited to being modelled by these fibre models.

The fibre model assumes the following simplifications (see Figure 5.5):

- The strain distribution across the section is assumed linear (the section remains plain).
- Cracking of concrete occurs mainly perpendicular to the axis of bending.
- It is expected that shear failure does not occur, so that the effect of shear force on the moment-curvature relations is not considered.



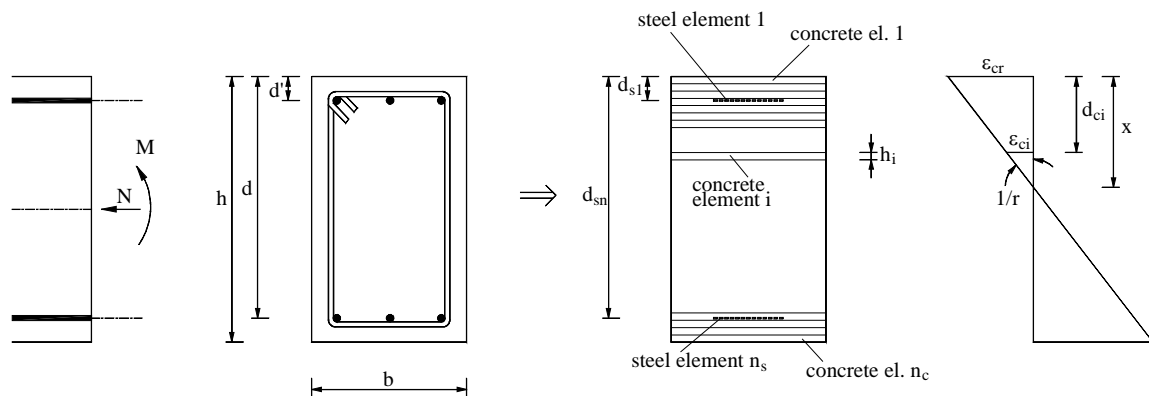


Figure 5.5 - General fibre method: section, discrete elements and curvature (adapted from CEB-161, 1983)

The general procedure to compute the internal forces at the section level consists on the following steps:

- i)* for the confined and unconfined concrete and for the steel positions the section is divided into an adequate number of elements, as shown in Figure 5.5;
- ii)* for a given curvature ( $\epsilon_{cr}$ ) and an assumed linear strain distribution, the average strain in each element is computed and subsequently the strain is obtained from the assumed stress-strain material models;
- iii)* in the case of cyclic loading, the stress-strain history of each element has to be stored in order to calculate the stress corresponding to the given strain, employing the rules of the cyclic stress-strain material model;
- iv)* the total internal forces are obtained by summing up the element forces over the section;
- v)* the equilibrium of the forces in the section is checked. In general, this is achieved by means of an iterative process with a new start in the assumed strain distribution and the above steps are repeated until the equilibrium equation has been satisfied, for the given moment and axial load.

The fibre model used in the numerical analyses was implemented by Guedes (1997) in the computer code CASTEM. The fibre model has been implemented in a Timoshenko beam element so that the distortional effect due to shear forces could be taken into account. However, classical fibre models, as the one used in CASTEM, do not consider non-linear behaviour laws for shear and this is the most important restriction of this model. If shear

strain exists and assumes an important role in the global behaviour of a structure, some attention must be taken in the numerical analysis. A detailed description of the used model can be found in Guedes (1997), namely the algorithm, the compatibility and equilibrium equations, the constitutive laws adopted for the materials, for monotonic and cyclic loading.

To reduce the computational effort involved in obtaining the moment-curvature diagram in the fibre method in the numerical analyses, and because we are working with 2D (plane) frames, the sections are considered to be composed of a number of horizontal element fibres, as illustratively represented in Figure 5.6 for a T-beam and for two column elements of the frame. As shown in the figure, a higher refinement was adopted for the columns when compared to the beams. This assumption is dictated by their relative importance in the structure response, and keeps in mind the inherent computational effort, without loss of accuracy. For the beams, the slab-participation with the respective significant slab reinforcement was considered, at its top and bottom layers. The concrete in the slab was considered as non-confined. For each steel group just one fibre element centred at its resultant position was considered.

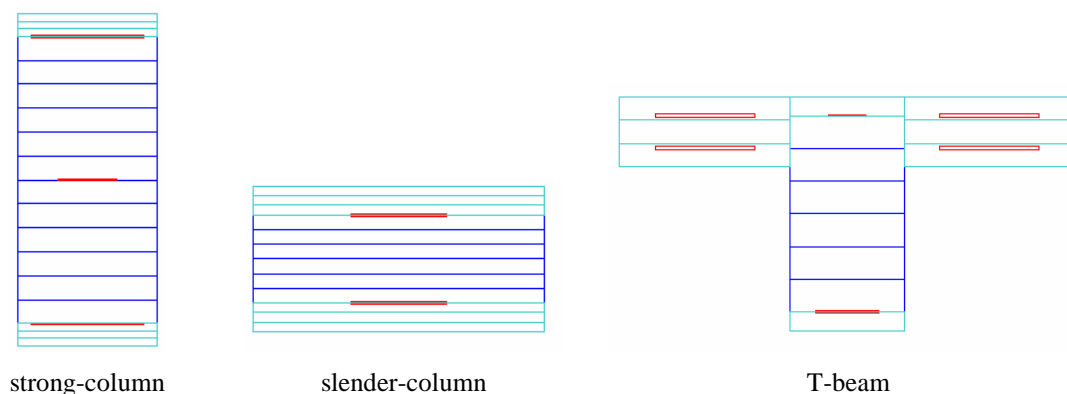


Figure 5.6 - Discrete elements for the fibre model

Concerning the concrete, different stress-strain relationships are used to differentiate between the confined concrete core of the sections and the unconfined concrete cover. In CEB-161 (1983) it is stated that once the concrete cover strain reaches the spalling strain, the concrete cover becomes ineffective. In addition, it is recommended a strain limit value of 0.004 for the limit since the concrete cover must be neglected. In the numerical analysis,

for all the elements (beams and columns), 2.5 cm for the concrete cover was considered, as employed in the construction of the frames. Therefore, the longitudinal steel reinforcement in beams and columns is centred at a level distant of about 4.0 cm of the external surface of the RC elements. For the Poisson ratio ( $\nu$ ) was considered the value of 0.3 for all the RC structural elements.

An exhaustive description of the material behaviour rules and models used in the numerical analyses can be found in Guedes (1997) and Menegotto and Pinto (1973) for the concrete and steel models, respectively. In the next section, the steel and concrete models for the cyclic stress-strain behaviour are summarised.

#### 5.3.4.1 - Concrete model

Figure 5.7 represents schematically the uniaxial concrete model. In compression, a parabolic curve is assumed from the initial unloaded stage up to the peak stress values, with initial tangent modulus equal to the concrete Young modulus. A straight line, which slope depends on the confinement degree, describes the softening branch. Under tensile stresses, the behaviour is described by a linear elastic branch with a subsequent softening branch, which accounts for tension stiffening effects.

The model representing the main features of the concrete behaviour under cyclic loading, takes secondary effects, such as crack closing, into account. The constitutive law for cyclic loading is sketched in Figure 5.7 together with the various loading-unloading-reloading paths. Analytical formulae and a detailed description of this model can be found in Guedes (1997).

For the concrete in the full-scale RC frames, relevant differences of strength were found between each casting phase. Therefore, in the numerical model different concrete mechanical properties and specific model parameters were adopted for each casting phase (storey columns and beams-girder floor levels). The mean value of the compressive strength was taken for the peak strength of the unconfined concrete. For the corresponding strain it was adopted 2.5‰. In the numerical models, the tensile ultimate strength was assumed to be 1/10 of the corresponding compressive ultimate strength. The residual

compressive strength is assumed to be 1/5 of the compressive ultimate strength for the confined concrete and zero for the unconfined concrete. Table 5.3 summarises the average relevant mechanical properties values of the concrete used in the numerical model (obtained from the concrete tests presented in Table 3.6, in Section 3.2.5).

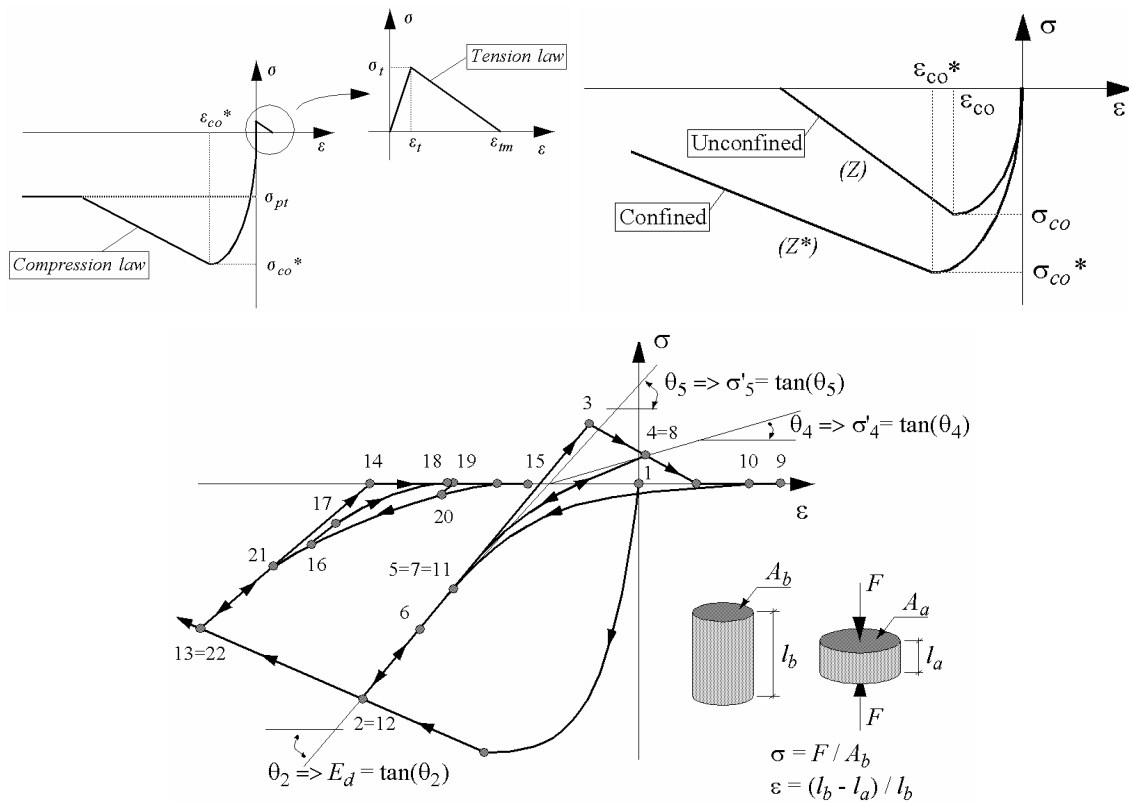


Figure 5.7 - Concrete axial stress-strain constitutive law: envelope monotonic curves for concrete under tension and compression with the effects of confinement and cyclic curves (Guedes, 1997)

Table 5.3 - Concrete: parameters to the numerical model

Mechanical parameter	zone (different casting phases)					
	columns				beams <sup>a</sup>	
	1 <sup>st</sup>	2 <sup>nd</sup>	3 <sup>rd</sup>	4 <sup>th</sup>		
Compressive ultimate strength, $f_{cu}$ (MPa)	13.90	13.80	9.20	11.00	17.00	
Compressive ultimate strain, $\varepsilon_{cu}$ (%)	0.3	0.3	0.3	0.3	0.3	
Young's modulus, $E_c$ (GPa)	22.8	22.8	19.9	21.1	24.4	
Residual compressive strength, $f_{c,res}$ (MPa)	confined	2.78	2.76	1.84	2.20	3.40
	unconfined	0.00	0.00	0.00	0.00	0.00
Tensile ultimate strength, $f_{tu}$ (MPa)	1.39	1.38	0.92	1.10	1.70	

a) For the beams and girders it was used the average values of this different casting phases, because they do not differ substantially and their minor influence in the structural response.

### 5.3.4.2 - Steel model

The steel model used supports an algebraic explicit stress-strain law, formulated on the basis of experimental tests on bars under cyclic load (Menegotto and Pinto, 1973). The steel model illustrated in Figure 5.8 includes typical curves for monotonic and cyclic loading, valid for tension and compression. The monotonic curve is characterised by an initial linear branch followed by a plateau and a hardening branch leading up to their failure point. The cyclic behaviour is described by the explicit formulation proposed by Giuffr  and Pinto and implemented by Menegotto and Pinto (1973). A detailed description of this model can be found in Guedes (1997).

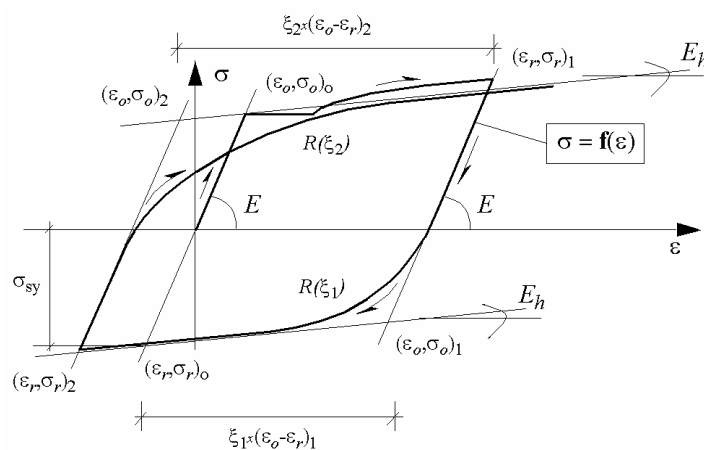


Figure 5.8 - Uniaxial constitutive model for steel (Guedes, 1997)

The mechanical properties (mean values) for the steel reinforcement adopted in the model for the numerical analyses are shown in Table 5.4 (based on the experimental results, see Table 3.8).

Table 5.4 - Steel: parameters to the numerical model

Mechanical parameters	Value
Yield stress, $f_{sy}$	343.6 MPa
Ultimate strength, $f_{su}$	451.5 MPa
Ultimate strain, $\epsilon_{su}$	22.9 %
Elastic Young's modulus, $E_s$	204.5 GPa
Hardening strain, $\epsilon_{sh}$	3.03 %

### 5.3.5 - Bond-slip modelling of the longitudinal reinforcing steel plain bars

Bond plays a fundamental role in the response of reinforced concrete members by allowing the stress transfer from the steel bars to the surrounding concrete. Perfect bond is usually assumed in the analyses of reinforced concrete structures. This implies full compatibility between concrete and reinforcement strains. This assumption is only valid in regions where negligible stress transfer occurs between the two components. Perfect bond between reinforcing steel and concrete can only exist at early loading stages and at low strain levels. As the load increases, cracking as well as breaking of bond unavoidably occurs and a certain amount of bond-slip takes place in the element, all of which will in turn affect the stress distributions in both steel and concrete. Near the cracks, high bond stresses develop at the steel-concrete interface causing relative displacements between concrete and reinforcement. Due to this bond-slip, different strains are observed in the steel rebars and in the surrounding concrete (Monti and Spacone, 1998; Keuser and Mehlhorn, 1987; Soleimani *et al.*, 1979). Berra *et al.* (1994) stated that the steel to concrete bond in RC structural elements subjected to cyclic loading can deteriorate, even before the stress state has attained the yield stress of the steel or the stress strength of the concrete.

Thoroughly reliable analytical models are needed to analyse reinforced concrete building frames subjected to strong earthquake motions. Indeed, one of the shortcomings of the current models is their inability to include the relative slippage of the main reinforcing bars in the joints. Since this effect causes fixed-end rotations of the elements, the stiffness of a structure is overestimated. Moreover, slippage of reinforcing bars within the joints increases the flexibility of the structure causing additional lateral displacements, which may contribute to frame instability (Sasani *et al.*, 1999; Soleimani *et al.*, 1979). As stated by Monti and Spacone (1998), the introduction of bond-slip of reinforcing bars in the numerical models proves to be a necessary enhancement towards a realistic description of the cyclic and the ultimate behaviour of reinforced concrete structures.

Several authors (e.g. Youssef and Ghobarah, 2001; 1999; Monti and Spacone, 1998; Abrishami and Mitchell, 1996; Murayama *et al.*, 1996; Berra *et al.*, 1994; Rodriguez and Park, 1994; Hawkins *et al.*, 1987; Keuser and Mehlhorn, 1987; Adham *et al.*, 1975; among countless others) developed work in the bond-slip of RC elements under cyclic loading. However, there is practically no investigation, experimental and numerical, on the cyclic

behaviour of RC members with smooth reinforcing steel bars. The bond-slip of smooth plain round bars gains vast significance considering that an important number of existing reinforced concrete structures in southern Europe (see for example LNEC, 2000) were constructed in the 1960's using these reinforcement steel bars.

The fibre element state determination is carried out at three levels: element, section and fibre. Stresses and corresponding stiffness are determined at all the three levels. In particular, the section state determination computes the axial forces  $N$  and bending moments  $M$  (generalised forces) corresponding to prescribed section deformations (see Figure 5.9), namely the average strain ( $\bar{\varepsilon}$ ) and the section curvature ( $\phi$ ). Assuming linear strain along the section, and that the deformed sections remain perpendicular to the longitudinal element axis, the strain at a fibre located at a distance  $y$  from the reference axis can be determined as follows

$$\varepsilon = \bar{\varepsilon} + \phi \cdot y \quad (5.4)$$

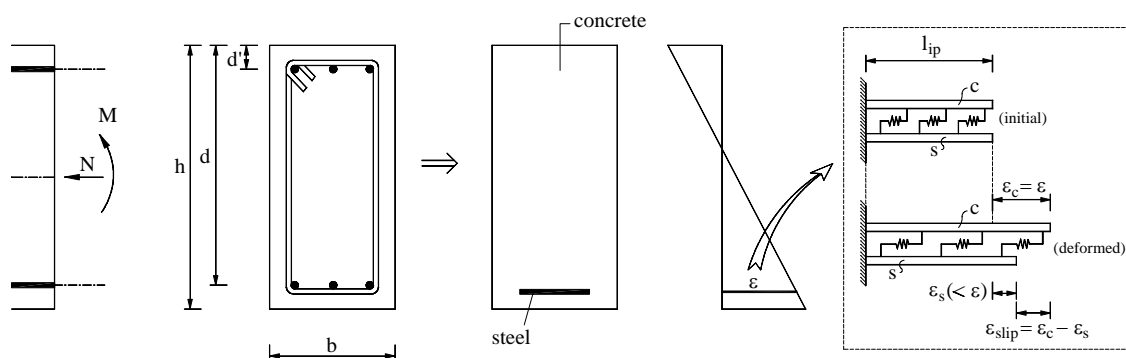


Figure 5.9 - Bond-slip deformation of the constituent materials

When perfect bond is assumed between concrete and steel longitudinal rebars, both concrete and steel fibres located at the same depth  $y$  have the same strain

$$\varepsilon_s = \varepsilon_c = \varepsilon \quad (5.5)$$

This assumption is no longer valid when the effect of longitudinal reinforcing bars slippage is observed (see Figure 5.9). The steel reinforcing constitutive laws are adjusted with slippage factors ( $\lambda$ ) in order to account for the slippage of the reinforcing steel bars relatively to the concrete

$$\lambda = \frac{\varepsilon_c}{\varepsilon_s} \quad (5.6)$$

Basically, the correction is carried out by purely adjusting the characteristics of the monotonic steel behaviour laws. considering the smaller steel strain for a certain level of concrete strain. Therefore, in the fibre model used, the bond-slip is modelled explicitly using a correction of the steel reinforcement constitutive law. Considering that steel hardening strain is not reached, the steel constitutive law can be assumed as a bi-linear law with an elastic perfect plastic behaviour (see Figure 5.10 and expressions 5.7 to 5.10).

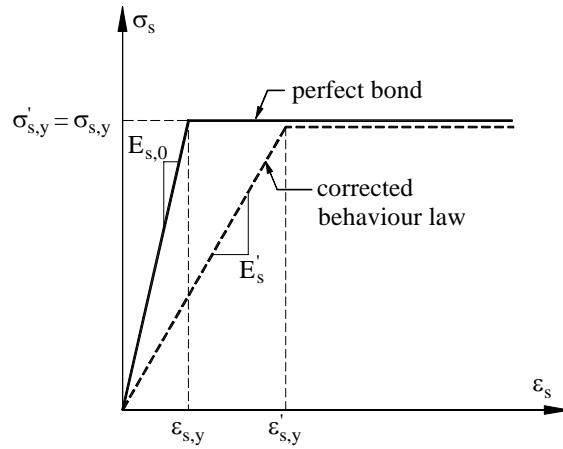


Figure 5.10 - Correction of the steel reinforcing constitutive law

$$\varepsilon'_{s,y} = \lambda \cdot \varepsilon_{s,y} \quad \sigma'_{s,y} = \sigma_{s,y} \quad E'_s = \frac{1}{\lambda} \cdot E_{s,0} \quad (5.7, 5.8, 5.9)$$

$$\sigma_s(\varepsilon_s) = \begin{cases} \text{if perfect bond} & \begin{cases} \varepsilon_s < \varepsilon_{s,y} \leftarrow \sigma_s(\varepsilon_s) = E_{s,0} \cdot \varepsilon_s \\ \varepsilon_s \geq \varepsilon_{s,y} \leftarrow \sigma_s(\varepsilon_s) = \sigma_{s,y} \end{cases} \\ \text{if not (not yielding steel occurs)} & \leftarrow \sigma_s(\varepsilon_s) = \frac{1}{\lambda} \cdot E_{s,0} \cdot \varepsilon_s \end{cases} \quad (5.10)$$

The bond-slip is accounted for by the slippage factor  $\lambda$  in the equations (5.7), (5.9) and (5.10), which is a correction factor of the strain in the steel stress-strain behaviour curve. The correction factor  $\lambda$  expresses the correction of the average steel strain in a RC finite element. The parameter  $\lambda$  assumes the value 1.0 when perfect adherence between steel and concrete is verified.



For analytical applications, several constant, linear and non-linear approximations of the bond stress-slip relationship are already published. Based on the bond stress-slip relationship proposed by Eligehausen *et al.* (1983), the CEB-FIP Model Code 90 (1990) adopts the model hereafter described. In the next,  $\tau$  stands for bond stress and  $s$  for bond-slip. It consists on an initial non-linear relationship  $\tau = \tau_{\max} \cdot (s/s_1)^\alpha$  valid for  $s \leq s_1$ , followed by a plateau  $\tau = \tau_{\max}$ , then a linearly decreasing branch and finally a constant line  $\tau = \tau_f$  (see Figure 5.11 and expression 5.11). Details on this model can also be found in CEB-217 (1993). In this model, the unloading branch of the bond stress-slip relationship is linear and valid for all parts of the diagram. The unloading modulus is independent of the bond-slip (Eligehausen *et al.*, 1983) and has an average value of  $200 \text{ N/mm}^3$ . The same bond stress-slip relationship is assumed regardless of whether the bar is pulled or pushed (CEB-217, 1993).

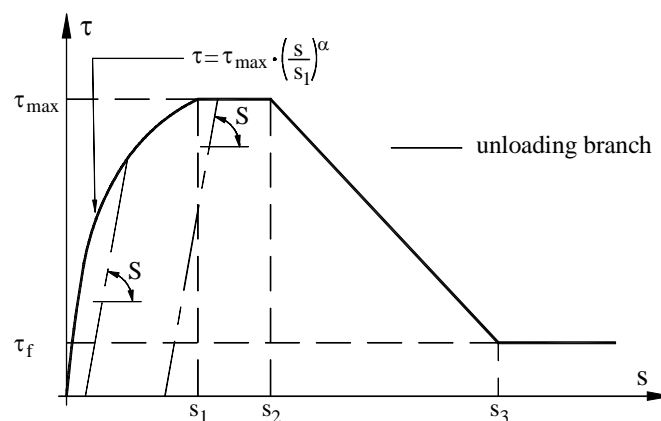


Figure 5.11 - Bond stress-slip relationship (CEB-217, 1993)

$$\tau = \begin{cases} \tau_{\max} \cdot (s/s_1)^\alpha & 0 \leq s \leq s_1 \\ \tau_{\max} & s_1 < s \leq s_2 \\ \tau_{\max} - (\tau_{\max} - \tau_f) \cdot \left( \frac{s - s_2}{s_3 - s_2} \right) & s_2 < s \leq s_3 \\ \tau_f & s_3 < s \end{cases} \quad (5.11)$$

Table 5.5 gives the proposal of CEB-217 (1993) for the model parameters of the bond stress-slip relationship for the case of smooth steel plain bars. The parameters depend on roughness of the bar surface, bond conditions and concrete strength. They are valid for both confined and unconfined concrete. Assuming  $s_1 = s_2 = s_3$ , as proposed in

CEB-217 (1993), the bond behaviour of smooth reinforcement is given by a constant line following a short non-linear increase till  $s_1$ . The bond stress-slip relationship for smooth reinforcing steel bars is represented in Figure 5.12 and expressed by equation (5.12).

Table 5.5 - Parameters for defining the bond stress-slip relationship of smooth bars (CEB-217, 1993)

Values <sup>a</sup>	cold drawn wire		hot rolled bars	
	bond conditions		bond conditions	
	good	all other cases	good	all other cases
$s_1=s_2=s_3$	0.01 mm		0.1 mm	
$\alpha$	0.5		0.5	
$\tau_{\max} = \tau_f (N/mm^2)$	$0.1\sqrt{f_{ck}}$	$0.05\sqrt{f_{ck}}$	$0.3\sqrt{f_{ck}}$	$0.15\sqrt{f_{ck}}$

a) The parameters given in the table are mean values.

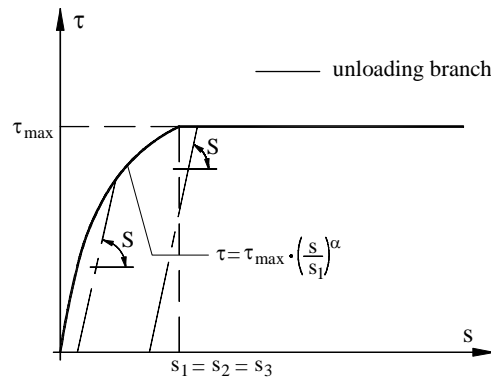


Figure 5.12 - Bond stress-slip relationship for smooth reinforcing steel

$$\tau = \begin{cases} \tau_{\max} \cdot (s/s_1)^\alpha & 0 \leq s \leq s_1 = s_2 = s_3 \\ \tau_f & s_3 < s \end{cases} \quad (5.12)$$

The relatively small values for the maximum bond stress  $\tau_{\max}$  given in Table 5.5 are based on the test results by Rehm (1961) (see Figure 5.13). In fact, for equivalent conditions, and according to CEB-217 (1993), the maximum bond stress for smooth reinforcing steel bars is just 12% of the maximum bond stress for ribbed bars. Even the residual bond strength of the ribbed bars is higher than the maximum for the smooth reinforcing bars. According to Figure 5.13, where  $f_{cc}$  means concrete strength measured on cubes of 200 mm side length, the bond strength of cold drawn wires is  $\approx 0.03 \cdot f_{cc}$  and that of hot rolled bars with some

scars is  $\approx 0.09 \cdot f_{cc}$ . As defended by Rehm (1961), the bond strength is proportional to  $f_{cc}$ , while in the CEB-FIP Model Code 90 (1990) it is assumed proportional to  $f_{ck}^{2/3}$ . In Figure 5.14 are represented the results from Rehm (1961), as well as the curve proposed in MC-90 (1990) for the bond stress-slip of plain reinforcing bars.

From cyclic tests on RC columns, both longitudinal and transversal reinforcement with plain round bars as typically used in Japan, Takiguchi *et al.* (1988) concluded that the bond stresses of the longitudinal bars were almost zero (less than  $f_{cm}/50$ ), when the specimens reaches their strength. The maximum stress founded by Takiguchi *et al.* (1988) for the maximum specimen's strength is inferior to the maximum bond stress proposed in the CEB-217 (1993).

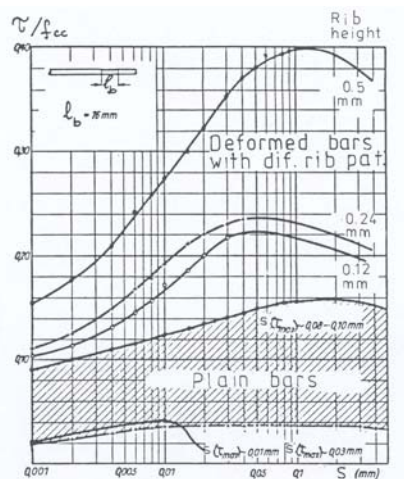


Figure 5.13 - Comparison of the bond stress-slip behaviour of plain and deformed bars (Rehm, 1961; CEB-217, 1993)

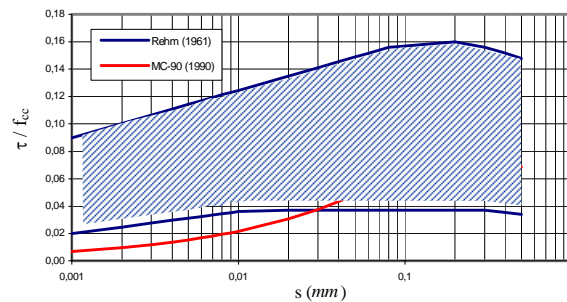


Figure 5.14 - Bond stress-slip behaviour of plain bars (Rehm studies, 1961; and, MC-90, 1990)

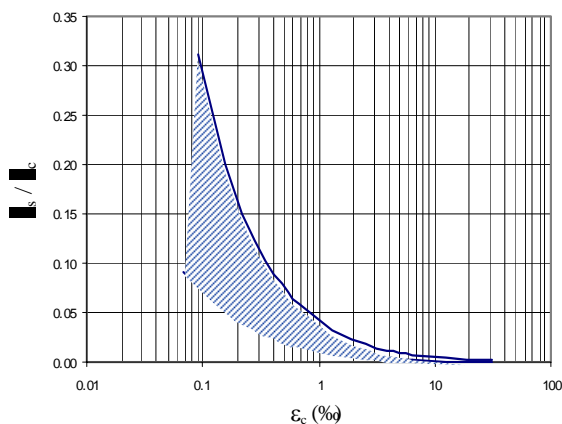


Figure 5.15 - Computed relative steel strain function of the total ('concrete') strain

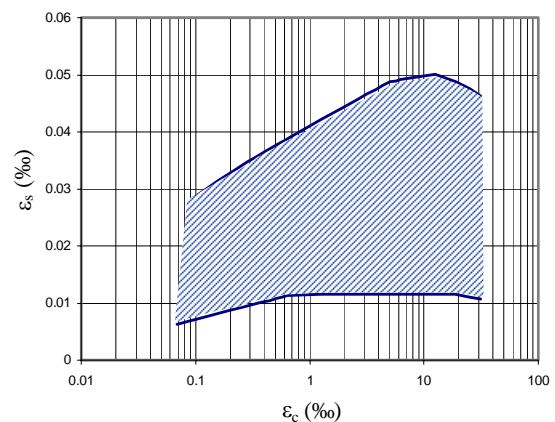


Figure 5.16 - Computed steel strain function of the total ('concrete') strain

Based on experimental data from Rehm (1961), the variation of the parameter  $\lambda$  (see equation 5.6) was estimated, and the results are represented in Figure 5.15. Further refinements in this relation, including taking into account spacing between cracks, the effect of cyclic loading and concrete strength, would be probably required from a theoretical point of view.

For the structure under study, a mean concrete strength of 16 MPa was found (see Section 3.2.5). Assuming good bond conditions for hot rolled bars, according to CEB-217 (1993), see Table 5.5, it was estimated a maximum bond stress  $\tau_{\max} \sim 1.10 \text{ MPa}$ .

Finally, from Rehm (1961) results, it was derived the variation of steel strain with the concrete strain. The results are plotted in Figure 5.16, where can be observed that for the range of strain studied, the maximum calculated steel strain is about 0.005%, which is much smaller than the yielding strain of the steel ( $\varepsilon_{\text{sy}} = 0.168\%$ ). These calculations are based on the hypothesis that steel yielding is not reached, which is here verified. The bond-slip does not allow the steel to mobilise its capacity. Furthermore, for poor bond conditions it is preferable to have smaller rebar diameters, for the same steel reinforcement, which conducts to higher bond strength.

In the numerical analyses with the refined finite element method, it was assumed for each element (beam or column), and for each earthquake, a constant value of  $\lambda$  in accordance to the maximum deformation experimentally observed at this element during the corresponding PsD test. A low slippage factor value was adopted for regions where low deformation was measured, while for regions with higher demands the slippage factor adopted reached values larger than 20. These high values of the slippage factor are corroborated by the experimental results of Rehm (1961). In fact, it can be observed in Figure 5.15 that for concrete deformation of about 1%, the reinforcing plain steel bars deformation is expected to be less than 5% of the concrete deformation. This corresponds to slippage factors bigger than 20. It was considered equal slippage correction factor  $\lambda$  for tension and compression.

As will be seen in Section 5.6, the numerical results obtained with the constant slippage factor  $\lambda$  are judged to be of good quality. However, it is presumed that more precise

numerical approximation can be achieved with a bond-slip model capable of adjusting the slippage factor to the maximum steel strain observed at each element. In fact, the bond-slip model should provide full bond at the beginning of loading (for tension and compression) being increased the slippage factor with the maximum strain observed. This model improvement is left to future research work. Figure 5.17 sketches a suitable function and expression (5.13) gives the slippage factor as a function of the maximum deformation,  $\lambda(\epsilon_s)$ .

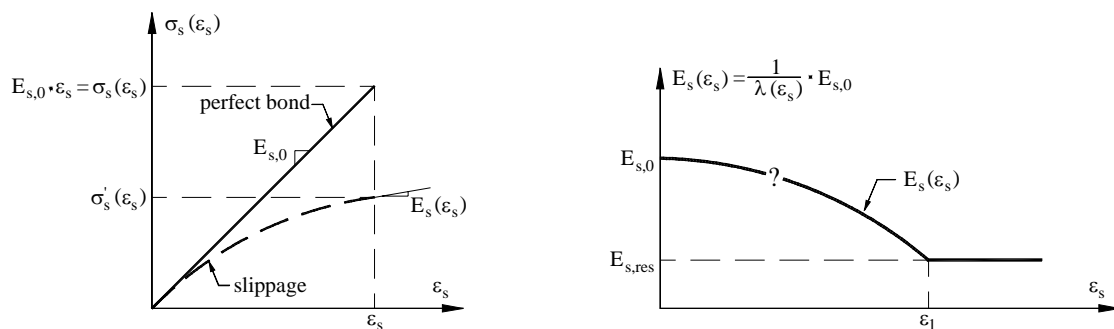


Figure 5.17 - Proposed bond stress-slip relationship for smooth reinforcing bars

$$\sigma'_s(\epsilon_s) = E_s(\epsilon_s) \cdot \epsilon_s = \frac{1}{\lambda(\epsilon_s)} \cdot E_{s,0} \cdot \epsilon_s \quad (5.13)$$

### 5.3.6 - Slab-participation

When reinforced concrete slab and beam floors are cast monolithically, the beam and the slab will act integrally with each other, contributing to both the strength and to the stiffness of the beams (Paulay and Priestley, 1992). As stated by Park and Paulay (1975), when the beam is subjected to positive bending moments, part of the slab will act as the flange of the beam, resisting the longitudinal compression, balancing the tensile force in the web reinforcement. When the spacing between the beams is large, it is evident that simple bending theory does not strictly apply because the longitudinal compressive stress in the flange will vary in accordance to the distance from the beam web, the flange being more highly stressed over the web than in the extremities. This variation in flange compressive stress, illustrated in Figure 5.18, occurs because of shear deformations in the flange (shear lag). The longitudinal compressive strain reduces with increasing distance from the web.

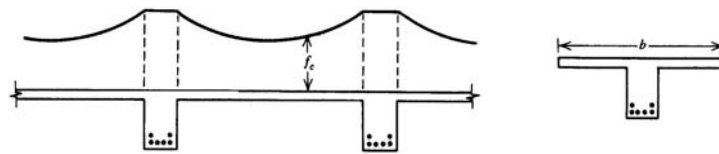


Figure 5.18 - Variation of sectional properties along the span of a beam (Paulay and Priestley, 1992)

The actual distribution of the beam compressive stress in the elastic range may be calculated using the theory of elasticity, and it depends on the relative dimensions of the cross section and of the span, and on the type of loading. At the flexural strength of the member, the distribution of longitudinal compressive stress across the flange will be more uniform than implied by the theory of elasticity. This happens because at near-maximum stress, the concrete stress-strain curve shows a smaller variation of stress with strain. In addition, the slab will usually bend transversely because of the load supported between the beams, and can cause cracking in the top of the flange parallel to the beam over the web-flange junction. Transverse reinforcement in the slab and shear-friction along the crack will allow longitudinal compression to be transferred out into the flange. Nevertheless, there are grounds for using a conservatively low effective width, as referred by Park and Paulay (1975).

Park and Paulay (1975) also advocate that in order to take into account the variation of compressive stress across the flange, it is convenient in design to use an effective flange width that may be smaller than the actual width, but uniformly stressed. The present code-specified effective widths are conservative estimates based on approximations to the elastic theory.

When the beam is subjected to negative bending moment, some of the longitudinal reinforcement in the flange clearly acts as tension steel, in parallel with the web main steel (see Figure 5.19). The tensile force is transferred across the flange into the web by shear in flange, much as the compressive force in the case of positive bending is transferred. Codes do not specify effective widths over which slab steel may be considered to be acting as tension reinforcement. Nevertheless, it is evident that a realistic appraisal of the beam strength for negative bending moment would include the effect of the slab steel. As an approximation, the slab steel within a width of four times the slab thickness each side of the web could be included with the tension steel of the beam (Park and Paulay, 1975).

During an earthquake action, the flange of a T-beam abutting against the two opposite faces of a column will be subjected to tension and compression, as illustrated in the moment distribution in Figure 5.19. In this figure, a typical variation of the sectional properties is shown along the beam span (Paulay and Priestley, 1992). As already stated, for monolithic slab-beam construction, the effective flange width and the stiffening effect of the slab depend on whether the slab is in tension or compression, and on the moment pattern along the beam. Diagonal cracking of a member due to shear, intensity and direction of axial load, and reversed cyclic loading are additional phenomena affecting member stiffness.

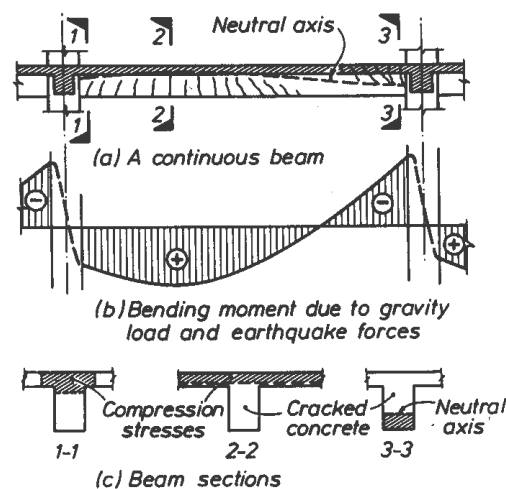


Figure 5.19 - Variation of sectional properties along the span of a beam (Paulay and Priestley, 1992)

Flange contribution to stiffness in T- and L-beams is typically lower than the contribution to flexural strength. This results from the moment reversal occurring across beam-column joints and of the low contribution of tension flanges to flexural stiffness. Consequently, it is recommended that for load combinations including seismic actions, the effective flange contribution to stiffness should be 50% of that commonly adopted for gravity load strength design (Paulay and Priestley, 1992).

Pantazopoulou *et al.* (1988) also developed a theoretical model to estimate the effective slab width. These authors proposed an effective slab width on each side of the beam equal to 1.5 times the beam depth up to yielding. For severe earthquake loading, they propose a slab width approximately 3 times the beam depth. Rodríguez and Díaz's (1987) study on

the development of buildings design codes in Mexico highlights the changes regarding slab-participation.

For the numerical analyses herein conducted, and in accordance to the geometrical section properties and to the reinforcing steel quantities previously presented in Chapter 3 (Figures 3.2 and 3.3), a total of seventeen different type-sections (fibre model) were identified and considered in the model. More specifically, eight for the columns and nine for the beams.

From the experimental PsD tests it was calculated a slab-participation width of approximately  $1.00\text{ m}$  (see Section 4.11.3). Therefore, in order to numerically account for the slab-participation,  $1.00\text{ m}$  was considered for the effective flange width  $b_s$  for all beam sections (see Figure 5.20)

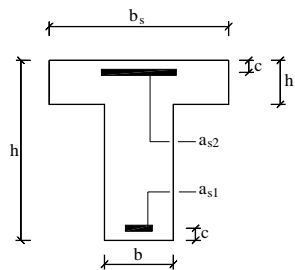


Figure 5.20 - Effective flange width of T-beam

where:  $b$  stands for beam width,  $h$  for beam height,  $b_s$  for slab-participation (if section rectangular:  $b_s = b$ ),  $h_s$  for slab height (if the section is rectangular thus:  $h_s = 0$ ),  $c$  represents the distance from the external beam face to the geometrical centre of the reinforcing steel (concrete cover plus half diameter of the longitudinal reinforcing steel bars;  $4\text{ cm}$  was considered as an average value),  $a_{s1}$  the inferior steel area (positive moment), and  $a_{s2}$  the superior steel area (negative moment).

As recommended by Park and Paulay (1975), in order to account for the contribution of the steel reinforcement existing in the slab, the steel within a width of four times the slab thickness ( $0.60\text{ m}$ ) each side of the beam was included with the tension steel of the beam. The steel detailing of the slab is represented in Figure 5.21.



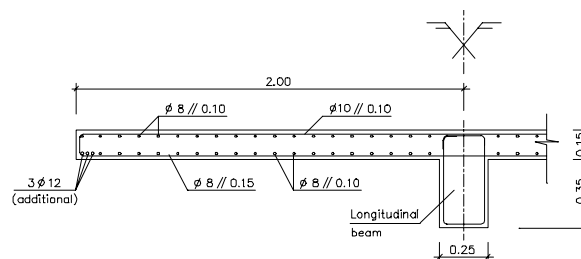


Figure 5.21 - Slab geometry and reinforcement details

### 5.3.7 - Infill masonry modelling

As stated in Section 2.4, the series of earthquakes in Turkey and Greece in 1999 have shown that seismic risk is still high in Europe. These earthquakes also emphasised the vulnerability of masonry infilled structures. In a recent workshop on the mitigation of seismic risk in Europe, Geradin and Pinto (2000), for example, concluded that the most vulnerable buildings to seismic risk are the masonry buildings and the infills of the unprotected frames.

As referred in Eurocode 8, the determination of the seismic effects on the structure shall be based on an idealised mathematical model, which is adequate for representing the actual behaviour. Moreover, the model shall also account for all non-structural elements that can influence the response of the main resisting system. Therefore, the modified response of a RC structure because of the stiffening effect of the infills shall be considered, taking however into account the 'some-how alleatoric' behaviour of the infills, namely the variability of their mechanical properties, the possible modifications of their integrity during the use of the building, as well as the non-uniform degree of their damage during the earthquake itself.

Infilled frame structures consist of brick masonry panels interconnected by a RC horizontal and vertical bracing (Borges and Ravara, 1969). At low levels of in-plane lateral force, the frame and infill panel will act in a fully composite fashion, as a structural wall with boundary elements (Paulay and Priestley, 1992), and the overall stiffness is very high. As lateral deformations increase, the behaviour becomes more complex because the frame attempts to deform in a flexural mode while the panel attempts to deform in a shear mode,

as shown in Figure 5.22-*a*. The result is separation between frame and panel at the corners in the tension diagonal, and the development of a diagonal compression strut in the compression diagonal. A considerable reduction of stiffness occurs. Contact between frame and panel occurs for a length  $z$ , as shown in Figure 5.22-*a*. This was also confirmed during the PsD earthquake tests on the infilled structure (see Section 4.5).

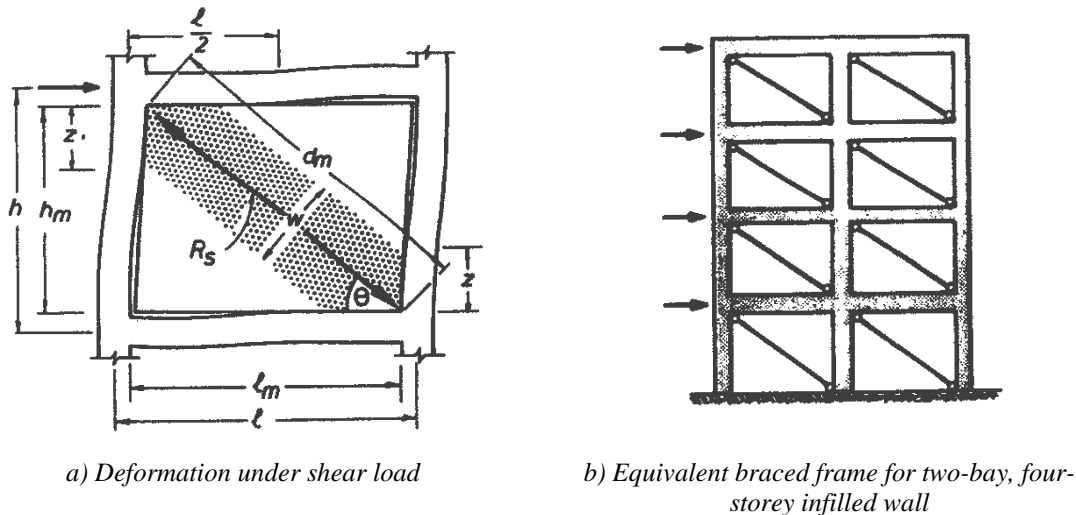


Figure 5.22 - Equivalent bracing action of masonry infill in the frame behaviour (Paulay and Priestley, 1992)

The separation may occur at 50% to 70% of the ideal lateral shear capacity of the infill. After separation, the effective width of the diagonal strut,  $w$  in Figure 5.22-*a*, is less than that of the full panel. Natural-period calculations should be based on the structural stiffness after separation has occurred.

In modelling infilled frames, the structure can be considered as an equivalent diagonally braced frame, where the diagonal compression strut is connected by pins to the frame corners. Figure 5.22-*b* shows the equivalent system for a two-bay, four-storeys frame. Analytical expressions, based on a beam-on-elastic-foundation analogy, have been developed by Stafford-Smith and Carter (1969). Their experimental results show that the effective width  $w$  of the diagonal strut depends on the relative stiffness of the frame and panel, on the stress-strain curves of the materials, and on the load level. However, since a high value of  $w$  will result in a stiffer structure, and, therefore, in a potentially higher seismic response, it is reasonable to take a conservatively high value of

---

$$w = 0.25 \cdot d_m \quad (5.14)$$

where:  $d_m$  is the diagonal length. Paulay and Priestley (1992) advocate that this expression agrees reasonably well with published charts, such as those by Stafford-Smith and Carter (1969), assuming typical masonry-infill properties and a lateral force level of 50% of the ultimate capacity of the infilled frame.

As stated by Paulay and Priestley (1992), there are several different possible failure modes for masonry infilled frames, including: *a*) tension failure of the tension column resulting from applied overturning moments; *b*) sliding shear failure of the masonry along horizontal mortar courses generally at or close mid-height of the panel; *c*) diagonal tensile cracking of the panel (this does not generally constitute a failure condition, as higher lateral forces can be supported by the following failure modes); *d*) compression failure of the diagonal strut; and, *e*) flexural or shear failure of the columns. In many cases, the failure may be a sequential combination of some of the failure modes above. For example, flexural or shear failure of the columns will generally follow a sliding shear failure, or a diagonal compression failure of the masonry.

As recalled by Borges and Ravara (1969), the dimensions and the reinforcement of the bracing system have a direct influence on the value of the force for which rupture occurs. In fact, slender bracing systems concentrate rupture in a small region. On the contrary, a stiff bracing system enlarges the rupture region and, consequently, increases the rupture force. Rupture can be caused not only by the crushing of the panels but also by the forces developed in the surrounding RC frame. The forces in the columns and beams and shear forces near the panel corners can be of particular relevance.

Modelling of infills has bounteous literature: Combescure *et al.* (1995), Oliveira (1995), Schuller *et al.* (1994), Abrams *et al.* (1993), Altin *et al.* (1992), Gavrilovic and Sendova (1992), Zarnic and Tomazevic (1985), Klingner and Bertero (1976) and Fiorato *et al.* (1970), among many others. Since the work performed by Klingner and Bertero (1976), the non-linear analysis of infilled frames is typically performed by replacing each individual panel by two or more diagonal struts with an uniaxial compressive law. Eurocode 8 also considers this model.

In order to model masonry infill panels it was used the strut model (equivalent bi-diagonal struts) represented in Figure 5.23, and implemented by Combescure and Pegon (1996) in CASTEM. The phenomena reproduced by the masonry law are: *a*) the stiffness degradation due to cracking mainly at the surface between the frame and the panel; *b*) the development of plastic strain due to crushing; *c*) the strength degradation under cyclic loading; and, *d*) the pinching associated with sliding. The behaviour law is described hereafter, considering positive strain and stress values for compression. In short, it is a general multi-linear model, which accounts for cracking, compression failure and strength degradation due to either monotonic or cyclic loading as well as for the pinching effects due the crack closing.

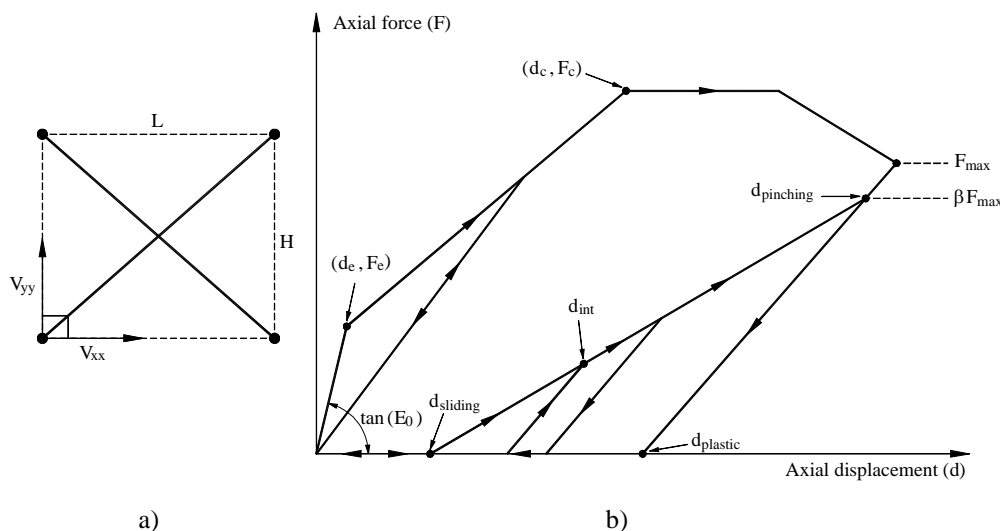


Figure 5.23 - Equivalent strut for the infill masonry model: a) geometric support of the strut diagonals; b) envelope and cyclic curves of the uniaxial behaviour law (Combescure and Pegon, 1996)

The model used assumes no tensile resistance, and the behaviour for monotonic compression is described by a multi-linear curve including a primary linear elastic behaviour, a second branch approximating the cracking process, and two final branches representing two phases of the masonry behaviour, which can be considered as plastic behaviour (crushing of the masonry panel) with positive and subsequently negative strain hardening. Cyclic behaviour is characterised by a linear unloading-reloading law without plastic displacement in the primary branches, before attaining the plastic point ( $d_c, F_c$ ). This hysteretical behaviour, after having reached the plastic point, is also governed by a multi-linear curve with specific rules to account for plastic deformations ( $d_{plastic}$ ), crack

closing ( $d_{sliding}$ ), and strength degradation ( $d_{pinching}$ ). Comberscure and Pegon (1996) provide full details on the cyclic behaviour model.

The equivalent axial stiffness and strength of each diagonal strut were calculated according to the empirical expressions suggested by Zarnic and Gostic (1998, 1997). This empirical model was already described in Section 3.4.4.1.

As already said, the infill panels in the investigated building were made from hollow bricks of 12 *cm* thickness laid with cement-lime mortar. Specimens were prepared in the laboratory by stacking five bricks joined with similar mortar, and tested under compression. The mean gross compressive strength obtained was 1.1 *MPa* and the mean modulus of elasticity was 991 *MPa* for the direction parallel to the holes, and 1873 *MPa* for perpendicular. A detailed description of the masonry properties has been provided in Section 3.4.3. The mechanical properties experimentally evaluated and empirical parameters for the Zarnic and Gostic (1998, 1997) model listed in Table 5.6 were considered in the numerical analyses. The meaning of these parameters was also given in Section 3.4.4.1.

Table 5.6 - Parameters for the Zarnic and Gostic numerical model

$C_R$	$\nu$	$\mu$
0.9	0.05	2.5

The structure has twelve infill panels, being each panel modelled by two diagonal struts. Therefore, twenty-four strut elements constitute the masonry mesh in the model, as represented in Figure 5.24. According to the presence, dimensions and location of the panel aperture in the infilled frame, four different infill panels, including three of them with apertures, can be identified. Strength and stiffness reduction for each panel due to the presence of apertures were modelled according to the methodology given in Section 3.4.4.2.

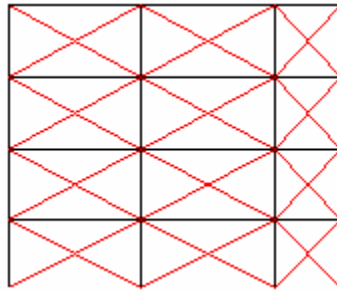


Figure 5.24 - Model of the plane infilled frame

### 5.3.8 - Retrofitting solutions modelling

One of the retrofitting solutions studied in the preliminary analysis was based on a strategy to improve the structural damping of the bare and infilled structures. More specifically, it was proposed to use a bracing system with rubber dissipation devices, which can increase stiffness and damping of the system, consequently reducing the deformation demands. This retrofitting solution was not experimentally verified but just numerical simulations were carried out. Section 5.3.8.1 provides details on this retrofitting technique and summarises the main results. It is underlined that the modelling of this solution is similar to the K-bracing with shear-link.

Another retrofitting technique that was successfully tested is based on the selective strengthening philosophy and was also numerically simulated. Relevant details on the modelling are presented in Section 5.3.8.2.

#### 5.3.8.1 - X- and K-bracing with dissipator retrofitting

Two alternative layouts were proposed for the bracing. One located in the central bay (K-bracing, see Figure 5.26), which leads to better distribution of the storey forces but interferes with the existing openings door and windows, and the other located in the shorter-external bay (X-bracing, see Figure 5.27).

The design of the bracing system, including the dissipation devices, was performed assuming 1% drift (27 mm inter-storey drift) as the ultimate limit state for the frame (see Griffith, 1999-a). It was also assumed that for these deformation levels the effects of the

infill panels are negligible. Furthermore, it was assumed that the peak base-shear strength of the frame for 1% drift was 150 kN, and that the effective stiffness (secant stiffness) of the equivalent SDOF system with the mass located at 2/3 of the total height of the building leads to a period ( $T_s = 1.8 \text{ sec}$ ).

The design displacement spectra for the different damping ratios were derived from a basic 5% damping (assumed to increase linearly from 0 for  $T = 0 \text{ sec}$ , to 200 mm for  $T = 2 \text{ sec}$ , and being constant for higher periods) using  $\sqrt{5/\xi}$  as 'correction factor'.

For a 50-years period non-exceeding probability of 10%, a device with the properties given in Table 5.7 is required on each storey (see also Figure 5.25).

Table 5.7 - Properties of the energy dissipation devices

1% ID	Location <sup>a</sup>	DLF	$F_u$ (kN)	$D_u$ (mm)	$F_y$	$K_1$
10% non-exceeding probability	storeys 1 2	0.35	80	25	$F_u / 3$	$K_0 / 10$
	storeys 3 4		50	25		

Energy dissipation device loss factor - DLF

$$DLF = \tan \delta; \delta = \sin^{-1} (2W/(\pi \Delta W))$$

$W$  – area surrounded by the hysteresis loop

$\Delta W$  – half of the area of the rectangle that inscribes the hysteresis loop ( $= 2F_{max} \cdot D_{max}$ )

Note: The devices are able to accommodate displacements and forces up to 140% of their nominal capacity ( $F_u, D_u$ )

a) One device per storey (see Figures 5.26 and 5.27).

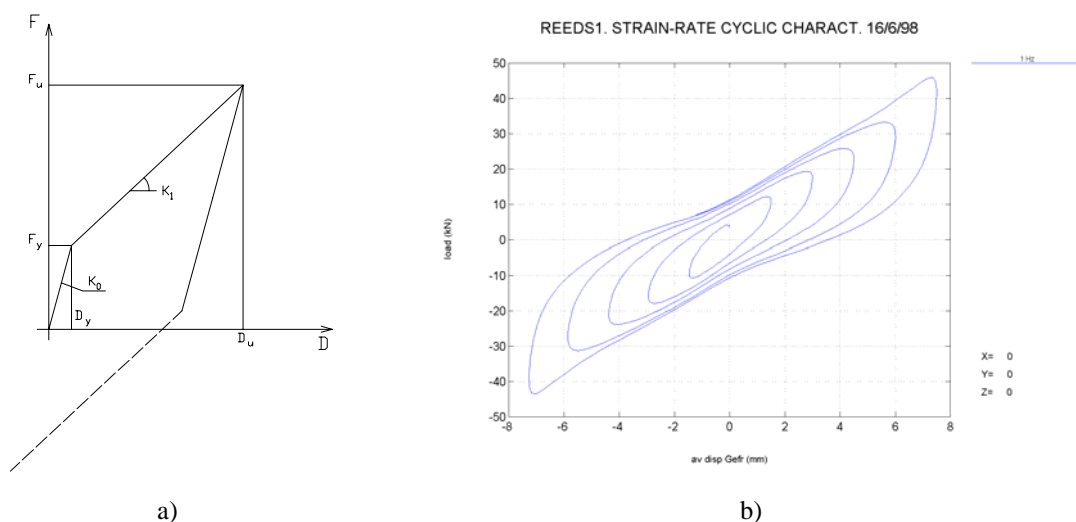


Figure 5.25 - Typical diagrams for a device: a) schematic, and b) typical diagram for a device tested at ELSA in the framework of the project REEDS (Molina *et al.*, 2000-a)

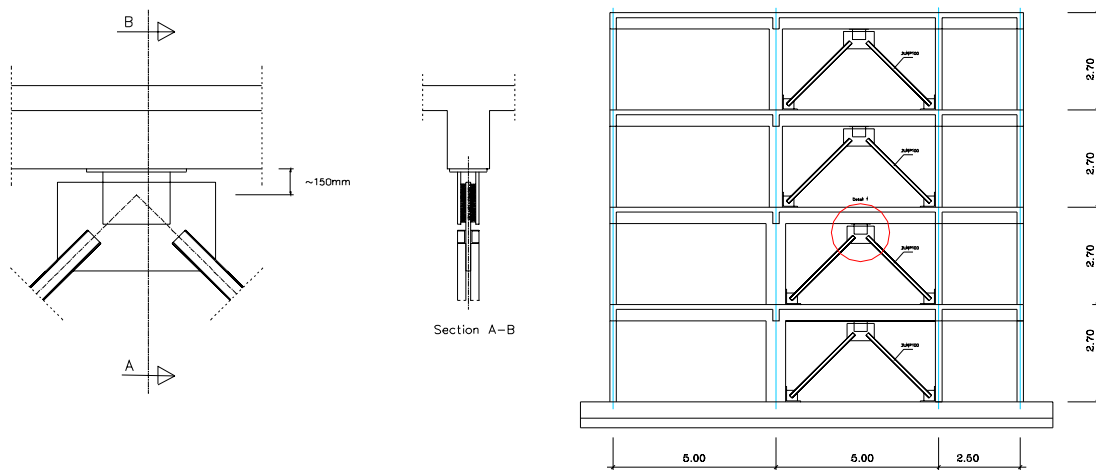


Figure 5.26 - Bracing system in the central bay: device details and general layout

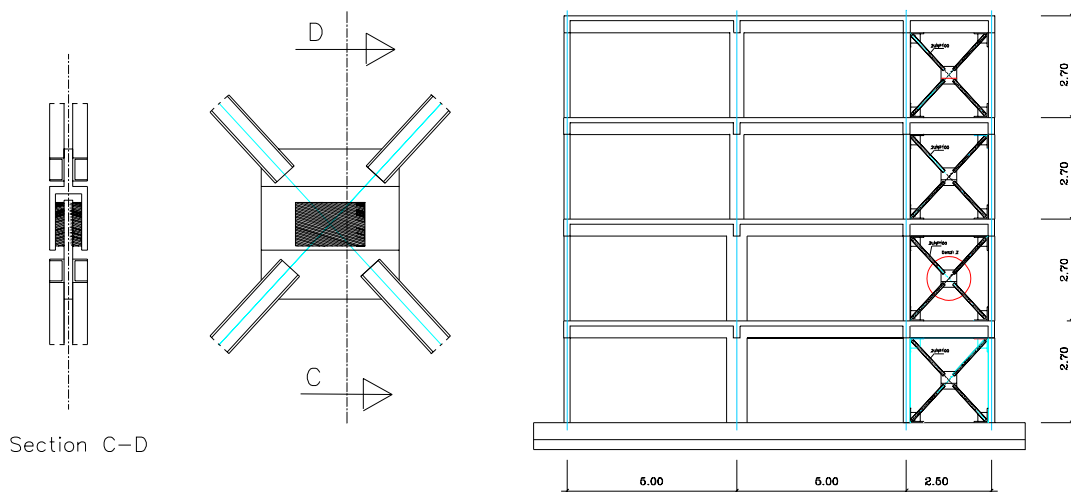


Figure 5.27 - Bracing system in the shorter-external bay: device details and general layout

The bracing system was simulated by bar elements (bracing), and a non-linear spring element was used to model the dissipator. As schematically represented in Figure 5.25-a, a bi-linear model simulated the dissipators. The steel uniaxial model was used to represent the constitutive uniaxial law of the dissipator, setting the model parameters according to the relevant requirements, namely a sharp transition between the linear and the 'post-yielding' curves and the tangent of the asymptotic curve defining the post-yielding range.

In Figures 5.28 and 5.29 are represented for the original bare and infilled frames, both with and without retrofitting, the vulnerability functions obtained in the preliminary analyses for increasing input motion of the top-displacement, base-shear and total energy dissipation.



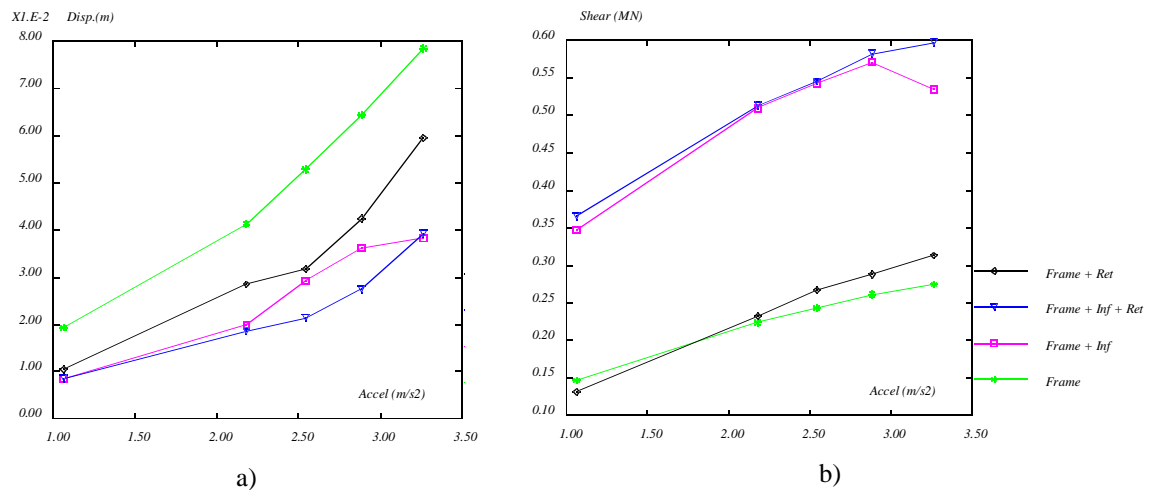


Figure 5.28 - Vulnerability functions: a) top-displacement; b) base-shear

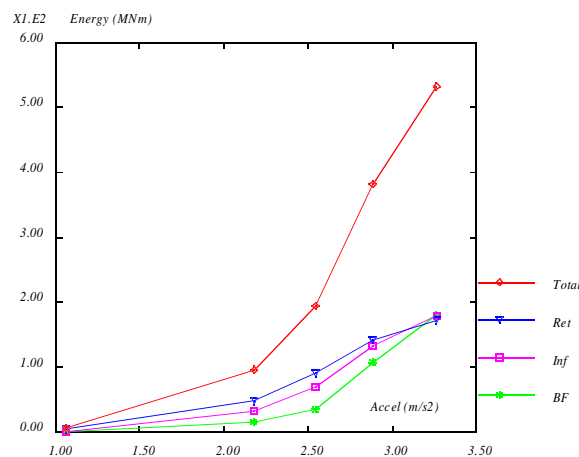


Figure 5.29 - Evolution of energy dissipation

The numerical analyses for the retrofitted frame case (K- and X-bracing with rubber dissipator) allow us to conclude that:

- The numerically studied light retrofitting solution seems to be effective for low, medium and high intensities, but not particularly effective for very high intensities when infill panels exist. This retrofitting system was designed for the bare frame and it is very effective for this case. However, a more accurate design shall consider the infill panels.
- The retrofitting system leads only to a small increase of storey shear forces.

- Important increase on energy dissipation capacity was observed. The contribution of the RC frame, of the infill panels and of the retrofitting devices to the total energy dissipation was approximately equal.

#### 5.3.8.2 - *Selective strengthening*

It was found a scarcity of rules and recommendations as well as of numerical models for modelling upgraded structures previously damaged by earthquakes. The insufficient experimental work and the difficulty in modelling the interaction and compatibility between existing elements and added retrofit ones might contribute to this circumstance. Compared to previous work, the numerical analysis conducted in this thesis models more precisely the sequence of damage and retrofitting.

Figure 5.30 represents the steps followed to model the sequence of loading and retrofitting applied to the non-infilled frame in the numerical analyses (static loading, earthquake input motions on the original structure, repair and strengthening, and finally, new earthquake input motions on the strengthened structure, see also Table 3.1).

Firstly, it were calculated the initial stresses and strains in the structure' elements with the dead and live loads (step 1).

Afterwards (step 2), in order to introduce in the numerical frame model a damage distribution corresponding to that observed experimentally during the previous damageable earthquake series (bare frame PsD earthquake tests), it were imposed increasing cyclic displacements. It was imposed a cyclic distribution of lateral displacements (storey displacement profile) up to the maximum inter-storey drift profile reached in the earthquake PsD tests of the non-retrofitted frame structure. The imposed displacement time-histories are composed by series of two equal complete symmetric cycles for displacement levels corresponding to 25%, 50%, 75% and 100% of the maximum storey displacement in the BF tests, as schematically represented in Figure 5.30. The maximum inter-storey drift for the PsD tests on the BF were 0.63%, 1.03%, 2.41% and 0.91%, for the 1<sup>st</sup> to 4<sup>th</sup> storeys, respectively. These values were given in Table 4.1 and are recalled in Figure 5.30.

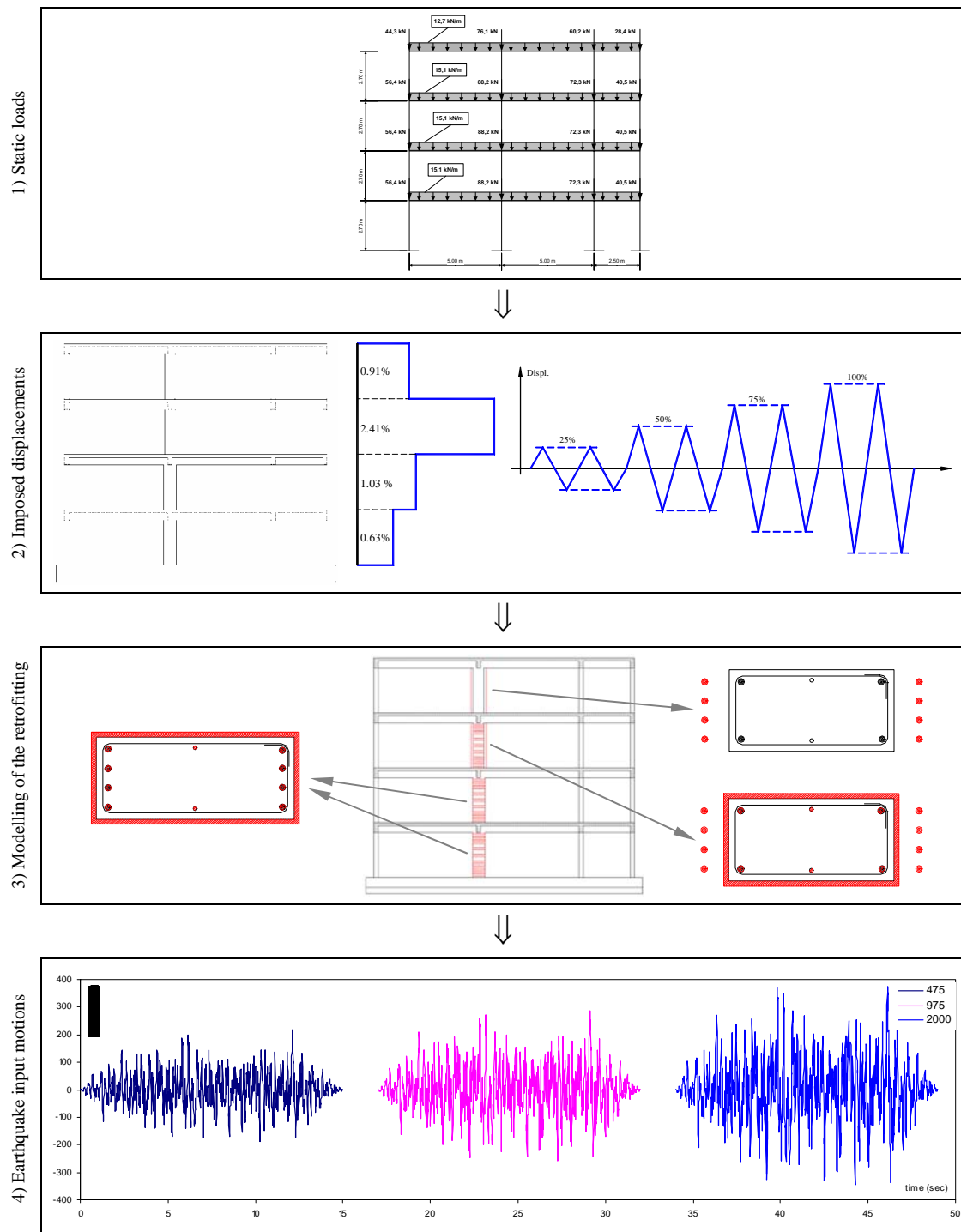


Figure 5.30 - Loading and modelling sequence for the SR numerical analyses

After accounting for the damage induced by the PsD tests, the repair and strengthening interventions are modelled (strengthened frame) at section level as represented in step 3 of Figure 5.30. An improved confinement effect of the strong-column at the first three storeys

is activated in the model of the strengthened structure accordingly to the scheme presented in Figure 5.30, where are presented the cross-section strengthening details (see also Section 3.3). It is assumed that the repair operations in the strong-column reinstate the original capacity of the concrete. Therefore, after the cyclic tests, the concrete properties for the strong-column are changed to the original non-damaged ones. As the reinforcing steel was not replaced, the steel properties are not altered. The parameters to model the retrofitting solutions adopted; i.e. improved ductility, flexural and shear strength of RC strong-column, are accurately estimated using the empirical formulas (see Pinho and Elnashai, 1999) in combination with measurements on the full-scale tests. For the remaining columns and all the beams, the damaged state for the steel and concrete was induced by the cyclic imposed displacements.

Finally, in step 4, the strengthened structure was numerically modelled, considering the same earthquake input motions as in the experimental test series on the SR.

### **5.3.9 - Vertical static loads, earthquake actions, masses and damping**

For the numerical analyses, constant vertical distributed loads on beams and concentrated loads on the column nodes were considered in order to simulate the dead load other than the self-weight of the frame (live-load, weight of partitions and finishings). Figure 3.7 gives details of the vertical static loads applied to the test experiments and considered in the numerical analysis.

The artificial accelerograms used in the PsD earthquake tests are also considered in the numerical analyses. It were considered accelerograms with 15 seconds duration and peak accelerations of 0.22g, 0.29g and 0.38g for 475, 957 and 2000 years return period, respectively (see Table 3.9 and Figure 3.8).

To assure that the numerically simulated structure considers the same conditions as in the PsD tests, the mass of the structure was assumed condensed at the storey level. Floor masses of 44.6 ton and 40.0 ton were considered for the three first storeys and for the roof storey, respectively. These masses were assumed to be uniformly distributed on the floors, and correspond to the weight of the slabs, beams, columns, masonry infill walls and

finishings, as well as to the correspondent quasi-permanent value of the live loads (as presented in Section 3.2.6). The mass matrix of the structure is diagonal.

A viscous damping ratio of 1.5% was considered in the numerical analysis for each mode of vibration. This value is smaller than those normally used in the linear dynamic analyses. This follows from considering that the damping values measured in real buildings increase with increasing amplitude of vibration mainly due to hysteretic phenomena (hysteretic damping) and not just to viscous forces (viscous damping). On the other hand, as referred by Tilly (1986), the values measured for small amplitude vibration are not much different from 1.0%. Thus, the adopted value for the damping of 1.5% is considered to represent the viscous component, while the hysteretic component is taken into account by the non-linear models of the structural members and components. As observed by Duarte and Campos-Costa (1988), this approach would be perhaps not totally adequate for vibrations with amplitudes bellow the elastic limits. Nevertheless, considering that in the present analysis a non-linear concrete model is activated from the beginning, and that much larger deformation amplitudes are expected, this value is judged to reproduce fairly well the reality.

The damping matrix,  $[C]$ , adopted in the experiments was also considered in the numerical analysis. Damping matrix was computed assuming Rayleigh damping and considering 1.5% damping ratio for the first two periods, for each structure, according with

$$[C] = \alpha \cdot [M] + \beta \cdot [K] \quad (5.15)$$

where the coefficients  $\alpha$  and  $\beta$  are calculated such that 1.5% damping ratio in the first two modes of vibration is achieved.  $[M]$  and  $[K]$  are the mass and stiffness matrices of the structure, respectively.

### 5.3.10 - Shear strength verification for the bare frame

The fibre model is able to reproduce the non-linearity due to flexural and axial deformations. However it does not consider the non-linear shear behaviour. The model considers axial stress versus strain constitutive laws uncoupled with linear elastic shear behaviour at each fibre. The basic assumption is that plane sections remain plane

(Bernoulli's kinematic) allowing to consider a uniaxial behaviour of each fibre. This is no longer satisfactory when shear strains take a major role. In this particular case, shear strains have to be introduced in the model. However, in the studied frames shear failure did not occur except at the extremities of the third storey strong-column at the end of the 975-yrp earthquake test (see Section 4.2.2).

Since the inelastic frame models are based on flexural capacities of the frame members, it is implicitly assumed that the shear capacities of the members are sufficient to develop flexural hinging. This assumption is verified here by performing shear control in the critical members of the columns. Maximum calculated values of the shear forces developed in the columns for the BF structure are summarised in Table 5.8.

Table 5.8 - Maximum calculated shear forces ( $kN$ ) in columns (BF calculations)

Storey	Column alignment			
	1	2 (strong-column)	3	4
4	11.14	53.82	11.55	8.34
3	20.77	100.42	21.71	15.42
2	25.30	148.85	30.27	19.17
1	28.80	203.84	33.42	21.82

Code equations for shear strength are excessively conservative, in many cases, and show a wide scatter when used to predict test results (CEB-240, 1998). As recommended in the CEB-240 (1998), the columns shear strength should be assessed using a more realistic formulation, than those incorporated in design codes, and it should reflect the dependence of shear strength on flexural ductility. Therefore, in this study, shear capacities of the columns are calculated by using the model proposed by Priestley and Xiao (1994). The shear strength of the columns  $V_R$  can be computed as the sum of the contributions of concrete  $V_c$ , steel  $V_s$  and the horizontal component of the inclined axial force  $V_p$

$$V_R = V_c + V_s + V_p \quad (5.16)$$

For the columns, rectangular cross sections with dimensions  $b$  and  $d$  are considered (see Table 5.1). The shear carried by the concrete is calculated from the equation

$$V_c = 0.8 \cdot b \cdot d \cdot k \cdot \sqrt{f_c} \quad (5.17)$$

where the value of  $k$  depends on the curvature ductility demand and varies from 0.29 to 0.05 (see Priestley, 1997; Priestley and Xiao, 1994),  $f_c$  is the mean compressive concrete strength (is taken as the measured value of 16 MPa, see Section 3.2.5).

The shear carried by the 6 mm diameter shear reinforcement stirrups at 15 cm spacing ( $s$ ) at the rectangular columns are calculated from the expression

$$V_s = \frac{d \cdot A_{sw} \cdot f_{yw}}{s} \quad (5.18)$$

where  $f_{yw}$  equals 343.6 MPa, the mean yielding stress of the steel (see Table 3.8), and  $A_{sw}$  is the cross sectional area of the shear reinforcement crossing the inclined shear crack.

The contribution of the inclined axial force, considered only for the strong-column and calculated by Combescure (2000), is based on the assumption that part of the shear is transmitted by the axial force, which can be represented by an inclined strut with an angle  $\alpha$  (Priestley, 1997)

$$V_p = P \cdot \tan \alpha \quad (5.19)$$

For the columns, the sum of the two shear strength components (three for the strong-column), listed in Table 5.9, guarantees the demanded shear capacities for the BF structure, given in Table 5.8. Therefore preventing shear failure, even when the flexural ductility demand becomes high. As already observed by Combescure (2000) for the slender-columns, the contribution of concrete and steel is sufficient to resist to the shear demand. The risk of shear failure of the strong column is minor for the BF structure. Although being insufficient the contribution of the concrete and steel, the inclination of the axial force increases significantly the shear strength of the columns (see Table 5.9), as verified during the PsD tests.

Table 5.9 - Maximum estimated shear strength ( $kN$ ) of the columns

Storey	Ductility demand	Column alignment			
		1	2 (strong-column)	3	4
4 <sup>th</sup>	low	80.12	190.05	80.12	65.27
	high	30.96	101.73	30.96	28.40
3 <sup>rd</sup>	low	80.12	220.05	80.12	65.27
	high	30.96	131.73	30.96	28.40
2 <sup>nd</sup>	low	80.12	317.96	80.12	65.27
	high	30.96	210.44	30.96	28.40
1 <sup>st</sup>	low	80.12	359.96	80.12	65.27
	High	30.96	252.44	30.96	28.40

#### 5.4 - NATURAL FREQUENCIES AND VIBRATION MODES

Well-established experimental techniques are available for determining the dynamic characteristics of structures. Moreover, numerous experimental and analytical determinations of natural frequencies of buildings have been performed. As argued by Borges and Ravara (1969), the comparison between experimental and analytical frequencies results allows the validity of the mathematical model, in the linear range, assumed to represent the structure to be assessed.

Computations of the elastic initial natural frequencies and of the corresponding mode shapes were performed with CASTEM. The four initial (undamaged) natural frequencies of the plane frame were numerically calculated and the obtained values for the bare and infilled frames are summarised in Figure 5.31, as well as, the shape of the first four natural vibration modes for the bare and infilled frames. The computed frequencies are compared with the experimentally obtained values.

Comparing the experimental frequencies measured before the PsD earthquake tests (see Tables 3.28 to 3.30) to the frequencies evaluated with the numerical model (Figure 5.31) a very good agreement was observed. From the results, it can be concluded that:

- The frequencies computed for the BF and IN frames are in accordance to the experimentally measured values (see Tables 3.28 to 3.30). This constitutes a first



confirmation of the model validity. For the BF structure, the eigenfrequencies calculated and experimentally measured coincide.

- The values of the eigenfrequencies registered in the tests on the IN frame for the four modes are slightly higher than those numerically obtained. For the first mode, the difference between them is 2% but it increases for higher modes (8%, 15% and 39% difference for the subsequent modes).
- The inclusion of the infill panels increases substantially the global stiffness of the structure, and, consequently, increases the modal frequencies, as can be observed in Figure 5.31. The ratio between the natural frequency for the infilled frame and for the bare frame for the first mode is 4.52. Experimental tests performed by other authors (e.g. Vintzeleou, 1987) confirm that this ratio usually assumes values between 3 and 5.

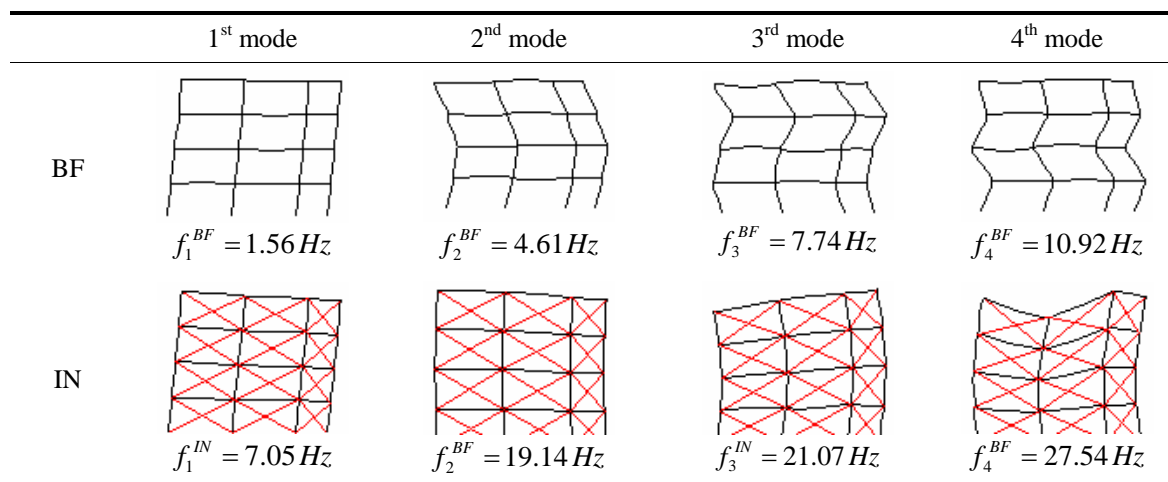


Figure 5.31 - Natural first four modal frequencies and mode shapes numerically evaluated for the BF and IN structures

## 5.5 - NUMERICAL PREDICTIONS OF THE PSEUDO-DYNAMIC TESTS

Each frame, with and without infill masonry walls, was pseudo-dynamically tested for increasing input motion intensities. Each PsD earthquake test was preceded by a predictive numerical calculation of the structural response. In this section, the relevant objectives of the predictive analyses are exposed. These calculations were performed with the models

and parameters described in the previous sections. The aim of the preliminary numerical studies were:

- To predict the response of the structures, and to establish which failure mechanisms are most likely to occur under seismic loading.
- To define an appropriate testing programme (testing sequence).
- To select the zones in the structure, where more damage is expected, and therefore, decide the density of the instrumentation to be used, in order to catch the local behaviour.
- To design the experimental test devices, actuators, load cells and instrumentation (transducers and inclinometers). Particularly, the capacity of load actuators (in terms of displacement and force) was defined from the maximum lateral storey capacity and deformation estimated. The capacity of each inclinometer or relative displacement transducer was selected based on the maximum deformation expected on the region it will be installed. The measurement capacity of the inclinometers located at the columns was five degrees, and for the beams and joints one degree. The measurement capacity of the relative displacement transducers for each location (slab, strong-column and beams) was defined from maximum deformation estimated with the preliminary analyses.
- To estimate the maximum forces, displacements and other parameters needed in the control system for the PsD and cyclic tests.
- To assist in the definition of suitable retrofitting solutions for the bare and infilled structures.

A comparison between experimental results and analytical predictions is not conducted here. Details on this comparison can be found in Varum *et al.* (2000; 1999). The comparison of the preliminary results with the experimental ones enabled to detect the inadequacies of the available numerical models, which were then improved for the posterior analysis (presented in Section 5.6).

## 5.6 - RESULTS OF THE NUMERICAL NON-LINEAR DYNAMIC ANALYSES

Using the implemented numerical models described in Section 5.3, the behaviour of the bare, selective strengthened and infilled frames were modelled. Reinforcement details of the beams and columns and material properties were used for the inelastic modelling. The used fibre model considers a rectangular cross-section for the columns and a T-beam to represent the girders. In the numerical analyses, the column bases of the first storey were fixed. Geometrical and material properties were chosen to be as close as possible to those of the tested structures.

The non-linear response of the RC frames was computed for each earthquake input motion applied in the pseudo-dynamic tests, as summarised in Table 5.10.

Table 5.10 - Non-linear dynamic analyses of the BF, SR and IN structures

Structure	Earthquake input motion
Bare	475-yrp + 975-yrp <sup>a</sup>
Selective strengthened	475-yrp + 975-yrp + 2000-yrp
Infilled	475-yrp + 975-yrp + 2000-yrp <sup>b</sup>

a) 7.5 seconds of the original 975-yrp earthquake.

b) 5.0 seconds of the original 2000-yrp earthquake.

Earthquakes of 15 seconds duration and increasing return periods, corresponding to 475, 975 and 2000-yrp, were applied to the frames. During the PsD tests, collapse was observed at 7.5 seconds of the 975-yrp earthquake for the bare frame, and at 5.0 seconds of the 2000-yrp earthquake for the infilled frame. Therefore, the numerical analyses were performed for the earthquake input motions given in Table 5.10. In the results analysis, the accelerograms will be systematically referred as their return period value in years.

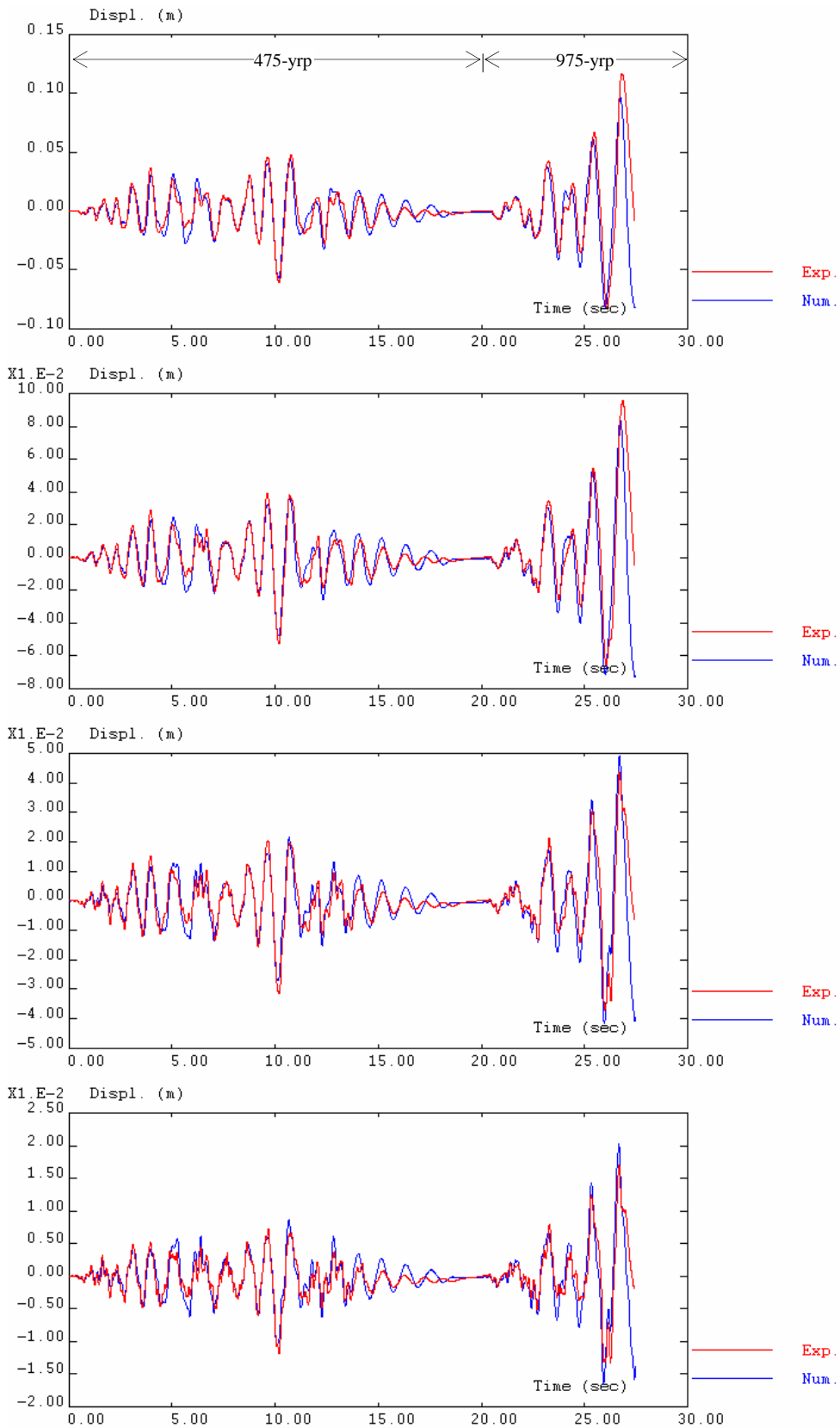
Time history analyses were performed for the original bare, strengthened and infilled frames. The following Sections 5.6.1, 5.6.2 and 5.6.3 highlight the main results of these numerical analyses. The numerical results comprise: *i*) time-histories of storey displacements, inter-storey drift and storey shear; *ii*) curves storey shear-drift and base-shear versus global-drift; *iii*) maximum drift and shear profiles; and, *iv*) energy dissipated at storey level and total dissipated energy. The post test non-linear numerical analyses are discussed and compared to the results of pseudo-dynamic tests.

### 5.6.1 - Bare frame numerical results

Figures 5.32, 5.33 and 5.34 provide the time histories (experimental PsD results and numerical calculations) of storey displacements, inter-storey drift and storey shear for the bare frame (BF). Figure 5.35 shows the computed and the experimentally measured relations between storey shear-force and inter-storey drift at storey level (shear-drift hysteresis diagrams). Figure 5.36 shows the evolution of the dissipated energy at storey level for the bare frame. In Figure 5.37 are represented the numerical and experimental curves of base-shear versus top-displacement, while Figure 5.38 contains the evolution of the total energy dissipated in the structure. Figures 5.39 and 5.40 show the distribution of maximum inter-storey drift and shear profiles of the BF.

Comparing the non-linear dynamic numerical results for the BF structure to the experimental ones, the following main conclusions can be drawn:

- It is found that the available non-linear fibre type models have serious limitations for the realistic prediction of the dynamic behaviour of existing RC structures. In fact, only with the inclusion of the bond-slip effect in the numerical models it was possible to reproduce well the experimental tests.
- The numerical results confirm the high vulnerability of the existing RC structure already experimentally observed. In fact, it was demonstrated that in spite of the very limited inter-storey drifts for the 475-yrp earthquake, the demands for a slightly higher intensity earthquake (1.3 times the reference earthquake, in terms of peak acceleration) led to much larger inter-storey drifts.
- The numerical model for the bare frame was able to reproduce quite well the experimental results, not only in relation to the storey shear and inter-storey drift evolutions, but also in relation to the dissipated energy in each storey.

Figure 5.32 - BF: storey displacement time histories (4<sup>th</sup>, 3<sup>rd</sup>, 2<sup>nd</sup> and 1<sup>st</sup> storeys)

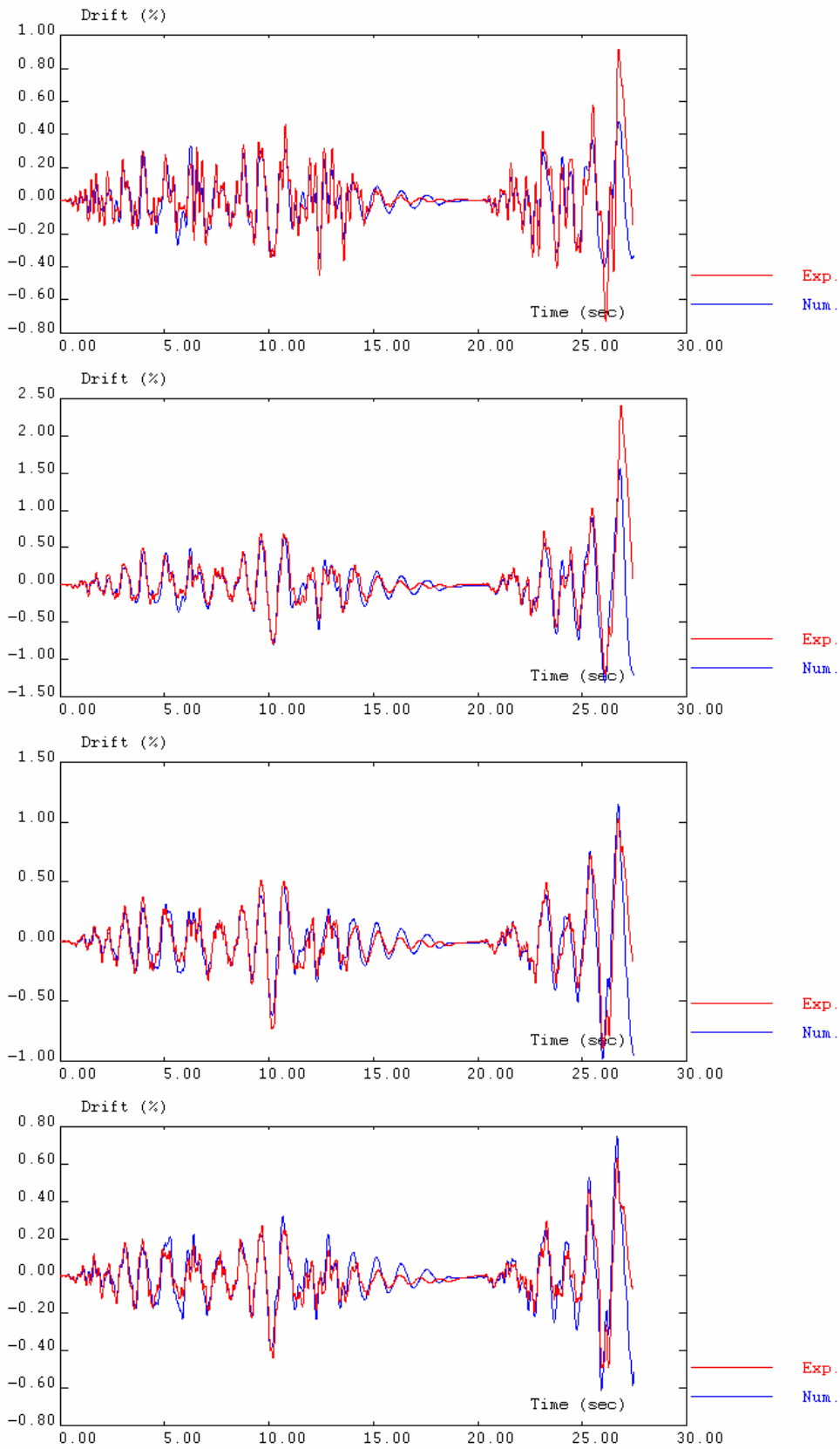
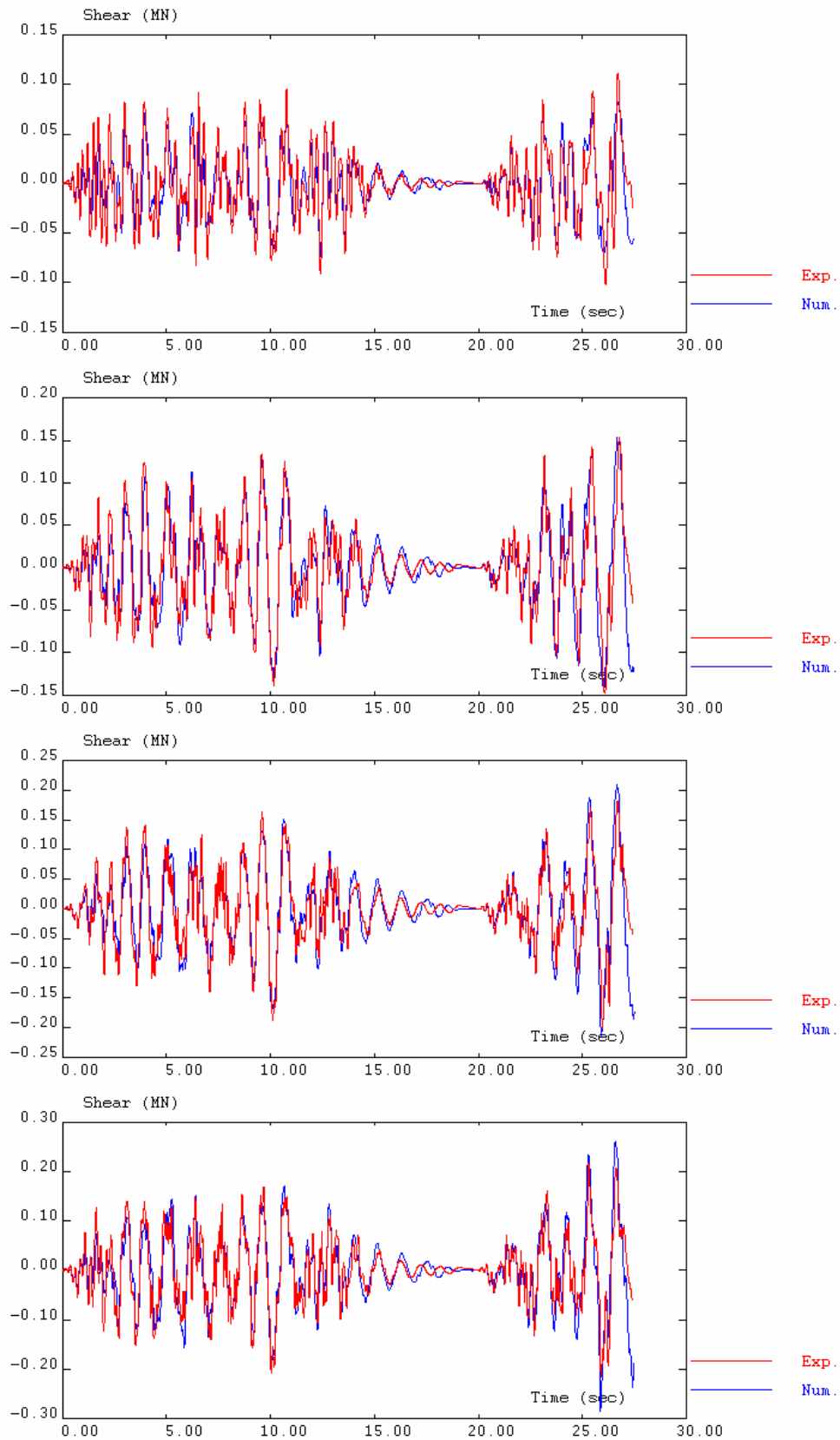


Figure 5.33 - BF: inter-storey drift time histories (4<sup>th</sup>, 3<sup>rd</sup>, 2<sup>nd</sup> and 1<sup>st</sup> storeys)

Figure 5.34 - BF: storey shear time histories (4<sup>th</sup>, 3<sup>rd</sup>, 2<sup>nd</sup> and 1<sup>st</sup> storeys)

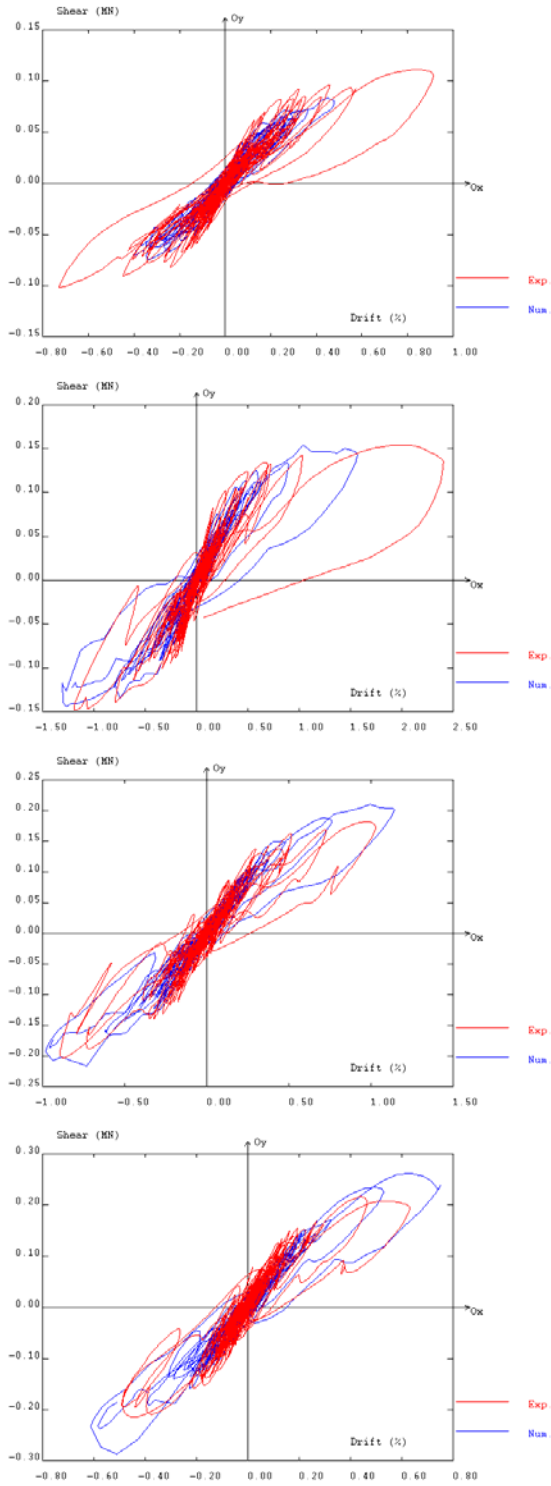


Figure 5.35 - BF: storey shear versus inter-storey drift (4<sup>th</sup>, 3<sup>rd</sup>, 2<sup>nd</sup> and 1<sup>st</sup> storeys)

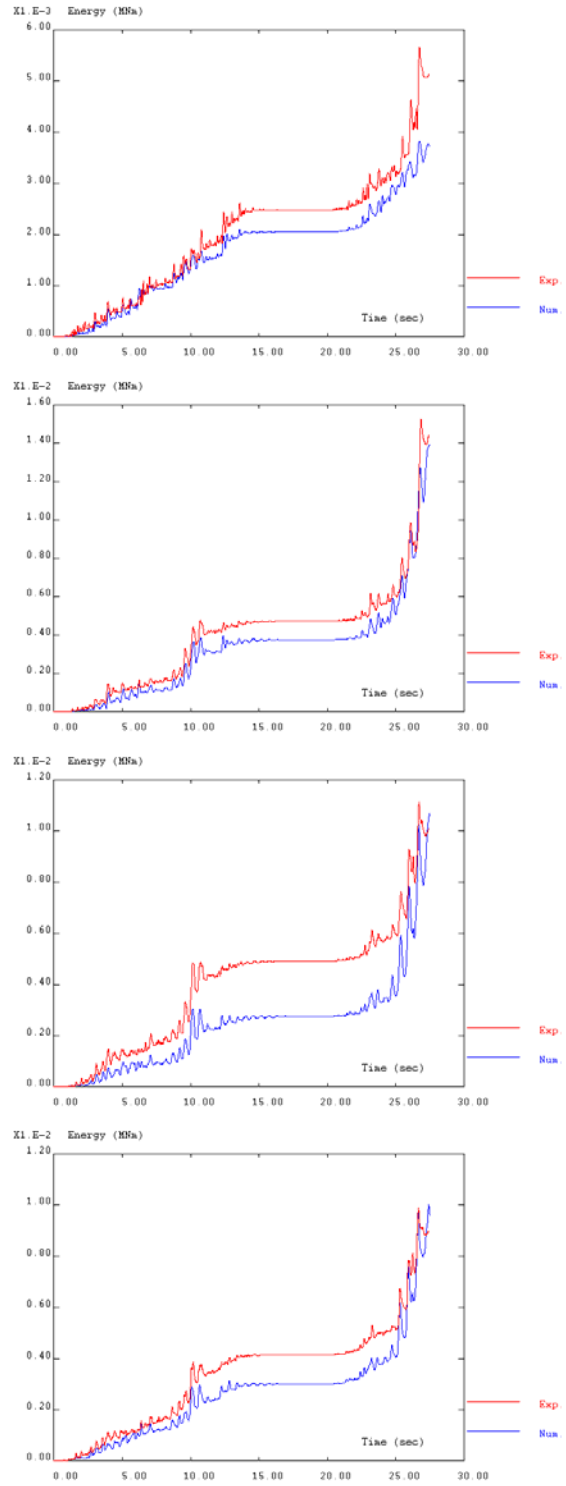


Figure 5.36 - BF: dissipated energy at storey level (4<sup>th</sup>, 3<sup>rd</sup>, 2<sup>nd</sup> and 1<sup>st</sup> storeys)



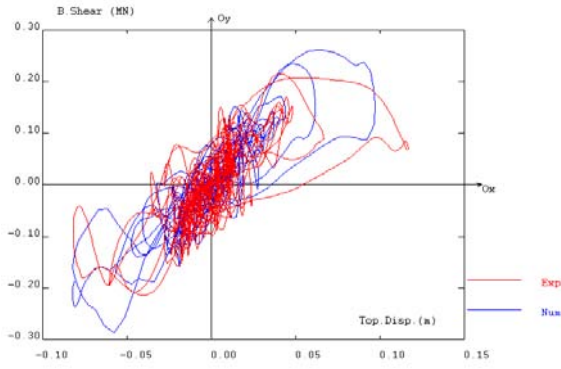


Figure 5.37 - BF: base-shear versus top-displacement

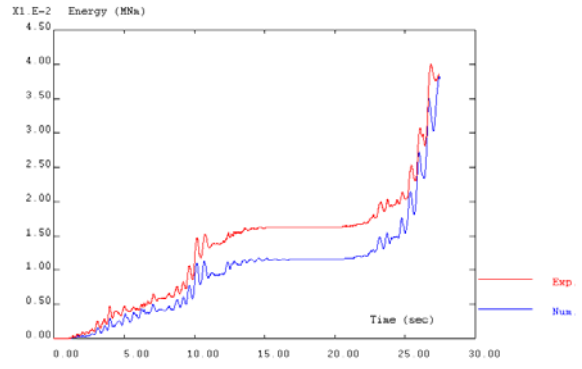


Figure 5.38 - BF: total dissipated energy

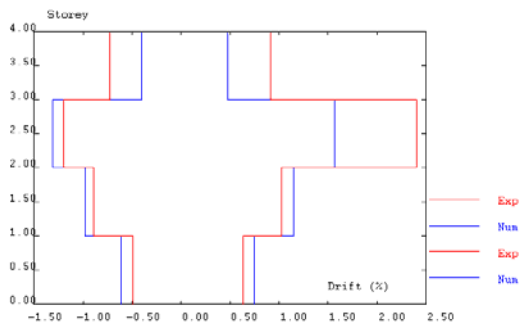


Figure 5.39 - BF: maximum drift profile

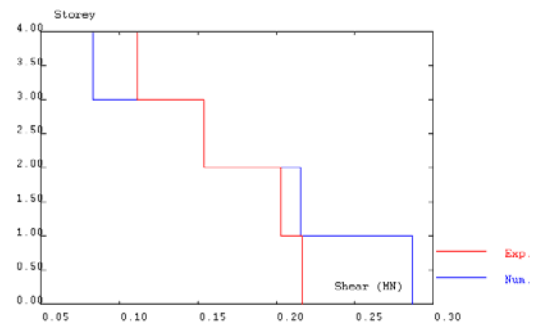


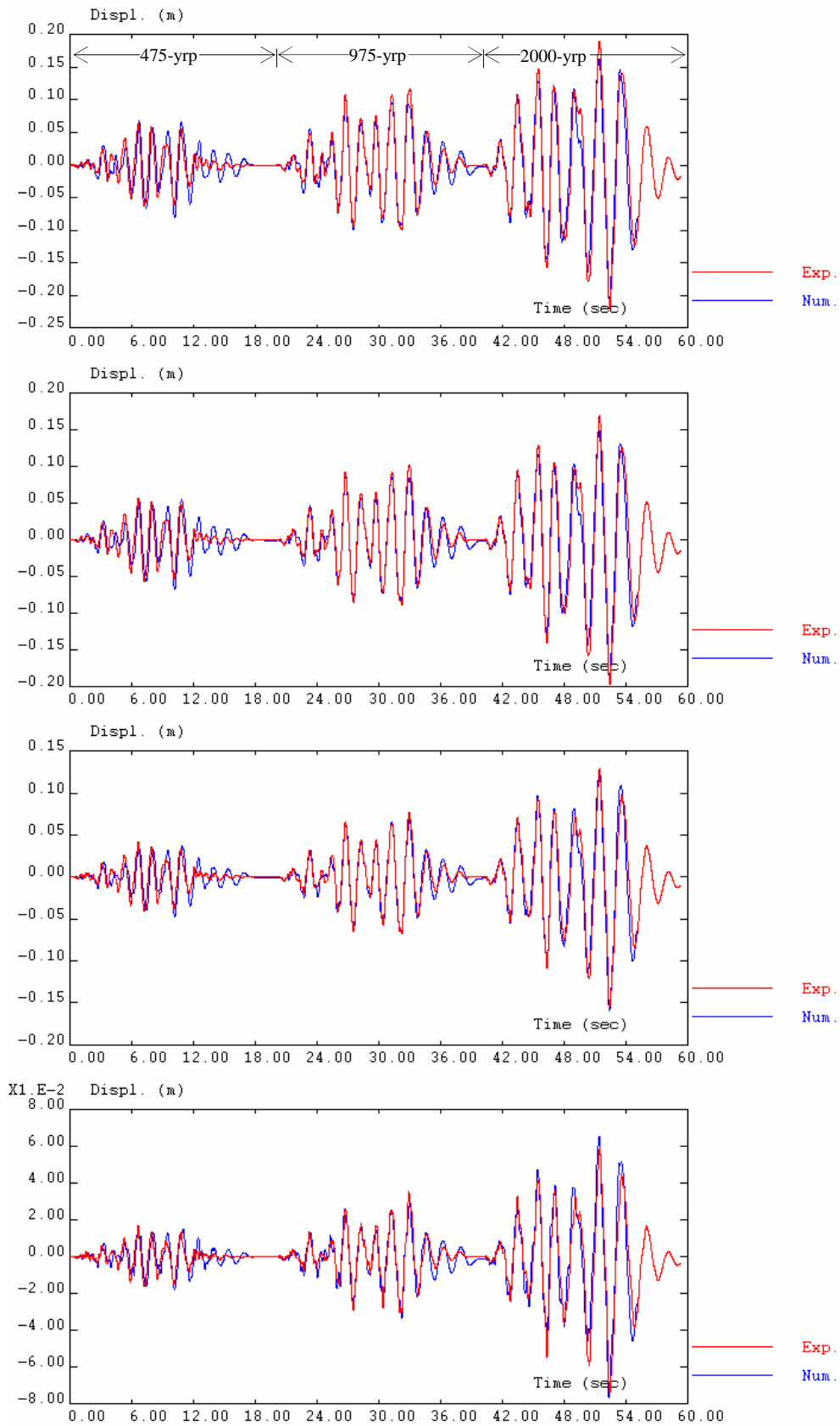
Figure 5.40 - BF: maximum shear profile

### 5.6.2 - Strengthened frame numerical results

Figures 5.41, 5.42 and 5.43 give the experimental and numerical time histories of storey displacements, inter-storey drift and storey shear for the strengthened frame (SR). Figure 5.44 shows the computed and the experimentally measured relations between storey shear force and inter-storey drift at storey levels (shear-drift hysteresis diagrams). Figure 5.45 shows the evolution of the dissipated energy at storey level of the strengthened frame. In Figure 5.46 are represented the numerical and experimental curves of base-shear versus top-displacement, while Figure 5.47 contains the evolution of the total energy dissipated in the structure. Figures 5.48 and 5.49 show the distribution of maximum inter-storey drift and shear profiles for the SR case.

Comparing the non-linear dynamic numerical results for SR structure to the experimental ones, the following main conclusions can be drawn:

- The beneficial effect of the strengthening solution was also well caught numerically. As can be observed in Figure 5.48, substantial reduction of the displacement demands, as well as a more uniform demands distribution were verified.
- The numerical model for the strengthened frame was able to reproduce well the experimental results, not only in relation to the storey shear and inter-storey drift evolutions, but also regarding the dissipated energy in each storey. The damage and respective changes in the structural behaviour induced during previous earthquake tests were also well reproduced numerically by the cyclic imposed storey displacement profile.

Figure 5.41 - SR: storey displacement time histories (4<sup>th</sup>, 3<sup>rd</sup>, 2<sup>nd</sup> and 1<sup>st</sup> storeys)

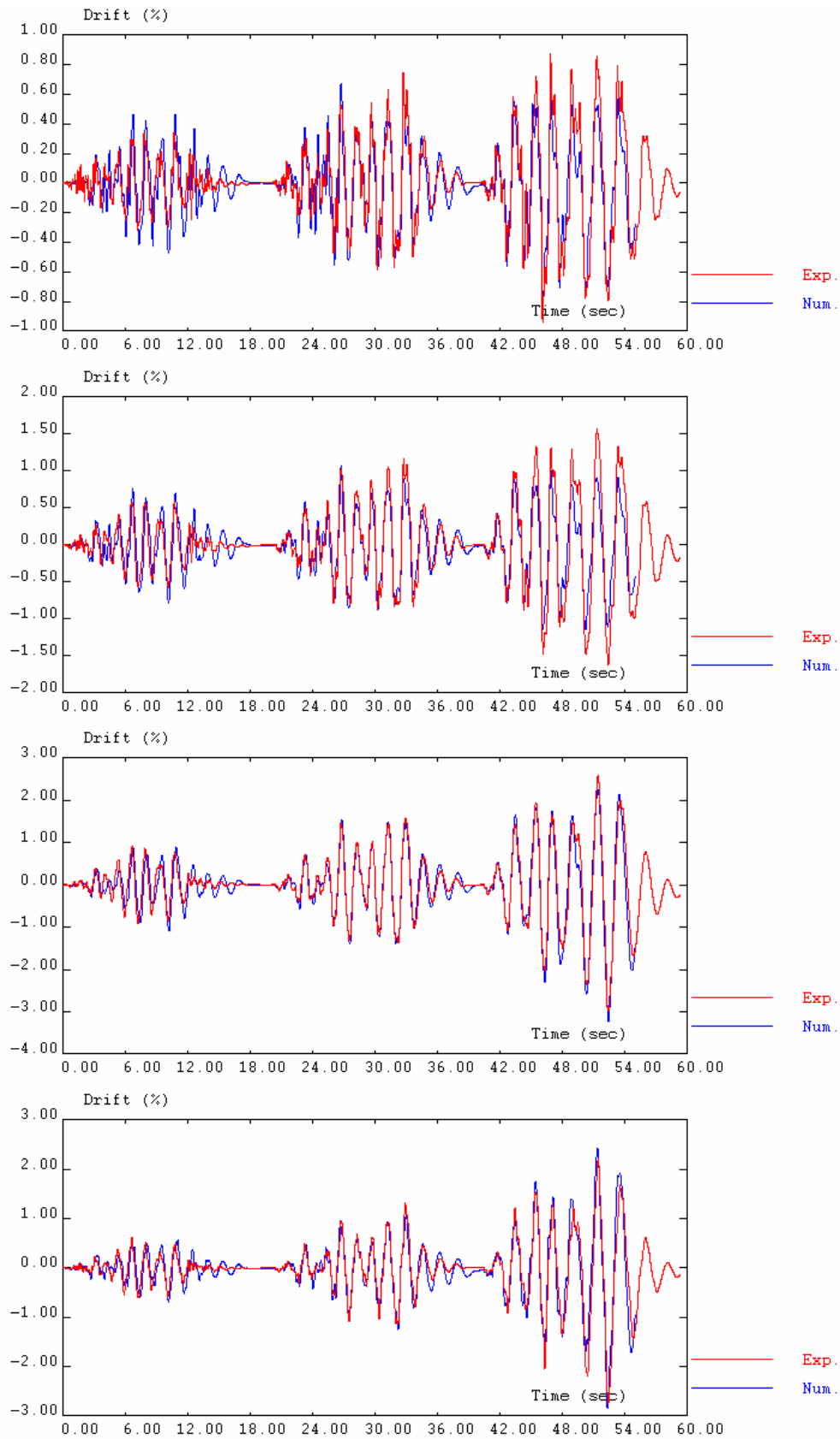
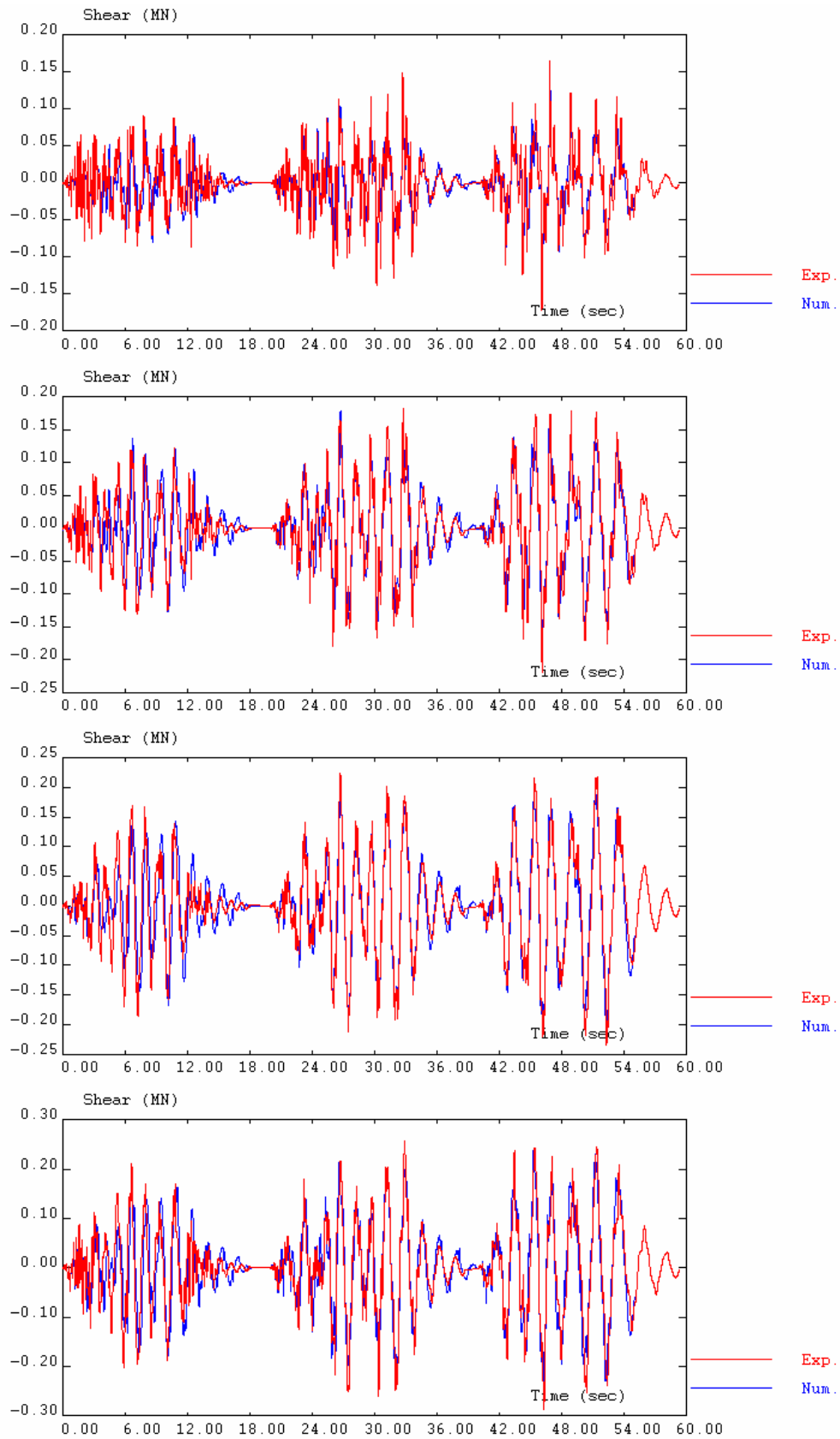


Figure 5.42 - SR: inter-storey drift time histories (4<sup>th</sup>, 3<sup>rd</sup>, 2<sup>nd</sup> and 1<sup>st</sup> storeys)

Figure 5.43 - SR: storey shear time histories (4<sup>th</sup>, 3<sup>rd</sup>, 2<sup>nd</sup> and 1<sup>st</sup> storeys)

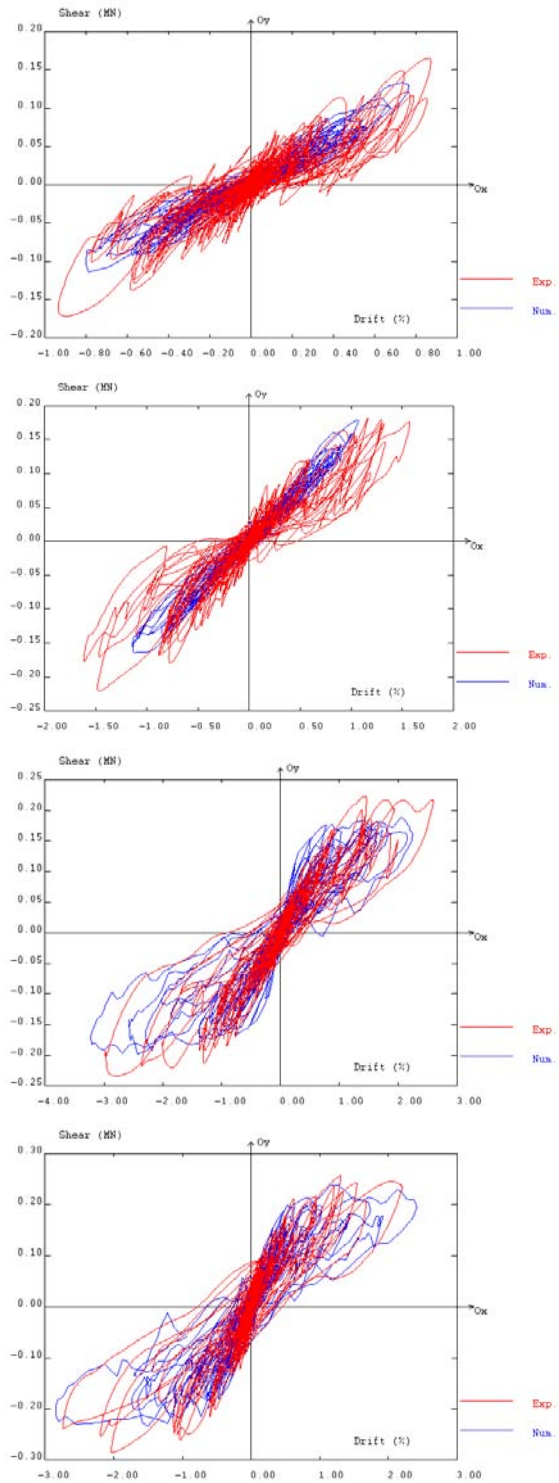


Figure 5.44 - SR: storey shear versus inter-storey drift (4<sup>th</sup>, 3<sup>rd</sup>, 2<sup>nd</sup> and 1<sup>st</sup> storeys)

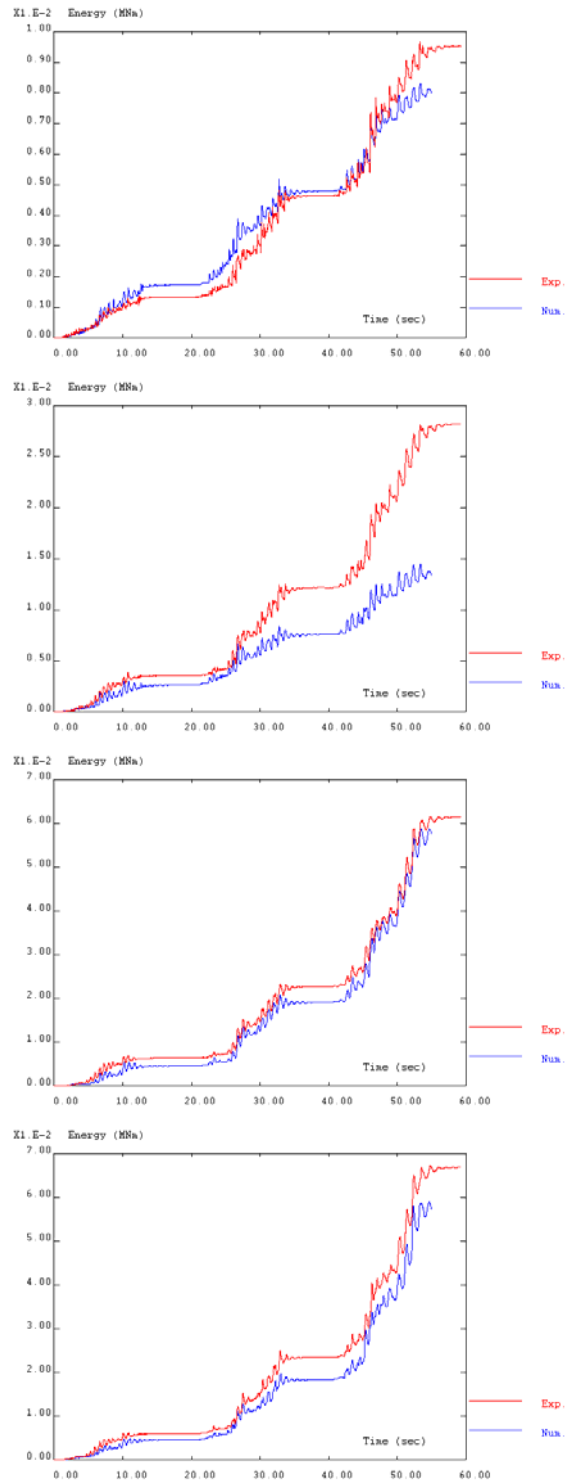


Figure 5.45 - SR: dissipated energy at storey level (4<sup>th</sup>, 3<sup>rd</sup>, 2<sup>nd</sup> and 1<sup>st</sup> storeys)

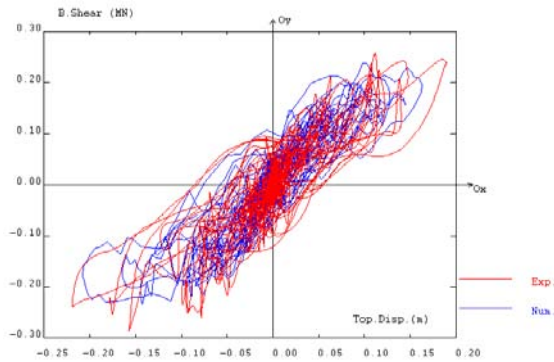


Figure 5.46 - SR: base-shear versus top-displacement

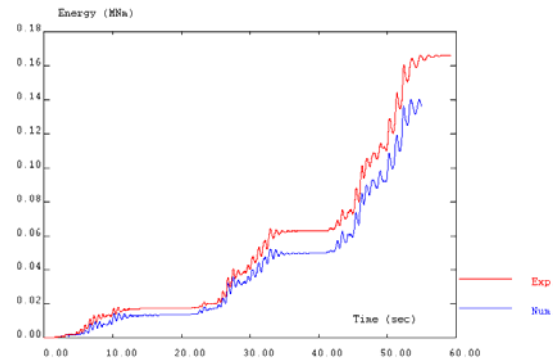


Figure 5.47 - SR: total dissipated energy

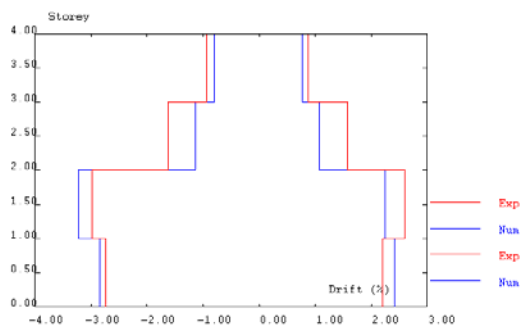


Figure 5.48 - SR: maximum drift profile

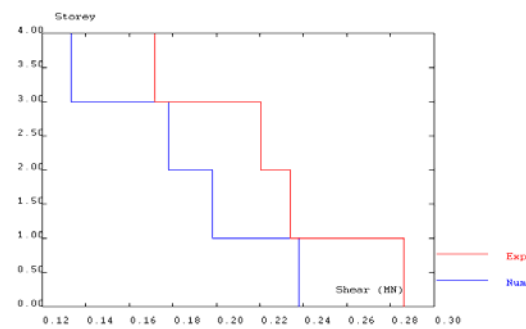


Figure 5.49 - SR: maximum shear profile

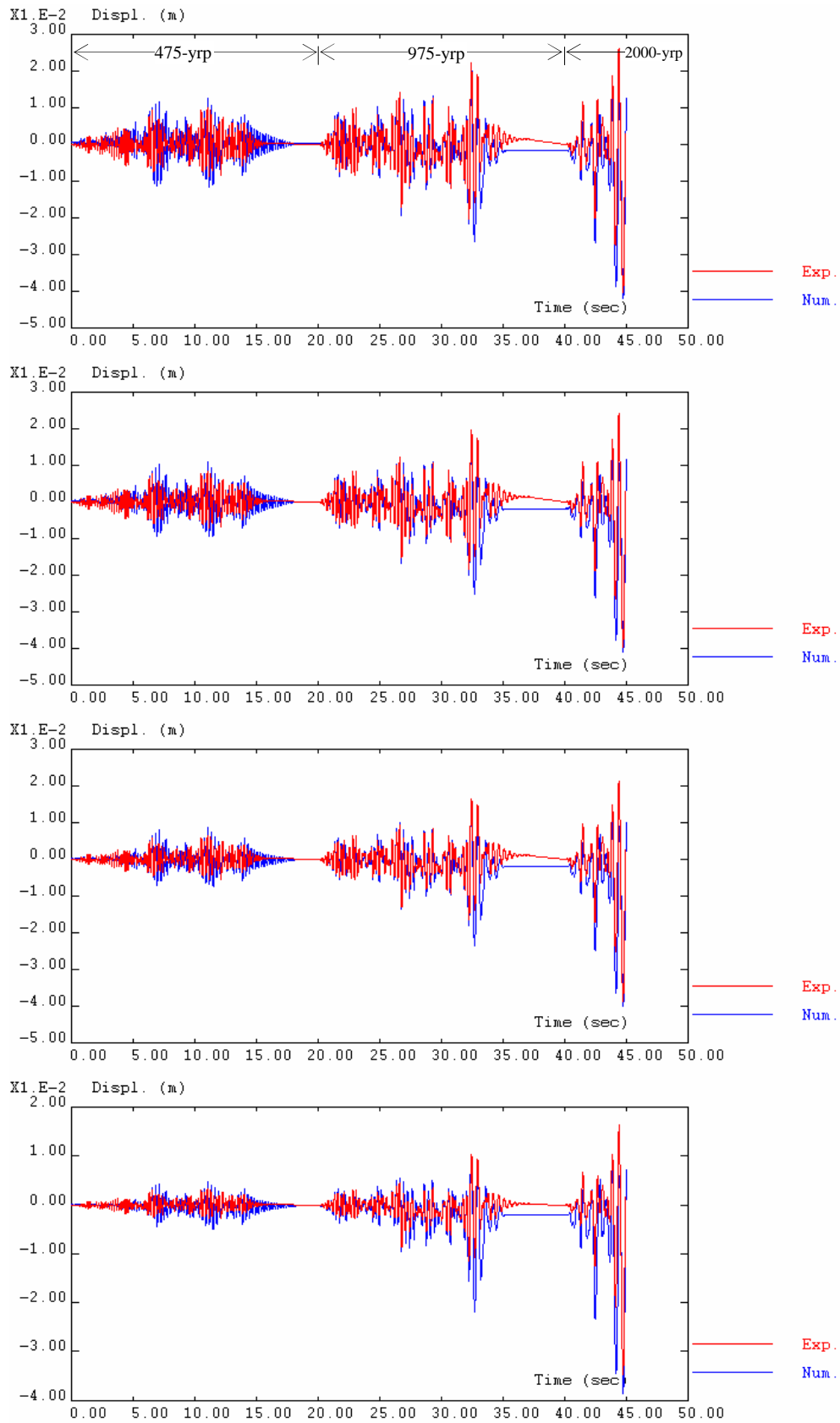
### 5.6.3 - Infilled frame numerical results

The time histories (experimental PSD results and numerical calculations) of storey displacements, inter-storey drift and storey shear for the infilled frame (IN) are given in Figures 5.50, 5.51 and 5.52, respectively. Figure 5.53 shows the computed and the experimentally measured relations between storey shear force and inter-storey drift at storey levels (shear-drift hysteresis diagrams). Figure 5.54 shows the evolution of the dissipated energy at storey levels for the infilled frame. In Figure 5.55 are represented the numerical and experimental curves of base-shear versus top-displacement, while Figure 5.56 contains the evolution of the total energy dissipated in the structure. Figures 5.57 and 5.58 show the distribution of maximum inter-storey drift and shear profiles for the infilled frame.

Comparing the non-linear dynamic numerical results for the infilled frame to the experimental ones, the following main conclusions can be drawn:

- The results of the numerical analyses confirm that the models adopted (elements with non-linearity concentrated at their extremities for the RC elements and equivalent strut elements for the infill panels) are adequate to simulate the non-linear seismic response of masonry infilled RC frames. The numerical analyses confirm that the infill panels protect the reinforced concrete frame for low intensity seismic input.
- The presence of infill panels increases the strength and the initial stiffness of the structure, as well as the total energy dissipated. The numerical model was able to reproduce the modifications in structural response induced by the infills. The natural frequencies of the infilled structure were considerably increased, when compared to the original bare frame. As already observed in Section 5.4, the numerical model also reproduces well the frequencies of the structural system.
- The numerical model was able to predict well the failure of the infill walls. In fact, the soft-storey mechanism is well identified with the numerical models.
- The numerical model for the infilled frame was able to reproduce well the experimental results, for the storey shear and inter-storey drift time-histories and envelopes. Nevertheless, significant differences were found for the dissipated energy at storey level. In fact, for the first and second storeys, the numerical model gives a dissipated energy approximately 20% lower than the experimental one. A possible justification for this effect is the non-smoothness of the spectrum in the zone of the frequencies corresponding to the infilled frame (see Figure 3.9). The equivalent bi-diagonal struts model adopted for the infills considers independent behaviour of the diagonal bars, i.e., the deterioration induced in one strut does not influence the behaviour of the other. For an infill wall, damage influences the global behaviour of the panel. As can be noted in Figure 5.53, for the first storey shear-drift numerical diagram, the curve indicates that when the global storey reached the maximum strength in one direction, corresponding to failure of the infill panels, the deformation in the other direction is protected, due to the conserved high stiffness. This effect can also be observed in Figure 5.57. The inter-storey drift at the first storey is dislocated towards the first damage direction.



Figure 5.50 - IN: storey displacement time histories (4<sup>th</sup>, 3<sup>rd</sup>, 2<sup>nd</sup> and 1<sup>st</sup> storeys)

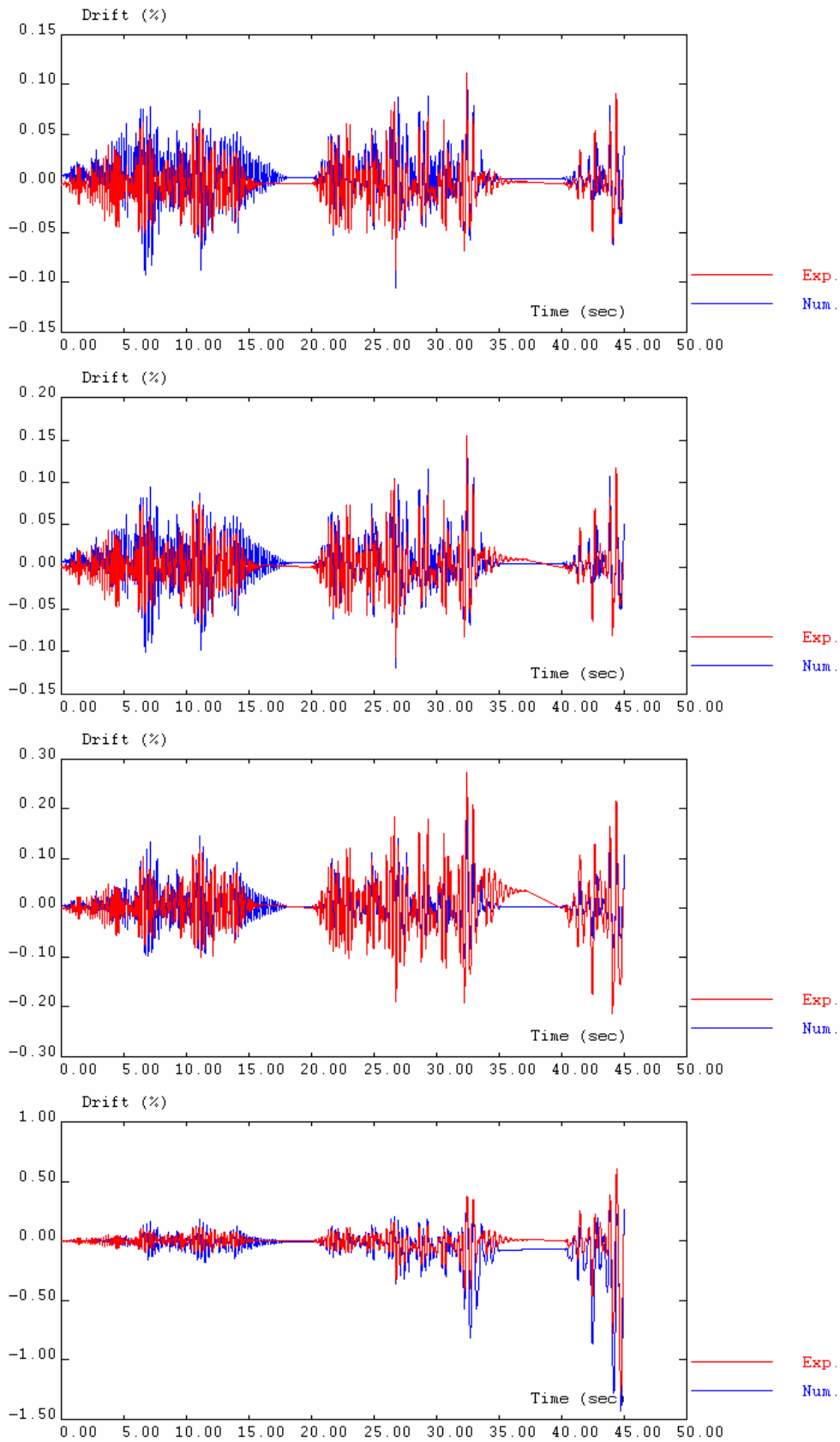
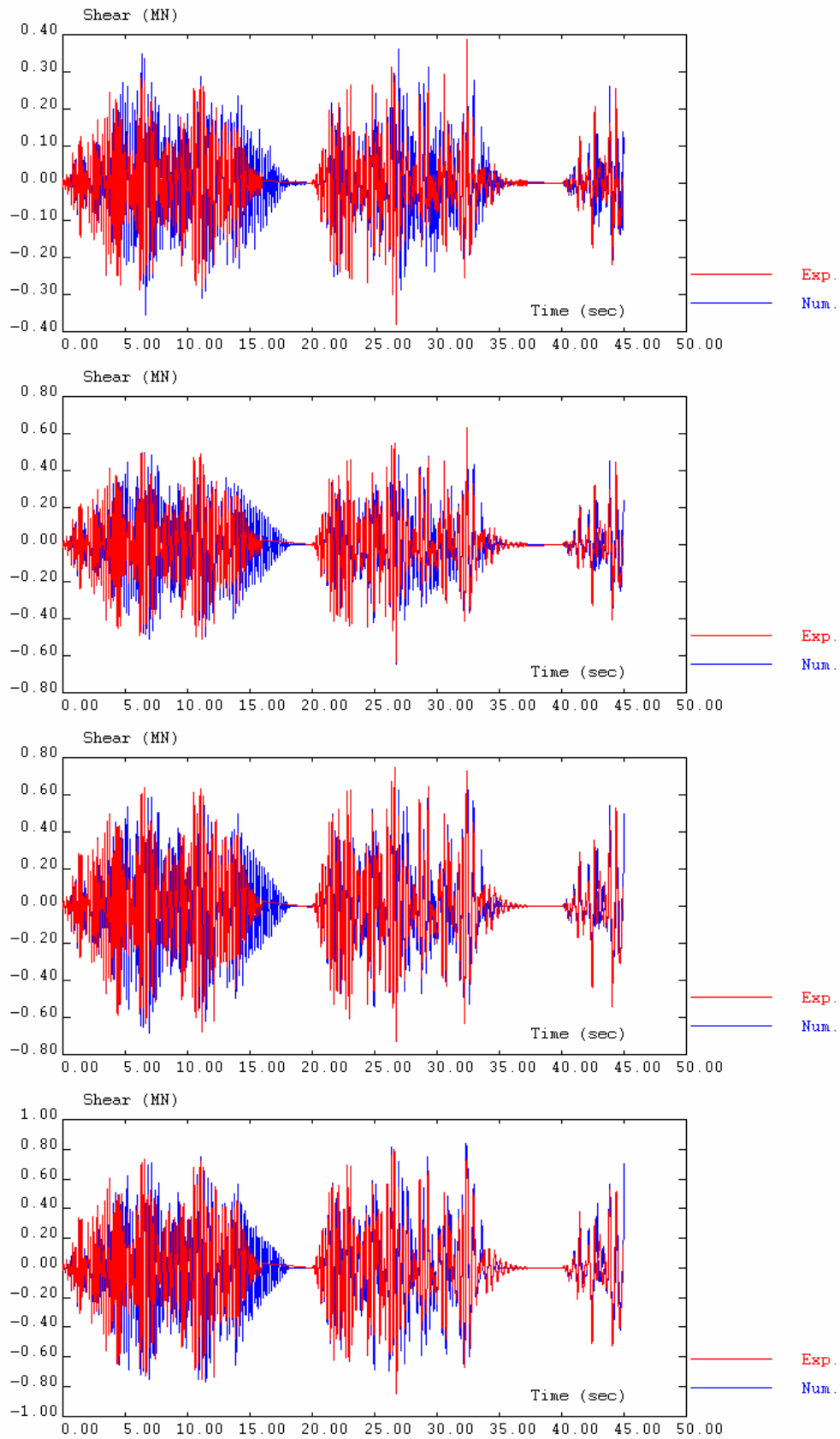


Figure 5.51 - IN: inter-storey drift time histories (4<sup>th</sup>, 3<sup>rd</sup>, 2<sup>nd</sup> and 1<sup>st</sup> storeys)

Figure 5.52 - IN: storey shear time histories (4<sup>th</sup>, 3<sup>rd</sup>, 2<sup>nd</sup> and 1<sup>st</sup> storeys)

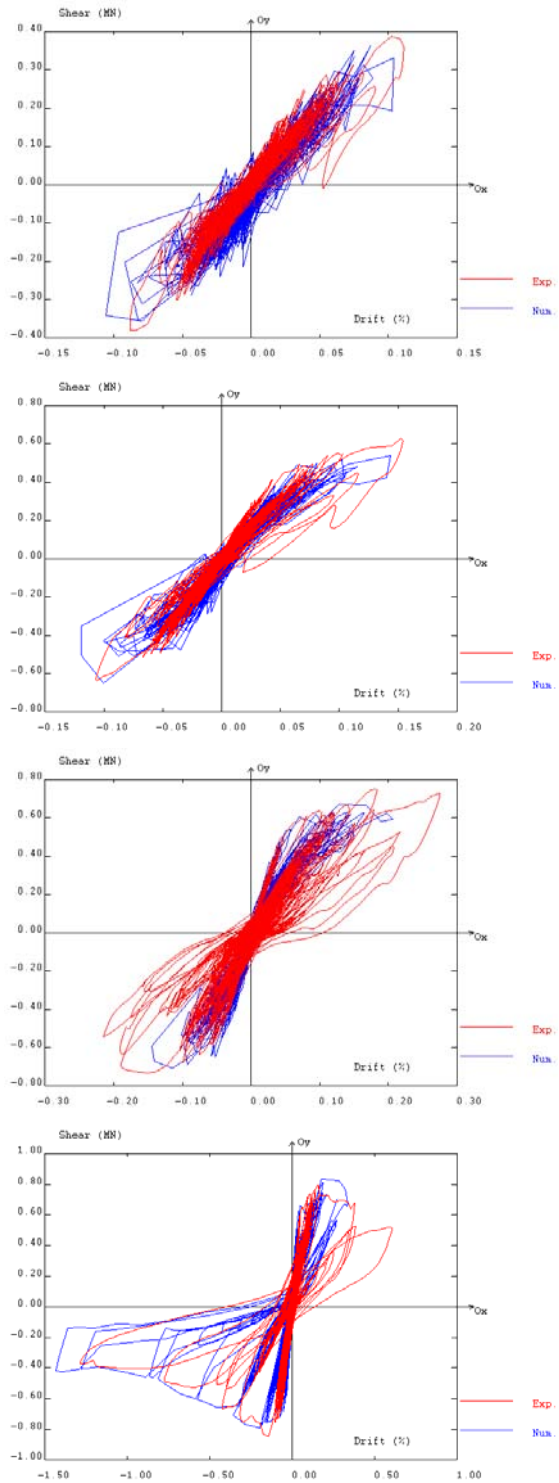


Figure 5.53 - IN: storey shear versus inter-storey drift (4<sup>th</sup>, 3<sup>rd</sup>, 2<sup>nd</sup> and 1<sup>st</sup> storeys)

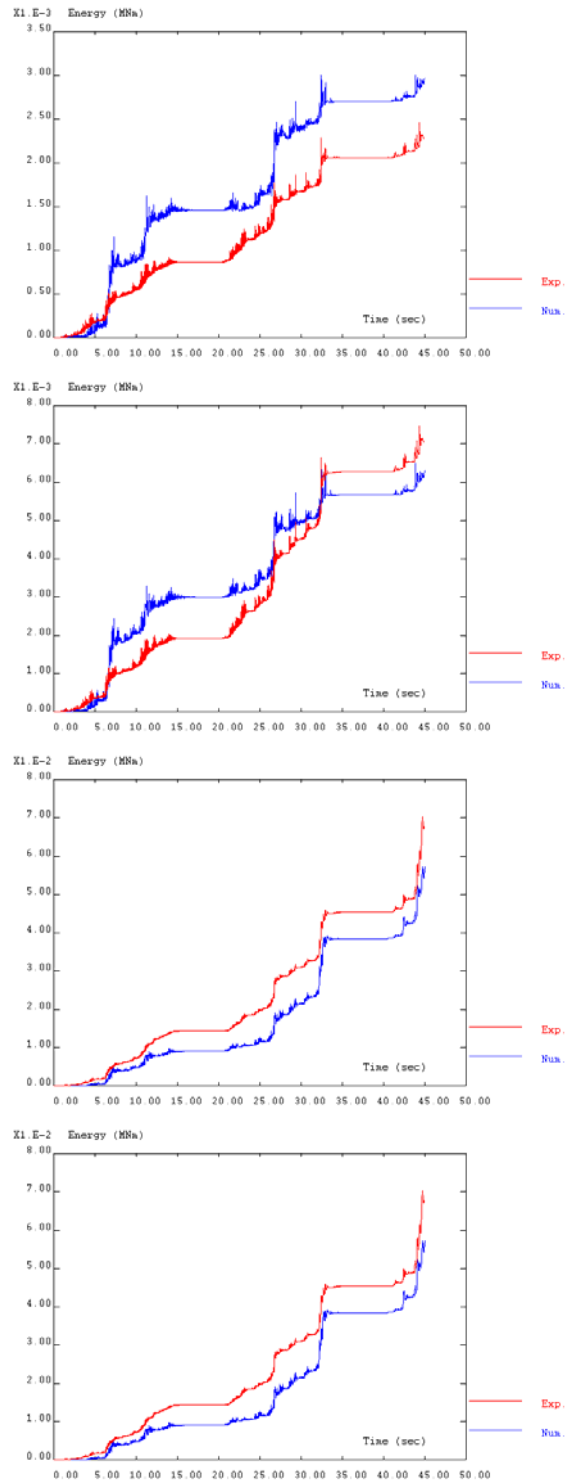


Figure 5.54 - IN: dissipated energy at storey level (4<sup>th</sup>, 3<sup>rd</sup>, 2<sup>nd</sup> and 1<sup>st</sup> storeys)

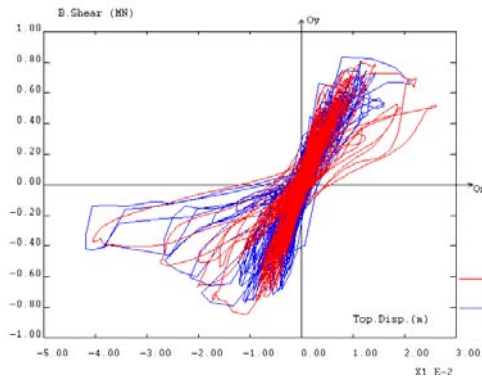


Figure 5.55 - IN: base-shear versus top-displacement

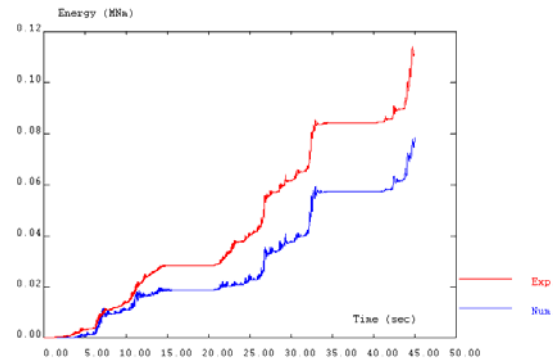


Figure 5.56 - IN: total dissipated energy

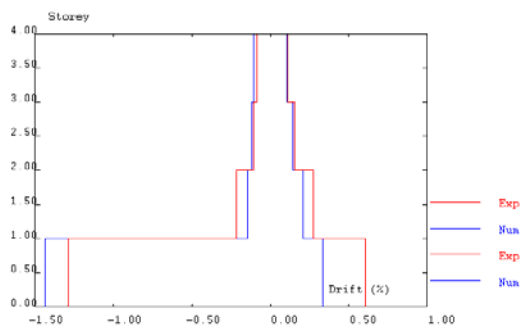


Figure 5.57 - IN: maximum drift profile

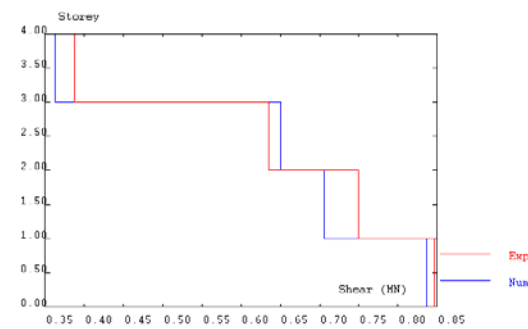


Figure 5.58 - IN: maximum shear profile

#### 5.6.4 - Discussion of the numerical results with refined FE models

Comparing the non-linear numerical results to the experimental ones, the following main conclusions, comments and recommendations can be drawn:

- As already stated, data on the real characteristics of buildings that have been subjected to earthquakes is generally difficult to obtain. In this numerical study, the vast experimental test results on the RC frame full-scale PsD tests are used to corroborate the numerical models, which is a significant advantage of the present study.
- In general, the experimental and analytical results are in good agreement not only in terms of peak storey displacement, inter-storey drift and storey shear, but also in terms of frequency content and dissipated energy at storey level. Nevertheless, significant differences in terms of dissipated energy were found for the infilled frame. As stated

earlier, this may result from considering independent behaviour between the two diagonal bars representing each infill panel.

- The original models used in the preliminary non-linear analyses do not take into account phenomena such as slippage of the steel rounded bars. As stated by Monti and Spacone (1998), the introduction of bond-slip of reinforcing bars in the numerical models proves to be a necessary enhancement towards a realistic description of the cyclic and the ultimate behaviour of reinforced concrete structures. As proven by the improved refined numerical results, including the proposed model for the bond-slip of the steel bars (slippage factor), this effect is crucial for proper modelling the structural response of the existing RC structures.
- The non-linear behaviour of the previously damaged structures (e.g. by precedent earthquakes) was well represented. Moreover, the numerical analyses demonstrate also that the upgraded models are able to well reproduce the non-linear structural behaviour of the repaired and strengthened structures.
- A higher slab-participation may dictate lower demands in the beams and higher demands in the columns, and, consequently, prompt the storey mechanism expected for these types of structures.
- Although the experimental tests are the best way to understand the behaviour of a structure and to check its capacity, the costs of such campaigns are very high. The numerical analyses are complementary to the experimental tests. The experimental results should be used to calibrate the numerical models, which should be then exploited in more extensive analyses.
- It is important to underline that much care should be taken in the modelling of these structures. In fact, due to the vast number of model parameters and rules, the use of refined models may lead to unrealistic results if the model parameters are not correctly chosen. It is also clear that the sensitivity of the response to such model parameters increases with the complexity of the models.
- Non-linear numerical analyses are in the line of use of several research groups around the World to study and assess the behaviour of structures subjected to earthquake

ground motions. In the academic and research communities, on the one hand, there is no doubt about the utility of these refined models in the structural assessment and design of retrofitting solutions. On the other hand, it is recognised that these powerful tools depend on a large amount of parameters not yet well calibrated. These powerful tools, if not carefully used, can be dangerous if in the hands of a common engineer. Therefore, work has to be done in order to produce and to implement calibrated non-linear models and related parameters that can be used safely and easily in the structural assessment and design by the technical community.

## **5.7 - STRUCTURAL RESPONSE AND ASSESSMENT USING SIMPLIFIED METHODS**

As already said, in Europe, many structures are potentially seismically vulnerable due to the late introduction of seismic loading into building codes. Therefore, there is a need to investigate the seismic behaviour of existing buildings and ultimately to assess their seismic vulnerability. As remarked by Peter and Badoux (1998), the seismic evaluation of buildings requires the prediction of the seismic performance, and, in consequence, the prediction of the inelastic deformations of the RC structures.

Despite the advantages of a refined non-linear dynamic structural fibre modelling, it must be admitted that this approach can frequently become elaborated and costly. This fact sustains the development of less complicated structural models without debasing the essential features of dynamic response. As remarked by Anderson *et al.* (1991), one main question is whether very sophisticated FE models are required or whether acceptable predictions can be obtained using simplified models. Many simplified non-linear models have been investigated in the past few years (see, for example, Calvi *et al.*, 2000; Calvi, 1998, Priestley, 1998).

This section is dedicated to structural assessment using simplified methods. In Section 5.7.1 are presented results of the equivalent damping evaluation, with the methodology exposed in Section 2.3.5, from the experimental tests.

In Section 5.7.2 it is verified the structural response and it is assessed the capacity of the bare original and of the strengthened structures, with the Capacity Spectrum Method (CSM). In Section 5.7.3 it is proposed and assessed a MDOF non-linear dynamic model for the assessment of irregular structures. Finally, in Section 5.7.4 are analysed the structural response for the BF and SR tests, in terms of seismic performance according to the performance levels proposed in the ATC-40.

### 5.7.1 Equivalent viscous damping from the experimental hysteretic curves

To perform a structural assessment, it is essential to define accurately the damping as a function of the deformation demand, as recalled in Section 2.3. There are some proposals for the damping of new buildings, but not for existing structures. In this study, it was possible to obtain, from the experimental tests, an estimation of the damping for the existing and strengthened structures.

For each test performed on the BF and SR structures, the structural equivalent damping was calculated, according to the methodology exposed in Section 2.3.5. Firstly, the equivalent viscous damping was evaluated at storey level from the curves inter-storey drift versus storey shear. Subsequently, the equivalent viscous damping of the global structure was computed as a function of the damping at storey level, weighted by the storey potential energy. The best-fit curves in terms of storey equivalent damping, as a function of the maximum inter-storey drift, obtained from the earthquake and cyclic tests on the bare and strengthened frames are plotted in Figure 5.59.

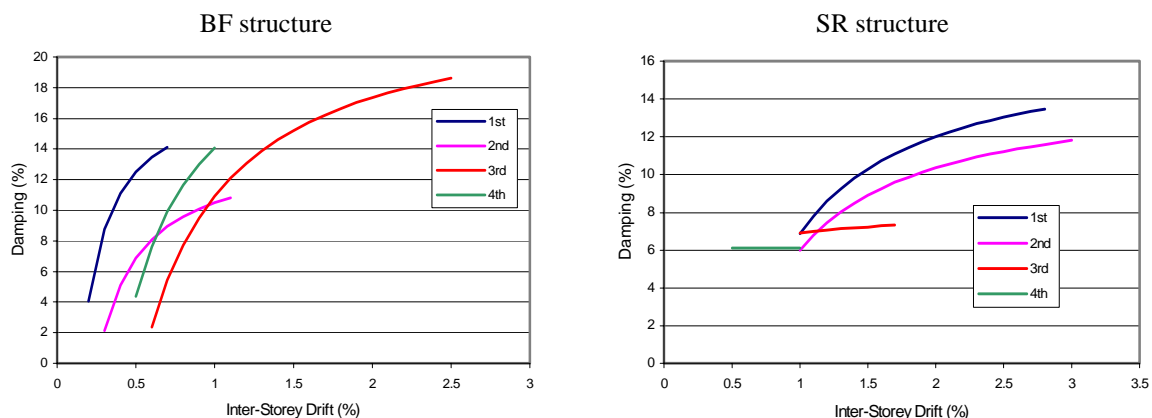


Figure 5.59 - Equivalent storey damping (%) for the earthquake and cyclic tests on the BF and SR structures



From Figure 5.59, the following can be observed:

- Generally, for smaller displacement amplitudes, the equivalent damping increases rapidly, while for larger displacement amplitudes the evolution is smoother, as confirmed by Priestley (1997).
- The minor cyclic hysteretic deformation detected in the 4<sup>th</sup> storey for the BF tests, and in the upper two storeys for the SR tests does not give enough data to estimate the damping function. Larger inter-storey drift would be very informative. However, the curves presented above are representative of the damping functions in the range of deformation reached during the tests.
- For the tests on the BF structure, larger damping values were observed at the 3<sup>rd</sup> storey level, where a concentration of drift was induced due to the structural irregularity.
- For the SR structure, a larger participation of the lower two storeys in terms of damping was observed, because the structure is more regular than the BF. The very low value of deformation reached at the 4<sup>th</sup> storey during the tests on the SR structure, was inadequate to estimate the damping function. Therefore, a constant average value was assumed.

The structural global equivalent damping, for the BF and SR test series, was computed as a function of the damping evaluated at storey level, weighted by the storey potential energy, as exposed in Section 2.3.5. In Figure 5.60 are plotted, for the BF and SR earthquake and cyclic tests, the estimated damping as a function of the global drift. The global drift is defined as the ratio between the top-displacement and the total height of the structure (10.80 m). The best-fit logarithmic curves were adjusted and are also represented in Figure 5.60. In Figure 5.60, are also represented, for each earthquake test, a point corresponding to the maximum global drift and global equivalent damping (see also Table 5.11).

From the Figure 5.60 and Table 5.11, it can be observed:

- For a specific global drift, the estimated equivalent global damping is higher for the bare original than for the strengthened structure, which can be explained by the more regular response of the last, which induces less non-linear demand at storey

level. Note that for the 475-yrp earthquake the BF and SR reached similar level of global drift (0.56% for the BF, and 0.59% for the SR), being the estimated equivalent global damping 8.5% for the BF and 7.1% for the SR tests. For the tests with the 975-yrp earthquake, the global drift reached by the BF and SR was equal (1.08%), being the global damping 10.9% and 8.9%, for the BF and SR frames respectively.

- An equivalent damping of 10.8%, for a global drift of 2.03%, was evaluated for the 2000-yrp earthquake test on the SR structure.
- Even for considerable deformation levels, for both BF and SR structures, a low value of damping was estimated (maximum value less than 11%), which confirms that existing structures, with reinforcing plain bars, have a small energy dissipation capacity.

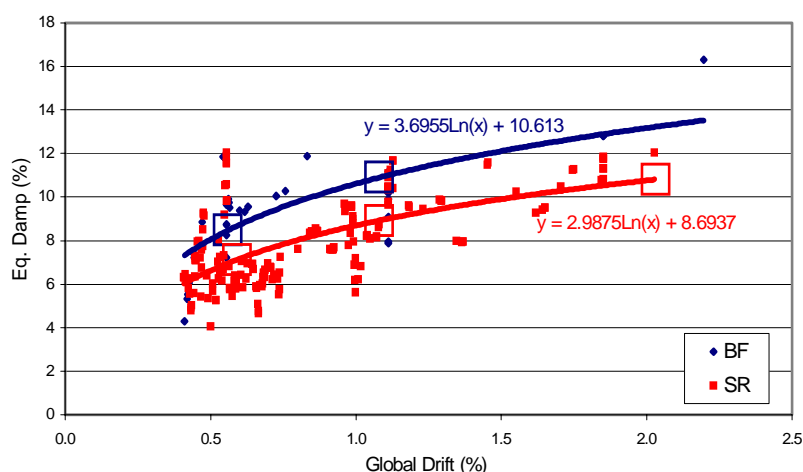


Figure 5.60 - Equivalent global damping (%) versus global drift for the earthquake and cyclic tests on the BF and SR structures

Table 5.11 - Maximum equivalent global damping (%) for the earthquake tests

Structure	Earthquake	Global drift (%)	Global damping (%)
BF	475-yrp	0.56	8.5
	975-yrp	1.08	10.9
SR	475-yrp	0.59	7.1
	975-yrp	1.08	8.9
	2000-yrp	2.03	10.8

## 5.7.2 Capacity spectrum method

The capacity spectrum method, summarized in Section 2.3.4, is here applied to the original bare and strengthened structures under analysis. The capacity curves and the capacity spectra are presented. The structural response is verified with the CSM, for the demand spectra of the earthquakes considered. Finally, the BF and SR structures are assessed using the elastic acceleration-displacement response spectra, proposed in the EC8.

### 5.7.2.1 Capacity curve and capacity spectra

As stated in Section 2.3.4.1, the capacity curves are usually determined by performing a pushover analysis of the building, with a numerical model accounting for the non-linear behaviour of the structure. Pushover analysis for the BF and SR structures was performed with the refined numerical model used in Section 5.6 to simulate the PsD tests. The pushover analysis was carried out imposing displacements at the roof level of the building and with a triangular-inverted distribution of forces.

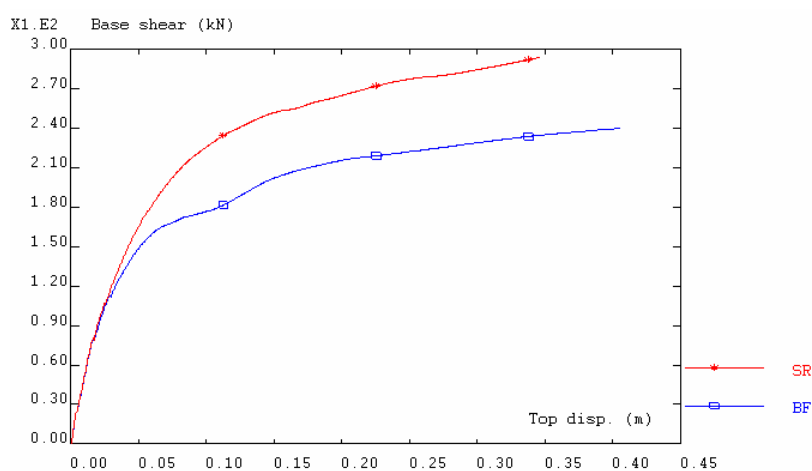


Figure 5.61 - Pushover capacity curves for the BF and SR structures

As can be observed from Figure 5.61, comparing the pushover capacity curves for the original structure to the strengthened structure, the strengthening intervention practically did not change the initial stiffness, but increased significantly its resistance, as was observed from the tests (see Section 4.4).

In Figure 5.62 are compared, for the BF structure and in terms of base-shear versus top-displacement, the pushover capacity curve (plot in blue) to the PsD tests results (plots in green) and to the results of the final capacity cyclic test (see plot in red). In Figure 5.63 are represented the storey shear-drift curves, also from the pushover analysis, from the PsD and from the cyclic tests on the BF structure. Finally, in Figure 5.64 are plotted the pushover capacity curve and the PsD test results in terms of base-shear versus top-displacement for the SR structure.

From the analysis of Figures 5.62 to 5.64, the following can be observed:

- The BF pushover capacity curve of the structure, in terms of base-shear versus top-displacement, follows the envelope of the cyclic tests, but not the envelope of the PsD tests (see Figure 5.62). Regarding the experimental results, the PsD and cyclic curves of base-shear versus top-displacement (Figure 5.62) are not comparable. But, looking at the results at storey level (see Figure 5.63), a better accordance is verified. The main differences are observed for the initial stiffness. Actually, the frame tested cyclically was previously tested with infills (see Section 4.5), and therefore, it was already installed a level of damage corresponding to each maximum inter-storey drift (see Table 4.8). Nevertheless, the storey envelope curves for the PsD and cyclic tests, do agree thoroughly.
- Regarding the SR structure, as can be observed in the plots of Figure 5.64, a better agreement between the PsD envelope test results and the pushover capacity curve was verified.
- Therefore, the pushover capacity curve could be representative of the global dynamic behaviour of regular buildings, as the studied SR structure, but it is believed that might be inappropriate to characterise the dynamic response of irregular buildings, as the studied bare frame. It is noted that a large number of existing buildings have irregular structures.
- Finally, the agreement verified between the PsD results (for the SR) and the cyclic test results (for the BF) with the pushover analysis illustrate (as already observed in Section 5.6) the ability of the refined FE numerical models in modelling these irregular structures.

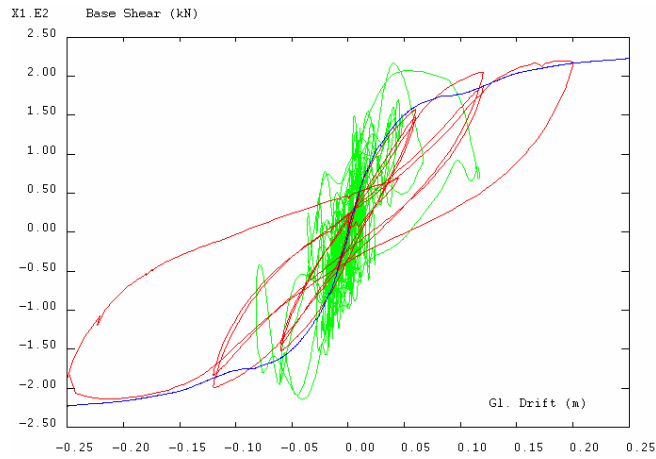


Figure 5.62 - BF structure: pushover capacity curve (blue), PsD tests (green), and cyclic test (red)

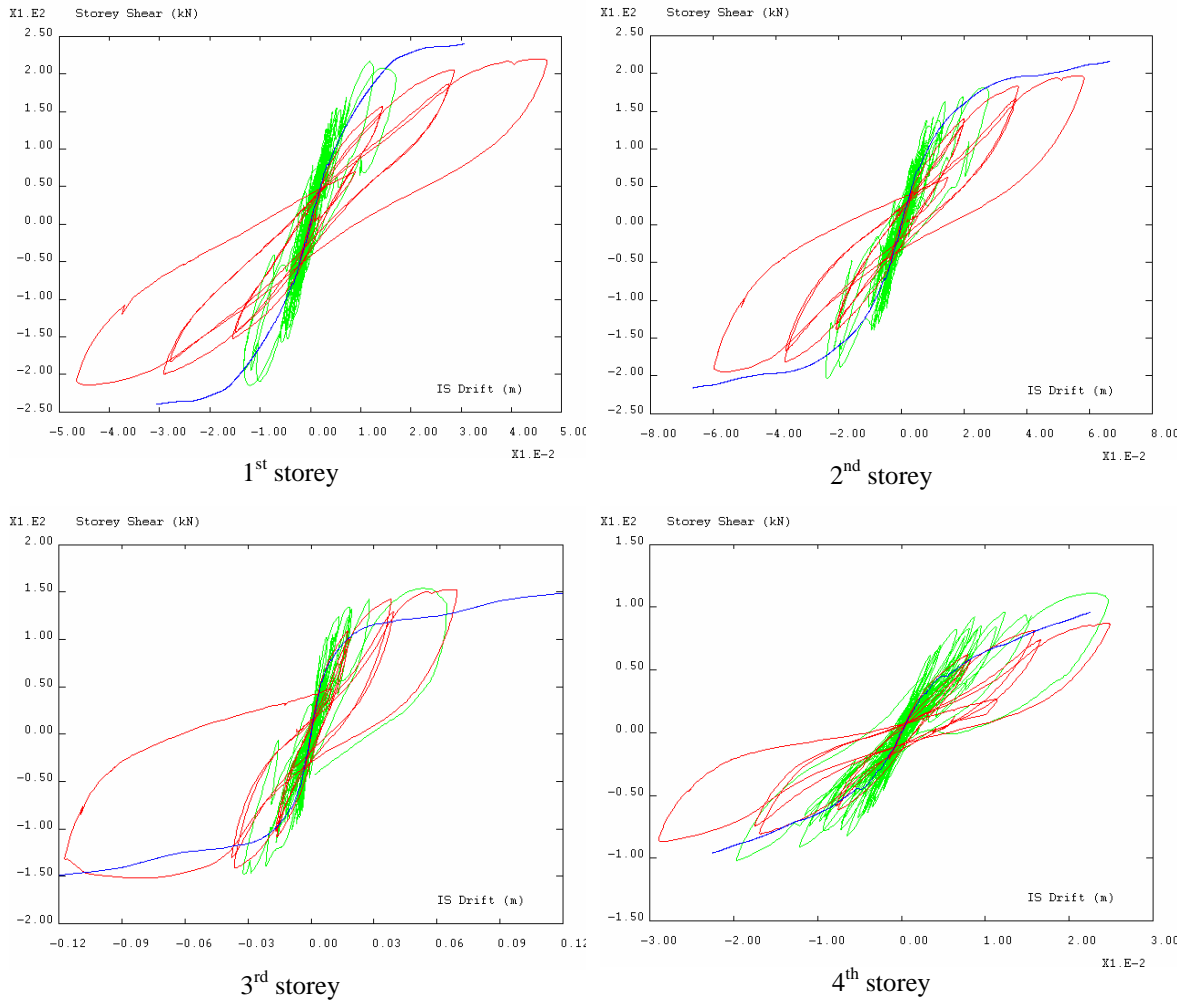


Figure 5.63 - BF storey shear-drift curves: pushover (blue), PsD tests (green), and cyclic test (red)

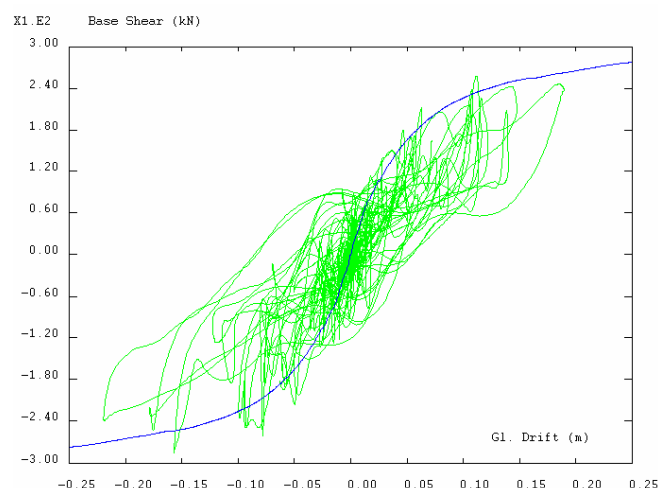


Figure 5.64 - SR structure: pushover capacity curve (blue) and PsD tests (green)

The capacity spectral curves for the BF and SR structures were calculated from the envelope of the base-shear top-displacement diagrams (in the positive and negative directions) of the PsD earthquake tests and from the pushover curve using the expressions (2.3) and (2.4). As refereed in ATC-40 (1996), the modal coefficients (modal participation factor and modal mass coefficient) should be selected in order to better correlate with the shape of the deformed structure at the maximum top-displacement. Therefore, using the maximum top-displacements verified in the PsD tests (see Table 4.1 for the BF, and Table 4.6 for the SR) and the expressions (2.5) and (2.6), the modal parameters were calculated (see Table 5.12).

Table 5.12 - Modal parameters for assessment of the BF and SR with the CSM

Modal parameter	Structure	
	BF	SR
Modal participation factor ( $PF_1$ )	$PF_1^{BF} = 1.26$	$PF_1^{SR} = 1.23$
Modal mass coefficient ( $\alpha_1$ )	$\alpha^{BF} = 0.72$	$\alpha^{SR} = 0.89$

### 5.7.2.2 Verification of the earthquake tests

In this section it is applied the CSM to estimate the response point for each PsD test performed on the BF and SR structures. The response estimation is represented in the ADRS spectral coordinates. The structures are represented by their pushover capacity curve (CC), represented in Figure 5.61, reduced to the corresponding capacity spectra, as presented in Section 5.7.2.1. The acceleration-displacement response spectra (ADRS) were computed for the earthquake time histories (corresponding to 475, 975 and 2000-yrp), and for several damping values. For the global structural damping, the curves represented in Figure 5.60 were assumed.

In Figures 5.65 and 5.66 are represented for the BF and SR structures the response estimation. In the figures are also represented, for comparison, the CC obtained from the envelope of the PsD tests (plots in red). Two curves are represented, one for each direction (positive and negative).

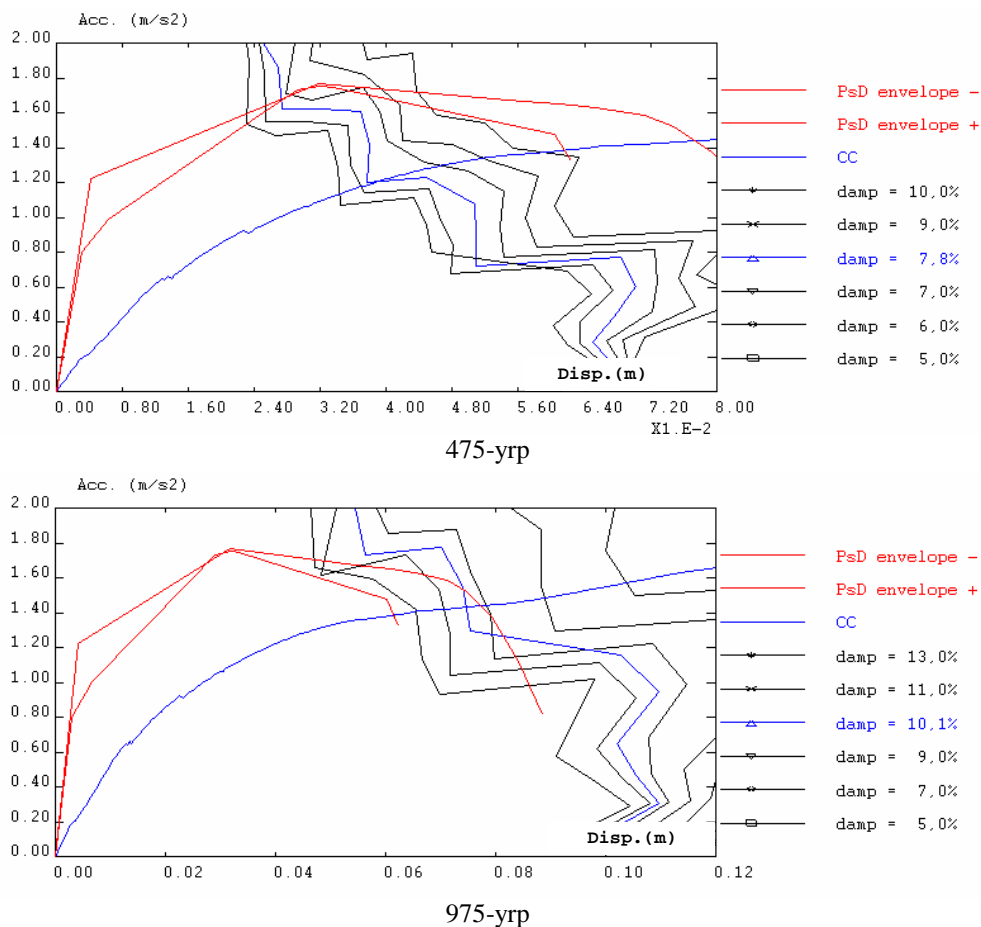


Figure 5.65 - BF response estimation with the CSM

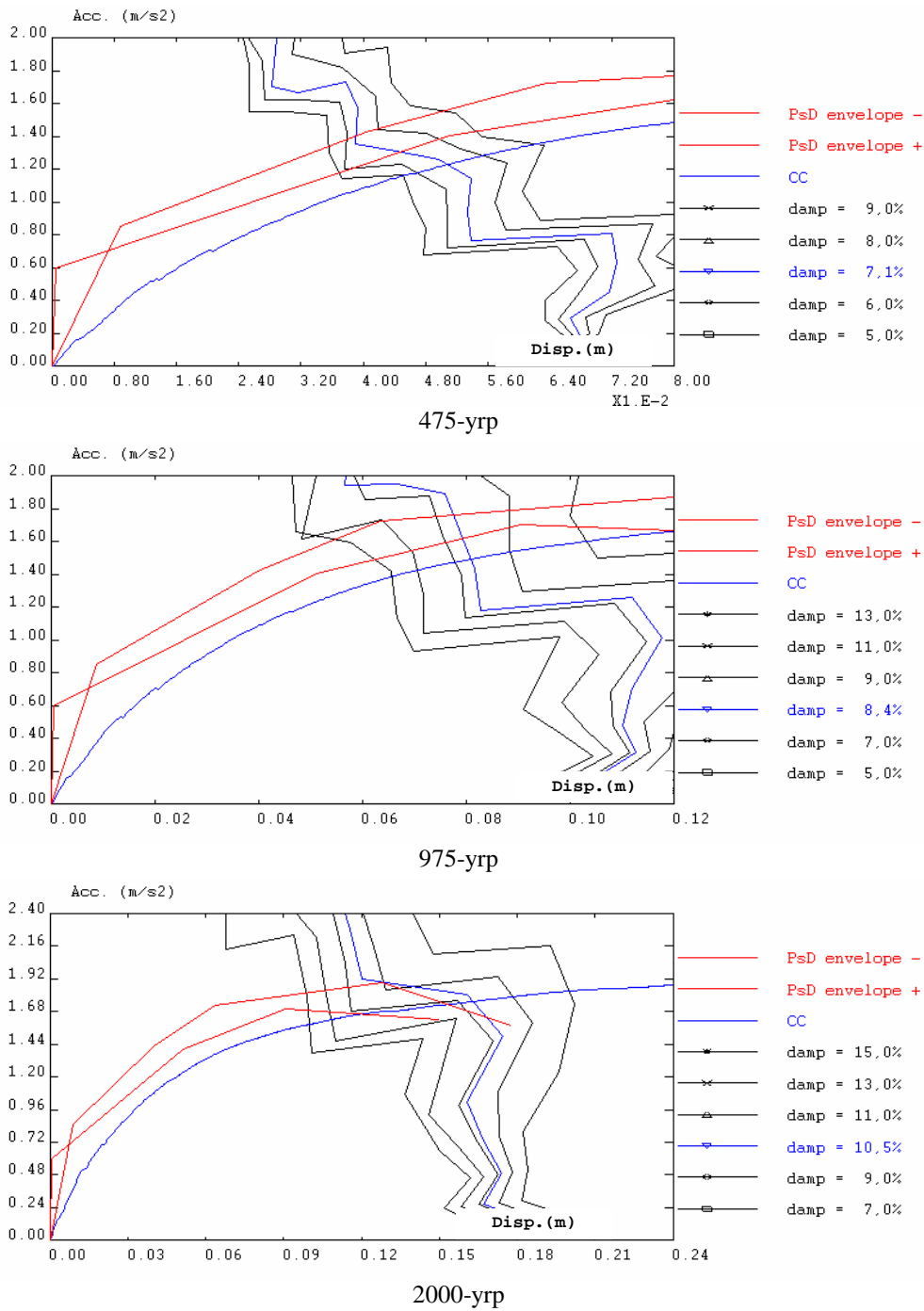


Figure 5.66 - SR response estimation with the CSM

In Table 5.13 the estimated with the CSM and the observed structural response in the PsD tests are compared, in terms of base-shear, top-displacement and global damping, for each test performed on the BF and SR structures.



Table 5.13 - Summary table of the response point (estimated with the CSM and PsD experimental results)

Structure	Input earthquake	Base-shear ( $kN$ )		Top-displacement ( $mm$ )		Global damping (%)	
		CSM	exp.	CSM	exp.	CSM	exp.
BF	475-yrp	149.3	209.0	50.4	60.8	7.8	8.5
	975-yrp	175.1	216.7	94.0	116.7	10.1	10.9
SR	475-yrp	187.1	212.2	63.4	63.2	7.1	7.1
	975-yrp	224.3	261.1	97.9	116.3	8.4	8.9
	2000-yrp	264.5	285.9	197.7	219.5	10.5	10.8

As already observed in Section 5.7.2.1, and from the analysis of Figures 5.65 and 5.66, and Table 5.13, it is confirmed that the CSM does not reproduce accurately the response of irregular structures. In fact, for the BF structure, despite a good approximation for the damping and for the global displacement, the base shear estimated with the CSM is very different than that measured in the PsD tests. Nevertheless, the CSM for the regular structure (SR) gives a better approximation, even in terms of base shear.

### 5.7.2.3 Assessment of the bare and strengthened structures

In this section, the BF and SR structures are assessed with the CSM. The structures are represented by their pushover capacity spectra (see Section 5.7.2.1). For the global structural damping it were assumed the functions represented in Figure 5.60. The seismic action is defined by the elastic acceleration-displacement response spectra (ADRS) proposed in the recent draft version of the Eurocode 8 (2003), where, for structures of long vibration period, it is proposed a revised form for the displacement response spectra.

In the analysis it was considered subsoil class A and response spectra type I. For the peak ground acceleration it was considered the maximum acceleration of the earthquake used for each PsD test (i.e. 2.180, 2.884 and 3.728  $m/s^2$ , for the return periods corresponding to 475, 975 and 2000 years, respectively). In Figure 5.67 are represented, for comparison, the ADRS (5% damping) obtained from the earthquake input motions and the ones proposed in the EC8 (and used in the assessment of the structures).

In Figures 5.68 and 5.69 are represented graphically the performance assessment of the BF and SR structures, respectively. The BF is assessed for two levels of demand ( $a_g = 2.180$

and  $2.884 \text{ m/s}^2$ ), while the SR structure is assessed for three levels of demand ( $a_g = 2.180$ ,  $2.884$  and  $3.728 \text{ m/s}^2$ ).

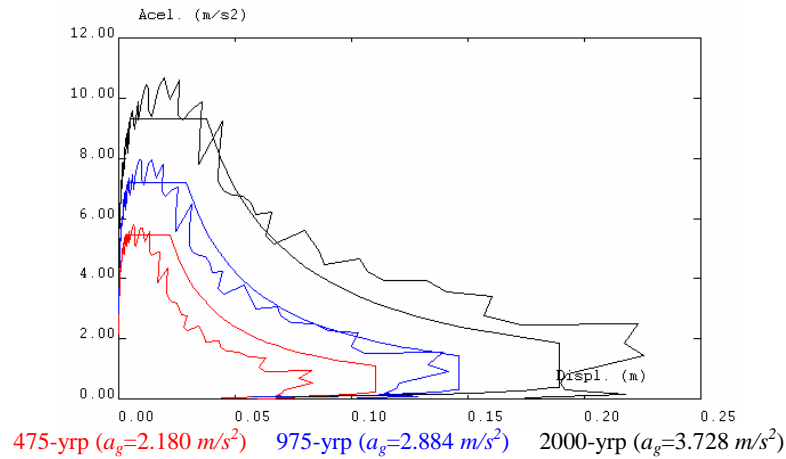


Figure 5.67 - ADRS: for the earthquake input motions and EC8 (5% damping)

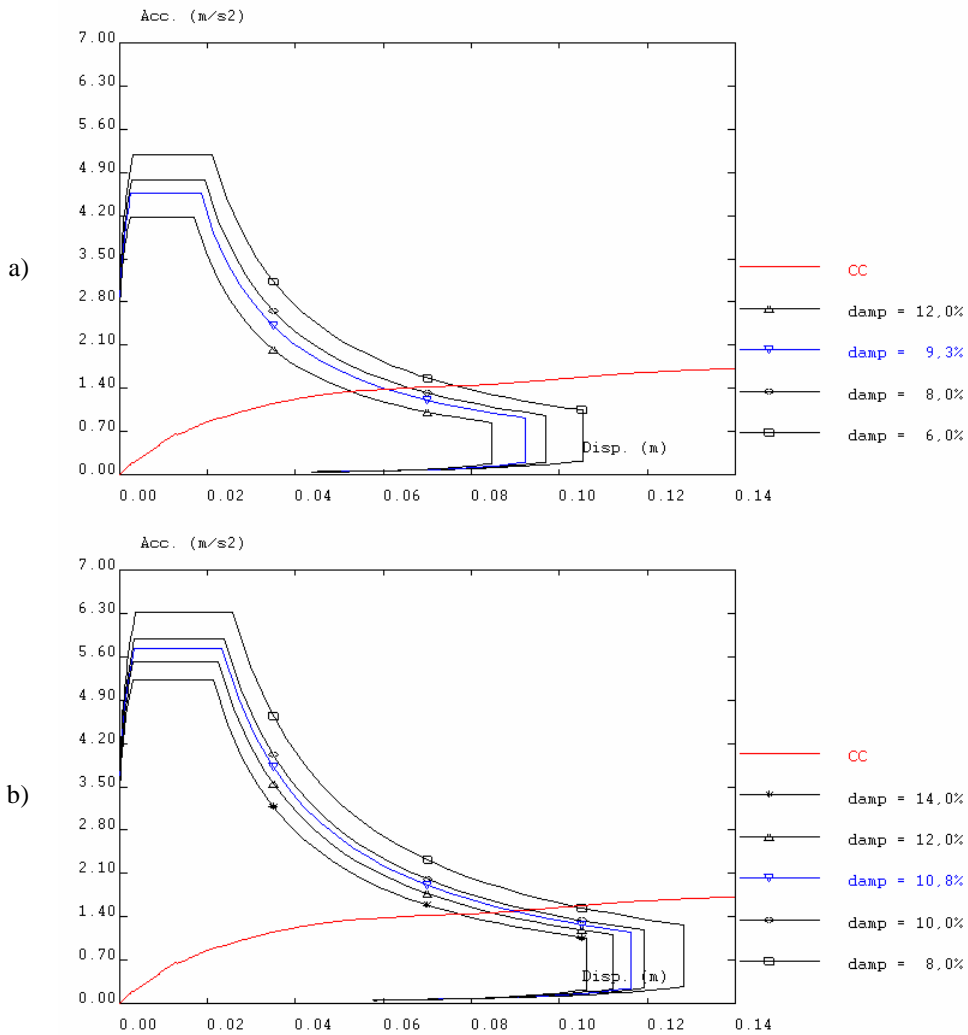


Figure 5.68 - Assessment of the BF with the CSM (subsoil class A; response spectra type I) for input motions: a)  $a_g = 2.180 \text{ m/s}^2$ ; b)  $a_g = 2.884 \text{ m/s}^2$

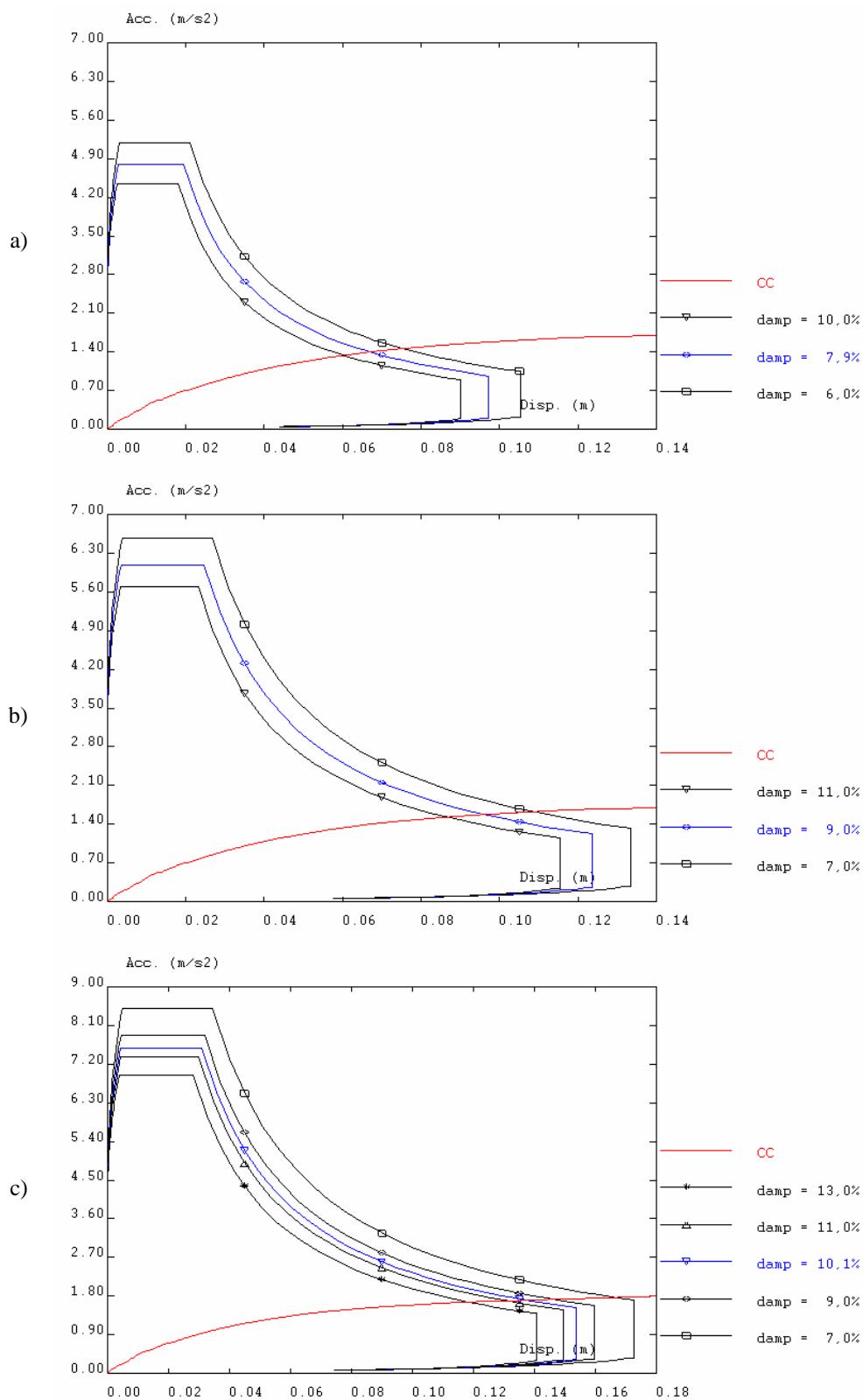


Figure 5.69 - Assessment of the SR with the CSM (subsoil class A; response spectra type I) for input motions: a)  $a_g = 2.180 m/s^2$ ; b)  $a_g = 2.884 m/s^2$ ; c)  $a_g = 3.728 m/s^2$

Figures 5.70 and 5.71 concentrate the response point estimations for the BF and SR structures, respectively. Table 5.14 summarises the response point, for the BF and SR structures, assessed with the CSM in terms of base-shear, top-displacement and global damping, for each level of seismic action.

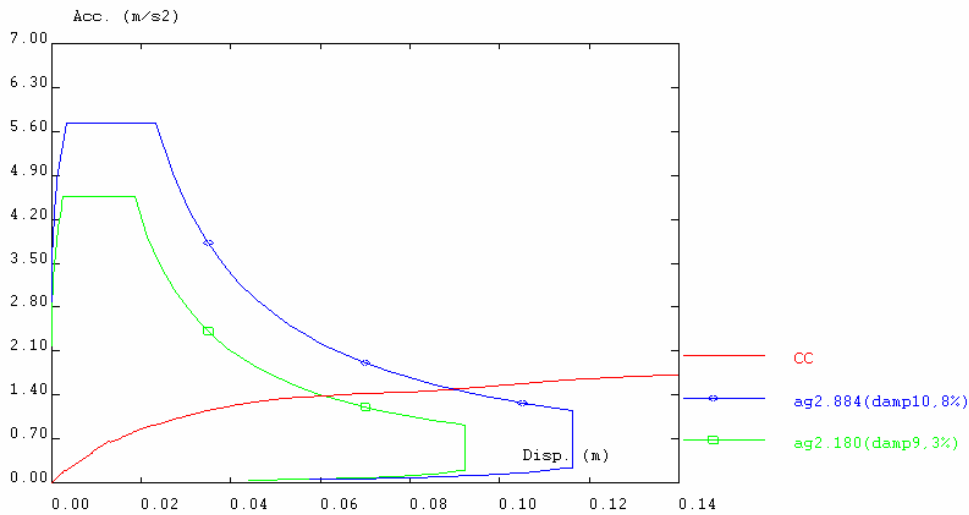


Figure 5.70 - Assessment of the BF with the CSM (subsoil class A; response spectra type I) for input motions:  $a_g = 2.180 \text{ m/s}^2$  and  $a_g = 2.884 \text{ m/s}^2$

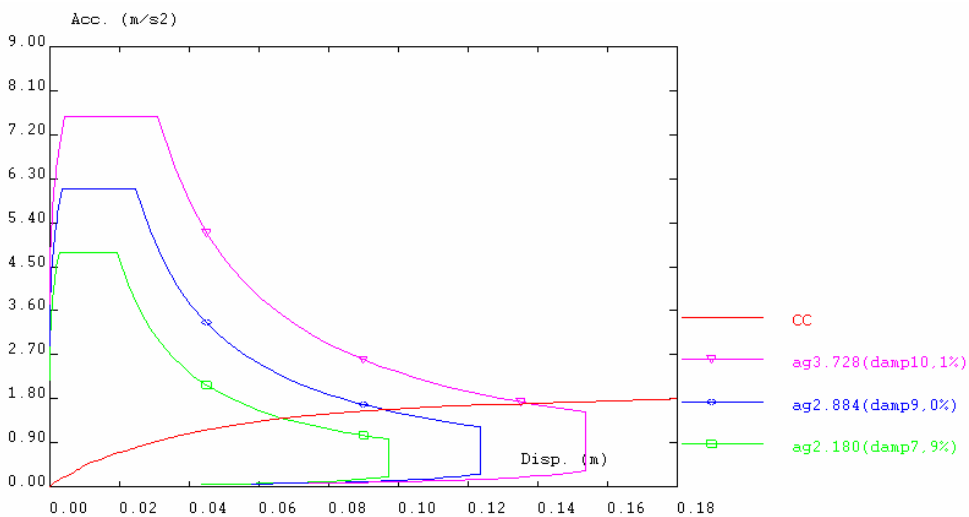


Figure 5.71 - Assessment of the SR with the CSM (subsoil class A; response spectra type I) for input motions:  $a_g = 2.180 \text{ m/s}^2$ ,  $a_g = 2.884 \text{ m/s}^2$  and  $a_g = 3.728 \text{ m/s}^2$

Table 5.14 - Summary table of the assessment response point (estimated with the CSM)

Structure	Input earthquake $a_g$ ( $m/s^2$ )	Base-shear ( $kN$ )	Top-displacement ( $mm$ )	Global damping (%)
BF	2.180	168.6	75.7	9.3
	2.884	182.4	113.6	10.8
SR	2.180	211.5	82.8	7.9
	2.884	238.4	119.7	9.0
	3.728	257.5	172.9	10.1

From the structural assessment summarised in Table 5.14, and comparing to the experimental PsD results (see Table 5.13), it can be observed that a rough estimation of the response global parameters, as top-displacement or base-shear, can be achieved with the capacity spectrum method.

#### 5.7.2.4 Final remarks

As observed in the application of the capacity spectrum method to the verification of experimental results and to the structural assessment, the global structural response parameters, as top-displacement or base-shear, can be achieved with this simplified non-linear static model.

However, it should be reminded that the main drawback of the capacity spectrum method is its incapacity to catch accurately the effect of irregularities (e.g. soft-storeys). Models that consider just one DOF (e.g. capacity curves) to describe the global behaviour of the structure have low sensitivity to local storey behaviour. Therefore, the response of irregular structures might be not adequately predicted with the CSM.

Nevertheless, the CSM can be considered a valuable tool for a first assessment of existing RC buildings and for parametric studies (assessment, redesign and retrofit decision strategies) of a certain class of buildings. Take for example, the work by Kölz and Bürge (2001), Badoux and Peter (2000), Peter and Badoux (2000, 1999) and Holmes (2000).

In the next section it is proposed a dynamic model to estimate the non-linear structural response of MDOF systems.

### 5.7.3 Improved MDOF non-linear dynamic model for structural assessment

As observed in Section 5.7.2.4, simplified non-linear static models considering just one DOF (such the CSM) are frequently not able to assess accurately irregular structural systems.

A simplified non-linear MDOF dynamic procedure, for structural assessment is here proposed and evaluated. The model accounts for two levels of non-linearities, namely: *a*) storey behaviour in terms of shear-drift; and, *b*) damping as a function of deformation. The procedure assumes that a non-linear MDOF system can be represented by an equivalent linearized system with element stiffness given the secant stiffness. Consequently, linear spectral analysis can be used and multi-modal response methods can be applied. The procedure is based on a generalization of the substitute-structure method, proposed by Shibata and Sozen (1976), which states that the response of a non-linear SDOF system can be accurately approximated by the response of an equivalent linear system with an equivalent period corresponding to the secant stiffness. The substitute-structure method constitutes the basis of the recently proposed direct displacement-based design methods (see for example Calvi, 1998).

The non-linear damping relationships can be modelled in two different ways, namely: *a*) variable (with damping functions defined for different structural components, e.g. for each DOF, storey); and, *b*) modal (global structural level). It was included the possibility of participation of several natural modes (multi-mode) for the structural response, with their quadratic combination.

The building structure is idealised as a bi-dimensional (2D) cantilever model (shear building), with a number of horizontal translational DOF's equal to the number of storeys. The structural model is fixed at the base, as represented in Figure 5.72, and the rotation of each node is fixed against rotation. The shear force-displacement relationship of each beam-element represents the curves storey shear versus inter-storey drift.

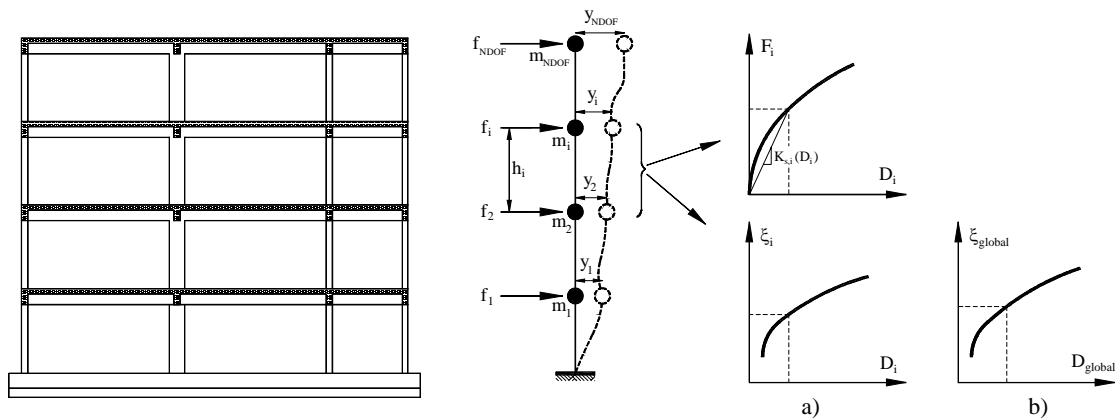


Figure 5.72 - MDOF structural simplified model with concentrated masses at storey levels being connected by shear beam elements: a) damping defined for each storey, b) global first mode structural damping

In this model, represented schematically in Figure 5.72, the mass distribution of the building is defined for each floor level accounting for the mid-height storey masses and lumped at floor level (equivalent total storey masses). Therefore, the  $i$ -th storey mass ( $m_i$ ) concentrates the total storey mass at node (storey)  $i$ , and these nodes are connected by shear-beam elements. The storey damping is labelled  $\xi_i$ . The force vector  $\{F\}$  is expressed in terms of the shear forces acting on the beam elements (storey shear), and the relative inter-node displacement vector  $\{D\}$  is expressed in terms of lateral deformation of the beam element (inter-storey drift). The storey shear force ( $F_i$ ) acting on a beam element and the inter-storey drift ( $D_i$ ) are related by the non-linear  $F_i$ - $D_i$  curve.

In the iterative step-by-step procedure, for each step, the calculations are made with constant secant stiffness and damping at the storey levels.

The required mechanical non-linear relationships can be obtained and calibrated from one or more of the following: *a)* experimental tests on structural specimens; *b)* simplified empirical expressions; and *c)* analytical calculations from a detailed structural model (pushover numerical analysis).

The proposed simplified MDOF non-linear dynamic method for assessment of multi-storey building structures calls for a relatively small number of DOF's (one per floor), compared to a detailed FE model. Evident advantages come out, for example, fast parametric studies with a good level of confidence can be carried out with the model. A practical application of this simplified method is made in the next section. Section 5.8 describes an optimization

algorithm for redesign of existing structures, which takes full advantage of the proposed simplified dynamic method. The method is described in the next section.

### 5.7.3.1 Description of the implemented algorithm

The basic steps of the proposed MDOF non-linear dynamic assessment iterative step-by-step procedure with two levels of non-linearities are:

#### *1<sup>st</sup> step: data, initial model and demand parameters*

- Structure geometry: number of DOF, inter-storey height,  $h_i$ .
- Set non-linear curves: monotonic storey shear-drift constitutive behaviour curves,  $F_i(D_i)$ , variable damping curves at storey,  $\zeta_i(D_i)$ , or global level,  $\zeta_{Global}(D_{Global})$  - (see Figure 5.72).
- Compute the non-linear storey behaviour curves for the uniform column with two ends fixed against rotation, which secant stiffness (see Figure 5.72), as a function of deformation  $k_{s,i}(D_i)$  is

$$k_{s,i}(D_i) = \frac{12 \cdot \overline{EI}_i(D_i)}{h_i^3} \quad (5.20)$$

where the coefficient  $\overline{EI}_i$  is a non-linear function of the level of deformation  $D_i$  as

$$\overline{EI}_i(D_i) = \frac{F_i(D_i)}{D_i} \cdot \frac{h_i^3}{12} \quad (5.21)$$

- Set storey masses,  $m_i$ .
- Define elastic seismic demand (see Figure 5.73),  $S_a(T, \zeta_0)$ , smoothed response spectra (e.g.: according to the spectra proposed in EC8).

#### *2<sup>nd</sup> step: starting point*

- Set the number of fundamental modes to be considered in the structural response,  $NMOD$ .
- Set the iteration index,  $k=0$ .



- Select the initial values for: the storey secant stiffness ( $K_{S,i}^0$ ) and for the storey ( $\xi_i^0$ ) or global ( $\xi_{Global}^0$ ) damping coefficient, on the basis of the constitutive relations.

3<sup>rd</sup> step: determine the seismic response

- Compute and assemble the stiffness matrix  $[K]$  and the diagonal mass matrix  $[M]$  of the MDOF system
- Compute the structural natural periods  $\{T\}$  and modal shapes  $[\Phi]$ , solving the eigenproblem

$$|[K] - \omega^2 \cdot [M]| = 0 \quad (5.22)$$

Solving the polynomial equation (characteristic equation) resulting from expression (5.22) of degree NDOF in  $\omega^2$ , are obtained NDOF values of  $\omega^2$ , which provide the natural frequencies  $\omega_j$  (and corresponding natural periods,  $T_j = 2\pi/\omega_j$ ).

For each value of  $\omega_j^2$  ( $j=1,2,\dots,NDOF$ ) satisfying the characteristic equation (5.22), it is solved the equation (5.23) for  $\phi_{1,j}, \phi_{2,j}, \dots, \phi_{NDOF,j}$  in terms of arbitrary constant, obtaining the modal shapes (eigenvectors) of the dynamic system

$$([K] - \omega_j^2 \cdot [M]) \cdot \{a\}_j = \{0\} \quad (5.23)$$

And dividing the components of the vector  $\{a\}_j$  by  $\sqrt{\{a\}_j^T [M] \{a\}_j}$ , we obtain the normalized eigenvectors  $\{\phi\}_j$

$$\{\phi\}_j = \frac{\{a\}_j}{\sqrt{\{a\}_j^T [M] \{a\}_j}} \quad (5.24)$$

- Compute the structural effective damping,  $\xi_{eff}$ .
- Compute the reduced elastic seismic response spectra  $S_a(T, \xi_{eff})$ , according to EC8, with the damping correction factor,  $\eta$

$$\eta = \sqrt{10/(5 + \xi)} \geq 0.55 \quad (5.25)$$

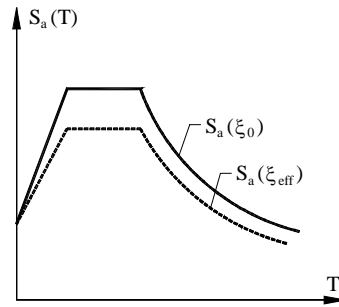


Figure 5.73 - Reduced spectral seismic demand

- Determine the structural response from the modal analysis with quadratic combination

$$u_{i,\max} = \sqrt{\sum_{j=1}^{NMOD} u_{ij,\max}^2} \quad (5.26)$$

- Determine storey shear forces  $\{F\}$ , from the storey restoring forces  $\{f\}$ , and the inter-storey drifts,  $\{D\}$ , from the storey lateral displacements  $\{y\}$ , for the MDOF system

$$F_i = \sum_{j=i}^{NDOF} f_j \quad D_i = \begin{cases} y_i - y_{i-1} & ; i > 1 \\ y_i & ; i = 1 \end{cases} \quad (5.27, 5.28)$$

4<sup>th</sup> step: check for convergence at two levels

- Check for convergence: in terms of storey shear-drift, and in terms of damping (at storey or global level)

$$\frac{\|X^{k+1} - X^k\|}{\|X^k\|} < \varepsilon ? \quad (5.29)$$

- If convergence is not satisfied, prepare new values for the next iteration point (for the secant stiffness and/or damping, on the basis of the constitutive relations and deformation demand), increase the iteration index  $k$  by one, and return to step 3.

5<sup>th</sup> step: graphical output of the converged response

- Graphical representation of the storey shear-drift response point, inter-storey drift profile, and damping.

### 5.7.3.2 Verification of the earthquake tests

In order to calibrate and verify the method in predicting global parameters (such as top-displacement, maximum inter-storey drift, maximum storey shear, and equivalent damping), the proposed MDOF non-linear dynamic seismic analysis methodology (described in Section 5.7.3.1) is applied to simulate the PsD tests performed on the bare and strengthened structures.

The structures were analysed for input motions corresponding to the maximum accelerations of the earthquakes considered in the tests, namely 2.180 and 2.884  $m/s^2$  for the BF (corresponding to 475 and 975-yrp), and 2.180, 2.884 and 3.728  $m/s^2$  for the SR (475, 975 and 2000-yrp). The description of the structure can be found in Section 3.2. Experimental results concerning these tests were given in Sections 4.2 and 4.3, for the BF and SR, respectively.

For the structure under analysis, four DOF are considered, being the storey masses considered for the first three storeys ( $m_1$ ,  $m_2$  and  $m_3$ ) 44.6 ton, and for the fourth storey ( $m_4$ ) 40.0 ton (as presented in Section 3.7.1). The envelope storey shear-drift behaviour curves, obtained from the PsD earthquake tests for the BF and SR structures, were here adopted as capacity curves (see Figure 4.5 and 4.23, for the BF and SR, respectively). As noted in Section 5.7.2.1, it is recalled that the storey shear-drift envelope curves of the PsD tests are in good agreement with the storey behaviour curves obtained with the pushover analysis. In these numerical analyses, it was considered the structural damping at storey level (see Figure 5.59).

The inter-storey drift profiles obtained from the numerical analyses performed with the proposed simplified MDOF non-linear dynamic method are plotted in Figures 5.74 and 5.75, for the BF and SR structures, respectively. In these figures are also plotted, for comparison, the maximum inter-storey drift profiles observed in the corresponding PsD tests.

The structural response was estimated considering the participation of one and four natural modes of the equivalent linear system, in order to analyse the influence of the number of natural modes in the global response. These two situations are also represented in the plots.

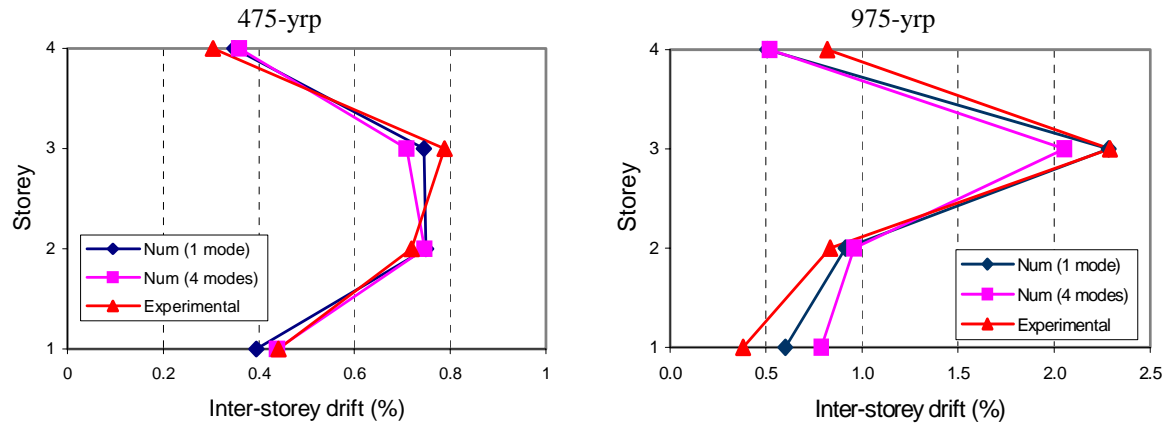


Figure 5.74 - Inter-storey drift profile computed and PsD test results for the BF structure

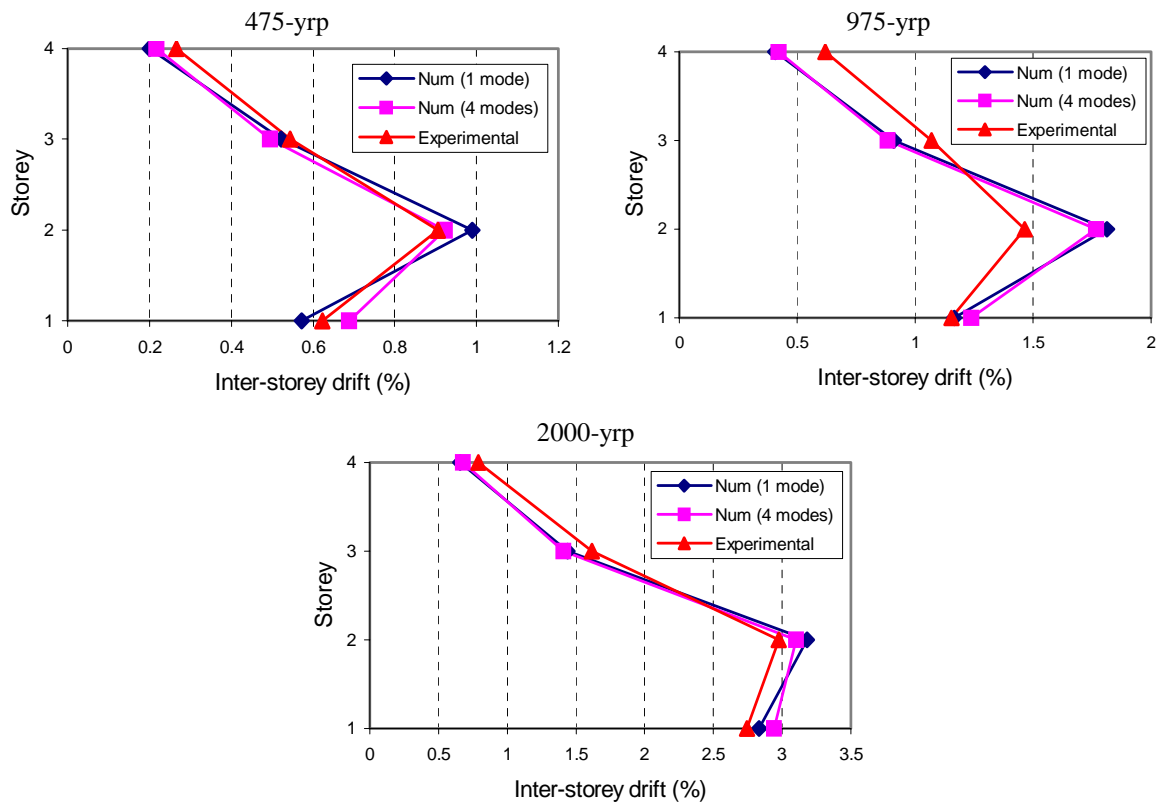


Figure 5.75 - Inter-storey drift profile computed and PsD test results for the SR structure

From the analyses of the results in Figures 5.74 and 5.75, the following can be observed:

- The results obtained with the proposed MDOF non-linear dynamic methodology are in good agreement with the maximum inter-storey drift demands observed in the PsD tests. This accordance was verified not only for the regular SR structure, but also for the irregular BF structure. Furthermore, with this model it is possible to

estimate the deformation demand at each storey level. Thus, this displacement-based methodology can be an efficient numerical tool for seismic vulnerability assessment.

- The higher mode effects were of relatively little importance in the global response of the studied BF and SR structures. That is, for both structures, it was not verified a significant variation considering one or four modes to the structural response.
- A good estimation of the maximum response was achieved, with the simplified non-linear dynamic model, considering a small number of DOF (4 versus 372 DOF's for the refined 2D FE model). Therefore, this model can be an effective tool to perform fast non-linear analyses, which could allow for parametric studies and rapid screening of existing building classes.

#### *5.7.3.3 Assessment of the bare frame structure*

A vulnerability assessment of the irregular BF structure is here performed with the proposed simplified non-linear MDOF dynamic model. For the storey behaviour curves it were used the storey shear-drift curves obtained with the pushover analysis of the building. The increasing input motion was defined considering the response spectra type I and subsoil class A, in accordance to the Eurocode 8.

The structural response was estimated for increasing input motions with the multi-mode model. In Figure 5.76 are represented the obtained vulnerability functions in terms of inter-storey drift and top-displacement. Considering the base-shear and top-displacement calculated for increasing levels of input motion, the capacity curve of the BF was then estimated. In Figure 5.77 are represented the capacity curves obtained with the simplified dynamic and pushover analysis, as well as the results of the PsD and cyclic tests on the BF structure.

From the application of the simplified non-linear analysis, it can be observed that the generated capacity curve gives a better approximation to the envelope of the dynamic test results for the irregular BF structure than the capacity curve obtained with the pushover analysis. This outcome sustains the utilization of this method in the seismic analysis of

structures. It is an accurate tool to determine the structural response even for irregular structures.

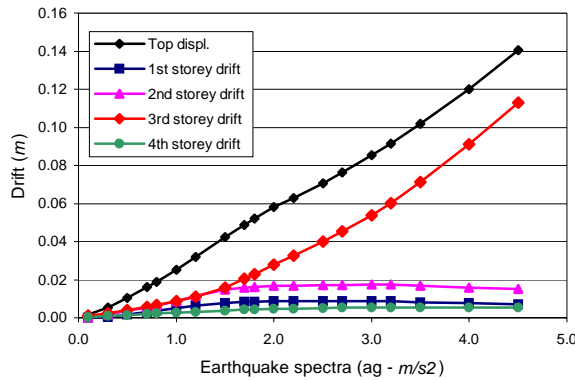


Figure 5.76 - Vulnerability functions of the top-displacement and storey drift for the BF structure calculated with the multi-mode model

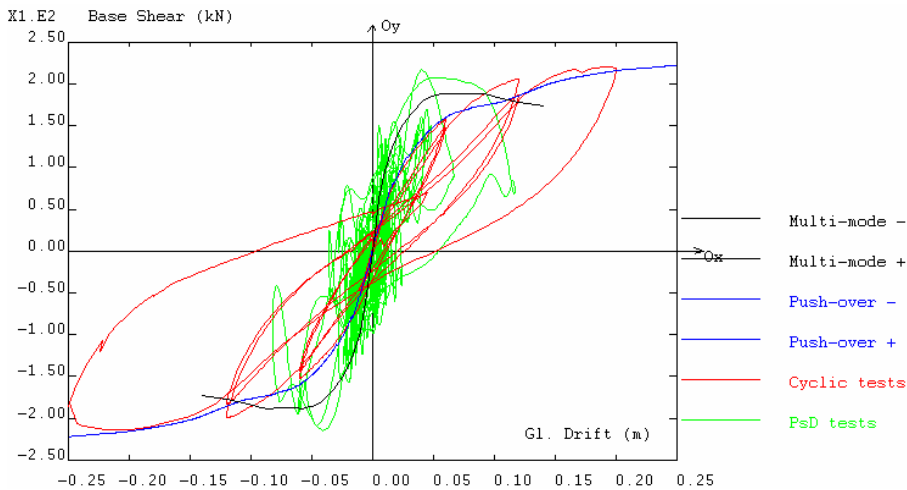


Figure 5.77 - BF capacity curves: multi-mode method (black), pushover (blue), PsD tests (green) and cyclic test (red)

### 5.7.4 Observed seismic performance in the earthquake tests

For each test series (bare and strengthened frames) the structure was subjected to increasing earthquake intensities (from moderate to high intensities, as given in Table 3.25), in order to reach different damage levels. As already stated in Chapter 3, the return periods for the input motions were chosen so as to test the structure under different seismic hazard levels specified in the VISION-2000 (SEAOC, 1995) and FEMA-273 (1997) documents. These correspond to the 'Rare' (475-yrp) and 'Very Rare'

(975 and 2000-yrp) events, under which a structure has to meet the 'Life Safety' and 'Collapse Prevention' performance levels, according to the minimum acceptable basic performance objectives for buildings of normal occupancy and use, proposed in the VISION-2000 (see Figure 2.1).

In Table 5.15 are presented for each performance level the representative damage in columns and beams, for non-ductile RC frame buildings (according to the ATC-40, 1996). In Table 5.16 are presented the storey deformation limits, also for each performance level, proposed at the ATC-40.

Table 5.15 - Representative damage descriptions for elements in non-ductile RC frame buildings (adapted from ATC-40, 1996)

Element	Nature of damage	Performance level			
		Immediate Occupancy	Damage Control	Life Safety	Structural Stability
Columns	Flexural and shear cracking	Very limited	Limited	---	---
	Hinges formed in the lower portions of the building	---	---	Yes	Yes
	Spalling (above and below beam-column joints)	No	No	Yes	Significant
	Pulverizing of concrete within the core	---	---	---	Yes
	Permanent horizontal offset	No	No	~2% <sup>a</sup>	~3.5% <sup>a</sup>
	Gravity capacity maintained	Yes	Yes	Yes	Yes <sup>b</sup>
Beams	Spalling around beam-column joint	Very limited	Limited	Yes	Extensive
	Spalling around hinge region	---	---	Yes	Extensive
	Flexural cracking in hinge region	Very limited	Very limited	Yes	Extensive
	Shear cracking in hinge region	---	---	Yes	Extensive
	Cracking progressing into the beam column-joint	---	---	Yes	Yes
	Damage of the shear stirrups adjacent to joint	---	---	Elongation	Rupture
	Permanent deflection	No	No	~L/175	~L/75
	Gravity capacity maintained	Yes	Yes	Yes	Yes

a) ID (%) with small areas marginally higher.

b) Throughout nearly all of the structure.

Table 5.16 - Storey deformation limits (adapted from ATC-40, 1996)

ID limit	Performance level			
	Immediate Occupancy	Damage Control	Life Safety	Structural Stability <sup>a</sup>
Maximum total drift	1%	1-2%	2%	$0.33 \frac{V_i}{P_i}$

a)  $V_i$  is the total lateral shear force in the storey  $i$ , and  $P_i$  is the total gravity load (i.e., dead load plus likely live load) at storey  $i$ .

The structural performance response for each PsD test on BF and SR structures is indicated in the seismic matrix of performance objectives in Table 5.17. In this table are also indicated the basic performance objectives for buildings of normal occupancy and use, proposed in the VISION-2000.

The performance response was classified according to the observed damage in beams and columns (see Tables 4.2 and 4.7, for BF and SR respectively) and to the maximum inter-storey drift (see Tables 4.1 and 4.6 for BF and SR respectively) verified for each pseudo-dynamic test. The classification of damages and drift limits, for each performance level, was based in the proposal of ATC-40 (1996), summarised in Tables 5.15 and 5.16, respectively.

From the analysis of Table 5.17, it is observed that for the 975-yrp test the original bare frame does not satisfy the VISION-2000 (SEAOC, 1995) basic design performance objective. For the strengthened structure the basic performance objectives are verified.

Table 5.17 - Matrix of the observed seismic performance for the BF and SR tests

		Fully Operational	Operational	Life Safe	Collapse Prevention	Collapse
Earthquake design level	Frequent (43-yrp)					
	Occasional (72-yrp)					
	Rare (475-yrp)			<b>BF475 SR475</b>		
	Very Rare (970-2000-yrp)				<b>SR975 SR2000</b>	<b>BF975</b>



---

## 5.8 - STRUCTURAL OPTIMIZATION PROBLEM IN SUPPORT OF BUILDING RETROFITTING DECISION

### 5.8.1 Introduction

Structural optimization problems consist on determining the configurations of structures that obey assigned constraints, and produce an extremum for a chosen objective function. In order to solve them, they are normally transformed into a mathematical form that can be solved by general optimization tools. Since structural optimization problems are characterized by computationally expensive function evaluations, it is common to generate a sequence of convex, separable sub-problems, which are then solved iteratively (Chickermane and Gea, 1996-*a*).

For structural strengthening, optimization is an obligatory stage, as stated by Verpeaux *et al.* (1991). It is therefore judged appropriate to have a methodology that can address the strengthening design of MDOF structural systems, generating optimal distribution (location) of the strengthening in the structure components (at storey level).

In this study, three methodologies for optimum redesign of existing structures are proposed and programmed. The optimization algorithms are based on the convex approximation methods, such as the CONvex LINearization method (CONLIN) developed by Fleury (1989; 1979) and Braibant (1985), and the Method of Moving Asymptotes (MMA). These optimization algorithms can deal with non-linear objective functions (minimum cost of intervention) and allows to impose constrains on the design variables (strength, stiffness or damping) and on any other response variable depending on the design variables, such as inter-storey drift, top-displacement, etc.

The optimization procedure requires several structural response evaluations, namely of the objective function, of constraints, and of their derivatives. The calculation of the structural response is required many times during the optimization process, which would be unfeasible with a refined FE model. The simplified model allows for spectral analysis, which constitutes a great advantage over the multi-series analyses. The model is able to estimate the response of irregular structures those we address with the optimization of the

retrofit. Therefore, the simplified MDOF dynamic method, presented in Section 5.7.3, was incorporated in the redesign optimization algorithms here proposed.

In these three structural optimization problems, the design variables, or control variables, are defined at storey level, and they are:

- The additional strength (Problem I);
- The additional pre-yielding stiffness (Problem II); and,
- The yielding strength of the energy dissipation device (Problem III).

In the next are revised the theoretical concepts related with the optimization problem. The three implemented optimization problems are explained. Strengthening design examples based on the structure under analysis are used to illustrate the capability of the proposed methodology. Finally, comments on the implemented methodology are given.

### 5.8.2 Theoretic mathematical background

As exposed by Chickermane and Gea (1996-*a*; 1996-*b*), in structural optimization problems, the performance and constraint functions can be selected from integral functions such as weight, mean compliance or natural frequency, and from local functions such as maximum Von Mises stress or maximum deflection. The design vector can consist of material properties or shape defining parameters, such as coordinates of vertices or control points of spline curve boundaries.

Consider  $x = \{x_1, x_2, \dots, x_n\}$  a vector of design variables and dimension  $n$ , and  $f_0(x)$  the function to be minimized. Here, the objective function  $f_0(x)$  represents the structural characteristic, and the additive inequalities  $g_j(x) \leq g_j$  ( $j = 1, \dots, m$ ) are the behaviour constraints. The lower and upper bounds of the design variables  $x_i$  are  $\underline{x}_i$  and  $\bar{x}_i$ , respectively. The structural optimization problem can be stated mathematically as

$$\begin{array}{ll} \text{Minimize} & f_0(x) \\ \text{Subject to} & \left\{ \begin{array}{l} g_j(x) \leq g_j \quad j = 1, \dots, m \\ \underline{x}_i \leq x_i \leq \bar{x}_i \quad i = 1, \dots, n \end{array} \right. \end{array} \quad \begin{array}{l} (5.30) \\ (5.31) \end{array}$$

For structure optimization, functions  $f_0(x)$  and  $g_j(x)$  are not always known in an explicit way, generally are non-linear and very expensive to evaluate (Verpeaux *et al.*, 1991). To reduce the computational cost, a general procedure is to generate a sequence of convex, explicit sub-problems and solve them in an iterative fashion (Fleury, 1989), i.e. a Sequential Convex Programming (SCP) approach is used. Various approximation schemes have been developed for this purpose.

The approximation schemes of interest to us are local function approximations (Barthelemy and Haftka, 1993), which generate an approximated formulation of the problem in the vicinity of the current design point. One of the earliest of such schemes is Sequential Linear Programming (SLP). In SLP, a linear approximation of the function is formulated using the first order derivative term of the Taylor Series expansion as

$$\tilde{f}(x) = f_0 + \sum_i (x_i - x_{i0}) \left. \frac{\partial f}{\partial x_i} \right|_{x_0} \quad (5.32)$$

In truss design problems, where the design variables are often chosen as the cross sectional areas of the bar structure, it is advantageous to use reciprocals of the design variables to formulate the approximation. This procedure was followed by the CONvex LINearization (CONLIN) method (Fleury and Braibant, 1986). This method linearizes each function using a properly selected mix of direct  $x_i$  and reciprocal  $1/x_i$  variables. The selection of the variables is made based on the signs of the first partial derivatives, that is, direct variables for positive first derivative and reciprocal for negative first derivatives. It is of the form

$$\tilde{f}(x) = f_0 - \sum \left. \frac{\partial f}{\partial x_i} \right|_{x_0} x_{i0} + \sum_+ \left. \frac{\partial f}{\partial x_i} \right|_{x_0} x_i - \sum_- x_{i0}^2 \left. \frac{\partial f}{\partial x_i} \right|_{x_0} \frac{1}{x_i} \quad (5.33)$$

where the symbols  $\sum_+$  and  $\sum_-$  mean summation over the positive and negative terms, respectively. The first two terms are the contribution of the zero-th order terms in the Taylor series expansion. This method yields convex and separable approximations. CONLIN employs conservative approximations and has shown good convergence properties in dealing with some structural optimization problems. However, in certain

problems, this convex approximation is either too conservative or not sufficiently conservative (Chickermane and Gea, 1996-a).

Svanberg (1987) proposed the Method of Moving Asymptotes (MMA), which is a modification of CONLIN method. In MMA method, the linearization variables can be used to adjust the degree of convexity and conservativeness depending on the problem. The variables take the form  $1/(x_i - L_i)$  and  $1/(U_i - x_i)$  where  $U_i$  and  $L_i$  are user selected variables called the moving asymptotes. The approximation is of the form

$$\tilde{f}(x) = d_0 + \sum_{+} \frac{b_i}{U_i - x_i} - \sum_{-} \frac{b_i}{x_i - L_i} \quad (5.34)$$

where

$$b_i = \begin{cases} (U_i - x_{i0})^2 \frac{\partial f}{\partial x_i} \Big|_{x_0} & ; \quad \frac{\partial f}{\partial x_i} \Big|_{x_0} > 0 \\ (x_{i0} - L_i)^2 \frac{\partial f}{\partial x_i} \Big|_{x_0} & ; \quad \frac{\partial f}{\partial x_i} \Big|_{x_0} < 0 \end{cases} \quad (5.35)$$

In this expression  $d_0$  collects the zero-th order terms. The moving asymptotes  $L_i$  and  $U_i$  can be used to control the optimization process. If the process oscillates, it can be stabilized by moving the asymptotes closer to the current iteration point. If it converges slowly, the asymptotes are moved away. On taking  $L_i = 0$  and  $U_i = +\infty$  MMA is reduced to the CONLIN method, while if  $L_i = -\infty$  and  $U_i = +\infty$  MMA is the same as SLP. MMA offers a great deal of flexibility in matching the curvature of the approximated function through the choice of  $L_i$  and  $U_i$ . However, empirical techniques have to be used to determine their values after each iteration.

A further extension of MMA was proposed by Fleury (1989). This method uses intermediate linearization variables of the form  $1/(x_i - d_{ij})$ . The approximated function is expressed as

$$\tilde{f}_i(x) = f_i(x^k) + \sum_{j=1}^n \left( \frac{1}{x_j - d_{ij}} - \frac{1}{x_j^k - d_{ij}} \right) (x_j^k - d_{ij})^2 \frac{\partial f_i}{\partial x_j} \Big|_{x^k} \quad (5.36)$$

The moving asymptote,  $d_{ij}$  determined from the second order derivative is

$$d_{ij} = x_j^k + 2 \frac{\partial f_i / \partial x_j}{\partial^2 f_i / \partial x_j^2} \Big|_{x^k} \quad (5.37)$$

In any structural optimization problem, an important consideration from the computational point of view is the number of function evaluations required to formulate the approximated problem. Besides this, to evaluate the quality of the approximation obtained it is crucial to determine the rate of convergence to the optimal solution (Chickermane and Gea, 1996-*a*).

### 5.8.3 Structural strengthening optimization problems' formulation

For the optimization problems here proposed, it is assumed that the behaviour of a multi-storey RC existing building (non-seismically designed) subjected to a certain earthquake action level can be represented by the multi-modal model proposed in Section 5.7.3. Buildings are modelled with one DOF per storey, linked by beam elements that represent the storey behaviour. The beam elements have an equivalent secant stiffness corresponding to the maximum deformation point in the non-linear storey constitutive curve. Furthermore, response spectra modal analysis with concentrated and/or distributed damping is used to compute the seismic response for each step of the optimization procedure.

The optimization procedure requires previous identification of simplified (bilinear) storey shear-drift constitutive relations made on the basis of pushover analysis, as represented in Figure 5.78.

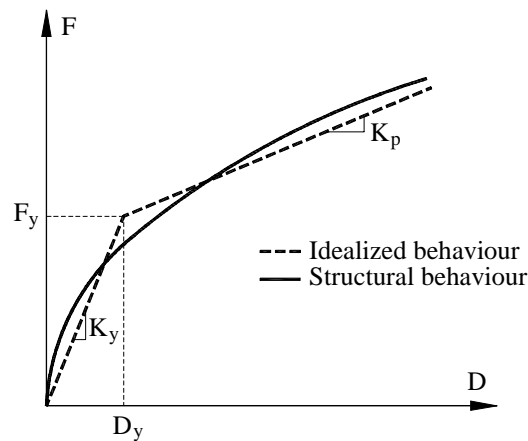


Figure 5.78 - Lateral storey shear versus inter-storey drift behaviour (exact and idealized bilinear behaviour)

As recalled in Section 2.3, a seismic performance objective is formed by combining a desired building performance level (a damage limit-state) with a given earthquake ground motion (level of hazard). The objective of this analysis is to find the optimum retrofitting solution in order to comply with a certain seismic demand-level defined for each limit-state.

The optimization problem, in generic terms, is to minimise the total strengthening requirements in the structure, whilst satisfying the limits for the inter-storey drifts and maximum strengthening at each storey, as given in the following

$$\begin{aligned} &\text{Minimise} \quad \text{The total strengthening costs} \\ &\text{Subject to} \quad \left\{ \begin{array}{l} \text{Upper limits of storey strengthening; and,} \\ \text{Upper limits of storey lateral deformation (inter-storey drift)} \end{array} \right. \end{aligned}$$

The objective function for each problem is the sum of the control variables (additional strengthening costs) at each storey level. The inequality constraints are upper inter-storey drift limits (to restrain the damage at storey level) and upper storey strengthening limits (to restrict the strengthening within acceptable values).

As already said, three design optimization structural strengthening problems were established in this work. They were conceptually based on the strengthening strategies commonly used in practice, which call for the control variables: the strength (controlled by

the yielding shear force,  $\Delta F_y$ ), the pre-yielding stiffness ( $\Delta K_y$ ), and the yielding strength of the energy dissipator devices ( $F_y^{dev}$ ), as will be explained in the subsequent sections.

### 5.8.3.1 Problem I: storey yielding strength

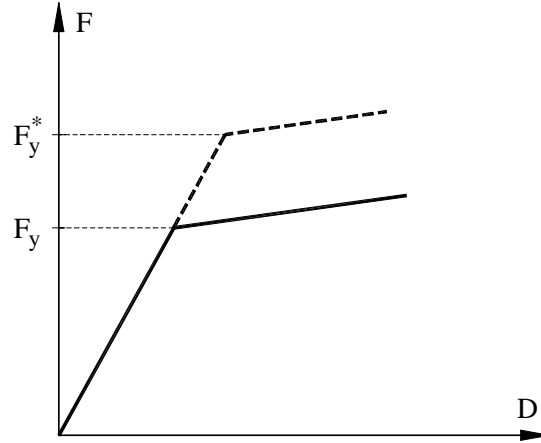


Figure 5.79 - Control variable: strength (yielding shear force –  $F_y$ )

Problem I (control variables: strength,  $\Delta F_y$ , see Figure 5.79) can be described in the following mathematical form

$$\text{Find} \quad \Delta F_y = \{\Delta F_{y,1}; \Delta F_{y,2}; \dots; \Delta F_{y,NDOF}\} \quad (5.38)$$

$$\text{Minimise} \quad Cost(\Delta F_y) = \sum_{i=1}^{NDOF} \Delta F_{y,i} = \sum_{i=1}^{NDOF} (F_{y,i} - F_{y,i}^0) \quad (5.39)$$

$$\text{Subject to} \quad \begin{cases} \Delta F_{y,i}^{\min} \leq \Delta F_{y,i} \leq \Delta F_{y,i}^{\max} & i = 1, 2, \dots, NDOF \\ D_i \leq D_i^{\max} & i = 1, 2, \dots, NDOF \end{cases} \quad (5.40)$$

in which:  $F_{y,i}^0$ ,  $\Delta F_{y,i}$  and  $F_{y,i}$  are the initial, incremental and total yielding strength of the storey  $i$ , respectively. NDOF represents the number of degrees of freedom of the problem, i.e. number of storeys.  $\Delta F_{y,i}^{\min}$  and  $\Delta F_{y,i}^{\max}$  are the lower and upper bound limits for each control variable ( $\Delta F_{y,i}$ ).  $D_i$  is the inter-storey drift at storey-level  $i$ .  $D_i^{\max}$  is the maximum admissible inter-storey drift for each storey-level.

In this problem, it were studied two possibilities for the variation of the curves force-displacement, namely (see schemes represented in Figure 5.80): *I-a*) yielding displacement constant; and, *I-b*) yielding stiffness constant.

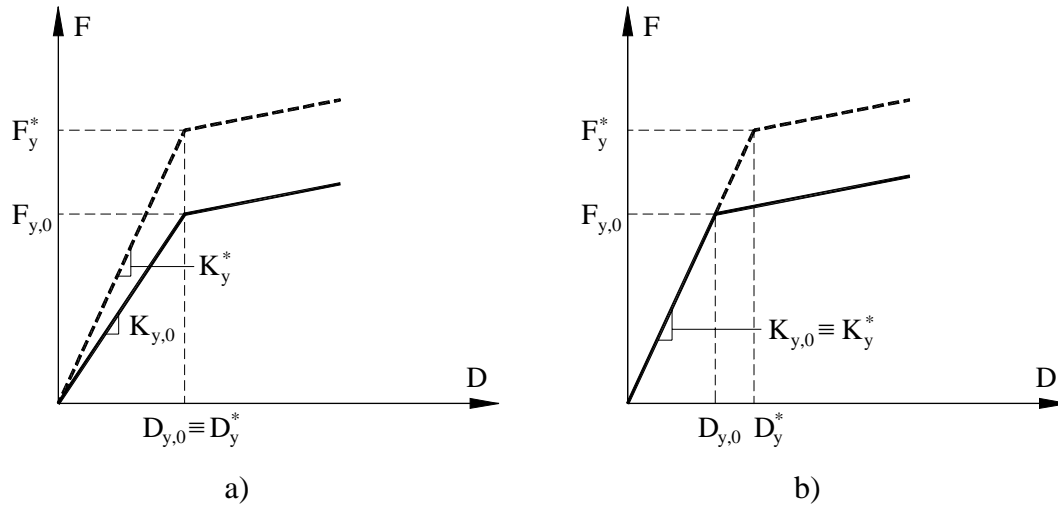


Figure 5.80 - Problem I: a) yielding displacement constant; b) yielding stiffness constant

For the pos-yielding stiffness ( $K_p$ ), two different possibilities were implemented in this optimization problem. The first option maintains constant the pos-yielding stiffness (expression 5.42), and in the second option it is imposed a constant ratio between the yielding stiffness ( $K_y$ ) and pos-yielding stiffness (expression 5.43)

$$K_p^* = K_p \qquad \frac{K_p^*}{K_y^*} = \frac{K_p}{K_y} \qquad (5.42, 5.43)$$

5.8.3.2 Problem II: storey yielding stiffness (initial stiffness)

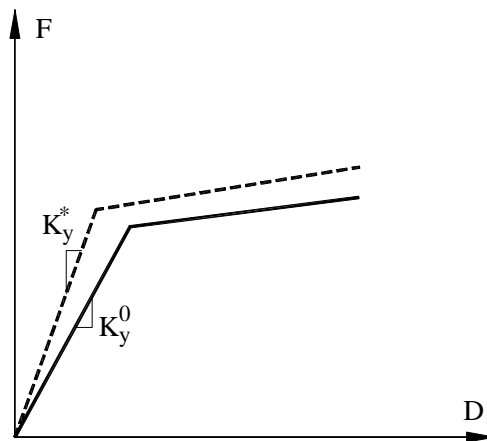


Figure 5.81 - Control variable: pre-yielding stiffness ( $K_y$ )



In Problem II, the task is to minimize the total pre-yielding stiffness,  $\Delta K_y$ , strengthening (see Figure 5.81). This optimum strengthening design problem can be mathematically stated in the form of

$$\text{Find} \quad \Delta K_y = \{\Delta K_{y,1}; \Delta K_{y,2}; \dots; \Delta K_{y,NDOF}\} \quad (5.44)$$

$$\text{Minimise} \quad \text{Cost}(\Delta K_y) = \sum_{i=1}^{NDOF} \Delta K_{y,i} = \sum_{i=1}^{NDOF} (K_{y,i} - K_{y,i}^0) \quad (5.45)$$

$$\text{Subject to} \quad \begin{cases} \Delta K_{y,i}^{\min} \leq \Delta K_{y,i} \leq \Delta K_{y,i}^{\max} & i = 1, 2, \dots, NDOF \\ D_i \leq D_i^{\max} & i = 1, 2, \dots, NDOF \end{cases} \quad (5.46)$$

in which:  $K_{y,i}^0$ ,  $\Delta K_{y,i}$  and  $K_{y,i}$  are the initial, incremental and total pre-yielding stiffness of the storey  $i$ , respectively. NDOF represents the number of degrees of freedom of the problem, i.e. number of storeys.  $\Delta K_{y,i}^{\min}$  and  $\Delta K_{y,i}^{\max}$  are the lower and upper bound limits for each control variable ( $\Delta K_{y,i}$ ).  $D_i$  is the inter-storey drift at storey-level  $i$ .  $D_i^{\max}$  is the maximum admissible inter-storey drift for each storey-level.

For the post-yielding stiffness ( $K_p$ ), this optimization problem, considers also the two different possibilities referred to in the Problem I (see expressions 5.42 and 5.43). It was also developed a strengthening intervention strategy defined as a combination of strength and stiffness upgrading.

### 5.8.3.3 Problem III: yielding strength of the energy dissipator devices

The Problem III (control variables: yielding force of the dissipator device,  $F_y^{dev}$ , see Figure 5.82) can be described in the following mathematical form

$$\text{Find} \quad F_y^{dev} = \{F_{y,1}^{dev}; F_{y,2}^{dev}; \dots; F_{y,NDOF}^{dev}\} \quad (5.48)$$

$$\text{Minimise} \quad \text{Cost}(F_y^{dev}) = \sum_{i=1}^{NDOF} F_{y,i}^{dev} \quad (5.49)$$

$$\text{Subject to } \begin{cases} F_{y,i}^{dev,min} \leq F_{y,i}^{dev} \leq F_{y,i}^{dev,max} & i = 1, 2, \dots, NDOF & (5.50) \\ D_i \leq D_i^{max} & i = 1, 2, \dots, NDOF & (5.51) \end{cases}$$

in which:  $F_{y,i}^{dev}$  is the total yielding strength of the dissipative device at storey  $i$ .  $NDOF$  represents the number of degrees of freedom of the problem, i.e. number of storeys.  $F_{y,i}^{dev,min}$  and  $F_{y,i}^{dev,max}$  are the lower and upper bound limits for each control variable ( $F_{y,i}^{dev}$ ).  $D_i$  is the inter-storey drift at storey-level  $i$ .  $D_i^{max}$  is the maximum admissible inter-storey drift for each storey-level.

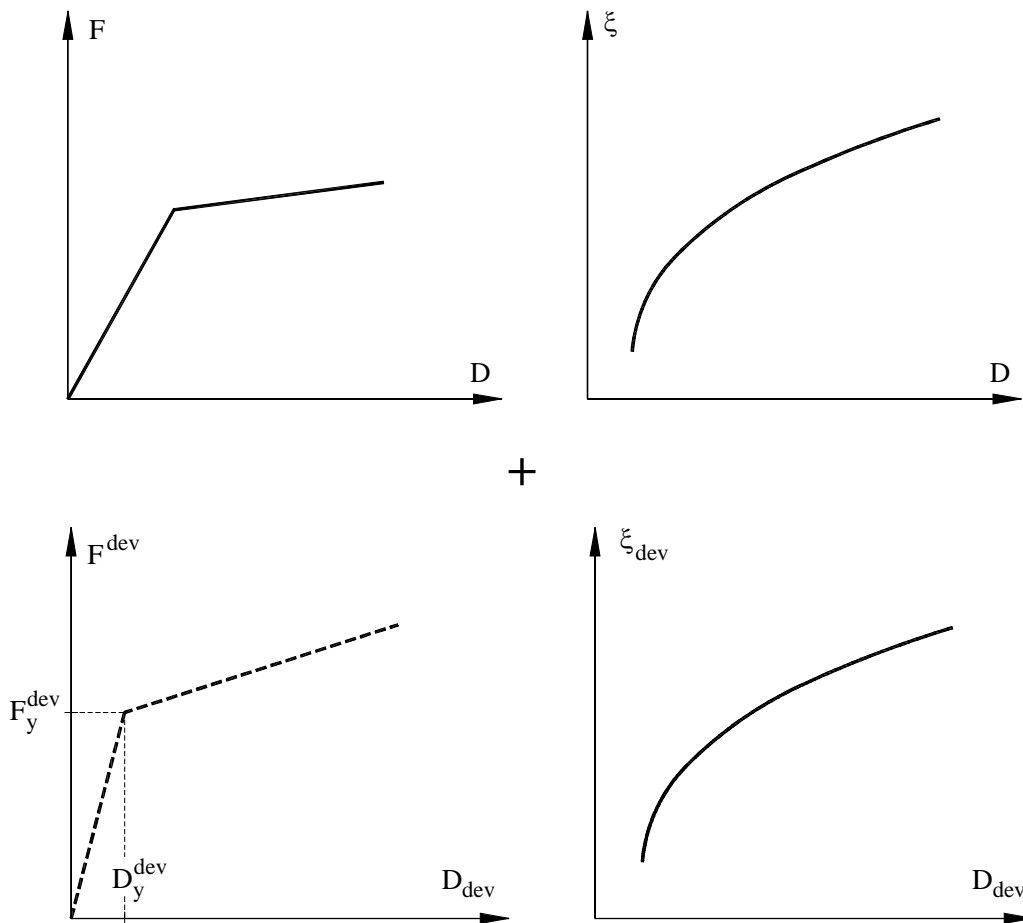


Figure 5.82 - Control variable: yielding force of the dissipator device

### 5.8.4 Implementation of the optimization problems

The optimization problems proposed in the previous section were implemented in the finite element code CASTEM (Millard, 1993). In CASTEM it is available an operator implemented by Verpeaux *et al.* (1991), called EXCE, which permits to solve numerically practical problems of optimization. The EXCE operator computes the minimum of a function with  $n$  independent variables, subjected to restrictions of the control variables and to other generic restrictions.

In this operator three methods of optimization are implemented, namely: *a)* 'LIN' – Method of Convex Linearization (without moving asymptotes) proposed by Braibant (1985). With the introduction of the moving asymptotes method (due to Svanberg, 1987), two different methods are implemented in CASTEM, for two different alternatives of the L and U functions, namely: *b)* 'STA'; and, *c)* 'MOV'.

The EXCE operator optimises the minimum of an approximate linear problem. The objective function and the restrictions are replaced with the linearized functions. With the linearized functions, the operator EXCE computes the converged minimum, which is employed to start with the next iteration. A more detailed description can be found in the CASTEM manual of the EXCE operator.

The philosophy of CASTEM is modular. Therefore, the optimization methodology was implemented in separate modules for pre-processing, structural analyses, optimization, pos-processing and graphical results visualisation. The basic steps of the iterative optimization process implemented can be summarised as follows (see also the schematic flowchart in Figure 5.83):

- 1) Select the design control variables, i.e. strengthening intervention strategy (strength, stiffness, or damping).
- 2) Define the structure geometry (NDOF storeys and inter-storey heights,  $h_i$ ), the original bilinear storey shear-drift behaviour curves,  $F_i(D_i)$ , and variable damping curves at storey,  $\zeta_i(D_i)$ , or global level,  $\zeta_{Global}(D_{Global})$ . Set storey masses,  $m_i$ .
- 3) Define design performance objective (design seismic demand,  $S_d(T, \zeta_0)$ , and inter-storey drift limit,  $D_i^{\max}$ , for each storey-level), based on commonly accepted values

for exceedance probabilities, as for example the given by ATC-40 (1996) or VISON-2000 (SEAOC, 1995).

- 4) Choose a starting point  $\{x^0\}$  and let the iteration index  $k = 0$ .
- 5) Given an iteration point  $\{x^k\}$  calculate the first order derivatives of the objective and constraint functions with respect to the design variables.
- 6) Generate the approximated sub-problems using one of the approximation methods available in CASTEM. Then the convex optimization problem is formulated and solved iteratively.
- 7) Get optimum design variables for the limit-state considered:  $\Delta F_y$  for additional yielding strength,  $\Delta K_y$  for additional yielding stiffness, or  $F_y^{dev}$  for K-bracing with dissipator device intervention.
- 8) With the obtained optimal design point  $\{x^*\}$ , the convergence is verified. If the solution does not converge, this solution is used as the next iteration point. The iteration index  $k$  is increased by one and the iterative process continues (go to step 5).
- 9) With converged solution (which minimizes the strengthening costs for a specific limit-state requirement), graphical output of the solution is prepared.

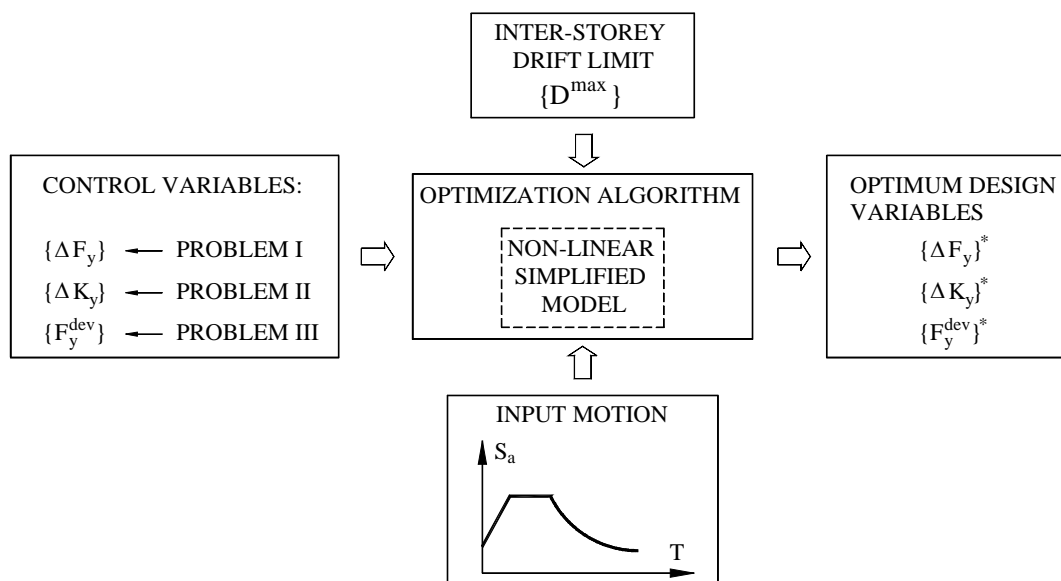


Figure 5.83 - Iterative optimization procedure

For the numerical optimization problem, the value of the objective function and of the restrictions as well as the respective first order derivatives at the starting point  $\{x^0\}$  are computed and given to start the optimization algorithm. At any design point, the implemented algorithm calculates the first order derivative information to formulate the approximation. The points chosen to calculate the derivatives in the vicinity of the current design point have to give a good approximation of the functions in the vicinity of the design point. In each of the structural optimization problems implemented, the first order derivatives are numerically calculated. Therefore, to calculate the first order derivatives for each design variable it is necessary to numerically evaluate each function (objective function and constraints functions) at two points in the vicinity of the current design point, as schematically represented in Figure 5.84. Then, the derivative value is calculated as generically expressed in equation (5.52).

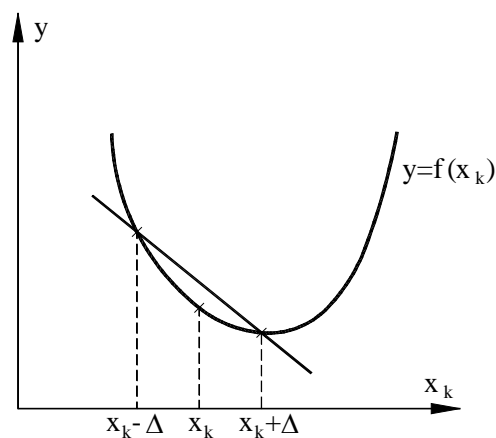


Figure 5.84 - First order derivatives – Numerical evaluation

$$\left. \frac{\partial f(x)}{\partial x} \right|_{x_k} \cong \frac{f(x_k + \Delta) - f(x_k - \Delta)}{2\Delta} \quad (5.52)$$

### 5.8.5 Illustrative examples

Numerical examples are herein presented in order to illustrate the proposed optimal retrofit design methodology. For each example, the computational optimal results are summarised in a table and the evolution of the control variables, objective function, storey displacement, inter-storey drift, and storey shear are provided graphically. The converged solution for each storey is also represented graphically in the storey shear-drift diagram.

### 5.8.5.1 Existing structure

From the experimental tests performed on the original bare frame, it were calculated the envelope curves of storey shear versus inter-storey drift and approximate for the best-fit idealized bi-linear curves. The original storey shear-drift curves were approximate for the idealized bi-linear curves, maintaining the dissipated energy and the maximum shear load. The adopted storey shear-drift curves are plotted in Figure 5.85 and are used in the optimization analyses. Table 5.18 summarises the characteristic values of the yielding shear force ( $F_y^0$ ), of the yielding inter-storey drift ( $D_y^0$ ), and of the pos-yielding stiffness ( $K_p^0$ ).

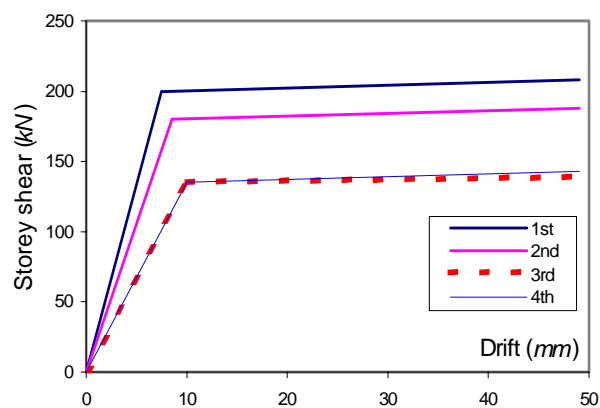


Figure 5.85 - Storey Shear-drift curves adopted from the experimental tests

Table 5.18 - Bi-linear storey shear-drift curves adopted

Storey $i$	$F_{y,i}^0$ (kN)	$D_{y,i}^0$ (mm)	$K_{y,i}^0$ (kN-mm)	$K_{p,i}^0$ (kN-mm)
4	135	10.0	13.5	0.2
3	135	10.0	13.5	0.1
2	180	8.5	21.2	0.2
1	200	7.5	26.7	0.2

### 5.8.5.2 Optimum design of the existing structure

The example of an optimization problem presented in this section assumes as control variables the additional storey strength. The structure under analysis is the four-storey RC building non-seismically designed. The objective function to be minimised is the total

structural additional strength, i.e., the sum of the storeys additional strength. It is intended to find the optimal distribution of strengthening in the building, whilst satisfying the restrictions in terms of maximum storey strengthening and maximum allowable inter-storey drift. The problem can be mathematically described as in the follows

$$\text{Find} \quad \Delta F_y = \{\Delta F_{y,1}; \Delta F_{y,2}; \Delta F_{y,3}; \Delta F_{y,4}\} \quad (5.53)$$

$$\text{Minimise} \quad \text{Cost}(\Delta F_y) = \sum_{i=1}^4 \Delta F_{y,i} \quad (5.54)$$

$$\text{Subject to} \quad \begin{cases} 0 \leq \Delta F_{y,i} \leq 500 \text{ kN} & i = 1, 2, 3, 4 \\ D_i \leq 3 \text{ cm} & i = 1, 2, 3, 4 \end{cases} \quad (5.55)$$

$$D_i \leq 3 \text{ cm} \quad i = 1, 2, 3, 4 \quad (5.56)$$

The start design point for each storey consisted on storey strength 1.4 times higher than the initial yielding strength in the existing structure, as can be observed in the second iterative point of Figure 5.86.

The constraint conditions for this structural optimization problem are: *a)* maximum admissible drift of 3.0 *cm*, for every storey; and, *b)* upper limit of 500 *kN* for each storey additional strength, that do not restraint the solution, and minimum zero (not additional strength).

The pre-yielding stiffness is assumed to be constant, i.e., the strengthened storey has higher strength, but the same pre-yielding stiffness. The pos-yielding stiffness is assumed constant.

The optimization problem converges after 12 iterations and the optimum result, for storey additional strength, is shown in Figure 5.86 and in Table 5.19. In Figure 5.86 to 5.89 are represented, for each iteration, the values of the control variables, of the objective function, of the storey displacements and of the inter-storey drifts. In Figure 5.90 are represented the storey shear-drift response for the converged optimal solution. In Figure 5.91 are represented the storey strength profiles of the original structure and of the optimum strengthening, to accomplish with a performance objective corresponding to an earthquake of 975-yrp and a drift limit of 3.0 *cm*.

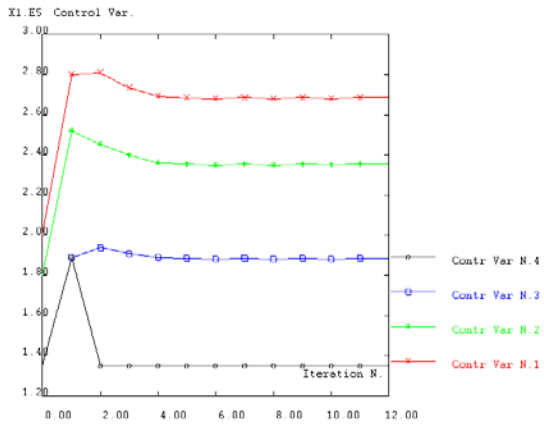


Figure 5.86 - Storey strength ( $N$ )

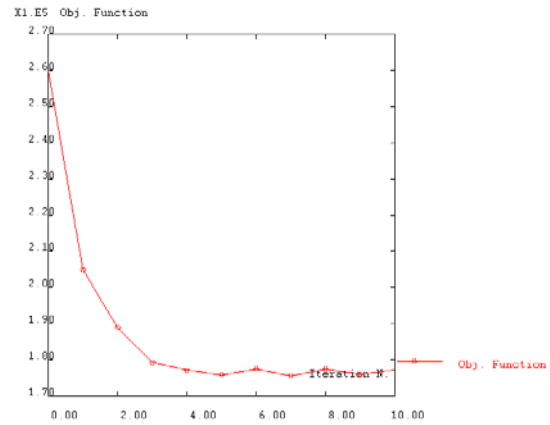


Figure 5.87 - Objective function ( $N$ )

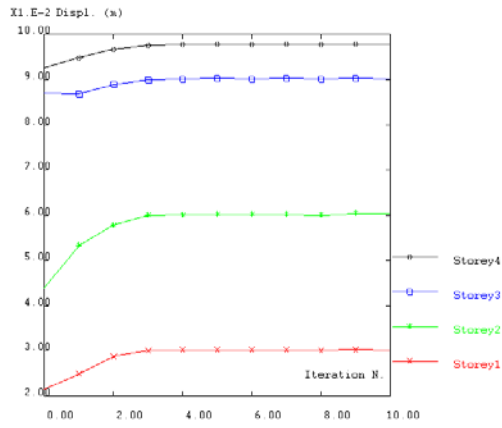


Figure 5.88 - Storey displacements ( $m$ )

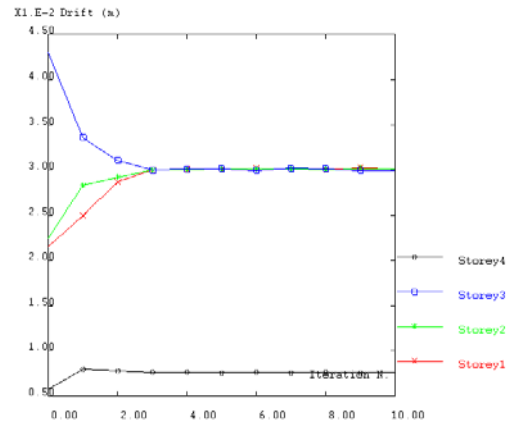


Figure 5.89 - Inter-storey drift ( $m$ )

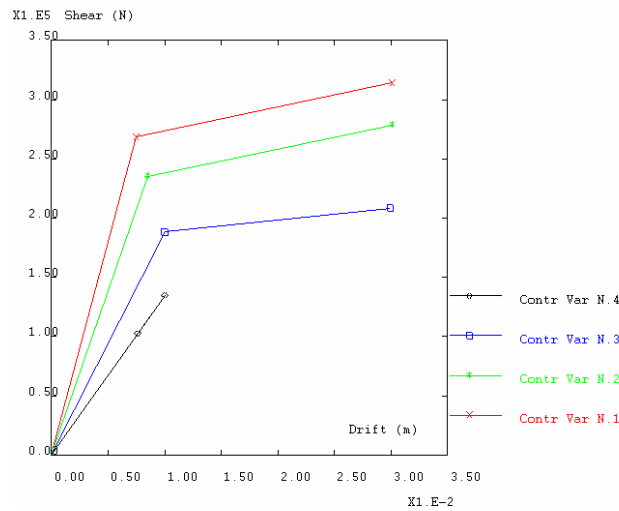


Figure 5.90 - Converged solution: shear-drift storey response



Table 5.19 - Converged solution: optimum distribution of the additional yielding strength  
(3 cm drift limit and earthquake 975-yrp)

Storey $i$	$F_{y,i}^0$ (kN)	$\Delta F_{y,i}$ (kN)
4	135	0.0
3	135	51.5
2	180	53.8
1	200	66.8
Total		172.1

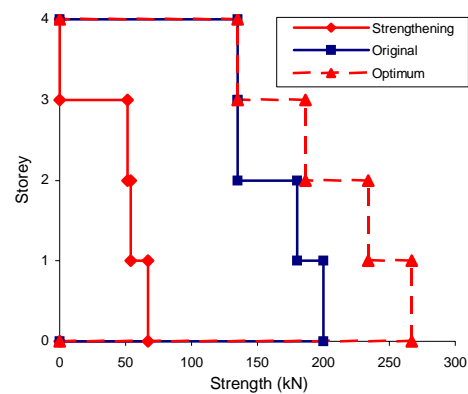


Figure 5.91 - Storey yielding strength of the existing structure and optimum strengthening distribution

### 5.8.5.3 Multiple optimum strengthening design

To illustrate the methodology proposed, a series of retrofitting design examples based on the non-seismic designed existing structure under analysis are presented here. The strength is the control variable used (Problem I). In this problem it was considered constant yielding displacement and constant post-yielding stiffness. Regarding the damping, the curves storey damping-drift, presented in Figure 5.59 were used. Additionally, it was considered that the storey damping functions do not change with the strengthening.

The optimal retrofit was calculated for a vast series of performance objectives (multiple performance objectives). Particularly, for the input motion, it were considered the seismic hazard levels corresponding to return periods of 73, 475, 975 and 2500 years (corresponding to the 'Serviceability Earthquake', SE, 'Design Earthquake', DE, 'Maximum

Earthquake', ME, and, 'Maximum Considered Earthquake', MCE, see Table 2.2), as recommended in the ATC-40 (1996). For the inter-storey drift limit (limit-states) it were considered several values. In this analysis, no upper limits were imposed for the strengthening.

In Figures 5.92 to 5.95 are represented for each redesign performance objective the results in terms of total and storey (1<sup>st</sup>, 2<sup>nd</sup> and 3<sup>rd</sup>) strengthening. For all redesign performance objectives, the obtained optimum strengthening distribution does not involve strengthening at the 4<sup>th</sup> storey level.

In Figure 5.96 are presented, as an example, the vulnerability performance functions for one designed optimum retrofitting structure. The strengthening was optimized using the storey strength as control variable, 2% as allowable drift limit, and a design seismic action corresponding to a return period of 2500 years (see also the optimum retrofitting solution signalled in Figure 5.92).

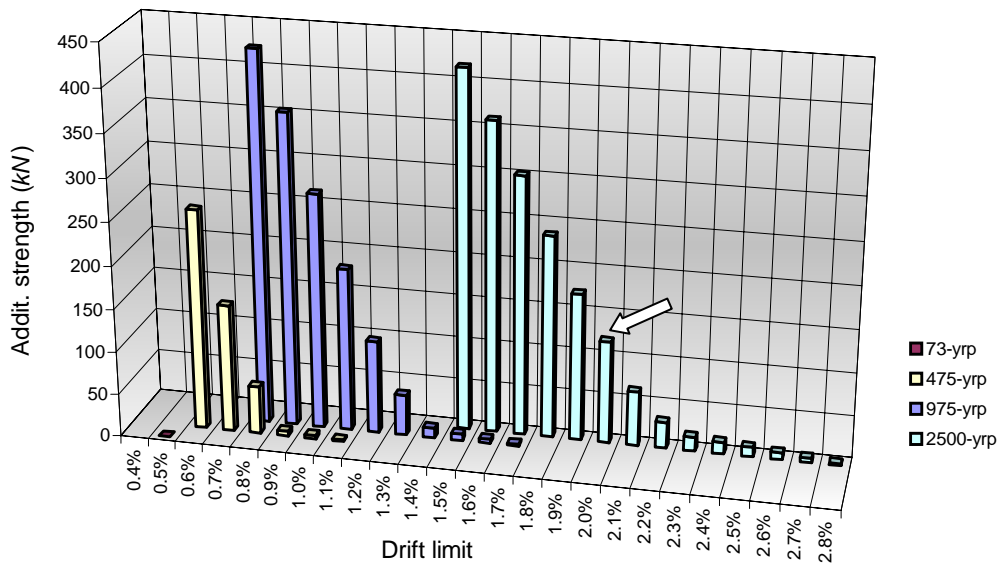


Figure 5.92 - Total additional strength

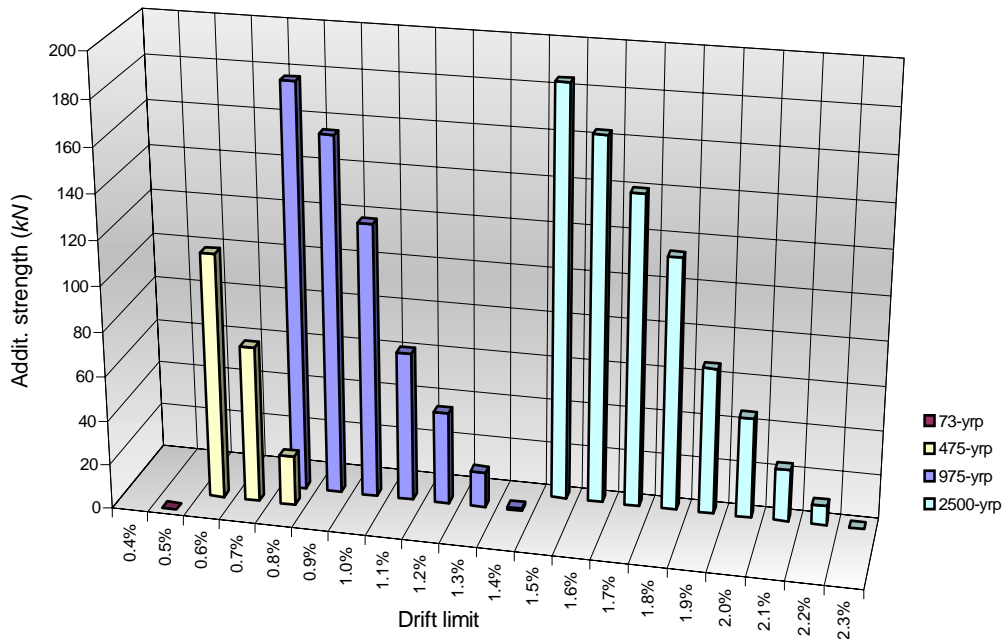


Figure 5.93 - 1<sup>st</sup> storey additional strength

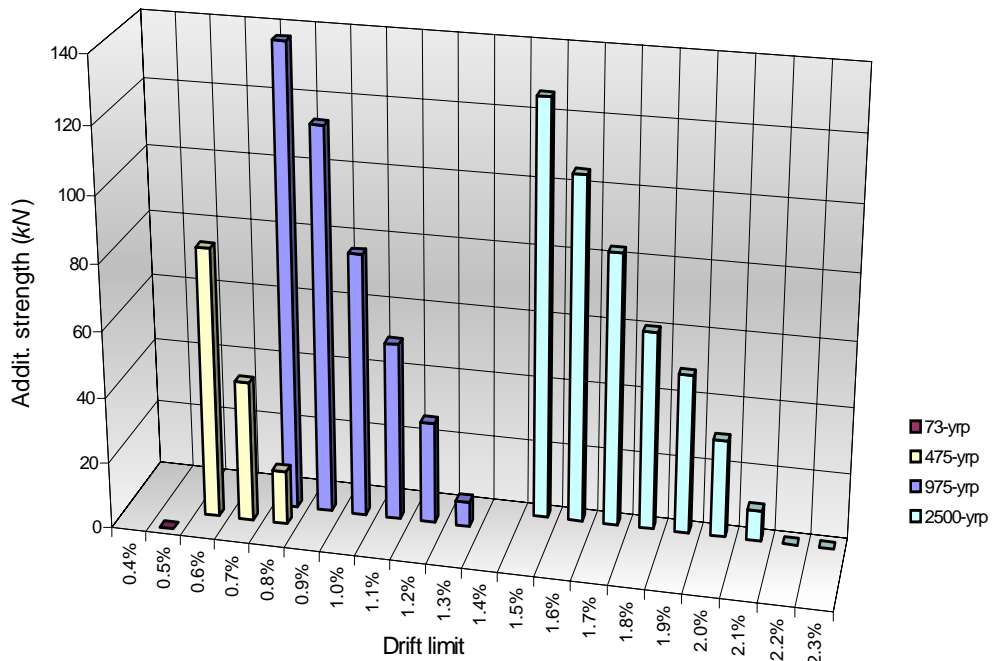


Figure 5.94 - 2<sup>nd</sup> storey additional strength

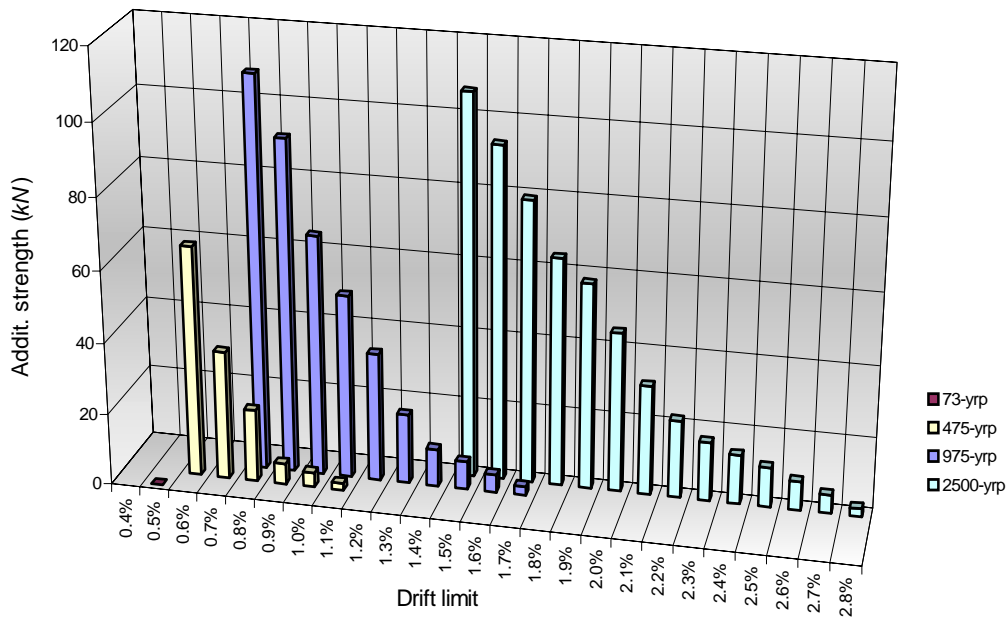


Figure 5.95 - 3<sup>rd</sup> storey additional strength

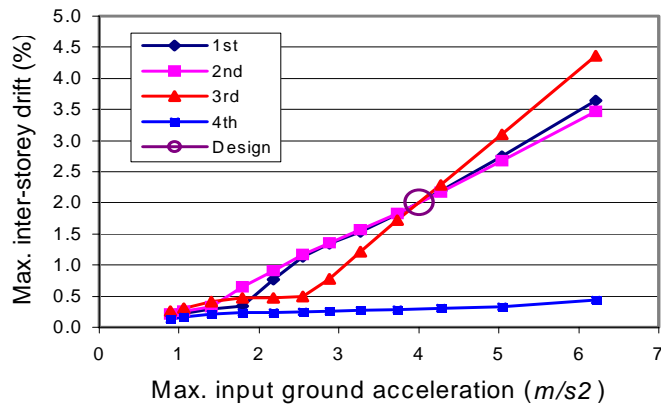


Figure 5.96 - Vulnerability function of the structure designed for 2% drift and 2500-yrp

### 5.8.6 Final remarks

From the optimum strengthening results for the existing structure, obtained with the proposed optimization methodology, the following can be observed:

- The proposed optimization methodology involves reduced computational costs. As observed in the studied strengthening structural optimization problems, this methodology leads to fast convergence (reduced number of iterations are required for convergence).
- The methodology can be a useful design tool, as a preliminary step, in the global structural strengthening decision, generating the optimum strengthening (strength, stiffness or damping) storey distribution, for one or multiple performance objectives.
- With this optimization procedure, it is possible to define optimum strengthening needs for different limit-states ('Fully Operational', 'Operational', 'Life Safe' and 'Collapse Prevention') as well as to achieve probabilistic sensitivity functions for specific limit-states, in terms of the basic design variables (storey strength, storey stiffness or additional damping). This procedure leads to a retrofit design, for each limit-state considered, which requires further considerations and possibly recourse to life-cycle cost analyses to identify the optimum design (see for example, the procedure proposed by Pinto, 1998).

# CHAPTER 6

## SUMMARY AND CONTRIBUTIONS, CONCLUSIONS, IMPLICATIONS AND FUTURE RESEARCH

*'It is a bitter and humiliating thing to see works, which have cost men so much time and labour, overthrown in one minute; yet compassion for the inhabitants is almost instantly forgotten, from the interest excited in finding that state of things produced in a moment of time, which one is accustomed to attribute to a succession of ages.'* (Charles Darwin, March 1835, reporting the ruin of Concepción in Chile by an earthquake)

### 6.1 - SUMMARY AND CONTRIBUTIONS

As recalled in Chapter 1, there is a lack of experimental results and associated calibrated numerical models for existing reinforced concrete structures designed without specific seismic resistance. The experimental work reported and discussed in the thesis intends to reduce this shortcoming.

A specific feature of this thesis relies on the combination of numerical and experimental work. The numerical models are calibrated against experimental PsD test results on RC full-scale structures (see Chapter 5). The tests on full-scale models of existing structures constitute an exceptional opportunity for improvement of knowledge on behaviour and capacity of RC structures designed and constructed in Europe until the late 1970's.

As reiterated by Coelho *et al.* (2000), seismic testing assumes a key role in the policies of earthquake risk mitigation. In this regard, the experimental programme defined and set-up by the ICONS researchers constitutes a major effort and can be considered as one of the largest co-ordinated experimental works performed in the world. In this thesis, conducted

within the ICONS project, a series of large-scale PsD seismic tests, described in Chapters 3 and 4, have been successfully carried out in the European reaction-wall facility (ELSA laboratory, of the Joint Research Centre, in Ispra, Italy). The experimental tests on the full-scale frames, representative of the construction practice until the late 1970's, aimed at: *i*) to assess the original capacity of bare structures; *ii*) to evaluate the influence of infill masonry in the structural response; *iii*) to assess different retrofitting solutions.

The results from these reference experimental PsD earthquake tests on full-scale structures produced a vast data set, useful to calibrate methodologies for the assessment of seismic fragility of buildings (as made by Coelho *et al.*, 2000), to calibrate refined non-linear numerical models (as made by the author in this thesis; Delgado *et al.*, 2002; Dolsek and Fajfar, 2001; Candeias, 2000; Combescure, 2000; Pinho, 2000; among others), and to design adequate retrofitting measures in order to enhance the seismic performance of existing RC structures (Elnashai and Pinho, 1999). The procedures for seismic assessment described in the literature require validation against experimental results from structures with typical reinforcement detailing, as those used a few decades ago. This data set is expected to contribute to set-up guidelines for the assessment and redesign of these structures in earthquake prone zones. In particular, the findings of the research can contribute as a basis for the calibration and further revision of EC8 Part 1-3. From the experimental PsD tests, slab-participation, plastic hinge length, damage indices and drift limits for each limit state, for existing and retrofitted RC structures, were studied.

The influence of physical phenomena and model parameters (such as the bond-slip, plastic hinge length and slab-participation) in the structural response was thoroughly understood due to the integrated numerical and experimental research approach. In the numerical study, it was proposed a simplified model to account for the slippage of the reinforcement in existing RC structures. The numerical models were able to properly simulate the retrofitted RC elements, even for the case of structures previously damaged by earthquakes. The refined model provides a valuable basis to simulate the behaviour of existing RC buildings and to adequately characterize strengthening solutions.

From the structural assessment performed with the Capacity Spectrum Method (CSM), it was concluded about the inadequacy of this method to predict the response of irregular structures. Therefore, it was proposed a simplified MDOF non-linear dynamic method for

---

the assessment of irregular structures. Based on the proposed MDOF non-linear model, it were developed optimization algorithms for the redesign of existing vulnerable structures. The proposed optimization procedure searches for the optimum storey strengthening distribution (strength, stiffness or damping) in order to meet specific performance requirements, in terms of maximum inter-storey drift for a given earthquake demand. Maximum strengthening values are also considered for each storey. With the proposed redesign methodology it is possible to define optimum retrofitting solutions for different limit-states.

The main conclusions drawn from the performed studies are here summarised. Implications for researchers, policy makers and owners are underlined. The chapter closes up suggesting possible future research topics and approaches.

## **6.2 - CONCLUSIONS**

Chapter 2 reviewed the worldwide experience from past and recent earthquakes showing that, by far, the major damages and even collapses of structures and human life losses come from deficiencies in existing non-ductile reinforced concrete buildings. Frame type RC structures were the most commonly structural system used until the late 1970's in the southern European countries, especially for buildings. Thus, this thesis concentrated in the study of seismic assessment and rehabilitation of RC constructions of that period.

Mentioning the recent earthquake occurred in 1999 in Izmit, Turkey (EQE, 1999), it has wide-ranging lessons for the earthquake engineering, building code development and application in earthquake regions, construction quality, risk management, and insurance. As declared in EQE (1999), almost all of the damage caused by the earthquake, and almost all of the deaths caused by the collapse of inadequately designed, detailed and constructed buildings were avoidable. The major sources of seismic weakness in old buildings were identified and studied. In spite of the current rather strict earthquake-resistant code requirements, on all continents around the world, serious deficiencies still take place in the design and construction of most buildings.



Another experience deeply analysed in Chapter 2 comes from the 1995 Kobe earthquake, in Japan. It was verified that pre-1981 concrete frame buildings performed very poorly, with many collapses. Post-1981 buildings performed much better. Many concrete buildings, similar to those that collapsed, have not been strengthened in other earthquake-prone regions in the world and are expected to collapse in future seismic events. For such buildings, similar damage and collapses have been reported in many recent earthquakes. As stated in EQE (1995), one of the most dangerous buildings' classes is the older non-ductile RC structure. From the performance of these buildings, it is obvious that a major strengthening and rehabilitation program also needs to be initiated in earthquake-prone regions.

In spite of the current knowledge in earthquake engineering, there are still many unidentified seismic sources and uncertainties. The damages caused by the 1999 earthquake that stroke Athens, a highly populated city and the heart of the economic and administrative activity of Greece, proves it.

A review of the lessons learned from these and others significant earthquakes that have occurred recently have led to the conclusion that the seismic risk in urban areas is increasing rather than decreasing. The disastrous consequences in terms of damages on RC buildings and human casualties resulting from seismic activity in a recent past, all around the world, reveal that research on repair and strengthening of structures is urgently needed.

One of the most effective ways to reverse this situation in future significant earthquakes is, first, through the development of more reliable seismic standards and code provisions than those currently available. Secondly, through their stringent implementation for the complete engineering of new civil engineering facilities and also for the evaluation of the seismic vulnerability and upgrading of existing hazardous facilities. A comprehensive approach for development and implementation of the next generation standards and codes must include consideration of all the main aspects involved in engineering of facilities to resist the effects of earthquakes. These main aspects involve not only those concerning the conceptual and numerical designs but also the proper structural detailing and construction of such conceptual and numerical designs, and the monitoring of the occupancy and maintenance of the whole facility.

---

The challenge to the scientific earthquake engineering community is: *a)* to develop rational assessment and redesign methods; *b)* to define appropriate decision criteria for retrofit of existing structures; and, *c)* to investigate and assess innovative cost-effective strengthening solutions and techniques.

As stated in Chapter 2, the selection of the retrofit strategy and its implementation should be guided by results of a detailed assessment or evaluation of the structure. The seismic rehabilitation of structures is based on two general approaches, namely system and member rehabilitation. In the majority of the retrofitting cases, both approaches need to be combined.

To study the vulnerability of existing RC structures a vast pseudo-dynamic and displacement cyclically imposed test campaign on a full-scale RC frame was performed (Pinto *et al.*, 2002). The efficiency of several retrofitting techniques was also experimentally evaluated (as exposed in Chapters 3 and 4). The experimental campaign was preceded by a set of preliminary numerical analyses performed with a refined fibre model. With the experimental results, the non-linear model was improved. It was concluded that bond-slip, slab-participation and lap-splices location and details are crucial in the structural response, and models have to accurately consider them. The improved refined numerical model proves to be very effective in reproducing the non-linear dynamic behaviour of existing RC structures, as demonstrated in Section 5.6. The main conclusions and the principal lessons learned from the experimental and numerical work performed in this thesis are summarised next.

### ***Experimental results***

Analyses of the PsD earthquake test results and comparison between the behaviour and earthquake vulnerability and performance of the different structures were deeply examined in Chapters 3 and 4. The main results from these test campaigns can be summarised as follows:

- The high vulnerability of the original bare frame was confirmed, which demonstrates that this type of structures effectively represents a major source of risk for human life. In spite of 'a satisfactory performance' for the nominal input

motion test corresponding to a return period of 475 years (10% exceeding probability in 50 years), where slight damage was observed, the structure reached imminent collapse for an input intensity slightly higher than the nominal one (1.3 times, in terms of PGA and corresponding to a 975-yrp input motion). The rather uniform distribution of demands for the nominal earthquake test was completely altered for the 975-yrp (5% exceeding probability in 50 years) earthquake. A drop of 20-25% for the four main eigenfrequencies was observed. The significant change in stiffness and strength from the 2<sup>nd</sup> to the 3<sup>rd</sup> storey, coupled with the inadequate lap-splice, induced the development of a soft-storey mechanism at the 3<sup>rd</sup> storey (2.4% inter-storey drift). Premature opening shear cracking in the strong-column at the 1<sup>st</sup> and 3<sup>rd</sup> storeys (where lap-splice exists) for storey drifts of approximately 0.4% were observed. Tests on a similar frame with infill panels have also shown shear crack initiation for 0.4% inter-storey drift, while severe (dangerous) shear cracking was apparent for drifts of 1.3%.

- The strengthened frame (SR frame) has shown rather improved seismic performance. In fact, it was subjected to the same input motions as the BF with limited structural damage and was able to withstand an input motion with intensity 1.8 times the nominal one (corresponding to a return period of 2000 years) maintaining its load carrying capacity with repairable damages (the four frequencies drop at about 35-40%, in contrast to the repaired structure). It should be noted that after repair and strengthening interventions, the initial first frequency was almost achieved (90% of the virgin structure) and the highest second, third and fourth eigenfrequencies were slightly enlarged due to the stiffening intervention in the 3<sup>rd</sup> and 4<sup>th</sup> floors. The strengthening operation addressed and solved the irregularity problem, and the confining steel plates definitively increased the limited deformation capacity of the central strong-column.
- The strong concentration of the inelastic demands at very small member ends observed during the tests leads to equivalent plastic hinge lengths much lower than the empirical values proposed in the literature (40% of the proposed values), due to the poor bond characteristics of the smooth round rebars.

- 
- The slab-participation is also much lower (approximately 45% lower) than the values proposed in the design codes and calculated from tests on building structures with improved bond steel, consequence also of the poor bond characteristics of the smooth round reinforcement of the slabs.
  - The test results confirmed that, for existing structures, with smooth round rebars with extremity hooks and poor detailing and amount of shear/confinement reinforcement, lap-splice at the base of the columns develop premature shear cracks at the bar termination zones for inter-storey drifts of approximately 0.4%. This shear cracks dictate dangerous shear failure of the columns for inter-storey drifts in the range of 1.3-1.8%.
  - The final capacity cyclic tests on the critical regions of the strengthened structure demonstrated that by using advanced composites (FRP's) the member strength and stiffness were recovered. The small variation of structural eigenfrequencies with the repair interventions with FRP's was expected and desirable considering the slight intervention without increasing the global stiffness of the structure. The strengthened frames were able to withstand storey deformations higher than the ones reached in the previous PsD earthquake tests, maintaining its load carrying capacity. Furthermore, improvement of energy dissipation capacity and the global ductility of the structure were also observed. It was shown that a very effective (cost/benefit) repair and/or strengthening operation can be used to repair local heavy damages.
  - It is well known that infills cause a completely different structural behaviour, when compared to the behaviour of a similar bare frame structure, and, therefore, infills must be taken into account in the assessment and redesign of existing structures. The masonry infill panels increase the frequencies about four times, comparing with the bare structure. The tests on the infilled frame confirmed that infill panels protect the RC frame structure for low and medium intensity earthquake input motions. The IN structure was able to withstand part of an earthquake corresponding to 2000-yrp, while the BF failed during the 975-yrp earthquake test. However, their abrupt (brittle) failure, with abrupt loss of loading carrying capacity (softening), for medium/high input levels, prompts dangerous soft-storey

mechanisms and consequently premature failure of the entire structure. In addition, infill walls cause shear-out of the external columns in the joint region. Any strengthening of the infills panels 'preventing' failure of the walls or conferring additional deformation capacity without abrupt loss of resistance would improve the earthquake behaviour of the infilled structures.

- The results from the tests on the infilled frame with strengthened infill walls (shotcrete) demonstrate better behaviour. Infill cracking was prevented and only slight crushing appeared in the corners. However, the higher strength of the panels led to premature shear failure of the external columns (shear-out of the columns in the interface column-joint) with dangerous loss of their vertical loading carrying capacity. This is a point that deserves special concern because it is a common practice to apply these strengthening techniques to repair and strengthening the infilled frame structures after earthquakes. Even renewals of walls plaster may increase substantially the strength of infill walls. Any strengthening intervention of infill walls in existing frame structures should provide appropriate doweling systems to transfer the shear forces developed in the walls directly from them to the surrounding beam/gird.
- It was also noted that after the tests on the original infilled frame, there was evidence of column/joint dislocation (shear-out) caused by the same phenomenon as in the SC frame tests. For existing structures, with poor column/joint detailing, this serious damage is likely to occur. Therefore, seismic assessment of this kind of structures shall take into account the possible negative effects of the infill in the global behaviour.
- Retrofitting solutions based on K-bracing with dissipative devices, such as a shear-link, can substantially improve storey behaviour and increase energy dissipation capacity. The basically similar shear capacities design objective (of the original and retrofitted structures) prevent the development of a retrofitted system, which may otherwise introduce excessively increased foundation loads. Other significant characteristics of this retrofitting system are the extremely effective energy dissipating properties of the shear-link, and the fundamental fact that cyclic shear-strain hardening of the shear-link web, under earthquake loads, leads to shear

resistance of the link equal to about twice the initial lateral resistance at its yield. Under increasing cyclic displacements, this development allows the shear-links, to compensate for the progressive failure and loss of resistance of the non-retrofitted walls. The technology used to anchor the steel retrofit assemblage to the surrounding concrete beams and columns of a retrofitted bay, was proven to be effective.

### ***Results with the refined numerical model***

From the non-linear dynamic numerical analyses, conducted in Chapter 5, the following was observed:

- The preliminary dynamic numerical analysis was very valuable, allowing to predict the behaviour of the structures, to evaluate the testing and instrumentation devices, and to investigate possible suitable retrofitting solutions for the bare and infilled structures.
- Comparing the experimental eigenfrequencies measured before the PsD earthquake tests to the frequencies evaluated with the refined numerical model, a very good agreement was observed, which constitutes a first confirmation of the model validity (in terms of stiffness).
- In general, the analytical results were in good agreement with the experimental ones in terms of peak storey displacement, inter-storey drift, storey shear, and storey dissipated energy.
- The numerical analyses performed demonstrate also that the upgraded refined numerical models are able to well reproduce the non-linear structural behaviour of the existing RC structures, as well as the repaired and retrofitted structures, and structures damaged by precedent earthquakes.
- The original models used in the preliminary non-linear analyses do not take into account the slippage of the steel rounded bars. As proven by the improved numerical results, including the proposed model for the bond-slip of the steel bars, this effect is crucial to the proper modelling of the structural response. Therefore, appropriate models should be used to consider the bond-slip.

- From the several analyses performed, it is important to underline that much care should be taken in the modelling of existing structures. Furthermore, due to the vast number of parameters and rules involved, the use of refined models may lead to unrealistic results, if the model parameters are not correctly chosen. It is also clear that the sensitivity of the response to such model parameters increases with the complexity of the models.

### ***Estimation of the equivalent damping***

The equivalent global damping was estimated from the experimental PsD tests for existing structures (bare original and strengthened) according to the procedure exposed in Section 2.3.5. Higher values of damping were observed for the original than for the strengthened structure. This finding can be explained by the fact that a more regular response of the strengthened structure induces less non-linear demand at storey level. However, even for the strengthened structure, a low value of damping was observed, which confirms that existing structures with reinforcing plain bars have a smaller energy dissipation capacity.

### ***Response estimation and assessment with the capacity spectrum method***

The capacity spectrum method was applied to the original bare and strengthened structures. First, a comparison to the experimental PsD test results for the demand spectra of the earthquakes allows to verify the method. Second, the BF and SR structures were assessed using the elastic acceleration-displacement response spectra proposed in the EC8.

From the application of the capacity spectrum method to the verification of experimental results and to the structural assessment, it was observed that an approximation of global structural response parameters, as top-displacement or base-shear, can be achieved. However, this simplified non-linear equivalent static model is not able to estimate accurately the response of irregular structures due to the low sensitive of the global structure behaviour curves (capacity curves) to the local storey behaviour.

---

### ***Results with the proposed simplified MDOF non-linear model***

In this line, it was proposed a simplified non-linear MDOF dynamic procedure for structural assessment of multi-storey building accounting for non-linear storey behaviour and storey damping.

The proposed MDOF non-linear seismic analysis methodology was applied to simulate the PsD tests performed on the bare and strengthened structures. A good agreement was verified between the numerical results given by the simplified method and the experimental results. These numerical results were verified not only in terms of global parameters (such as top-displacement, base-shear and equivalent damping) but also in terms of maximum inter-storey drift, and maximum storey shear. The proposed model calls for a relatively smaller number of DOF's (one per floor) compared to a detailed FE model, and proved to be able to predict accurately the response, even for irregular systems. Therefore, this model can be an effective tool to perform fast non-linear analyses, which allows for parametric studies and rapid seismic vulnerability assessment of existing building classes. The dynamic method was incorporated in the optimization algorithms proposed for the redesign of existing structures.

### ***Building retrofitting decision based on the optimization problems***

In this study, it were proposed and programmed three problems for optimum redesign of existing structures based on the convex linearization method and on the method of moving asymptotes. The three problems implemented have as storey design variables: *a*) the additional strength; *b*) the additional pre-yielding stiffness; and, *c*) the yielding strength of the energy dissipation device. These optimization algorithms deal with non-linear objective functions and allow to impose constrains on the design variables (strength, stiffness or damping) and on any other response variable depending on the design variables, such as inter-storey drift, top-displacement, etc.

With this optimization procedure, it is possible to define optimum strengthening needs in terms of the basic design variables (storey strength, storey stiffness or additional damping) for different limit-states ('Fully Operational', 'Operational', 'Life Safe' and 'Collapse Prevention').



From the redesign examples of the non-seismically designed structure under analysis, it was illustrated the capability of the proposed optimization methodology. The proposed optimization methodology involves reduced computational costs, and, therefore, can be a useful tool, as a preliminary step, in the global structural strengthening decision for one or multiple performance objectives.

Lastly, the tests have shown that the vulnerability of existing RC frames designed without specific seismic resisting characteristics, which are an important part of the existing buildings in European earthquake prone regions, constitute a source of high risk for human life. Furthermore, it was demonstrated that advanced retrofitting methods, solutions and techniques substantially reduce that risk to levels currently considered in modern seismic design. The improved refined numerical model proves to be very effective in reproducing the non-linear dynamic behaviour of existing RC structures. Simplified tools can be systematically used in the vulnerability assessment and optimum strengthening design for this kind of structures.

### **6.3 - IMPLICATIONS FOR RESEARCHERS, POLICY MAKERS AND OWNERS**

There is a wide agreement that an extensive action is necessary in order to reduce the seismic risk. The studies conducted in this thesis, summarised in the previous section, have shown that the vulnerability of existing non-ductile buildings, which are an important part of the existing buildings in seismically active areas throughout the world, constitute a source of high risk for human life. As recalled in EQE (1995), unless these buildings are retrofitted, many lives will be needlessly lost in future major earthquakes.

From the experimental tests presented in Chapter 4, it was demonstrated that advanced retrofitting methods, solutions and techniques could reduce substantially that risk to levels currently considered in modern seismic design.

In spite of some activities oriented in this sense, which led to positive results, there is a wide discontent due to the too low actual volume and results of these activities. The first reason for this relies on the lack of appropriate financial resources aimed at supporting risk

---

reduction activities, as has been widely emphasised. Nevertheless, a more in-depth examination shows that there are several cases when the severely limited financial resources available could not be properly used due to other obstacles. In this regard, it is clear that the practical implementation of possible solutions certainly presents challenges.

The best way to promote standards of safety of the existing constructions is based on the complementary work of the researchers, policy makers and the citizens' communities. Therefore, a global partnership between international organizations, national governments, academic institutions (universities and research centres), the private industrial sector, and civil society organizations should be arranged aiming at reducing earthquake disaster impacts in society, through the implementation of rehabilitation plans. The involved parts must become more dynamic, share the same goals and upgrade their efforts, as clearly encouraged by the concept of the European Research Area (ERA - Busquin, 2002). The main tasks of each agent are presented and discussed below.

### **6.3.1 - Implications for academic community, practitioner engineers and code makers**

Over the past years, researchers have put together a more complete picture of how the new structures behave during earthquakes. This increased knowledge over time has enabled engineers to improve earthquake requirements in actual building design standards, so that new structures are more able to survive strong earthquakes. The prime responsibility for researchers is to conduct studies on structural safety of building stock, industrial facilities and infrastructures constructed before the implementation of new codes, particularly in the development of appropriate upgrading and strengthening techniques for the different types of constructions.

World researchers involved in vulnerability assessment and retrofitting studies, working directly with city officials and building owners, and in order to develop a consistent structural evaluation and rehabilitation action plan for our cities, should systematically work on the following subjects: *a*) classification and inventory of various types of existing constructions (structural and architectural characterization); *b*) development of a comprehensive data file on inventory of buildings of the populated centres (towns and cities); *c*) preparation of vulnerability zoning maps (towns and cities) of vulnerable

structures; *d*) vulnerability analysis of buildings, giving particular attention to important and vital facilities (as hospitals, fire stations, schools, hotels, and many other major buildings) for the purpose of future strengthening; *e*) improvement of solutions for seismic strengthening, conducting both full-scale and component tests to determine the effects of retrofitting scheme; and, *f*) definition of adequate strategies for seismic strengthening of each type of buildings.

On the education side, researchers should prepare instruction manuals on various general and cost-effective strengthening solutions for different types of structures and for low-income constructions. Research institutes and organisations, university departments and enterprises should promote the exchange of information through the organization of scientific meetings, workshops, technical courses and conferences, specialist scientific journals, technical reports and dynamic websites.

Setting standards for the education, training and competence for those entering the profession of structural engineering and maintaining a policy of continuing professional development for those already qualified. Thus, improving knowledge of structural engineers in fields of structural assessment and retrofitting.

Building codes are the public's first line of defence against earthquakes, as reiterated by Celebi *et al.* (1995). As already stated, structures built to modern seismic standards are much safer in earthquakes than structures built 50 or even 25 years ago. In recent earthquakes, buildings built to modern codes have generally sustained relatively little damage. Nonetheless, it will still be necessary to refine the earthquake requirements in building codes in the future. Each major earthquake produces new strong-motion records that expand our knowledge of ground shaking. For example, observations from the devastating 1994 Northridge, California, earthquake and other recent temblors have led engineers to propose an increase in the seismic standards for structures built near dangerous faults (Celebi *et al.*, 1995). Furthermore, the lack of codified criteria and rules for redesign of buildings increase the average rehabilitation costs.

Although many seismic assessment procedures have been proposed worldwide in the last decades for RC buildings, none of them has been codified. To facilitate the stringent implementation of the code or standards, Bertero and Bertero (2002) suggest that the

---

vulnerability assessment strategies and techniques included in these codes must be simple enough so that they can be applied effectively according to the education of the professionals involved, as well as, the owners. Thus, radical changes should be included in the present code by incorporating the most reliable and user-friendly procedure that can be developed according to the state-of-the-art in seismic engineering.

### **6.3.2 - Implications for policy makers and government agencies**

The ultimate objective of the vulnerability assessment and retrofitting studies is to assist in obtaining seismically safer structures. As previously stated, RC buildings represent a considerable percentage of the worldwide inventory of seismically deficient buildings. Rehabilitation of existing constructions is urgent. It is cost effective, as the potential economic losses are much higher than the cost of retrofit. Therefore, policy makers should encourage and support programmes to reduce seismic risk, as the one proposed by the Portuguese Society for Earthquake Engineering (SPES, 2001) in cooperation with the Society for Conservation and Rehabilitation of the Architectural Heritage (GECORPA).

The following key-actions could be taken by policy makers, at national and local levels, for mitigation of seismic risk in existing hazardous buildings: *a)* instruction of competent professionals (engineers, architects) linked to the seismic risk reduction; *b)* gathering information on owners' needs and on major barriers (such as renting policies and funding costs) for their engagement in rehabilitation, so that a better policy framework can be designed; *c)* analyse and introduce incentives for the retrofitting of buildings, as tax incentives; *d)* development and divulgation of the adequate legislative framework for retrofitting of city safety; *e)* make the population aware of about the economical and social importance of the seismic upgrading of buildings; *f)* pre-earthquake preparation of emergency response plans, as well as pos-earthquake search and rescue capabilities; and, *g)* planning, execution and accompaniment control of the strengthening works.

These tasks cannot be enforced without an appropriate supporting configuration. At the local level, a technical office with appropriate responsibilities and authority should be designed. These offices should also ensure the coordination between local authorities, national governments and international institutions.

Demographic forecast analysis indicate that probably 70-80% of humanity will live in just a few dozen large metropolis by 2030-2050 and even Western countries will have to cope with continuous changes in environmental and social conditions in the large cities that can weaken the relationship between citizens and the town or city in which they live (Anselmi and Mocchi, 2002). In this context, policy makers need better monitoring systems in order to acquire a fuller knowledge of their city's building problems, contributing to a more effective provisions for safety constructions assessment and to an economic definition of strengthening techniques for each class of buildings structural system. Therefore, applications of ICTs (Information and Communication Technology), such as the Internet, can be used in order to provide rapid and efficient solutions to citizen's global safety information. The implementation of advanced web-based interactive systems for city monitoring (e.g. the project in progress 'Aveiro digital city', in Portugal) can create a new opportunity, giving the citizens an active and central role in the city safety information and evaluation, as well in finding optimal buildings retrofit solutions.

### **6.3.3 - Implications for building owners**

Owners have the main responsibility on the buildings upgrade. In the majority of the cases, owners give exclusive attention to the non-structural aspects, such as aesthetics and functionality of the construction. As stated by Brenner (2001), many 'obsolete' buildings can be successfully upgraded for contemporary use. The addition of multiple computers, servers, networks, and peripherals, as well as, poor lighting, insufficient vertical and horizontal cabling infrastructures, and inadequate HVAC systems are common afflictions nowadays.

By contrast, it is well known that the market is prepared to pay a low premium for higher safety, which makes difficult the seismic vulnerability reduction. Nevertheless, the high cost of retrofitting or upgrade of existing buildings, including those of disruption of use and of removal and/or replacement of non-structural parts, makes the cost of seismic retrofitting diminutive. Owners should consider this in their strategy for buildings upgrade.

## 6.4 - FUTURE RESEARCH LINES

*'Science has no limits, the horizons get wider and wider. There are no boundaries, they outgrow up to the infinite.'* (Egas Moniz, Nobel Prize of Medicine and Physiology, 1949)

As expressed above by Egas Moniz, we cannot consider in anyway that the research is at its end. In fact, in the fields of the seismic engineering and structural rehabilitation we are just at the first step of a long way. There are many exciting and new directions for future research related to the evaluation of seismic performance of existing structures and to the optimum retrofit design. A few potential research topics believed to be relevant to protect citizens from loss of life and property in future earthquakes, are outlined:

- Information gained from past (see Chapter 2) and future earthquakes should be used to study the factors that affect the seismic capacity of different types of existing structures, to estimate the losses in economic terms and human life, and to study the most efficient retrofitting technique for each structural type system. In fact, strong earthquakes put to a severe test the existing building stock, as well as, assess the adequacy of the seismic code of each époque and the efficiency of the common structural retrofitting techniques. After earthquakes, meticulous report on the ground in the damaged area should be done, investigating and researching the damage, documenting the lessons learned to prevent catastrophic losses in future earthquakes.
- Strong-motion data collected around the world have contributed to the improvement of building codes over the decades (as stated in Section 2.4). These improved codes have saved many lives and reduced damage in recent earthquakes. A growing network of instruments will provide even more extensive and reliable data in earthquakes to come. Using this information, scientists and engineers will be able to suggest further improvements to building codes.
- As stated by Anderson *et al.* (1991), the best experiment is when earthquakes occur and there are properly instrumented structures which can record the actual building response to ground motions recorded at its base. Instrumentation in representative existing RC buildings (original and retrofitted) should be set up. The potential benefits of the structural measurements express inferior costs in the installing of instrumentation.

- The vast experimental data obtained from the PsD and cyclic full-scale tests (presented and discussed in Chapter 4) should be exhaustively exploited. Particularly, numerical models have to be implemented to model: *a*) the infill strengthened PsD tests; *b*) the cyclic tests on the frame retrofitted with K-bracing with shear-link; *c*) the final capacity cyclic tests on the BF and SR frames repaired with FRP's; *d*) modelling of the repaired column with FRP's.
- The bond-slip reveals to have an important influence in the structural behaviour of ancient RC structures, as commented in Sections 5.3.5 and 5.6. However, there is a lack of relevant experimental studies on the bond-slip for this kind of RC elements. Therefore, calibration of the bond-slip effect in the numerical models for old RC structures based on experimental results is vital. It is considered of extreme importance the development of an experimental research programme on a series of specimens (columns, beams and joints) made with smooth reinforcing bars, in order to better investigate the bond-slip for this kind of ancient structures.
- The shear failure mode (due to the lack of confining reinforcement) proves to be important in a significant number of buildings damaged by earthquakes (as referred in Section 2.5.5). The damage mechanisms of the used model are entirely based on flexural capacities of frame members, not including the inelastic behaviour in shear (see Section 5.3.4). Therefore, further experimental research is needed to develop and calibrate the shear behaviour of RC members of existing structures.
- Experimental calibration of empirical formulae to estimate the plastic hinge length in RC elements with smooth reinforcing steel bars should be developed, as already commented in Section 5.3.3.
- From comparisons of the load-deformations relationships in a series of tests on specimens with different end anchorage detailing, Hassan and Hawkins (1977) conclude that the presence of hook caused a marked deterioration in behaviour. The effect of the standard 180° hook on the end anchorage of the bar, traditionally used in the existing RC buildings, needs to be further investigated.
- The equivalent bi-diagonal struts model is commonly adopted to simulate the effect of infill panels in the structural response. However, the behaviour laws and hysteretic rules of each diagonal do not influence the other. Since damage of an infill panel in one

---

direction, reduces the global stiffness and strength of the panel for any direction, there is a need to obtain an improved infill model that accounts for a connected behaviour of both struts, as recalled in Section 5.6.3.

- Experimental research done in the 1990's decade has improved our knowledge on the behaviour of jacketed members. As referred by Ersoy (1998), most of the questions related to jacketed beams have been answered by the research work. However, such a statement cannot be made for columns. Further experimental research is needed to clarify the behaviour of jacketed columns, especially for jacketing made under load, as already referred in Section 5.3.8.2. Analytical studies to predict the strength of rehabilitated member and structures should also be enforced.
- As already exposed in Section 2.5.6.4, common structural conceptions lead to a presence of a soft-storey at the ground storey, which induces excessive inter-storey drift at this storey level when earthquake happens. Regardless of the need for a structural detailing accounting for this intensity of inelastic deformation, a correct consideration of the geometric non-linearity should be considered. Therefore, it is considered of vital importance the inclusion of the  $P-\Delta$  effect in the non-linear models and a meticulous sensibility analysis should be developed for these kind of irregular structures.
- Numerical evaluation of the effect of the vertical component of seismic action in existing structures, non-seismically designed, should be considered.
- Several research groups around the world are currently using extensively refined non-linear numerical analyses to study the real behaviour of structures subjected to earthquake ground motions. In the academic community, on the one hand, there is no doubt about the utility of these refined models in the structural assessment and design of retrofitting solutions. Yet, on the other hand, it is recognised that these powerful tools depend on a large amount of parameters not yet well calibrated (as in the examples studied in Chapter 5). Therefore, work has to be done in order to produce and to implement calibrated refined non-linear models and related parameters that can be used in the structural assessment and design.
- The dilemma of the inclusion of non-linear numerical analyses methods for structural design in engineering education studies plan, at the graduate and post-graduate levels,



also needs to be resolved. It is recognised that the available models are quite complex and time consuming, and, consequently, difficult to put into practice in teaching at the graduate level. Fortunately, today we can take advantage of the interminable facilities given by the Information Technology (IT) to enhance the learning practice. Using, for example, dynamic figures and practical examples, the concepts and ideas can be conveyed instantly, as sustained by Shepherdson (2001). Traditional teaching methods delay the learning process. Additionally, learning based on IT allows access to so many more users and to the handicaps, with the convenience of continual access and repeatability, what makes the e-learning possible. Such sophistication is extremely challenging and can be the source of much research. In summary, Information Technology offers exciting opportunities, and its influence on the future of education is welcome.

- However, it is recognised that refined models for rapid assessment of existing structures are quite unfeasible and time consuming. Rapid seismic assessment procedures are required for low-to-medium-rise regular buildings. Such procedures should be influenced by the spirit of the recent US documents (e.g. ATC-40, 1996; FEMA-274, 1997) and by the displacement-based philosophy (Calvi, 1999; Fajfar, 2000). Development and calibration of numerical tools, as the MDOF simplified non-linear model, proposed in Section 5.7, that allow doing a preliminary screening and empirical evaluation methods to the existing structures, yet still maintaining an adequate accuracy, is and will be an area of rich research.
- Parametric studies with the MDOF simplified non-linear model should be enforced to determine the priority for strengthening intervention in the building stock.
- The proposed MDOF simplified non-linear model for the response evaluation and assessment was developed for plane frames. To account for the in plan building irregularities, an extension of the method to structures modelled by three DOF's per storey (one rotation and two horizontal displacements) should be developed and calibrated.
- The decision related to vulnerability can only be made by the judgement of experienced engineers. Therefore, we need to develop some simple methods and

---

criteria for initial screening of the building inventory. Such methods and criteria should not be time consuming and should not require expert opinion.

- Currently, highly efficient mathematical programming and analysis capabilities are available to the designer (as the methodology proposed in Section 5.8). However, the widespread use of optimization techniques to real life engineering problems is still not a reality. One area that has shown tremendous progress in the past few years is the optimal design of new structural systems. The optimal design of structural retrofitting systems is a relatively new area and is still not extensively addressed. This is a subject of great relevance, since an increasing number of real life engineering design problems involve retrofitting of structures. Furthermore, the structural changes made in the redesign of one component (storey) may influence the global behaviour of the structure. So, it may not be possible to divide properly the design of a multi-component structural system into design of single components (storeys). It is therefore necessary to use a methodology that can tackle the optimal multi-component system as a whole, while generating designs for the optimal layouts of the retrofit components. In this line, a simplified tool to determine the optimum retrofit need for each storey, in order to comply with certain performance objectives was proposed in Section 5.8. As already said, the optimal design of retrofitting is still not extensively researched. Further evaluation of the proposed methodology, with experimental results, will allow further refinement and the development of specific and practical guidelines for its use by engineers enrolled in the retrofitting design of existing structures.
- As stated by Fardis (2000), complete and clear provisions for the design and detailing of the strengthening of existing elements need to be developed for EC8, including simple procedures for dimensioning of the retrofitting for the most common and effective strengthening techniques.

Lastly, in order to encourage balanced and sustained retrofitting decision to preserve our patrimony, our lives and of the successive generations, it is salutary to recognise that policy makers, engineers and building owners should remain the focus on the task and not on the tools. A quote found in the Izmit (Turkey) post-earthquake report (EQE, 1999) is herein used as conclusive thought:

*'Loss of life and building collapse was avoidable.'*

**Appendix A**

*PHOTOGRAPHIC DOCUMENTATION AND  
STRENGTHENING DETAILS*



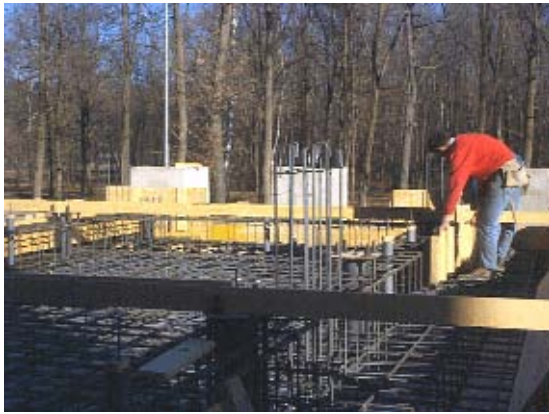


Figure A.1 - Base foundation reinforcement (general view) and reinforcement of the columns (lap-splice at the columns base)



Figure A.2 - Base foundation (detail): slender-column reinforcement and tubes to apply the vertical jacks (for structure uplift)



Figure A.3 - General view of the base foundation (concrete casting)



Figure A.4 - Base foundation (concrete casting) and column longitudinal reinforcement at the base with  $180^\circ$  bends



Figure A.5 - Slab reinforcement, reinforcement added in the attachment zone and plastic tubes for connection to the steel loading frame



Figure A.6 - Joint detail



Figure A.7 - Casting of the 1<sup>st</sup> floor (general view)



Figure A.8 - Casting of the 1<sup>st</sup> floor (general view): the 1<sup>st</sup> to 2<sup>nd</sup> floor transition without lap-splice in the columns reinforcement.

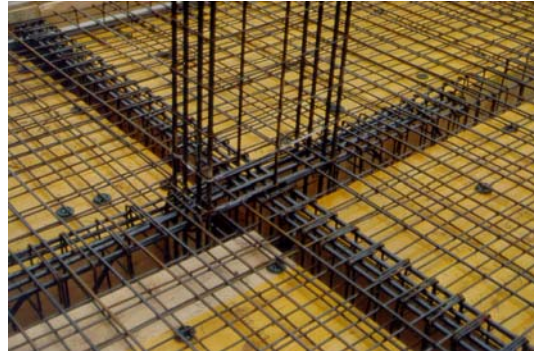


Figure A.9 - Joints and columns reinforcement details



Figure A.10 - Construction at various phases (general views)



Figure A.11 - Transport: vertical jacks





Figure A.12 - Transport: general view of the frames at the external area of the ELSA laboratory



Figure A.13 - Frames transportation



Figure A.14 - Vertical connectors pre-stressing (to attach the actuators at the steel load frame)



a)



b)

Figure A.15 - Steel frames: a) pined bars connecting the two frames and fixings to the reaction-wall; b) frame to control out-of-plane deformation in the frame extremity opposite to the reaction-wall



Figure A.16 - Fixings to the reaction-wall, steel pined bars connecting the two frames and actuators



Figure A.17 - Additional loads (2.7 ton concrete blocks and 1.2 ton steel plates) and floor attachment steel bars system with pre-stressed connectors



Figure A.18 - Actuators (double acting servo-hydraulic actuator linked at the extremity to piezoresistive load cell)



Figure A.19 - Displacement controllers (HEIDENHEIN optical transducers)



Figure A.20 - Acquisition, control and monitoring system



Figure A.21 - Instrumentation: strong-column at 1<sup>st</sup> storey



Figure A.22 - Instrumentation: slab (below)



Figure A.23 - Instrumentation: inclinometers

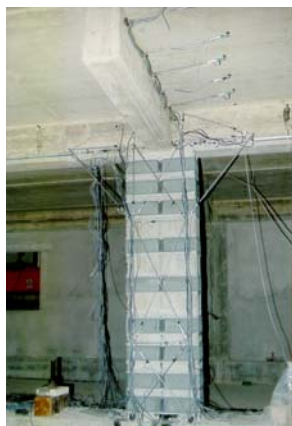


Figure A.24 - 1<sup>st</sup> storey strong-column: selective retrofitting (ductility and shear resistance improvement) and instrumentation (strong-column, slab, joint and beam deformation)



Figure A.25 - Strength improvement: connection of the steel bars to columns



Figure A.26 - Construction of the infill masonry walls: sequential phases and detail



Figure A.27 - Four-storey full-scale reinforced concrete infilled frame: a) construction of the masonry infill walls; b) general views of the structure



Figure A.28 - Infill strengthening construction: sequential operations and details of the reinforcing steel mesh



Figure A.29 - Infills instrumentation installed for the IN and SC tests: panels and local instrumentation at the panel corners of the short external panel



Figure A.30 - Concrete specimens extraction from the frame structure



Figure A.31 - Additional masses (water reservoirs)



Figure A.32 - Instrumentation in repaired external joints (relative displacement transducer)



Figure A.33 - Instrumentation at the 1<sup>st</sup> storey strong-column for the final capacity cyclic test



Figure A.34 - Storey displacement measurement systems: HEIDENHEIN and PSITRONIX displacement transducers





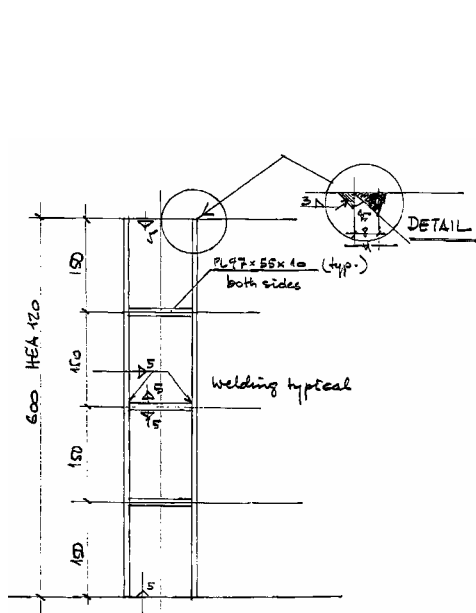


Figure A.37 - K-bracing and shear-link: shear-link details

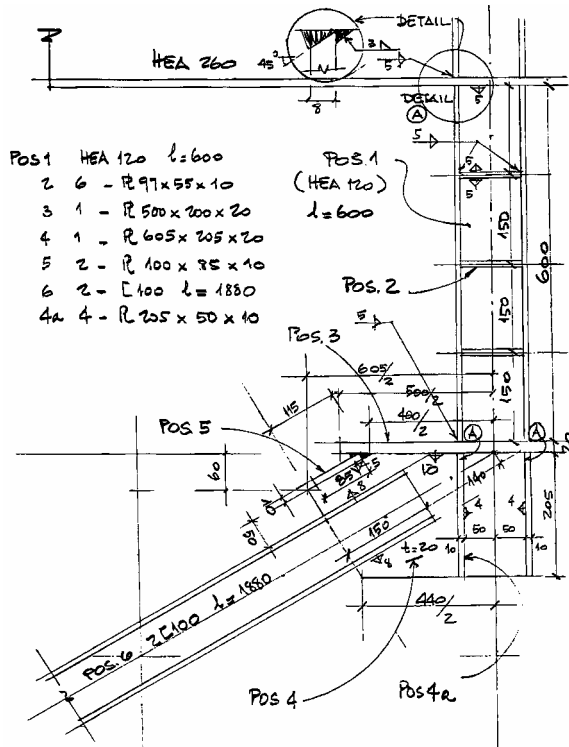
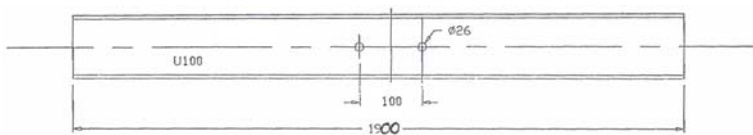
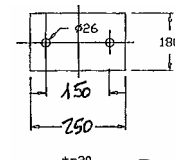


Figure A.38 - K-bracing and shear-link: details of shear-link and adjacent connections



Pos. 6



t=20

Pos. 6a

Figure A.39 - K-bracing and shear-link: detail of braces

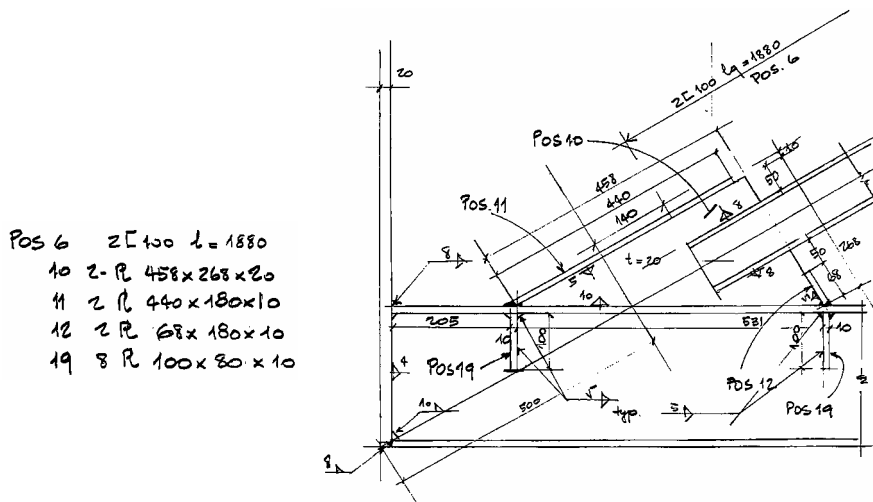


Figure A.40 - K-bracing and shear-link: detail of the bottom braces connection

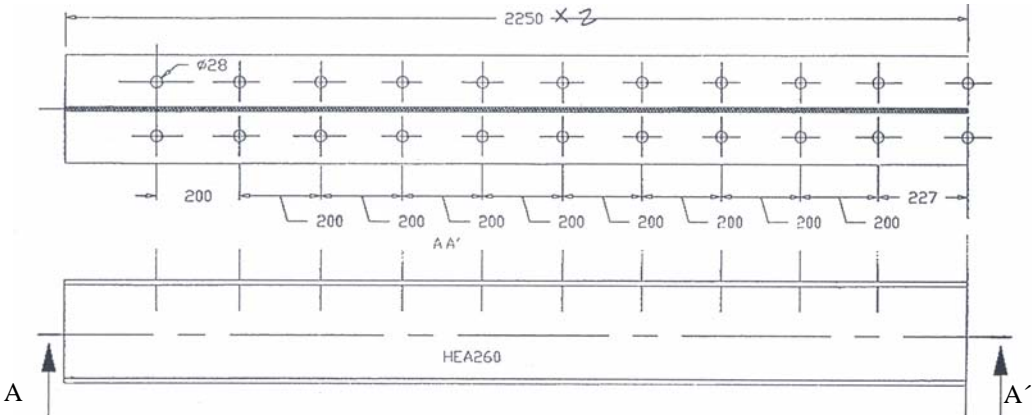


Figure A.41 - K-bracing and shear-link: detail of Pos. 8

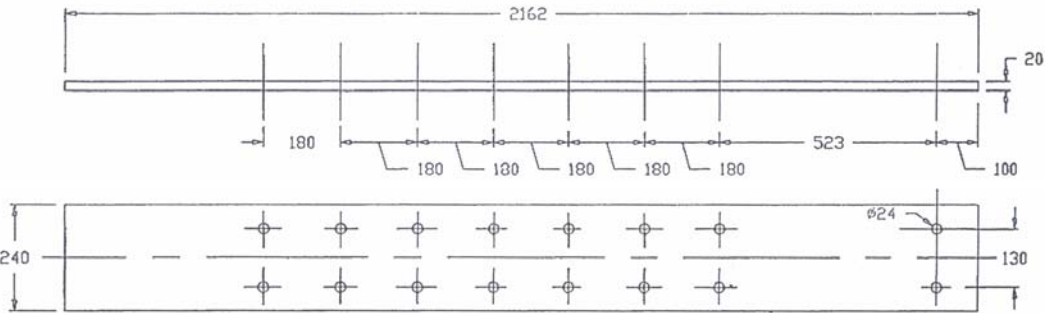


Figure A.42 - K-bracing and shear-link: detail of Pos. 14

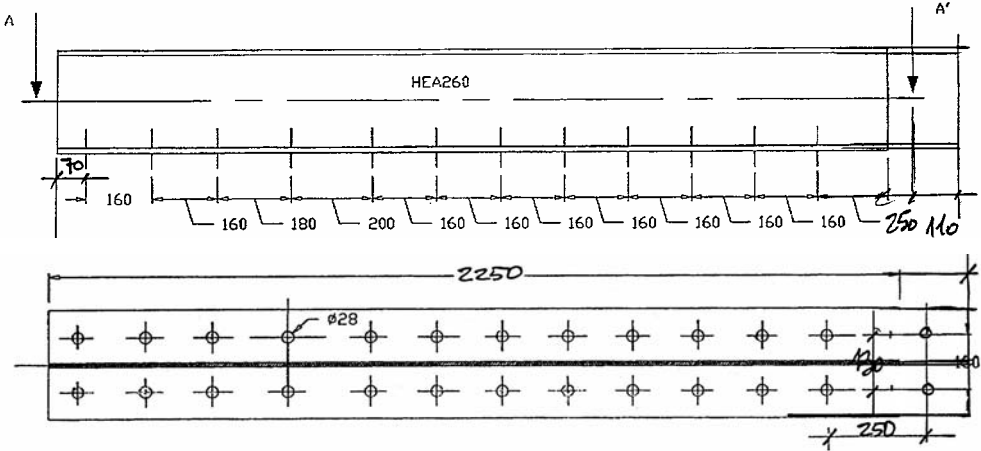


Figure A.43 - K-bracing and shear-link: detail of Pos. 15

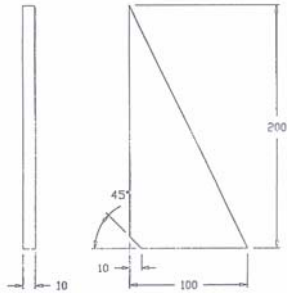


Figure A.44 - K-bracing and shear-link: detail of Pos. 16

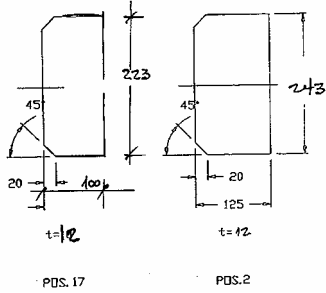


Figure A.45 - K-bracing and shear-link: detail of Pos. 17 and Pos. 2



Figure A.46 - Columns drilling: strong-column (left) and weak column (right)



Figure A.47 - Anchoring of the top-beam to the existing RC frame



Figure A.48 - Bottom-beams: drilling



Figure A.49 - Shear-link with the surrounding beam and braces



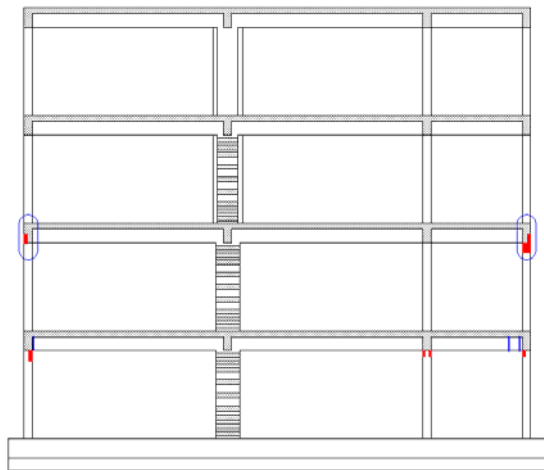
Figure A.50 - Bracing instrumentation (strain-gauges)



Figure A.51 - Instrumentation: relative displacement transducer (detail of the zone nearest to the shear-link)

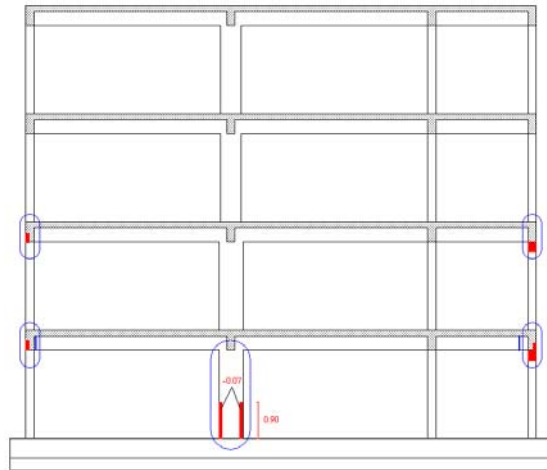


Figure A.52 - Repair operations (steps): 4 – remove concrete at the top of the damaged column; 5 – relocation of the column; 6 – concreting of the column/joint; 7 – strengthening with carbon fibre



LEGEND:  
— Crack injected with resin  
■ Reconstruction (repair) with mortar  
○ Fiber-Carbon strengthening zone

Figure A.53 - Repair intervention: frame B



LEGEND:  
— Crack injected with resin  
■ Reconstruction (repair) with mortar  
○ Fiber-Carbon strengthening zone

Figure A.54 - Repair intervention: frame A



Figure A.55 - Damages on the first storey strong-column: frame A



Figure A.56 - Column repaired with carbon fibre materials

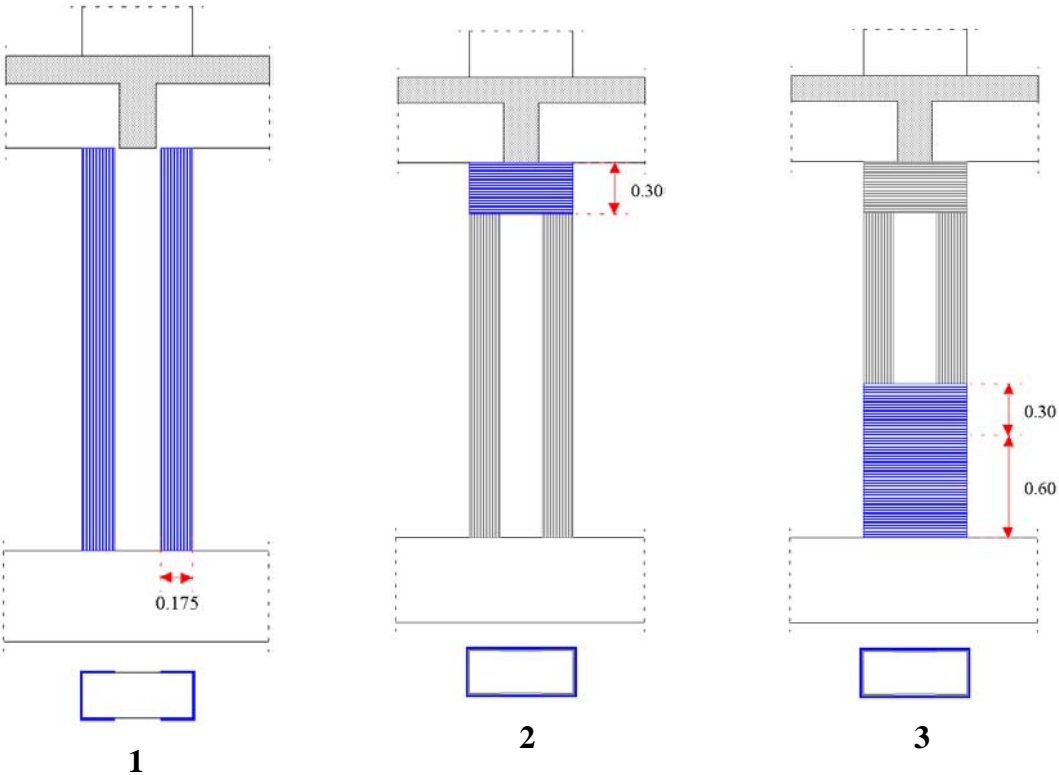


Figure A.57 - Strong-column (frame B) repair intervention (schematic sequential operations): 1– longitudinal fibres; 2 – confinement of the column upper-part; 3 – confinement of the column low part (including bar termination zone)

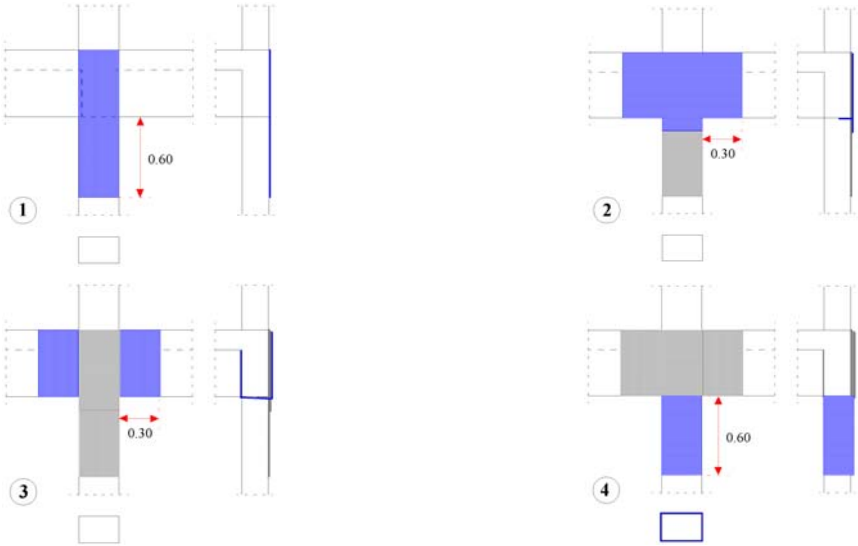


Figure A.58 - Joints repair intervention: schematic sequential operations





Figure A.59 - Sequential operation phases for the joints intervention

## **Appendix B**

### *TEST RESULTS AND PHYSICAL DAMAGE PATTERNS*

*Visual inspection and photographic documentation*



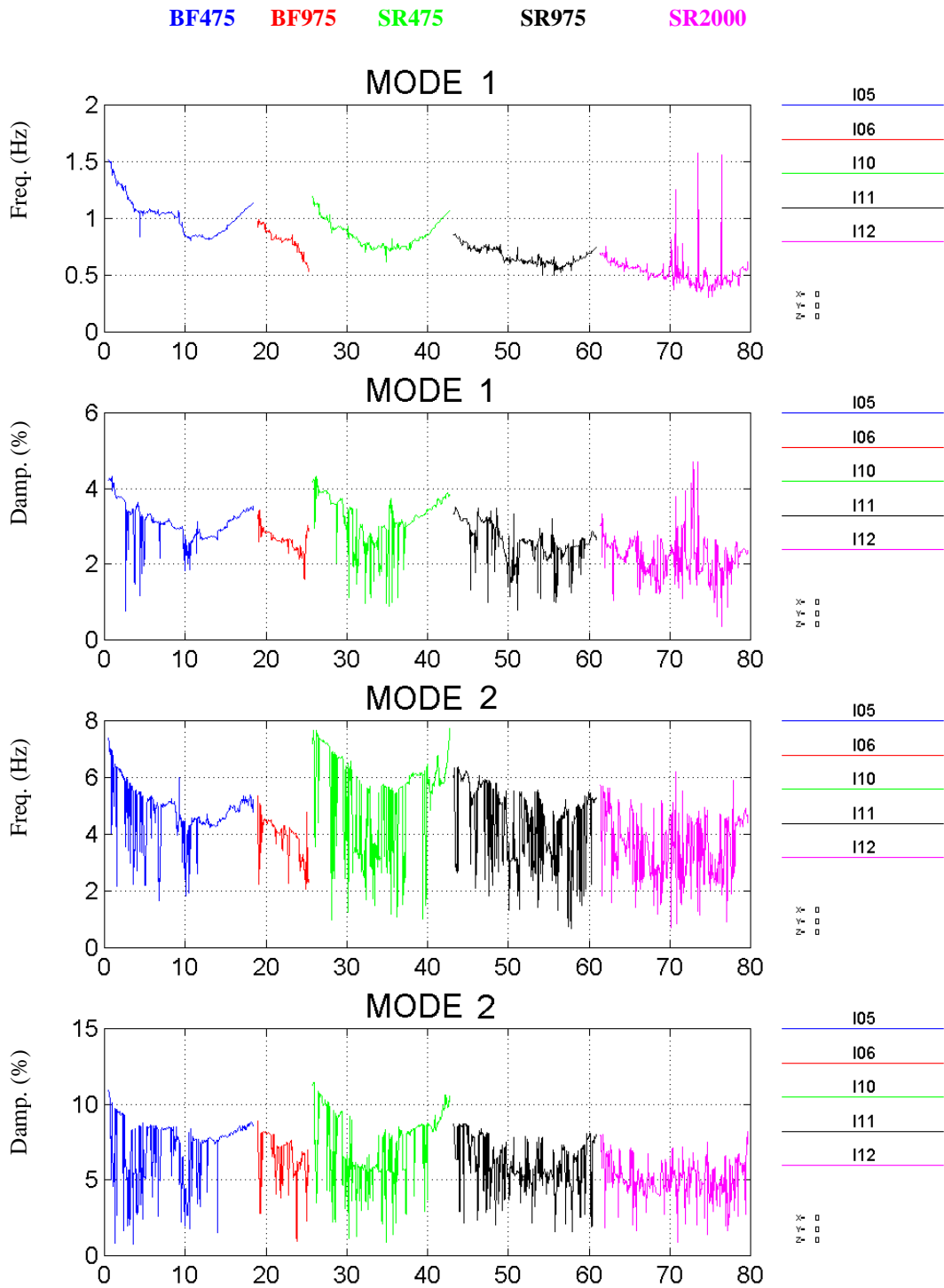


Figure B.1 - Plots of the time-domain identified frequency and damping ratio for the first two vibration modes of BF475 (L05), BF975 (L06), SR475 (L10), SR975 (L11) and SR2000 (L12)

L04: ASR PsD 10% 475-yrp 13/07/99

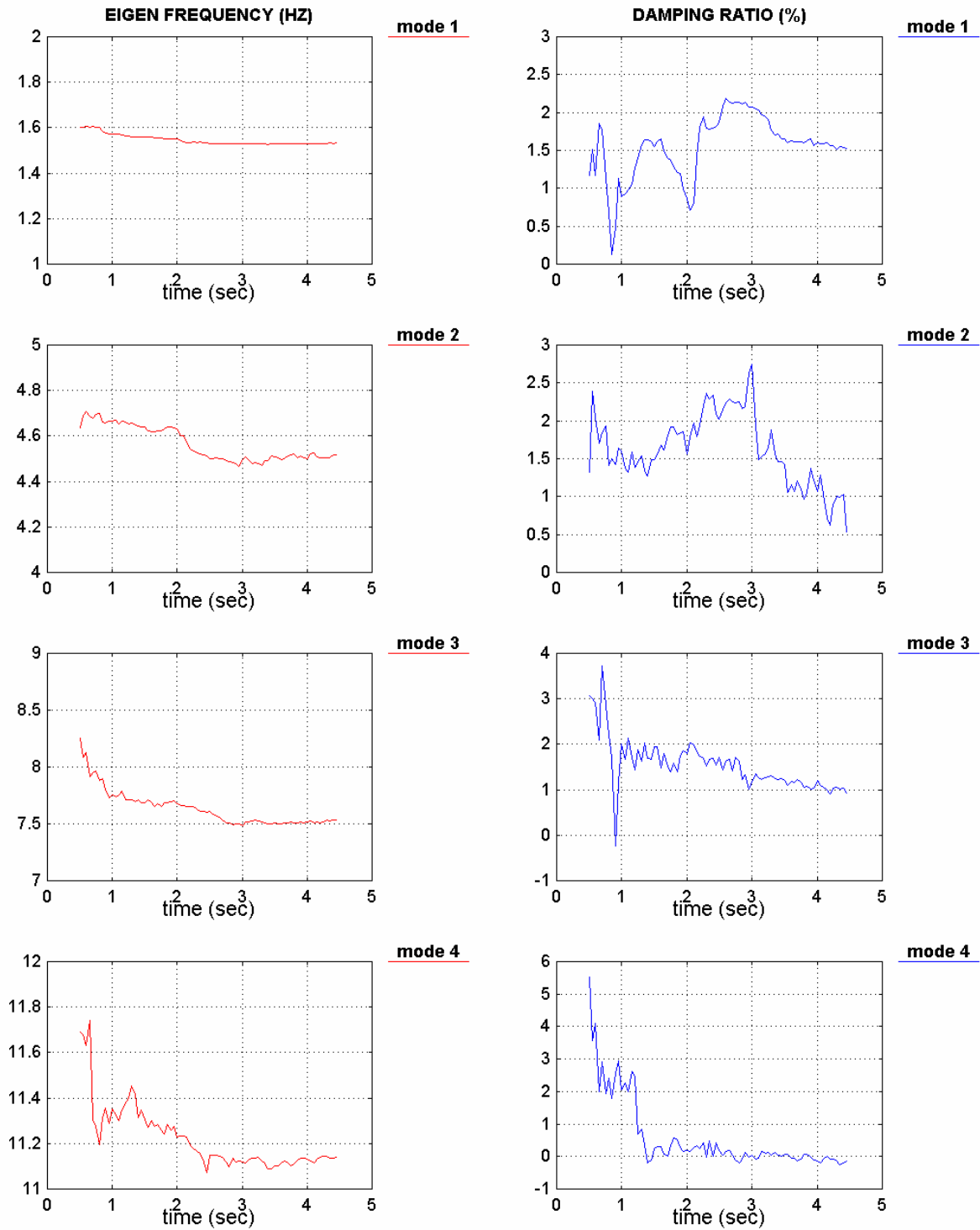


Figure B.2 - Equivalent modal frequency and damping for the virgin bare frame (10% intensity of 475-yrp earthquake)

## L05: ASR PsD 100% 475-yrp 13/07/99

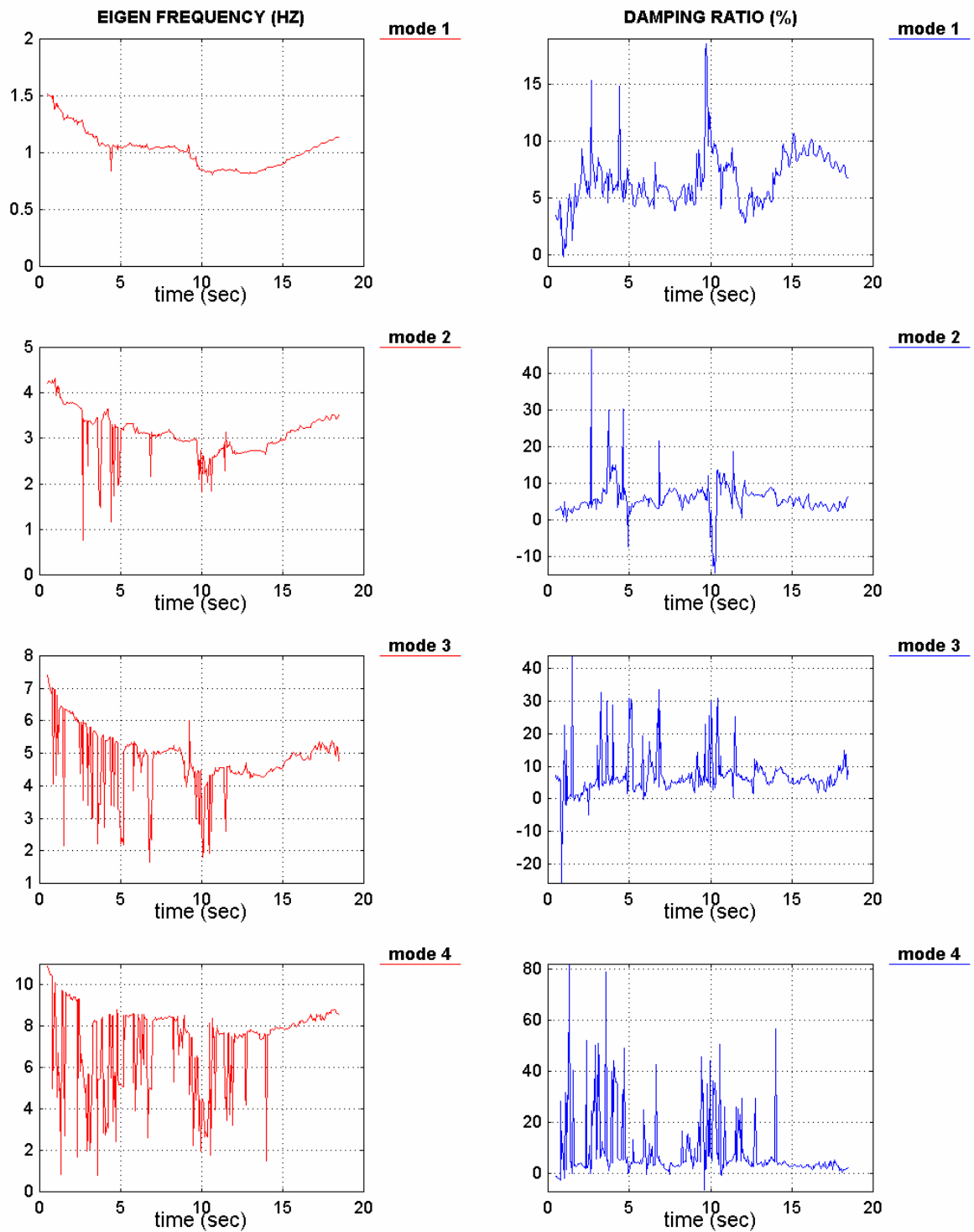


Figure B.3 - Equivalent modal frequency and damping for the BF 475-yrp test

L06: ASR PsD 100% 975-yrp 14/07/99

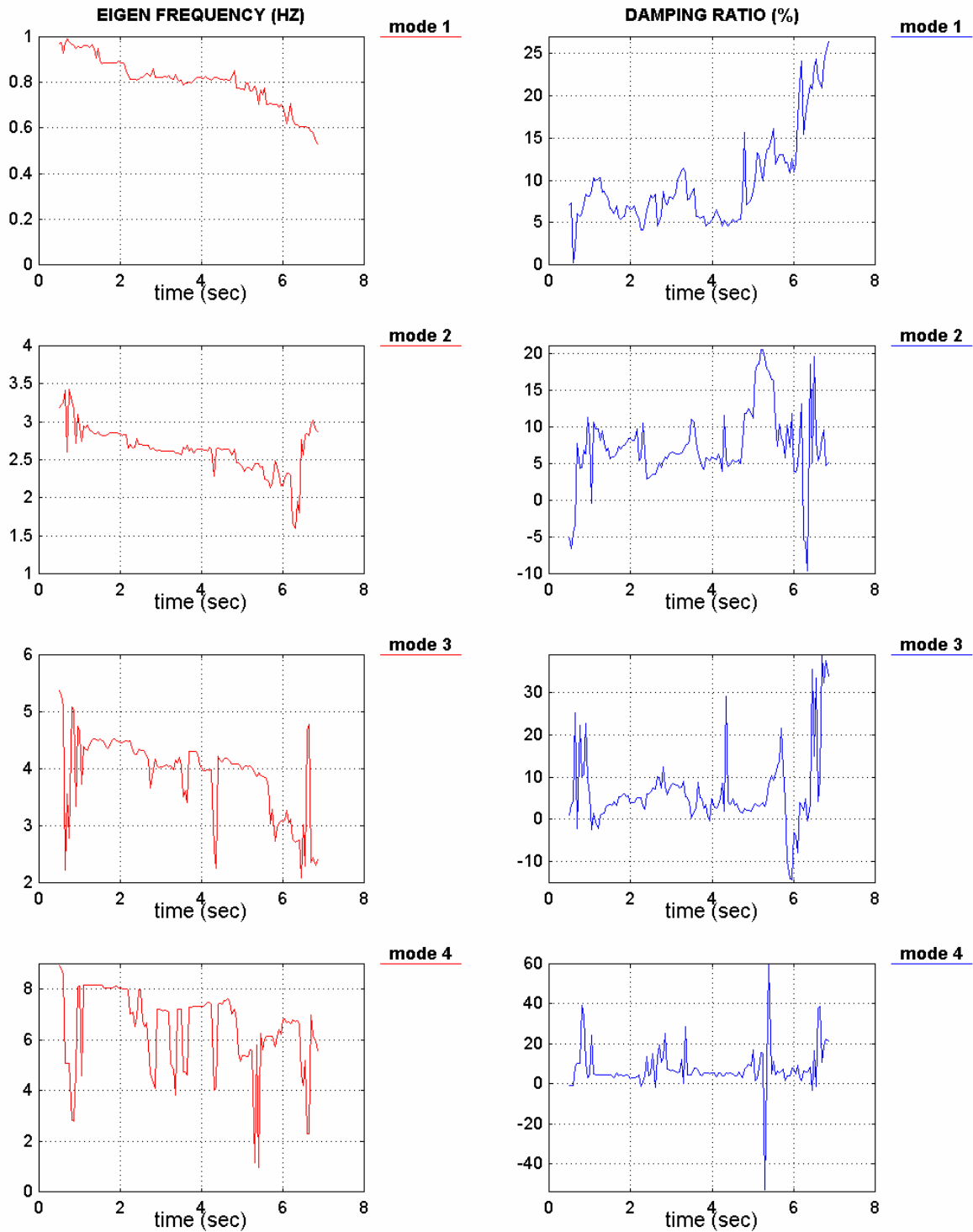


Figure B.4 - Equivalent modal frequency and damping for the BF 975-yrp test

## L08: ASR PsD 5% 475-yrp 20/07/99

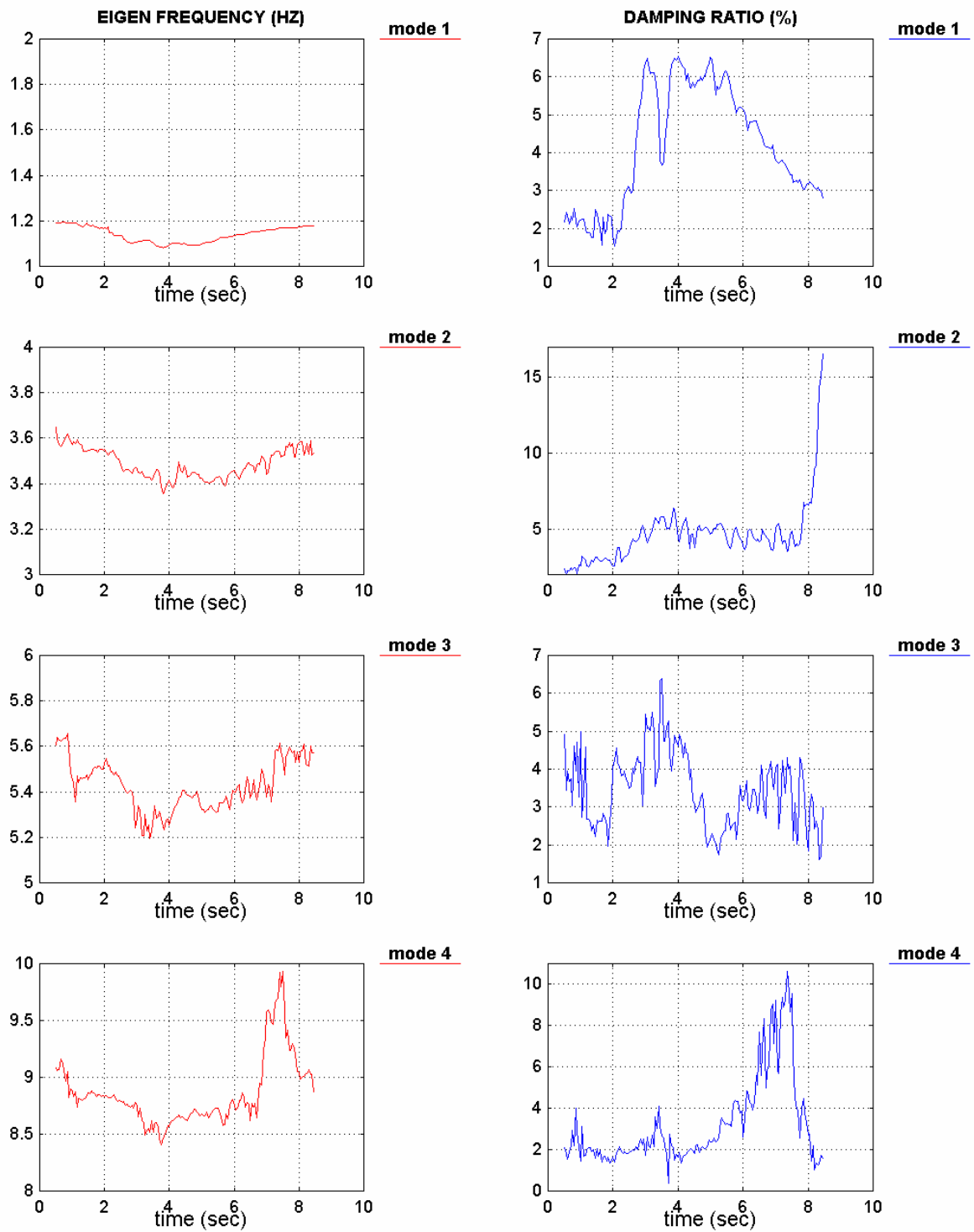


Figure B.5 - Equivalent modal frequency and damping for the BF after 975-yrp earthquake test (5% intensity of 475-yrp earthquake)



L09: ASR REPAIRED PsD 5% 475-yrp 14/09/99

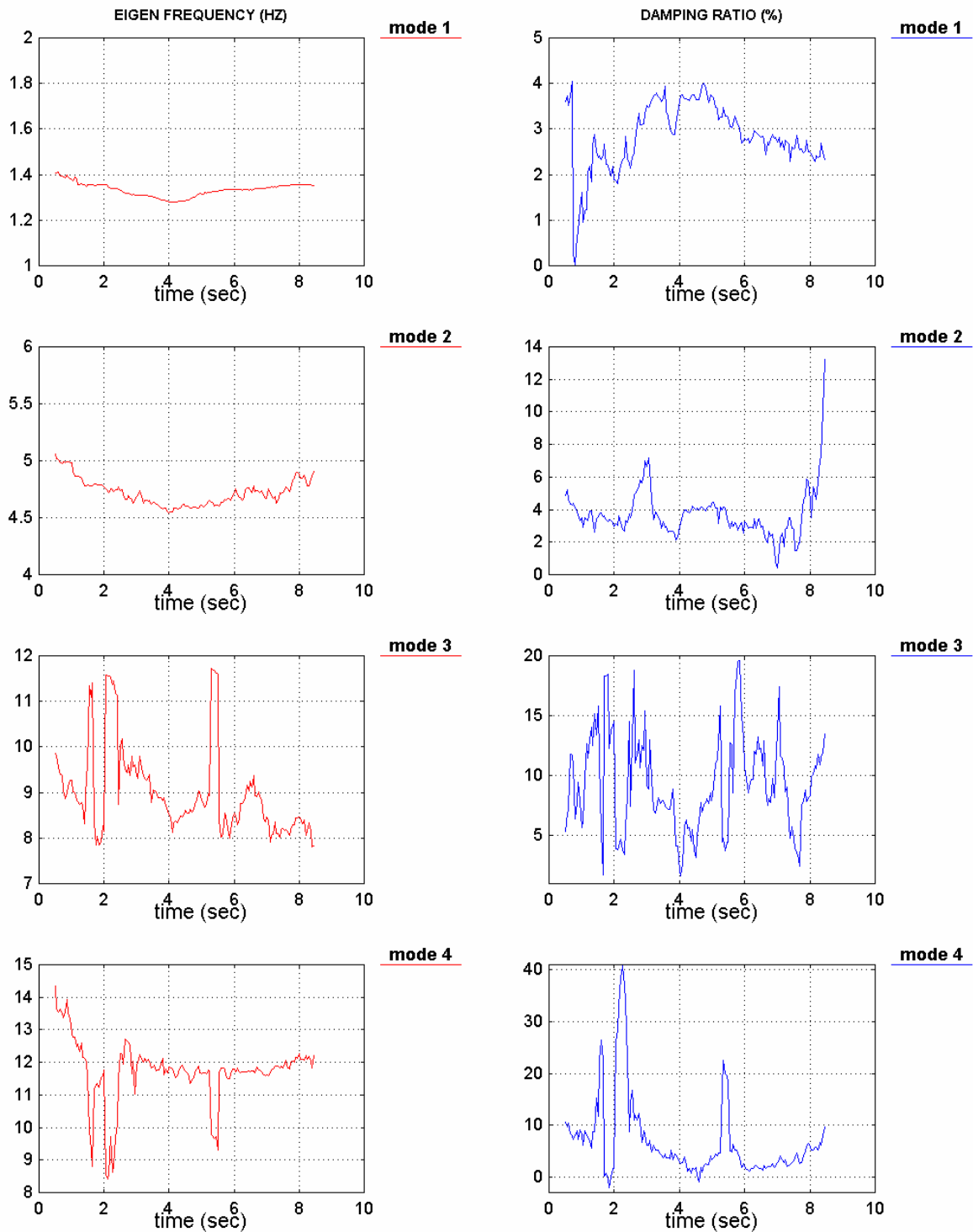


Figure B.6 - Equivalent modal frequency and damping for the SR - 5% intensity of 475-yrp earthquake (before full-intensity earthquake tests)

## L10: ASR REPAIRED PsD 100% 475-yrp 16/09/99

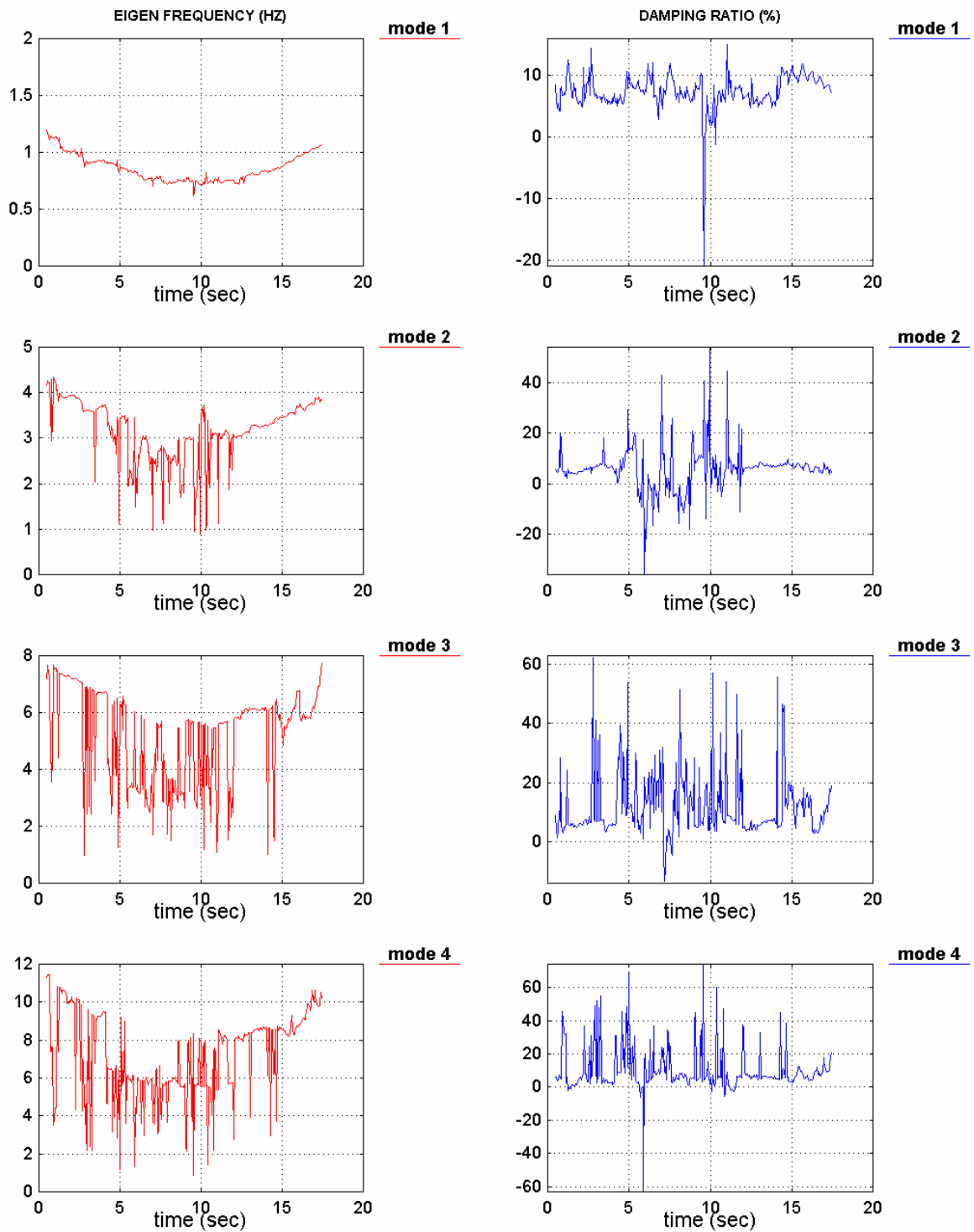


Figure B.7 - Equivalent modal frequency and damping for the SR 475-yrp test

L11: ASR REPAIRED PsD 100% 975-yrp 16/09/99

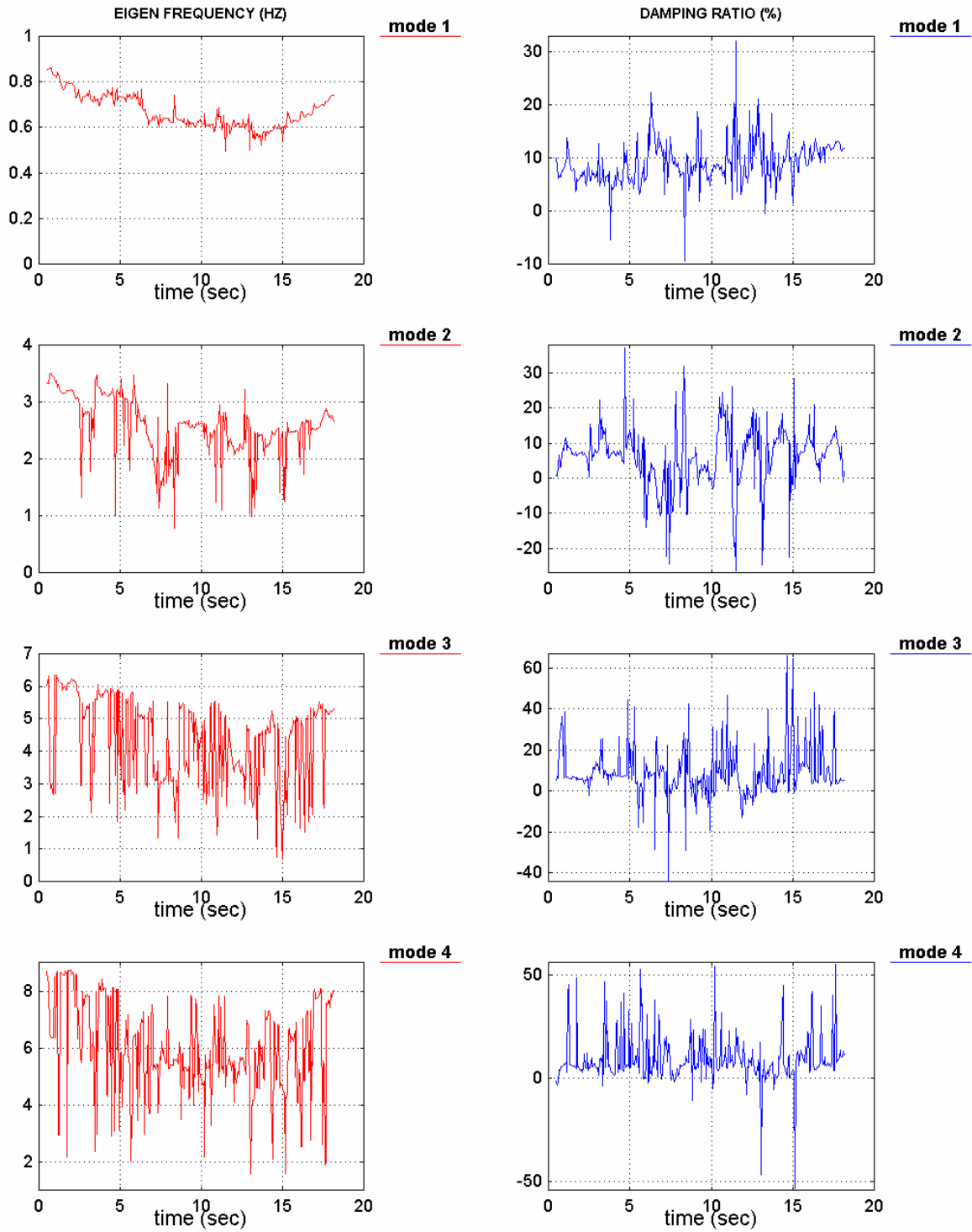


Figure B.8 - Equivalent modal frequency and damping for the SR 975-yrp test

## L12: ASR REPAIRED PsD 100% 2000-yrp 17/09/99

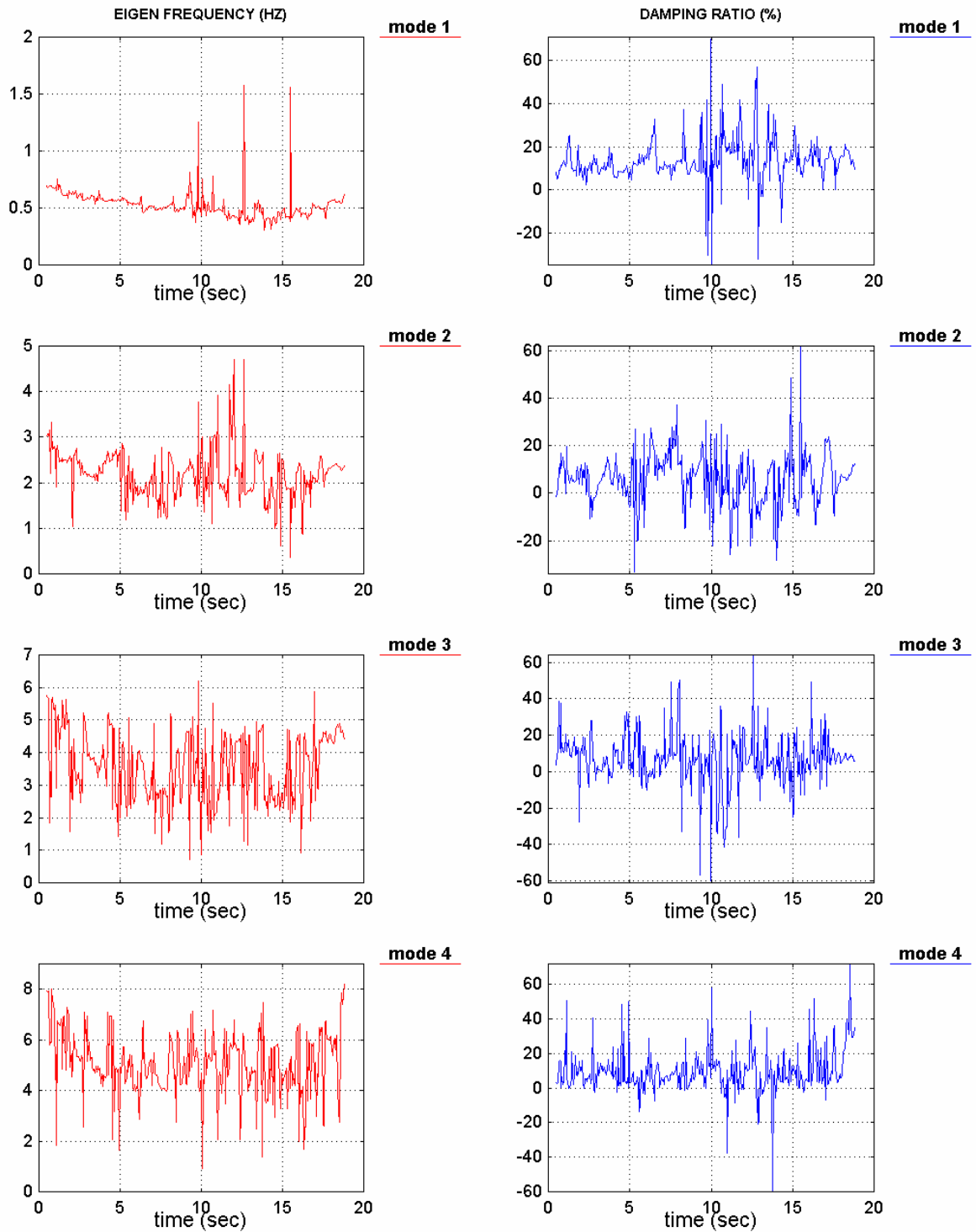


Figure B.9 - Equivalent modal frequency and damping for the SR 2000-yrp test

L13: ASR REPAIRED PsD 5% 475-yrp 17/09/99

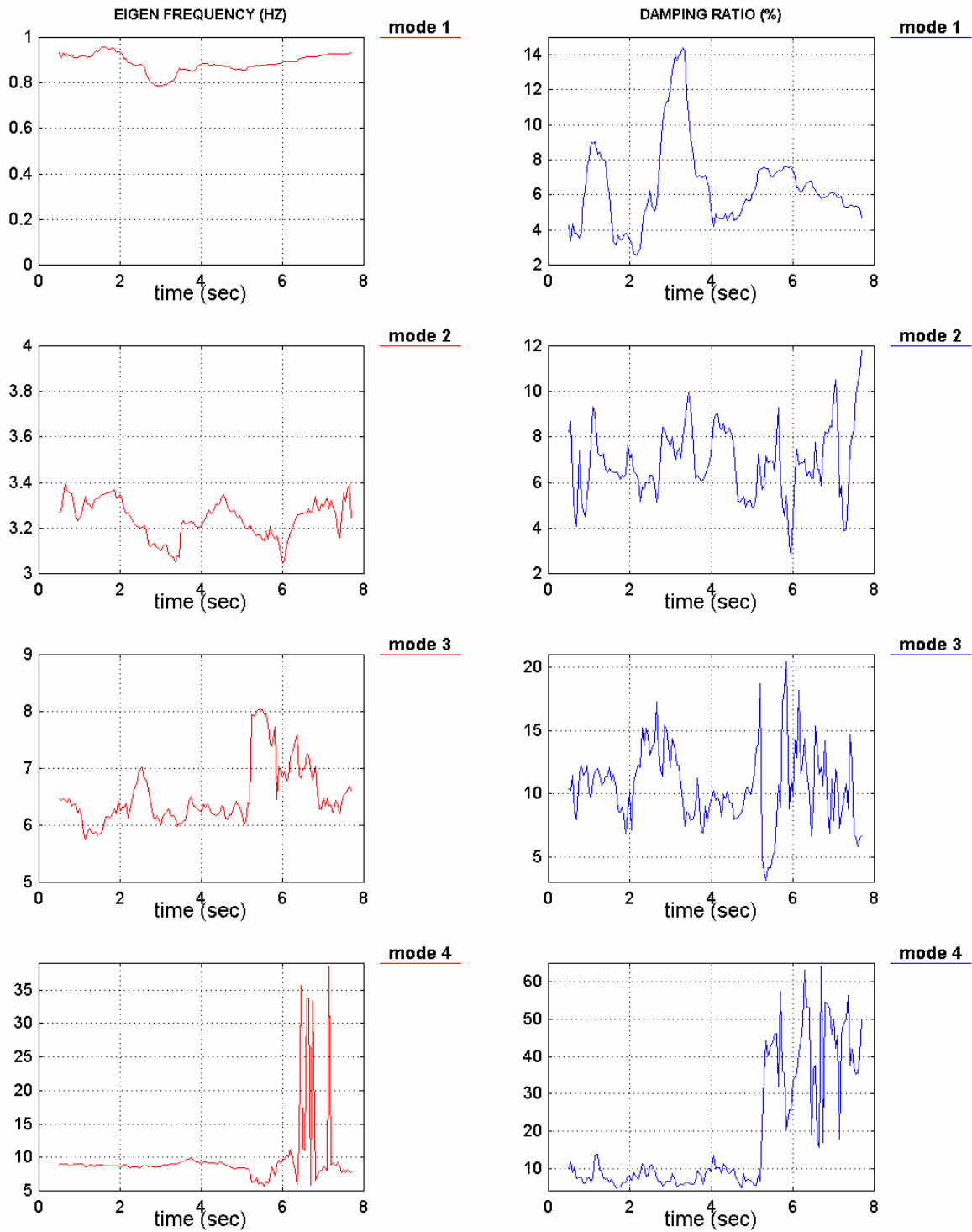


Figure B.10 - Equivalent modal frequency and damping for the SR after 2000-yrp earthquake test (5% intensity of 475-yrp earthquake)

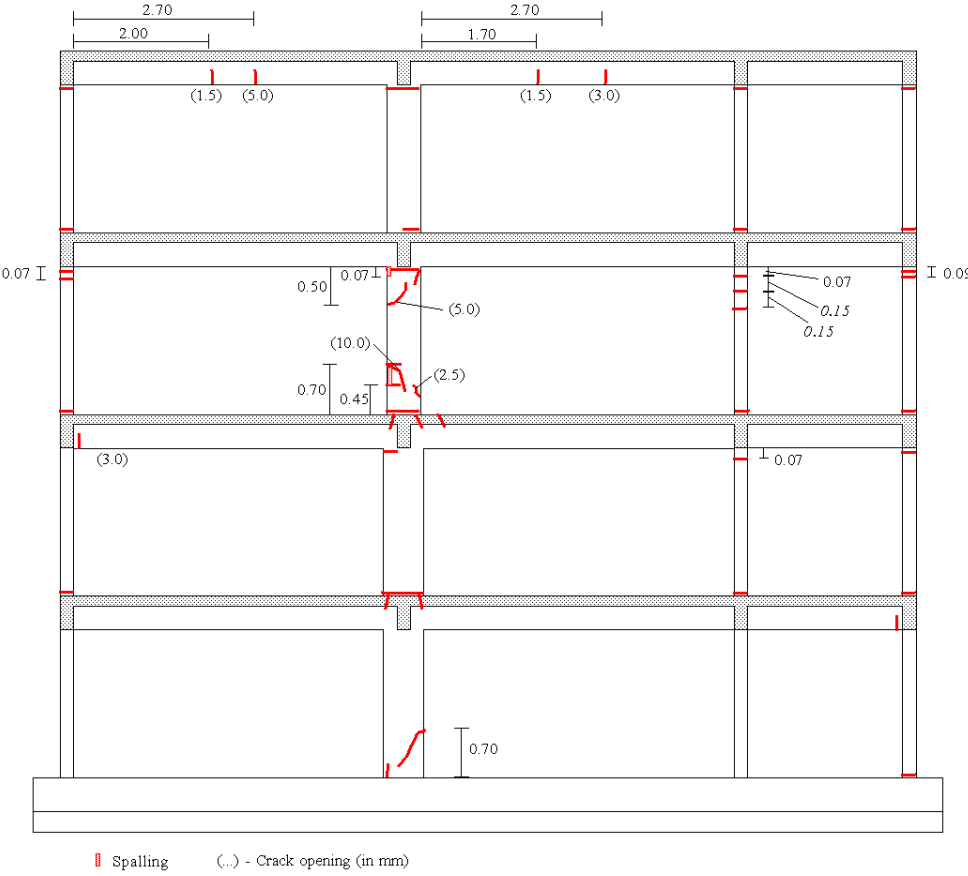


Figure B.11 - Damage pattern after the bare frame tests (general layout)

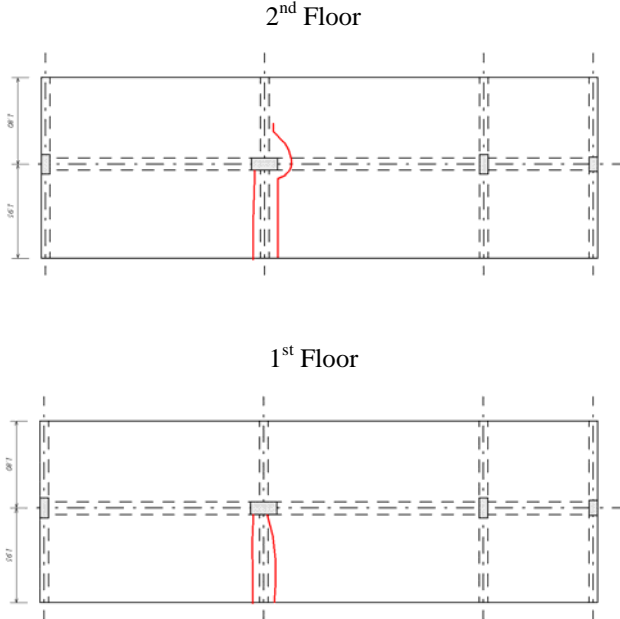


Figure B.12 - Slab damage pattern after the bare frame tests



Figure B.13 - BF975: the horizontal storey displacement is evidenced (comparing the relative position of the transversal beams of the two frames)



Figure B.14 - BF975: Damage (spalling) at the top of the 3<sup>rd</sup> storey strong-column (beginning)



Figure B.15 - BF975: damage (spalling) at the bar termination zone of the 3<sup>rd</sup> storey strong-column



Figure B.16 - BF975: damage (spalling) at the top of the 3<sup>rd</sup> storey strong-column



Figure B.17 - BF975: damage (spalling) at the bar termination zone of the 3<sup>rd</sup> storey strong-column

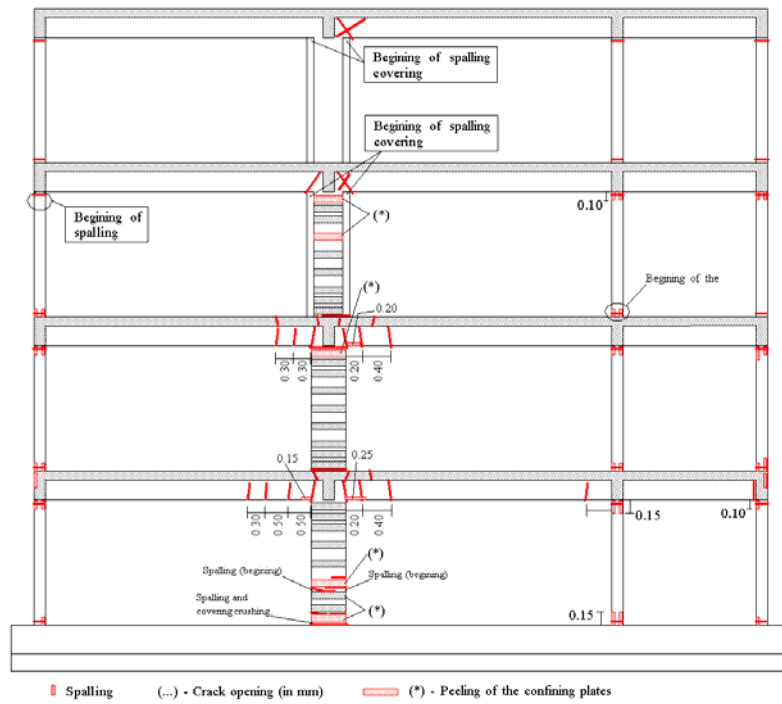


Figure B.18 - Damage pattern after the selective strengthened frame tests (general layout)

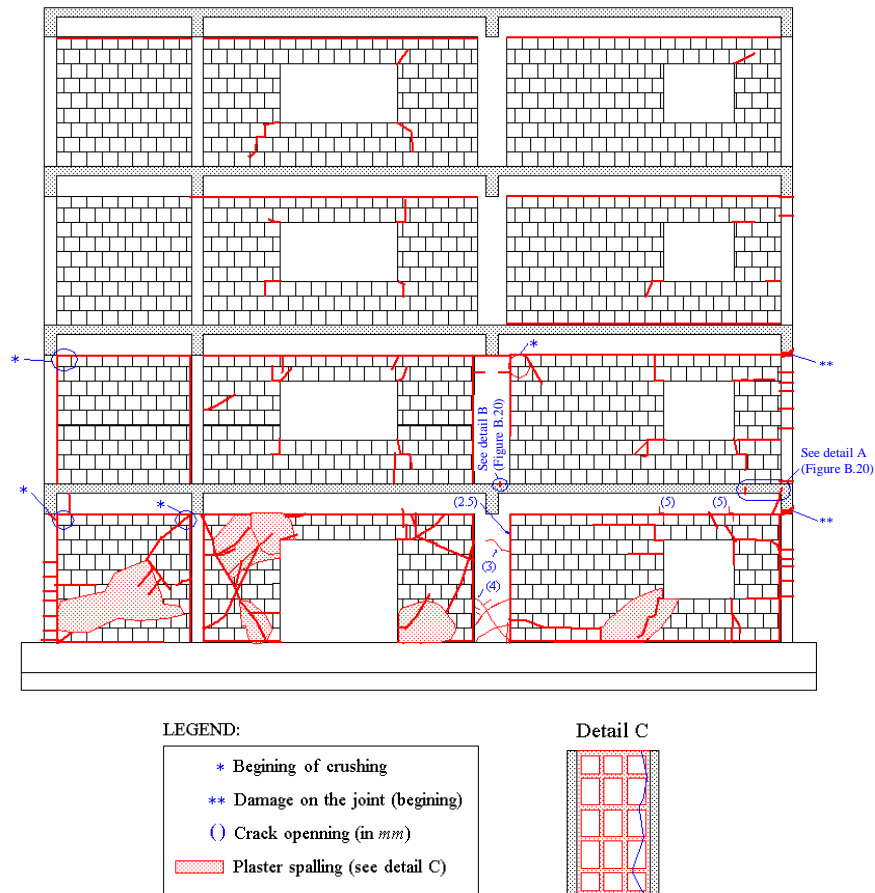
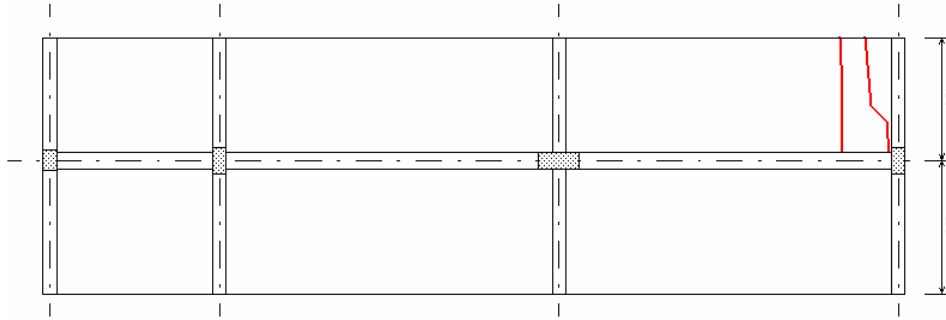


Figure B.19 - Damage pattern after the infill frame tests (general layout)



Detail A (floor 1, bellow)



Detail B (floor 1, above)

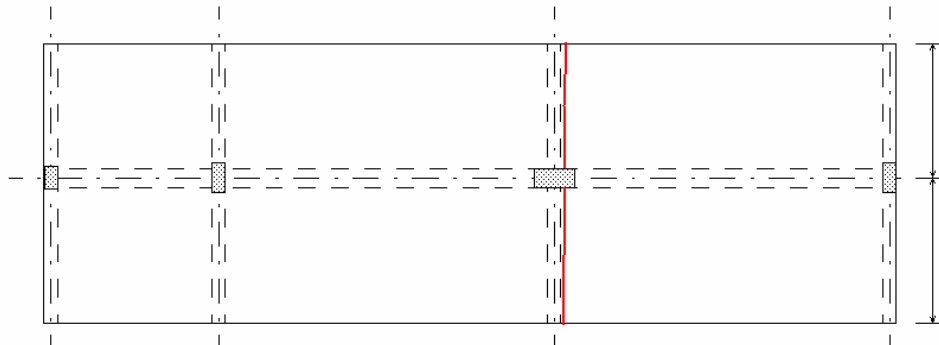


Figure B.20 - Slab damage pattern after the infill frame tests



Panel with window opening



Panel with door opening



Short panel (south view)



Short panel (north view)



Short panel (detail)

Figure B.21 - IN975: damages at the 1<sup>st</sup> storey infill panels and RC strong-column at the base

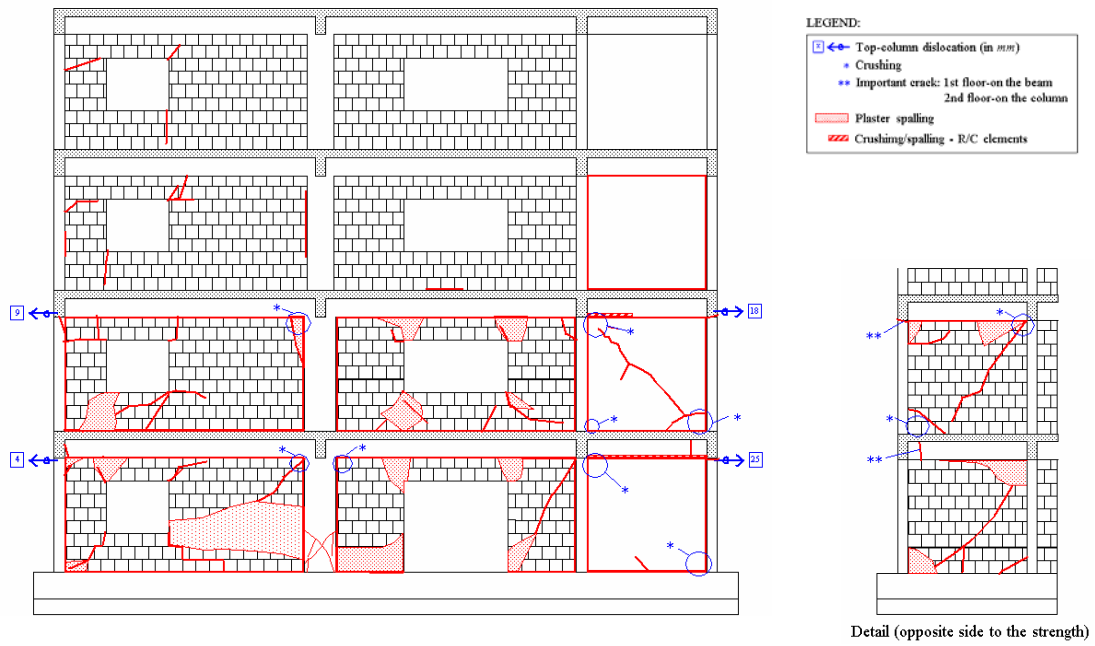


Figure B.22 - Damage pattern after the infill strengthened frame tests (general layout)



Figure B.23 - Damage on the reinforced concrete frame, infill and infill strengthened panels after the SC earthquake tests



Figure B.24 - KB-cyclic test: damage pattern in the shear-link



Figure B.25 - KB-cyclic test: damaged external columns ('shear-out')

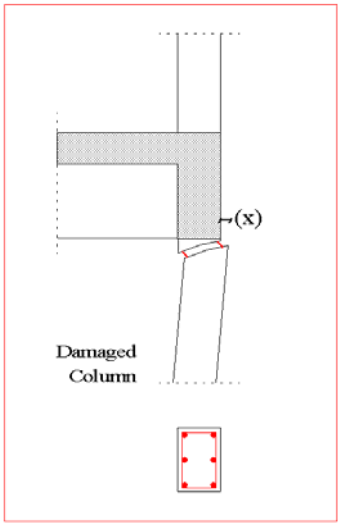


Figure B.26 - KB-cyclic test: details of the damaged external columns ('shear-out')

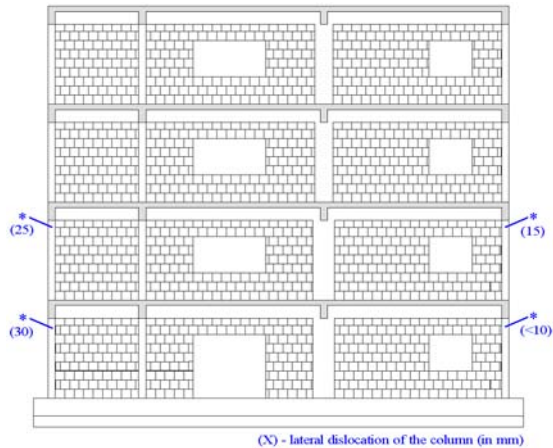


Figure B.27 - Frame A (brick infilled frame): damaged joints after the PsD tests

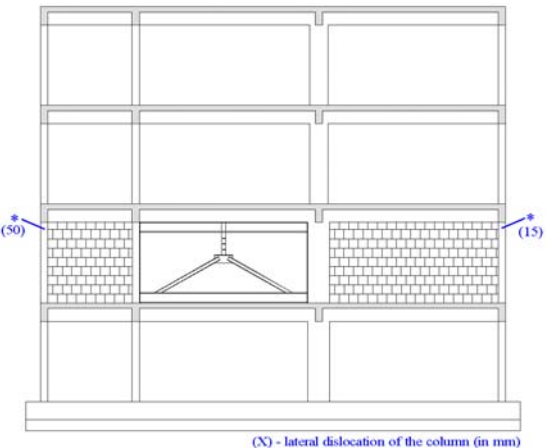


Figure B.28 - Frame B (brick infilled 2<sup>nd</sup> storey and K-bracing with shear-link in the internal bay): damaged joints after cyclic tests

## **Appendix C**

### *GLOSSARY*



At the outset, some basic concepts and information are necessary in order to better understand the contents of this thesis. These are a number of terms that are used, or are particularly related to the studied field, in the thesis. The terms themselves have been chosen, bent or created in order to describe something that our common language and thought pattern is incapable of describing. Also, the connotations of each term described would be the far better understood when viewed as a part of a whole, therefore is suggested to browse through the entire glossary and text if you wish to understand the concept of any individual term. Where as volumes could be written on any one of these terms, are briefly offered here a few hopefully clarifying paragraphs for explanation on the vocabulary used on this thesis (terms related with the studied topics).

### ***Assessment***

Consists on the verification of the resistance of an existing damaged or undamaged building, taking into account both non-seismic and seismic actions, for the period of its intended lifetime (EC8 Part 1-3).

### ***Bond-slip***

Slip (relative displacement) occurs along a reinforcing bar under loading, relatively to the contiguous concrete, and the produced bond stress is a function of the slip. The bond behaviour of reinforcement is usually described by the bond stress-slip relationship. The magnitude of bond stress is influenced by a large number of parameters, such as: the rib pattern of rebar, concrete strength, concrete cover, position of bar during casting, rate and type of loading (CEB-217, 1993).

### ***Building Performance Level***

A limiting damage state, considering structural and non-structural building components, used in the definition of Rehabilitation Objectives (FEMA-274, 1997).

### ***Capacity***

The permissible strength or deformation for a component action (FEMA-274, 1997).

***Capacity design method***

Design method in which elements of the structural system are chosen and suitably designed and detailed for energy dissipation under severe deformations while all other structural elements are provided with sufficient strength so that the chosen means of energy dissipation can be maintained (EC8).

***Civil engineering structural damage***

Any natural disaster can destroy or severely damage civil engineering structures: buildings; water structures (such as pipelines, pumping stations, intake structures, and dams); retaining walls; electrical poles; roads; and platforms. Damage of these structures can cause casualties to nearby individuals, and it may lead to either partial or total disruption of lifeline services to the communities they serve. Making advance preparations for the possibility of destruction and modifying existing facilities are major ways in which the damage can be reduced or eliminated. Structures can be reinforced to withstand the impact of a disaster. Likewise, the anchorage and support of machinery, equipment, and storage tanks can be improved. Bypass facilities can be provided; for example, in preparation for the possibility that a water plant, its equipment, or processes may fail, the plant can be bypassed to a point where raw water can be chlorinated. Finally, the adoption of standard operating rules and procedures will maximize readiness for any disaster. Another way to reduce the impact of disaster on civil engineering structures is to improve the planning of the database and of design standards. Conducting meteorological, topographical, hydrological, geological, and soil engineering studies in newly chosen sites will enable planners to avoid vulnerable locations. Vital structures can be located in areas known to be protected from the impact of disasters. Specific design methods can be prepared, used, and updated to protect structures, equipment, and supplies from disaster. For example, water distribution reservoirs can be sized with a storage factor of 1 1/2 to 2 times their normal capacity in order to guarantee emergency supplies.

***Composites***

A matrix of polymeric material reinforced by fibres with a discernable aspect ratio of length to thickness (Wabo MBrace, 2002).



***Constraints***

Limitations on the range over which the objective function may be minimized, represented as equality or inequality relations (Richards, 1995).

***Corrective measure***

Any modification of a component or element, or the structure as a whole, intended to reduce building vulnerability (FEMA-274, 1997).

***Critical regions***

Predetermined parts of a dissipative structure where the dissipative capabilities are mainly located (also called dissipative zones, EC8).

***Deformability***

Capability of a material, structural component, or entire structure to deform before rupture (Bertero *et al.*, 1991).

***Demand***

The amount of force or deformation imposed on an element or component (FEMA-274, 1997).

***Design variables***

The entities which may be modified during the optimization process. If the values of the design variables are known the design is fully defined (Richards, 1995).

***Dissipative structure***

Structure, which is able to dissipate energy by means of ductile hysteretic behaviour (EC8).

***Drift***

Relative lateral displacement between two points (e.g.: two floors).

***Ductility***

Capability of a material, structural component, or entire structure to undergo deformation after its initial yield without any significant reduction in yield strength. While ductility is a useful concept, it has a precise definition and quantitative meaning only for the idealised case of monotonic, linear elasto-perfectly plastic behaviour. Its use in real cases where behaviour significantly differs from this idealised case leads to much ambiguity and confusion. It is thus difficult to make valid comparisons of 'available' ductility values reported by different researchers because they are often based on different response parameters or on yielding values determined using definitions that are different or unexplained or both. These experimentally obtained 'available' ductility values are also often misused in analytical studies of the 'demand' or 'required' ductility due to the difficulty of establishing realistic values for the 'linear-elastic stiffness and yielding strength'. Attempts should be made to integrate the definitions of response parameters that are used in experimental test programs and in analytical investigations. Furthermore, it is highly questionable whether the performance of different building systems can be properly described and evaluated on the sole basis of elastic stiffness, yielding strength, and ductility. Consequently, there is a need to introduce additional parameters for describing the total hysteretic energy dissipation, number of cycles of reversed deformations, and the degradation in stiffness and strength that has been observed under seismic conditions (Bertero *et al.*, 1991).

***Ductility ratio or ductility factor***

The ratio of the maximum deformation that a structure or element can undergo without a significant loss of initial yielding resistance to the initial yield deformation (Bertero *et al.*, 1991).

***Durability***

The ability of a material or system to maintain its physical and mechanical properties over time (Wabo MBrace, 2002).

***Effective damping***

The value of equivalent viscous damping corresponding to the energy dissipated by the building, or element thereof, during a cycle of response (FEMA-274, 1997).

***Energy dissipation device***

Non-gravity-load supporting element designed to dissipate energy in a stable manner during repeated cycles of earthquake demand (FEMA-274, 1997).

***Energy dissipation system***

Complete collection of all energy dissipation devices, their supporting framing, and connections (FEMA-274, 1997).

***Evaluation***

(see *Assessment*).

***Exposure***

Quality and distribution of goods over the area.

***Failure***

The termination of the ability of an item to perform a required function (BS-4778, 1987).

***Framed structure***

Consist of members that are long in comparison with their cross-sectional dimensions, such as width and depth (Yang and Kuo, 1994).

***Global drift***

Roof-displacement divided by the frame height.

***Hazard***

Nature, number and intensity of seismic events occurring in a given area over a given period of time. A hazard is a phenomenon which, when it manifests itself in a given area

over a specific period of time, has the potential for severe social disruption, trauma, property damage and loss. The potential impact of a hazard is normally expressed in terms of its magnitude or intensity, which are expressed as a probability function over a specified time period according to hazard type. Hazard functions can be derived for different sites if there are sufficient relevant records going back over a significant period of time. For example, if we analyse the known history of earthquake occurrences in the Eastern Caribbean countries, and we measure their size in terms of the intensities given by the Modified Mercalli Intensity Scale, we will find that not all countries are under the same seismic hazards.

***Hazard level***

Earthquake shaking demands of specified severity, determined on either a probabilistic or deterministic basis (FEMA-274, 1997).

***Hollow masonry unit***

A masonry unit whose net cross-sectional area in every plane parallel to the bearing surface is less than 75% of the gross cross-sectional area in the same plane (FEMA-274, 1997).

***Inter-storey drift***

The relative horizontal displacement of two adjacent floors in a building. Inter-storey drift can also be expressed as a percentage of the storey height separating the two adjacent floors (FEMA-274, 1997).

***Jacketing***

A method in which a concrete column or beam is covered with a steel or concrete 'jacket' in order to strengthen and/or repair the member by confining the concrete (FEMA-274, 1997).

***Load path***

A path that seismic forces pass through to the foundation of the structure and, ultimately, to the soil. Typically, the load travels from the diaphragm through connections to the vertical lateral-force resisting elements, and then proceeds to the foundation by way of additional connections (FEMA-274, 1997).

***Masonry***

The assemblage of masonry units, laid in a specified pattern, joined together with mortar and possibly grout and/or reinforcement. Types of masonry can be classified with respect to the type of the masonry units such as clay-unit masonry, concrete masonry, or hollow-clay tile masonry (EC6; FEMA-274, 1997).

***Masonry infill***

An unreinforced or reinforced panel of masonry wall construction placed within a steel or reinforced concrete frame. Panels separated from the surrounding frame by a gap are termed 'isolated infills'. Panels that are in tight contact with a frame around its full perimeter are termed 'shear infills' (FEMA-274, 1997; GSREB, 2001).

***Moment frame***

A building frame system in which seismic shear forces are resisted by shear and flexure in members and joints of the frame (FEMA-274, 1997).

***Mortar***

A mixture of inorganic binders, aggregates and water, together with additions and admixtures if required (EC6).

***Non-dissipative structure***

Structure designed for the seismic load case without taking into account the non-linear material behaviour (EC8).

***Non-linear modelling***

Analysis based on and including both elastic and post-yield force-versus-displacement relationships (FEMA-274, 1997).

***Non-structural elements***

The non-structural elements of a building include every part of it and all of its contents with the exception of the structure. Architectural, mechanical, plumbing or electrical element, system and component or item of interior equipment and furnishing, permanently installed in the building which, whether due to lack of strength or to the way it is connected to the structure, is not considered in the seismic design as load carrying element. Common non-structural items include ceilings, windows, laboratory equipment, inventory stored on shelves, computers, electrical equipment, furnishings and light fittings. (EC8; FEMA-274, 1997).

***Optimization***

The act or process of making something as fully functional or effective as possible (Richards, 1995).

***Performance-based engineering***

Is defined as consisting of the selection of the design criteria, of the appropriate structural systems, of the layout, proportioning, and detailing for a structure and its non-structural components and contents, and the assurance and control of construction quality and long-term maintenance, such that at specified levels of all the excitations (that can act on the buildings) and with defined levels of reliability, the building or facility will not be damaged beyond certain limit states. The PBE process begins with the first concepts of a project and lasts throughout the life of the building (Bertero and Bertero, 2002).

***Performance-based seismic engineering***

Is defined as the application of PBE to the case that seismic hazard controls the design. Hence, PBSE involves the complete design, construction and control (monitoring) of the maintenance and function of the building to assure that the constructed buildings will resist

the effects of earthquake ground motions of different severities within specified limiting levels of damage (Bertero and Bertero, 2002).

***Performance-based seismic design***

Is the subset of activities of PBSE that focus on the design process. Therefore, it includes identification of seismic hazards, selection of the performance levels and performance design objectives, determination of the site suitability, conceptual design, numerical preliminary design, final design, acceptability checks during design, design review, specification of quality assurance during the construction and of monitoring of the maintenance and occupancy (function) during the life of the building. The term design applying to the whole building system, including the foundation, non-structural components, contents, equipment and the utility lines serving the facility (Bertero and Bertero, 2002).

***Performance design objectives***

Expected levels of damage resulting from expected levels of earthquake ground motions (Bertero and Bertero, 2002).

***Pseudo-dynamic testing***

A testing methodology that uses on-line computer calculation and control together with the experimental measurement of the structure restoring forces providing a realistic simulation of the dynamic structural response, which enables, for, instance, the simulation of earthquake loading of full-scale structures (Pegon and Pinto, 2000; Donea *et al.*, 1996).

***Rehabilitation method***

A procedural methodology for the reduction of building earthquake vulnerability (FEMA-274, 1997).

***Rehabilitation objective***

A statement of the desired limits of damage or loss for a given seismic demand, which is usually selected by the owner, engineer, and/or relevant public agencies (FEMA-274, 1997).

***Rehabilitation strategy***

A technical approach for developing rehabilitation measures for a building to reduce its earthquake vulnerability (FEMA-274, 1997).

***Reliability***

The ability of an item to perform a required function under stated conditions for a stated period of time (BS-4778, 1987).

***Repair***

Any operations to recover the original performance (or capacity) of a damaged structural element or structure.

***Resistance***

The capacity of a structure, component, or connection to resist the effects of loads. It is determined by computations using specified material strengths, dimensions, and formulas derived from accepted principles of structural mechanics, or by field or laboratory tests of scaled models, allowing for modelling effects and differences between laboratory and field conditions (FEMA-274, 1997).

***Restoration***

Making the building or its part to be usable by repairing or strengthening.

***Retrofitting***

Structural retrofitting can be defined as the operation to bring the structural system or some of the structural members to a specified performance level. Depending on the state of the



structure and in the purpose, rehabilitation can simply be classified as repair strengthening (Ersoy, 1998).

***Risk***

Risk is a measure of the probability of expected loss for a given hazardous event.

***Softening***

The reduction in the strength capacity under cyclic loading after reaching the ultimate strength limit (Ghobarah *et al.*, 1999).

***Shotcrete***

Mortar or concrete pneumatically projected at high velocity onto a surface (ACI 506R-90, 1995).

***Strengthening***

Any operations to increase the performance or capacity (in strength, ductility or stiffness), of an undamaged element or structure, over the original performance to a specified higher performance level.

***Strong-column weak-beam***

The capacity of the column at any moment frame joint must be greater than those of the beams, in order to ensure inelastic action in the beams, thereby localizing damage and controlling drift (FEMA-274, 1997).

***Structural elements***

The portions of a building that support it and resist gravity, earthquakes, hurricane winds and other type of loads are said to be the structural elements. The structural elements of buildings include columns, beams (girders and joints), floor or roof sheeting, slabs or decking, load bearing walls and foundations.

***Structural model***

The idealisation of the structural system used for the purposes of analysis and design (EC8).

***Vertical irregularity***

A discontinuity of strength, stiffness, geometry, or mass in one storey with respect to adjacent storeys (FEMA-274, 1997).

***Vulnerability***

Propensity of any given good to be damaged or lost by any of the occurring events. Vulnerability is a measure of the intrinsic susceptibility of structures, contents and processes to fail once they are exposed to potentially damaging natural phenomena. Vulnerability is generally expressed as the degree of expected damage or loss, given in a certain scale, as a function of hazard intensity.

***Yield storey drift***

The lateral displacement of one level relative to the level above or below at which yield stress is first developed in a frame member (GSREB, 2001).

***Zero-th order***

An optimization method that does not use derivatives (Richards, 1995).

## REFERENCES AND RECOMMENDED READING

- 'Who's been repeating all that hard stuff to you?'  
- 'I read it in a book' - said Alice.  
(Lewis Carrol, Through the Looking Glass)

### 1. REFERENCES

#### A

- Aboutaha, R.S.; Engelhardt, M.D.; Jirsa, J.O.; Kreger, M.E. (1996) - *Retrofit of concrete columns with inadequate lap splices by the use of rectangular steel jackets* - Earthquake Spectra, Vol. 12, No. 4, pp. 693-714.
- Abrams, D. (2000) - *Performance-based rehabilitation of unreinforced masonry buildings* - International Seminar on Evaluation of Seismic Risk and Reduction of Vulnerability of Historical Structures, Pavia, 18<sup>th</sup>-30<sup>th</sup> June.
- Abrams, D.; Angel, R.; Uzarski, J. (1993) - *Transverse strength of damaged URM infills* - Journal of The Masonry Society, Boulder, Colorado - Vol. 12, No. 1, pp. 45-52.
- Abrishami, H.H.; Mitchell, D. (1996) - *Analysis of bond stress distributions in pullout specimens* - Journal of Structural Engineering, Vol. 122, No. 3, pp. 255-261, March.
- ACI-318 (1971) - *Building code requirements for reinforced concrete* - American Concrete Institute, Detroit, 78 pp.
- ACI 506R-90 (1995) - *Guide to shotcrete* - Reported by ACI Committee 506, Reapproved 1995.
- ACI 506.2-95 (1995) - *Specification for shotcrete* - Reported by ACI Committee 506.
- Adham, S.; Bhaumik, A.; Isenberg, J. (1975) - *Reinforced concrete constitutive relations* - Agbabian Associates, AD-A007 886, US Department of Commerce, National Technical Information Services, Springfield, VA.
- AISC (1986) - *Manual of steel construction-load & resistance factor design* - 1<sup>st</sup> edition - American Institute of Steel Construction, Inc., Chicago, IL.
- Albanesi, T.; Nuti, C.; Vanzi, I. (2002) - *State-of-the-art on non-linear static methods* - 12<sup>th</sup> ECEE, London, UK, Paper No. 602, Elsevier Science Ltd., 9<sup>th</sup>-13<sup>th</sup> September.
- Allen, E.W.; Bailey, J.S. (1988) - *Seismic rehabilitation of the Salt Lake City and County building using base isolation* - 9<sup>th</sup> WCEE, Tokyo-Kyoto, Japan, Vol. 5, pp. 639-644.

- Altin, S.; Ersoy, U.; Tankut, T. (1992) - *Hysteretic response of reinforced concrete infilled frames* - Journal of the Structural Engineering Division, ASCE, New York, New York, Vol. 118, No. 8, pp. 2133–2150.
- Anagnostopoulos, S.A. (2000) - *Policy issues for seismic risk mitigation* - Workshop on Mitigation of Seismic Risk: Support to Recently Affected European Countries, JRC, Belgirate, Italy, November.
- Anderson, J.C.; Miranda, E.; Bertero, V.V.; The Kajima Project Research team (1991) - *Evaluation of the seismic performance of a thirty-storey RC building* - Report No. UCB/EERC-91/16, EERC, University of California, Berkeley, July.
- Anselmi, G.; Mocci, U. (2002) - *Applying ICTs to public participation in enhancing the urban environment* - IPTS, No. 69, JRC, Seville, November.
- Aoyama, H. (1981) - *A method for the evaluation of the seismic capacity of existing reinforced concrete buildings in Japan* - Bulletin of the New Zealand National Society for Earthquake Engineering, Vol. 14, No. 3, September, pp. 105-130.
- Aoyama, H.; Kato, D.; Katsumata, H.; Hosokawa, Y. (1984) - *Strength and behaviour of postcast shear walls for strengthening of existing reinforced concrete buildings* - 8<sup>th</sup> WCEE, San Francisco, US, Vol. 4, pp. 485-492.
- Arêde, A. (1997) - *Seismic assessment of reinforced concrete frame structures with a new flexibility based element* - PhD thesis, FEUP, University of Porto, October.
- Aschheim, M. (2001) - *The Izmit (Kocaeli) earthquake of 17<sup>th</sup> August 1999: Preliminary observations* - EERI Reconnaissance Team - Mid-America Earthquake Center - University of Illinois at Urbana-Champaign.
- ASTM-97 (1997) - *Standard test method for diagonal tension (shear) in masonry assemblages - E 519-81 (reapproved 1993)* - ASTM Standards on Masonry - ASTM Publication code: 03-315097-60.
- ATC-13 (1985) - *Earthquake damage evaluation data for California* - Applied Technical Council - Redwood City, California, US.
- ATC-21 (1989) - *A handbook for seismic evaluation of existing buildings* - Applied Technology Council, Redwood City, California, US.
- ATC-40 (1996) - *Seismic evaluation and retrofit of concrete buildings* - Applied Technical Council - California Seismic Safety Commission, Report No. SSC 96-01 (two volumes), Redwood City, California, US.
- Aviles, N.B.; Maruyama, K.; Rojas, L.E. (1996) - *Improving strength and ductility by using steel plate wrapping* - 11<sup>th</sup> WCEE, Acapulco, Mexico, Paper No. 742.
- Ayala, A.G.; Tayebi, A.K.; Ye, X.G. (1996) - *Dynamic response of a reinforced concrete frame compared with observed earthquake damage* - 11<sup>th</sup> WCEE, Acapulco, Mexico, Paper No. 697.

**B**

- Badoux, M.; Peter, K. (2000) - *Seismic vulnerability of older Swiss RC buildings* - 12<sup>th</sup> WCEE, Auckland, New Zealand, January.
- Barthelemy, J.-F.M.; Haftka, R.T. (1993) - *Approximation concepts for optimum structural design - A review* - Structural Optimization, Vol. 5, pp. 129-144.
- Bento, R.; Azevedo, J. (2000) - *Behaviour coefficient assessment for soft storey structures* - 12<sup>th</sup> WCEE, Auckland, New Zealand, January.
- Bento, R.; Lopes, M. (2000) - *Evaluation of the need for weak-beam strong-column design in dual frame-wall structures* - 12<sup>th</sup> WCEE, Auckland, New Zealand, January.
- Berra, M.; Castellani, A.; Ciccotelli, S.; Coronelli, D. (1994) - *Bond slip effects on reinforced concrete elements under earthquake loading* - European Earthquake Engineering, Vol. 8, No. 3, pp. 3-10.
- Bertero, V.V. (1997) - *Earthquake engineering* - Structural Engineering Slide Library - (available at [http://nisee.berkeley.edu/bertero/html/earthquake-resistant\\_construction.html](http://nisee.berkeley.edu/bertero/html/earthquake-resistant_construction.html)) - W.G. Godden (ed.), Godden Collection, Earthquake Engineering Library, University of California, Berkeley.
- Bertero, V.V. (1992) - *Seismic upgrading of existing structures* - 10<sup>th</sup> WCEE, Madrid, Spain, Vol. 9, pp. 5101-5106.
- Bertero, V.V. (1982) - *State-of-the-art in seismic resistant construction of structures* - 3<sup>rd</sup> International Earthquake Microzonation Conference, University of Washington, Seattle, Washington, Vol. II, pp. 767-805.
- Bertero, V.V. (1979) - *Seismic performance of reinforced concrete structures* - Anales de la Academia Nacional de Ciencias Exactas, Física y Naturales, Buenos Aires, Argentina, Tomo 31, pp. 75-144.
- Bertero, R.D.; Bertero, V.V. (2002) - *Performance-based seismic engineering: the need for a reliable conceptual comprehensive approach* - Earthquake Engineering and Structural Dynamics, Vol. 31, pp. 627-652, March.
- Bertero, V.V.; Anderson, J.C.; Krawinkler, H.; Miranda, E.; The CUREe and The Kajima Research Teams (1991) - *Design guidelines for ductility and drift limits: Review of state-of-the-practice and state-of-the-art in ductility and drift-based earthquake-resistant design of buildings* - Report No. UCB/EERC-91/15, EERC, University of California, Berkeley, July.
- Borges, J.F.; Ravara, A. (1969) - *Earthquake engineering: Seismic design of reinforced concrete buildings* - Course 113, LNEC, Lisbon, November.
- Bouwkamp, J.; Pinto, A.V.; Molina, F.J.; Varum, H. (2000) - *Cyclic tests on RC frame retrofitted with K-bracing and shear-link dissipator* - EUR Report No. 20136 EN, ELSA, JRC-Ispra, EC, Italy.

Braibant V. (1985) - *Optimisation de forme des structures en vue de la conception assistée par ordinateur* - Publication de la Faculté des Sciences Appliquées, No. 102, Liège, Belgique (in French).

Brenner, P. (2001) - *Reclaiming buildings: Strategies for change* - Buildings.com - @ the moment (available at <http://www.buildings.com/Articles/detail.asp?ArticleID=445>), 28<sup>th</sup> November.

BS-4778 (1987) - *Glossary of terms used in quality assurance (including reliability and maintainability)* - British Standards Institution, London.

Buchet, P.; Capéran, P.; Pegon, P. (2000) - *Visual Cast3m for Windows NT: User manual* - JRC Special Publication No.I.00.142, ELSA, JRC-Ispra, EC, Italy, December.

Busquin, P. (2002) - *Message from EU Research Commissioner* - CORDIS focus, Community Research and Development Information Service, Office for Official Publications, EC, Luxemburg.

## C

Calderón, E.V. (1980) - *Some lessons from the March 14, 1979 earthquake in Mexico City* - 7<sup>th</sup> WCEE, Istanbul, Turkey, Vol. 4, pp. 545-552.

CALTRANS (1998) - *Bridge design specifications manual* - California Department of Transportation, Division of Structures, Sacramento, California, US.

Calvi, G.M. (1999) - *A displacement-based approach for vulnerability evaluation of classes of buildings* - Journal of Earthquake Engineering, Imperial College Press, Vol. 3, No. 3, pp. 411-438.

Calvi, G.M. (1998) - *Performance-based approaches for seismic assessment of existing structures* - 11<sup>th</sup> ECEE, Paris, France, Invited lecture, ISBN 90 5809 027 2, A.A. Balkema, Rotterdam, 6<sup>th</sup>-11<sup>th</sup> September.

Calvi, G.M.; Pavese, A. (1997) - *Conceptual design of isolation system for bridge structures* - journal of Earthquake Engineering, Vol. 1, pp. 193-218.

Calvi, G.M.; Pampanin, S.; Ward, J.; Fajfar, P. (2000) - *New methods for assessment and design of structures in seismic zones: Present state and research needs* - Workshop on Mitigation of Seismic Risk: Support to Recently Affected European Countries, JRC, Belgirate, Italy, November.

Campos-Costa, A.; Pinto, A.V. (1999) - *European seismic hazard scenarios - an approach to the definition of input motions for testing and reliability assessment of civil engineering structures* - JRC Special Publication No. X.99.XX, ELSA, JRC-Ispra, EC, Italy.

Candeias, P. (2000) - *Avaliação sísmica de edifícios existentes: Contribuição para a avaliação da Vulnerabilidade em Portugal* - Master thesis, IST, Technical University of Lisbon, December (in Portuguese).

- Carvalho, E.C.; Bairrão, R. (2000) - *Experimental activity at LNEC under ECOEST II - Workshop on Mitigation of Seismic Risk: Support to Recently Affected European Countries*, JRC, Belgirate, Italy, November.
- Carvalho, E.C.; Coelho, E.; Campos-Costa, A. (1999) - *Preparation of the full-scale tests on reinforced concrete frames - Characteristics of the test specimens, materials and testing conditions. ICONS report, Innovative Seismic Design Concepts for New and Existing Structures, European TMR Network - LNEC, Lisbon.*
- Carvalho, E.C.; Coelho, E.; Pinto, A.V.; Molina, F.J.; Varum, H. (2000-a) - *Avaliação e reforço sísmico de estruturas de betão armado - Encontro Nacional Betão Estrutural 2000 - FEUP, Porto, 22-24 de Novembro (in Portuguese).*
- Carvalho, E.C.; Coelho, E.; Campos-Costa, A.; Sousa, M.L.; Candeias, P.; Carvalho, A.; Massena, B.; Castro, S. (2000-b) - *Seismic risk mitigation in Portugal - Workshop on Mitigation of Seismic Risk: Support to Recently Affected European Countries, JRC, Belgirate, Italy, November.*
- CEB-131 (1979) - *Bulletin d'Information N. 131 - Structural concrete under seismic actions - Comité Euro-International du Béton.*
- CEB-161 (1983) - *Bulletin d'Information N. 161 - Response of RC critical regions under large amplitude reversed actions - Comité Euro-International du Béton.*
- CEB-217 (1993) - *Bulletin d'Information N. 217 - Selected justification notes - Comité Euro-International du Béton, April.*
- CEB-240 (1998) - *Bulletin d'Information N. 236 - Seismic design of reinforced concrete structures for controlled inelastic response - Comité Euro-International du Béton, Thomas Telford Ltd, ISBN 0-7277-2641-2.*
- CEB-FIP MC-90 (1990) - *Model code for concrete structures - Comité Euro-International du Béton.*
- Celebi, M.; Spudich, P.A.; Page, R.A.; Stauffer, P.H. (1995) - *Saving lives through better design standards - USGS Fact Sheet-176-95 (available at <http://quake.usgs.gov/prepare/factsheets/BetterDesign/>).*
- CEN (2003) - *Eurocode 8: Design of structures for earthquake resistance - Part 1-3: Strengthening and repair of buildings - European prEN 1998-1-3, European Committee for Standardization, Brussels, Belgium.*
- CEN (1995) - *Eurocode 6: Design of masonry structures - Part 1-1: Rules for reinforced and unreinforced masonry - European prENV 1996-1-1, European Committee for Standardization, Brussels, Belgium.*
- CEN (1994) - *Eurocode 8: Design provisions for earthquake resistance of structures - Part 1-1 and 1-2 - European prENV 1998-1-1, 1-2, European Committee for Standardization, Brussels, Belgium.*
- CEN (1991) - *Eurocode 2: Design of concrete structures - European prENV 1992-1-1, CEN/TC 250/SC 2, European Committee for Standardization, Brussels, Belgium.*

- Chai, Y.H.; Priestley, M.J.N.; Seible, F. (1991) - *Seismic retrofit of circular bridge columns for enhanced flexural performance* - ACI Structural Journal, Vol. 88, No. 5, pp. 572-584.
- Chickermane, H.; Gea, H.C. (1996-a) - *A new local approximation method for structural optimization problems* - International Journal for Numerical Methods in Engineering, Vol. 39, pp. 829-846 (available at <http://www.rci.rutgers.edu/~hemant/ijnme/paper.html>).
- Chickermane, H.; Gea, H.C. (1996-b) - *Design of multi-component structural systems for optimal layout topology and joint locations* - ASME Design Automation Conference, Irvine, CA, August (available at <http://www.rci.rutgers.edu/~hemant/ijnme/paper.html>).
- Chopra, A.K. (2001) - *Dynamics of structures: Theory and applications to earthquake engineering* (2<sup>nd</sup> edition) - Englewood Cliffs, New Jersey: Prentice Hall, Inc.
- Coelho, E. (1992) - *Comportamento sísmico de estruturas em pórtico de betão armado: Avaliação da resposta não-linear histerética* - PhD thesis, Instituto Superior Técnico, Lisbon (in Portuguese).
- Coelho, E.; Campos-Costa, A.; Carvalho, E.C. (2000) - *Assessment of experimental seismic response through damage evaluation* - 12<sup>th</sup> WCEE, Auckland, New Zealand, January.
- Combescure, D. (2000) - *Étude d'une structure portique de 4 étages en béton armé ayant de mauvaises dispositions constructives (portique Ispra) - Influence des remplissages en maçonnerie sur le comportement sismique* - Rapport DMT, SEMT/EMSI/RT/00-009/A, CEA - Laboratoire d'Études de Mécanique Sismique (in French).
- Combescure, D. (1996) - *Modélisation du comportement sous chargement sismique des structures de bâtiment comportant des murs de remplissage en maçonnerie* - PhD thesis (in French).
- Combescure, D.; Pegon, P. (1996) - *Introduction of two new global models in CASTEM-2000 for seismic analysis of civil engineering structures* - Special Publication No. I.96.34, ELSA, JRC-Ispra, EC, Italy.
- Combescure, D.; Pegon, P.; Anthoine, A. (1995) - *Modelling of the in-plane behaviour of masonry infilled frames* - Proceedings of the European Seismic Design Practice Conference, Chester, October.
- Costa, A.G. (1989) - *Análise sísmica de estruturas irregulares* - PhD thesis, FEUP, University of Porto (in Portuguese).
- Cowell, A.D.; Popov, E.P.; Bertero, V.V. (1980) - *Repair of bond in RC structures by epoxy injection* - 1<sup>st</sup> Seminar on Repair and Retrofit of Structures - US/Japan Co-operative Earthquake Engineering Research Program, Department of Civil Engineering, University of Michigan, Ann Arbor, Vol. 1, pp. 234-240.



**D**

- Delgado, P.; Silva, B.; Ribeiro, D.; Delgado, R.M. (2002) - *Análise numérica da reabilitação sísmica de uma estrutura de betão armado* - Congresso Nacional da Engenharia de Estruturas, Estruturas 2002, LNEC, Lisbon (in Portuguese).
- Delgado, R.M. (1984) - *O método dos elementos finitos na análise dinâmica de barragens incluindo a interação sólido-líquido* - PhD thesis, FEUP, University of Porto (in Portuguese).
- Dimitriu, P.; Karakostas, C.; Lekidis, V. (2000) - *The Athens (Greece) earthquake of 7 September 1999: The event, its effects and the response* - 2<sup>nd</sup> Euro-Conference on Global Change and Catastrophe Risk Management: Earthquake Risks in Europe, IIASA, Laxenburg, Austria, 6<sup>th</sup>-9<sup>th</sup> July.
- Dolsek, M.; Fajfar, P. (2001) - *Soft storey effects in uniformly infilled reinforced concrete frames* - Journal of Earthquake Engineering, Imperial College Press, Vol. 5, No. 1, pp. 1-12.
- Donea, J.; Magonette, G.; Negro, P.; Pegon, P.; Pinto, A.V.; Verzeletti, G. (1996) - *Pseudo-dynamic capabilities of the ELSA laboratory for earthquake testing of large structures* - Earthquake Spectra, Vol. 12, No. 1, pp. 163-180.
- Duarte, R.T.; Campos-Costa, A. (1988) - *Earthquake behaviour of reinforced concrete frame structures infilled with masonry panels* - LNEC Report (contract No. 86/7750/023), Lisbon.
- Dyngeland, T. (1998) - *Retrofitting of bridges and building structures: A literature survey* - Special Publication No. I.98.33, ISIS, SSMU, ELSA, JRC-Ispra, EC, Italy.

**E**

- EASY (1997) - (available at <http://www.ikpir.fgg.uni-lj.si/easy/tour.htm>) - *Earthquake engineering slide information system*.
- EERI (1996) - *Spectra theme issue: Repair and rehabilitation research for seismic resistance of structures* - Jirsa, J.O. (ed.), Earthquake Spectra, Vol. 12, No. 4.
- Eligehausen, R.; Popov, E.P.; Bertero, V.V. (1983) - *Local bond stress-slip relationships of deformed bars under generalized excitations* - Report No. UCB/EERC 83-23, Earthquake Engineering Research Center, University of California, Berkeley, California, October.
- Elnashai, A.S. (2000) - *The Kocaeli (Turkey) earthquake of 17<sup>th</sup> August 1999: Assessment of Spectra and Structural Response Analysis* - Personal PowerPoint Presentation. (7.5Mb, 117 slides). (available at <http://www.isesd.cv.ic.ac.uk/esd/frameset.htm>).
- Elnashai, A.S.; Pinho, R. (1999) - *ICONS Topic 2 - Pseudo-dynamic testing of RC frames - Proposal for selective repair/strengthening of specimen B* - Report Imperial College of London.

Elsesser, E. (2002) - *The search for the perfect seismic protection system* - Forell/Elsesser Engineers, Inc. - San Francisco.

EN-196-1 (1987) - *Methods of testing cement. Determination of strength* (Portuguese version: NP-1990).

ENV-206 (1993) - *Concrete: Performance, production, placing and compliance criteria* - European Standards, CEN, European Committee for Standardisation, Brussels.

EQE (2001) - (available at <http://www.eqe.com/revamp/HiroshimaEQ.htm>). *Report of the M6.9 Geiyo earthquake, southwest Japan, March 24<sup>th</sup>*.

EQE (1999) - (available at <http://www.eqe.com/revamp/izmitreport/index.html>). *Report of the M7.4 Izmit earthquake, Turkey, August 17<sup>th</sup>*.

EQE (1995) - (available at <http://www.eqe.com/publications/kobe/building.htm>). *The January 17, 1995 Kobe earthquake - An EQE summary report*.

Ersoy, U. (1998) - *Seismic rehabilitation* - Second Japan-Turkey Workshop on Earthquake Engineering: Repair & Strengthening of Existing Buildings - Istanbul.

## F

Fajfar, P. (2002) - *Structural analysis in earthquake engineering: A breakthrough of simplified non-linear methods* - 12<sup>th</sup> ECEE, London, UK, Paper No. 843, Elsevier Science Ltd., 9<sup>th</sup>-13<sup>th</sup> September.

Fajfar, P. (2000) - *A non-linear analysis method for performance based seismic design* - Earthquake Spectra, Vol. 16, No. 3, pp. 573-592, August.

Fajfar, P. (1998) - *Trends in seismic design and performance evaluation approaches* - Bisch, Ph.; Labbé, P.; Pecker, A. (eds.), 11<sup>th</sup> ECEE, Paris, France, Invited lecture, ISBN 90 5809 027 2, A.A. Balkema, Rotterdam, 6<sup>th</sup>-11<sup>th</sup> September.

Fajfar, P.; Gaspersic, P. (1996) - *The N2 method for the seismic damage analysis of RC buildings* - Earthquake Engineering & Structural Dynamics, Vol. 25, pp. 31-46.

Fajfar, P.; Krawinkler, H. (eds.) (1997) - *Seismic design methodologies for the next generation of codes* - Proceedings of the International Workshop, Bled, Slovenia, Rotterdam, Balkema, 24-27 June.

Fajfar, P.; Krawinkler, H. (eds.) (1992) - *Nonlinear seismic analysis and design of reinforced concrete buildings* - Proceedings of the Workshop, Bled, Slovenia, Yugoslavia, Elsevier Applied Science, 13-16 July.

Fajfar, P.; Gaspersic, P.; Drobnic, D. (1997) - *A simplified nonlinear method for seismic damage analysis of structures* - Proceedings of the International Workshop Seismic design methodologies for the next generation of codes, Fajfar, P. and Krawinkler, H. (eds.), Slovenia, Rotterdam, Balkema, 24-27 June.

- Fardis, M.N. (2000) - *Eurocode 8: Present state, pre-normative and co-normative research needs (including design seismic actions)* - Workshop on Mitigation of Seismic Risk: Support to Recently Affected European Countries, JRC, Belgirate, Italy, November.
- Fardis, M.N. (1998) - *Seismic assessment and retrofit of RC structures* - Bisch, Ph.; Labbé, P.; Pecker, A. (eds.), 11<sup>th</sup> ECEE, Paris, France, Invited lecture, ISBN 90 5809 027 2, A.A. Balkema, Rotterdam, 6<sup>th</sup>-11<sup>th</sup> September.
- FEMA-273 (1997) - *NHERP Guidelines for the seismic rehabilitation of buildings* - Federal Emergency Management Agency, Applied Technology Council, Washington, DC, October.
- FEMA-274 (1997) - *NHERP Commentary on the guidelines for the seismic rehabilitation of buildings* - Federal Emergency Management Agency, Applied Technology Council, Washington, DC, October.
- FEMA-310 (1998) - *Handbook for the seismic evaluation of buildings: A prestandard* - American Society of Civil Engineers.
- Filiatrault, A.; Uang, C.M.; Folz, B.; Christopoulos, C.; Gatto, K. (2001) - *Reconnaissance report of the February 28, 2001 Nisqually (Seattle-Olympia) earthquake* - Report No. SSRP-2001/02, Department of Structural Engineering, University of California, San Diego, La Jolla, California.
- Fiorato, A.E.; Sozen, M.A.; Gamble, W.L. (1970) - *Investigation of the interaction of reinforced concrete frames with masonry filler walls* - Report UILU, Structural Research Series 370, University of Illinois, Urbana, Illinois.
- Fleury, C. (1989) - *CONLIN: An efficient dual optimizer based on convex approximation concepts* - Structural Optimization, Vol. 1, pp. 81-89.
- Fleury, C. (1979) - *Structural weight optimization by dual methods of convex programming* - International Journal for Numerical Methods in Engineering, Vol. 14, pp. 1761-1783.
- Fleury, C.; Braibant, V. (1986) - *Structural optimization: a new dual method using mixed variables* - International Journal of Numerical Methods in Engineering, Vol. 23, No 3, pp. 409-429.
- Foutch, D.A.; Hjelmstad, K.D.; Calderón, E.V. (1988) - *Seismic retrofit of a RC building: A case study* - 9<sup>th</sup> WCEE, Tokyo-Kyoto, Japan, Vol. 7, pp. 451-456.
- Freeman, S.A. (1978) - *Prediction of response of concrete buildings to severe earthquake motion* - Proceedings of Douglas McHenry International Symposium on Concrete Structures, Detroit, pp. 589-605.
- Frosch, R.J.; Li, W.; Jirsa, J.O.; Kreger, M.E. (1996) - *Retrofit of non-ductile moment-resisting frames using precast infill wall panels* - Earthquake Spectra, Vol. 12, No. 1, pp. 163-180.

**G**

- Gavrilovic, P.; Sendova, V. (1992) - *Experimental and analytical studies of infill walls in reinforced concrete structures* - 10<sup>th</sup> WCEE, A.A. Balkema, Rotterdam, The Netherlands, Vol. 6, pp. 3309-3315.
- Geradin, M.; Pinto, A.V. (eds.) (2000) - *Workshop on mitigation of seismic risk: Support to recently affected European countries* - JRC, Belgirate, Italy, November.
- Ghobarah, A. (2000) - *Seismic assessment of existing RC structures* - Progress in Structural Engineering and Materials, Vol. 2, No. 1, pp. 60-71, January-March.
- Ghobarah, A.; Aziz, T.; Abou-Elfath, H. (1999) - *Softening effects on the seismic response of non-ductile concrete frame* - Journal of Earthquake Engineering, Imperial College Press, Vol. 3, No. 1, pp. 59-81.
- Griffith, M. (1999-a) - *Seismic retrofit of RC frame buildings with masonry infill walls - Literature review and preliminary case study* - JRC-Special Publication (in print).
- Griffith, M. (1999-b) - *Description of damage in block masonry infill frame* - (personal notes).
- GSREB (2001) - *Guidelines for the seismic retrofit of existing building* - International Conference of Building Officials, US, ISBN 1-58001-076-8, July.
- Guedes, J. (1997) - *Seismic behaviour of reinforced concrete bridges. Modelling, numerical analysis and experimental assessment* - PhD thesis, FEUP, University of Porto.

**H**

- Hall, J. (1994) - *Northridge earthquake January 17, 1994: Preliminary reconnaissance report* - Earthquake Engineering Research Institute, Oakland, CA, March.
- Hanson, R.D. (ed.) (1981) - *Proceedings of the first seminar on repair and retrofit of structures* - US-Japan Co-operative Earthquake Engineering Research Program, Dept. of Civil Engineering, University of Michigan, Ann Arbor, Vol. 1.
- Hassan, F.M.; Hawkins, N.M. (1977) - *Anchorage of reinforced bars for seismic forces* - ACI Special Publication, SP 53-15, pp. 387-416.
- Hawkins, N.M.; Lin, I.; Ueda, T. (1987) - *Anchorage of reinforced bars for seismic forces* - ACI Structural Journal, Technical Paper, Title No. 84-S43, pp. 407-418, September-October.
- Higashi, Y.; Endo, T.; Shimizu, Y. (1984) - *Experimental studies on retrofitting of reinforced concrete buildings* - 8<sup>th</sup> WCEE, San Francisco, US, Vol. 4, pp. 477-484.
- Holmes, W.T. (2000) - *Risk assessment and retrofit of existing buildings* - 12<sup>th</sup> WCEE, Auckland, New Zealand, January.

**I**

- ICONS WebPages (1999) - available at <http://elsa.jrc.it/ICONS/> - *WebPages of the project ICONS* - Developed and maintained by Varum, H. and Pinto, A.V.
- Iglesias, J.; Aguilar, J. (1996) - *Rehabilitation of buildings after the 1985 Mexico city earthquake* - 11<sup>th</sup> WCEE, Acapulco, Mexico, Paper No. 2091.
- Imanbekov, S.; Uranova, S.; Iwan, W. (1999) - *Earthquake resistance of multi-storey residential buildings in Central Asian capital cities* - Seismic Hazard and Building Vulnerability in Post-Soviet Central Asian Republics, King, S.A.; Khalturin, V.I.; Tucker, B.E. (eds.), Kluwer Academic Publishers, pp. 45-65.
- ISO-1000 - SI Units and recommendations for the use of their multiples and of certain other units.
- ISPMNH (2002) - *Catastrophic Athens (Greece) earthquake of 7 September 1999: An unexpected event in a low seismicity region* - Special Issue of the Journal of the International Society for the Prevention and Mitigation of Natural Hazards, Vol. 27, No. 1 and 2, October.
- Iwan, W.D.; Gates, N.C. (1979) - *Estimating earthquake response of simple hysteretic structures* - Journal of engineering Mechanics, ASCE, Vol. 105, No. EM3, pp. 391-405, June.

**J**

- Jara, J.M.; Miranda, E.; Ayala, A.G. (2001) - *Limit states of behaviour for structures with energy dissipating systems in Mexico* - 7<sup>th</sup> International Seminar on Seismic Isolation, Passive Energy Dissipation and Active Control of Vibration of Structures - Assisi, Italy, 2-5 October.
- Jara, J.M.; Ayala, A.G.; Miranda, E. (2000) - *Seismic behaviour of structures with energy dissipating systems in Mexico* - 12<sup>th</sup> WCEE, Auckland, New Zealand, January.
- Jaramillo, J.D.; Campos, A. (2000) - *Seismic vulnerability of Pereira city, Colombia* - 12<sup>th</sup> WCEE, Auckland, New Zealand, January.
- JBDPA (1977) - *Standard for evaluation of seismic capacity and guidelines for seismic retrofit design of existing reinforced concrete buildings* - Japan Building Disaster Prevention Association.
- Jirsa, J.O.; Kreger, M.E. (1989) - *Recent research on repair and strengthening of reinforced concrete structures* - Seismic Engineering, ASCE, pp.679-688.
- JSCE (1996) - *Standard specification for design and construction of concrete structures* - Japanese Society of Civil Engineers (in Japanese).

**K**

- Kagami, H. (1999) - *Reconnaissance report on the 1999 Quindio, Central Western Colombia, earthquake and its disasters* - Hokkaido University, Japan.
- Karadogan, F. (ed.) (1998) - *Repair and strengthening of existing buildings* - 2<sup>nd</sup> Japan-Turkey Workshop on Earthquake Engineering, Istanbul, Turkey, Vol. 1.
- Karayannis, C.G.; Chalioris, C.E.; Sideris, K.K. (1998) - *Effectiveness of RC beam-column connection repair using epoxy resin injections* - Journal of Earthquake engineering, Vol. 2, No. 2, pp. 217-240.
- Katayama, T. (1996) - *Lessons from the 1995 Great Hanshin earthquake of Japan with emphasis on urban infrastructure systems* - Structural Engineering in consideration of Economy Environment Energy, 15<sup>th</sup> Congress, Copenhagen, Denmark (available at <http://rattle.iis.u-tokyo.ac.jp/kobenet/report/pub1/pub1-1.html>).
- Kelly, J.M. et al. (1979) - *Aseismic base isolation: A review* - 2<sup>nd</sup> US National Conference on Earthquake Engineering, Stanford University, Stanford, California, pp. 823-837.
- Keuser, M.; Mehlhorn, G. (1987) - *Finite elements models for bond problems* - Journal of Structural Engineering, ASCE, Vol. 113, No. 10, pp. 2160-2173.
- Klingner, R.E.; Bertero, V.V. (1976) - *Infilled frames in earthquake-resistant construction* - Report 76-32, University of California, Berkeley.
- KOBENet (1995) - *Buildings collapsed in many ways* - (available at <http://rattle.iis.u-tokyo.ac.jp/kobenet/picture/damage6/Building.html>).
- KOERI (1999) - *Izmit earthquake (Turkey)* - Kandilli Observatory & Earthquake Research Institute, Boğaziçi University, Istanbul - (available at [http://www.eas.slu.edu/Earthquake\\_Center/TURKEY/](http://www.eas.slu.edu/Earthquake_Center/TURKEY/)).
- Kölz, E.; Bürge, M. (2001) - *Priorities in earthquake upgrading of existing structures* - Structural Engineering International, IABSE, Vol. 11, No. 3.
- Kowalsky, M.J.; Priestley, M.J.N.; MacRae, G.A. (1994) - *Displacement-based design: A methodology for seismic design applied to single degree of freedom reinforced concrete structures* - Structural Systems Research, University of California, San Diego, La Jolla, California, Report No. SSRP-94/16, October.
- Kunnath, S.K.; Reinhorn, A.M.; Park, Y.J. (1990) - *Analytical modelling of inelastic seismic response of RC structures* - Journal of Structural Engineering, ASCE, Vol. 116, No. 4.

**L**

- Lafuente, M.; Molina, A.; Genatios, C. (2000) - *Seismic-resistant behaviour of minor reinforced concrete frames with masonry infill walls* - 12<sup>th</sup> WCEE, Auckland, New Zealand, January.

- Leuchars, J.M.; Scrivener, J.C. (1976) - *Masonry infill panels subjected to cyclic in-plane loading* - Bulletin of the NZSEE, Vol. 9, No. 2, pp. 122-131.
- Liu, A.; Park, R. (2001) - *Seismic behaviour and retrofit of pre-1970's as-built exterior beam-column joints reinforced by plain round bars* - Bulletin of the New Zealand Society for Earthquake Engineering, Vol. 34, No. 1, pp. 68-81, March.
- Liu, A.; Park, R. (2000) - *Seismic behaviour of existing moment-resisting frames with plain round reinforcing bars designed to pre-1970's codes* - 12<sup>th</sup> WCEE, Auckland, New Zealand, January.
- LNEC (2000) - *Levantamento do parque habitacional de Portugal continental para o estudo da sua vulnerabilidade sísmica com base nos CENSOS-91* - Relatório 260/00 - C3ES, LNEC, Lisbon, October (in Portuguese).

## M

- Magonette, G.; Pegon, P.; Molina, F.J.; Buchet, P. (1998) - *Development of fast continuous substructuring tests* - 2<sup>nd</sup> World Conference on Structural Control, Kyoto.
- Martinez-Romero, E. (1993) - *Experiences on the use of supplementary energy dissipators on building structures* - Earthquake Spectra, Vol. 9, No. 3, pp. 581-626.
- Martinez-Rueda, J.E. (1997) - *Energy dissipation devices for seismic upgrading of RC structures* - PhD thesis, Imperial College, University of London, UK.
- Meier, U. (1992) - *Carbon fiber-reinforced polymers: Modern materials in bridge engineering* - Structural Engineering International, IABSE, Vol. 1, pp. 7-12.
- Menegotto, M.; Pinto, P.E. (1973) - *Methods of analysis for cyclically loaded reinforced concrete plane frames including changes in geometry and non-elastic behaviour of elements under combined normal force and bending* - IABSE Symposium on Resistance and Ultimate Deformability of Structures acted on by well-defined repeated loads, Lisbon.
- Millard, A. (1993) - *CASTEM-2000 - Guide d'utilisation* - Rapport CEA 93/007, Saclay, France.
- Miranda, E.; Bertero, V.V. (1990) - *Post-tensioning technique for seismic upgrading of existing low-rise buildings* - 4<sup>th</sup> US National Conference on Earthquake Engineering, Palm Springs, California, Vol. 3, pp. 393-402.
- Moehle, J.P.; Mahin, S.A. (1991) - *Observations on the behaviour of reinforced concrete buildings during earthquakes* - ACI publication SP-127, Earthquake-Resistant Concrete Structures: Inelastic Response and Design - Ghosh, S.K. (ed.).
- Mokha, A.S.; Amin, N.; Constantinou, M.C.; Zayas, V. (1996) - *Seismic isolation retrofit of large historic building* - Journal of Structural Engineering, Vol. 122, No. 3, pp. 298-308.
- Molina, F.J.; Pegon, P.; Verzeletti, G. (1999-a) - *Time-domain identification from seismic pseudodynamic test results on civil engineering specimens* - 2<sup>nd</sup> International

Conference on Identification in Engineering Systems, University of Wales Swansea, Cromwell Press Ltd.

Molina, F.J.; González, M.P.; Varum, H.; Pinto, A.V. (2001) - *Frecuencias propias y índices de amortiguamiento durante la respuesta de un pórtico de cuatro pisos en diferentes estados de daño o reparación* - 2º Congreso Iberoamericano de Ingeniería Sísmica, Madrid, 16-19 October (in Spanish).

Molina, F.J.; Verzeletti, G.; Magonette, G.; Taucer, F. (2000-a) - *Dynamic and pseudo-dynamic responses in a two storey building retrofitted with rate-sensitive rubber dissipators* - 12<sup>th</sup> WCEE, Auckland, New Zealand, January.

Molina, F.J.; Gonzalez, M.P.; Pegon, P.; Varum, H.; Pinto, A.V. (2000-b) - *Frequency and damping evolution during experimental seismic response of civil engineering structures* - COST F3 Conference on System Identification & Structural Health Monitoring, Madrid, 6<sup>th</sup>-9<sup>th</sup> June.

Molina, F.J.; Verzeletti, G.; Magonette, G.; Buchet, P.; Géradin, M. (1999-b) - *Bi-directional pseudo-dynamic test of a full-size 3-storey building* - Journal of Earthquake Engineering and Structural Dynamics, No. 28, pp. 1541-1566.

Monti, G.; Spacone, E. (1998) - *Insertion of bond-slip into RC beam fiber finite elements* - 11<sup>th</sup> ECEE, Paris, France, ISBN 90-5410-982-3, A.A. Balkema, Rotterdam, 6<sup>th</sup>-11<sup>th</sup> September.

Murayama, Y.; Suda, K.; Toshimichi, I.; Shimbo, H. (1996) - *Stress-slip model of the longitudinal reinforcing bars in a reinforced concrete column joint* - 11<sup>th</sup> WCEE, Acapulco, Mexico, Elsevier Science, Paper No. 1750, ISBN 0-08-042822-3.

## N

Naeim, F. (1994) - *Northridge earthquake ground motions: Implications for seismic design of tall buildings* - 3<sup>rd</sup> Conference on Tall Buildings in Seismic Regions, Los Angeles, Los Angeles Tall Buildings Structural Design Council, May.

NAHB (1994) - *Assessment of damage to residential buildings caused by the Northridge earthquake* - NAHB Research Center, Upper Marlboro, Maryland, US Department of Housing and Urban Development Office of Policy Development and Research, July.

Nakano, Y. (1995) - *Damage to buildings due to 1994 Sanriku-harukaoki earthquake* - Building disaster, Japan Building Disaster Prevention Association, Vol. 211, pp. 6-15 (in Japanese).

Negro, P.; Verzeletti, G.; Magonette, G.; Pinto, A.V. (1994) - *Tests on a four-storey full-scale RC frame designed according to Eurocodes 8 and 2: Preliminary Report* - EUR 15879 EN, ELSA, JRC-Ispra, EC, Italy.

NIST (1994) - *1994 Northridge earthquake: Performance of structures, lifelines, and fire protection systems* - National Institute of Standards and Technology, Washington.



---

NZNSSEE (1996) - *The assessment and improvement of the structural performance of earthquake risk buildings: Draft for general release* - New Zealand National Society for Earthquake Engineering.

## O

OECD (2001) - *OECD science, technology and industry scoreboard: Towards a knowledge-based economy* - Organisation for Economic Co-operation and Development, ISBN 92-64-18648-4.

Okada, T.; Nakano, Y.; Kumazawa, F. (1992) - *Experimental study of 1/10 scaled RC frames retrofitted with steel framed Y-shaped bracing system* - International Symposium on Earthquake Disaster Prevention, Mexico City, pp. 200-209.

Oliveira, D.V.C. (1995) - *Comportamento de pórticos de betão armado preenchedos com paredes de alvenaria* - MSc thesis, FEUP, University of Porto (in Portuguese).

Oliveira, C.S.; Azevedo, J.; Delgado, R.; Costa, A.G.; Campos-Costa, A. (1995) - *O sismo de Northridge, Los Angeles, 17 de Janeiro de 1994: Ensinamentos para Portugal* - Edition of IST and FEUP, ISBN 972-96893-0-X (in Portuguese).

## P

Pantazopoulou, S.J.; Moehle, J.P.; Shahrooz, B.M. (1988) - *Simple analytical model for T-beams in flexure* - Journal of Structural Engineering, ASCE, Vol. 114, No. 7, pp. 1507-1523, July.

Papadopoulos, G.A.; Ganas, A.; Pavlides, S. (2002) - *The problem of seismic potential assessment: Case study of the unexpected earthquake of 7 September 1999 in Athens, Greece* - Earth Planets Space, Vol. 54, pp. 9-18.

Park, R. (1992) - *Seismic assessment and retrofit of concrete structures - United States and New Zealand developments* - Technical Conference of New Zealand Concrete Society, Wairakei, pp. 18-25.

Park, R.; Paulay, T. (1975) - *Reinforced concrete structures* - John Wiley & Sons, Inc.

Park, Y.J.; Ang, A.H.S. (1985) - *Mechanistic seismic damage model for reinforced concrete* - Journal of Structural Engineering, Vol. 111, No. 4, ISSN 0733-9445/85/0004-0722, Paper No. 19670, April.

Park, Y.J.; Ang, A.H.S.; Wen, Y.K. (1987) - *Damage-limiting aseismic design of buildings* - Earthquake Spectra, Vol. 3, No. 1.

Park, Y.J.; Ang, A.H.S.; Wen, Y.K. (1984) - *Seismic damage analysis and damage-limiting design of RC buildings* - Technical Report of Research, University of Illinois at Urbana-Champaign, ISSN 0069-4274, October.

Paulay, T.; Priestley, M.J.N. (1992) - *Seismic design of reinforced concrete and masonry buildings* - John Wiley & Sons, Inc., ISBN 0-471-54915-0.

- Pegon, P. (1998) - *The numerical simulation of buildings subjected to seismic loading: Application of an integrated modelling strategy* - 11<sup>th</sup> ECEE, Paris, France, Invited lecture, ISBN 90 5809 027 2, A.A. Balkema, Rotterdam, 6<sup>th</sup>-11<sup>th</sup> September.
- Pegon, P.; Pinto, A.V. (2000) - *Pseudo-dynamic testing with substructuring at the ELSA laboratory* - Earthquake Engineering and Structural Dynamics, Vol. 29, pp. 905-925.
- Perera, R.; Carnicero, A.; Alarcón, E.; Gomez, S. (2000) - *A fatigue damage model for seismic response of RC structures* - Computers and Structures, Elsevier Science, Vol. 78, pp. 293-302.
- Peter, K.; Badoux, M. (2000) - *Application of the capacity spectrum method to RC buildings with bearing walls* - 12<sup>th</sup> WCEE, Auckland, New Zealand, January.
- Peter, K.; Badoux, M. (1999) - *Seismic evaluation of existing reinforced concrete buildings in Switzerland* - 11<sup>th</sup> ECEE, Paris, France, ISBN 90-5410-982-3, A.A. Balkema, Rotterdam, 6<sup>th</sup>-11<sup>th</sup> September.
- Pichard, P. (1984) - *Emergency measures and damage assessment after an earthquake* - Studies and documents on the cultural heritage - UNESCO, CLT/84/WS/14.
- Pinho, R. (2000) - *Selective retrofitting of RC structures in seismic areas* - PhD thesis, Imperial College, London, UK.
- Pinho, R.; Elnashai, A.S. (1999) - *Analytical assessment of multi-storey RC frame before and after repair* - ICONS-Topic 2 Report, Imperial College, London, UK.
- Pinho, R.; Elnashai, A.S.; Pinto, A.V.; Varum, H. (2000) - *Pseudo-dynamic testing of a selectively retrofitted full-scale RC frame* - ESEE-00/8, December.
- Pinto, A.V. (1998) - *Earthquake performance of structures: Behaviour, safety and economical aspects* - PhD thesis, JRC-Special Publication, No. I.98.111, September.
- Pinto, A.V.; Varum, H. (2000) - *Repair of two RC frames at the ELSA laboratory (external joints and column: Fibre carbon based technique)* - Personal Notes, ELSA, JRC-Ispra, EC, Italy.
- Pinto, A.V.; Molina, F.J.; Varum, H. (2000-a) - *Tests on the shotcrete infilled frame: Short presentation of the test results* - ELSA, JRC-Ispra, EC, Italy (internal document).
- Pinto, A.V.; Molina, F.J.; Varum, H. (2000-b) - *Final capacity cyclic tests on non-seismic resisting RC frames: Bare and selective retrofitted frames* - EUR Report, ELSA, JRC-Ispra, EC, Italy.
- Pinto, A.V.; Molina, F.J.; Varum, H. (1999-a) - *Assessment, strengthening and repair (tests on the shotcrete infilled frame)* - Short presentation of the test results - ELSA, JRC-Ispra, EC, Italy, December.
- Pinto, A.V.; Varum, H.; Molina, F.J. (2002) - *Experimental assessment and retrofit of full-scale models of existing RC frames* - 12<sup>th</sup> ECEE, London, UK, Paper No. 855, Elsevier Science Ltd., 9<sup>th</sup>-13<sup>th</sup> September.

- Pinto, A.V.; Molina, F.J.; Pegon, P.; Varum, H. (2001-a) - *Actividades do laboratório ELSA no domínio da avaliação e reforço de estruturas em zonas sísmicas - SISMICA2001*, Açores, Portugal, 24-27 October (in Portuguese).
- Pinto, A.V.; Negro, P.; Colombo, A.; Varum, H. (2001-b) - *The use of FRP's in seismic repair and retrofit: Experimental verification - CCC2001-International Conference on Composites in Construction*, 10-12 October, FEUP, Porto.
- Pinto, A.V.; Verzeletti, G.; Molina, F.J.; Varum, H.; Carvalho, E.C.; Coelho, E. (2001-c) - *Pseudo-dynamic tests on non-seismic resisting RC frames (infilled frame and infill strengthened frame tests)* - EU Special Publication (in preparation), ELSA, JRC-Ispra, EC, Italy.
- Pinto, A.V.; Verzeletti, G.; Molina, F.J.; Varum, H.; Coelho, E.; Pinho, R. (1999-c) - *Pseudo-dynamic tests on non-seismic resisting RC frames (bare and selective retrofit frames)* - EUR Report 20244 EN, ELSA, JRC-Ispra, EC, Italy.
- Pinto, A.V.; Verzeletti, G.; Pegon, P.; Magonette, G.; Negro, P.; Guedes, J. (1996) - *Pseudo-dynamic testing of large-scale RC bridges* - Report EUR 16378 EN, ELSA, JRC-Ispra, EC, Italy.
- Pinto, P. (2000) - *Seismic assessment of existing structures: Present state and research needs* - Workshop on Mitigation of Seismic Risk: Support to Recently Affected European Countries, JRC, Belgirate, Italy, November.
- Prakash, V.; Powell, G.H.; Campbell, S. (1993) - *DRAIN-2DX (static and dynamic analysis of inelastic plane structures): Basic program description and user guide* - Report No UCB/SEMM-93/ 17, University California, Berkeley.
- Priestley, M.J.N. (1998) - *Displacement-based approaches to rational limit states design of new structures* - 11<sup>th</sup> ECEE, Paris, France, Invited lecture, ISBN 90 5809 027 2, A.A. Balkema, Rotterdam, 6<sup>th</sup>-11<sup>th</sup> September.
- Priestley, M.J.N. (1997) - *Displacement-based seismic assessment of reinforced concrete buildings* - Journal of Earthquake Engineering, Imperial College of London, Vol. 1, No. 1, pp. 157-192.
- Priestley, M.J.N.; Xiao, R.V. (1994) - *Seismic shear strength of reinforced concrete columns* - ASCE, Journal of Structural Engineering, Vol. 120, No. 8, pp. 2310-2329.
- Priestley, M.J.N.; Seible, F.; Calvi, G.M. (1996) - *Seismic design and retrofit of bridges* - Wiley-Interscience.
- Priestley, M.J.N.; Seible, F.; Xiao, Y.; Verma, R. (1994) - *Steel jacket retrofitting of reinforced concrete bridge columns for enhanced shear strength - Part 1: Theoretical considerations and test design* - ACI Structural Journal, Vol. 91, No. 4, pp. 394-405.

## R

- Rehm, G. (1961) - *Über die Grundlagen des Verbundes zwischen Stahl und Beton* - Deutscher Ausschuss für Stahlbeton, Heft 138 (in German).

- Richards, R. (1995) - *Zero-th order shape optimization utilizing a learning classifier system* - Ph.D. dissertation, Mechanical Engineering Department, Stanford University (available at <http://www.stanford.edu/~buc/SPHINcsX/book.htm#RTFToC0>).
- RILEM (1992) - *Technical recommendations for the testing and use of construction materials* - International Union of testing and Research Laboratories for Materials and Structures, E&FN SPON.
- Rodríguez, M.; Díaz, C. (1987) - *Análisis sísmico de edificios de concreto reforzado* - Revista IMCYC, Vol. 25, No. 198, pp. 15-30 (in Spanish).
- Rodríguez, M.; Park, R. (1994) - *Seismic lead tests on reinforced concrete columns strengthened by jacketing* - ACI Structural Journal, Technical Paper, Title No. 91-S116, pp. 150-159, March-April.
- Rodríguez, M.; Park, R. (1991) - *Repair and strengthening of reinforced concrete buildings for seismic resistance* - Earthquake Spectra, Vol. 7, No. 3, pp. 439-459.
- Rosenblueth, E.; Meli, R. (1986) - *The 1985 earthquake: Causes and effects in Mexico city* - Concrete International, Vol. 8, No. 5, May, pp. 23-34.
- RSA (1983) - *Regulamento de segurança e acções para estruturas de edifícios e pontes* - Decreto-Lei N.º 235/83, Imprensa Nacional, Casa da Moeda, Lisbon, Portugal (in Portuguese).

## S

- Saadatmanesh, H.; Ehsani, M.R.; Jin, L. (1997) - *Seismic retrofitting of rectangular bridge columns with composite straps* - Earthquake Spectra, Vol. 13, No. 2, pp. 281-304.
- Saadatmanesh, H.; Ehsani, M.R.; Li, M.W. (1994) - *Strength and ductility of concrete columns externally reinforced with fiber composite straps* - American Concrete Institute, Structures Journal, Vol. 91, No. 4, pp. 434-447.
- Saatcioglu, M.; Gardner, N.J.; Ghobarah, A. (1999) - *The Kocaeli earthquake of August 17, 1999 in Turkey* - (available at <http://www.genie.uottawa.ca/profs/murat/KocaeliEQ.html>).
- Saiidi, M.; Sozen, M.A. (1981) - *Simple nonlinear seismic analysis of RC structures* - Journal of Structural Division, ASCE, Vol. 107, pp. 937-952.
- Salama, A.I. (1993) - *Repair of earthquake-damaged RC structures* - PhD thesis, Imperial College, University of London, London.
- Sasani, M.; Bertero, V.; Anderson, J. (1999) - *Rehabilitation of non-ductile RC frame building using encasement plates and energy-dissipating devices* - PEER Report 1999/12, Pacific Earthquake Engineering Research Center, University of California, Berkeley.
- Schuller, M.; Mehrabi, A.B.; Noland, J.L.; Shing, P.B. (1994) - *Performance of masonry-infilled RC frames under in-plane lateral loads: experiments* - NCEER Workshop on Seismic Response of Masonry Infills, San Francisco, California.

- SEAOC (1995) - *Performance based seismic engineering of buildings, Part 2: Conceptual framework* - Vision 2000 Committee, Structural Engineers Association of California, Sacramento, California.
- Seible, F.; Hegemier, G.A.; Innamorato, D. (1995) - *Developments in bridge column jacketing using advanced composites* - National Seismic Conference on Bridges and Highways: Progress in Research and Practice, Federal Highway Administration, California Department of Transportation, San Diego, California, 10<sup>th</sup>-13<sup>th</sup> December.
- Seible, F.; Priestley, M.J.N.; Hegemier, G.A.; Innamorato, D. (1997) - *Seismic retrofit of RC columns with continuous carbon fiber jackets* - Journal of Composites for Construction, ASCE, Vol. 1, No. 2, pp. 52-62, May.
- Severn, R.T. (2000) - *Earthquake engineering research infrastructures* - Workshop on Mitigation of Seismic Risk: Support to Recently Affected European Countries, JRC, Belgirate, Italy, November.
- Severn, R.T.; Juhasova, E.; Franchioni, G.; Popa, G.; Sofronie, R.A. (2000) - *Mitigation of seismic risk by composing masonry structures* - Workshop on Mitigation of Seismic Risk: Support to Recently Affected European Countries, JRC, Belgirate, Italy, November.
- Shepherdson, E. (2001) - *Teaching concepts utilizing active learning computer environments* - PhD thesis, Massachusetts Institute of Technology, February.
- Shibata, A.; Sozen, M.A. (1976) - *Substitute-structure method for seismic design in reinforced concrete* - Journal of Structural Division, ASCE, Vol. 102, pp. 1-18.
- Silva-Araya, W.F.; Rincón, O.T.; O'Neill, L.P. (eds.) (1997) - *Repair and rehabilitation of reinforced concrete structures: The state-of-the-art* - International Seminar, Workshop and Exhibition, Maracaibo, Venezuela, April 28<sup>th</sup>-May 1<sup>st</sup>, Published by ASCE.
- Soleimani, D.; Popov, E.; Bertero, V. (1979) - *Hysteretic behaviour of reinforced concrete beam-column subassemblages* - ACI Journal, Technical paper, Title No. 76-48.
- Sortis, A.; Pasquale, G.; Nasini, U. (1999) - *Criteri di calcolo per la progettazione degli interventi - Terremoto in Umbria e Marche del 1997* - Servizio Sismico Nazionale, Editrice Sallustiana, Roma (in Italian).
- Souza, V.C.M.; Ripper, T. (1998) - *Patologia, recuperação e reforço de estruturas de concreto* - PINI, São Paulo, Brazil (in Portuguese).
- SPES (2003) - *Políticas de reconstrução sísmica nos Açores: Lições para o continente* - IST, Lisbon, Portuguese Society for Earthquake Engineering, February (in Portuguese).
- SPES (2001) - *Encontro sobre redução da vulnerabilidade sísmica do edificado em Portugal* - LNEC, Lisbon, SPES/GECORPA, April (in Portuguese).
- Stafford-Smith, B.; Carter, C. (1969) - *A method of analysis for infilled frames* - Proceedings ICE, Vol. 44, pp. 31-44.

Stephens, J.E.; Yao, J.P.T. (1987) - *Damage assessment using response measurements* - ASCE Journal of Structural Engineering, Vol. 113, No. 4, pp.787-801, April.

Sucuoglu, H. (2000) - *The 1999 Kocaeli and Düzce-Turkey earthquakes* - Workshop on Mitigation of Seismic Risk: Support to Recently Affected European Countries, JRC, Belgirate, Italy, November.

Sugano, S. (2000) - *Seismic rehabilitation of existing concrete buildings in Japan* - 12<sup>th</sup> WCEE, Auckland, New Zealand, January.

Sugano, S. (1996) - *State-of-the-art in techniques for rehabilitation of buildings* - 11<sup>th</sup> WCEE, Acapulco, Mexico, Paper No. 2178.

Svanberg, K. (1987) - *The method of moving asymptotes - A new method for structural optimization* - International Journal for Numerical Methods in Engineering, Vol. 24, pp. 359-373.

## T

Tamijani, M.H.V. (1998) - *Seismic behaviour, analysis and design of eccentrically braced frames with vertical shear-links* - Dissertation CE Department, University of Technology Darmstadt, Darmstadt.

Takiguchi, K.; Ichinose, T.; Hotta, H. (1988) - *Earthquake damage evaluation and repair techniques of RC columns with round bars* - 9<sup>th</sup> WCEE, Tokyo-Kyoto, Japan, Vol. VII, pp. 285-291, 2<sup>nd</sup>-9<sup>th</sup> August.

Tankut, T.; Ersoy, U. (1998) - *Seismic repair/strengthening of RC structures - METU research and practice* - Second Japan-Turkey Workshop on Earthquake Engineering: Repair & Strengthening of Existing Buildings, Istanbul.

Taucer, F. (2000) - *Performance based design of infilled frames protected with energy dissipation devices* - Personal presentation at the ELSA, JRC-Ispra, EC, Italy.

Tilly, G.P. (ed.) (1986) - *Dynamic behaviour of concrete structures* - Elsevier, Amsterdam.

Tjebbes, M.R. (1994) - *Determination of the equivalent slab width from experimental data* - Technical Note No. I.94.139, JRC-Ispra, EC, Italy.

Triantafillou, T.C. (1998) - *Strengthening of structures with advanced FRP's* - Progress in Structural Engineering and Materials, Vol. 1, No. 2, pp. 126-134 - Construction Research Communications Limited, ISSN 1365-0556.

Trigo, J.A. (1968) - *Estruturas de painéis sob acção de solicitações horizontais* - LNEC, Lisbon (in Portuguese).

## U

UBC-97 (1997) - *Uniform Building Code: Structural engineering design provision* - International Conference of Building Officials, 1997 Edition, Whittier, California.

- Umemura, H.; Takizawa, H. (1982) - *Dynamic response of reinforced concrete buildings* - Structural Engineering Documents, ISBN 3 85748 029 7, IABSE, Zürich, Switzerland.
- UNESCO (1968) - *Recommendations concerning the preservation of cultural property endangered by public and private works* - Adopted on 10<sup>th</sup> November (available at <http://www.unesco.org/whc/nwhc/pages/part/main.htm>).
- USGS (2000) - *Implications for earthquake risk reduction in the United States from the Kocaeli, Turkey, earthquake of August 17, 1999* - US Geological Survey Circular 1193.
- USGS (1995) - *Reducing earthquake losses throughout the United States* - US Geological Survey Fact Sheet-169-95 - (available at <http://quake.wr.usgs.gov/QUAKES/FactSheets/BayArea/>).

## V

- Varum, H. (1995) - *Modelo numérico para a análise sísmica de pórticos planos de betão armado* - MSc thesis, FEUP, University of Porto (in Portuguese).
- Varum, H.; Costa, A.G. (1997) - *Modelo não-linear para a análise estática e/ou dinâmica de pórticos de betão armado* - 3<sup>o</sup> Encontro de Sismologia e Engenharia Sísmica, Instituto Superior Técnico, Lisbon, 3<sup>rd</sup>-5<sup>th</sup> December (in Portuguese).
- Varum, H.; Costa, A.G. (1996) - *Modelo numérico para a análise de pórticos planos de betão armado* - XXVIII Jornadas Sul-Americanas de Engenharia de Estruturas, Escola de Engenharia de S. Carlos, University of S. Paulo, Brasil, 1<sup>st</sup>-5<sup>th</sup> September (in Portuguese).
- Varum, H.; Oliveira, D. (1994) - *Métodos de reabilitação e reforço de estruturas: State-of-the-art* - Human Capital and Mobility Programme, Laboratory of Reinforced Concrete, National Technical University of Athens, Greece (in Portuguese).
- Varum, H.; Pinto, A.V. (2001-a) - *Utilização do aço na reabilitação e reforço de edifícios existentes: Avaliação da sua eficiência em testes à escala real* - III Encontro de Construção Metálica e Mista, organized by Associação Portuguesa de Construção Metálica e Mista (CMM) and SAECivil of University of Aveiro, Aveiro, Portugal, 6<sup>th</sup>-7<sup>th</sup> December (in Portuguese).
- Varum, H.; Pinto, A.V. (2001-b) - *Simplified methods for the assessment and redesign of existing structures* - EU Special Publication (in preparation), ELSA, JRC-Ispira, EC, Italy.
- Varum, H.; Pinto, A.V. (1999) - *Dynamic non-linear analyses for the 4-storey RC frame: Bare, infilled and retrofitted frames* - Special Publication No. I.00.132, ISIS, SSMU, ELSA, JRC-Ispira, EC, Italy.
- Varum, H.; Pinto, A.V.; Coelho, E.; Carvalho, E.C. (2000) - *Seismic analyses of a RC building: Study of a retrofitting solution* - Conference on Abnormal Loading on Structures: Experimental and Numerical Modelling - Joint Institution of Structural

Engineers/City University London International - London - Viridi, K.S.; Mathews, R.S.; Clarke, J.L.; Garas, F.K. (eds.) - Spon Press; ISBN 0419259600 - March.

Varum, H.; Carvalho, E.C.; Coelho, E.; Pinto, A.V. (1999) - *Dynamic non-linear analyses for the 4-storey infilled RC frame: Study of a retrofiting solution* - 4<sup>o</sup> Encontro Nacional sobre Sismologia e Engenharia Sísmica and 2.<sup>ème</sup> Rencontre en Génie Parasismique des Pays Méditerranéens - SISMICA 99 - University of Algarve - Faro - 28<sup>th</sup>-30<sup>th</sup> October.

Verpeaux, P.; Millard, A.; Charras, T. (1991) - *A modern solution of optimization problem using CASTEM-2000* - European Conference on New Advances in Computational Structural Mechanics, Ladeveze, P.; Zienkiewicz, O.C. Chairmans), Giens (Var), France, 2<sup>nd</sup>-5<sup>th</sup> April.

Vintzeleou, E. (1987) - *Behaviour of infilled frames subject to lateral actions* (a state-of-the-art report).

## W

Wabo MBrace (2002) - *Composite strengthening system: Engineering design guidelines* - Third Edition, May.

Warner, J. (1996) - *Shotcrete in seismic repair and retrofit* - Seismic rehabilitation of concrete structures, ACI, Sabnis, G.M.; Shroff, A.C.; Kahn, L.F. (eds.), Farmington Hills, Michigan, pp. 299-313.

## Y

Yamazaki, F. (1993) - *The January 15, 1993 Kushiro-Oki earthquake: A quick look report* - (available at <http://incede.iis.u-tokyo.ac.jp/Newsletter/1.3sp/1-3-2sp.htm>), INCEDE Newsletter, Supplement to Vol. 1, No. 3.

Yang, Y.B.; Kuo S.R. (1994) - *Theory & analysis of non-linear framed structures* - Prentice Hall, ISBN 0-13-109224-3.

Youssef, M.; Ghobarah, A. (2001) - *Modelling of RC beam-column joints and structural walls* - Journal of Earthquake Engineering, Imperial College Press, Vol. 5, No. 1, pp. 93-111.

## Z

Zarnic, R.; Gostic, S. (1998) - *Non-linear modelling of masonry infilled frames* - 11<sup>th</sup> ECEE; Paris, France, ISBN 90 5410 982 3, A.A. Balkema, Rotterdam, 6<sup>th</sup>-11<sup>th</sup> September.

Zarnic, R.; Gostic, S. (1997) - *Masonry infilled frames as an effective structural sub-assembly* - Proceedings of the International Workshop Seismic design methodologies for the next generation of codes, Fajfar, P. and Krawinkler, H. (eds.), Slovenia, Rotterdam, Balkema, 24-27 June.



Zarnic, R.; Tomazevic, M. (1985) - *Study of behaviour of masonry infilled reinforced concrete frames subjected to seismic loading* - 7<sup>th</sup> International Brick Masonry Conference, Brick Dev. Res. Inst. & Dept. of Arch. and Bldg., University of Melbourne, Vol. 2, pp. 1315-1325.

## 2. RECOMMENDED READING

Next are listed other references, not necessarily quoted in the thesis, of particular interest and complementary to better comprehend the subjects herein studied.

Ang, A.H.-S.; Tang, W.H. (1984) - *Probability concepts in engineering planning and design* - Vol. II, John Wiley and sons, Inc., New York.

Balendran, R.V.; Rana, T.M.; Nadeem, A. (2001) - *Strengthening of concrete structures with FRP sheets and plates* - Structural Survey, Vol. 19, No. 4, pp. 185-192.

Campos-Costa, A. (1993) - *A acção dos sismos e o comportamento das estruturas* - PhD thesis, FEUP, University of Porto, Oporto, October (in Portuguese).

Castellani, B.M.; Ciccotelli, A.; Coronelli, D. (1994) - *Bond slip effects on reinforced concrete elements under earthquake loading* - European Engineering Earthquake, Vol. 8, No. 3, pp. 3-10.

Castellani, A.; Negro, P.; Colombo, A.; Castellani, M. (2000) - *Experimental response of a non-ductile RC building rehabilitated by means of fibre-reinforced polymers* - 12<sup>th</sup> WCEE, Auckland, New Zealand, January.

Chai, Y.H.; Romstad, K.M.; Bird, S.M. (1995) - *Energy-based linear damage model for high-intensity seismic loading* - Journal of Structural Engineering, pp. 857-864, May.

Chen, J.-J.; Duan, B.-Y. (1999) - *Reliability aspects in dynamic and structural optimization* - Structural Dynamic Systems Computational Techniques and Optimization: Reliability and Damage Tolerance, C. Leondes (ed.), Gordon and Breach Science Publishers, ISBN 90-5699-652-5.

Christopher, A. (1998) - *The nature of ground motion and its effect on buildings* - (available at <http://nisee.ce.berkeley.edu/lessons/arnold.html>) - General Lessons in Earthquake Engineering (NISEE).

Chung, Y.S.; Meyer, C.; Shinozuka, M. (1987) - *Seismic damage assessment of reinforced concrete members* - Technical Report NCEER-87-0022, National Center for Earthquake Engineering Research.

Clark, P.W.; Higashino, M.; Kelly, J.M. (2002) - *Performance of seismically isolated structures in the January 17, 1994 Northridge earthquake* - NISEE online library, University of California, Berkeley.

- COLA (1995) - *Earthquake hazard reduction in existing reinforced concrete buildings and concrete frame buildings with masonry infills* - City of Los Angeles, January.
- Cosenza, E.; Manfredi, G.; Verderame, G.M. (1999) - *Problemi di verifica sismica di telai progettati per carichi verticali* - 9<sup>th</sup> Convegno Nazionale L'Ingegneria Sismica in Italia, Torino, 20-23 September (in Italian).
- Costa, A.G. (2003) - *Aspectos técnicos da reconstrução dos Açores* - Políticas de Reconstrução Sísmica nos Açores: Lições para o Continente - IST, Lisbon, SPES, February (in Portuguese).
- Delgado, P. (2000) - *Vulnerabilidade sísmica de pontes* - MSc thesis, FEUP, University of Porto (in Portuguese).
- DiPasquale, E.; Cakmak, A.S. (1990) - *Detection of seismic structural damage using parameter-based global damage indices* - Probabilistic Engineering Mechanics, Vol. 5, No. 2, pp. 60-65.
- Ellingwood, B.; Hwang, H. (1985) - *Probabilistic descriptions of resistance of safety-related structures in nuclear power plants* - Nuclear Engineering and Design, Vol. 88, pp. 169-178.
- Fardis, M.N. (1996) - *Experimental and numerical investigations on the seismic response of RC infilled frames and recommendations for code provisions* - ECOEST/PREC8, Report No. 6.
- Fardis, M.N.; Bousias, S.N. (1999) - *Engineering aspects of the Mt. Parnes (Athens) earthquake of 7/9/99* - Structures Laboratory, Department of Civil Engineering, University of Patras, Greece.
- Faria, R. (1994) - *Avaliação do comportamento sísmico de barragens de betão através de um modelo de dano contínuo* - PhD thesis, FEUP, University of Porto (in Portuguese).
- Faza, S.S.; Gangarao, H.V.S. (1994) - *Fiber composite wrap for rehabilitation of concrete structures* - Infrastructures: New Materials Engineering Conference, San Diego, CA, US.
- Fletcher, R. (1995) - *Practical methods of optimization* - John Willey & Sons, ISBN 0-471-91547-5.
- Ghobarah, A.; Abou-Elfath, H. (1998) - *Damage assessment of non-ductile reinforced concrete frames* - 11<sup>th</sup> ECEE, Paris, France, ISBN 90-5410-982-3, A.A. Balkema, Rotterdam, 6<sup>th</sup>-11<sup>th</sup> September.
- Ghobarah, A.; El-Attar, M. (1998) - *Seismic performance evaluation of reinforced concrete buildings* - 11<sup>th</sup> ECEE, Paris, France, ISBN 90-5410-982-3, A.A. Balkema, Rotterdam, 6<sup>th</sup>-11<sup>th</sup> September.
- Ghobarah, A.; Youssef, M. (1999) - *Response of an existing RC building including concrete crushing and bond slip effects* - 8<sup>th</sup> Canadian Conference on Earthquake Engineering, Vancouver.

- Ghobarah, A.; Aly, N.M.; El-Attar, M. (1997) - *Performance level criteria and evaluation* - International Workshop on Seismic Design Methodologies for the Next Generation of Codes, Bled, Slovenia, pp. 207-215.
- Guedes, J.; Pegon, P.; Pinto, A.V. (1994) - *A fibre-Timoshenko beam element in CASTEM-2000* - JRC-Special Publication, No. I.94.31, ELSA, JRC-Ispira, EC, Italy.
- Haftka, R.; Grandhi, R. (1986) - *Structural shape optimization: A survey* - Computer Methods in Applied Mechanics and Engineering, Vol. 57, pp. 91-106.
- Hamburger, R.O.; Cole, C.A. (2001) - *Seismic upgrading of existing structures* - Naeim, F. (ed.) - The seismic design handbook - Kluwer Academic Publishers, ISBN 0-7923-7301-4.
- Hoskin, C.B.; Baker, A.A. (1986) - *AIAA education series* - American Institute of Aeronautics and Astronautics, Inc., New York.
- Hwang, H.; Jaw, J.-W.; Shau, H.-J. (1988) - *Seismic performance assessment of code-designed structures* - Technical Report NCEER-88-0007, National Center for Earthquake Engineering Research, State University of New York at Buffalo.
- Krawinkler, H. (1996) - *Pushover analysis: why, how, when, and when not to use it* - 65<sup>th</sup> Annual Convention of the Structural Engineers Association of California, Maui, Hawaii, pp. 17-36.
- Kunnath, S.K.; El-Bahy, A.; Taylor, A.W.; Stone, W.C. (1997) - *Cumulative seismic damage of reinforced concrete bridge piers* - NISTIR 6075, National Institute of Standards and Technology, US Department of Commerce Technology Administration, October.
- Leite, A.N.; Lopes, M. (2003) - *Viabilidade económica do reforço sísmico das construções* - Políticas de Reconstrução Sísmica nos Açores: Lições para o Continente - IST, Lisbon, SPES, February (in Portuguese).
- LNEC (1993) - *Cooperative research on the seismic response of reinforced concrete structures* - Contract No. 4504-91-10 ED ISP P, Final Report, Lisbon, Proc. 035/11/10778, October.
- Mahin, S.A.; Bertero, V.V. (1976) - *Problems in establishing and predicting ductility in aseismic design* - International Symposium on Earthquake Structural Engineering, St. Louis, Missouri, August.
- Mainstone, R.J. (1971) - *On the stiffness and strength of infilled frames* - Institution of Civil Engineers, Supplement iv.
- Manfredi, G.; Peccem M. (1998) - *Effectiveness of the plastic hinge in the assessment of the rotation capacity of RC columns* - 11<sup>th</sup> ECEE, Paris, France, ISBN 90-5410-982-3, A.A. Balkema, Rotterdam, 6<sup>th</sup>-11<sup>th</sup> September.
- Maxwell, J. (1872) - *On reciprocal figures, frames, and diagrams of force* - Transactions of the Royal Society of Edinburgh, Vol. 26.

- Meier, U.; Deuring, M. (1991) - *The application of fiber composites in bridge repair* - Strasse and Verkehr, No. 9.
- Meier, U.; Kaiser, H.P. (1991) - *Strengthening of structures with CFRP laminates* - Advanced Composite Materials in Civil Engineering Structures, MT Div/ASCE/ Las Vegas.
- Melchers, R. (1999) - *Structural reliability analysis and prediction* - ISBN 0-471-98324-1, John Willey & Sons, Inc.
- Michell, A. (1904) - *The limits of economy of material in frame structures* - Phil Mag, Vol. 8, pp. 589-597.
- Miranda, E.; Ruiz-García, J. (2002) - *Evaluation of approximate methods to estimate maximum inelastic displacement demands* - Journal of Earthquake Engineering and Structural Dynamics, No. 31, pp. 539-560.
- Mola, E.; Tsionis, G.; Taucer, F.; Pinto, A.V. (2003) - *The Molise (Italy) earthquakes of 31 October and 1 November 2002: Report and analysis from a field mission* - Draft report, ELSA, JRC-Ispira, EC, Italy.
- Monti, G.; Pinto P.E. (1999) - *Deterministic assessment of a multi-storey reinforced concrete frame through pushover* - ICONS Report, Dipartimento di Ingegneria Strutturale e Geotecnica, Università di Roma 'La Sapienza', Rome, Italy.
- Negro, P.; Pinto, A.V.; Verzeletti, G.; Magonette, G. (1996) - *PsD test on four-storey RC building designed according to Eurocodes* - Journal of Structural Engineering.
- Nielsen, S.R.K.; Cakmak, A.S. (1992) - *Evaluation of maximum softening damage indicator for reinforced concrete under seismic excitation* - 1<sup>st</sup> International Conference on Computational Stochastic Mechanics, Spanos and Brebbia (eds.), pp. 169-184.
- Nunez, I.L. (2000) - *Compound growth or compound seismic risk of destruction? Some vulnerability lessons from the Izmit, Turkey earthquake of 17 August 1999* - 2<sup>nd</sup> Euro-Conference on Global Change and Catastrophe Risk Management: Earthquake Risks in Europe - IIASA, Laxenburg, Austria, 6<sup>th</sup>-9<sup>th</sup> July.
- Oliveira, D.V.C. (2002) - *Experimental and numerical analysis of blocky masonry structures under cyclic loading* - PhD thesis, University of Minho, October.
- Pinto, A.V.; Pegon, P.; Campos-Costa, A. (1999-b) - *Pseudo-dynamic testing of bridges with asynchronous input motions* - JRC-Special Publication.
- Powell, G.H.; Allahabadi, R. (1988) - *Seismic damage prediction by deterministic methods: Concepts and procedures* - Earthquake Engineering and Structural Dynamics, Vol. 16, pp. 719-734.
- REBAP (1984) - *Regulamento de estruturas de betão armado e pré-esforçado* - Decreto-Lei N.º 349-C/83, Imprensa Nacional, Casa da Moeda, Lisbon (in Portuguese).
- Recla, M.; Calvi, G.M. (1999) - *Oral presentation* - ICONS-Topic 2 Meeting.

- Romão, X.N. (2002) - *Novos modelos de dimensionamento sísmico de estruturas* - Master thesis, FEUP, University of Porto, April (in Portuguese).
- Rossetto, T.; Elnashai, A. (2002) - *Derivation of vulnerability functions for RC buildings based on observational data* - SAFFER research report, EC (available at [http://www.saferr.net/reports/Vulnerability\\_Paper2.pdf](http://www.saferr.net/reports/Vulnerability_Paper2.pdf)).
- Saadatmanesh, H. (1999) - *Seismic retrofitting of concrete columns with fiber composite wrap: An analytical and experimental study* - Structural Dynamic Systems Computational Techniques and Optimization: Reliability and Damage Tolerance, C. Leondes (ed.), Gordon and Breach Science Publishers, ISBN 90-5699-652-5.
- Sabetta, F. (2000-a) - *Elements of seismology* - International Seminar on Evaluation of Seismic Risk and Reduction of Vulnerability of Historical Structures, Pavia, Italy, 18<sup>th</sup>-30<sup>th</sup> June.
- Sabetta, F. (2000-b) - *Seismic risk assessment and reduction in Italy* - International Seminar on Evaluation of Seismic Risk and Reduction of Vulnerability of Historical Structures, Pavia, Italy, 18<sup>th</sup>-30<sup>th</sup> June.
- Schmit, L. (1960) - *Structural design by systematic synthesis* - 2<sup>nd</sup> ASCE Conference Electr Comp (Pittsburg, PA), pp. 105-122.
- Seidel, M.J.; Reinhorn, A.M.; Park, Y.J. (1989) - *Seismic damageability assessment of RC buildings in eastern US* - Journal of Structural Engineering, Vol. 115, No. 9, September.
- Singh, M.P.; Moreschi, L.M. (2001) - *Optimal seismic response control with dampers* - Earthquake Engineering and Structural Dynamics, Vol. 30, pp. 553-572.
- Skjaerbaek, P.S.; Nielsen, S.R.K.; Kirkegaard, P.H. (1997) - *Earthquake tests on scale 1:5 RC-frames* - Fracture & Dynamics, Paper No. 86, ISSN 1395-7953 R9713, Department of Building Technology and Structural Engineering, Aalborg University, Aalborg, Denmark.
- Skjaerbaek, P.S.; Nielsen, S.R.K.; Kirkegaard, P.H.; Cakmak, A.S. (1997) - *Experimental study of damage indicators for a 2-bay, 6-storey RC-frame* - Journal of Structural Engineering, ASCE.
- Tanabe, T.A. (1999) - *Comparative performances of seismic design codes for concrete structures* (two volumes) - Elsevier Publisher, ISBN 0 08 043021 X.
- Tasai, A. (1992) - *Effective repair with resin for bond failure of RC members* - 10<sup>th</sup> WCEE, Balkema, Rotterdam, ISBN 90-5410-060-5, pp. 5211-5216.
- Taucer, F. (1999) - *A displacement based design methodology for retrofitting of frame structures using dissipation devices* - JRC-Publication.
- Tsionis, G.; Negro, P.; Molina, F.J.; Colombo, A. (2001) - *Pseudo-dynamic tests on a 4-storey RC dual frame building* - Report EUR 19902 EN, ISIS, SSMU, ELSA, JRC-Ispra, EC, Italy.

- Varum, H.; Neves, A.S. (1995) - *Modelo linear para a optimização de estruturas articuladas* - XVI Congresso Ibero-Latino-Americano sobre Métodos Computacionais para Engenharia (CILAMCE), Curitiba, Brasil, 29<sup>th</sup> November to 1<sup>st</sup> December (in Portuguese).
- Vitiello, E.; Pister, K.S. (1974) - *Application of reliability-based global cost optimization to design of earthquake resistant structures* - Report No. EERC 74-10, EERC, Berkeley, California, August.
- Williams, M.S.; Sexsmith, R.G. (1995) - *Seismic damage indices for concrete structures: A state-of-the-art review* - Earthquake Spectra, Vol. 11, No. 2, pp. 319-349, May.
- Youssef, M.; Ghobarah, A. (1999) - *Strength deterioration due to bond slip and concrete crushing in modelling of reinforced concrete members* - ACI Structural Journal, Technical Paper, Title No. 96-S105, pp. 956-966, November-December.
- Zarnic, R. (1994) - *Inelastic model of RC frame with masonry infill: Analytical approach* - Engineering Modelling, Vol. 1, No. 2, pp. 47-54.
- Zerbe, H.E.; Durrani, A.J. (1990) - *Seismic response of connections in two-bay reinforced concrete frame subassemblies with a floor slab* - ACI Structural Journal, Vol. 87, No. 4.

### 3. WEB RESOURCES

Apart from those cited in the references list, here are listed a series of web-sites related to the subject herein studied (links to earthquake engineering related web-sites, news groups, general and specific information applications, etc.). These web-pages were last visited in October 2002.

Advanced Technology for Large Structural Systems (Lehigh University, Pennsylvania, US)

<http://www.atlss.lehigh.edu/>

All about Earthquake Engineering

<http://users.hol.gr/~tbp/ee/>

Applied Technology Council (Structural Engineers Association of California, US)

<http://www.atcouncil.org/>

Automatic monitoring of regional seismic events

<http://www.fi.uib.no/~antonych/IRIS.html>

Building Seismic Safety Council (Washington, US)

<http://www.bssconline.org/>

California Seismic Safety Commission (CSSC)

<http://www.seismic.ca.gov/>

Civil and Mechanical Systems (US)

<http://www.eng.nsf.gov/cms/default.htm>

Computational Structural Mechanics (NCSA, US)

<http://archive.ncsa.uiuc.edu/EP/CSM/>

Concrete Repair Association (UK)

<http://www.concreterepair.org.uk/cra/>

Council of the National Seismic System (CNSS, US)

<http://www.cnss.org/>

Earthquake Database

<http://www.mysteries-megasite.com/main/bigsearch/earth-1.html>

Earthquake Engineering Research Centre (Bristol University, UK)

<http://www.cen.bris.ac.uk/civil/research/eerc/>

Earthquake Engineering Research Centre (University of California, Berkeley)

<http://eerc.berkeley.edu/>

Earthquake Engineering Research Institute (EERI)

<http://www.eeri.org/>

Electronic Journal of Structural Engineering (University of Melbourne, Australia)

<http://www.civag.unimelb.edu.au/ejse/>

Engineering Consultation & 3D Finite Element Structural Analysis Software (CADRE)

<http://www.cadreanalytic.com/>

EQ Prediction

<http://users.otenet.gr/~thandin/index.htm>

EQECAT

<http://www.eqecat.com/>

EQNET - Earthquake Information Network

<http://www.eqnet.org/>

European Laboratory for Structural Assessment (ELSA, JRC, EC, Italy)

<http://elsa.jrc.it/>

European Macro-Seismic Scale

<http://www.gfz-potsdam.de/pb5/pb53/projekt/ems/index.html>

European School of Advanced Studies in Reduction of Seismic Risk (ROSE School)

<http://www.roseschool.it/>

European Seismological Commission

<http://www.gserg.nmh.ac.uk/esc>

European Strong-Motion Database (ESD)

<http://www.isesd.cv.ic.ac.uk/>

European School of Advanced Studies in Preservation of the Architectural Heritage (Italy)

<http://www.unipv.it/iuss/esascpsa/>

GALBIS (Spain)

<http://www.galbis.org/>

GEOCID (Portugal)

<http://geocid-snig.igeo.pt/Portugues/sismos.html>

Global Earthquake Response Center

<http://www.earthquakes.com/>

IDARC - Computer Program for Seismic Inelastic Structural Analysis

<http://civil.eng.buffalo.edu/idarc2d50/>

INFILTEC - Inexpensive Seismometer Project

<http://www.infiltec.com/seismo/>

Information Technology in Construction (Slovenia)

<http://itc.fgg.uni-lj.si/>

Institute of Earthquake Engineering and Engineering Seismology (Republic of Macedonia)

<http://www.iziis.ukim.edu.mk/>

Institute of Geological and Nuclear Sciences (New Zealand)

<http://www.gns.cri.nz/>

International Association of Seismology & Physics of the Earth's Interior

<http://www.seismo.com/iaspei/>

International Centre for the Preservation of the Architectural Heritage (Italy)

<http://soalinux.comune.firenze.it/cicop/>

International Council on Monuments and Sites

<http://www.international.icomos.org/>

International Networks

[http://wwwneic.cr.usgs.gov/neis/station\\_book/NETWORK.html](http://wwwneic.cr.usgs.gov/neis/station_book/NETWORK.html)

International Seismological Centre (UK)

<http://www.isc.ac.uk/>

IRIS Headquarters

<http://www.iris.edu/>

ITSAK (Greece)

<http://www.itsak.gr/index.html>

John A. Blume Earthquake Engineering Center

<http://blume.stanford.edu/>

Laboratory of Earthquake Engineering (Athens, Greece)

<http://frida.transport.civil.ntua.gr/earthquake/index.htm>



Mid-America Earthquake Center (MAE, US)

<http://mae.ce.uiuc.edu/>

Multidisciplinary Center for Earthquake Engineering Research (MCEER, US)

<http://mceer.buffalo.edu/>

National Information Center of Earthquake Engineering (NICEE, Kanpur, India)

<http://www.nicee.org/>

National Information Service for Earthquake Engineering (NISEE, California)

<http://nisee.berkeley.edu/>

National Research Institute for Earth Science and Disaster Prevention (NIED, Japan)

<http://www.bosai.go.jp/>

Natural Disaster Reference Database (NASA)

<http://ndrd.gsfc.nasa.gov/>

Network for Earthquake Engineering Simulation (NEES)

<http://www.eng.nsf.gov/nees/>

New Zealand Society for Earthquake Engineering (NZSEE)

<http://www.nzsee.org.nz/index.htm>

NOAA - National Geophysical Data Center (US)

<http://www.ngdc.noaa.gov/seg/hazard/earthqk.html>

Pacific Earthquake Engineering Research Centre (PEER, California, US)

<http://peer.berkeley.edu/>

Prototype International Data Centre (US)

<http://www.pidc.org/>

Queensland University Advanced Centre for Earthquake Studies (QUAKES)

<http://quakes.earth.uq.edu.au/>

Reinforced Concrete Column Tests Database

<http://maximus.ce.washington.edu/~peera1/>

Safety Assessment for Earthquake Risk Reduction (SAFERR, EC)

<http://www.saferr.net/scope.htm>

Saving Lives Through Better Design Standards (US Geological Survey)

<http://geopubs.wr.usgs.gov/fact-sheet/fs176-95/>

Seismic stations around the world

<http://www.pidc.org/web-gsett3/Network/seismic.shtml>

Seismograph Station Codes and Coordinates

[http://wwwneic.cr.usgs.gov/neis/station\\_book/](http://wwwneic.cr.usgs.gov/neis/station_book/)

SeismoLinks

<http://www.seismlinks.com/>

SeismoSoft

<http://www.seismosoft.com/>

Seismosurfing (Pacific Northwest Seismograph Network)

<http://www.geophys.washington.edu/seismosurfing.html>

SISMO - Spanish thematic portal

<http://www.sismo.info/>

Spanish Association of Earthquake Engineering

<http://www.aeis.es/>

Structural Dynamics Control & Earthquake Engineering Laboratory (Indiana, US)

<http://www.nd.edu/~quake/>

Swiss Seismological Service list of worldwide AutoDRM sites

<http://seismo.ethz.ch/autodrm/>

Techdata - Engineering technical data sources

<http://ourworld.compuserve.com/homepages/MJVanVoorhis/techdata.htm>

The Masonry Society

<http://www.masonrysociety.org/>

The Worldwide Earthquake Locator

<http://www.geo.ed.ac.uk/quakexe/quakes>

TNO Building and Construction Research (Holland)

<http://www.bouw.tno.nl/homepage.html>

USGS - United States Strong Motion Program (US)

<http://nsmg.wr.usgs.gov/>

USGS Earthquake Hazards Program (US)

<http://earthquake.usgs.gov/>

USGS National Earthquake Information Center (NEIC, US)

<http://wwwneic.cr.usgs.gov/>

Washington University Structural Control & Earthquake Engineering Laboratory (WUSCEEL)

<http://wusceel.cive.wustl.edu/quake/>

Workshop on Mitigation of Seismic Risk in Europe (2000, ELSA)

<http://elsa.jrc.it/workshop2000/>